Current Problems in Computational Fluid Dynamics

Edited by
O.M. BELOTSERKOVSKII and V.P. SHIDLOVSKY

Advances in Science and Technology in the USSR

Mathematics and Mechanics Series

MIR Publishers
Moscow

Mir Publishers Moscow

Advances
in
Science
and
Technology
in
the USSR

Mathematics and
Mechanics Series

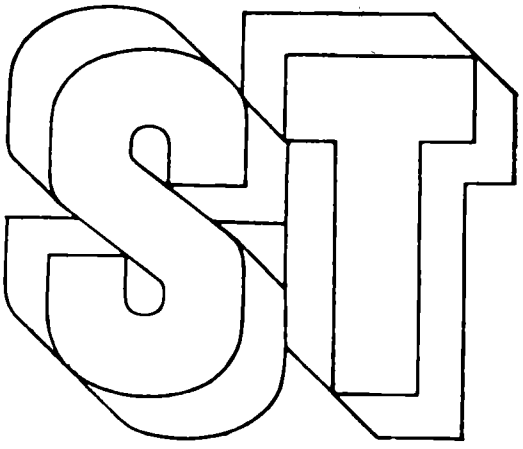

Current Problems in Computational Fluid Dynamics

Edited by O. M. BELOTSERKOVSKII,
Mem. USSR Acad. Sc., and
V. P. SHIDLOVSKY, D.Sc. (Phys.-Math.)

Translated from Russian by
Ram S. Wadhwa, Ph.D.

MIR Publishers
Moscow

Современные проблемы вычислительной гидродинамики

Под редакцией академика *О. М. Белоцерковского*
и д-ра физ.-мат. наук *В. П. Шидловского*

Издательство «Мир» Москва

First published 1986

На английском языке

© Издательство «Мир», 1986
© English translation, Mir Publishers, 1986

Contents

	Preface	7
1	**Numerical Models in Fluid Dynamics** *by O. M. Belotserkovskii*	9
2	**Computations of Supersonic Flow past Lifting Bodies** *by P. I. Chushkin and G. P. Voskresensky*	71
2.1.	Introduction	71
2.2.	Finite-difference Grid Methods	73
2.3.	Method of Characteristics	97
2.4.	Method of Integral Relations and Method of Straight Lines	108
2.5.	Conclusion	117
	References	118
3	**Grid-characteristic Methods in Multidimensional Problems of Gas Dynamics** *by O. M. Belotserkovskii, A. S. Kholodov, and L. I. Turchak*	125
3.1.	Difference Schemes for Simple One-dimensional Hyperbolic Equations	126
3.2.	Grid-characteristic Methods for One-dimensional Quasilinear Hyperbolic Systems	145
3.3.	Grid-characteristic Methods for Multidimensional Systems of Hyperbolic Equations	165
3.4.	Some Results of Numerical Investigations of Multidimensional Problems	170
3.5.	Conclusion	186
	References	187
4	**Method of Difference Potentials for Numerical Solution of Problems in Mechanics of Continuous Media** *by V. S. Ryaben'ky*	190
4.1.	An Example Illustrating the Method	192
4.2.	Green's Formula, Potential, Projector, and Calderón's Boundary Conditions Generalized on the Basis of the Concept of Sharp Trace	200
4.3.	Difference Green's Formula, Potential, Projector, and Internal Boundary Conditions on the Basis of the Concept of Sharp Difference Trace	207
4.4.	Scheme of Approximation of Generalized Continual Potentials by Difference Potentials	212
4.5.	Preliminary Nonconstructive Discretization of Boundary Equations	215
4.6.	Examples of Specific Algorithms	217
	References	223

5	**Higher-accuracy Methods for Solving Fluid Dynamics Problems** *by A. I. Tolstykh*	225
5.1.	Introduction	225
5.2.	Nonsymmetric Compact Schemes for One-dimensional Transport Equations	226
5.3.	Compact Schemes for Equations Containing Diffusive Terms	242
5.4.	Higher-accuracy Algorithms for Multidimensional Problems	254
5.5.	Application of Compact Schemes to the Analysis of Viscous Gas Flows	262
5.6.	Conclusion	271
	References	272
6	**Three-dimensional Boundary Layer at the Surface of a Dihedral Corner** *by V. P. Shidlovsky*	273
6.1.	Introduction	273
6.2.	Formulation of the Problem	274
6.3.	Asymptotic Behaviour of the Solution	277
6.4.	Numerical Solution and Results of Calculations	279
	References	285
7	**On the Stability of a Compressible Boundary Layer Against Three-dimensional Disturbances with Self-induced Pressure Gradient** *by O. S. Ryzhov and V. I. Zhuk*	286
7.1.	Statement of the Problem	286
7.2.	Dispersion Relation	290
7.3.	Three-dimensional Steady Disturbances in Supersonic Boundary Layer	294
7.4.	Supersonic Boundary Layer Instability to Three-dimensional Periodic Disturbances	297
7.5.	Three-dimensional Disturbances in a Subsonic Boundary Layer	301
	References	307
	Name Index	308
	Subject Index	313

Preface

Although computational fluid dynamics is a comparatively new branch of science, more than half books and articles on fluid dynamics now published are devoted to computational methods. The appearance of several new scientific journals dealing exclusively with problems of computational fluid dynamics over the last few years also indicates the rapid expansion of the subject. The number of papers appearing in publications traditionally associated with classical fluid dynamics and involving some application of numerical methods continues to increase.

The Soviet school of computational fluid dynamics has made quite a significant contribution to the formation and growth of this branch of science. The international conferences on the application of numerical methods in fluid dynamics that were initiated by Soviet scientists and are held regularly confirm the world recognition of the Soviet school. The results of leading Soviet scientists, such as Yanenko, Marchuk, Tikhonov, and Samarsky, are widely used all over the world for numerically solving complicated problems in fluid dynamics.

Quite frequently, however, latest Soviet results in computational fluid dynamics reach foreign readers after a considerable delay. This is because the material published in Russian can only be used by a few and there is a considerable time lag before it is translated. Moreover, translated periodicals are not popular. Like other books in the "Advances in Science and Technology in the USSR" series, this collection of articles aims at acquainting foreign scientists with results obtained by Soviet scientists over the last few years in computational fluid dynamics. When we compiled this collection, we took into account that this series also contains books dealing with similar topics. The methods and results described in this book are not presented in any other volume of the series.

At the same time, this collection also includes review of results obtained by both Soviet and foreign scientists. This book is compiled in such a way that after going through the articles, the reader can choose his own approach to the numerical solution of any new fluid-dynamics problem.

Naturally, the choice of the method depends on the problem. The articles preferred for this collection involve those methods and applications which best meet today's requirements, i.e. those involving three-dimensional physical processes, taking into account possible time dependence or nonlinear effects. However, the analysis of many fluid-dynamics phenomena is often hampered due to the ambiguity of the form of the basic equations, and not due to the complexity of their mathematical description. This is the case, for example, for some problems in rarefied gas dynamics or for turbulent or separated flows. These problems can be solved with the help of numerical experiments. In other words, a phenomenon is numerically investigated on the basis of a test model (or a series of models). The ultimate choice of model comes by comparing the results either with experimental data or with the solution of the test problem. The technique of numerical experiment and the choice of hydrodynamic model are thoroughly investigated in the paper by O. M. Belotserkovskii, which opens this collection and is a review of some of the fruitful approaches now used and

which are based on selected numerical models. Several types of problems are considered to illustrate the numerical methods. These include turbulent flow problems, which are solved using an essentially new approach.

The article by P. I. Chushkin and G. P. Voskresensky is a detailed review of the numerical investigations of steady supersonic flow past lifting bodies, carried out in recent years.

The next three articles are devoted to the substantiation and application of numerical methods in fluid dynamics as developed in the USSR. The articles cover the grid-characteristic method by O. M. Belotserkovskii, A. S. Kholodov, and L.I. Turchak, the difference potential method by V.S. Ryaben'ky, and the higher-accuracy methods for solving fluid-dynamics problems by A.I. Tolstykh. In addition to the mathematical principles for constructing the respective methods, these articles also contain specific application examples.

The article by V.P. Shidlovsky describes the formulation, methodology, and results for the numerical solution of three-dimensional boundary layer problems on the surface of a dihedral corner.

The article by O.S. Ryzhov and V.I. Zhuk analyzes the stability of compressible boundary layers to three-dimensional perturbations on the basis of the asymptotic theory of free interaction.

We express our deep gratitude to the authors who contributed to this collection and to all those who rendered scientific and technical assistance in preparing the manuscript. We are especially thankful to Dr. Ram S. Wadhwa for his careful work in the difficult task of translating these articles which were sometimes very different both in style and content. It is hoped that this book will be helpful to readers interested in the numerical solution of current problems in fluid dynamics. Any comments, suggestions or remarks concerning the content of the book will be welcome.

O. M. Belotserkovskii
V. P. Shidlovsky

1 Numerical Models in Fluid Dynamics

O. M. Belotserkovskii, Mem. USSR Acad. Sc.

One of the most important tasks of modern nonlinear mechanics is to investigate the so-called "transient" processes which are frequently encountered in fluid dynamics. These investigations include, for example, transonic and diffraction problems with complex internal structures, flow in separation zones and in the wake of a moving object, problems of the dynamics of rarefied gases (when the Knudsen number $\mathrm{Kn} \simeq 1$), processes associated with Rayleigh-Taylor instability, and, of course, turbulent flows. Being multidimensional in nature, these phenomena are characterized by time-dependence and nonlinearity of the processes, a complex mechanism of interaction, a large deformation of the medium, etc. Their complete investigation (especially in the multidimensional case) became possible only after the advent of high-speed computers.

The achievements of modern theoretical and applied fluid dynamics over the past few years are mainly (and justifiably) associated with the progress in the field of computational mathematics. Today we can rightly adduce computational hydrodynamics and computational physics as fully developed branches of scientific activity. The *numerical experiment*, used in fluid dynamics to consider complex nonlinear problems, stands at present on equal footing with the traditional physical experiment.

The apparent simplicity of the numerical experiment, however, conceals considerable difficulties associated with the construction of the corresponding mathematical model, i.e. a numerical algorithm for solving the problem, and the need to justify the results obtained. The experience gained so far shows that the success of the numerical experiment depends on the choice of the appropriate model for the phenomenon under consideration, the numerical method of solving the corresponding mathematical problem and the method of realizing the algorithm on a computer. The algorithm which in a certain sense is adequate for the phenomenon is deemed successful.

Thus, the choice and construction of an appropriate "*optimal*" (for a given problem) method of solving the mathematical problem seems to us to be the decisive factor in theoretical approaches even today. It should be emphasized once again that the creation of numerical models is of primary importance for the problems of non-

linear mechanics as well. We believe that in near future, the development of rational models rather than high-speed computers will determine the effectiveness of the computational experiment in various branches of science and technology.

We shall describe in this paper the results of numerical investigations of some problems in fluid dynamics[1]. We shall mainly consider the separated flows under "*limiting*" conditions for large values of Reynolds number (Re). This essentially involves the construction of new numerical models for this type of flows. These models must be adequate for the problem under consideration, i.e. they must incorporate its most characteristic properties (the side effects should be eliminated). On the other hand, such models must be adequate for investigation at the present level of growth of computer technology.

1.1. For a long time, the main objective of our investigations was to study the properties of flows and to determine the flight characteristics of vehicles (Fig. 1.1). This constitutes a whole spectrum of

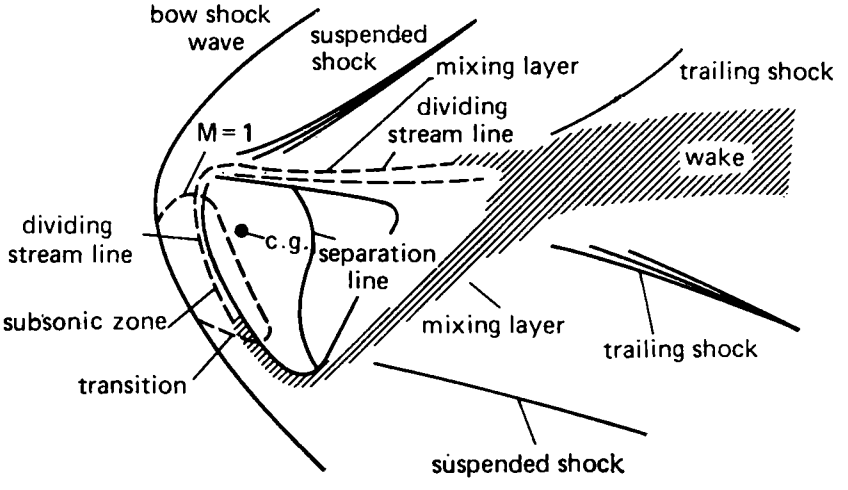

Fig. 1.1. General pattern of flow past a descending space vehicle

problems in nonlinear mechanics, associated with the formation of shock waves, contact discontinuities and their interaction, investigation of flow separation zones and, finally, the wake of an object. The complexity of investigation of this problem will become clear if we consider that a reentry vehicle is successively exposed to a whole lot of conditions from supersonic flow (characterized by physical and chemical conversions in a gas) to purely subsonic flow,

[1] This review contains the material of the paper presented by the author on 19 May, 1981 at the conference held to commemorate the 80th birth anniversary of Academician N.E. Kochin.

including a transition through the sonic barrier, "supercritical" and transonic regions. The vehicle flies at different heights, and hence we must consider not only the continuum models, but also the processes which generally occur in a rarefied gas.

To our mind, the problems associated with the investigation of separated (generally, turbulent) flows are of special interest and significance. We shall consider such problems below.

Various numerical algorithms are constructed by using essentially the same approach which seems to have a clear physical meaning and is adequate for the transition phenomena under consideration. This approach is called the *splitting method* [1.1, 1.2]. Following the standard computational practice, the domain of integration is covered by a fixed computational grid. The medium being simulated can be replaced by an aggregate of so-called liquid (Lagrangian) particles contained in each elementary cell or, if the medium is discrete, by a set (ensemble) of some particles ("molecules"). The imitation model, describing the stochastic process under consideration, is constructed by using the Monte-Carlo methods. Note that the numerical simulation on a computer in this case is carried out with the help of the methods of statistical tests without using the initial kinetic equation. Thus, one of the main problems in such an approach is to prove the adequacy of a given initiation process and the corresponding kinetic equation. At present, this approach is also being developed for investigating turbulent flows on a kinetic level.

Let us formulate the general principle of splitting [1.1]. The entire idea of this method allows us to successively carry out computations in Euler-Lagrangian variables, thus providing a possibility of using the "strong" points of such methods. A certain iterative process is constructed at each time step Δt: to begin with, we consider "adaptation", i.e. the motion of a subsystem only within each cell which remains fixed (there is no exchange with the neighbouring cells in the case of a continuous medium, while collision relaxation is considered in the spatially homogeneous case for a discrete model of the medium). The "displacement", which involves the motion of these subsystems (collisionless relaxation) but without a change in their internal state, is then simulated.

We shall illustrate specific methods of constructing multidimensional splitting schemes for two "extreme" types of models, viz. the time-dependent Euler and Boltzmann equations. To our mind, the universal nature of the method of constructing a computational process can be perceived most clearly in these cases, although these two approaches differ considerably in the realization of algorithms.

1.2. For numerical models constructed on the basis of *Euler equations* ("coarse particle" method [1.2-1.5], etc.), the mass of the entire liquid (Euler) cell ("coarse particle", hence the name of the

method) is considered instead of an aggregate of particles in a cell. Further, with the help of the finite-difference representations of the conservation laws, the nonsteady and continuous flows of coarse particles through an Euler grid are considered. Essentially, this involves the conservation laws in the form of difference balance equations for a finite-size cell (as is usually the case while deriving the gasdynamic equations, but without the subsequent limiting transition from a cell to a point)[2].

Let us consider the flow of an ideal compressible gas. For the initial equations, we can take either Euler's differential equations in a divergent form (continuity, momentum and energy equations)

$$\begin{aligned}
&\frac{\partial \rho}{\partial t} + \nabla(\rho \mathbf{V}) = 0,\\
&\frac{\partial(\rho u)}{\partial t} + \nabla(\rho u \mathbf{V}) + \frac{\partial p}{\partial x} = 0,\\
&\frac{\partial(\rho v)}{dt} + \nabla(\rho v \mathbf{V}) + \frac{\partial p}{\partial y} = 0,\\
&\frac{\partial(\rho E)}{\partial t} + \nabla(\rho E \mathbf{V}) + \nabla(p \mathbf{V}) = 0,
\end{aligned} \tag{1.1}$$

or the integral equations of motion in the form of conservation laws. To close this system, we use the equation of state

$$p = p(\rho, I), \quad I = E - V^2/2, \tag{1.2}$$

where $\mathbf{V}$ is the velocity (u and v are its components along x and y-axes, respectively), ρ is the density, while I and E are the specific internal energy and the total energy, respectively.

The main idea behind this approach is that the calculation for each time layer for the initial multidimensional operator (1.1) is "split" according to physical processes into several stages for which simpler equations are solved in principle[3].

The *first stage* of calculations considers the effects of acceleration of the fluid only due to pressure: the quantities corresponding to the cell as a whole vary while the fluid is assumed to be instantaneously arrested. Hence the convective terms corresponding to the displacement effects are eliminated from the equations. It then follows, in particular, from continuity equations that the density

---

[2] A detailed description of the coarse particle method and the results of calculations are given in the monograph [1.5].

[3] One of the first computer realizations of splitting schemes was carried out by Harlow in the "particle-in-cell" method (see, F. Harlow: "The particle-in-cell computing method for fluid dynamics" in *Fundamental Methods in Hydrodynamics*, eds. B. Alder, S. Fernbach and M. Rotenberg, vol. 3 of *Methods in Computational Physics*. Academic Press, New-York-London, 1964). A fairly complete description of this method and its modifications is contained in [1.5].

field will be "frozen" and the initial system of equations will assume the form

$$\rho \frac{\partial u}{\partial t} + \frac{\partial p}{\partial x} = 0, \quad \rho \frac{\partial v}{\partial t} + \frac{\partial p}{\partial y} = 0, \quad \rho \frac{\partial E}{\partial t} + \nabla(p\mathbf{V}) = 0. \quad (1.3)$$

Here, calculations are essentially made in locally Lagrangian coordinates and the initial (fixed) grid is deformed. Various finite-difference representations were used to approximate (1.3) [1.3, 1.5]. In order to improve the computational stability at this stage, schemes of the integral relations method were also used. According to the accepted practice in Lagrangian methods, it is possible to introduce into the scheme explicit terms with artificial viscosity q, i.e. we can replace the thermodynamic pressure p by the sum $p + q$. To our mind, schemes with internal dissipation (scheme viscosity) are the most promising ones.

The *second stage* involves the calculation of transport phenomena taking into account the exchange between cells upon their reorganization to the original Euler grid. Here, we find for $t^n + \Delta t$ the mass flows ΔM^n through the cell boundaries. It is assumed that the entire mass is transported only due to the component of velocity normal to the boundary, for example,

$$\Delta M^n_{i+1/2,\, j} = \langle \rho^n_{i+1/2,\, j} \rangle \langle u^n_{i+1/2,\, j} \rangle \Delta y \Delta t, \text{ etc.} \quad (1.4)$$

The angle brackets contain the values of ρ and u at the cell boundary. The choice of these quantities is very important for organizing the computational process, since it strongly influences the stability and accuracy of computation. The flow direction at the given boundary is taken into account in all versions of formula (1.4). For the flows ΔM^n, first- and second-order approximations are used in the form of the central differences, etc. Besides, a discrete model represented by an aggregate of particles in a cell of fixed mass is used for the continuous medium [1.3, 1.5].

Lastly, at the *third* and *final stage*, the computational grid is "regularized" and the final fields of Euler flow parameters are determined on the fixed initial grid at the instant $t^{n+1} = t^n + \Delta t$. The equations of this stage are the laws of conservation of mass M, momentum $\mathbf{P}$ and the total energy E, written for the given cell in the difference form

$$F^{n+1} = F^n + \sum \Delta F^n_{\mathrm{b}}, \quad (1.5)$$

where $F = (M, \mathbf{P}, E)$.

These expressions state, in particular, that there are no sources or sinks of M, $\mathbf{P}$ and E in a flow field, and their variation over the time Δt is due only to interaction on the external boundary of the flow region.

The *homogeneous* finite-difference schemes constructed in this way are divergently conservative and dissipatively stable. They allow a single algorithm for a "through" count in the regions where smooth solutions exist, as well as in discontinuity zones. The stability of computations is ensured only by internal dissipation (approximation viscosity), and this allows these schemes to be used for curvilinear boundaries, as well as for nonstationary three-dimensional problems [1.4, 1.5].

For constructing the numerical algorithms, we can also use as the initial system an approximation of the well-known *conservation laws written in the integral form* (method of "flows", [1.2, 1.6-1.8])

$$\frac{\partial F}{\partial t} = -\oint\limits_{S_\Omega}\oint \mathbf{Q}_F \cdot \mathbf{n}\, ds, \quad F = \{M,\ \mathbf{P},\ E\}, \tag{1.6}$$

where S_Ω is the lateral surface of the volume Ω and $\mathbf{Q}_F$ is the flux density vector of the quantity F.

Equations (1.6) are written (for a viscous compressible gas, as well as for an ideal medium) taking into account the boundary conditions and are numerically solved for each calculated cell in the computational domain.

The following circumstances are of importance in the approximation of the flux density vectors $\mathbf{Q}_F$: the distribution density of the additive characteristics like the densities of the quantities F are calculated nonsymmetrically at the boundary S_Ω of the volume Ω (by extrapolation in the direction of a gas flow). The remaining quantities like the pressure, rate of transport of additives, derivatives of u, v and T in the viscosity stress tensor and the law of thermal conduction are calculated with the help of symmetric formulas. Because of convective transport, various directions in space are not equivalent, and this circumstance should be taken into account while constructing difference schemes. We feel that this permits a proper consideration of the domains of influence and the nature of interaction of quantities, which is an important factor in the investigation of the physical patterns of flows.

It can be easily observed that the method of "flows" is essentially of a conservative nature. When using integral laws of conservation derivatives must be approximated to an order of magnitude lower than that used for numerically solving Navier-Stokes equations. Splitting the flux density vector $\mathbf{Q}_F$ into "convective" and "viscous" components permits us to easily use this method for calculating an ideal flow, separation phenomena, etc. [1.8-1.10].

While numerical methods based on the models of an ideal medium allow us to consider "global" phenomena (when minor effects do not significantly affect the flow pattern as a whole), the approaches based on Navier-Stokes equations permit a detailed "resolution"

of inner flow structures determined by the mechanism of molecular diffusion. Thus, for investigations of the flow of a viscous incompressible liquid on the basis of *Navier-Stokes equations*, natural variables like "velocity-pressure" were used [1.2, 1.11-1.14]. This allowed an extension of the method to the case of three-dimensional fluid flows [1.13], and helped to avoid formulation of the boundary condition for a vortex on the surface of a body, which is characteristic of variables (ω, ψ) and is absent in the physical formulation of the problem. The splitting scheme (of the second order of accuracy) has the following form [1.12]:

Stage I: determination of the intermediate values of velocities $\tilde{\mathbf{V}}(\tilde{u}, \tilde{v})$:

$$\frac{\tilde{\mathbf{V}}-\mathbf{V}^n}{\tau} = -(\mathbf{V}^n\nabla)\,\mathbf{V}^n + \nu\Delta\mathbf{V}^n.$$

Stage II: calculation of the pressure field:

$$\Delta p = \nabla\tilde{\mathbf{V}}/\tau \quad (\nabla\mathbf{V}^{n+1} = D^{n+1} = 0). \tag{1.7}$$

Stage III: determination of the final values of velocities:

$$\mathbf{V}^{n+1} = \tilde{\mathbf{V}} - \tau\nabla p.$$

Here, ν is molecular viscosity, and τ is the time step. Stages I and III lead to a fulfilment of Navier-Stokes equations, while stages II and III result in the solenoid conditions.

The methods described above were found to be effective for investigation of a wide range of nonlinear problems in continuum mechanics and plasma physics [1.1, 1.2, 1.10] and, in particular, for calculating the flows in the wake of a moving object [1.3-1.5, 1.8, 1.9, 1.12-1.14]. Some results of such calculations are given below. It is important to note that this group of algorithms can be realized on medium-power computers.

1.3. Let us now consider the other limiting case of a discrete medium, viz. the flow of a rarefied gas described by the *Boltzmann kinetic equation*. We assume that the problem of flow of a rarefied gas past a body may be solved by using a distribution function, and that the gas is monatomic. Then, any macroscopic parameter $\Psi(t, \mathbf{x})$ of the gas flow, associated with the molecular criterion $\psi(\mathbf{c})$, is a functional of the form

$$\Psi(t, \mathbf{x}) = \frac{1}{n(t, \mathbf{x})} \int \psi(\mathbf{c})\, f(t, \mathbf{x}, \mathbf{c})\, d\mathbf{c},$$

where $f(t, \mathbf{x}, \mathbf{c})$ is the distribution function of molecules in the six-dimensional space of $(\mathbf{x}, \mathbf{c})$-coordinates and velocities of particles.

If Ω is a domain of the control volume and Γ is the boundary of the domain Ω including the surface of the body in a flow, the problem is reduced to finding the solution $f(t, \mathbf{x}, \mathbf{c})$ of the Boltzmann equation

$$\frac{\partial f}{\partial t} + \mathbf{c}\,\frac{\partial f}{\partial \mathbf{x}} = \int (f'f_1' - ff_1)\, g\, d\sigma\, d\mathbf{c}_1 \equiv I(ff_1). \tag{1.8}$$

This solution satisfies the given initial conditions

$$f(t + 0, \mathbf{x}, \mathbf{c}) = f_0(\mathbf{x}, \mathbf{c}), \quad x \in \Omega,$$
$$-\infty < c_{x, y, z} < +\infty \tag{1.9}$$

and the boundary conditions

$$f(t, \mathbf{x}_b, c) = \int K(\mathbf{c}, \mathbf{c}_1)\, f(t, \mathbf{x}_b, \mathbf{c}_1)\, d\mathbf{c}_1,$$
$$\mathbf{c}\cdot\mathbf{n}(\mathbf{x}_b) > 0, \quad \mathbf{c}_1\cdot\mathbf{n}(\mathbf{x}_b) < 0. \tag{1.9'}$$

Here $\mathbf{n}(\mathbf{x}_b)$ is the inward normal to the surface Γ of the volume Ω at the point $\mathbf{x}_b \in \Gamma$. The form of the kernel K is determined by the law of "gas-surface" interaction [1.15].

To approximately solve the problem (1.8)-(1.9') formulated above, we construct the *statistical model* of an ideal monatomic gas consisting of N particles with coordinates $\mathbf{r}_i$ and velocities $\mathbf{c}_i$ ($i = 1, \ldots, N$), such that the equation for the evolution of this model approximates equation (1.8) under the only additional assumption of molecular chaos [1.15]:

$$f_2(t, \mathbf{x}, \mathbf{c}_1, \mathbf{c}_2) = f_1(t, \mathbf{x}, \mathbf{c}_1)\, f_1(t, \mathbf{x}, \mathbf{c}_2), \tag{1.10}$$

where

$$f_s(t, \mathbf{x}, \mathbf{c}_1, \ldots, \mathbf{c}_s) \equiv \frac{N}{(N-S)!}\, F_s(t, \mathbf{r}_1, \ldots, \mathbf{r}_s, \mathbf{c}_1, \ldots, \mathbf{c}_s)$$

for $\mathbf{r}_1 = \mathbf{r}_2 = \ldots = \mathbf{r}_s = \mathbf{x}$. Here F_s is the distribution function for S particles in the $6N$-dimensional phase space.

It is well known that the Boltzmann equation (1.8) is a complex integro-differential equation, closed with respect to the density distribution function. It is practically impossible to directly solve this equation with the exception of, perhaps, one-dimensional or simple two-dimensional problems. The main difficulty here lies in the calculation of the collision integral $I(f, f_1)$. In the general case, it is a five-fold multiple integral containing seven independent variables $(t, \mathbf{x}, \mathbf{c})$ with a quadratic nonlinearity of the integrand; moreover, $I(f, f_1)$ depends on the "primed" values of the distribution function f' (determined after a collision).

In the statistical interpretation, a combination of Bird's ideas of splitting [1.16, 1.17] and Kac's mathematical model [1.18] (which is asymptotically equivalent to the Boltzmann equation without

a convective derivative) can be used to construct an effective numerical approach for the statistical modelling of Boltzmann's kinetic equation in the multidimensional case [1.2, 1.19-1.23], and of some turbulence problems [1.23, 1.24].

We shall consider this statement in greater detail. The medium being simulated (discrete in the present case) is replaced by a system of a finite number N of "particles" of finite mass. A direct numerical modelling of statistical characteristics is carried out for this system with the help of the Monte Carlo method. At a given instant t_α of time, each cell j contains N (α, j) particles with certain velocities. The main computational cycle consists of two stages: at the first stage, particles only collide with other particles in the cell (collision relaxation), while in the second stage they only move and interact with the boundary of the control volume and the surface of the body in a flow (collisionless relaxation).

In the *first stage*, the variation of the internal state of the subsystems in the cells is simulated for a gas at rest (spatially homogeneous medium): the collisions of the particles in each cell (with other particles in the same cell) are modelled independently for the subsystems $\{\mathbf{c}_1, \ldots, \mathbf{c}_N\}$ as a result of which the particles acquire new velocities.

The vector $\mathbf{c} = \{\mathbf{c}_1, \ldots, \mathbf{c}_N\}$ is considered as the statistical state of the Kac model. Suppose that $\varphi(t, \mathbf{c})$ is the probability distribution density of the state $\mathbf{c}$ (t). In this case, the "master equation" for this model [1.18] has the form[4]

$$\frac{\partial \varphi(t, \mathbf{c})}{\partial t} = \frac{1}{V^0} \sum_{1 \leqslant l < m \leqslant N} g_{lm} \int [\varphi(t, \mathbf{c})]\, d\sigma_{lm} \equiv K[\varphi(t, \mathbf{c})]. \qquad (1.11)$$

Here K is the collision operator in Kac's equation, $g_{lm} \equiv |\mathbf{c}_l - \mathbf{c}_m|$ ($\mathbf{c}_l$ and $\mathbf{c}_m$ being the velocities of the lth and mth particles after their collision), $d\sigma_{lm}$ is the differential cross section of elastic scattering of the pair of particles $(\mathbf{c}_l, \mathbf{c}_m)$, and the normalization parameter V^0, which depends on the choice of the units of measurement, can be interpreted as the volume of a cell. When a collision is simulated with the help of this approach, the Monte Carlo numerical method is used for solving the master equation in the Kac model [1.11] allowing a computation of the intervals between collisions of particles in exact correspondence with the statistics of collisions in an ideal monatomic gas. Unlike the methods proposed earlier [1.16, 1.17], this approach is a strictly Markov process[5].

Unlike the Boltzmann equation, Eq. (1.11) is linear, and this considerably simplifies the numerical realization of the algorithm.

[4] Here $[\varphi(t, \mathbf{c})] = \varphi(t, \mathbf{c}'_l, m) - \varphi(t, \mathbf{c})$.

[5] This means that the time T_m between successive collisions of a given pair of particles is an arbitrary quantity which is distributed according to an exponential law which is the same for any pair of particles m [1.22].

From the property of spreading of molecular chaos it follows that the Kac model is asymptotically equivalent to the Boltzmann equation without the convective derivative. Integration of the Kac master equation leads (as long as the assumption (1.10) concerning molecular chaos is valid) to the Boltzmann equation for the spatially homogeneous case [1.21, 1.22].

In the *second stage*, the collisionless displacement of particles from a given cell to any neighbouring cell is simulated (without a change in the internal state of the subsystems), and their interaction with the boundary of the control volume and the surface of the body in a flow is considered. This stage corresponds to the Monte Carlo numerical method for solving Boltzmann's free-molecular equation in the following form:

$$\frac{\partial f}{\partial t} + \mathbf{c}Lf = 0, \tag{1.12}$$

where L is a finite-difference operator approximating the derivative $\partial/\partial \mathbf{x}$. The introduction of this operator is closely linked with the inadequacy in the description of the state of systems in the coordinate space.

Thus, two ideas are successively used here, viz. the splitting principle and the representation of the spatially homogeneous Boltzmann equation in the form of the Kac model (1.11) (Fig. 1.2). It can be seen that on the whole, this computational scheme helps avoid the direct calculation of the collision integral in the Boltzmann equation. The simplest numerical algorithms for the approach considered here [1.19-1.21] correspond to the solution of quasi-stationary first-order finite-difference schemes that are explicit in time, for the Kac equations and the Boltzmann free-molecular equation.

To calculate the second stage of the evolution of a simulation gas, it is proposed to apply numerical algorithms for the displacements of particles, using the incomplete information on the position of particles in the coordinate space. This considerably decreases storage requirements of the computer and significantly improves the effectiveness of the method.

The approach described above can be naturally extended to the case of a multidimensional space. The generalization to the two-dimensional and three-dimensional flows consists in a sequence of one-dimensional displacements along the coordinate axes [1.22]. This corresponds to the splitting of the multidimensional transport equation (1.12) into a sequence of one-dimensional finite-difference schemes, which can be easily accomplished.

It is well known that the Boltzmann equation (1.10) involves the concept of molecular chaos or the statistical independence of particles. Our model has the same prerequisites as the Boltzmann

equation, but does not contain the assumption of molecular chaos or the statistical independence. Thus, in the model under consideration, there exists in principle a *statistical dependence of particles*, which can lead to a perturbation in the form of molecular chaos. It should be noted that the statistical dependence is governed by mathematical and physical prerequisites and does not depend on the grid size (it exists even when $\Delta x \to 0$).

The results of calculations for a rarefied gas flow showed that the data obtained for different numbers of particles in a cell (for example,

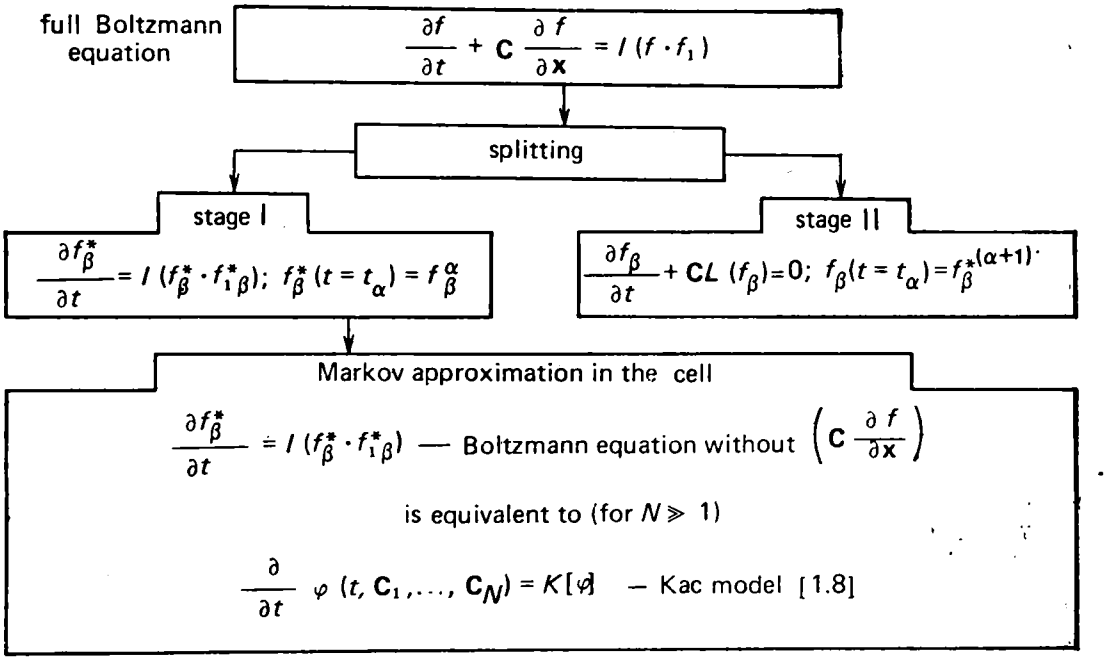
full Boltzmann equation
$\frac{\partial f}{\partial t} + C\frac{\partial f}{\partial x} = I(f \cdot f_1)$
splitting
stage I
$\frac{\partial f^*_\beta}{\partial t} = I(f^*_\beta \cdot f^*_{1\beta});\ f^*_\beta(t = t_\alpha) = f^\alpha_\beta$
stage II
$\frac{\partial f_\beta}{\partial t} + CL(f_\beta) = 0;\ f_\beta(t = t_\alpha) = f^{*(\alpha+1)}_\beta$
Markov approximation in the cell
$\frac{\partial f^*_\beta}{\partial t} = I(f^*_\beta \cdot f^*_{1\beta})$ — Boltzmann equation without $\left(C\frac{\partial f}{\partial x}\right)$
is equivalent to (for $N \gg 1$)
$\frac{\partial}{\partial t}\varphi(t, C_1, \ldots, C_N) = K[\varphi]$ — Kac model [1.8]

Fig. 1.2. Splitting scheme for the Boltzmann equation

$N = 3$ and $N = 20$) are almost the same (in several cases calculations made for the case when the average number of particles in a cell $N \simeq 1$ are found to be acceptable). Moreover, these results are in good agreement with the solution of the Boltzmann equation (results obtained by Cheremisin and Rykov) [1.21, 1.22]. Consequently, perturbation in the form of molecular chaos in the problems under consideration is weak (although statistical dependence of particles does exist, it is manifested weakly in the case of a rarefied gas and can be obviously neglected).

The model worked out in this way was tested in the analysis of the structure of the forward shock wave in a gas consisting of elastic spheres in the range of the Mach number $M_\infty = 1.25$-4 [1.21]. Examples of calculations for two-dimensional and three-dimensional problems of the dynamics of a rarefied gas (including transient regimes) are given in [1.22-1.24].

Upon a certain modification of the method, this approach can be also used for considering nonstationary turbulence problems on the kinetic level [1.23, 1.24].

1.4. Let us consider some "*internal*" properties of the algorithms mentioned above [1.2, 1.10]. It is well known that when problems involving discontinuities are considered in the framework of an ideal gas, the concept of generalized solution has to be introduced. This concept follows from the uniform description of hydrodynamic flow, and the corresponding difference schemes are called *homogeneous*.

Such a uniformity in the description of flows can be achieved in two ways: by considering gasdynamic equations with dissipative terms, and by using the integral laws of conservation.

In the first approach, equations with dissipation are taken into consideration (in the difference equations of gas dynamics, terms with higher-order derivatives contain a small parameter, viz. viscosity). This dissipation causes a smoothing of the discontinuities. For the generalized solution, we take the limit of the solutions of parabolic equations obtained in this way, when the coefficients of the viscosity terms tend to zero. The generalized solution defined by integral laws of conservation in Euler or Lagrangian coordinates is homogeneous, since the equations of gas dynamics and the compatibility conditions at the discontinuities are consequences of the laws of conservation.

It follows from the above that the approaches described here involve the application of homogeneous difference schemes constructed in accordance with the two approaches described above. In the framework of an ideal gas, this allows a "through" count in the region of smooth flows, as well as at discontinuities, by using a single algorithm. The difference schemes approximating Euler equations must have certain dissipative properties in order to admit solutions analogous to a shock wave. This is attained with the help of corresponding dissipatively stable uniform finite-difference schemes which approximate the initial equations written in divergent (1.1) or integral (1.6) form.

Thus, "Euler difference" equations (obtained with the help of differential approximations for splitting schemes of type (1.3)-(1.5)) have the following form[6] [1.5]:

$$\frac{\partial \rho}{\partial t} + \nabla(\rho V) = 0,$$

[6] Here, we have written expansions to within $O(\Delta t, h^2)$. It is interesting to note that the structure of the coefficients of the approximation viscosity $\varepsilon \sim |V| h$ in (1.13) resembles the structure of the coefficient of turbu-

$$\frac{\partial \rho u}{\partial t}+\nabla(\rho u \mathbf{V})+\frac{\partial p}{\partial x}=\frac{\partial}{\partial x}\left(\rho \varepsilon_x \frac{\partial u}{\partial x}\right)+\frac{\partial}{\partial y}\left(\rho \varepsilon_y \frac{\partial u}{\partial y}\right),$$

$$\frac{\partial \rho v}{\partial t}+\nabla(\rho v \mathbf{V})+\frac{\partial p}{\partial y}=\frac{\partial}{\partial x}\left(\rho \varepsilon_x \frac{\partial v}{\partial x}\right)+\frac{\partial}{\partial y}\left(\rho \varepsilon_y \frac{\partial v}{\partial y}\right), \qquad (1.13)$$

$$\frac{\partial \rho E}{\partial t}+\nabla(\rho E \mathbf{V})+\nabla(p \mathbf{V})=\frac{\partial}{\partial x}\left(\rho \varepsilon_x \frac{\partial E}{\partial x}\right)+\frac{\partial}{\partial y}\left(\rho \varepsilon_y \frac{\partial E}{\partial y}\right),$$

where $\varepsilon_x=\frac{1}{2}|u|\Delta x$, $\varepsilon_y=\frac{1}{2}|v|\Delta y$ are the approximation viscosity coefficients.

The left-hand sides of Eq. (1.13) contain exact expressions for the initial Euler equations (1.1), while the right-hand sides contain dissipative terms which are obtained through an approximation of the initial system of differential equations to finite-difference equations and which depend on the internal properties of the representations used. It can be seen that in the two-dimensional case, the "viscosity pressure" has the form of a tensor.

Thus, it follows from the above expressions that the "smoothed" equations (1.13) obtained as a result of computations are dissipative, although the model of an ideal medium was used for initial equations. The form of the dissipative mechanism depends on the nature of approximations introduced and, generally speaking, can be "controlled".

An exact simulation of the time process in (1.13) enables us to study the dynamics of nonstationary phenomena. The approximate dissipation mechanism (with approximation viscosity) permits a quite accurate determination of the characteristics of averaged flows, as well as the position, velocity of propagation and the nature of interaction of discontinuities, viz. shock waves, contact surfaces, narrow mixing layers in the wake of a body, etc. However, the internal structures of these processes (which are determined by molecular effects) are not "captured" by such an approach, since the influence of approximation viscosity in the Navier-Stokes difference equations "suppresses" the molecular effects.

For comparison with (1.13), let us consider the "Navier-Stokes difference" expression. The equation for momentum in the splitting schemes of the coarse particle method can be written as follows with

---

lent viscosity for λ-scale: $\nu_{\text{turb. }\lambda} \simeq v_\lambda \lambda$ (apparently, there is but one reason behind their emergence, viz. the nonlinearity of the processes). If we put a turbulent vortex of scale λ moving with a velocity v_λ into correspondence with a "coarse particle" of size h moving with a velocity v_h, the expressions for ε and $\nu_{\text{turb. }\lambda}$ will be absolutely identical. If we put $\varepsilon_x \simeq \varepsilon_y \simeq \nu_{\text{turb. }\lambda}$, Eqs. (1.13) or $\rho = \text{const}$ (incompressible liquid) will assume the form of exact Navier-Stokes equations in which the molecular viscosity ν is replaced by the "effective" turbulent viscosity $\nu_{\text{turb. }\lambda}$ [1.10].

the help of differential approximations [1.25]:

$$\frac{\partial \rho u}{\partial t}+\frac{\partial (p+\rho u^2)}{\partial x}$$
$$=\left[\mu(A+2)+\rho|u|\frac{h}{2}\right]\frac{\partial^2 u}{\partial x^2}+O(\Delta t,\ h^2), \qquad (1.14)$$

where $A=\lambda/\mu$, $\mu=\rho\nu$, and λ is the second viscosity coefficient. For the schemes (1.7), we have the following expression [1.12]:

$$\frac{\partial u}{\partial t}+\frac{\partial u^2}{\partial x}+\frac{\partial uv}{\partial y}$$
$$=\left(\nu-\frac{\Delta t}{2}u^2\right)\frac{\partial^2 u}{\partial x^2}+\left(\nu-\frac{\Delta t}{2}v^2-\frac{h^2}{4}\frac{\partial v}{\partial y}\right)\frac{\partial^2 u}{\partial y^2}, \qquad (1.14')$$

and so on.

We see that the approximation of viscosity terms is also influenced by scheme viscosity $\varepsilon(\rho\,|\,u\,|\,h/2)$ in (1.14) or $\varepsilon(\Delta t\,u^2/2,\ \Delta t\,v^2/2,\ \ldots)$ in (1.14′). Thus, to attain the required accuracy and to fulfill the conditions of stability of computations, it is necessary to employ smaller and smaller steps in the computational grid with increasing Reynolds number.

Thus, a discrete representation of a medium in the form of cells or particles is manifested in difference equations in the form of a dissipation mechanism with an "effective" viscosity. The structure of this mechanism must ensure an approximation of initial equations and stability of computations. At the same time (during simulation of turbulence phenomena) this mechanism must generally reflect the contribution of the small-scale "subgrid" pulsations.

The construction of difference schemes with an approximate description of the dissipation mechanism for the limiting types of flows under consideration should preferably be carried out on the basis of Euler's equations. As a matter of fact, when flows are calculated for large values of Reynolds number, the stability of the computational procedure is ensured only if the effective viscosity is quite large and suppresses fluctuations which would otherwise increase due to convective terms. For flows at small Reynolds numbers, this condition may be ensured in different ways. Naturally, for this purpose, it is highly desirable to use reliable values of viscosity, or to decrease the diffusive (second order) rounding errors. However, it follows from (1.14) that for large Reynolds numbers molecular viscosity is too small a quantity to be used for ensuring computational stability. In this case, we must use larger values of effective viscosity and consider a dissipation mechanism other than molecular.

Thus, investigations and computations show that if dissipative terms are introduced in the equations for an ideal gas, the generalized solution for a large class of problems under limiting flow conditions ($\nu \to 0$) may be obtained for quite wide assumptions concerning the nature of dissipation, with a certain degree of accuracy (by carrying

out limiting transition), from equations with an approximate dissipation mechanism rather than the Navier-Stokes equations [1.1, 1.10].

However, it should be borne in mind that convective terms of a difference scheme may generate positive dissipation of a nonphysical nature, which is admissible if the influence exerted by it on the averaged motion is negligibly small. Strictly speaking, with the help of approximation viscosity we can claim to obtain solutions in those domains where the effect of this viscosity is insignificant.

Numerical solution of boundary value problems on the basis of Navier-Stokes equations for large Reynolds numbers involves not only technical problems, but apparently difficulties of a more serious nature. Investigations have revealed [1.25] that as Re exceeds a certain critical value (of the order of 10^3-10^4), most of the difference schemes for analyzing the Navier-Stokes equations become unstable. Even if the computational algorithm actually allows a stable "through" count for large values of Re, the results obtained generally no longer correspond to the Navier-Stokes equations.

Apparently, such a situation is also observed in the dynamics of rarefied gases while solving problems with a small Knudsen number Kn. Transition from free-molecular to continuous medium regime (i.e. a decrease in the value of Kn) leads to computational difficulties analogous to those appearing in the Navier-Stokes equations upon a decrease in the molecular viscosity.

The presence of small parameters in equations of gas dynamics leads to the existence of their *critical values* in the difference schemes, when the influence of the corresponding terms on the solution becomes comparable with the order of approximation viscosity [1.25]. Finer computational grids and an increase in the accuracy of difference schemes do not lead to the desired results in many cases (at least for the class of problems under investigation). All this predetermines the difficulties that arise during the simulation of transient processes in fluid dynamics for large Reynolds numbers [1.26].

Thus, it seems quite justified and expedient to simulate large-scale macroscopic structures of separated flows for limiting ("turbulent") cases on the basis of time dependent equations for an ideal medium ([1.2, 1.5, 1.9, 1.10] and others).

The method of mathematical modelling described here for simulating macroscopic structures of separated flows of a compressible gas is quite similar to [1.27], where Belotserkovskii and Nisht used the ideal medium model and the method of discrete vortices to investigate a wide range of separated flows appearing when an incompressible fluid flows past a lifting surface with a vortex wake.

1.5. Let us now consider the construction of *numerical models of separated flows and turbulence problems.* This is probably one of the

most vital branches of aerodynamics involving an ever increasing application of mathematical modelling. In the analysis of the above-mentioned flows, it seems theoretically possible and physically justified to investigate averaged large-scale macroscopic structures and statistical characteristics of turbulence. To our mind, the main issue here consists in the following: *what type of equations (Euler's, Navier-Stokes, or kinetic equations) should be used for modelling turbulent flows under limiting flow conditions (for* $\mathrm{Re} \to \infty$)?

For a wide range of such phenomena, the molecular viscosity and small flow elements in most of the perturbation region for large values of Re have practically no effect on the mean characteristics of macroscopic flow structures and on the flow pattern as a whole. These phenomena include jet-stream problems, flows in the wake of a moving object, motion of fuselages with a trailing edge, and the formation of leading separation zones in a flow past a blunt-nosed object with jets or needles pointing against the flow, etc. On the other hand, flows in boundary layers and narrow mixing layers for small and moderate Reynolds numbers are mainly determined on viscous turbulence interval by molecular diffusion. Pulsating turbulence flows are unstable and irregular, and form a stochastic process.

The main difficulty encountered in the investigation of this type of problems involves the development of *general ideas* for creating *constructive* numerical models of turbulence. Before carrying out a detailed investigation of these questions, let us briefly put forth our point of view on the problems under investigation:

in view of the individual nature of "ordered" unsteady motion of large-scale macroscopic structures of turbulence, their investigation on the inertial interval should be carried out in the entire perturbation range by direct numerical modelling based on an analysis of complete dynamic equations for an ideal medium, viz. Euler's time-dependent equations (or the corresponding conservation laws) with an approximate dissipation mechanism reflecting the contribution of "small-scale" pulsations;

investigation of local turbulence effects ("stochastic components"), viz. the nature of distribution of Reynolds stresses, turbulence energy density, the rate of its dissipation, etc., is carried out in the regions of large gradients statistically or by using some turbulence model;

investigation of the properties of turbulent flows on small (internal) scales of viscous turbulence interval should naturally be carried out with the help of Navier-Stokes equations.

In the following, we shall mainly consider the methods in which the description of turbulent flows for large time intervals employs a *complete* (and *closed*) system of dynamic equations for actual values of velocities and pressure, as well as statistical methods. A combined application of these two approaches leads to a deeper understanding

of the turbulence structure and helps in finding rational means for constructing appropriate mathematical models.

Naturally, the numerical modelling of turbulence must reflect to the largest possible extent the main properties of turbulent flows, viz. the nonstationarity and nonlinearity of the processes, the possibility of transporting groups of molecules ("molar" transport), a continuous energy flow along a vortex cascade, different mechanisms of interaction for various scales of motion, viscosity dissipation, etc.

Numerical realization of general concepts of the turbulence theory is carried out in different directions (see, for example, [1.10] and other works):

integration of complete Navier-Stokes time-dependent equations without additional assumptions concerning the nature of transport finite-difference methods, Fourier spectral methods, etc. are used for comparatively simple problems on convection, diffusion, modelling of the "disintegration" of laminar flow, etc.;

calculation of the same models for a coarser difference grid using semi-empirical variable transport coefficients (effective viscosity, etc.);

solution of Reynolds or Boussinesq's equations for mean flow elements and Reynolds stresses together with approximate transport equations;

application of differential equations for moments of different orders with different types of "closure", etc.

It is well known that the methods of investigation of turbulence, based on *Navier-Stokes equations*, are closely linked with the analysis of the properties of these equations (in particular, energy dissipation) for a low viscosity, i.e. for $\nu \to 0$[7]. The main difficulty in the modeling of turbulence is associated (for large "supercritical" Reynolds numbers) with the construction of a stable time-dependent numerical solution (for average characteristics) adequate for Navier-Stokes equations. As a matter of fact, the approximation conditions and the stability of the solution during calculations are ensured if the grid step is such that the error in the approximation of convective terms in Navier-Stokes equations is much smaller than the difference representation of viscosity terms. Estimates for model equations [1.26] show that an approximation to the real solution can be attained

---

[7] The following assumption is made in [1.28] about the nature of a fully developed uniform isotropic turbulent flow: turbulence is not a result of increased instability due to an increase in the Reynolds number of viscous flow; rather, it appears in a finite time interval t_0 due to the "energy catastrophe" in an inviscid flow (up to t_0, the spatial covariance is analytic, the spectrum has finite moments of all orders and energy is conserved; beyond t_0, covariance is no longer analytic, the spectrum obeys Kolmogorov's law for large wave numbers, and a finite dissipation of energy occurs at zero viscosity).

under the condition $\mathrm{Re}\, h < \alpha \ll 1$. In other words, even if it is possible to calculate flows with a molecular dissipation mechanism for large ("turbulent") values of Re, it can be done only on very fine difference grids (generally comparable with pulsation moles)[8].

It is also important to note that a different (non-molecular) molar transport mechanism is realized for $\mathrm{Re} > \mathrm{Re}_{cr}$. Here, a chaotic motion of individual molecular groups is observed, and the fraction of molecular viscosity in the *effective turbulence viscosity* corresponding to turbulent exchange is insignificant (usually $\nu_{turb}/\nu_{mol} \simeq 10^4$-$10^6$). Besides, in order to investigate turbulence problems, it is generally necessary to consider three-dimensional (in spatial variables) time-dependent Navier-Stokes equations. The solution of such problems may not be unique for large Reynolds numbers (although it has been proved that one-dimensional and two-dimensional nonstationary problems for Navier-Stokes equations always have a unique solution over the entire time interval $t > 0$ [1.29]. Hence the conditions for the emergence of turbulence should generally correspond to the conditions of ambiguity of time-dependent solutions of Navier-Stokes equations [1.30]. Thus, in its direct formulation, the problem of a detailed investigation of turbulent structures on the basis of Navier-Stokes model seems hardly solvable even if high-speed computers are used.

In calculations of the same models on real ("*coarse*") grids stability of the averaged solution can be ensured for large Reynolds numbers by using higher values of effective (or approximation) viscosity and considering an approximate dissipation mechanism differing from molecular dissipation. Generally, such an approach is valid for problems in which the similarity principle is obeyed for Reynolds numbers.

Using the modern concepts concerning turbulence structure, we consider it justified and promising to investigate the properties of turbulent flows with the help of "global" numerical models based on the splitting principle for Euler, Navier-Stokes and kinetic equations [1.2, 1.10, 1.23, 1.24].

Before considering the general scheme of such investigations, we would like to make a few comments. While in the first investigations of turbulence these phenomena were treated as completely stochastic processes (determined by a random distribution of pulsation quantities), their concepts have undergone a fundamental change at present. It was found that the *ordered motion of coherent structures is also one of the elements of turbulence*, and the relation between de-

---

[8] Computation with a grid step of the order of the internal turbulence scale is impracticable (even on modern high-speed computers) and unadvisable for most of the problems. Small-scale pulsations must be "smoothed" over the cells of computational grid and over a time step.

terministic and chaotic nature of turbulence is being actively investigated at present (see [1.31-1.36, etc.]).

A large number of experiments and investigations have shown (see, for example, [1.31-1.35])[9] that a wide range of turbulent flows with shear (for free flows as well as in the region near the wall) are characterized by a nonstationary ordered motion of large-scale formations ("large vortices") with a weak pulsation, i.e. by an ordered motion of coherent structures which have a stable and typical form for a given problem. The inner zone of such flows (for example, in jet-stream problems) has a turbulent (stochastic) nature and consists of disordered small-scale pulsations of very high intensity, albeit of a uniform structure.

Thus, in free shear flows (wakes, jets), a dual "alternating" turbulence structure is observed (see Townsend [1.31]). The main turbulence zone of the fluid has a comparatively small scale, is uniform and contains the main part of energy. This zone is subjected to an external system of slow stable (nonturbulent) large vortices, which transports the turbulized fluid completely from one part of the flow to another.[10]

Thus, *coherent structures form a proper basis for turbulent flow*[11]. Following [1.36], we can classify the turbulence structure as follows:

"*dynamic*" *coherent structures* which exist near the point of transition from laminar flow to turbulent flow and are of bifurcative origin;

"*quasiequilibrium*" *structures* which are formed in the regions with a developed turbulence, when the chaotic motion is so pronounced that the system is close to thermodynamic equilibrium;

"*flow*" *structures* which occupy a position intermediate between the first two types of structures.

In free turbulent flows, viz. jets, wakes and mixing layers, coherent structures are observed for arbitrarily large values of Reynolds numbers. Structures of this type often have a two-dimensional (or quasi-two-dimensional) form [1.36]. The form, intensity and scale of such a low-frequency ordered flow are quasi-determined (i.e. "individual") for a given type of flows, and in the statistical aggregate under consideration. It is expedient to use equations of fluid dynamics (rather than the statistical approaches) to describe these char-

---

[9] I am grateful to Prof. O.S. Ryzhov for drawing my attention to these works and for a discussion of the problems considered here.

[10] The reason behind the alternating turbulence is the creation by large vortices of a curved boundary surface between nonturbulent and turbulent liquids, i.e. between the region with a zero (or low) vortex pulsation and a field with considerable pulsations. After corrections are introduced for the coefficient of alternation, the main turbulence characteristics are found to be practically constant in a considerable part of the transverse wake [1.33].

[11] Results of recent investigations by Soviet scientists in the field of structural turbulence theory are described in [1.36].

acteristics. Moreover, the dimensions of "large vortices" are comparable with the characteristic flow dimension and much larger than the size of energy-carrying vortices that constitute the proper turbulent flow [1.31, 1.32]. The turbulence in a wake also has a fairly high degree of local isotropy (relative to the intensities of velocity pulsations in various directions; and hence relative to energy characteristics as well) [1.33].

The main contribution to *turbulent transport* is naturally made by the motion of large-scale structures, which absorb the energy of the main stream and transfer a part of their energy to small vortices over a cascade. In turn, a large-scale transport of a turbulent fluid is apparently carried out by the ordered motion of a group of large vortices which are responsible for the distortion of the boundary of a turbulized field and transport the turbulent fluid across the flow [1.31, 1.32]. Consequently, the motion of ordered coherent structures mainly forms dynamic and energy characteristics of the flow "as a whole", which naturally determines the properties of "depth" turbulence where dissipation of energy takes place. The opposite effect of small-scale turbulence (and molecular diffusion) on the basic properties of ordered flow for free turbulent shear flows is apparently insignificant, since these effects are of different orders and the process of energy transfer itself is one-sided.

Thus, a study of the properties of nonstationary movement of ordered and large-scale structures as a determining factor for flow seems to us to be the main link in the analysis of a wide range of turbulent shear flows. Large-scale structures must be investigated separately, while statistical approximation should be used for small vortices.

The statements made above essentially determine the organization of the computational process in the direct numerical modelling of turbulence problems. The entire cycle of investigations can generally be divided into two mutually connected problems:

1. *Calculation of unsteady flow of ordered and large-scale structures.* The large-scale and ordered motion of such a flow allows us to describe it with the help of numerical schemes based on time-dependent equations of fluid dynamics for the model of an ideal medium ("Euler difference") and having some approximate dissipation mechanism. This mechanism must ensure the stability of the averaged solution and reflect (in "smoothed" form) the contribution of small-scale pulsations. The properties of large-scale flows are mainly determined by bulk convection and generally depend on the solution "as a whole". Consequently, calculations must be directly carried out in the entire flow field on real difference grids and followed by the determination of the required averaged flow characteristics (for example, moments of various orders) by corresponding statistical treatment of the obtained results.

Here, naturally, we come across the question of *correctness* of the formulation of the problem of numerical simulation of a large-scale turbulent flow, i.e. we must find the relationship between the real situation and the results of these computations. It was shown by Ievlev (see also [1.37]) and others that in principle it is possible to obtain correct statistical results by "smoothing" the equations of motion, in which the contribution of small vortices is expressed approximately (without the requirement for exactly calculating the "true" fields of the pulsating quantities).

2. *Numerical simulation of the stochastic component of turbulent shear flow (small-scale turbulence).* Calculation of this type of flows is naturally carried out by statistical methods [1.23, 1.24] or phenomenologically by introducing appropriate turbulence viscosities [1.10]. It is also possible to use algorithms based on pulsation equations (see, for example, [1.38]), where the mean flow parameters are obtained from a solution of the first problem.

Here, it is important to note that the calculations of these flows should be carried out only in bounded subdomains, "picking out" the large gradient zones in the general flow pattern. Such an approach is based on the probable assumption that for a turbulence scale which is small in comparison with the average motion scale, the local structure of turbulence is universal for different flows and is determined only by local conditions (turbulent transport is characterized here by gradient diffusion) [1.31]. All this allows us to use quite definite models and quite fine computational grids in calculations. Moreover, the demand on the computer facilities is sharply reduced in this case.

It is well-known that the averaging of Navier-Stokes equations according to Reynolds method is carried out simultaneously over all turbulence scales for large time intervals, and this requires a simultaneous modelling of all structures. Thus, it is not feasible to construct a *universal* turbulence model for *different* types of flows. In contrast to this approach, the concept described above is based on the "splitting" of the total flow into large-scale and small-scale structures. The motion of large vortices (of size $\lambda \geqslant h$, where h is the resolution of the difference grid) is determined by directly integrating the equations of hydrodynamics[12]. Modelling ("smoothing") is applied only to a small-scale subgrid pulsations, which cannot be solved explicitly during numerical integration and, as was mentioned above, have quite universal properties. This concept is quite adequate for the so-called models for "*overgrid*" *closure* ([1.39, 1.40], etc.). However, the crux of the matter is to organize a certain split-

[12] For such an approach, averaging is essentially carried out only over time intervals characterized by the occurrence of events of the same kind (method of "random options").

ting (averaging) process, and to choose the models which are used for constructing approximate ("smoothed") equations describing the motion of large-scale structures. Naturally, this raises problems associated with the choice of approximations for small vortices and an estimate of their influence on large-scale flows. Of course, the most important aspects here are those associated with the realization of the approaches mentioned above.[13]

1.6. Using the general numerical methods described here and the basic concepts of structural turbulence, let us consider a *constructive scheme for direct numerical simulation of turbulence problems* [1.2, 1.10]. The main idea behind this approach for investigating anisotropic free turbulence lies in the fact that for studying of various structures of turbulent flows, it seems quite reasonable to "split" the total effect into regions (intervals) with different scales of interaction and accordingly with different numerical models.[14]

For inertial interval of motion (vortex scales $l > \lambda \gg \lambda_0$, where λ_0 is the inner turbulence scale, $\mathrm{Re}_{\lambda_0} \simeq 1$), the transfer of kinetic energy through a vortex cascade with a velocity $\mathscr{E}$ will be the principal process, and the breaking-up of vortices will take place only under the action of inertial forces while the viscosity will be insignificant (Kolmagorov's second similarity hypothesis regarding the conservation of energy flux[15]). This type of motion takes place for very large Reynolds numbers, and local turbulence relations should be used for vortex scales $\lambda \gg \lambda_0$ [1.41-1.43].

Essentially, simulation starts in this case from the local turbulence scale, while the computation of ordered structures and large-scale flows is carried out directly.

The *viscous* (*dissipative*) *flow interval* ($\lambda \leqslant \lambda_0$) is entirely determined by viscous forces. The smallest turbulence scale λ_0 is characterized by the fact that the local Reynolds number for it is of the order of unity ($\mathrm{Re}_{\lambda_0} \simeq 1$), and turbulent flow is possible only in

---

[13] In many cases, for example, in models of "overgrid" turbulence ([1.39, 1.40], etc.), the mathematical difficulties encountered during a consideration of the problems mentioned above are nearly identical to the problems associated with the solution of the Reynolds averaged equations.

[14] Instead of introducing a unified (for the entire flow field) coefficient of effective turbulent viscosity in the "smoothed" equations, the spectrum of such coefficients depending on the order of length of the scales under consideration is essentially proposed here.

[15] It is mentioned in [1.41] that all the quantities corresponding to the turbulent flow of the scale $\lambda \gg \lambda_0$ cannot depend on molecular viscosity ν; to be more precise, these quantities must not change with a change in ν, other flow conditions remaining fixed. Distances of the order of $\lambda_0 = l/\mathrm{Re}^{3/4}$ are the boundaries of applicability of Euler equations to a turbulent flow. Thus, turbulent flows of the scale $\lambda \gg \lambda_0$ can be generally investigated on the basis of Euler equations with an approximate dissipation mechanism which must incorporate the contribution of small vortices.

quite large volumes, where $\mathrm{Re} > 1$. Viscosity hinders the evolution of turbulence in smaller volumes, and hence the flow of the smallest vortices is laminar. Besides, these vortices are responsible for a large part of the total energy scattering. Thus, the smallest-scale flows and viscous losses (energy dissipation) are described by the time-dependent Navier-Stokes equations for small values of Reynolds numbers.

The isolation of viscosity interval is analogous to a boundary layer. It is investigated independently, but on the basis of the data corresponding to the "main" (inertial) interval of motion of large-scale structures. Such a division of a phenomenon into regions of "large" and "small" turbulence structures with different types of exchange (and hence different values of effective viscosity) is quite physical; it can be seen that this does not require the solution of Navier-Stokes equations for large values of Re.

Let us discuss the possibility of quantitatively estimating the properties of turbulent flows by using the scheme described above [1.2, 1.10].

On the *inertial turbulence interval*, the role of viscosity is insignificant. In this case, it is natural to investigate the ordered and large-scale processes directly by constructing a generalized solution for Euler's nonstationary model with a certain approximate dissipation mechanism for exact simulation of the process in time ("Euler difference process" of the type (1.13)). An exact simulation of the transient nature of motion helps in the investigation of the dynamics of the process evolution. Essentially, the approximate dissipation mechanism in Euler's difference equations permits the determination of the effective values of transport coefficients from the stability conditions. In principle, the dissipation mechanism can be "controlled" in such a way that it will reflect (for appropriate resolution scales) the "contribution" of subgrid structures for various values of λ.

If the analysis of the *averaged motion of nonstationary ordered macroscopic structures* (which depends on the entire flow region) is carried out with the help of "Euler's difference schemes" with a scheme viscosity of the type

$$\varepsilon \simeq |V| \cdot h, \tag{1.15}$$

the investigation of large ("energy-carrying") turbulent vortices in the domain of large gradients can be introduced into the approximate dissipation mechanism of turbulent viscosity in the form

$$\hat{\nu}_{\text{turb.}} \simeq \Delta u \cdot l, \tag{1.16}$$

where Δu is the variation in the mean velocity at distances of the order l; for *local turbulence* zones which are defined by local gradients, it is expedient to use in the "Euler difference" the effective viscosity $\hat{\nu}_{\text{turb.}\,\lambda}$ satisfying the well-known Kolmogorov-Obukhov law [1.41,

1.43]:

$$v_\lambda \simeq (\mathscr{E}\lambda)^{1/3} \quad \text{or} \quad \mathscr{E} \simeq \frac{v_\lambda^3}{\lambda} \simeq \hat{\hat{\nu}}_{\text{turb. }\lambda} \left(\frac{v_\lambda}{\lambda}\right)^2, \tag{1.17}$$

whence

$$\hat{\hat{\nu}}_{\text{turb.}\lambda} \simeq \mathscr{E}\lambda^2/\nu_\lambda^2. \tag{1.18}$$

Here, $\mathscr{E}$ is the rate of dissipation of turbulence energy over the vortex cascade (this quantity can be directly obtained from calculations for large-scale formations); v_λ is the change in velocity (mainly in its pulsating component) over a distance $\simeq\lambda$.[16]

Introducing the relations (1.15)-(1.18) into the computational scheme (1.13), we can correctly simulate the law of turbulence damping for different scales λ. In the regions of viscous flow interval where a complete dissipation of energy takes place (over distances $\simeq h$ for $\mathrm{Re}_h \simeq 1$), the effect of molecular viscosity becomes significant and we must go over to the computation of Navier-Stokes equations with molecular dissipation mechanism.

Thus, new coefficients of turbulence viscosity, corresponding to their "own" scale of flow, are successively introduced.

The smaller the resolution scale, the "rougher" the estimates of pulsations in the subgrid (an ever increasing part of the spectrum "falls" in the region of direct resolution). A "change" in the type of effective viscosity ("splicing" of the solution) takes place when the condition of energy flow conservation over the vortex cascade is satisfied in the regions where the "old" solution becomes unstable and it becomes necessary to use finer steps (scale) for the computational grid. We believe that this idea of constructing a numerical experiment is quite similar to Landau's turbulence evolution theory [1.41, 1.44].

The following circumstances must be borne in mind:

(1) the choice of the computational grid step in "Euler's difference" must ensure that the main part of the energy spectrum is contained in it for $\lambda \geqslant h$ (the grid must not be a rigid filter);

(2) it can be seen that for such an approach it is not necessary to solve Navier-Stokes equations for large values of Reynolds numbers;

(3) the "true" scale of turbulence (and the corresponding transport coefficients) are worked out during the calculations for unsteady flows.[17]

---

[16] In local turbulence zones ($\lambda \gg \lambda_0$), the relative motion of liquid particles is considered on this segment (instead of the absolute motion, when the entire "cell" moves as a whole; the latter situation is characteristic of large scales and follows from (1.15)) [1.41].

[17] The author is grateful to Acad. A.M. Obukhov, Corr. Member of the USSR Academy of Sciences Prof. V.M. Ievlev and Prof. A.T. Onufriev for the discussion of the problems mentioned here.

Computations for "smoothed" equations with a reduced dissipation mechanism are carried out on large intervals of time up to the formation of characteristic (generally, nonstationary) structures. After this, an appropriate statistical analysis of the obtained results is essential for determining the averaged characteristics of pulsating flow (moments). This statistical analysis can be carried out directly from the results of computations or by using probabilistic methods.

It was shown by Ievlev [1.37] and others that calculations made by using "smoothed" equations can, in principle, ensure the determination of the right statistical flow parameters which depend on large-scale turbulence, although a detailed space-time pattern for such a pulsation flow will not duplicate any real process.[18]

We shall call this fundamental result "*Ievlev's process*". Essentially, this result provides an affirmative answer to the question of a direct numerical simulation of nonsteady (pulsating) large-scale turbulent flow with the help of "smoothed" equations of motion. Naturally, this requires a correct specification of the mathematical expectation conditions on the right-hand sides of "smoothed" equations (see the conditions in Sec. 4 of [1.37]). We also note that the right-hand sides of "smoothed" equations are *uniquely* determined from the values of flow parameters at the nodes of the computational grid (in contrast to the exact equations in which the right-hand sides also contain random oscillations). Thus, "closure" of approximate equations is carried out by an appropriate simulation ("smoothing") of the effects of small-scale subgrid vortices. Such a representation must approximate the right-hand sides of these equations with a certain degree of accuracy and reflect the effect of small vortices.

The values of energy flux and turbulent viscosity were estimated for various scales of flow in the wake of a body by the method described above for a flow past a rectangular obstacle (compressible gas, $M_\infty = 2.00$). The formation of mean flow (characterized by the emergence of a typical flow pattern) occurred after about 1500 time steps ($T = 1500\ \Delta t$). We shall give here the values of effective viscosity in the separation zone behind a body [1.10] corresponding to the preliminary data for various turbulence scales. The value of scheme viscosity in the calculations of ordered macroscopic structures with the help of (1.15) is $\varepsilon \simeq |V| h \simeq 10^{-2}$; the turbulence

---

[18] The equations describing the evolution of probability densities f_n (for real values) and $\tilde{f}_n$ (for the aggregate of their approximate values determined from "smoothed" equations) are identical. If we prescribe similar initial and boundary conditions for f_n and $\tilde{f}_n$, these functions become completely identical, i.e. all statistical flow characteristics, defined in terms of f_n and $\tilde{f}_n$ respectively, coincide (although the time dependence of real and approximate values of pulsating quantities will not be the same for identical initial conditions).

viscosity coefficients for large vortices, obtained from (1.16), are also of the same order:

$$\hat{\nu}_x \simeq \Delta u \cdot \Delta x \simeq 0.009, \quad \hat{\nu}_y \simeq \Delta v \cdot \Delta y \simeq 0.0075,$$

while for local turbulence scales (where the effect of mean flow is comparatively weak), we get in accordance with (1.18)

$$\hat{\hat{\nu}}_x \simeq \frac{\mathscr{E}(\Delta x)^2}{(\Delta u)^2} \simeq 3 \times 10^{-5}, \quad \hat{\hat{\nu}}_y \simeq \frac{\mathscr{E}(\Delta y)^2}{(\Delta v)^2} \simeq 6 \times 10^{-5}.$$

The energy flux is

$$\mathscr{E} \simeq 3 \times 10^{-5}.$$

Here, Δu and Δv are the variations in velocity in a cell at distances Δx and Δy, respectively. Thus, we see that for various turbulence scales, our "cascade" model gives a qualitatively correct (in orders of magnitudes) estimate of "viscosity effects" in turbulent flows: as we go over to smaller and smaller scales, the values of effective turbulence viscosity, tend to their values ν f the molecular flow. Of course, these results need to be refined.

1.7. The above method and splitting schemes were used for carrying out a large number of numerical experiments to calculate the motion of *large-scale ordered structures in the wake* of a body ([1.2, 1.5, 1.9, 1.10, 1.13, 1.14], etc.). While the analysis for moderate Reynolds numbers (on the basis of Navier-Stokes equations) characterizes the origin of the first bifurcation process in a coherent dynamic structure ("pseudoturbulence", [1.33]), calculations made for limiting flow conditions with the help of "Euler difference" method illustrate the evolution of ordered and large-scale equilibrium structures for "supercritical" and supersonic flows. As expected, local and small-scale formations have an insignificant effect on the kinetic characteristics and the overall flow pattern. Thus, one can expect to obtain objective quantitative information in this case. The results described are also in good agreement with the experimental data (see, for example, [1.34], etc.).

Estimate of flow parameters for the "*stochastic component*" *of turbulence* was obtained with the help of statistical methods [1.2, 1.10, 1.23, 1.24].

We shall describe some results of computations. Let us consider *steady* separation flows first. For supersonic values of Mach number for the incoming flow (which stabilizes the flow), stationary separation regimes are observed under natural conditions and can be analyzed theoretically. Such calculations were made by Davydov ([1.2-1.5, 1.9, 1.10], and others) with the help of the coarse particle method.

Figure 1.3*a* shows the general pattern of supersonic flow of air past a sharp axisymmetric body ("missile") [1.45]. When a statistically steady state is attained, the characteristics in the wake can be numerically simulated as shown in Fig. 1.3*b* which depicts the isotherms T/T_∞ for $M_\infty = 1.89$. Essentially, this involves the solution

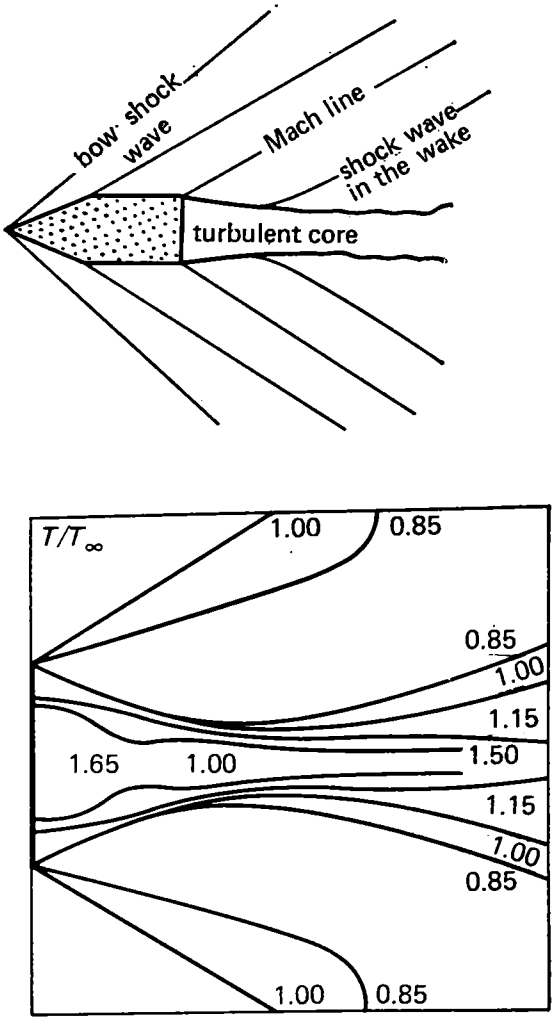

Fig. 1.3. Supersonic air flow past a missile ($M_\infty = 1.89$): (*a*) general pattern of flow; (*b*) field of isotherms T/T_∞ in the wake after the establishment of statistically steady state (calculated).

of the problem of diffraction of the shock wave at the bottom edge of the missile; the waves meet at the mid-point of the bottom edge and an averaged pattern is established after some time, when the local flow parameters undergo only weak fluctuations. Such calculations were essentially of a methodical nature. Although real turbulence is three-dimensional and the method described above does not allow small structures to be "captured", the computation appar-

ently simulates the initial stage of transition to turbulence (Kelvin-Helmholtz type instability), which is in good agreement with the data given in [1.45].

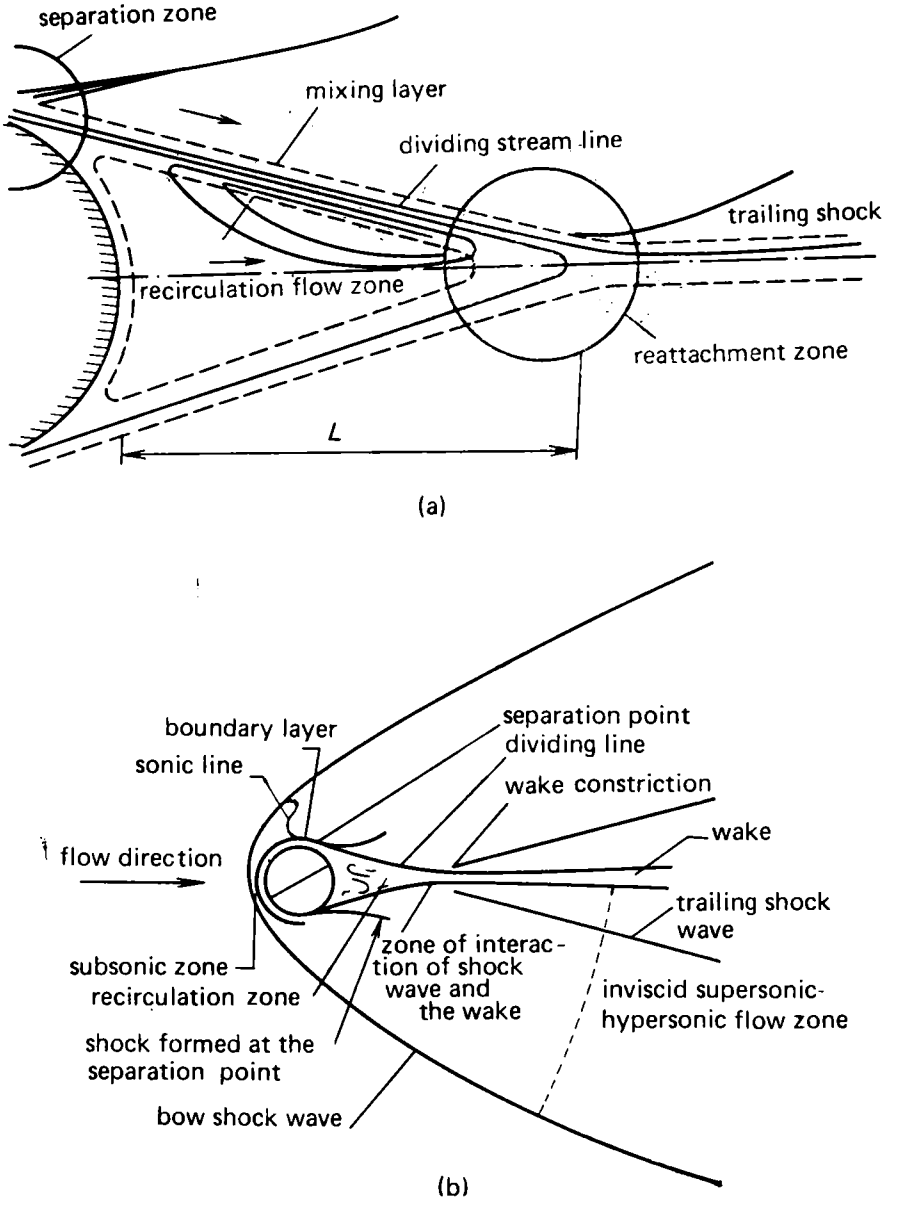

Fig. 1.4. Separation zones in the flow of a compressible gas past a blunt body: (*a*) Chapman's scheme [1.46] for large Reynolds numbers; (*b*) McCarthy and Kubota experiment (circular cylinder, $M_\infty = 5.7$, $Re_d \simeq 66 \times 10^3$) [1.47].

Figure 1.4*a* shows Chapman's classical scheme [1.46] for a separation zone behind a blunt body subjected to a hypersonic flow of a compressible gas. Figure 1.4*b* shows the experiment by McCarthy

and Kubota [1.47] on the flow past a circular cylinder for $M_\infty = 5.7$. It was found that this type of patterns can also be obtained with the help of a numerical experiment.

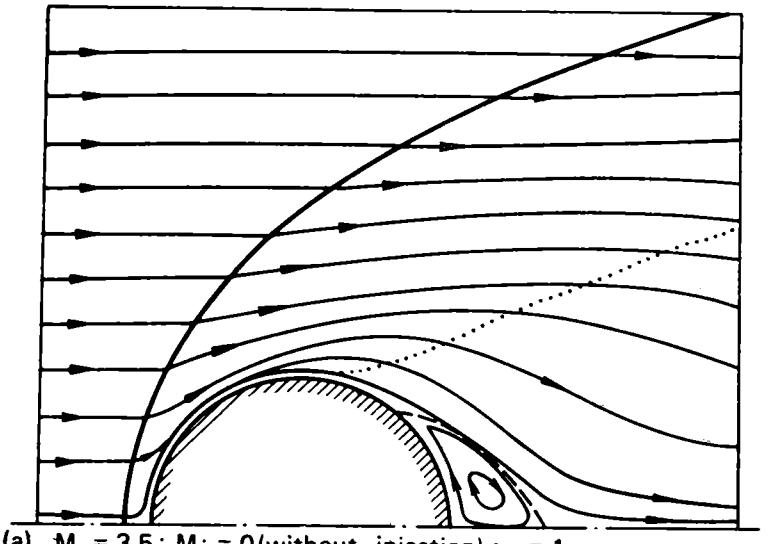

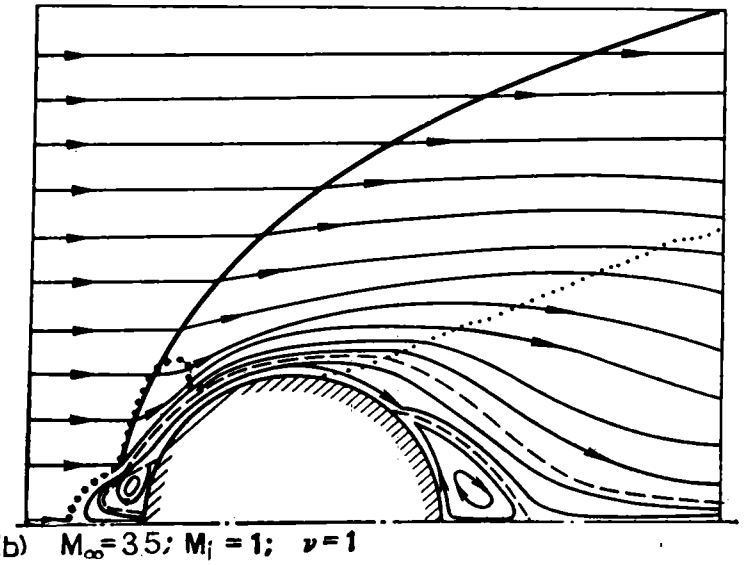

Fig. 1.5. Supersonic gas flow past a sphere ($M_\infty = 3.5$): (*a*) without jet-stream injection; (*b*) for sonic jet-stream injection from the leading critical point (—— shock wave, —→ stream lines, ... sonic lines, ——— separation line, ... velocity vector horizontality line).

Figure 1.5 shows the "visualization" of the flow field in the vicinity of a sphere with a sonic jet-stream injection (from the leading critical point) and without it. This visualization is realized by the coarse particle method based on complete Euler equations for a compres-

sible gas. The formation of separation zones can be clearly seen in this figure (the position of the point of separation is determined by the oblique shock generated at the midsection of the body [1.34]

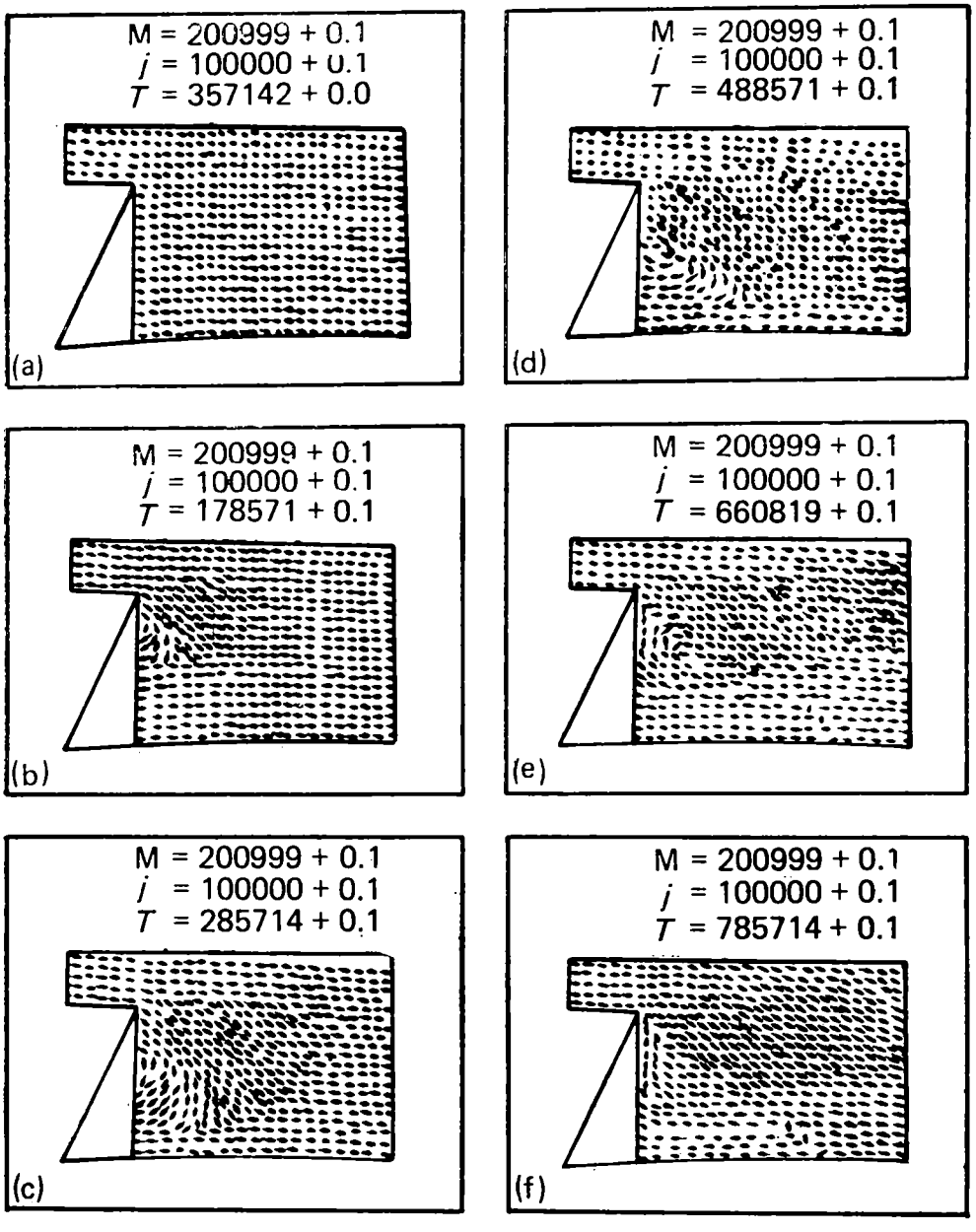

Fig. 1.6. Formation of the separation zone behind a flat shoulder (calculated), $M_\infty = 2.01$, $\nu = 1$, T = var.

$\varphi_{sep} \simeq 110\text{-}120°$, where the angle φ is measured from the leading critical point); in the case of a jet-stream injection, the bow shock wave is "blown" towards the flow and the wave deviation is consider-

ably increased. A stagnation zone with a complex eddy structure is formed in front of the body, and so on.

The following conclusions can be drawn while considering this type of problems:

1. From the multitude of approximate solutions of Euler equations (1.13), the scheme dissipation mechanism "selects" those which have a physical meaning (apparently, the value of viscosity is not significant here). On the other hand, it follows from the estimates that the scheme viscosity of "Euler difference" is quite small in the separation zone, and this ensures an adequate description of the flow pattern.

2. A comparison with the experimental data shows that there is a good qualitative as well as quantitative agreement between the results of physical and numerical experiments.

The "coarse particle" method permits a simulation of quite complex (including three-dimensional) flows for large values of Re. It was used to solve various types of problems on separation [1.2, 1.4, 1.5, 1.9]. For the sake of illustration, we shall mention just a few of these results.

The process of formation of separation zones behind a flat shoulder ("snapshots" of flow at successive instants of time) is shown in Fig. 1.6. Figure 1.7 illustrates the flow pattern past a plane rectangular body with injection of jets of various intensities in its front part.

So far, we have been considering steady flows at supersonic velocities. The situation is more complicated for *subsonic* flow rates. Experiments show that at least two flow patterns are possible in this case, viz. symmetric steady flow and asymmetric periodic flow. Numerical simulation of this type of problems has the following specific feature: in view of the symmetry of the body, initial and final conditions, as well as the algebraic symmetry of the approximating equations, the solution is found to be symmetrical. Apparently, perturbation of purely schematic nature (for example, rounding errors) cannot violate the symmetry which is easily violated by real perturbations under natural conditions. That is why a nonsymmetric (oscillatory) flow with a developed vortex road is usually observed ([1.34, 1.48-1.50], etc.). For numerical imitation of periodic regime for flow past finite-sized bodies, the initial flow asymmetry is introduced in the form of instantaneous perturbations (for example, eddies in front of the body, rotation of the body, flow displacement, momentary injection, etc.).

Thus, the possibility of existence of two separation regimes in a compressible gas, viz. stationary symmetric regime[19] (Fig. 1.8)

[19] The flow separation from the surface of the body occurs behind the shock closing the local supersonic zone, which is in agreement with the experiment [1.34].

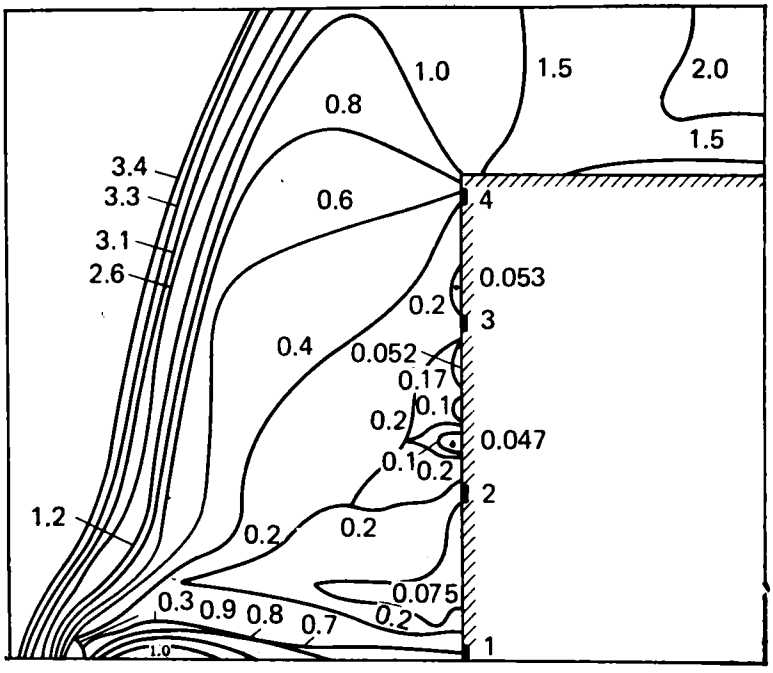

Fig. 1.7. Pattern of flow past a plane rectangular body (calculated, M = const lines) for $M_\infty = 3.5$ with jet injection of various intensities: (*1*) $\rho = 2.9$, $E = 1.826$; (*2*) $\rho = 2.3$, $E = 1.785$; (*3*) $\rho = 1.7$, $E = 1.756$; (*4*) $\rho = 1.1$, $E = 1.717$; $u = -0.286$ and $V = 0$ everywhere.

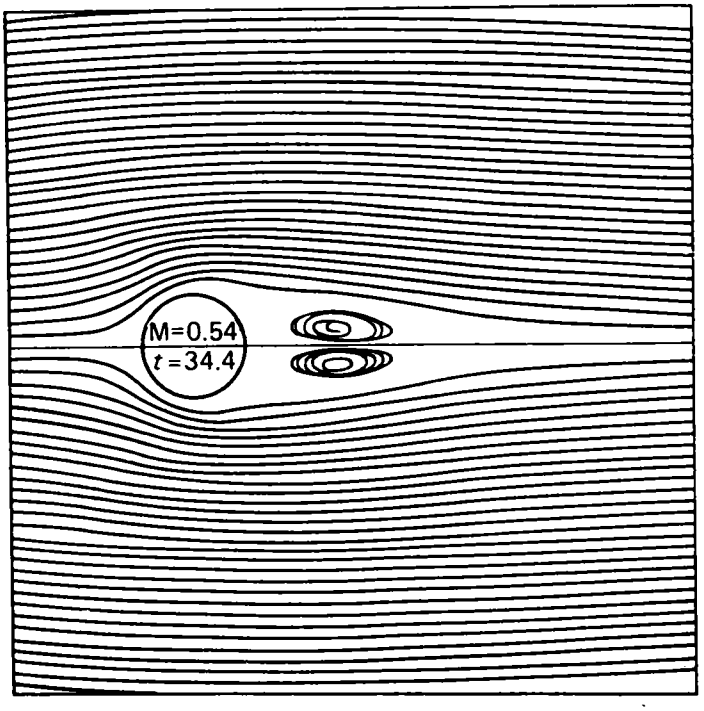

Fig. 1.8. Steady flow of a compressible gas past a circular cylinder (calculated, $M_\infty = 0.54$, stream lines).

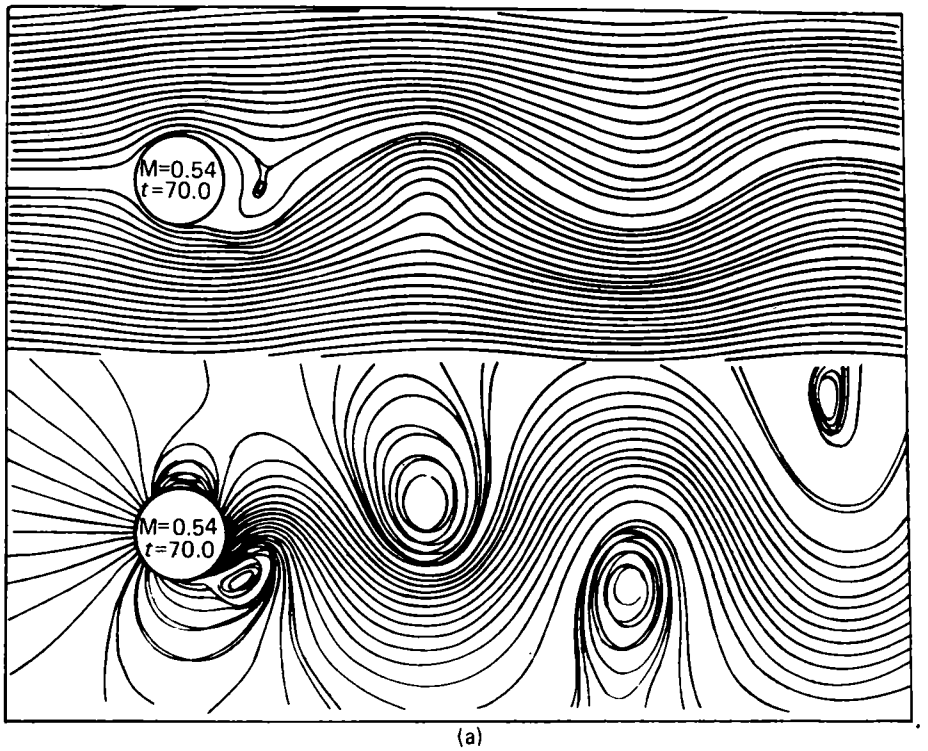

(a)

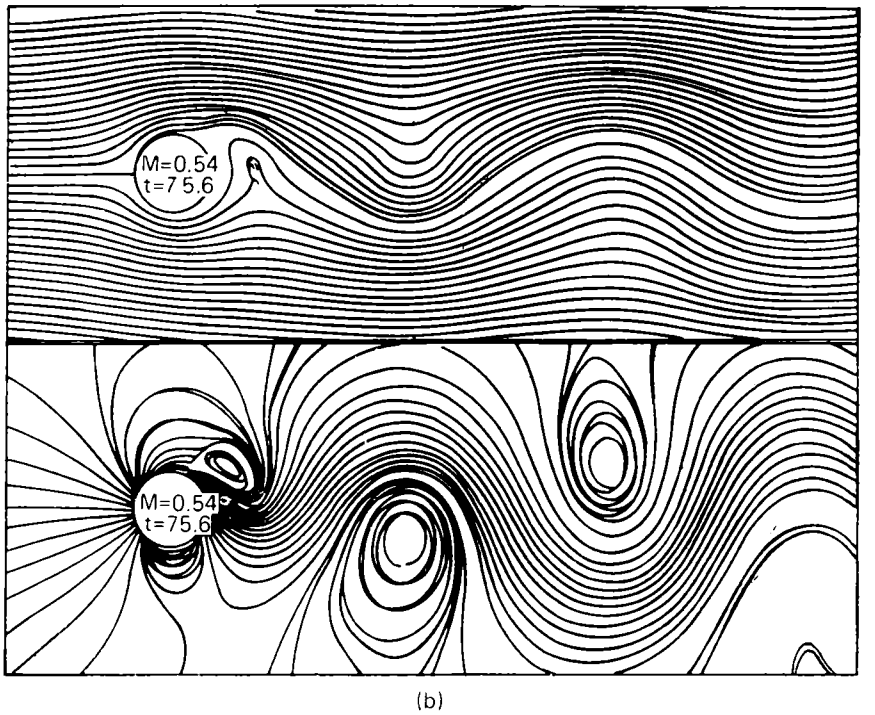

(b)

Fig. 1.9. Unsteady (periodic) flow of a compressible gas past a circular cylinder (calculated, $M_\infty = 0.54$, stream lines; in the coordinate system fixed to the cylinder-top, with incoming flow-bottom).

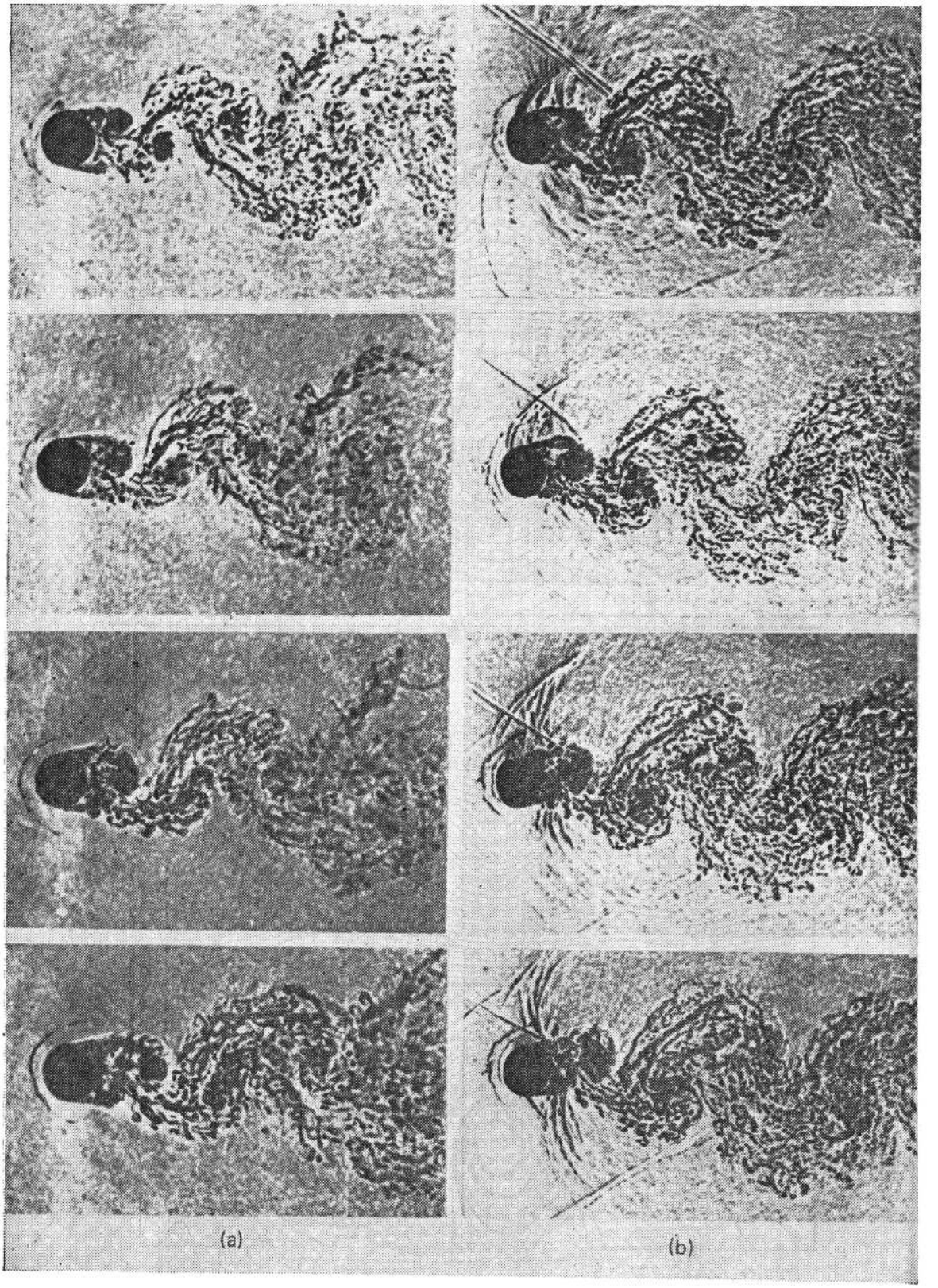

Fig. 1.10. Pattern of flow past a circular cylinder (experiment [1.34]): (*a*) $M_\infty = 0.45$, $Re = 1.1 \times 10^5$; (*b*) $M_\infty = 0.64$. $Re = 1.35 \times 10^6$.

and periodic nonsymmetric regime (Fig. 1.9) was clearly observed during numerical simulation of limiting subsonic (supercritical) flow past a circular cylinder. Babakov and Zyuzin [1.2, 1.9, 1.51] used conservative scheme (1.6) of the method of flows for solving complete time-dependent equations for a compressible medium (the effect of viscosity on the motion of macroscopic structures in such phenomena is insignificant).

It turned out that we can also obtain a second stable regime here, in which a vortex road is formed behind the body. For a circular

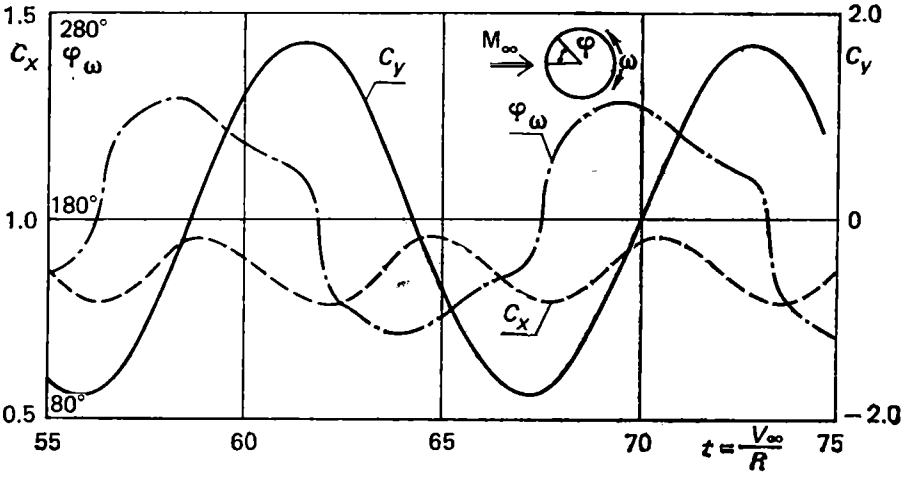

Fig. 1.11. Time variation of aerodynamic coefficients C_x, C_y and the position of the separation point φ_ω in the flow past a circular cylinder (calculated, $M_\infty = 0.54$).

cylinder ($M_\infty = 0.54$), it is characterized by the removal of a vortex sheet from a point on the surface, performing periodic oscillations from 120° to 240°. Figure 1.9 shows an instantaneous visualization of the flow field in the coordinate system fixed to the cylinder (upper field) as well as the incoming flow where the evolution of eddy structure is clearly manifested. In order to attain this regime, an instantaneous perturbation was applied at the beginning and then withdrawn. Irrespective of the form (and type) of perturbations, the same stable periodic flow pattern was observed and was found to be in good agreement with the experimental results [1.34] (Fig. 1.10).

It is interesting to compare the qualitative characteristics for the "nonstationary" regime with the experimental results. Figure 1.11 shows the time variation of aerodynamic coefficients C_x and C_y, as well as the position of the point of separation φ_ω. The value of Struchal number Sh characterizing the frequency of vortex separation is found to be 0.178 in calculations, while experiments [1.48] give a value Sh = 0.18. A comparison of the values of drag coefficient

C_x with experiment [1.49, 1.50] also points towards the adequacy of the real flow pattern. The following mean values (averaged over a period) are obtained in the nonstationary regime: experimental—$C_x \simeq 0.9$; calculated—$C_x \simeq 0.88$-0.9 (in the steady flow conditions, the experimental and calculated values of this coefficient are $\simeq 0.45$ and $\simeq 0.34$, respectively). Note that the experiment [1.49, 1.50] was carried out in a low-noise wind tunnel with a flow turbulence not exceeding 0.5%, which apparently helped in the establishment of a stationary regime.

Calculations and experiments [1.34] have shown that as the Mach number increases ($M_\infty \to 1$), the flow becomes more and more stable and attains a kind of steady state. The deviations in the values of C_y ($|C_y|_{max} \to 0$) decrease[20], the vortex road becomes "narrower" and gradually "moves away" from the stern of the body where it is replaced by a stationary zone (for $M_\infty > 1$) of reverse circulation flow (Figs. 1.4, 1.5).

Apparently, this type of flow can be characterized as the motion of coherent equilibrium macroscopic structures in the turbulent wake behind a body (in particular, this is indicated by a comparison with experiment (Fig. 1.10), the position of separation points on the body, as well as the behaviour of pressure along the surface of a circular cylinder[21]).

The application of Euler's difference equations allows the construction of an overall "macroscopic pattern" of flow without resorting to the low molecular viscosity effect. If, however, it is necessary to obtain a thin flow structure which depends on this viscosity (for example, the friction and thermal flux characteristics), the *Navier-Stokes equations* are the most reliable tool for investigations.

The main difficulty associated with the application of Navier-Stokes equations, as mentioned above, lies in the exact "resolution" of the flow structure for not-too-small values of Re. This difficulty can be partially overcome by using finer grids (wherever necessary) and higher-accuracy schemes. Figures 1.12 and 1.13 show certain examples of numerical simulation of *laminar stationary separation* at supersonic velocities (see Tolstykh *et al* [1.9, 1.52]).

---

[20] It follows from the calculations of flow past a circular cylinder that as M_∞ increases from 0.54 to 0.64, the maximum value $|C_y|_{max}$ decreases by about an order of magnitude ($|C_y|_{max} \simeq 2.0$ for $M_\infty = 0.54$ and $|C_y|_{max} \simeq 0.2$ for $M_\infty = 0.64$). For $M_\infty \simeq 0.8$, the value of $|C_y|_{max} < 0.1$.

[21] In their article "On Turbulent Separation" in *Zh. Vychisl. Matem. i Mat. Fiz.*, 20, 6: 133 (1980), Sychev and Sychev have shown (without putting forth any hypothesis concerning the closure of Reynolds equations) that the separation of turbulent boundary layer of an incompressible liquid from a smooth surface is self-induced and takes place under the action of a large local pressure gradient. In principal terms, the separation is determined by the interaction due to the influence of the nonlinear part of the boundary layer, where the action of friction forces is insignificant.

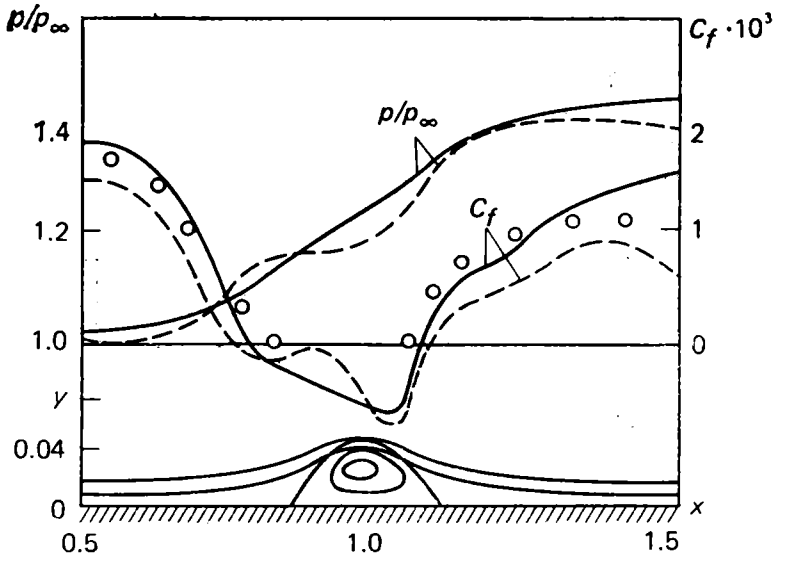

Fig. 1.12. Interaction of an oblique shock wave with the boundary layer on a plate ($M_\infty = 2$, $Re = 5 \times 10^4$, angle of incidence of the shock wave is 32.6°; —— calculated, ○○○○, - - - - experiment [1.52]).

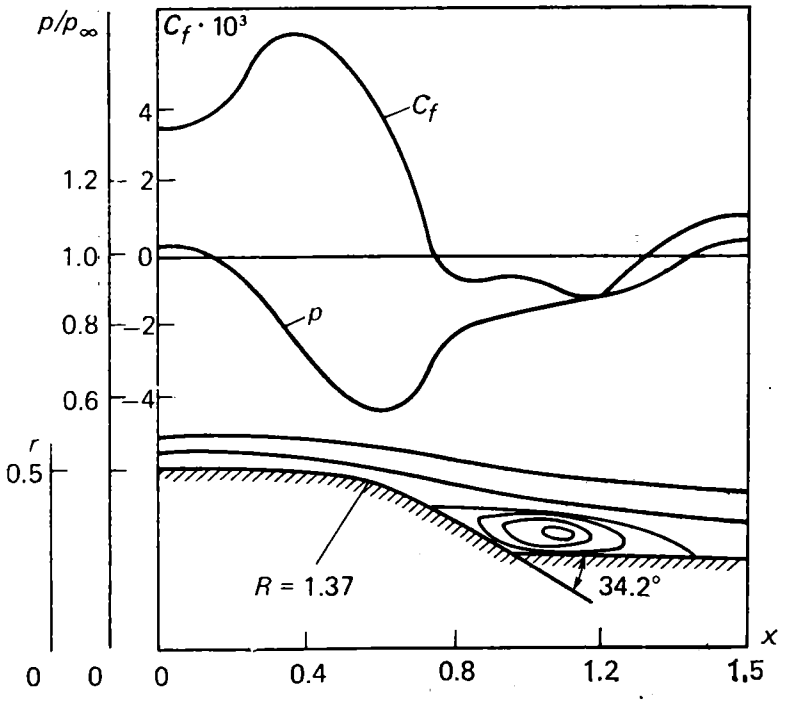

Fig. 1.13. Flow past the aft nacelle of a body of revolution (calculated, $M_\infty = 1.7$, $Re = 10^4$, $Pr = 0.72$).

Figure 1.12 shows the fragment of the flow pattern obtained by solving the classical problem of the incidence of an oblique shock wave (at an angle of 32.6°) on a plate with a sharp leading edge for $M_\infty \simeq 2$. The Navier-Stokes equations were solved with the help of the so-called "compact" scheme of fourth-order accuracy with

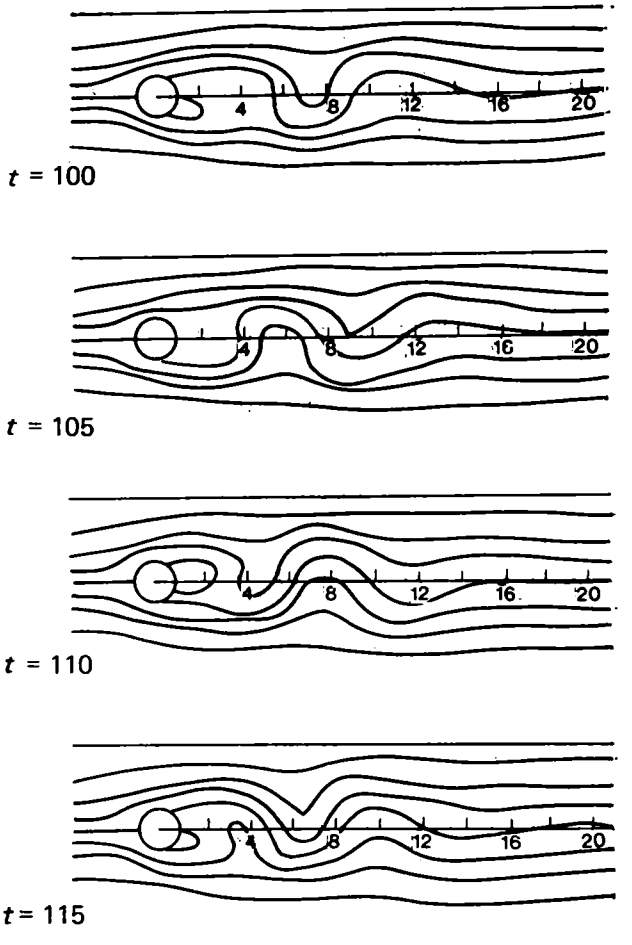

Fig. 1.14. Pattern of flow of a stratified incompressible viscous fluid past a circular cylinder (calculated, Re = 100, Fr = 0.315, Sh = 0.133).

a finer difference grid [1.52]. In spite of the fact that Reynolds number was 10^5 in this case, the method permitted a "resolution" of even a thin near-wall layer inside the boundary layer (the figure shows the flow lines in the neighbourhood of a separation, distribution of pressure p/p_∞ along the plate and friction coefficient C_f, as well as the experimental results). It can be seen that the numerical solution correctly describes the position of the separation zone in the vicinity of the incidence of shock wave, as well as the distribution of the main flow parameters.

Figure 1.13 shows the separation zone formed during the axisymmetric flow past a body with a curvilinear generatrix. This configuration can be interpreted as the aft nacelle of an aircraft engine with a jet imitator.

S. Belotserkovskii and V. Gushchin [1.9, 1.14] have endeavoured to simulate the flow of a *viscous incompressible fluid* as a periodic

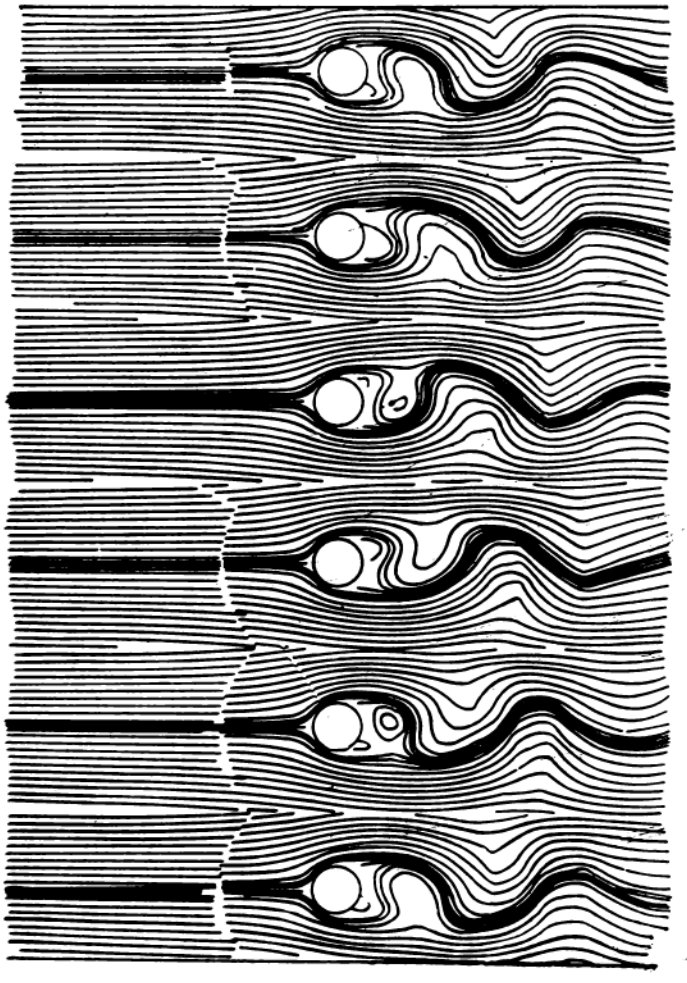

Fig. 1.15. Pattern of flow of a homogeneous incompressible viscous fluid past a circular cylinder (calculated, Re = 100).

flow structure in the wake of a body, without introducing an artificial initial asymmetry of the flow, but employing natural conditions instead, viz. a stable density stratification.

Figure 1.14 shows the flow of a stratified incompressible viscous fluid past a circular cylinder for $\mathrm{Re} = 100$ and $\mathrm{Fr} = \frac{U_\infty^2}{dg} = 0.315$. Calculations were carried out on the basis of Navier-Stokes equations

with the help of the difference scheme (1.7) employing splitting according to physical criteria [1.12, 1.14]. The creation of a periodic separation (alternately in the upper and lower parts of the cylinder) with the formation of flow structure of "Karman's vortex road" type can be seen in the figure. The calculated value of Struchal's number for this periodic regime was found to be 0.133.

The results of calculations for the flow of a homogeneous viscous incompressible fluid past a circular cylinder for Re = 100 (nullifying

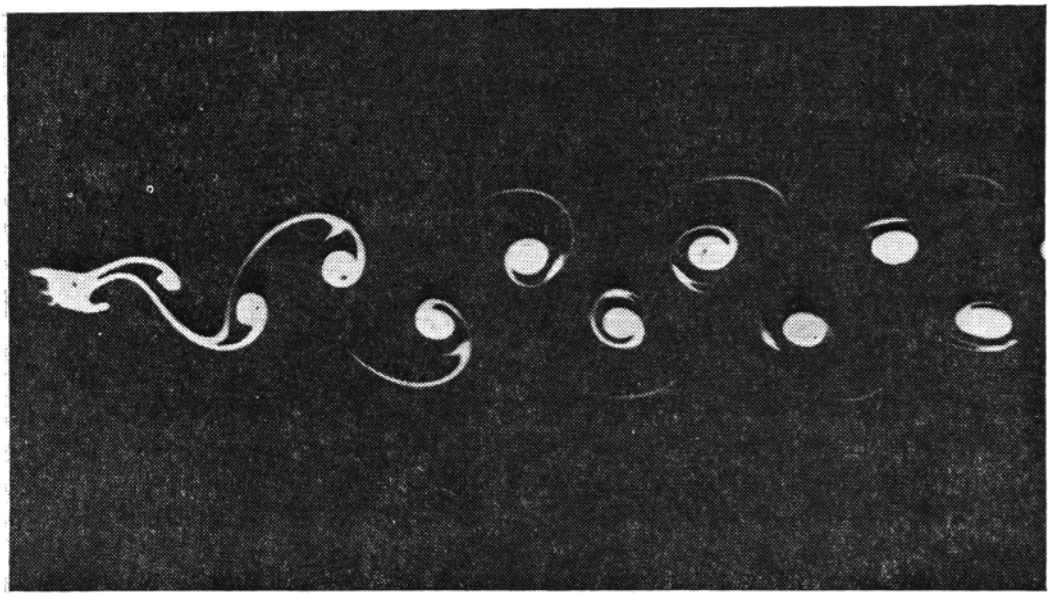

Fig. 1.16. Pattern of flow of an incompressible viscous fluid past a circular cylinder (Re = 105, experiment [1.34]).

the stratification) are shown in Fig. 1.15. For the sake of comparison, Fig. 1.16 shows the flow pattern obtained experimentally in [1.34]. Note that the value of Sh obtained in experiments and by calculations for a homogeneous fluid varies from 0.14 to 0.17.

1.8. While the results described above illustrate the simulation of averaged large-scale macroscopic flow structures, the investigation of *statistical characteristics* ("*stochastic component*") *of turbulence* should naturally be made with the help of the Monte Carlo method by constructing imitation models for the corresponding kinetic equations. We shall describe some results for the problem of "*disintegration*" *of turbulence spots*, obtained by Yanitskii [1.23, 1.24].

As in the dynamics of a rarefied gas (DRG), the problem is solved in this case on the level of distribution function. However, the distribution will now correspond to the pulsations of velocity $\mathbf{v}'$ of a "liquid" particle. In the case of turbulence, the idea of construc-

tion of a computational process on the basis of the splitting method remains the same (compare with the DRG problems [1.19-1.22]). However, each particle in the cell has a new meaning (see the table in Fig. 1.17). A particle is characterized by its "position" and "velocity" in this case too, but it now serves as a model for a fluid particle. The difficulties in creating such a model are associated with the nonstationary nature of the phenomenon itself and with the absence

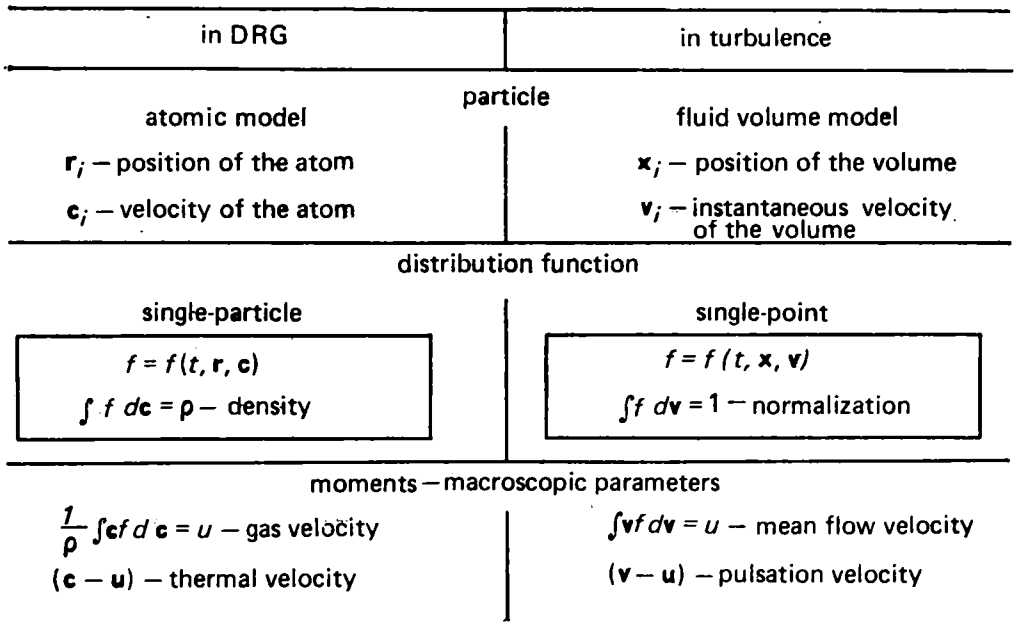
in DRG
in turbulence
particle
atomic model
fluid volume model
$\mathbf{r}_i$ – position of the atom
$\mathbf{x}_i$ – position of the volume
$\mathbf{c}_i$ – velocity of the atom
$\mathbf{v}_i$ – instantaneous velocity of the volume
distribution function
single-particle
single-point
$f = f(t, \mathbf{r}, \mathbf{c})$
$\int f\, d\mathbf{c} = \rho$ – density
$f = f(t, \mathbf{x}, \mathbf{v})$
$\int f\, d\mathbf{v} = 1$ – normalization
moments – macroscopic parameters
$\frac{1}{\rho}\int \mathbf{c} f\, d\mathbf{c} = u$ – gas velocity
$\int \mathbf{v} f\, d\mathbf{v} = u$ – mean flow velocity
$(\mathbf{c} - \mathbf{u})$ – thermal velocity
$(\mathbf{v} - \mathbf{u})$ – pulsation velocity

Fig. 1.17. Comparative description of a medium by the distribution function for the problems in the dynamics of a rarefied gas (DRG) and turbulence.

of a universal kinetic equation in turbulence, analogous to Boltzmann's equation (1.8) in DRG. In principle, simulation can be carried out for different types of kinetic equations. We shall demonstrate one of such attempts here. Our main aim is to solve nonstationary turbulence problems in such a way as to retain the main principles of the method of statistical simulation, although expressing them in other terms.

At a given stage, an imitation model was constructed on the basis of Onufriev's relaxation kinetic equation [1.53] for a one-point distribution function $f(t, \mathbf{r}, \mathbf{v}')$ for the pulsation velocity $\mathbf{v}'$

$$\frac{\partial f}{\partial t} + \mathbf{v}\frac{\partial f}{\partial \mathbf{x}} - \frac{1}{2\tau_1}\frac{\partial}{\partial \mathbf{v}}(\mathbf{v}' f) = \frac{f_M - f}{\tau_2}, \tag{1.19}$$

where

$$f_M = \left(\frac{3}{4\pi E}\right)^{3/2} \exp\left[-\frac{3(v')^2}{4E}\right]$$

is the normal distribution law;

$$\tau_1 = \mathscr{L}_1/\sqrt{E}, \quad \tau_2 = \mathscr{L}_2/\sqrt{E}$$

are the relaxation times;

$$\mathscr{L}_1 E^{(2\gamma_1-1)/2} = \text{const}_1, \quad \mathscr{L}_2 E^{(2\gamma_2-1)/2} = \text{const}_2$$

are the relations determining the laws of variation of integral scales $\mathscr{L}_1$ and $\mathscr{L}_2$, and E is the turbulent energy density. The analogy of the kinetic equation (1.19) with Boltzmann's and Crook's equations is known.

The main empirical constants of the model are the exponents γ_1 and γ_2 in the laws of variation of integral scales as functions of the turbulence intensity E:

$$\mathscr{L}_1^- \simeq E^{(2\gamma_1-1)/2} \quad \text{and} \quad \mathscr{L}_2^{-1} \simeq E_2^{-1} \simeq E^{(2\gamma_2-1)/2}.$$

The simulation scheme employed here is the same as in the dynamics of rarefied gases, viz. fluid particles in cells and the splitting of the evolution of the model at the step Δt into the following fundamental physical processes:

convective transport $\left(\mathbf{v}\frac{\partial f}{\partial \mathbf{x}}\right)$,

dissipation of turbulence energy $-\frac{1}{2\tau_1}\frac{1}{\partial \mathbf{v}}(\mathbf{v}'f)u$, and

redistribution of energy over degrees of freedom $\frac{f_M - f}{\tau_2}$.

Numerical solution was obtained for the *problem on turbulence diffusion*, in which the energy was initially concentrated in the region with characteristic radius r_0 (the problem of a "spot", see Fig. 1.18). With the passage of time, the characteristic radius $r(t)$ of the spot changes as well as the turbulence energy density $E_m(t)$ at the centre of the spot. The following are the initial parameters for this problem ($t = 0$):

the energy field:

$$E_0(r) = E_m^{(0)} \exp\left(-\frac{r^2}{r_0^2}\right), \quad E_m^{(0)} = E_m(0);$$

the distribution function $f(0, \mathbf{r}, \mathbf{v}') = f_0(\mathbf{r}, \mathbf{v}')$ for the pulsations of $\mathbf{v}'$:

$$f_0(\mathbf{r}, \mathbf{v}') = \left[\frac{3}{4\pi E_0(r)}\right]^{3/2} \exp\left[-\frac{3(v')^2}{4E_0(r)}\right].$$

For the case of a uniform spot, Fig. 1.18 gives a comparison of the results of calculations with the results obtained from Naudasher's experiment [1.54]. Figure 1.18*a* shows the time variation of the relative characteristic radius $\bar{r}_{1/2} = r_{1/2}/r_0$ of the spot ($r_{1/2}$ indicates

the radius at which the energy density $E\ (t,\ r_{1/2})$ is half its value at the centre of the spot ($E\ (t,\ r_{1/2}) = \frac{1}{2} E_m\ (t)$). Figure 1.18*b* shows a similar comparison for the turbulent energy density in the centre of the spot $\bar{E}_m\ (t) = E_m\ (t)/E_m\ (0)$. We find that a good agreement between the numerical and physical experiments is observed.

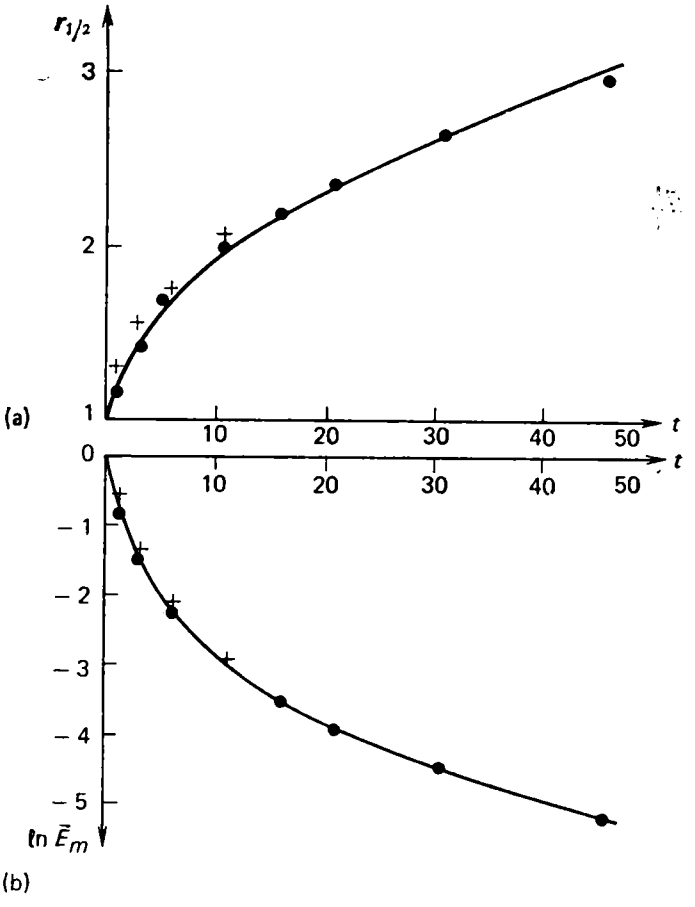

Fig. 1.18. Time variation (*a*) of the characteristic radius $r_{1/2}$ and (*b*) the turbulence energy density E at the centre of a homogeneous spot: •••• Naudasher's experiment [1.54]; ——— root-mean-square approximation of the experiment; direct numerical simulation.

The distribution of energy along the radius of the spot is self-similar (Fig. 1.19): $\bar{E} = f\ (\xi)$, where $\bar{E} = E\ (t,\ r)/E_m\ (t)$, $\xi = r/r_{1/2}$ is the relative radius. The physical experiment [1.54] for the self-similarity law $f\ (\xi)$ gives the following representation: $f\ (\xi) = \exp\ (-0.69\xi^2)$. In numerical computations, this relation is usually specified as the initial condition. The dependence mentioned here assumes the form of a more rapidly decreasing function which can be approximated quite well by the expression $\tilde{f}\ (\xi) \simeq I_0\ (a\xi^2)$,

where $a \simeq 1.5$ and I_0 is a zero-order Bessel function (this is illustrated in Fig. 1.19).

Such a discrepancy between numerical results and the physical experiment is characteristic of most numerical models, and this shows the inadequacy of our concepts about the physical nature of the phenomenon under consideration. The deviation of the turbulence-variation coefficient from unity (characteristic of all numerical models of this problem) is probably the general drawback which is responsible for the indicated discrepancy with the experiment.

The method of direct statistical simulation allows us to obtain a one-point pulsation distribution function or its moments. Figure

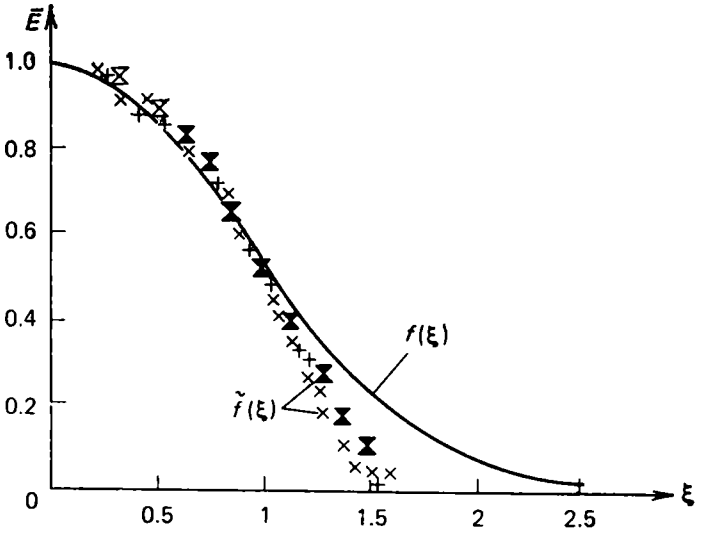

Fig. 1.19. Energy distribution along the spot radius: ——— experiment [1.54]; ⧗ ($t = 3$), + ($t = 6$), × ($t = 11$) direct numerical simulation.

1.20 shows (in different time intervals for the relative spot radius $\xi = r/r_{1/2}(t)$) the distribution of asymmetry and excess indices α_r and β_r. The asymmetry index $\alpha_r(\xi) = \mu_3/\mu_2^{3/2}$ characterizes the third moment of the distribution function (turbulence energy flow), while the excess index $\beta_r(\xi) = \mu_4/3\mu_2^2 - 1$ corresponds to the fourth moment of the distribution function (according to Millionshchikov's hypothesis, $\beta_r = 0$). The spot boundary, the nature of turbulence energy distribution, etc. are clearly seen. Calculations were also made for (density) stratification of the spot.

The prospect of the application of direct statistical simulation to turbulence problem is due to the possibility of using kinetic models which are closed at the level of the pulsation distribution function. As a rule, such models have a smaller number of empirical constants (there are two such constants in the present case, viz. γ_1

and γ_2, while the constants $\mathcal{L}_1^{(0)}$ and $\mathcal{L}_2^{(0)}$, i.e. the integral scales at the initial moment of time, are associated with the initial conditions). However, kinetic models are more informative, since they allow us to determine the pulsation distribution function.

This trend is being pursued vigorously and, in particular, one can hope to solve more complicated turbulence problems in which the

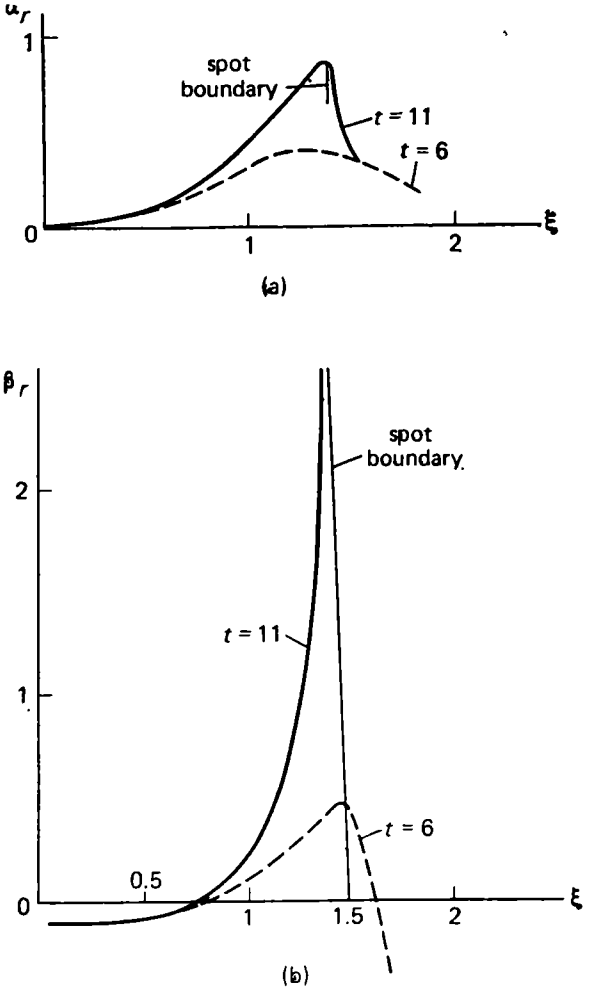

Fig. 1.20. Indices of (*a*) asymmetry α_r and (*b*) excess β_r for a homogeneous turbulence spot.

motion of ordered and large-scale macroscopic structures is directly computed from splitting schemes for finite-difference transport equations (for example, with the help of coarse particle method or the method of flows), while the local small-scale fluctuations of the "stochastic component" of turbulence are simulated (Euler cells inside a "coarse particle") with the help of statistical methods [1.2, 1.10].

1.9. It is undoubtedly interesting to investigate the *hydrodynamic stability of a fluid flow* while considering atmospheric phenomena, in the problems of turbulence generation, in the evolution of the Rayleigh-Taylor instability, etc.

Investigation of the laminar flow stability against small perturbations which always exist in nature is quite interesting from theoretical point of view, as well as for practical applications. Thus, according to Landau [1.44] (see also [1.41, 1.43, 1.55]), as the Reynolds number (or any other parameter characterizing the flow) passes through its critical value, the main steady flow loses its stability and a new, generally periodic and oscillatory regime (secondary flow) is established. In turn, this secondary flow is stable only in a certain interval of values of the parameter, beyond which it again loses its stability and so on. It is assumed that as the value of the parameter increases, new types of perturbations may appear successively and a quasi-periodic motion with an ever increasing number of frequencies emerges. Hence the flow can be assumed as turbulent for a quite large value of the parameter.

Landau considers the emergence of a periodic oscillatory regime as the first step in a transition from the laminar flow of a fluid to turbulent flow. It is well known that in the two-dimensional case, there is generally no fixed transition point: laminar flow is always transformed into a completely turbulent flow over a certain transition region where secondary (as a rule, oscillatory) flows are imposed on the main flow. Without changing the laminar nature of the main flow on the whole, these flows considerably influence its averaged characteristics.

It seems especially important to obtain the general flow patterns in the transition region for stationary as well as oscillatory regimes, investigate the dynamics of their behaviour, determine the critical values of the flow parameters, and find the periods of oscillatory periodic flows.

Mathematical models for this type of flows are boundary value problems for nonlinear partial differential equations (in the general case, this is a multidimensional time-dependent system of Navier-Stokes equations). The problem of the *two-dimensional flow of an incompressible viscous fluid under the action of a periodic (transverse) force* is considered in [1.14, 1.56, 1.57]. This problem was proposed by Kolmogorov [1.58] and was investigated for the linear case in [1.59, 1.60], etc., where the loss of stability of the main laminar flow with respect to spatial-periodic perturbations with a large wavelength along the flow was proved. The problem of nonlinear evolution of perturbations and the onset of secondary or periodic flows upon the loss of stability of laminar flow of an incompressible viscous fluid is investigated in [1.61-63]. Experimental investigations of a two-dimensional periodic flow are described in [1.64].

However, the question of the existence of stable steady or oscillatory secondary flows remains open to a considerable extent.

We shall describe the main results of the investigations of this problem, carried out by S. Belotserkovskii and Gushchin [1.14, 1.56, 1.57].

Let us consider the flow of an incompressible viscous fluid under the action of an external force which is spatially periodic, directed along the x-axis and equal to $\gamma \sin \eta y$ (the parameter $\gamma > 0$). Such a motion is described by a system of Navier-Stokes equations. Introducing scales of length η^{-1}, velocity $\eta^{-2}\nu^{-1}\gamma$, time $\eta\nu\gamma^{-1}$ and going over to dimensionless variables, we can write the equations of motion and the continuity equation in the following form:

$$\begin{aligned} &\frac{\partial u}{\partial t}+\frac{\partial u^2}{\partial x}+\frac{\partial uv}{\partial y}=-\frac{\partial p}{\partial x}+\frac{1}{\mathrm{Re}}\Delta u+\frac{1}{\mathrm{Re}}\sin y, \\ &\frac{\partial v}{\partial t}+\frac{\partial uv}{\partial x}+\frac{\partial v^2}{\partial y}=-\frac{\partial p}{\partial y}+\frac{1}{\mathrm{Re}}\Delta v, \\ &\frac{\partial u}{\partial x}+\frac{\partial v}{\partial y}=0. \end{aligned} \tag{1.20}$$

Here, $\mathrm{Re} = \gamma^2/\nu^2\eta^3$ is the Reynolds number and ν is the kinematic viscosity. The flow is investigated in a rectangular domain $\Omega = \{(x, y), |x| \leqslant \pi/\alpha, |y| \leqslant \pi\}$, at whose boundary we impose the conditions of periodicity in x (with a period $2\pi/\alpha$, the wave number α being positive) and in y (with a period 2π) [1.14, 1.56].

The average flow velocity of the fluid

$$\mathbf{q} = \frac{\alpha}{4\pi^2}\int_{\Omega}\mathbf{V}\,dx\,dy \tag{1.21}$$

will be assumed to be given.

To begin with, let us consider the case $\mathbf{q} = 0$ corresponding to zero flow rate across the sides of a rectangle Ω. The differential problem formulated for (1.20) has the following stationary solution corresponding to laminar flow along the x-axis:

$$u = \sin y,\ v = 0,\ p = \text{const}. \tag{1.22}$$

In terms of the "stream function-eddy" variables, this solution can be written as follows:

$$\Psi = -\cos y. \tag{1.22'}$$

Let us investigate the stability of time-dependent solution (1.22)-(1.22') in the domain Ω with respect to perturbations that are harmonic in x with a wavelength $2\pi/\alpha$ and in y with a wavelength 2π. After this, the solution obtained initially in the domain Ω is periodically continued in x and y (with periods $2\pi/\alpha$ and 2π, respectively).

For a numerical solution of the problem (1.20), we use the difference method based on the splitting of the complete system of Navier-

Stokes equations on each time layer into physical factors. This method was earlier developed for solving the problems of external flow of a viscous homogeneous fluid past bodies [1.12, 1.14].

It was shown in [1.59, 1.60] (for a linear formulation of the problem) that for $\alpha < 1$, the stationary solution (1.22′) for the laminar flow is unstable with respect to longwave longitudinal perturbations for a definite value of the parameter Re. This value will be called the critical Reynolds number Re_{cr}. Moreover, $\mathrm{Re}_{cr}(\alpha) \to +\infty$ as $\alpha \to 1 - 0$; for $\alpha \to +0$, $\mathrm{Re}_{cr} \to \sqrt{2} + 0$. With the help of the asymptotic technique for solving the corresponding Orr-Sommerfeld periodic problem, we can find [1.14, 1.63] an expression for $\mathrm{Re}_{cr} = \mathrm{Re}_{cr}(\alpha)$ for small values of α:

$$\mathrm{Re}_{cr} = \sqrt{2} + \frac{3}{2}\sqrt{2}\cdot\alpha^2 + O(\alpha^4) \tag{1.23}$$

The flow pattern (lines $\Psi = \text{const}$) corresponding to subcritical regime in accordance with the analytic solution (1.22′) for $\alpha = 0.5$ is shown in Fig. 1.21*a*. A similar flow pattern is also observed for a direct numerical solution of the complete problem (1.20) for $\alpha = 0.5$, $\mathrm{Re} = 0.5$ and $\mathbf{q} = 0$. This solution is stationary and coincides completely with the asymptotic solution (1.22′) (the relative error is less than 1%). The flow obtained for $\mathrm{Re} < \mathrm{Re}_{cr}$ will be called the *mainstream* flow.

Motion in the supercritical region, resulting from the loss of stability of mainstream flow shown in Fig. 1.21*a*, is investigated analytically and numerically in [1.14, 1.56].

The procedure of analytic investigation of the secondary flow for $\mathrm{Re} > \mathrm{Re}_{cr}$ is based on the approximation of hydrodynamic equations to a finite-dimensional system of ordinary differential equations (Galerkin's method). For the basis functions, we use the most unstable modes obtained from the linear theory of flow stability (1.22′). A general expression has been obtained in [1.63] (at $\mathbf{q} = 0$) for the flow function of secondary flow, taking into account the dependence of Re_{cr} on the wave number α:

$$\Psi(x, y) = -\frac{\mathrm{Re}_{cr}}{\mathrm{Re}}\cos y - \frac{\sqrt{\mathrm{Re}_{cr}(\mathrm{Re} - \mathrm{Re}_{cr})}}{\mathrm{Re}} \times \left\{\frac{1}{\alpha}\sin\alpha x + \frac{2}{\mathrm{Re}_{cr}}\cos\alpha x\cdot\sin y\right\}. \tag{1.24}$$

Here the first term corresponds to the stream function for the mainstream flow, and the second term to the stream functions for finite perturbations. Formula (1.24) describes various secondary flow regimes for $\mathbf{q} = 0$.

Analysis of the secondary flow (1.24), carried out in [1.63], shows that there exist certain *characteristic* values of Reynolds numbers

$\mathrm{Re}_1(\alpha)$ and $\mathrm{Re}_2(\alpha)$, and each of the three intervals $\mathrm{Re}_{cr} < \mathrm{Re} \leqslant \mathrm{Re}_1$, $\mathrm{Re}_1 < \mathrm{Re} \leqslant \mathrm{Re}_2$ and $\mathrm{Re} > \mathrm{Re}_2$ has its own secondary flow pattern. A qualitative reconstruction of the flow structure takes place

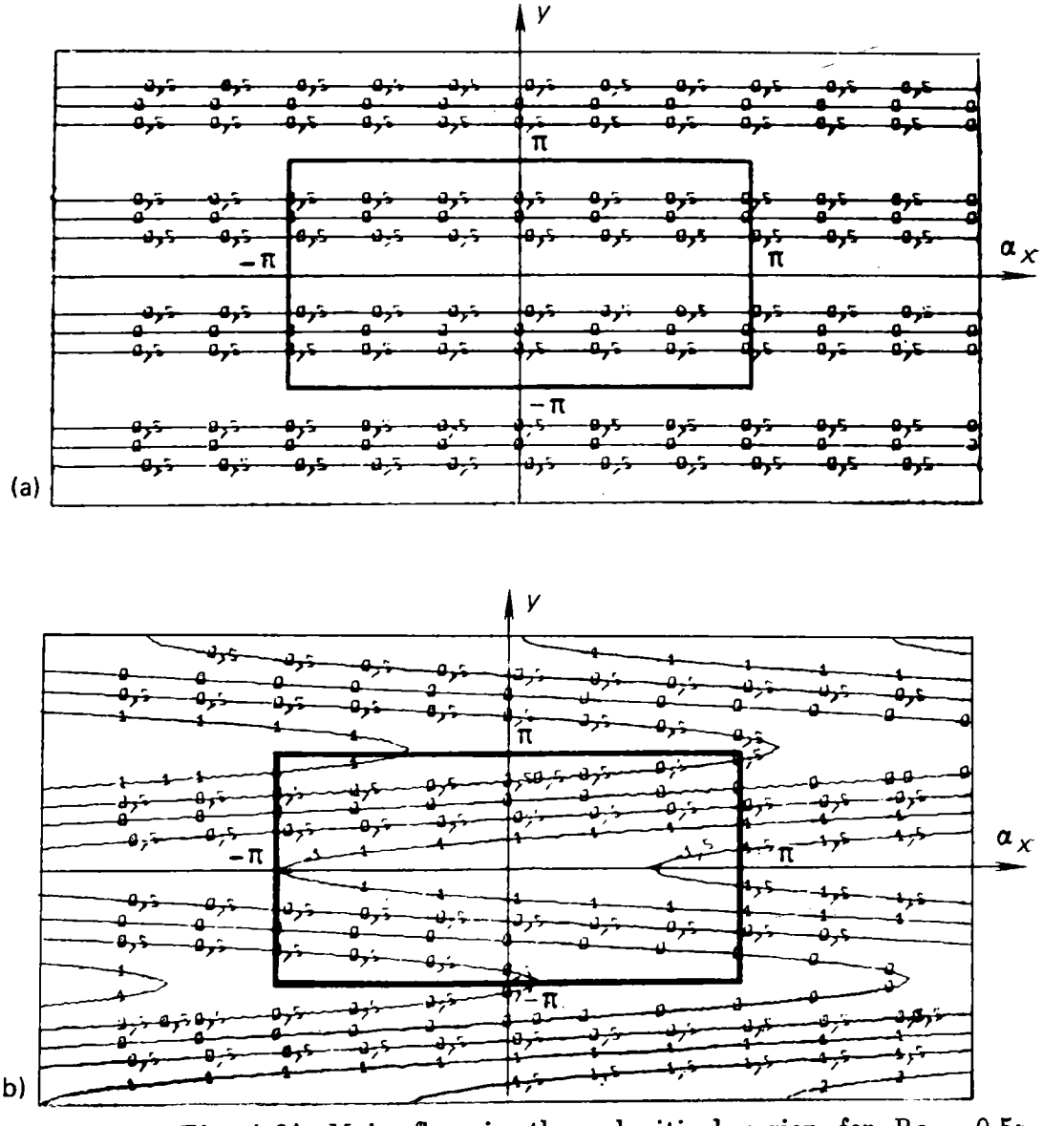

Fig. 1.21. Main flow in the subcritical region for Re = 0.5: (*a*) **q** (0, 0) = 0; (*b*) **q** (0.05, 0.05) $\neq$ 0.

upon a transition through these boundaries. According to [1.63], the values of Re_1 and Re_2 are determined with the help of the following relations:

$$\mathrm{Re}_1(\alpha) = \mathrm{Re}_{cr}(\alpha)(1+\alpha^2);$$

$$\mathrm{Re}_2(\alpha) = \mathrm{Re}_{cr}(\alpha)\left(1+\frac{\mathrm{Re}_{cr}^4}{16\alpha^2}\right). \qquad (1.25)$$

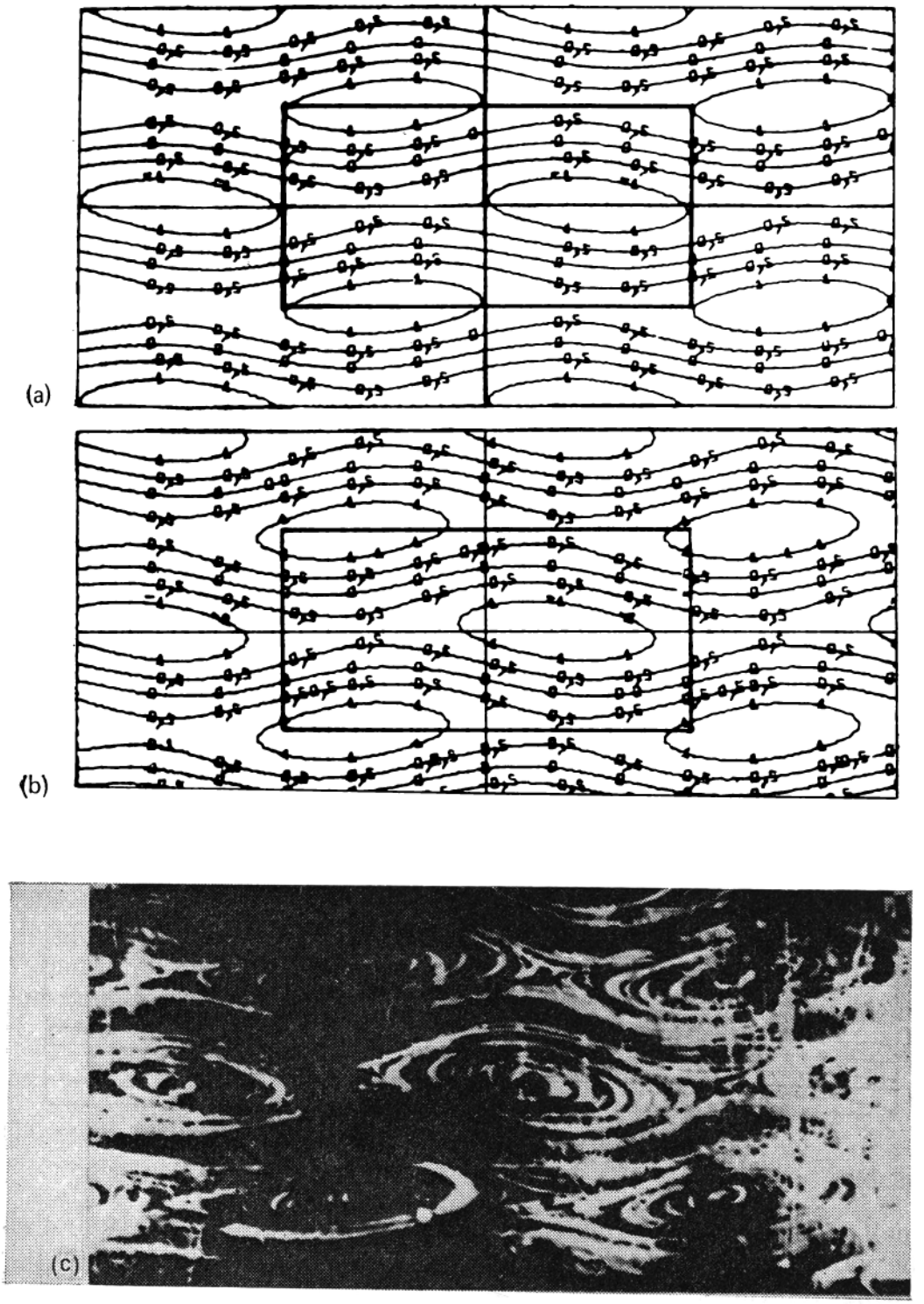

Fig. 1.22. Secondary steady flow in the first interval ($Re_{cr} < Re \leqslant Re_1$) for $\alpha = 0.5$, $\mathbf{q}\ (0,\ 0) = 0$: (*a*) $Re = 2.0$ (analytic solution); (*b*) $Re = 3.1$ (calculated), (*c*) experiment [1.64] for $Re > Re_{cr}$.

(For $\alpha = 0.5$ in the present case, it follows from (1.23) and (1.25) that $\mathrm{Re}_{cr} \simeq 1.9$, $\mathrm{Re}_1 \simeq 2.4$ and $\mathrm{Re}_2 \simeq 8.8$). We shall now investigate each interval of Reynolds numbers separately.

In the *first case* ($\mathrm{Re}_{cr} < \mathrm{Re} \leqslant \mathrm{Re}_1$), a stationary system of vortex chains which are parallel to the x-axis and are separated by horizontal jet-stream zones is observed. Figure 1.22*a* shows the pattern of analytical solutions of (1.24) (the lines $\Psi = \text{const}$) for this case ($\mathrm{Re} = 2$). In can be seen that the vortex axis is inclined under the action of shear, while the directions of angles of rotation alternate upon a successive transition from one vortex band to another. With increasing Reynolds number (as $\mathrm{Re} \to \mathrm{Re}_1$), the maximum width of a vortex band increases while the jet-stream zones become smaller.

For the sake of comparison, Fig. 1.22*b* shows the steady flow pattern in the supercritical regime, obtained by a direct numerical solution of the complete initial problem (1.20) for $\mathrm{Re} = 3.1$ after the loss of stability of the mainstream at $\mathbf{q} = 0$ (shown in Fig. 1.21*a*). Although the numerical solution is obtained for $\mathrm{Re} = 3.1$, the flow pattern shown in Fig. 1.22*b* corresponds to the first type of flow. Figure 1.22*c* shows the results of experimental investigations [1.64]. A quite good agreement between the experimental and computed results is observed.

Results of computations showed that as the Reynolds number Re changes from 3 to 3.1, the mainstream constructed numerically for the complete system (1.20) of Navier-Stokes equations loses its stability and a new (first) stationary regime corresponding to the secondary flow is established (although in accordance with the linear theory, the critical Reynolds number defined by formula (1.23) for $\alpha = 0.5$ is $\mathrm{Re}_{cr} \simeq 1.9$). This discrepancy in the value of Re_{cr} is apparently due to the fact that the value (1.23) of the critical Reynolds number is introduced in the linear approximation for small values of α, while in numerical simulation we solve the complete system of time-dependent equations when the wave number $\alpha = 0.5$.

In the *second case* ($\mathrm{Re}_1 < \mathrm{Re} \leqslant \mathrm{Re}_2$), a stationary system of vertical vortex bands separated by vertical jet-stream regions is formed in accordance with (1.24). The vortex axes in the same band have the same slope, while the direction of rotation angles is reversed upon a transition to the adjoining band. Moreover, the vortices are somewhat elongated in the transverse direction (Fig. 1.23*a*, $\mathrm{Re} = 5$).

For the sake of comparison, Fig. 1.23*b* shows the steady flow pattern (1.20) obtained numerically ($\alpha = 0.5$, $\mathrm{Re} = 5$). Figure 1.23*c* shows the experimental results obtained in [1.64]. It can be seen that the results are in good agreement in this case also.

In the *third case*, as Re passes through its limiting value Re_2 ($\mathrm{Re} > \mathrm{Re}_2$), another reconstruction of the flow structure (1.24) takes place and the flow pattern becomes extremely complicated (Fig. 1.24*a*, $\mathrm{Re} = 50$). Although the system of vertical vortex bands

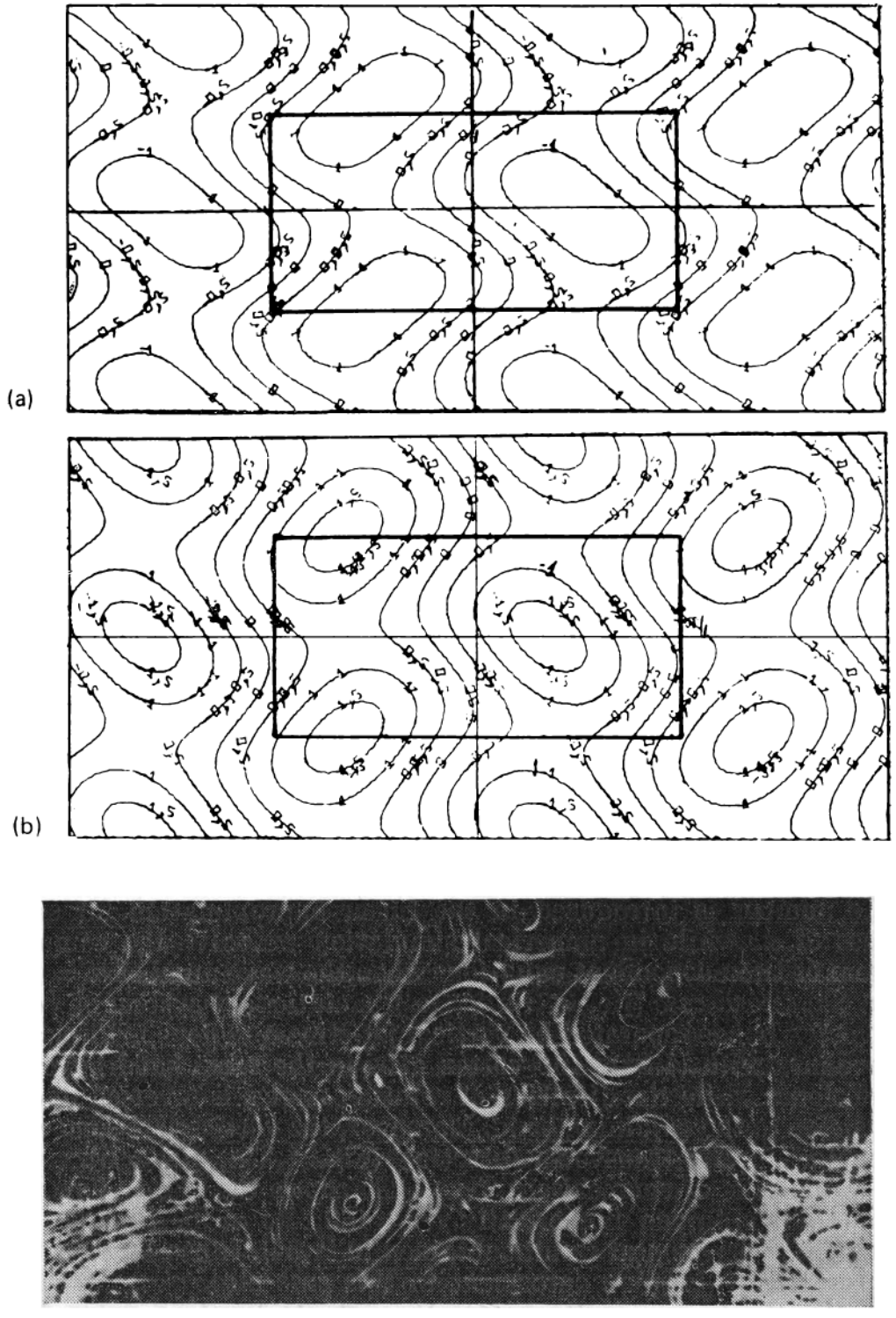

Fig. 1.23. Secondary steady flow in the second interval ($Re_1 < Re \leqslant Re_2$) for $\alpha = 0.5$, $\mathbf{q}\ (0,\ 0) = 0$: (*a*) $Re = 5$ (analytic solution); (*b*) $Re = 5$ (calculated); (*c*) experiment [1.64] for $Re > 1.25Re_{cr}$.

in this case is analogous to that in the second case, the slope of main vortices increases and a new sub-system of "8-shaped" vortices is formed inside them. It can be seen from Fig. 1.24*a* that this regime differs considerably from all the previous cases in that the flow has a fine vortex structure in this case.

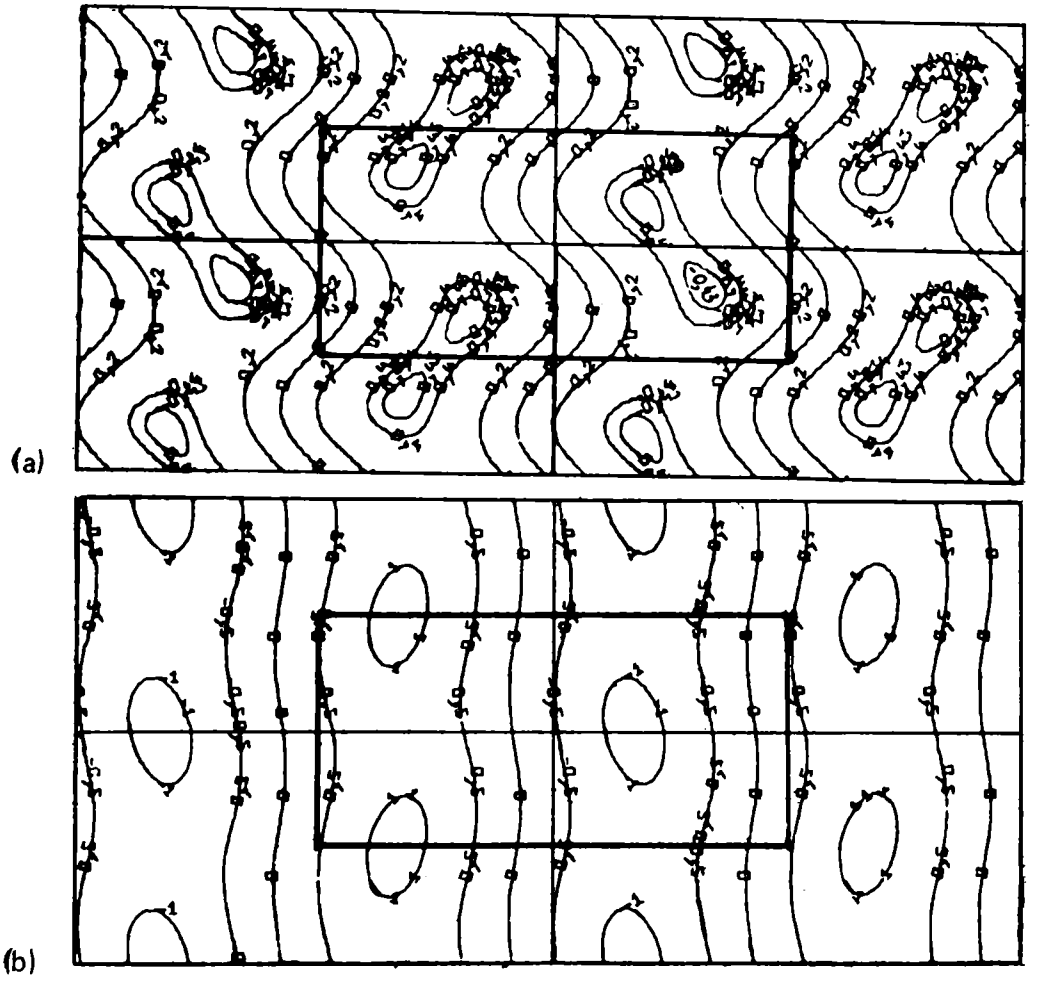

Fig. 1.24. Secondary steady flow in the third interval ($Re > Re_2$) for $\alpha = 0.5$, $\mathbf{q}$ (0, 0) = 0: (*a*) Re = 50 (analytic solution); (*b*) Re = 50 (calculated).

Figure 1.24*b* shows the steady flow pattern obtained as a result of the numerical solution of the complete problem (1.20) for Re = 50. This situation is qualitatively different from the analytic solution in that there is no fine structure. This can be explained by the fact that new types of perturbations may appear for large Reynolds numbers and we can no longer confine the analytic investigations to the consideration of one harmonic in x and harmonics in y with numbers $n = 0 \pm 1$ only.

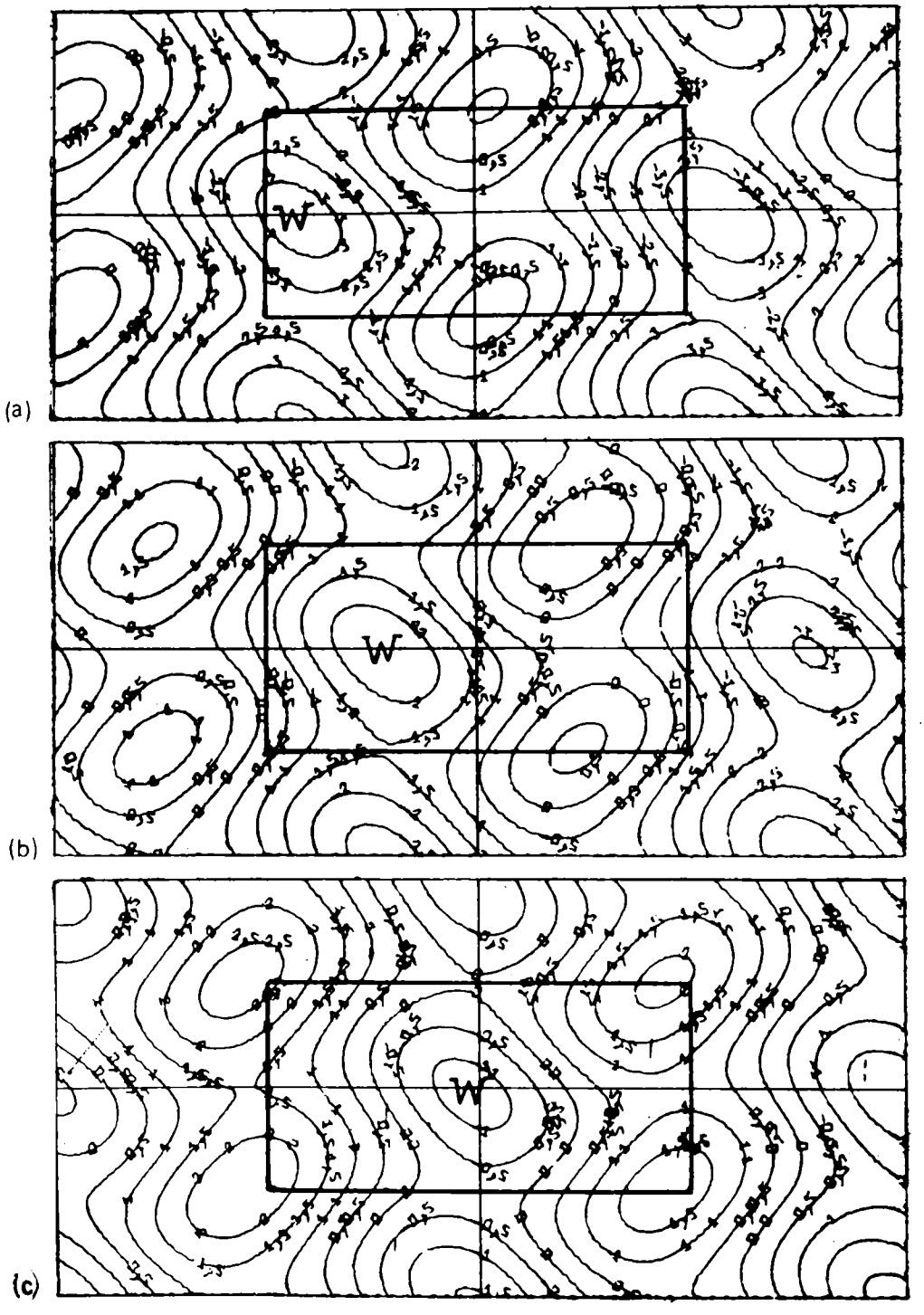

Fig. 1.25. Secondary unsteady flow (calculated) for Re = 5, α = 0.25, **q** (0.05, 0.05) $\neq$ 0: (*a*) t = 75; (*b*) t = 125; (*c*) t = 175, (*d*) t = 255; (*e*) t = 275; (*f*) t = 325.

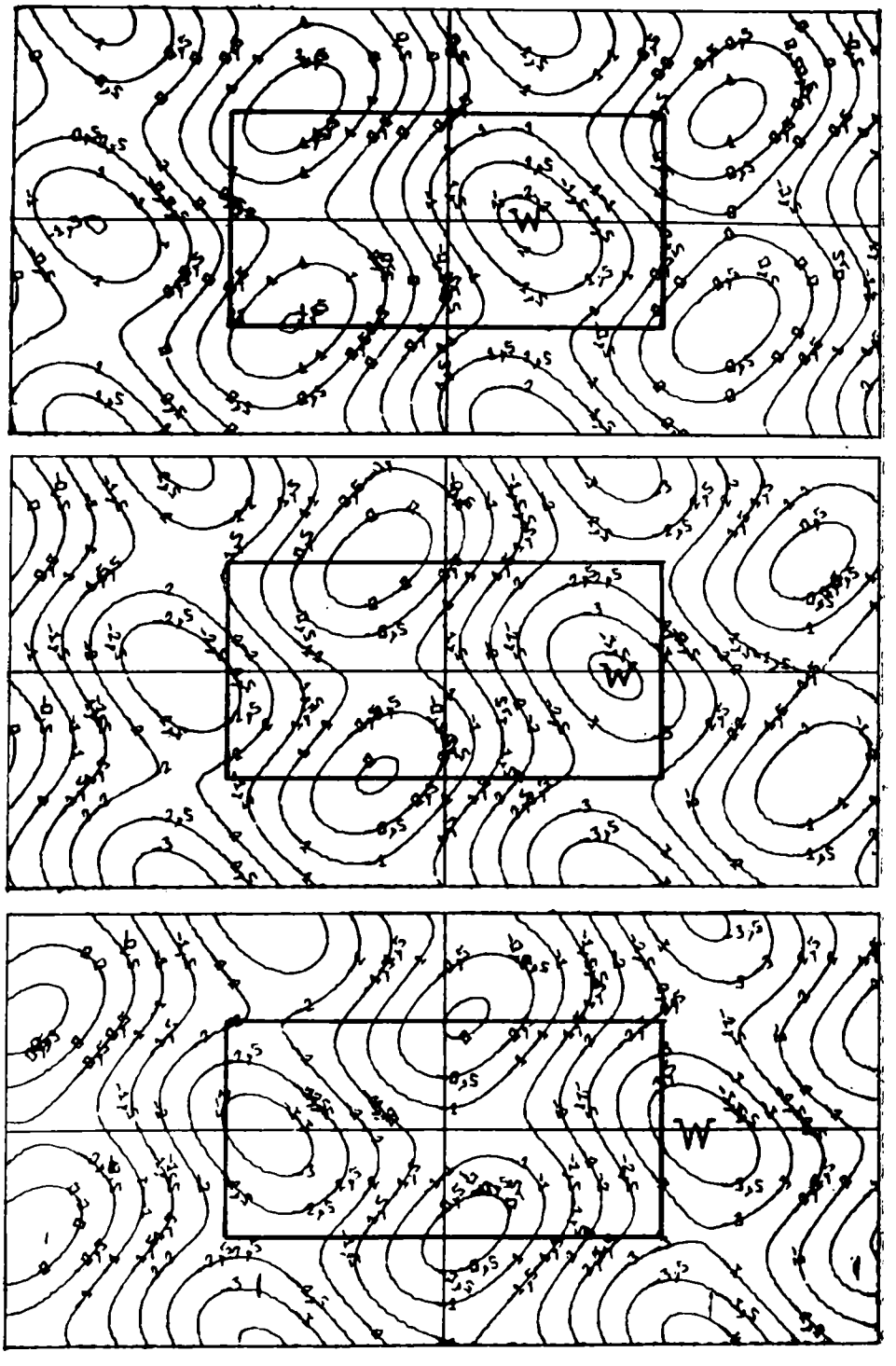
(d)
(e)
(f)

It can be seen that when the mean flow rate of the liquid is equal to zero, all solutions in the supercritical regime are stable and stationary. Thus, it is also shown numerically that as Reynolds number varies from 0.5 to 50, a qualitative reconstruction of the flow structure takes place. This confirms the fact (which was proved analytically and investigated experimentally in [1.64]) that there exist various qualitative regimes of steady flow in the supercritical region.

A quite good agreement exists between the secondary flow patterns obtained from a numerical solution of the problem (on the basis of the complete system of equations (1.20)) and the flow patterns obtained analytically by taking only the first harmonics into consideration (perturbations in x). This confirms the correctness of the description of the analytic expression (1.24) for the secondary flow in the case when Re is close to Re_{cr}.

Let us now suppose that the *mean flow velocity* (1.21) of the fluid is $\mathbf{q} \neq 0$ [1.14, 1.57]. We shall assume that the laminar (subcritical) flow is steady. In this case, the solution of the system of equations (1.20) can be written in the form

$$u(x, y, t) = u(y) + U,\ v(x, y, t) = V,\ p(x, y, t) = \text{const},$$

where U and V are the components of the flow velocity vector $\mathbf{q}$ (U, V) describing the main stream, and $U = \text{const}$, $V = \text{const}$. In this case we obtain an ordinary second-order linear differential equation with constant coefficients, while for the stream function, the solution has the form

$$\Psi = -\frac{1}{1 + (\mathrm{Re}\, V)^2}(\cos y + \mathrm{Re}\, V \sin y) + Uy - Vx. \qquad (1.26)$$

The general solution (1.26), describing the laminar flow in the subcritical regime for any value of $\mathbf{q}$, will be called *basic* solution (if $U = V = 0$, the flow described by the formula (1.26) coincides with the solution (1.22′)).

For $U = V = 0.05$, $\mathrm{Re} = 0.5$ and $\alpha = 0.5$ $(\mathrm{Re} < \mathrm{Re}_{cr})$, the laminar flow pattern corresponding to the solution (1.26) (the lines $\Psi = \text{const}$) is shown in Fig. 1.21*b*. Numerical solution of the problem on the basis of the complete system of equations (1.20) for the same values of the parameters U, V, Re and α confirms that the flow in the subcritical regime is stable and steady. Both flow patterns are completely identical. Numerical computations also show that the initial field for pressure does not influence the solution obtained in this case.

Let us now consider the flow in the supercritical region $(\mathrm{Re} > \mathrm{Re}_{cr})$, which is obtained due to the loss of stability of the main solution (1.26) shown in Fig. 1.21*b* for $\mathbf{q} \neq 0$. The secondary flow can be constructed in this case only numerically.

Numerical solution of the problem (1.20) for Re = 5 ($\mathbf{q}$ (0.05, 0.05) $\neq 0$, $\alpha = 0.5$) is found to be stable, but time-dependent, and hence the subsequent flow pattern is considered as a function of time (Figs. 1.25*a-f*). It follows from Fig. 1.25 that the flow stream lines form a system of vertical vortex bands separated by vertical jet-stream strips. The secondary flow pattern for the case when the mean velocity vector for the initial flow $\mathbf{q} \neq 0$, has a quite complex structure and the flow function does not satisfy the periodicity condition in x and y. Moreover, this flow is transient and the system of vortices moves in the positive direction of the x-axis. It can be seen that the pattern of stream lines for the secondary flow is repeated in time after about 250 dimensionless units; in other words, an oscillatory regime with a period $T \simeq 250$ (dimensionless units) is obtained.

It is interesting to follow the variation of the secondary flow pattern for Re = const (Re = 5) upon a variation of the components of the flow velocity vector $\mathbf{q}$ $(U, V) \neq 0$, which is responsible for the main stream.

If $U = 0.05$ and $V = 0$, the flow remains oscillatory with the same period $T \simeq 250$[22]. For $U = 0.005$ and any $V > 0$, the period of oscillatory regime $T \simeq 2500$ for the same Re = 5 ($\alpha = 0.5$), which is ten times more than in the first case where $U = 0.05$. Thus, it follows from calculations that $T_2/T_1 = U_1/U_2$. Hence, while U, $V \to 0$ for $\mathrm{Re} > \mathrm{Re}_{cr}$, $T \to \infty$ and the numerical solution becomes independent of time (Figs. 1.22*b*, 1.23*b*, 1.24*b*). Apparently, the period of oscillatory motion should not change upon a variation in the value of Reynolds number (for $\mathrm{Re} > \mathrm{Re}_{cr}$).

Thus, it is shown in [1.14, 1.57] that the period of oscillatory motion does not depend on the component V of the initial flow and is determined only by the component U. The accuracy of the results obtained is confirmed by the theorem given in [1.60].

For values of Reynolds numbers Re *at which the system of equations* (1.20) *has nontrivial solutions in the case* $q = 0$, *the same equations* (1.20) *for* $\mathbf{q}$ $(U, 0) \neq 0$ *have nontrivial solutions which are periodic in time with a period*

$$T = 2\pi/\alpha U. \tag{1.27}$$

It can be hoped that this formula is applicable to all supercritical flow patterns.

Thus, depending on the average value of the initial flow velocity $\mathbf{q}$, which determines the main laminar flow, we obtain in the supercritical region stable (all regimes discussed in this paper are stable with respect to small perturbations), stationary (for $T \to \infty$), or oscillatory regimes with a period $T = 2\pi/\alpha U$.

---

[22] For $U = 0$ and $V = 0.05$, the secondary flow is stable and steady (it coincides with the flow depicted in Fig. 1.23*b*).

The numerical results presented here show that stable flows for supercritical regimes can be constructed through a direct numerical solution of the complete system of Navier-Stokes equations (1.20).

Finally, we shall describe the results of calculations for the evolution of *three-dimensional perturbations in the case of Rayleigh-Taylor instability (RTI)*. These results were obtained by Davydov and Panteleev [1.65] with the help of the coarse particle method.

Investigation of RTI is a very important problem. Apart from the undoubted theoretical interest, it is also quite significant for several practical problems which are associated, for example, with the investigation of stability of compression of shells in the problems of laser thermonuclear fusion, creation of ultrahigh magnetic fields, etc.

The following distinct stages are traced in the evolution of Rayleigh-Taylor instability: linear, intermediate nonlinear, regular asymptotic, and turbulent stages [1.66]. The linear stage is characterized by a small amplitude a (compared to the perturbation wavelength L) and an exponential growth rate. When the quantity $a \simeq 0.4L$, the process enters an intermediate stage between linear and regular asymptotic stages. The regular asymptotic stage (for $a \simeq 0.75L$) involves the final formation of "peaks" of a heavy fluid, sinking downwards, and "bubbles" of a light fluid, rising upwards. In turn, this stage of RTI is hydrodynamically unstable and is replaced by the "turbulent stage" in which a strong interaction between perturbations of different wavelengths and an agitation of the fluid take place.

For a direct numerical simulation of RTI by the coarse particle method, we can generally use two formulations of the problem [1.67]: kinematic and dynamic. In kinematic formulation of the problem, the velocity perturbation at the interface is specified; in the dynamic formulation, the boundary (in the fluid which was initially at rest) has a perturbed form. In both cases, the coarse particle method permits a numerical analysis of linear and considerably nonlinear stages. In the kinematic formulation, the solution of the problem generally requires less computer time, and hence this approach was used to study the evolution of perturbations in three-dimensional space [1.65][23].

Figure 1.26 shows the geometrical projection of the interfaces constructed at successive instants of time. For $t = 0$, the following initial conditions were specified: the upper half-space contained a heavy fluid with density ρ_2, while the lower half-space contained a light

[23] Earlier, while analyzing the RTI problems (analytically or by computational methods), we considered only the two-dimensional case (see [1.68] and others). However, the two-dimensional model is not adequate for the physics of the phenomenon. Thus, in experiment, two-dimensional structures collapse due to shortwave transverse instability and are transformed into three-dimensional structures.

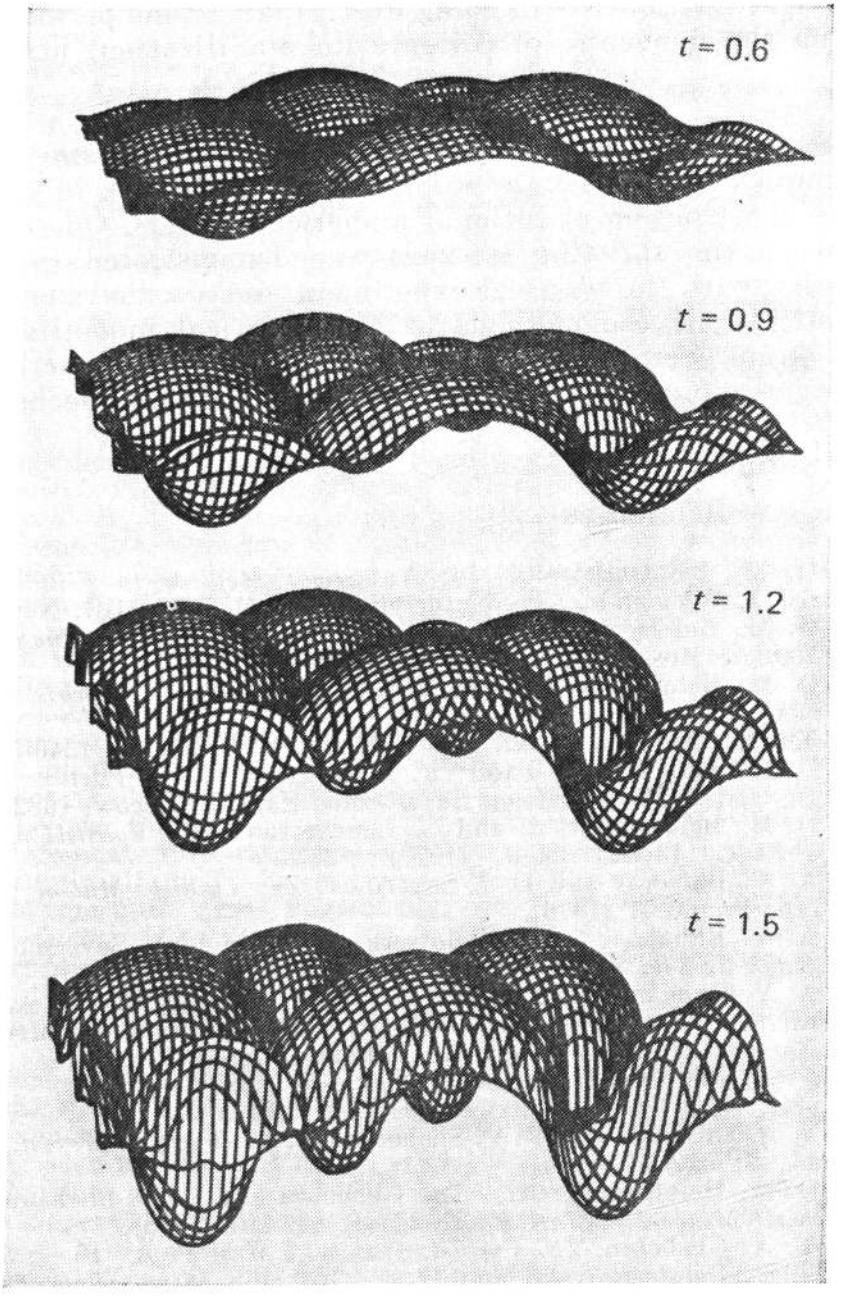

Fig. 1.26. Geometrical projection of the interface for the three-dimensional Rayleigh-Taylor instability ($\rho_2/\rho_1=10$).

fluid with density ρ_1 ($\rho_2/\rho_1 = 10$); initial perturbation was introduced at the interface of the two media in the form of a velocity field [1.65].

The "rising" of broad "bubbles" and "sinking" of sharp "peaks", etc. can be seen quite clearly in this diagram. The main problem in such

investigations consists in going over to large time periods and establishing the moments of collapse (or stabilization) of the process.

Thus, computational experiment methods allow an investigation of complex hydrodynamic problems. The main link in such methods is the construction of rational numerical models. One of the trends based on the splitting schemes was demonstrated in this paper. Together with the physical experiment and a wide range of analytic investigations, the methods of mathematical modelling are being used on an ever increasing scale in scientific and practical applications for solving complex problems of nonlinear mechanics.

References

1.1. O. M. Belotserkovskii, in: *Numerical Methods in Fluid Dynamics* (H. J. Wirz and J. J. Smolderen, Eds.), McGraw-Hill, New York, 1978.
1.2. O. M. Belotserkovskii, *Numerical Simulation in Continuum Mechanics*, Nauka, Moscow, 1984 (in Russian).
1.3. O. M. Belotserkovskii and Yu. M. Davydov, *Zh. Vychisl. Mat. i Mat. Phys.*, **11**, 1: 182-207 (1971).
1.4. Yu. M. Davydov, *Dokl. Akad. Nauk SSSR*, **247**, 6: 1346-50 (1979).
1.5. O. M. Belotserkovskii and Yu. M. Davydov, *Coarse Particle Method in Gas Dynamics. Computational Experiment*, Nauka, Moscow, 1982 (in Russian).
1.6. O. M. Belotserkovskii and L. I. Severinov, *Zh. Vychisl. Matem. i Mat. Phys.*, **13**, 2: 385-97 (1973).
1.7. A. V. Babakov and L. I. Severinov, *Zh. Vychisl. Matem. i Mat. Phys.*, **16**, 1; 140-51 (1976).
1.8. A. V. Babakov, O. M. Belotserkovskii and L. I. Severinov, *Izv. Akad. Nauk SSSR, Ser. Mekh. Zhidk. i Gaza*, 33: 112-24 (1975).
1.9. A. V. Babakov, V. A. Gushchin, Yu. M. Davydov and A. I. Tolstykh, in: *Proc. of the* V *All-Union Congr. on Theor. and Appl. Mech., Abstracts*, Nauka, Alma-Ata, 1981 (in Russian).
1.10. O. M. Belotserkovskii, in: *Mechanics of Turbulent Flows*, V. V. Struminskii, Ed., Nauka, Moscow, 1980 (in Russian).
1.11. V. A. Gushchin and V. V. Shchennikov, *Zh. Vychisl. Matem. i Mat. Phys.*, **14**, 2: 512-20 (1974).
1.12. O. M. Belotserkovskii, V. A. Gushchin and V. V. Shchennikov, *Zh. Vychisl. Matem. i. Mat. Phys.*, **15**, 1: 197-207 (1975).
1.13. V. A. Gushchin, *Zh. Vychisl. Matem. i Mat. Phys.*, **16**, 2: 529-34 (1976).
1.14. S. O. Belotserkovskii and V. A. Gushchin, *Simulation of Some Viscous Flows*, Vychisl. Tsentr Akad. Nauk SSSR, Moscow, 1982 (in Russian).
1.15. M. N. Kogan, *Dynamics of Rarefied Gas*, Nauka, Moscow, 1967 (in Russian).
1.16. G. A. Bird, *Phys. Fluids*, **13**, 11: 2677-81 (1970).
1.17. G. A. Bird, *Molecular Gas Dynamics*, Clarendon Press, Oxford, 1976.
1.18. M. Kac, *Probability and Related Topics in Physical Sciences*, Interscience Publishers, London-New York, 1959.
1.19. V. E. Yanitskii, *Zh. Vychisl. Matem. i Mat. Phys.*, **13**, 2: 505-10 (1973).
1.20. V. E. Yanitskii, *Zh. Vychisl. Matem. i Mat. Phys.*, **14**, 1: 259-62 (1974).
1.21. O. M. Belotserkovskii and V. E. Yanitskii, *Zh. Vychisl. Matem. i Mat. Phys.*, **15**, 5: 1195-1208 (1975) (part I); **15**, 6: 1553-67 (1975) (Part II).

1.22. O. M. Belotserkovskii, A. I. Erofeev, and V. E. Yanitskii, *Zh. Vychisl. Matem. i Mat. Phys.*, 20, 5: 1174-1204 (1980).
1.23. O. M. Belotserkovskii, A. I. Erofeev, and V. E. Yanitskii, in: *Theor. and Appl. Mech., Proc. of the IV Nat. Congr. on Theor. and Appl. Mech., Varna, 1981*, Bolg. Acad. Sciences, Sofia, 1982.*
1.24. O. M. Belotserkovskii, A. I. Erofeev, and V. E. Yanitskii, in: *XIII Int. Symp. on Rarefied Gas Dynamics, Novosibirsk, 1982*; Abstracts, Novosibirsk Inst. of Thermophysics, p. 152-3, 1982.
1.25. Yu. M. Davydov, in: *Direct Numerical Simulation of Gas Flows*, Vychisl. Tsentr Akad. Nauk SSSR, 1978 (in Russian).
1.26. A. A. Dorodnitsyn, *A Review of Methods for Solving the Navier-Stokes Equations, Lect. Notes in Phys.*, Springer-Verlag, 18, 1: 23-47 (1973).
1.27. O. M. Belotserkovskii and M. I. Nisht, *Separated and Unseparated Flow of an Ideal Liquid Past Thin Wings*, Nauka, Moscow, 1978 (in Russian).
1.28. A. Brissaud, V. Frisch, I. Leorat, *et al.*, *Ann. géophys.*, 29, 4: 539-46 (1973).
1.29. O. A. Ladyzhenskaya, *Mathematical Problems of the Dynamics of a Viscous Incompressible Fluid*, Nauka, Moscow, 1970 (in Russian).
1.30. V. M. Lyakhter, in: *Turbulent Flows*, Nauka, Moscow, 1974 (in Russian).
1.31. A. Townsend, *The Structure of Turbulent Shear Flow*, Cambridge Univ. Press, 1956.
1.32. B. J. Cantwell, *Ann. Rev. Fluid Mech.*, 13: 457-515 (1981).
1.33. J. O. Hinze, *Turbulence*, McGraw-Hill, New York, 1959.
1.34. M. Van Dyke, *Album of Fluid Motion*, Parabolic Press, Stanford, California (USA), 1982.
1.35. *Structure and Mechanisms of Turbulence, Parts I and II, Lect. Notes in Phys.*, 75: 295 (1978); 75: 406 (1978).
1.36. M. A. Goldshtik, Ed., *Structural Turbulence*, collected works, Izd. Severn. Otd. Akad. Nauk SSSR, Novosibirsk, 1982 (in Russian).
1.37. V. M. Ievlev, *Turbulent Flow of High-temperature Continuum Media*, Nauka, Moscow, 1975 (in Russian).
1.38. V. V. Struminskii, in: *Turbulent Flows*, Nauka, Moscow, 1977 (in Russian).
1.39. J. W. Deardorff, *J. Fluid Engineering*, Ser. I, 95: 429-38 (1973).
1.40. J. H. Ferziger, *AIAA Journal*, 15, 9: 1261-67 (1977).
1.41. L. D. Landau and E. M. Lifshitz, *Fluid Mechanics*, Ed. I, Pergamon Press, Oxford, 1959.
1.42. A. N. Kolmogorov, *Izv. Akad. Nauk SSSR, Ser. Phys.*, 6, 1-2: 56-8 (1942).
1.43. A. S. Monin and A. M. Yaglom, *Statistical Hydromechanics*, Nauka, Moscow, 1965 (part I), 1967 (part II) (in Russian).
1.44. L. D. Landau, *Doklady Akad. Nauk SSSR*, 44, 8: 339-42 (1944).
1.45. A. A. Amsden and F. H. Harlow, *AIAA Journal*, 3, 11: 2081-6 (1965).
1.46. D. R. Chapman, D. M. Kuehn, and H. K. Larson, *Investigation of Separated Flow in Supersonic and Subsonic Streams with Emphasis on the Effect of Transition*, NASA Report No. 1356, 1956.
1.47. J. F. McCarthy, Jr., and N. Kubota, *AIAA Journal*, 2, 4: 629-36 (1964).
1.48. O. M. Kuznetsov and S. G. Popov, *Izv. Akad. Nauk SSSR, Ser. Mekh. Zhidk. i Gaza*, 2: 112-13 (1967).
1.49. D. V. Bazhenov and L. A. Bazhenova, in: *Proc. II All-Union Symp. on Phys. of Acoustic-hydrodynamic Phenom. in Opto-acoustics*, Nauka, Moscow, 1982.

---

* See also: *Advances in Mechanics*, Warszawa, 5, 3-4: 11-40 (1982).

1.50. D. V. Bazhenov, L. A. Bazhenova, and A. V. Rimskii-Korsakov, in: *Synops. of pap. to V All-Union Cong. on Theor. and Appl, Mech.*, Izd. Nauka, Kazakh SSR, Alma-Ata, 1981.
1.51. A. V. Babakov, O. M. Belotserkovskii, and A. P. Zyuzin, *Doklady Akad. Nauk SSSR*, **279**, 2: 315 (1984).
1.52. O. M. Belotserkovsii, A. P. Byrkin, A. P. Mazurov, and A. I. Tolstykh, *Zh. Vychisl. Matem. i Mat. Phys.*, **22**, 6: 1480-90 (1982).
1.53. A. T. Onufriev, *Prikl. Mekh. i Tekhn. Fiz.*, 2: 66-71 (1970).
1.54. E. Naudasher, *J. Fluid Mech.*, **22**, 4: 625-56 (1965).
1.55. F. V. Dolzhanskii, V. I. Klyatskin, A. M. Obukhov, and M. A. Chusov, *Nonlinear Systems of Hydrodynamic Type*, Nauka, Moscow, 1974 (in Russian).
1.56. S. O. Belotserkovskii and V. A. Gushchin, *Izv. Akad. Nauk SSSR, Ser. Fizika Atmos. i Okeana*, **20**, 9: 810-19 (1984).
1.57. S. O. Belotserkovskii, *Izv. Akad. Nauk SSSR, Ser. Fizika Atmos. i Okeana*, **20**, 10: 915-21 (1984).
1.58. V. I. Arnold, L. D. Meshalkin, and A. N. Seminar, *Usp. Mat. Nauk*, **15**, 1: 247-50 (1960).
1.59. L. D. Meshalkin and Ya. G. Sinai, *Prikl. Mat. i Mekh.*, **25**, 6: 1140-5 (1961).
1.60. V. I. Yudovich, *Prikl. Mat. i Mekh.*, **29**, 3: 453-67 (1965).
1.61. V. I. Yudovich, *Izv. Akad. Nauk SSSR, Ser. Mekh. Zhidk. i Gaza*, **1**: 32-5 (1973).
1.62. V. I. Klyatskin, *Prikl. Mat. i Mekh.*, **36**, 2: 263-71 (1972).
1.63. S. O. Belotserkovskii, A. P. Mirabel, and M. A. Chusov, *Izv. Akad. Nauk SSSR, Ser. Fizika Atmos. i Okeana*, **14**, 1: 11-20 (1978).
1.64. N. F. Bondarenko, M. Z. Gak, and F. V. Dolzhanskii, *Izv. Akad. Nauk SSSR. Ser. Fizika Atmos. i Okeana*, **15**, 10: 1017-26 (1979).
1.65. Yu. M. Davydov and M. S. Panteleev, *Zh. Prikl. Mekhan. i Tekhn. Fiz.*, 1 (125): 117-22 (1981).
1.66. G. Birkhoff, in: *Proc. of the 13th Sympos. in Appl. Math. of the Amer. Math. Soc.*, Providence, Amer. Math. Soc., 1962.
1.67. Yu. M. Davydov, in: *Numerical Methods in Continuum Mechanics*. Sibirsk. Otd. Akad. Nauk SSSR, Novosibirsk, 1978 (in Russian).
1.68. B. J. Daly, *Phys. Fluids*, **10**, 2: 297 (1967).

2 Computations of Supersonic Flow past Lifting Bodies

P. I. Chushkin, *D.Sc. (Phys.-Math.) and*
G. P. Voskresensky, *D.Sc. (Eng.)*

2.1. INTRODUCTION

Numerical simulation is an important tool for investigations and design in aeronautics and space research. The main advantages of numerical simulation over physical experiments in wind tunnels, ballistic installations or during flights are a high degree of accuracy, applicability under diverse conditions, possibility of separate analysis of the basic parameters, rapid realization and relatively low cost. Numerical methods involving the application of computers in aerodynamic research were first used in early fifties. At present, computational aerodynamics is a separate branch of scientific activity.

One of the basic problems in supersonic aerodynamics is the calculation of flow fields, forces, moments and heat fluxes acting on a vehicle and its units. These problems can be solved successfully owing to modern computational methods and the technical efficiency of computers. The most significant advances have been made in solving the inviscid gas flow problem. Complex cases like the three-dimensional flow about aerodynamic configurations simulating aircraft, or the flows involving high-temperature phenomena in gases can be calculated quite successfully. Integration of the Euler equations describing such flows provides useful and often sufficient information for actual designing without any cumbersome computations. Using the solutions obtained in this case, we can take into account the effect of viscosity with the help of the boundary-layer theory. Although numerical methods for solving the Navier-Stokes equations for viscous gas flows are being worked out intensively at present, serious limitations are imposed by the power of the existing computers.

This paper is a review of the development and present-day state-of-the-art of numerical computation of the external three-dimensional steady supersonic flow of an inviscid non-heat-conducting gas past lifting aerodynamic bodies. The formulation of this problem is familiar: it is required to integrate the system of Euler equations in the region between the body surface and the bow shock wave. For simple bodies, it is expedient to consider two computational subdomains, viz. the nose and the subsequent (supersonic) subdomains which are separated by a space-type surface. In the first subdomain the nature of flow (mixed or supersonic conical) depends on the form of the

body nose (bluntness or sharpness; the latter is then approximated by a corresponding cone). In the second subdomain, we encounter a problem with known initial data on a space-type surface and boundary conditions on the body and the bow shock wave. For complex configurations, we can consider a larger number of computational subdomains. For example, separate subdomains should be used for front and lateral edges in the case of a wing with a blunted airfoil, while for a flow with several local subsonic regions we should consider an appropriate number of subdomains.

While choosing a computational algorithm, the specific nature of flow in the given subdomain must be taken into consideration. In order to calculate the steady supersonic flow about bodies accompanied by formation of local subsonic regions, the time-dependent stationing principle is often used, where a steady solution is obtained as the limit of the corresponding unsteady solution as the time tends to infinity. In this case, the complex steady elliptic-hyperbolic problem is transformed into a simpler unsteady hyperbolic problem by introducing time as an additional independent variable. The latter problem can be solved with the help of the time-marching method in which the existence of subsonic regions is not explicitly supposed. For conical flows, as a rule the self-similar stationing principle is used.

Soviet scientists have made a significant contribution to the formulation and numerical solution of the problem of flow past lifting bodies in a supersonic free stream. We shall endeavour to acquaint the readers with the achievements of Soviet specialists in this field. Keeping this in mind, we shall confine ourselves mainly to the results published in this country, beginning with the first publications on the subject. The works of foreign authors will be mentioned only if they are directly connected with the investigations by Soviet scientists.

The main attention in this review will be paid to the numerical solution of applied problems of supersonic aerodynamics, and purely computational aspects will not be discussed. The description will be carried out in accordance with the numerical methods used. We shall successively consider the application of several finite-difference methods, the method of characteristics and the method of integral relations (including the method of straight lines). The method of finite elements will not be considered since there is no information on its application for calculating three-dimensional supersonic flows past bodies with shock waves. The linearization method and other approximate approaches will also be disregarded.

After a brief description of the basic idea and properties of the numerical method in question, we shall discuss its application for calculating various cases of supersonic flow past bodies at an angle of attack. The results of numerical calculations are given for classical

aerodynamic forms (spherical or ellipsoidal bluntness, sharp or blunt cone, delta plate, etc.) as well as more complicated configurations used for modelling separate elements of an aeroplane (fuselage, wing, engine nacelle, etc.) or a vehicle as a whole. Supersonic flows of a perfect gas with a constant adiabatic exponent as well as a gas with equilibrium or nonequilibrium physical and chemical properties are discussed. A large number of plots illustrate the flow pattern and the behaviour of aerodynamic characteristics of bodies under various flight conditions.

It should be noted that this paper contains a lot of new material and thus considerably supplements the earlier reviews [2.1-2.3] published by the authors on numerical solutions of supersonic flow problems.

2.2. FINITE-DIFFERENCE GRID METHODS

2.2.1. Basic Concepts of the Methods

In finite-difference methods, differential equations are approximated by difference equations on a given grid which is not a characteristic net. In view of their universal nature, these methods are widely used for solving problems of supersonic aerodynamics. There are many methods of this type and all of them are being continuously improved in order to meet the conflicting demands of high accuracy and low cost of computations.

Supersonic flow past bodies is calculated with the help of difference schemes which have various structures: explicit or implicit, single-step or multistep, etc. Explicit schemes are simple, but in this case the Courant stability condition determines the integration step size in the marching direction. Implicit schemes do not suffer from this drawback but lead to a more complicated computational algorithm in which direct or iterative methods are used for solving systems of difference equations. Generally speaking, the choice of the best difference scheme is far from obvious. However, while solving the supersonic flow problems, it seems preferable to use implicit schemes since they have a greater economical efficiency. Such problems contain narrow zones in which the gasdynamic functions vary rapidly. For reasons of accuracy, a finer computational difference grid must be used in this case. In explicit schemes, this leads to a sharp decrease in the permissible integration step in the marching direction over the entire computational domain.

Two-step "predictor-corrector" schemes are often used for flow computations. These belong to splitting type of schemes and the splitting can be analytical, geometrical or physical, or a combination of all three. Splitting schemes can be explicit or implicit. Three-dimen-

sional problems of supersonic flow are usually solved with the help of difference schemes having second order of accuracy, although schemes having first order of accuracy are also used. Schemes with third order of accuracy have certain advantages (higher accuracy in the smooth solution domain, smaller spreading of discontinuities), but they are not used in practice for solving these problems because of realization difficulties, particularly in the case of irregular cells.

Two alternative approaches can be used for computation of shock waves. In the first approach, all shock waves in the flow field are treated as strong discontinuity surfaces on which the Rankine-Hugoniot relations are satisfied and which serve as the boundaries of subdomains of the solution. In the second approach, all discontinuities are spread into some narrow zones either by introducing terms containing artificial viscosity into the equations, or due to the presence of an approximation viscosity in the difference scheme. If there are discontinuities, it is desirable to use conservative difference schemes which ensure that the basic conservation laws are obeyed. In problems of supersonic flow, the combined approach is the most suitable, when the bow shock wave is treated as a strong discontinuity, while a "through counting" is carried out in the perturbed flow field.

A significant factor in computations is the choice of the difference grid which must be flexible and take into account the behaviour of the solution. It is convenient to introduce special variables in which the computational domain is straightened out, i.e. the body surface and the bow shock wave surface coincide with the corresponding grid surfaces. It was mentioned above that for a flow with a complicated structure, a reliable and detailed description of its properties can be obtained with the help of nonuniform grids or hybrid grids which are constructed in different subdomains of the solution by using different coordinate systems, including nonorthogonal ones. It is desirable to use movable three-dimensional grids for finding solutions with the help of the time-dependent stationing principle.

2.2.2. Explicit First-order Method

This method was first proposed by Godunov for unsteady one-dimensional flows. It was then developed by Godunov, Zabrodin and Prokopov [2.4] for investigating two-dimensional supersonic unsteady flows past bodies. Later, Ivanov and Kraiko [2.5] worked out an analogue of this method for computing steady three-dimensional supersonic flows. A systematic description of the method and its application to various gasdynamic problems were given in the monograph by Godunov *et al.* [2.6]. A brief account of the unsteady three-dimensional version of the method is also contained in this monograph, as well as in the article by Lutsky, Prokopov and Cherkashin [2.7].

This method is based on an explicit monotonic difference scheme which ensures the first order of accuracy on smooth solutions and a uniform grid. In the steady three-dimensional case, the gasdynamic equations in integral form are written in a discrete form, and the difference solution is advanced through successive reference planes along the body. The quantities on the right-hand sides of the difference equations are taken either from the preceding reference plane or from the reference plane being computed. Since the scheme is no longer explicit in the latter case, we have to resort to iteration procedure. The computational algorithm of this method includes a preliminary stage with a very interesting construction. Some auxiliary quantities are determined from the solution of the self-similar problem on the interaction of two uniform semi-infinite supersonic flows. These flows have parameters corresponding to two adjacent elementary cells on the preceding reference plane and meet on the boundary between these two cells. This interaction may be accompanied by the generation of shock waves, rarefaction waves or tangential discontinuities. Separate branches of the algorithm are used for calculating each type of interaction.

This method allows a "through counting" of discontinuity surfaces which are treated more physically in this method than in methods with artificial viscosity. If required, the discontinuities can be treated exactly. This is done during the calculations of the interaction of two flows without any additional computational procedure.

A great deal of computational experience has proved the efficiency and universality of this method in numerical investigations of multidimensional flows with complicated structures and various types of inner discontinuities. The method is well adapted to the features of the flows being computed and allows a simple application of irregular mobile grids associated with the subdomain boundaries. However, the first order of accuracy and the restriction on the integration step in the marching direction imposed by the stability condition considerably decrease the efficiency of this method. Besides, the algorithm of the method is quite complicated and cannot be extended easily to nonequilibrium flows.

The method described above found a wide application for computing supersonic flow past lifting bodies of classical aerodynamic forms as well as configurations modelling whole aircraft or spacecraft. We shall first discuss papers in which the bow shock wave was explicitly treated and the inner discontinuities were spread. All the results refer to a perfect gas with ratio of specific heats $\varkappa = 1.4$.

Ivanov and Kraiko [2.8] carried out computations for many supersonic non-axisymmetric conical flows, including cases of circular, elliptical and quasi-pyramidal cones, delta and V-shaped wings of zero thickness, as well as a combination of a circular semicone and a delta plate. The three-dimensional pattern of flow past a sharp nose

of a schematic model of vehicle was investigated by Ivanov and Nikitina [2.9].

Rozin [2.10] studied the aerodynamic properties of an axisymmetric body with a tail in a supersonic flight, with Mach number $M_\infty = 3$ and at different angles of attack α. He investigated the cross-shaped and X-shaped positions of the tail. Shock waves propagating from the tail panels interacted in the second case without reaching the bow shock wave, and did not interact in the first case. The shape of the body, the plots of the normal force coefficient C_n and the pitch moment coefficient C_m for the entire body (referred to the area of two tail panels) are shown in Fig. 2.1 as functions of the angle of attack α. The numerical results are compared with the experimental data (shown by triangles). Curves 1-3 correspond to values of C_m for any isolated tail panel inclined to the symmetry plane at angles 90°, 135° and 45° respectively.

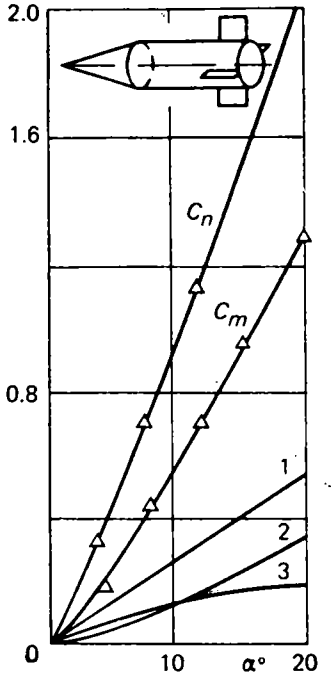

Fig. 2.1. Aerodynamic coefficients for a body with a tail, $M_\infty = 3$.

Flow calculations for $M_\infty = 2.56$ of a schematic model of a hypersonic aeroplane, consisting of an axisymmetric fuselage and a delta wing of zero thickness were carried out by Aukin and Tagirov [2.11]. The model and the shock wave in top and cross-sectional ($x = 0.8$) views are shown in the left-hand part of Fig. 2.2. The right-hand part shows the calculated aerodynamic characteristics of the model (curves *1*), which are compared with the experimental results (circles *3*) obtained in [2.12]. A good agreement between calculated (curves *5*) and experimental data for the total drag coefficient C_D is obtained if the friction is approximately taken into account. For the induced drag coefficient, the theoretical curve *2* is in good agreement with the experimental points *4*.

Aukin and Tagirov [2.13] have also made calculations for the three-dimensional complex flow past a more complete model of an aeroplane with a non-axisymmetric fuselage, two engine nacelles, swept wings and four tail surfaces. The wings and tail surfaces had zero thickness, and the engines were supposed to have no ducts. The

computational domain was divided into a number of subdomains, and an appropriate grid was constructed in each of them. The model of the aeroplane is shown in Fig. 2.3, where the distribution of the pressure coefficient C_p along the windward side (upper curves) and leeward side (lower curves) of the fuselage are plotted. Curves *1*, *2* and *3* correspond to angles of attack $\alpha = 10°$, $5°$ and $0°$ respectively, $M_\infty = 2.3$. It was assumed that a cylindrical jet of elliptic cross section is ejected through the nozzle exit at the end of the fuselage ($x = 1$).

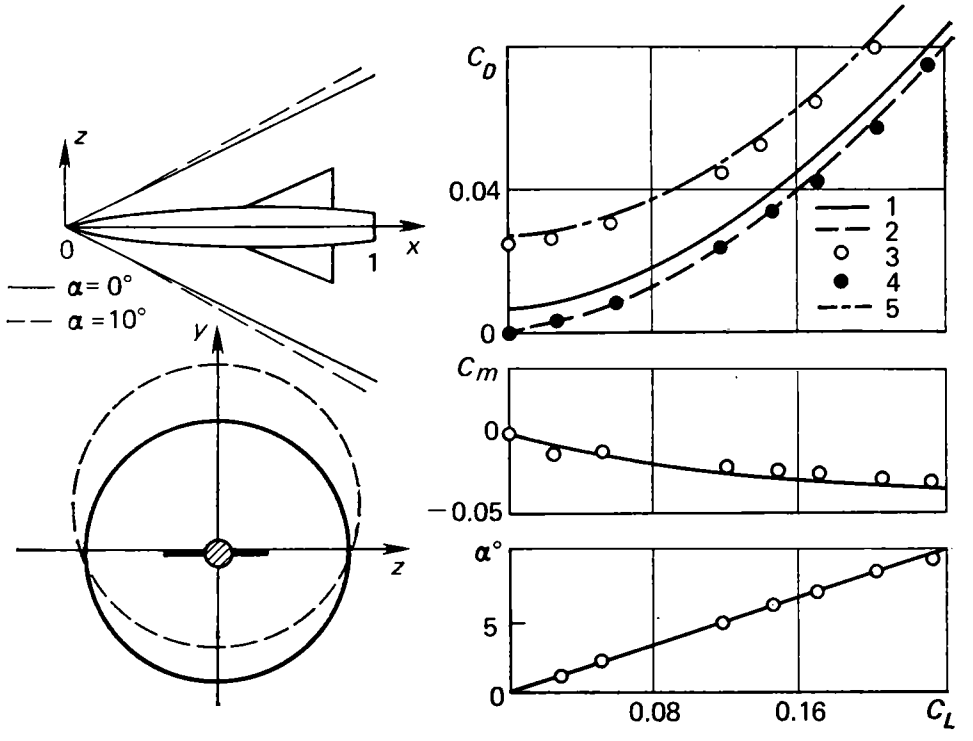

Fig. 2.2. Flow past the model of a hypersonic aeroplane, $M_\infty = 2.56$. Aerodynamic coefficients.

Calculation of the mixed three-dimensional flow in front of a bluntness requires the application of the nonstationary three-dimensional version of the method together with the time-dependent stationing principle (see [2.7]). Figure 2.4 shows the results of calculations carried out by Gusev and Lutsky for the flow past the nose part of an aeroplane for $M_\infty = 3.5$ and $\alpha = 5°$. Isomachs are depicted in the region between the bow shock wave and the body in the symmetry plane. Sonic lines are marked by points. The crowding of isomachs in front of the cockpit ledge characterizes the smeared inner shock wave. It can be seen that this shock wave interacts with the bow shock wave and is followed by a subsonic region.

The two-dimensional nonstationary version of the method described here was somewhat modified by Kolgan [2.14] who proposed that the gasdynamic function inside a cell should be represented by piecewise linear, and not piecewise constant, approximations in geometric variables. Such an approach helps increase the order of accuracy of a scheme in these variables, although the scheme itself has

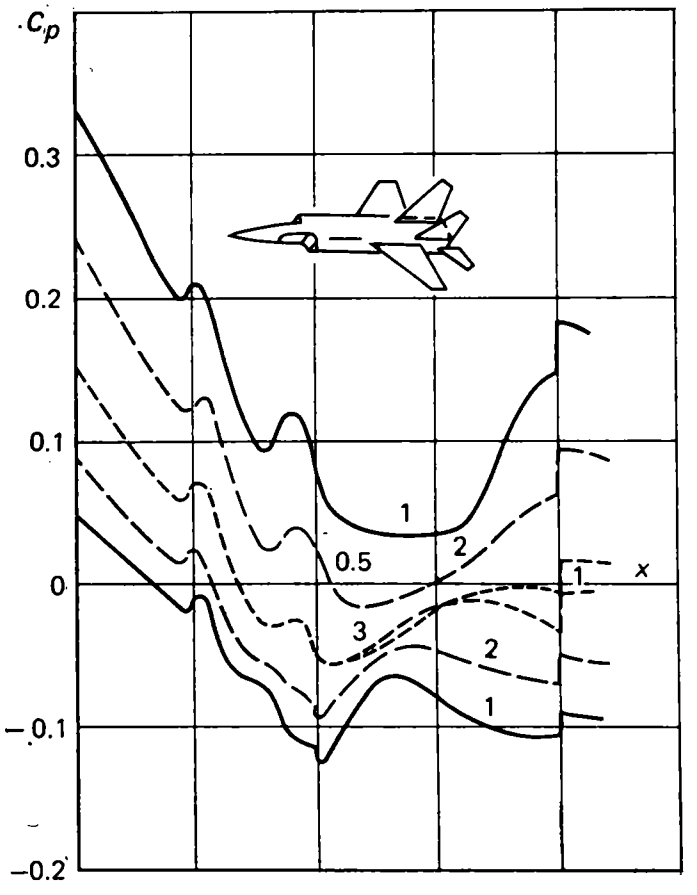

Fig. 2.3. Distribution of pressure coefficient for an aeroplane at various angles of attack, $M_\infty = 2.3$.

still the first order in terms of the marching variable (time). By way of an illustration, the supersonic flow past a cylinder with a hemispherical bluntness at an angle of attack has been computed in [2.14]. Naturally, the next step was to apply this method to the steady three-dimensional case, which was indeed done by Kosykh and Minailos [2.15]. Such a numerical approach was followed for solving a number of problems on the three-dimensional supersonic flow of a perfect gas, as well as for some cases involving a real gas. "Through counting" was carried out in this case, and even the bow shock wave was spread.

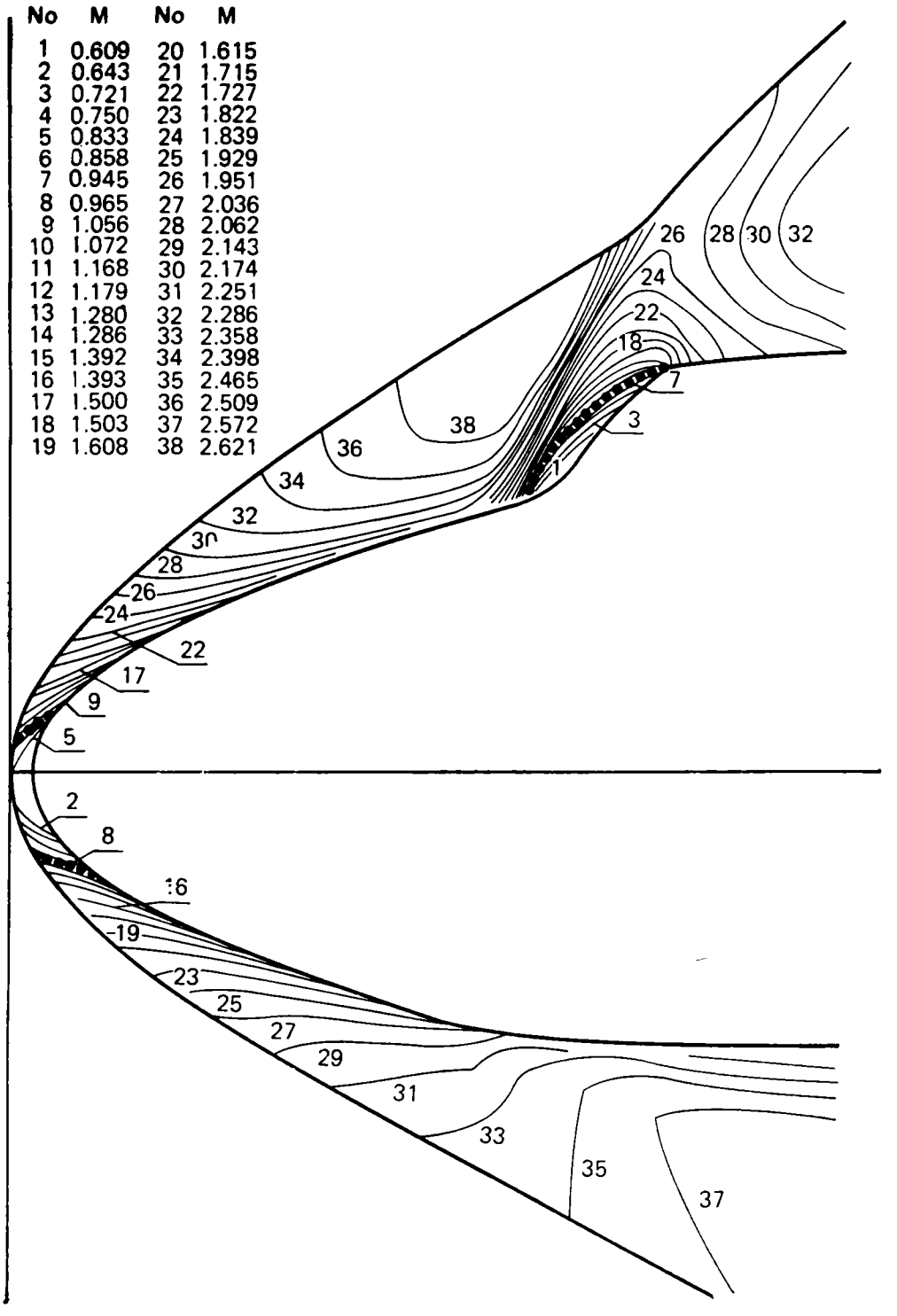

Fig. 2.4. Flow past the nose part of an aeroplane, $M_\infty = 3.5$, $\alpha = 5°$. Isomach field.

Kosykh and Minailos [2.15] computed the flow at an angle of attack past different types of wings, including plane and nonplane delta wings of rectangular and trapezoidal plane forms, and double swept wings. The same authors [2.16] considered the flow past a delta-shaped vehicle with the bow shock wave attached to the apex. Under the same flow regimes, Kosykh [2.17] has investigated the flow past a wing having a curvilinear (hyperbolic) leading edge and a triangular cross section.

The interference of a delta-shaped wing at small angles of attack (up to 10°) with other aerodynamical elements simulating the rudders, tails, additional wings, etc. was estimated by Minailos on the

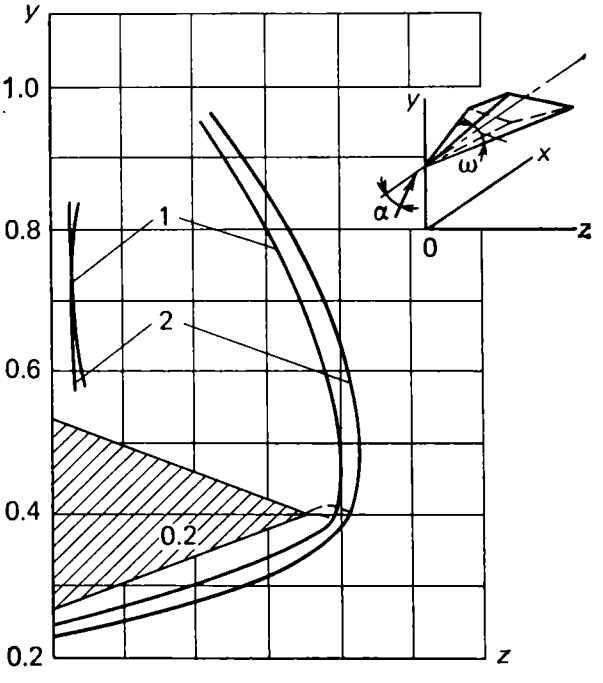

Fig. 2.5. Flow past a delta wing with $\chi = 70°$, $M_\infty = 20$, $\alpha = 30°$, and $H = 5$ km.

basis of his numerical computations [2.18, 2.19]. In one case, the main wing was followed by another wing which could have a different angle of attack. In another case, two small delta-shaped wings were mounted over the main wing in the vicinity of its rear edge symmetrically with respect to the central wing axis.

Golubinsky and Kosykh [2.20] have calculated the supersonic conic flow about a delta-shaped wing with a swept $\chi = 70°$ and a rhombic cross section (angle $\omega = 15°$), flying at an angle of attack $\alpha = 30°$ with Mach number $M_\infty = 20$ at a height $H = 5$ km. At such a hypersonic velocity, equilibrium high-temperature processes in air were taken into consideration. Figure 2.5 shows the cross sections

of a wing, the bow shock wave, the inner shock wave on the leeward side and the sonic surface (dashed line). For the sake of comparison, the corresponding results for the equilibrium reactive air (curves *1*) and a perfect gas (curves *2*) are plotted on the figure.

Zarubin [2.21] considered the supersonic flow at a large angle of attack past an elliptical cone whose semiaxes have the ratio 1:10. He also took into account the real properties of air in the thermodynamic equilibrium model, but calculated flow only for the windward surface of the body, where the effects of a real gas are not pronounced.

2.2.3. Implicit Second-order Method

This method for calculating three-dimensional supersonic flows past smooth bodies was proposed and first applied by Babenko and Voskresensky [2.22]. For over 20 years of wide application, this method was developed and generalized and was found to be quite effective for numerical analysis of flows. In the book by Babenko, Voskresensky, Lyubimov and Rusanov [2.23], the computational algorithm of the method was improved, its stability and convergence were analyzed, and modifications were made to take into account the high-temperature equilibrium processes in a gas.

Later, owing to a transition to time-dependent equations and the determination of the solution on the basis of the time-dependent stationing principle, this method was extended to the case of supersonic flows with local subsonic regions. At first Babenko and Rusanov [2.24] suggested appropriate modifications for plane and axisymmetric flows. Later, the method was generalized to the case of three-dimensional supersonic flow past a bluntness by Rusanov [2.25] and by Babenko et al. [2.26]. Finally, Ivanova and Radvogin [2.27] worked out and included in the method an algorithm for calculating nonequilibrium physical and chemical processes at high gas temperatures.

We proceed in this method from a cylindrical or other system of coordinates. The region between the bow shock wave (considered as a sharp discontinuity) and the surface of the body is then straightened out by coordinate transformation. The solution is advanced through successive reference planes along the axis of the body. Since the difference scheme is implicit in the marching direction, the computational algorithm includes an iterative process consisting of several cycles embedded into one another. In the stationary version of the method, there are two such cycles corresponding to a ray and a reference plane. In the nonstationary version of the method, another time cycle is added to these cycles. The local boundary value problem is solved on each ray for five difference equations with one condition on the body and four conditions on the shock wave. These equations

are solved by a special elimination method called the sweep method and known in Russian literature as the "progonka" method.

In order to ensure the correctness of the boundary value problem on a ray for a wide class of flows, several authors have depeloped appropriate modifications of the initial algorithm. Dyakonov (see [2.28]) proposed that in the sweep method the marching direction on different parts of the ray should be chosen in accordance with the orientation of the stream line with respect to the side of the cell. In the modification proposed by Mikhailov [2.29] the differential equations along the stream line are approximated according to a special implicit difference scheme. The sweep version with a varying number of sweep relations was worked out by Radvogin [2.30].

A characteristic feature of this method is that it has the second order of accuracy. The use of an implicit difference scheme in the marching direction enables us to avoid the hard constraints on the corresponding integration step required by the stability conditions. Owing to these two circumstances for the calculation of supersonic flow of a gas with a smooth structure this method is several times more efficient than the explicit method discussed above. Strictly speaking, the second order of accuracy is not preserved in this method, since the difference scheme for ensuring stability now contains additional terms with second differences. The presence of these terms which create an artificial dissipation makes it possible to calculate the internal shock waves, as was done by Lyubimov and Rusanov [2.62] for supersonic flow past blunted bodies. On account of its nonmonotonic and nonconservative nature this method can be used for flows with internal shock waves of low intensities only. The representation of equations in a conservative form widens the potentialities of the method in this respect. This approach was adopted by Weiland [2.31] who obtained a satisfactory pattern of embedded shock waves by computing the supersonic flow past a long blunt-nosed cylinder at an angle of attack.

We shall describe various applications of this method, and shall successively give results for three-dimensional problems involving supersonic flow past sharp-nosed bodies, for purely supersonic flow region behind the bluntness and, finally, for complete subsonic-supersonic flow past lifting bodies with detached bow shock wave. We shall consider cases relating to aerodynamic elements of simple type, as well as to the concrete forms of fuselages and wings. Most of the results given here have been obtained for the perfect air, and appropriate remarks will be made while discussing examples of real high-temperature gas flows.

The first significant application of the method in the sense of the amount of computations and of practical importance of the numerical solutions obtained, was the compilation of tables for supersonic flow past a circular cone at an angle of attack. These tables were first

published in the above-mentioned book by Babenko et al. [2.23] and contain detailed information on the conical flow field for different cases covering a wide range of cone semi-angle ω (from 10° to 45°), Mach number M_∞ (from 2 to 7) and angle of attack (from 0° to 20°). In all cases, the value of ω was greater than α. The computed solution was found to be quite accurate from the practical point of view.

Gonidou [2.32] has presented examples of supersonic non-axisymmetric flows past circular and thick elliptical cones. Serious computational difficulties are encountered in the case of a strongly oblate elliptical cone, which is similar in form to a delta wing. Large gradients of gasdynamic functions appear on the lateral sides of the body. Numerical investigations of the flow past such a cone with the ellipse semi-axes ratio 1:8 were carried out by Voskresensky, Tatarenchik and Shepetievsky [2.33], who obtained the solution by using the self-similar stationing principle. They demonstrated the formation of a local overexpansion zone of flow on the leeward side due to a strong transverse flow of gas. Vetlutsky and Ganimedov [2.34] also considered an elliptical cone with the semiaxes ratio 1:5. They found the solution by using time-dependent stationing principle but were unable to obtain the complete flow pattern on the leeward side at large angles of attack in view of the violation of hyperbolicity condition which must be satisfied for the functioning of the algorithm. Calculations for thicker bodies were successfully carried out by these authors both for perfect air and equilibrium air.

The sharpened nonconical bodies about which the supersonic flow with a shock wave attached to the tip takes place were investigated by several scientists. A body having the shape of a delta plane was considered in [2.33]. Voskresensky [2.35] and later Voskresensky, Ivanov and Stebunov [2.36] calculated the flow about the non-axisymmetric nose parts of fuselages of supersonic aeroplanes. Figure 2.6 illustrates an example of such calculations, corresponding to Mach number $M_\infty = 2.5$, angle of attack $\alpha = 6°$, and angle of slip $\beta = 5°$. The figure shows a fuselage-shaped body with root part of wings. For one cross section (marked by a solid line), the field of isobars is plotted in the perturbed flow region bounded by the bow shock wave. The isobars 1-6 correspond to the values $p/p_\infty = 0.75$, 0.85, 0.96, 1.06, 1.17 and 1.27 respectively.

Voskresensky et al. have carried out several numerical investigations of supersonic flow past flat and profiled delta wings at an angle of attack in the regime when the bow shock wave is attached to sharp leading edges. Later, this method was extended to calculate the compression flow on the windward side [2.37] and the expansion flow on the leeward side [2.38] by treating these problems separately in view of the fact that these flows do not affect each other in the case of a supersonic edge. Tables of supersonic flow past flat delta wings,

containing the distribution of gasdynamic functions and the values of aerodynamic coefficients have been published by Voskresensky, Ilyina and Tatarenchik [2.39]. These tables cover the cases with angles of sweep $\chi = 45°$-$75°$ for $M_\infty = 1.7$-10 and $\alpha \leqslant 15°$. Subsequently, the same authors [2.40] considered delta, swept and rhombic wings having parabolic profiles. In particular, they showed the importance of taking into account the wing profiling which has a profound influence on the aerodynamic load distribution over the wing.

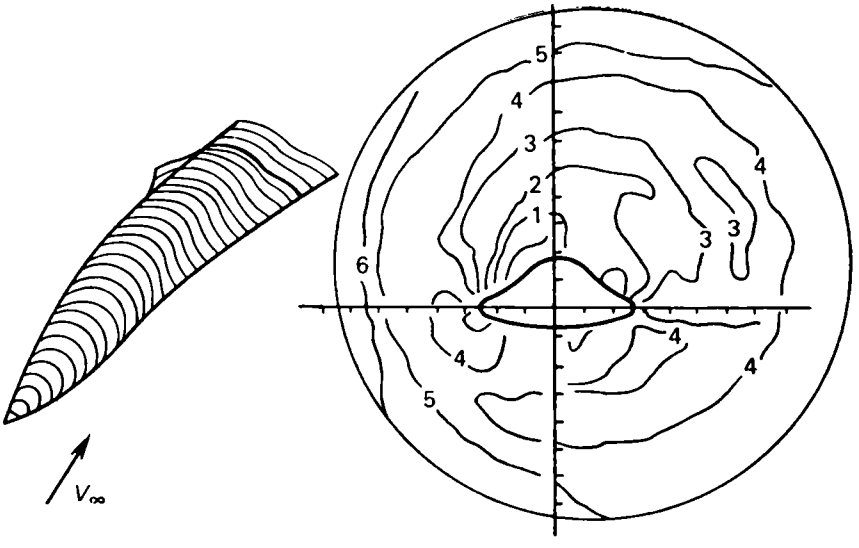

Fig. 2.6. Flow past the fuselage of an aeroplane, $M_\infty = 2.5$, $\alpha = 6°$, $\beta = 5°$. Isobar field for a marked cross section.

Voskresensky, Ivanov and Stebunov have calculated the supersonic flow past delta wings having a blunted airfoil for the case when the bow shock wave is attached to the pointed apex of the wing but is detached from the blunted leading edge. Figure 2.7 shows the results obtained by them for a delta wing with an angle of sweep $\chi = 69.5°$, having an elliptical cross section and a biconvex central airfoil with a relative thickness 3.8%. The pressure profiles for different cross sections on the upper (solid line) and lower (dashed line) parts of the wing are shown for $M_\infty = 1.5$ and $\alpha = 3°$. Besides, the figure also shows the shock wave whose form is found to be close to a circular cone.

A number of papers were devoted to the computation of purely three-dimensional supersonic flow in the region which lies downstream behind the sharpened or blunted nose part of the body. The initial data required for the computation are taken from the solutions of the corresponding gasdynamic problems. Dyakonov *et al.* [2.41-2.43, 2.187] have studied the flow past spherically blunted direct and in-

verse cones. Results of calculations of supersonic three-dimensional flow region on smooth blunted bodies were presented by Rusanov [2.188]. Antonets and Marinin [2.44] have computed the flow past the lateral surface of an inverse cone having a spherical segment as its nose in the range $\alpha = 0°$-$40°$ of the angle of attack. A comparison

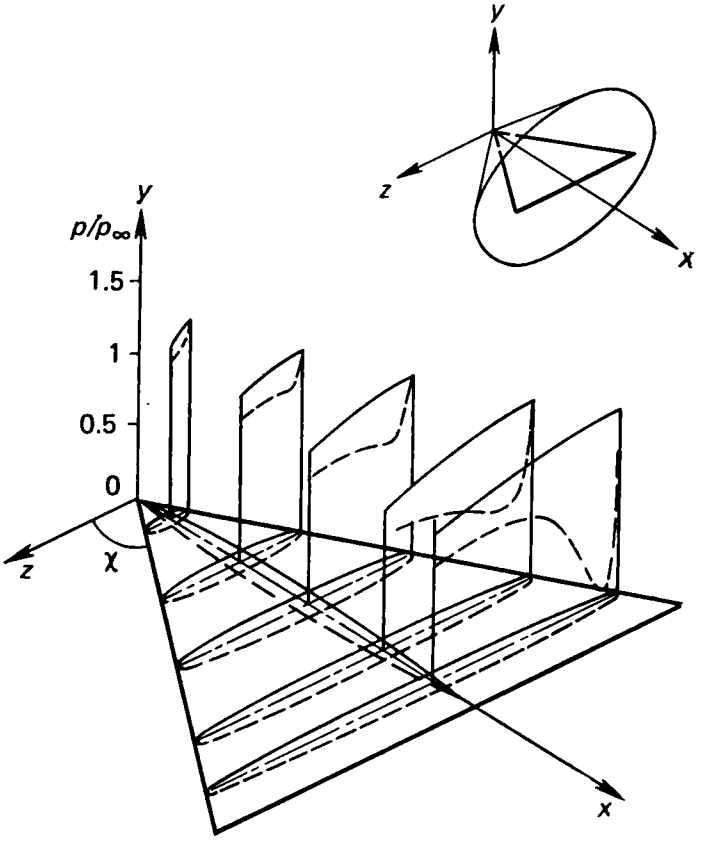

Fig. 2.7. Pressure profiles on the upper (solid lines) and lower (dashed lines) surfaces of a delta wing with $\chi = 69.5°$, $M_\infty = 1.5$, $\alpha = 3°$.

of the theoretical and experimental pressure profiles revealed a considerable discrepancy between them. Vishnevetsky and Ivanov [2.45] have investigated the three-dimensional supersonic flow past a small-angle cone with an asymmetric nose. The nose was in the form of a sharp or blunted large-angle cone and had an oblique rounded conjugation with the main cone. The number of computation points had to be increased in order to suppress the oscillations of the solution in the region of conjugation. The numerical results were compared with the experimentally measured values.

Mikhailov, Nersesov and Chelysheva [2.46-2.48] analyzed delta-shaped bodies with a spherical bluntness and a combined bielliptic cross section whose smooth contour was formed by two different semi-ellipses. This family of bodies includes, in particular, a circu-

lar cone and a delta wing with elliptical cross section. The authors determined the aerodynamic characteristics for the bodies of this family at different angles of attack and different slip angles. Bazzhin and Mikhailov [2.49] have reported several examples of such calculations including the case of flow past a very thin wing, which is quite difficult from computational point of view.

The method described above was also used for numerical simulation of the three-dimensional supersonic flow past bodies, taking into consideration high-temperature effects of a real gas. In their book [2.23] Babenko *et al.* describe the results for a cylinder with a nose cone which is located in a hypersonic flow of equilibrium air at an angle of attack. Dyakonov [2.50] has analysed the flow of air in the same thermodynamic state, past blunted cones. An equilibrium and frozen air flow past a lifting body in the form of a blunted cylinder with two conical flared tails ("skirts") arranged one behind the other was studied by Antonets [2.51]. Here the shock wave arisen at the bending of the generatrix was treated as a strong discontinuity.

Computations of three-dimensional mixed subsonic-supersonic flow past blunted bodies with the help of the nonstationary three-dimensional version of this method are quite complicated and cumbersome, especially for flows with a complex structure. Lipnitsky, Mikhailov and Savinov [2.52] proposed a simplified approach which has certain advantages. In this approach, the gasdynamic functions are represented by trigonometric approximations in the meridional angle. As a result, the solution is reduced to the computation of the flow over a number of interconnected meridional interpolation planes. Thus, we have to actually deal with the two-dimensional nonstationary version of the computational algorithm.

This approach was applied in several cases where the flow does not have a symmetry plane and is essentially three-dimensional. Lipnitsky *et al.* [2.52] have calculated the mixed subsonic-supersonic flow past the nose part of a triaxial ellipsoid at an angle of attack and a slip angle. Burdelnyi *et al.* [2.53] investigated such a flow both numerically and experimentally. One of the results is shown in Fig. 2.8 where the pressure distribution has been plotted over the surface of a triaxial ellipsoid with the semi-axes ratio of 3:1:2. The stream had Mach number $M_\infty = 3$, angle of attack $\alpha = 15°$ and roll angle $\gamma = 45°$. The figure contains curves for different values of x. The x-axis runs from the front point of the ellipsoid along its major axis, the distances x are referred to the minor axis, and $\psi = 0$ corresponds to the leeward plane. Here the experimental points are marked by various symbols. It can be seen that the flow has a complex structure and the experimental results are in good agreement with the theoretical values.

The effect of the essentially three-dimensional nature of the flow was also studied by Antonets and Lipnitsky [2.54] who considered

an elongated elliptical cone with a bluntness in the form of a corresponding ellipsoid, at an angle of attack and a roll angle. The authors presented the numerical values of aerodynamic coefficients for such bodies as functions of the roll angle and compared them with experimental results in some cases. Minostsev and Savinov [2.55]

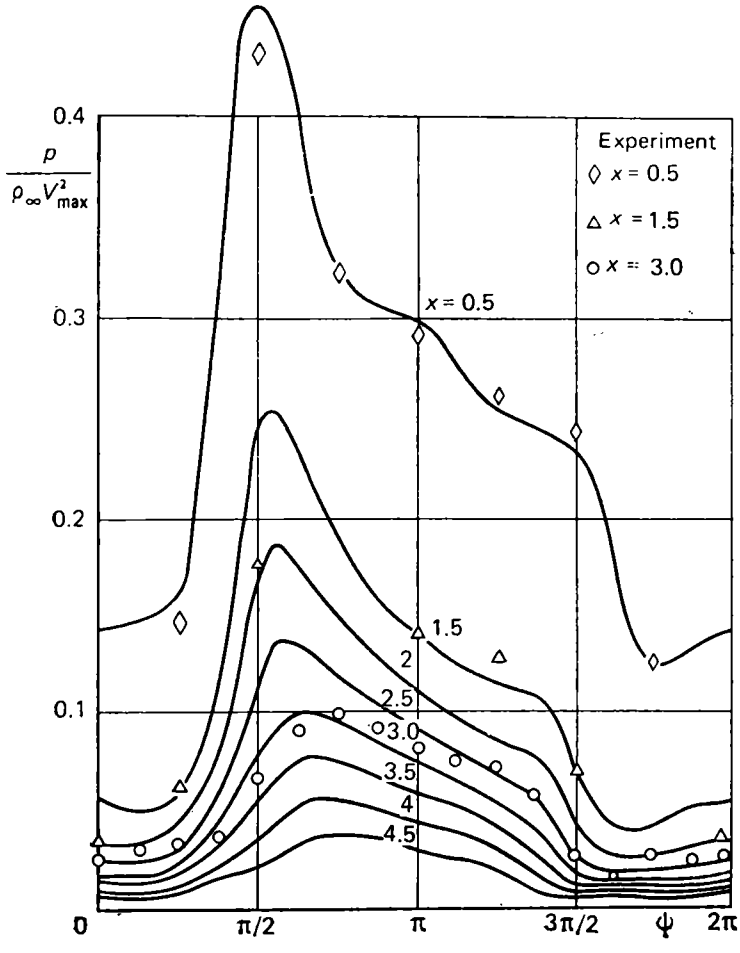

Fig. 2.8. Distribution of pressure over a triaxial ellipsoid, $M_\infty = 3$, $\alpha = 15°$, $\gamma = 45°$.

numerically analyzed the flow past a spherically blunted cylinder at $M_\infty = 6$ at large angles of attack, when elongated subsonic zones are formed on the windward side of the shock layer. They showed that as the angle of attack increases in the interval $40° < \alpha < 49°$, the flow is rearranged and the configuration of subsonic zones changes. At first only one such zone exists near the spherical part of the body. Then the second subsonic zone whose length increases with α appears at the lateral surface of the cylinder and finally these two zones merge into one.

The solution of the problem of the three-dimensional flow past a bluntness at a hypersonic free-stream velocity taking into account nonequilibrium physical and chemical transformations in a gas at high temperatures imposes especially stringent requirements on computer facilities. Therefore, an approximate nonstationary approach [2.52] is quite expedient in this case. Savinov and Shkadova [2.56] used this approach by extending their symmetric algorithm to the three-dimensional case. This algorithm includes an iterative process: on one step, the gasdynamic equations are solved with the help of time-dependent stationary principle and on the other step, the relaxation equations are integrated along the stream lines with the help of Shkadova's two-point implicit scheme [2.57]. However, the relaxation equations are solved only in two meridional planes, viz. windward and leeward, while interpolation of such a solution is carried out for the remaining meridional planes under consideration. Such an approach was earlier followed by Burdelnyi and Minostsev [2.58] for calculating the supersonic region on a blunted body. The nonequilibrium flow of carbon dioxide past the front part of a blunted cone with a large angle and a bluntness in the form of spherical segment at an angle of attack and for different pressures of free streams has been investigated in [2.56].

A more rigorous numerical simulation of flows with subsonic regions in the shock layer is possible with the aid of the complete three-dimensional nonstationary method. One of its versions [2.25] was used by Rusanov and Lubimov (see, for example, [2.59-2.61]) for studying the properties of three-dimensional shock layer for various bluntness. The results of these investigations were compiled by the authors in a monograph [2.62] which also contains a detailed description of the computational algorithm. In this book the results for the three-dimensional flows past the front part of a circular paraboloid and two elliptical paraboloids for M_∞ ranging from 4 to 10 and $\alpha \leqslant 15°$ are given in the form of tables and plots along with the numerical two-dimensional solutions. Using a modification of the method [2.26] Babenko et al. [2.63] have calculated the non-axisymmetric flow past the front parts of several ellipsoids of revolution and published their results in the form of tables for M_∞ ranging between 6 and 20.

Ivanova and Radvogin [2.64, 2.65] have adapted this method for the case of flow at an angle of attack past sharp nose parts with a detached bow shock wave. The modification of the algorithm involved the elimination of the coordinate singularity and the construction of the difference scheme in the case of the cusp of coordinate lines. The authors have made calculations for three large-angle conical tips but only at a small angle of attack ($\alpha = 5°$).

The nonstationary three-dimensional algorithm [2.26] was extended by Ivanova and Radvogin [2.27] to nonequilibrium high-temper-

ature flows past blunted noses. The system of equations of chemical kinetics in the difference form are solved at the nodal points of the difference grid simultaneously with the system of equations of gas dynamics. Figure 2.9 shows calculations for the flow past the nose part of an ellipsoid of revolution with axes $a = b = 1$ m and $c = 2$ m. The flow of nonequilibrium air which was treated as a mixture of six

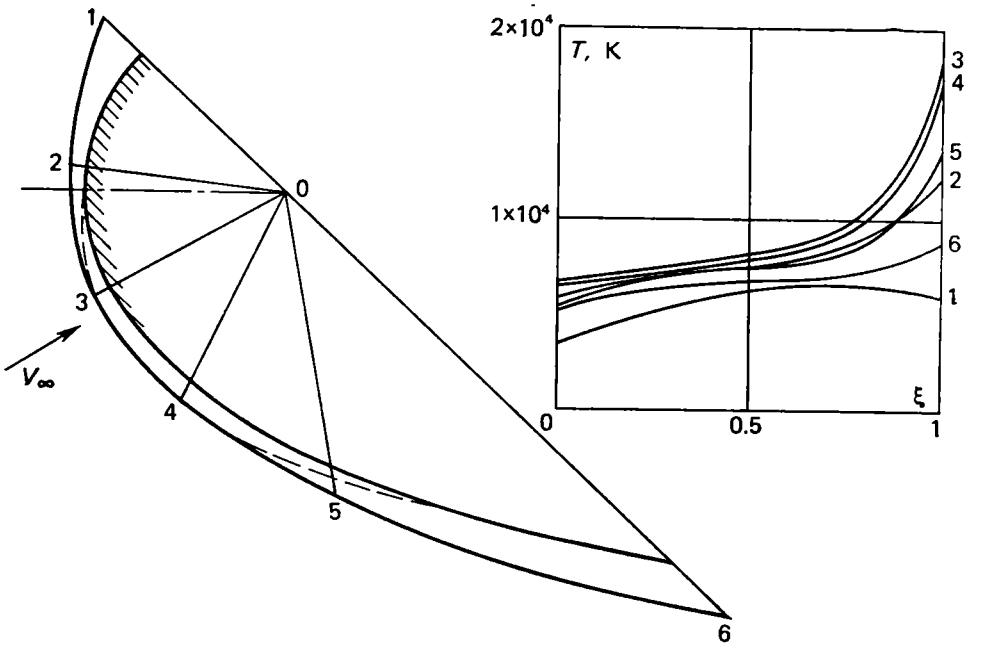

Fig. 2.9. Nonequilibrium air flow past the nose part of an ellipsoid of revolution, $M_\infty = 23$, $\alpha = 34°$, $H = 71$ km. Temperature distribution across the shock layer.

gas components had parameters corresponding to the height of flight $H = 71$ km, Mach number $M_\infty = 23$, and angle of attack $\alpha = 34°$ with respect to the rotational axis of the body (shown by a dash-dot line in the figure). The contours of the body ($\xi = 0$), the shock wave ($\xi = 1$) and the sonic surface (dashed line) on the symmetry plane are drawn in the figure. Besides, the figure also shows the distribution of temperature T across the shock layer along several enumerated rays.

In the works by Voskresensky [2.66], and Voskresensky, Orlova and Stebunov [2.67] this method was modified for the problem of supersonic flows past a lifting wing having an arbitrary plan form and an arbitrary blunted airfoil when the shock wave detaches from the front edge and the apex of the wing. In [2.66] the three-dimensional mixed subsonic-supersonic flow in subdomain I on the front part of the wing (Fig. 2.10) is determined with the help of time-dependent stationing principle. In [2.67] the supersonic flow in subdomain II on the lateral part and subdomain III on the central part of the wing

is obtained as the solution of the gasdynamic system of steady three-dimensional equations. The complete algorithm of the solution of this problem is presented in the work [2.189] by Voskresensky. The coordinate transformation which is carried out for each of the above-mentioned parts of the wing plays an important role in this case and makes it possible to obtain computational subdomains with simple fixed boundaries. A typical example of computations at free-stream parameters $M_\infty = 2$ and $\alpha = 5°$ is presented in Fig.

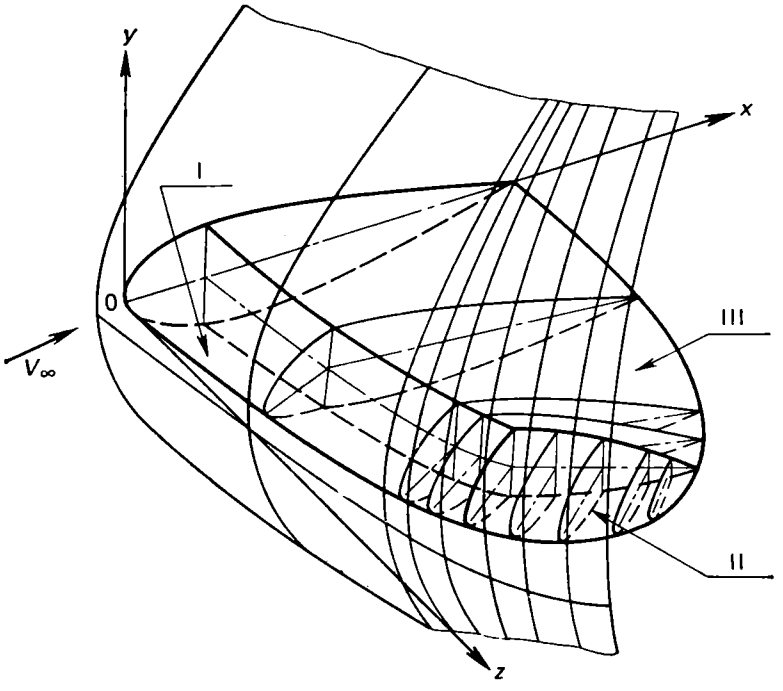

Fig. 2.10. Flow past a wing with blunted profile, $M_\infty = 2$, $\alpha = 5°$.

2.10. The wing under investigation has an elliptical plan form with the aspect ratio $\lambda = 2.56$, and a blunted symmetric airfoil with relative thickness 26%. This figure also shows the bow shock wave surface whose cross sections correspond to the nose parts drawn on airfoils. The computational subdomains are bounded by solid lines.

2.2.4. Splitting Methods and Other Methods

In order to obtain the practically required accuracy in numerical computation of three-dimensional supersonic flows past aerodynamic configurations (especially if they have a complex geometry), high-efficiency computers with a large operating memory must be used. However, estimates show that the solution of three-dimensional aerodynamic problems requires computers with one or two decimal

orders higher speed and storage capacity in comparison with the two-dimensional case.

In this connection, economical and efficient finite-difference schemes applied in the splitting methods are of interest. In these methods, the solution of the initial multidimensional problem is reduced to the solution of a sequence of simpler problems. Splitting also may improve the accuracy, stability and other properties of the difference scheme. Three main types of splitting are distinguished.

1. Analytical splitting, in which different procedures are applied at different stages of the computational algorithm. This type of splitting is used in two-step (predictor-corrector type) and multistep difference schemes.

2. Geometrical splitting, in which the multidimensional difference operators are transformed into a time-dependent sequence of operators of lower dimensions (usually one-dimensional operators). This approach is realized in the method of alternating directions or in the method of fractional steps (Yanenko [2.68]).

3. Physical splitting, in which the difference operators are split according to physical processes and the contribution from each of these processes is calculated separately. This splitting forms the basis of various particle methods.

It is also possible to construct difference methods in which two types of splitting are carried out simultaneously as, for example, splitting in spatial directions and splitting in accordance with physical processes (Kovenya and Yanenko [2.69]).

Among the difference schemes of predictor-corrector type the second-order explicit scheme proposed by MacCormack [2.70] has been widely used, especially outside the USSR, for solving two-dimensional and three-dimensional problems of aerodynamics. For the one-dimensional equation $\partial U/\partial t + \partial V/\partial x = 0$, this scheme is formulated as follows:

$$\overline{U_i^{n+1}} = U_i^n - \frac{\Delta t}{\Delta x}(V_{i+1}^n - V_i^n),$$

$$U_i^{n+1} = \frac{1}{2}\left[U_i^n + \overline{U_i^{n+1}} - \frac{\Delta t}{\Delta x}(\overline{V_i^{n+1}} - \overline{V_{i-1}^{n+1}})\right].$$

Various modifications have been worked out for this scheme; in particular, a monotoniser is introduced in it and geometrical splitting at the fractional time steps is used for the multidimensional problem.

The MacCormack scheme was used by several Soviet scientists for calculating the supersonic flow of a perfect gas past conical bodies. The solution was determined either with the help of time-dependent stationing principle or by stationing with respect to the self-similar variable. Bazzhin and Chelysheva [2.71] investigated the flow past a flat delta wing at small angles of attack when bow shock wave was attached only to the tip. Later, Chelysheva [2.72] treated a combina-

tion of such a wing and a wedge having a small apex angle and attached symmetrically to a flat delta wing with a subsonic leading edge. The flow in the corner at the intersection of the wing and wedge planes is conical and represents the simplest model of flow near the junctions of different elements of an aeroplane or a space vehicle. The author has investigated the interaction between the shock wave from the wedge and the shock wave or the rarefaction wave arisen at the leading edge of the wing in accordance with the sign of the angle of attack ($\alpha = \pm 5°$).

Blokhin [2.73] has calculated the flow past a conical body with a cross section in the form of an equilateral triangle. The computations of the supersonic flow past a lifting configuration consisting of a cone with two flat delta plates having the same apex were carried out by Lobanovsky [2.74] who proposed a shock wave attached to the leading edges of the plates. In a later work [2.75] he considered a flat delta wing with a semi-cone, assuming that the shock wave is attached only to the apex of the wing.

A modified version of the two-step MacCormack scheme was used for calculating the supersonic flow past sharp-nosed lifting bodies. Volkov [2.76, 2.77] considered a configuration consisting of a sharp conical nose, a cylindrical body and a conical flared tail, as well as an elongated fuselage-shaped body with a bielliptic cross section and a straight or slightly curved axis. Vasenov, Volkov and Vorobyov [2.78] have presented numerical and experimental results for a body of revolution with an ogive nose part conjuncted with a long cylinder; the values of angle of attack were up to 20°.

Kotenev, Sakharov and Tirsky [2.79] have published the results of numerical computations for the hypersonic flow past a three-dimensional configuration in the shape of a sharp-nosed body with delta wing. They considered the conditions of flight at the height 65 km and velocity 6.7 km/s, and used the six-component model of air for taking into account the nonequilibrium physical and chemical transformations. The kinetic equations were integrated with the help of the Crank-Nicolson implicit scheme having second order of accuracy [2.80].

The MacCormack scheme, together with the time-dependent stationing principle, was also applied to solve the problem of three-dimensional supersonic flow of a perfect gas past a blunted body. Sakharov and Tirsky [2.81] determined the flow field in the vicinity of a bluntness in the form of an elliptical paraboloid at an angle of attack. For large angles of attack, it is expedient to use nonorthogonal coordinates which are chosen in accordance with the physical flow pattern. This allows us to extend the range of applicability of the algorithm to large values of α because the system of equations in such variables remains hyperbolic in the marching direction. Such an algorithm was developed by Pogorelov and Shevelev [2.82]

and Sakharov, Kotenev and Tirsky [2.83], who computed the flow past the spherically-blunted nose of a body with a bielliptical cross section at an angle of attack $\alpha = 30°$. The stationary version of the method was adopted in the purely supersonic region.

We shall now discuss the numerical investigations in which the two-step predictor-corrector scheme was used for computing the flow past a blunted lifting fuselage having a delta wings with blunted leading edges and flying at supersonic speed. The fuselage bluntness was spherical and therefore only the supersonic flow region was actually calculated with the help of the stationary version of the MacCormack

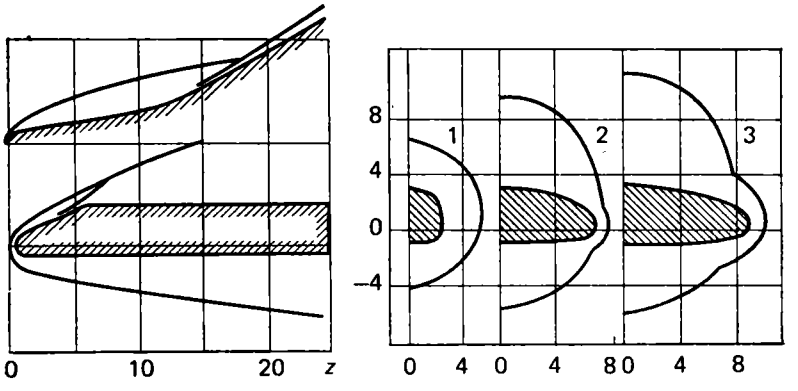

Fig. 2.11. Shock waves taking place in a flow past the nose part of a vehicle, $M_\infty = 6$, $\alpha = 5°$.

scheme using the initial data from the known solution for the flow past a sphere. Similar computations were also carried out in the USA (see, for example, [2.84]).

Figure 2.11 shows the geometry of the body investigated by Sakharov and Shevelev [2.85]. Two projections and three cross sections of the body are shown for $z = 11$, 20 and 24 (all lengths are referred to the bluntness radius). For Mach number $M_\infty = 6$ and an angle of attack $\alpha = 5°$, the bow shock wave and two inner shock waves arising in front of the cabin and the wing edge are drawn in the figure. At distance $z \approx 19$, the latter shock wave starts interacting with the bow shock wave. This problem is fraught with computational difficulties caused in the first place by a strong entropy layer and, secondly, by the appearance of local subsonic zones near the leading edges of the wings. In order to overcome these difficulties, a characteristic algorithm [2.85] was used for calculating the flow on the body surface (this eliminates the first drawback), and a special artificial reduction of the entropy on the body was carried out in the second case [2.84].

Galinsky and Timoshenko [2.86-2.88] have carried out numerical computations for the three-dimensional supersonic flow past the

front part of a similar configuration modelling a vehicle. They assumed a bielliptical cross section of the body but, unlike other authors mentioned above, took different values of horizontal semiaxes of the upper and lower ellipses, i.e. assumed the existence of corner points in the body contour (these corner points were actually smoothed during computations). The plan form of the configuration was determined by varying the lengths of these semiaxes. The results of computations for free stream parameters $M_\infty = 6$ and $\alpha = 0°$ are reproduced in Fig. 2.12, which shows for the cross section $z = 6$ the distribution of the relative pressure $p/\rho_\infty V_\infty^2$ along several rays passing between the body and the bow shock wave. The pressure peaks indicate the secondary shock wave from the wings. Apparently, the oscillations (which are especially noticeable at $\psi = 90°$) are due to the nonmonotonic nature of the difference scheme employed in this case. It should be noted that on the windward side and up to $\psi < 110°$, the bow shock wave and the flow in its vicinity at $\alpha = 0°$ still remain axisymmetric, since they are determined by the spherical bluntness of the body.

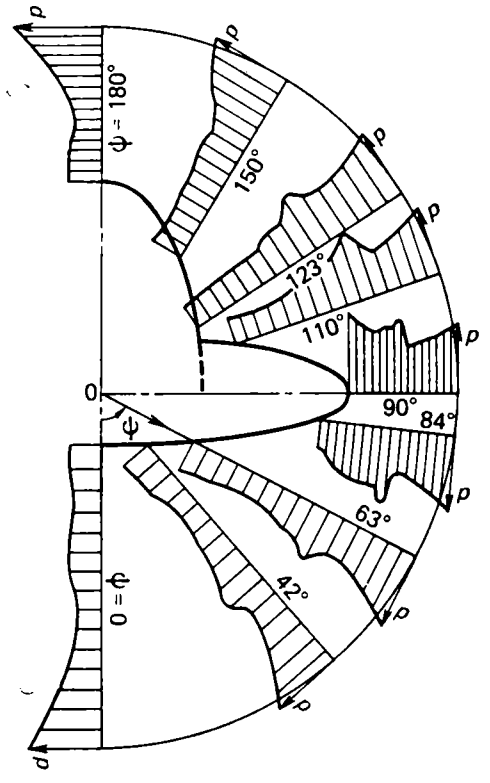

Fig. 2.12. Flow past the nose part of a vehicle, $M_\infty = 6$, $\alpha = 0°$. Pressure distribution over a cross section.

Kovenya, Tarnavsky and Yanenko [2.89-2.91] proposed and developed an implicit difference scheme for numerically solving the time-dependent equations of gas dynamics. This scheme is based on splitting according to physical processes and spatial directions, and was also extended in [2.69] for integrating the Navier-Stokes equations. In the divergent or non-divergent form of the equations, the convective flow matrices, the matrices due to pressure forces (as well as the dissipative force matrices in the viscous case) are treated separately and splitting with respect to spatial variables is carried out. A scheme of splitting into six fraction steps is used for the momentum equations and the energy equation, while splitting into three fraction steps along spatial directions is used for the continuity equation. The difference scheme on fraction steps is realized either by scalar sweep method or by an implicit through-counting scheme. The exam-

ples of computation of supersonic free stream flow past a blunted cone at a large angle of attack, and past a sharp-nosed body of revolution with a detached bow shock wave, as well as triaxial ellipsoid at small angles of attack are given in [2.91].

Various particle methods involve splitting in accordance with physical processes. The coarse particle method developed by Belotserkovskii and Davydov [2.92] is the most thoroughly investigated and widely used method which serves as an effective tool in numerical experiments. These authors have devoted a monograph [2.93] to a detailed description of the method, its development and analysis, as well as various applications.

At each time step, the computational algorithm in the coarse particle method is split into three stages. At the first ("Euler") stage, the work done by the pressure forces is considered only and the fluid is assumed to be at rest. At the second ("Lagrangian") stage, the flows of mass, momentum and energy across the cell boundaries are calculated. The third stage involves the calculation of the final values of gasdynamic functions on the basis of the conservation laws. A fluid cell as a whole serves as a coarse particle in this method. The distinguishing features of the coarse particle method are the use of a conservative difference scheme and the presence of a sufficiently high artificial viscosity which permits a through count without treating the shock waves as strong discontinuities.

The coarse particle method has been adapted successfully for computation of flows with a complicated structure and involving large distortion of streamlines. This method was also widely employed for solving two-dimensional nonstationary problems of aerogasdynamics. A scheme has also been worked out for computing three-dimensional nonstationary flows (Davydov [2.94]). However, the applications of the last scheme to the problem of supersonic flows are limited for the time being. Davydov has calculated the complex flow pattern in the vicinity of a parallelepiped of finite length at zero and nonzero angles of attack. Pyzik and Tarnogrodzky [2.95] have considered a similar body at $\alpha = 0°$ in the supersonic stream inside a duct with a square cross section.

Let us now consider other numerical methods employed in the USSR for calculating the flow past lifting bodies in the case of supersonic flights in perfect air. Using an explicit one-step scheme, which is a modification of the scheme proposed by Lax [2.98], Bazzhin and Pirogova [2.96, 2.97] have numerically integrated the time-dependent three-dimensional system of equations of gas dynamics in spherical coordinates. These investigations were carried out for flows past large-angle cones with spherically blunted apex and toroidally rounded edges at the mid section. Non-axisymmetric bodies which had the radius of curvature of the rounded edges depending on the meridian angle were also considered. Aerodynamic character-

istics have been calculated for such bodies at different angles of attack.

Some authors have calculated supersonic conical flows by using the Rusanov explicit difference scheme [2.99] in which forward differences in time and central differences in space variables are taken. An artificial dissipation of general type is introduced and thus calculations with shock wave smearing become possible. Since the scheme is applied to each equation from the system of gasdynamic equations, there are not only artificial viscosity, but also artificial mass diffusion and artificial thermal conductivity in this approach.

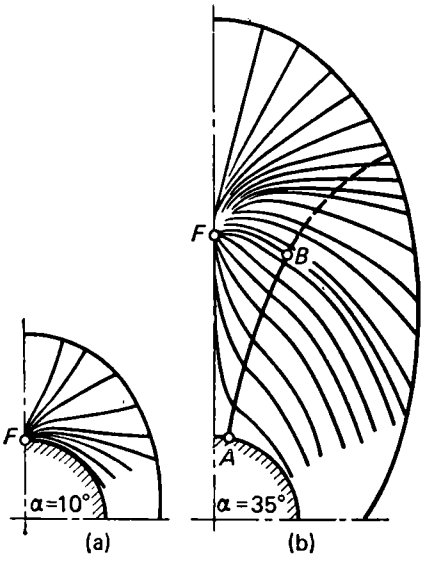

Fig. 2.13. Pattern of transverse stream lines for a circular cone, $M_\infty = 5$, $\alpha = 10°$ and $\alpha = 35°$.

Bachmanova, Lapygin and Lipnitsky [2.100] have used this scheme to study the supersonic flow past circular cones at large angles of attack which are much larger than the cone semiangle and attain values for which the conic flow is violated. The authors obtained the solution with the help of time stationing principle using a fictitious time variable. A local region with supersonic velocity of transverse flows emerges in the shock layer on the leeward side. This region is closed by the inner shock wave. Figure 2.13, which has been borrowed from [2.100], shows the streamlines of the transverse flow on the leeward side of the shock layer for a cone with the semiangle $\omega = 10°$ at $M_\infty = 5$ and two different values of the angle of attack $\alpha = 10°$ and 35°. In the second case, the inner shock wave AB is generated, but does not reach the bow shock wave. The sonic line of transverse flow is shown by the dashed line. It can be seen that the nodal singular point F (the Ferri point) moves with increasing angle of attack from the body surface into the flow field. The authors also revealed several interesting properties of conical flows at large angles of attack. In particular, they found that in certain regimes, the longitudinal velocity on the windward side is directed towards the apex of the cone.

In the works of Lapygin [2.101, 2.102] and Lapygin and Ostapenko [2.103] the Rusanov scheme has been used for calculating the flow past a V-shaped conic wing with supersonic leading edges. The wing geometry as well as the angle of attack were varied. Numerical results demonstrated the possibility of existence of different types of flow

on the leeward side of such a wing. At large angles of attack, the bow shock wave has the Mach triple configuration with the stem (inner shock wave). As the value of α increases, the wave attains a position in which it becomes plane and lies on the leading edges. This is followed by a strong shock wave regime. As the angle of attack is further increased, the shock wave is detached from the edges.

One of the first solutions of the problem of supersonic conical flow on the windward and leeward sides of a flat delta wing was obtained by Babaev [2.104, 2.105], who considered the shock wave attached to the edges of the wing. In the regions adjoining the edge from above and below, the Prandtl-Mayer flow and the flow past the corresponding wedge respectively take place. The central, upper and lower domains of the flow were calculated with the help of difference scheme using iterations. Subsequent computations by other authors revealed that the results obtained by Babaev are not quite accurate.

Finally, we would like to mention the work done in this direction by Shashkin [2.106], who considered a circular cone with three triangular plates, flying with a supersonic velocity at an angle of attack. Calculations in which the bow shock wave was smearing were carried out with the aid of an explicit time-dependent conservative scheme described by Samarsky and Popov [2.107].

2.3. METHOD OF CHARACTERISTICS

2.3.1. Basic Concepts of the Method

Since the system of equations of gas dynamics belongs to hyperbolic type in the case of steady supersonic flows of an inviscid non-heat-conducting gas, its solution can be obtained by using the numerical method of characteristics. It is well known that in a three-dimensional hyperbolic flow domain, a one-parametric family of wave characteristic surfaces passes through each point. The envelope of these surfaces is the characteristic conoid which is formed by the corresponding tangent lines called bicharacteristics and restricts the domain of dependence and the domain of influence of the solution at this point. The stream surfaces also possess characteristic properties.

The initial system of equations in three variables is considerably simplified on the characteristic surfaces. Here it is replaced by an equivalent system of characteristic compatibility relations which explicitly contain derivatives in two directions only. The compatibility relations for non-isentropic three-dimensional supersonic flows were derived and investigated by Rusanov [2.108, 2.109]. The compatibility relations on wave surfaces and stream surfaces are similar for a perfect gas and for a gas in equilibrium, the differences between them being due only to the form of caloric and thermal equations of state.

In the nonequilibrium case (see Chushkin [2.110, 2.111]) the compatibility relations on wave surfaces contain an additional term which takes into account the physical and chemical processes. The relaxation equations describing these processes are valid along the stream lines.

In the method of characteristics, the compatibility relations are expressed in finite-difference form on a number of characteristic surfaces forming a computational grid. Unlike the two-dimensional case, it is possible to choose different elementary computational cells in the three-dimensional case. Besides, we can construct the characteristic grid of direct or inverse type. In the former case, the characteristic surfaces are issued downstream and the grid points are obtained as a result of intersection of the surfaces in the course of solution. In the latter case, the grid points are fixed beforehand on certain reference planes and the characteristic surfaces are issued upstream from the reference plane under consideration to the preceding known reference plane where all the data at the points of intersection are obtained by interpolation. In the grids of inverse type, the grid points are ordered and their mutual arrangement can be easily varied during the course of solution (for example, their distribution can be made denser in the regions where the functions have large gradients). However, the interpolation increases the computational work and also introduces additional errors in the solution. If there are weak or strong discontinuities inside the flow field, separate grids of inverse type can be constructed for the regions with quite smooth properties of the flow.

In the three-dimensional case, an effective and widely used approach involves a combination of the method of characteristics in two geometrical variables with the finite-difference representations in the third variable. Calculating the flow past bodies of revolution at an angle of attack, the meridional angle is usually taken as such third variable. In this case, we consider the characteristic lines on a selected system of meridional planes. The grid-characteristic method also is based on the combination approach.

The advantage of the method of characteristics is that the finite-difference approximations are simplified owing to the use of compatibility relations whose dimension is lower by unity than that of the initial system. Even in the schemes involving the grid of inverse type, the domain of dependence and the domain of influence of solution are taken into consideration in a better way, and the numerical stability is ensured more easily. Characteristic algorithms for calculating grid points on the body and on the shock wave are quite convenient and effective, and are therefore included in the finite-difference methods. Some disadvantages of the method of characteristics should be mentioned. The accuracy of solution deteriorates for small angles of intersection of characteristic surfaces. The character-

istic grids of direct type are irregular and require the storage of additional quantities, viz. the coordinates of the grid points.

The three-dimensional method of characteristics can be applied advantageously for computing supersonic flows with a not-too-com plicated structure. In this case, the shock waves and other discontinuities are treated strictly. This method is always used for solving the variational problems of supersonic aerodynamics when very accurate calculations have to be made by strictly taking into account the domains of dependence and influence of the solution. The method is also quite effective for numerical investigation of nonequilibrium flows, since it includes the determination of stream lines along which the relaxation equations are integrated. In its pure form, the three-dimensional method of characteristics is confined to steady supersonic flows. In order to solve multidimensional problems where time is involved as the fourth variable, the method of characteristics is normally used in grid-characteristic form although in principle bicharacteristic schemes are also quite suitable for these problems.

We shall discuss the applications of the method of characteristics for calculating the supersonic flows past lifting bodies, and define two classes of algorithms, viz. schemes using bicharacteristics and schemes using characteristic lines on coordinate surfaces. It should be noted that a detailed review and analysis of the three-dimensional method of characteristics is given in [2.110, 2.111].

2.3.2. Schemes Using Bicharacteristics

In this type of schemes, the calculation of an inner grid point involves the participation of not less than three bicharacteristics belonging to the characteristic conoid whose apex lies at this point. In schemes with first order of accuracy, the characteristic conoid is approximated by a Mach cone. A smaller number of bicharacteristics are used for calculating the boundary points (on the body and on the shock wave).

In the direct tetrahedral scheme, a tetrahedron circumscribed around the Mach cone serves as an elementary cell. The base of this tetrahedron is constructed by three grid points on the surface with given data and the intersection of the faces of the tetrahedron determines the fourth grid point. Compatibility relations, in which one of the directions is a bicharacteristic, are written for each face of the tetrahedron, which represents a characteristic plane. Besides, we employ the condition of constant entropy along the segment of the stream line passing through the vertex and the mid-point of the tetrahedron base.

The direct tetrahedron scheme of the method of characteristics was developed by Rusanov [2.108]. For calculating the supersonic flow past bodies at an angle of attack, a modified version of this scheme

was used by Podladchikov [2.112], who calculated, in particular, the three-dimensional supersonic flow past a blunted inverse cone whose generatrix had a corner point at the mid-section. It is this kind of local singularities that can be exactly taken into account in the direct tetrahedral scheme. However, the irregularity of the grid, which becomes more pronounced with increasing angle of attack and the length of the body, and which ultimately leads to a breakdown of the computational process due to rapidly increasing errors, quite seriously limits the practical application of this scheme.

A numerical scheme of tetrahedral type, having the first order of accuracy but, unlike the previous scheme, operating on a grid of inverse type was proposed by Minostsev [2.113] (see also Zapryanov and Minostsev [2.114]). The calculations of the flow are fulfilled in cylindrical coordinates x, r, ψ, and the solution is advanced along the reference planes $x = \text{const}$. On each reference plane between the body and the shock wave the main gasdynamic functions are represented by continuous interpolation expressions containing double sums with terms like $a_{nk}(x)\,\xi^n \cos k\psi$ or $b_{nk}(x)\,\xi^n \sin k\psi$ depending on whether the function is odd or even in ψ. Here ξ is the normalized variable replacing the radius r. In computations for a new inner nodal point, three bicharacteristics (edges of the tetrahedron) and a stream line are issued from this point up to their intersection with the known preceding reference plane. The adopted interpolations are used to find the functions and their derivatives appearing in the compatibility relations at the points of intersection.

This scheme is more economical and effective as compared to the direct tetrahedral scheme. It is sufficient to take in this case a small number of nodal points on reference planes. Interpolation expressions in two geometrical variables provide all the information about the flow field in a compact form. However, in view of continuous character of these interpolations, the scheme cannot be used directly for nonsmooth bodies. A local analytical smoothening of the contour should be carried out at the location of the discontinuity of derivatives or (if possible) the entire body should be approximated to an identical body with an analytic contour.

This approach was used by Lebedev, Minostsev, Telenin and Tinyakov [2.113, 2.115-2.117] for calculating the three-dimensional supersonic flow past smooth bodies with a nearly-spherical front part and with the lateral surface resembling an inverted cone. Short and long bodies were investigated, and the gas was assumed to be perfect, but high-temperature effects were considered in some cases by introducing the effective value of the adiabatic exponent. Dyakonov and Minostsev [2.118] have considered elongated bodies of such a type (as well as a blunted cylinder) in a supersonic free stream at an angle of attack, but in this case the aft part had a flare ("skirt"). They analyzed the effect of the displacement of the flare on the pressure distri-

bution over the body and the position of the centre of pressure. Calculations in the region between the bluntness and the flare were carried out by the method of characteristics using the scheme described above, while the finite-difference method [2.23] with modification [2.28] was used for the aft part.

To illustrate the possibilities of the characteristic scheme described above, two projections of the flow pattern are shown in Fig. 2.14

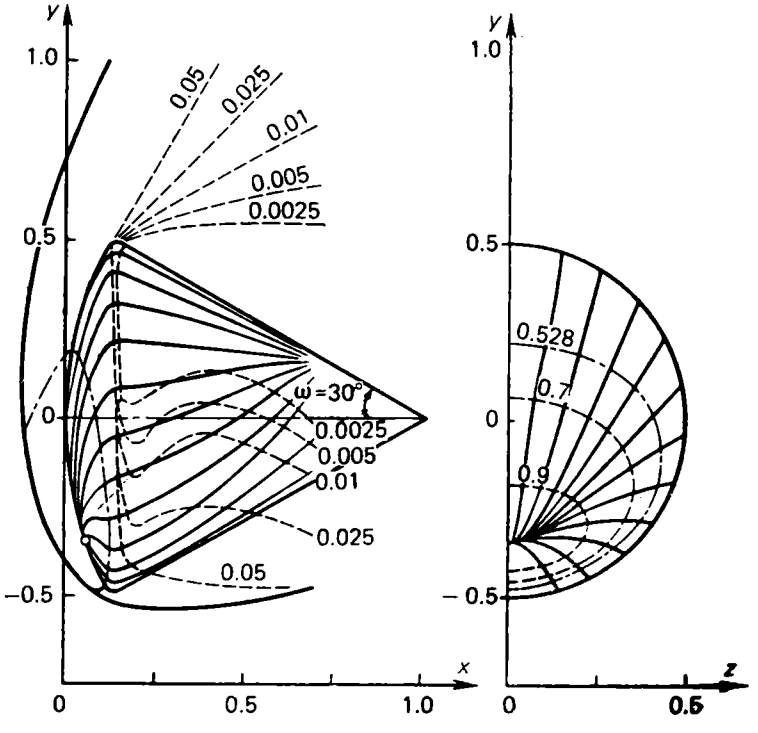

Fig. 2.14. Two projections of flow past a segmental-conic body, $M_\infty = \infty$, $\alpha = 30°$. Stream lines (solid lines) and isobars (dashed lines).

for $M_\infty = \infty$, $\alpha = 30°$ and $\varkappa = 1.4$, for an analytical body which closely resembles a spherical sector with semiangle $\omega = 30°$ [2.116, 2.117]. Solid lines show the shock wave in the symmetry plane and the stream lines which are projected onto the surface of the body. It can be seen that all the stream lines (except the two lines in the symmetry plane) approach the stagnation point and have a common tangent which is perpendicular to the symmetry plane. It is found that for small angles of attack ($\alpha = 15°$), the stream line pattern at the stagnation point is different and is reminiscent of a subcritical nodal point. The dashed lines show the isobars on the body, which are extended to the symmetry plane. The sonic line, which is also an isobar on the surface of the body, is drawn by a dot-and-dash line. The numbers at the isobars indicate the pressure referred to the pressure at

the stagnation point. The pressure on the leeward side of the inverse cone is practically equal to zero.

It was mentioned before that in the three-dimensional case the compatibility relations contain, besides the derivatives with respect to the bicharacteristic, the derivatives with respect to the non-bicharacteristic directions. In order to eliminate the latter quantities, Butler [2.119], who analyzed the unsteady plane motions of a gas, proposed that four bicharacteristics should be used for calculating the inner field point, and combinations of compatibility relations for these bicharacteristics should be composed.

On the basis of this idea, Magomedov [2.120, 2.121] developed a pentahedral bicharacteristic scheme with an inverse grid, applicable for calculating the steady three-dimensional supersonic flow of an equilibrium gas. He analyzed this explicit scheme and established that unlike the corresponding two-dimensional scheme, the order of difference approximation here is lowered to first. It was also shown [2.122] that for calculating a point on the shock wave, it is necessary and sufficient in the three-dimensional case to take (besides the conservation laws on the shock wave) the compatibility relation for only one bicharacteristic and the geometrical condition (the equality of second mixed derivatives of the coordinates of the shock wave).

The computational algorithm of the pentahedral scheme is more standardized as compared with the tetrahedral scheme, although it requires additional interpolations. This somewhat increases the amount of computations as well as the errors associated with them. This scheme was applied in different cases. It was used for calculating the supersonic flow of a perfect gas and a thermodynamic equilibrium gas past a spherical bluntness at an angle of attack. Some versions of such a solution for small angles of attack were compiled in the form of tables by Lunev, Magomedov and Pavlov [2.123]. This scheme was also adapted by Magomedov and Kholodov [2.124] for solving the problem of supersonic flow past a delta wing of finite thickness at an angle of attack. Such a wing had a spherically blunted nose while the lateral edges were blunted in the form of a circular cylinder.

2.3.3. Schemes Using Characteristic Lines on Coordinate Surfaces

To calculate supersonic flow past bodies at an angle of attack with the help of the three-dimensional method of characteristics, it was found advantageous to use the idea once proposed by Ferrari [2.125] for potential flows. This idea involves the consideration of two-dimensional traces of characteristic surfaces on coordinate surfaces (meridional planes in the case of a body of revolution). The functions in the direction connecting these planes are represent-

ed by some interpolation expressions with nodal points on these planes.

Especially simple computational algorithms are obtained in schemes where the elimination of the third variable associated with the transverse flow is carried out in the initial three-dimensional system of gasdynamic equations. The approximating system of equations obtained in this way (its order depends on the number of interpolation planes) retains its hyperbolic form under some not very stringent supersonic conditions. On each interpolation plane two-dimensional characteristics of opposite families and "stream lines" are drawn. The compatibility relations on these characteristics and "stream lines" form a system of ordinary differential equations that is similar to the system in the axisymmetric case.

Katskova and Chushkin [2.126, 2.127] proposed an effective scheme of this type for supersonic flows of a perfect and an equilibrium gas. In the cylindrical system of coordinates, this scheme employs continuous trigonometric interpolations in meridional angle ψ, an inverse grid with fixed nodal points and a normalized independent variable ξ which straightens the calculated domain between the body and the shock wave. This scheme is implicit and has the second order of accuracy. Hence its algorithm contains an iterative counting procedure whose cycle includes all the points on the computational reference plane $x = \text{const}$ that have the same coordinate ξ and all the values of ψ under consideration. The second order of the scheme and continuous trigonometric approximations make it possible to reduce the number of reference planes as well as the number of interpolation planes.

The efficiency and accuracy of this scheme was demonstrated in various applications involving the computation of sufficiently smooth supersonic three-dimensional flows, in particular, past blunted cones [2.127]. Katskova and Chushkin [2.128, 2.129] have carried out numerical investigation of the flow past ducted bodies flying at supersonic speeds at an angle of attack. They considered the case when the shock wave is attached to the leading edge of the body. The geometry of the body, the free stream Mach number and the angle of attack were varied in calculations. Figure 2.15 shows the variation of the coefficient of the tangential force C_t, the coefficient of normal force C_n and the coefficient of longitudinal moment C_m referred to the difference in the exit and entrance areas, along the outer surface of a ducted body in the form of a truncated cone with the semi-angle $\omega = 15°$. These results correspond to $\alpha = 10°$ and two values of Mach number $M_\infty = 5$ and $M_\infty = \infty$ (shown by solid and dashed lines respectively). With increasing distance, the aerodynamic coefficients approach the corresponding values for a sharp cone with the same angle (these values are shown in the figure by circles for $M_\infty = 5$ only).

Katskova and Chushkin [2.110, 2.130] later extended their scheme of characteristics to flows with nonequilibrium physical and chemical transformations. In this case, the relaxation equations are represented according to a special difference formula which can be used for calculations near the equilibrium conditions or under other conditions. Elliptical coordinates were used instead of cylindrical ones, thus considerably widening the scope of the algorithm. This scheme was used to calculate for the first time the three-dimensional nonequilibrium supersonic flows about blunted circular [2.131] and elliptical [2.132] cones with an exact consideration

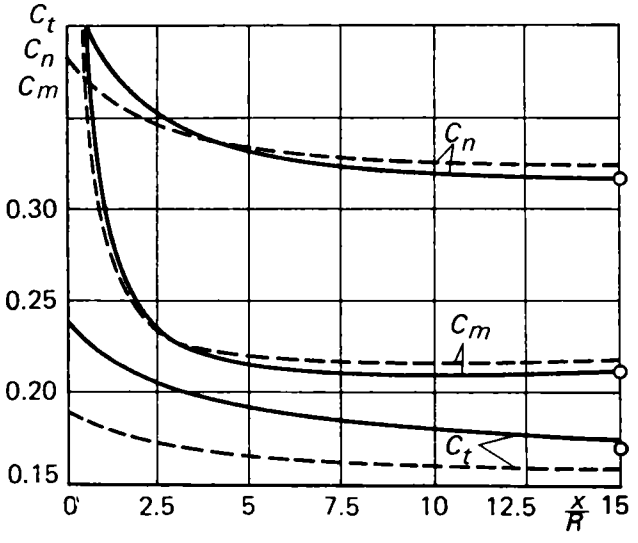

Fig. 2.15. Aerodynamic coefficients for a ducted body, $M_\infty = 5$ (solid lines) and $M_\infty = \infty$ (dashed lines), $\alpha = 10°$.

of dissociation of oxygen. The three-dimensional supersonic nonequilibrium flows past sharp cones with modelling reactions of combustion of hydrogen-air mixtures were computed by Chushkin [2.133]. To this date, this characteristic scheme remains the most effective for solving such problems.

Figure 2.16 illustrates some results of calculations for direct ($\omega > 0$) and inverted ($\omega < 0$) elliptical cones with different semiangles and an ellipsoidal bluntness with the ratio b/a of semiaxes equal to 1.5 and $b = 1$ m. Here, the flow of nonequilibrially dissociating oxygen is considered at $M_\infty = 10$, $\alpha = 10°$, the free-stream pressure $p_\infty = 0.001$ atm and temperature $T_\infty = 300$ K. The temperature distribution along the windward and leeward sides are plotted by solid and dashed lines respectively; the left and right branches of the curves correspond to the bluntness and aft conical part of the body respectively. The influence of nonequilibrium dissociation can

be judged from the frozen-flow data shown by crosses on the curve for a cone with $\omega = -30°$. The form of the shock wave is also shown. The pressure and temperature increase sharply on the leeward side near the rear corner point of the body; this effect must be manifested in the form of a secondary shock wave.

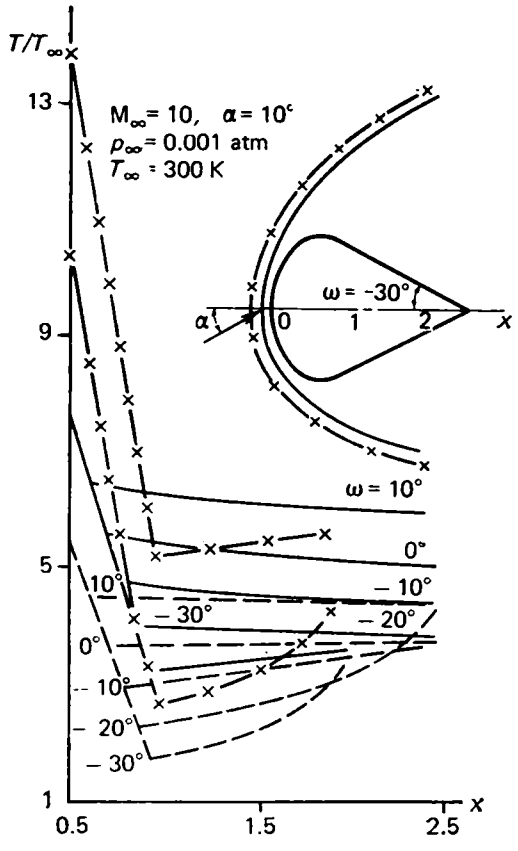

Fig. 2.16. Temperature distribution on the windward (solid lines) and leeward (dashed lines) generators of a blunted elliptical cone in the flow of nonequilibrially dissociating oxygen, $M_\infty = 10$, $\alpha = 10°$, $p_\infty = 0.001$ atm, $T_\infty = 300$ K.

Moretti [2.134] earlier proposed his version of the scheme of this type, which differs from the scheme presented in [2.127]. The Moretti scheme, however, has the first order of accuracy and suffers from a number of drawbacks (the linear interpolation in ψ, the grid of direct type, the absence of coordinate transformation and the Neumann instability). The author later adopted a more effective algorithm of the scheme [2.127]. Rakich [2.135] essentially used the same algorithm [2.127] but with a modification according to which the reference planes are planes normal to the surface of the body rather than to its axis. Rakich et al. [2.136] calculated the three-dimensional supersonic flow of nonequilibrium air past the nose of a space vehicle. The scheme proposed in [2.127] was also used by Camarero [2.137].

Grigoryev and Magomedov [2.138] have worked out a different three-dimensional scheme employing traces of characteristic surfaces on a selected system of meridional planes. In this scheme, a direct grid is constructed in each meridional plane by the intersection of characteristic surfaces of opposite families. The compatibility relations contain derivatives along mentioned characteristic traces as well as derivatives along a certain vector which lies on the characteristic surface and connects adjoining meridional planes. The latter derivatives are represented by central difference formulas. In the case of an axisymmetric flow, this scheme is transformed into the classical direct scheme of the two-dimensional method of characteristics.

This scheme can be used expediently when it is required to take into account more accurately the physical peculiarities of flow, for example, a corner point of the generatrix of a body, as was done by Grigoryev and Magomedov [2.138]. It can also be used for continuing a solution with initial data on a characteristic surface or for obtaining initial data on non-characteristic reference planes, as was done by Chushkin et al. [2.132]. Borisov and Mikhailov [2.139], who developed a similar scheme for potential flows, investigated various methods of approximating transverse derivatives (central differences, interpolation trigonometric polynomials, cubic splines).

A grid-characteristic method has been worked out in the Soviet Union. This method can be used successfully for solving various steady and unsteady problems of supersonic aerogasdynamics. The first publication on this subject was made by Magomedov and Kholodov [2.140]. In order to solve multidimensional equations, they constructed explicit difference schemes generalizing the scheme proposed by Courant, Isaacson, and Rees [2.141] for two-dimensional hyperbolic equations. The grid-characteristic method was developed and applied by many authors. A comprehensive analysis of this method and a review of the numerical results for supersonic flow past bodies, obtained with the help of this method, are given in the monograph by Belotserkovskii et al. [2.142].

The grid-characteristic method is based on finite-difference approximations of characteristic compatibility relations following from equations of gas dynamics, as well as the interpolation with respect to nodal points of a given fixed grid. Two-dimensional "characteristics", which are the lines of intersection of characteristic surfaces with two coordinate planes, are considered in the three-dimensional case. The solution is advanced along reference planes on which the third coordinate is constant. Two-dimensional "characteristics" pass from the point under consideration to the preceding reference plane where the functions at the meeting points are determined by linear or quadratic interpolation. Accordingly, the schemes are constructed with the first or the second order of accuracy. Since the interpolations establish the connection between the values of functions at these meeting points of the "characteristics" and their values at fixed nodal points on a reference plane, the entire scheme can be put in a form inherent in schemes of finite-difference method. This is why the method is called the grid-characteristic method.

Calculations proved that due to approximation viscosity, the scheme with linear interpolations allows one to carry out a through count of weak inner shock waves. In this respect, the applicability of the grid-characteristic method was extended by the explicit divergent scheme of the first order of accuracy, proposed by Kosarev and Magomedov [2.143]. This publication, as well as the papers by Magomedov and Kholodov [2.140] and Kosarev [2.144], contain

examples of calculation of supersonic flow ($\alpha = 5°$, $10°$) past bodies of revolution having a small discontinuity of the contour slope in front of which a secondary shock wave emerges.

The nonstationary three-dimensional version of the grid-characteristic method makes it possible to calculate the flow past blunted lifting bodies in the case of a detached shock wave. The monograph [2.142] contains results applied to a cylinder with a spherical-conical bluntness, and to an inverse cone with the nose part in the

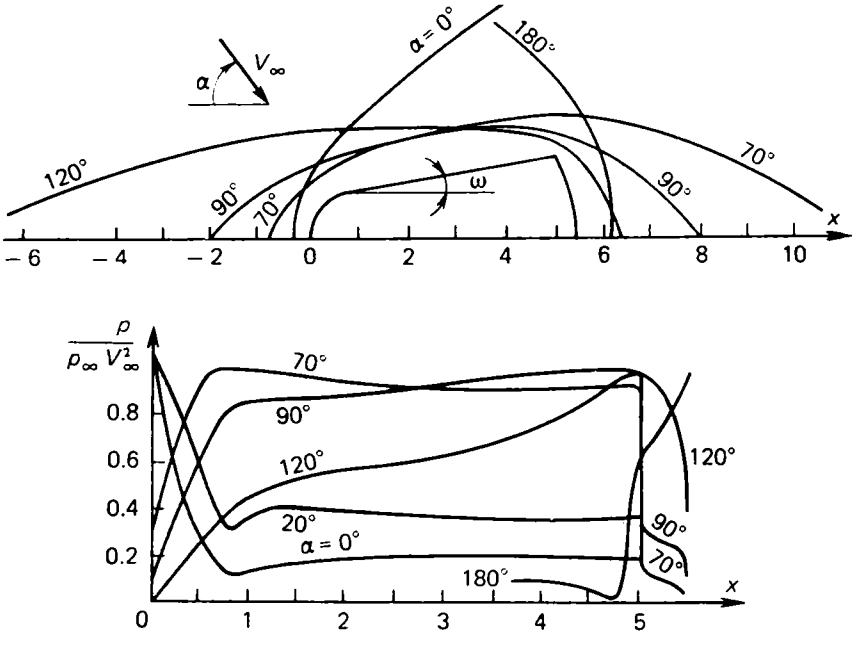

Fig. 2.17. Flow past a blunted body of revolution at various angles of attack, $M_\infty = 2$. Shock wave profile and pressure distribution over the body.

form of a spherical segment for various values of the free-stream parameters. The angles of attack reached values up to 25° and equilibrium high-temperature processes were taken into account in some cases. Reshetin et al. [2.145] have considered a lifting axially symmetric blunted body with a plane oblique base at the stern and presented graphs of aerodynamic coefficients as functions of α, calculated with the aid of the grid-characteristic method. Figure 2.17 shows an interesting example of calculations made by Kholodov [2.146]. This figure shows a conic body with a semi-angle $\omega = 10°$, having a spherical bluntness of the nose part and a spherically segmental bluntness of the aft part. For flows at Mach number $M_\infty = 2$, the shock waves in the symmetry plane and the pressure distribution over the surface of the body have been plotted for the angles of attack α varying between 0° and 180°.

The grid-characteristic method was used for solving three-dimensional problems of flow past a bluntness under complicated conditions. Computations for the flow in shock layer on the front part of the ellipsoid of revolution in a nonuniform supersonic flow were made by Kamenetsky and Turchak [2.147] who particularly considered nonzero angles of attack. Onufrieva, Pirogov, and Kholodov [2.148] investigated blunted bodies when jet flow was ejected out of the body nose part into a supersonic free stream. Various types of jet flow, including that at an angle of attack to the free stream, were considered. Belotserkovskii et al. [2.149] (see also [2.142]) generalized the grid-characteristic method to flows of a radiating gas. Kostuzik [2.150] has reported the application of this method for computing the three-dimensional radiation field in the shock layer in the case of a bluntness in hypersonic free stream of air. The interaction of radiation field and the gasdynamic field was considered and the selectivity of radiation was taken into account within the framework of the ten-group model for absorption coefficients. In the analysis of a segmental bluntness, the flight velocity V_∞ was varied between 12 and 18 km/s, while the angle of attack varied from 0° to 25°. An increase in the value of α entails a considerable change in the distribution of radiative heat flow on the surface of the body.

2.4. METHOD OF INTEGRAL RELATIONS AND METHOD OF STRAIGHT LINES

2.4.1. Basic Concepts of the Method

In the method of integral relations, from which the method of straight lines is obtained as a special case, the original system of partial derivative equations is reduced to an approximating system of ordinary differential equations which is then numerically integrated. This method was proposed in 1951 by Dorodnitsyn [2.151] for numerical solution of nonlinear problems of aerohydrodynamics. Later, Dorodnitsyn [2.152] gave a generalized form for the method of integral relations. Here certain weight functions which are chosen in accordance with the expected behaviour of the solution are introduced. The approximating system obtained provides a better approximation of the solution. Belotserkovskii and Chushkin [2.153] have made a significant contribution to the development, analysis and application of the method of integral relations. This method was subsequently used by many authors for numerical computation of various types of gas flows.

The application of the method of integral relations to the problems of three-dimensional supersonic flow past bodies is based on the approach described in [2.153] and involving an additional trigono-

metric approximation of functions in meridional angle on an accepted system of meridional planes. We are thus actually dealing with the two-dimensional version of the method of integral relations for each meridional plane. Hence we shall describe the essence of this method by considering the two-dimensional case.

The gasdynamic equations are taken in the divergent form

$$\frac{\partial P}{\partial x}+\frac{\partial Q}{\partial y}=F,$$

where P, Q, and F depend on x, y and the sought functions. Considering the Nth approximation, we divide the domain of integration into N nonintersecting strips. For this purpose, we draw $N-1$ intermediate lines, $y=y_n(x)=y_0(x)+(n/N)[y_N(x)-y_0(x)]$ between the boundaries $y=y_0(x)$ and $y=y_N(x)$ of the integration domain. For each equation, we take a certain complete system of N linearly independent piecewise continuous functions $f_n(y)$ and multiply this equation successively by each of these functions. Integrating with respect to y across the entire domain, we obtain the integral relations

$$\frac{d}{dx}\int_{y_0}^{y_N} f_nP\,dy-f_{nN}P_N\frac{dy_N}{dx}+f_{n0}P_0\frac{dy_0}{dx}$$

$$-f_{nN}Q_N-f_{n0}Q_0-\int_{y_0}^{y_N} Q\frac{df_n}{dy}\,dy=\int_{y_0}^{y_N} f_nF\,dy,$$

$$n=1,\ 2,\ \ldots,\ N.$$

The integrands are represented with the help of some interpolation formulas with nodes on strip boundaries. Thus, the original system of equations is reduced to an approximating system of ordinary differential equations in x for the values of the sought functions on all strip boundaries.

The functions $f_n(y)$ can be chosen in different ways. In the particular case when they are chosen in the form of the Dirac delta function $f_n(y)=\delta(y-y_n)$, we get the method of straight lines in which the derivatives are represented by the accepted interpolation formulas. In another case, when these functions are in the form of step functions, i.e. when $f_n(y)=1$ for $y_{n-1}<y<y_n$ and $f_n(y)=0$ for $y<y_{n-1}$ and $y>y_n$, we obtain the simple method of integral relations where the original equations are integrated across each of the N strips.

The use of the divergent form of equations (this enables the exact integration with respect to one variable), the approximation of integrals (and not derivatives), and the possibility of choosing such a class of interpolation formulas and weight functions which have

the best correspondence to the behaviour of the solution are the circumstances that make the method of integral relations quite effective. Due to simplicity of the computational algorithm this method is especially attractive when computers with low efficiency and small storage computers are used. The boundary conditions are realized easily in the method, in particular, if there are singularities at the boundaries (discontinuities of the slope or curvature of the body surface, singularity on the axis in cylindrical coordinates). A fairly high accuracy of solution is obtained in many cases by using a small number of strips ($N = 1$-3). The realization of the method, however, becomes laborious if the boundary value problem of a high order arises for the approximating system.

2.4.2. Method of Integral Relations

This method has been used for computing the supersonic flow past various bodies. It was employed successfully as an effective tool for determining the mixed subsonic-supersonic flow behind detached shock wave in front of a bluntness. Belotserkovskii [2.154] developed the method of integral relations for calculating such a mixed flow past a blunted body and was the first to obtain the solution of this problem in a direct formulation. In particular, he computed the tables [2.155] of flow fields behind the detached shock wave in front of spherical and ellipsoidal bluntness. Other authors used these tables as the initial data for continuing the computation of the flow in the supersonic region for various bodies including lifting ones. Belotserkovskii et al. [2.156] have published a monograph devoted to the development of the algorithm for the method of integral relations and its applications to different blunted bodies in supersonic free stream.

The numerical solution of the problem of three-dimensional mixed steady flow past the nose parts of bodies with a detached shock wave can be obtained (as in the two-dimensional case) by using two schemes of the method of integral relations which differ in the direction of strips. In the first scheme, the strips are arranged along the shock layer. The approximating system in this case has singular points of saddle type, the number of these points increases with the order of approximation. The integration of the system starts at a certain point where the unknown quantities are uniquely determined from the condition of boundedness of the derivatives of velocity at singular points. The first scheme can be advantageously used for free streams with a large supersonic velocity, when the shock layer is thin and even a single-strip solution with linear approximations may be quite satisfactory. This scheme is also applicable for bodies with a sharp change in their form and for non-smooth bodies; it provides detailed information on the body surface and on the shock wave.

In the second scheme, we consider the minimum region of bluntness influence bounded by two characteristic surfaces on the windward and leeward sides of the flow. This region is divided into strips passing across the shock layer. The approximating system, to which compatibility relations along the boundary characteristics are added, is integrated from the shock wave towards the body. In the Nth approximation, there is a boundary value problem in which $N + 1$ unknown parameters on the shock wave (the detachment distances on the strip boundaries) are determined from the conditions that the normal velocity vanishes at $N + 1$ corresponding points on the body surface. The position of the shock wave is found with the help of the Newton method. This scheme can be advantageously used for a free stream with a low supersonic velocity, when the shock layer is thick, as well as for nonequilibrium flows when the physical properties of the gas may change rapidly across the shock layer.

Several authors have applied the first scheme to calculate the three-dimensional supersonic steady flow past bluntness. The entire shock layer was considered as a single strip and three meridional planes of interpolation were taken. A disc in a perfect gas (Minailos [2.157]), a spherical segment and a blunted cone in equilibrium reactive air (Kozlova and Minailos [2.158]) have been considered at an angle of attack. A similar approach was also adopted by Waldman [2.159]. Minitsky [2.160] has considered bodies in the form of triaxial ellipsoids which do not differ significantly from bodies of revolution and are set at zero angle of attack. The approximating system was solved in this case by iteration.

Chushkin [2.161] numerically analyzed conical bodies of revolution in a supersonic free stream at an angle of attack. The cone had a finite length (bounded by the base section), the semiangle was larger than the limiting value, and the apex had a very small bluntness. The detached shock wave appearing in this case was mainly determined by the lateral surface of the cone rather than the bluntness. The solution was obtained in special variables which allowed to capture large gradients of gasdynamic functions in the neighbourhood of the apex. A comparison with the experimental results for $\alpha = 0°$ proved that for $M_\infty \geqslant 2.5$, the first scheme gave the distribution of functions on the body and the shape of the shock wave with a reasonable accuracy. During computations, the Mach number, the angle of attack and the cone semiangle ω were varied, and the cases of a disc ($\omega = 90°$) and cone-shaped concave noses ($\omega > 90°$) were also covered. One of the results obtained is presented in Fig. 2.18 where the distribution of velocities referred to the critical velocity of sound is plotted for the cone with $\omega = 60°$ at $M_\infty = 3$ and various values of α. The figure shows the behaviour of the longitudinal velocity v along the cone generators in the symmetry plane of flow, and of the

peripheral velocity w along the cone generator in the plane perpendicular to the symmetry plane. For large values of α, a sharp nonmonotone local change in the velocity takes place near the apex of the body. The longitudinal velocity becomes sonic at the base section. The shape of the shock wave at $\alpha = 20°$ is also drawn.

The problem of supersonic flow past smooth bluntness at an angle of attack is better solved with the aid of the second scheme of the method of integral relations, where higher-order approximations can be realized more easily. For three-dimensional flow of a perfect

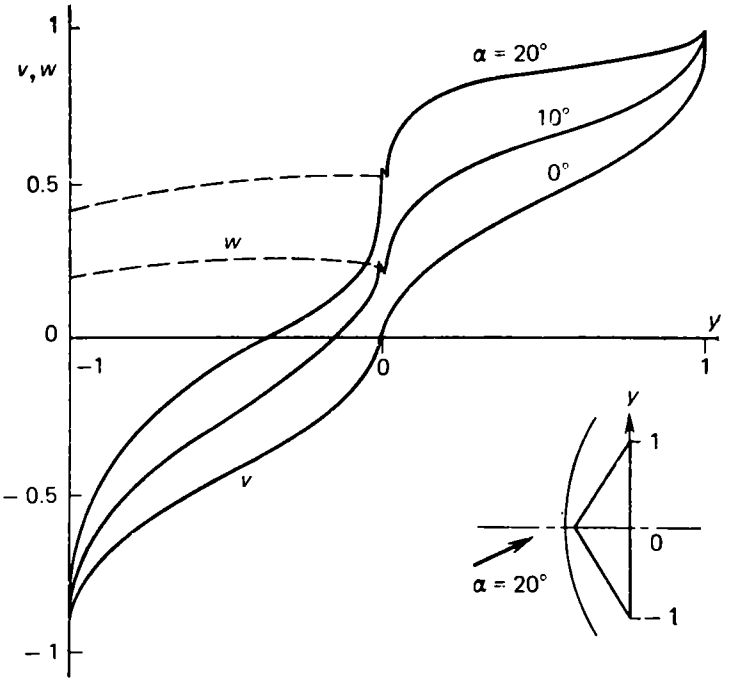

Fig. 2.18. Flow past a cone with a detached shock wave at various angles of attack, $M_\infty = 3$. Velocity distribution over the body.

gas, such a scheme was developed and applied in the book by Belotserkovskii *et al.* [2.156]. Golomazov [2.162, 2.163] computed by this scheme some equilibrium and nonequilibrium flows. To illustrate these results, we reproduce the plot from [2.163], describing the nonequilibrium flow past the front part of the ellipsoid of revolution with the ratio of the semiaxes $b/a = 1.5$. To simulate the atmosphere on Mars, two chemical compositions for the gas were considered: 50% CO_2 + 25% N_2 + 25% Ar, or 100% CO_2. Figure 2.19 corresponds to the free-stream parameters $M_\infty = 10$, $\alpha = 15°$, $p_\infty = 0.001$ atm and $T_\infty = 300$ K. The calculated dependences for the first gas mixture are shown by solid lines and dashed lines, while the dependences for pure carbon dioxide are depicted by dot-and-dash lines. For various values of the semi-axis b (in metres), the pro-

files of temperature T and of weight concentration c of carbon monoxide across the shock layer in the direction of the ellipsoid axis are also shown in the figure, where $\xi = 0$ and $\xi = 1$ correspond to the shock wave and the body respectively. It can be seen that the nonequilibrium grows with increasing size of the body. The addition of argon raises the temperature and hence the dissociation of the carbon dioxide molecules occurs more intensively.

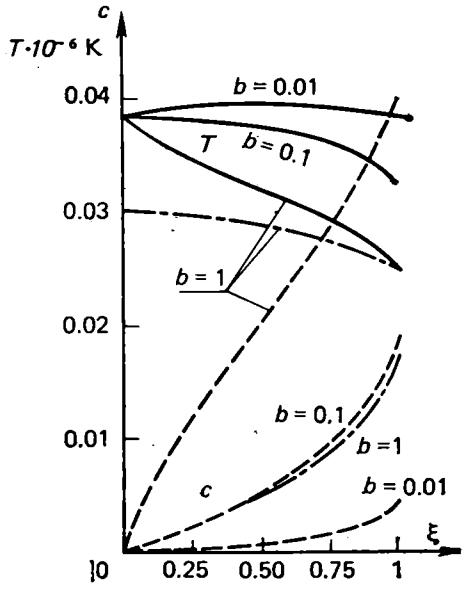

Fig. 2.19. Nonequilibrium flow past ellipsoids, $M_\infty = 10$, $\alpha = 15°$, $p_\infty = 0.001$ atm, $T_\infty = 300$ K. Distribution of temperature (solid lines) and carbon dioxide concentration (dashed lines) across the shock layer.

The supersonic conical flows without axial symmetry are another class of flows which was calculated by using the method of integral relations. The problem was solved in conic variables as a two-dimensional problem. For this purpose, Chushkin and Shchennikov [2.164] worked out a scheme with approximations across the shock layer. The approximating system was integrated from the windward plane of symmetry to the leeward one and the solution was determined by satisfying the necessary boundary conditions on these planes. Computations in the single-strip approximation were made for elliptical and circular cones at small angles of attack, when the parabolicity line has not yet reached the surface of the body. As in the case of flow past a blunted body, the problem of supersonic conical flow can be solved more effectively by using the scheme with approximations along the shock layer, in which the approximating system is integrated from the shock wave to the body. Such a scheme was proposed and realized by Chushkin [2.133, 2.165] who used the generalized form of the method of integral relations for the approximations $N = 3$ and $N = 4$. He also extended this scheme to cover the equilibrium case.

Following the first of these schemes and considering the limiting case of an infinitely thin elliptical cone, Bazzhin [2.166] computed the flow past the windward side of a flat delta wing which was set in a supersonic free stream at a large angle of attack. The regime when the shock wave is attached only to the apex of the wing was studied. For the same case, Kennet [2.167] developed a somewhat different single-strip scheme, where quadratic approximations were employed

under the assumption that the functions had zero gradients on the surface of the wing. Some results obtained from computations using such an approach were published by Bazzhin [2.168]. This scheme was used by Akinrelere [2.169] to calculate the flow on the windward side of a lifting flat delta wing in the regime when the shock wave is attached to the leading edge.

Chushkin [2.170] has worked out the algorithm for applying the method of integral relations to the computation of a supersonic three-dimensional flow past lifting bodies. This region is straightened out and K meridional planes with N strips in each of them are taken; trigonometric approximations and approximations by power polynomials (piecewise or continuous) are used. This algorithm constructed for any values of K and N was applied for calculating the external flow past ducted conical bodies at an angle of attack with a shock wave attached to the leading edge.

2.4.3. Method of Straight Lines

To numerically solve the two-dimensional problem on the mixed flow past the front part of a smooth blunted body, Telenin (see [2.171]) modified the well-known method of straight lines. Later on, Telenin and Tinyakov [2.172] generalized this method to the three-dimensional case. The solution is usually calculated in spherical coordinates with the pole displaced with respect to the bluntness axis. A system of meridional planes is introduced and the strips are formed in each of them by rays arranged either uniformly or in accordance with the position of zeros of the Chebyshev polynomials. Characteristic surfaces bounding the minimum domain of influence are not considered in this approach, and hence, generally speaking, the position of the rays bounding this domain has to be corrected in the course of solution. The use of trigonometric representations in one geometrical variable and of continuous power interpolating polynomials in the other variable (this is what makes this method different from the classical method of straight lines where piecewise linear approximations are used across each strip) leads to an approximating system of ordinary differential equations along all the rays. This system is numerically integrated from the shock wave to the body in the same way as in the second scheme of the method of integral relations. Thus, the method of straight lines differs from the latter scheme in that no integral relations are set up and the minimum domain of influence is not taken exactly, which somewhat simplifies the form of the approximating system, though a certain loss of accuracy has to be incurred.

The work [2.172] contains the first examples of the application of this method for calculating the mixed flow behind a detached shock wave in front of a bluntness which is set in supersonic free stream

of a perfect gas at an angle of attack. The three-dimensional flow past ellipsoids was then analyzed. A whole cycle of investigations, started in the article by Minostsev, Telenin and Tinyakov [2.115], was devoted to the three-dimensional flow past bodies with a nose part close to the spherical segment. The contour of the body is approximated by an analytic function. The properties of such a flow under various conditions were described in the articles [2.116, 2.117] mentioned in Sec. 2.3.2.

Shkadova [2.174] extended the method described in [2.172] to calculate the mixed flow past a bluntness at an angle of attack in the case when the air behind the shock wave becomes chemically active and the processes occurring in it are nonequilibrium, i.e. proceed at a finite speed. The state of the gas in the shock layer changes from nearly frozen to nearly equilibrium conditions. Near the equilibrium, the relaxation equations become the equations with small parameter at the highest derivative. Besides, in the method applied in [2.172], the coefficients of derivatives in the gasdynamic equations of the approximating system tend to zero near the surface of the body. Therefore, all differential equations of the system are represented according to a two-point implicit difference scheme which was worked out by Shkadova [2.157] earlier for the two-dimensional case. This scheme contains normalizing factors, which are chosen in accordance with the flow conditions and whenever it is possible, enable one to reduce the scheme to a simpler explicit one. The solution of implicit equations is carried out with the aid of iterations.

This method was used in [2.174] (see also Semenikhina and Shkadova [2.175]) to compute the flow of nonequilibrium air past a spherical segmental bluntness at angles of attack $\alpha \leqslant 10°$. Burdelnyi, Shkadova and Minostsev [2.176] later advanced these results up to the angle of attack $\alpha = 25°$. They also considered the flow about the lateral surface of the body. Figure 2.20 shows the plots presented in this paper for the spherical segment with the angle 60° and the radius 1 cm, in the free stream of air with the Mach number $M_\infty = 20$, the pressure $p = 10^{-4}$ atm and the temperature $T_\infty = 250$ K, when the nonequilibrium behind the shock wave is highly pronounced. The figure represents the shock waves, the sonic lines and the stagnation points in the symmetry plane of flow for various angles of attack. The change in the electron concentration c_e along the body is also shown. At large angles of attack, a considerable influence of the three-dimensional nature of flow on the thermochemical structure of the shock layer is observed.

To numerically solve the problem of three-dimensional flow past a bluntness, Golomazov and Zyuzin [2.177] have proposed a modified version of the method of straight lines, which is similar to the method described in [2.172]. However, it does consider the boundary characteristic surfaces to which strips are attached. Moreover, it

uses piecewise approximations of various types (most often, cubic spline-functions are taken) rather than continuous approximations. Another distinguishing feature of this method is the use of a special algorithm which simplifies calculations near the body surface (such an algorithm was proposed by Grudnitsky for the unsteady axisymmetric problem, see [2.142]).

This modification of the method of straight lines was applied by several authors for parametric investigation of the mixed flow past

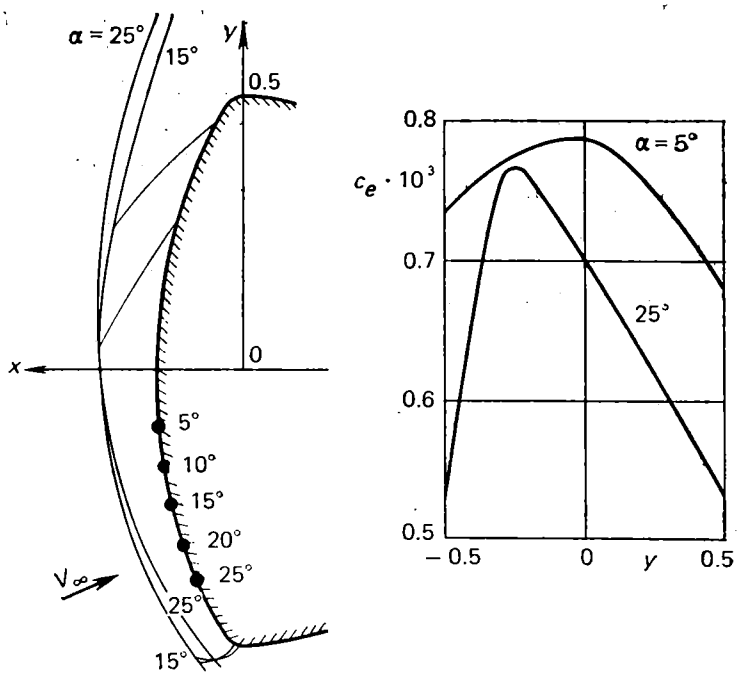

Fig. 2.20. Flow of nonequilibrium air past a segmental bluntness at various angles of attack, $M_\infty = 20$, $p_\infty = 0.0001$ atm, $T_\infty = 250$ K. Distribution of electron concentration along the body.

the front part of different types of bluntness at an angle of attack. Golomazov and Zyuzin considered the flows about an ellipsoid [2.177] and a large-angle blunted cone with sonic shoulder [2.178]. The behaviour of the sonic surface was analyzed in the latter case. It was found that in a very narrow interval of angles of attack, the subsonic part of the shock layer on the leeward side contains a local supersonic zone in the vicinity of the shock wave.

Belotserkovskii, Golomazov and Zhuravleva [2.179] have used this method for investigating the flow of a freely expanding supersonic jet past the end face of a cylinder under various angles of attack. The numerical simulation of problems involving jets in gas dynamics is the subject of a paper by Belotserkovskii [2.180]. One of the numerical examples discussed there is presented in Fig. 2.21. This

figure shows in the symmetry plane the flow past a spherically blunted cone $\omega = 60°$, at whose surface the main flow of a perfect gas ($\varkappa = 1.4$) is injected by a uniformly distributed normal flow of the same gas at a velocity $v/v_{max} = 0.1$. The results pertain to the flow with Mach number $M_\infty = 10$ at $\alpha = 0°$ and 5° (curves *1* and *2* respectively). The shock wave is depicted by the solid line while the dashed line represents the contact surface separating the gas being injected.

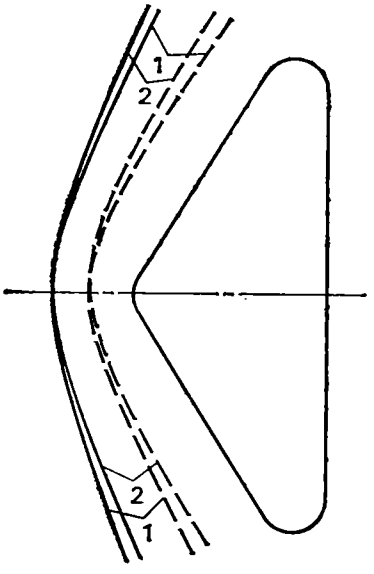

Fig. 2.21. Flow past a blunted cone with an injection from the surface, $M_\infty = 10$, $\alpha = 0°$ and $\alpha = 5°$. Shock wave (solid line) and contact surface (dashed line).

The method of straight lines was also applied for solving problems of supersonic conical flow in the two-dimensional formulation. While Makhin and Syagaev [2.181] utilized the traditional form of this method, the authors listed below used the form presented in [2.171]. Bazzhin and Chelysheva [2.182], and Bazzhin et al. [2.183, 2.184] have considered elliptical cones at large angles of attack when the flow on the windward side is not affected by the motion of the gas on the leeward side. In the case of perfect air [2.183] and equilibrium air [2.184], the mixed flow region on the windward side was calculated by the method of straight lines and the calulation in the hyperbolic region was made by the method of characteristics. However, the leeward symmetry plane could not be reached on account of the secondary embedded shock. Holt and Ndefo [2.185] have computed the supersonic flow past a circular cone at moderate angles of attack, while Fletcher [2.186] has carried out calculations at angles of attack exceeding the semiangle of the cone. In the latter work, the method of straight lines was combined with the method of characteristics. The Ferri singular point shifted from the body surface and the internal secondary shock wave, treated as a strong discontinuity, were taken into account in this case, and their positions were determined with the help of the iteration process.

2.5. CONCLUSION

We have given a fairly complete and detailed review of the research carried out during the last two decades or more by Soviet scientists for numerical solution of the problem of three-

dimensional flow of an ideal gas past lifting bodies flying at supersonic velocities. Aerodynamic forms which simulate a whole aircraft, or its individual components were considered.

This review demonstrates the significant progress made in the USSR in the development of effective numerical methods and their applications to solve problems of aerohydrodynamics. Earlier methods, which were developed, modified and generalized in the course of time, serve even today as effective tools for computing three-dimensional supersonic gas flows. Three main types of methods have been worked out for numerical simulation of supersonic flow past bodies. These are: the finite-difference grid method, the method of characteristics and the method of integral relations (including the method of straight lines). With advancing computer techniques, various finite-difference grid methods are being widely applied, although the other methods, for example, the grid-characteristic method, are also receiving due attention.

At the present time, we can assume that the problem of computation of flow past classical aerodynamic shapes at an angle of attack in the supersonic free stream of an inviscid perfect or real high-temperature gas has been solved in principle. In a number of simpler cases (sharp cones, spherically blunted cones, certain types of bluntness, delta wings, etc.), tables for flow fields have been computed with sufficient accuracy.

A great deal of progress has also been made in the numerical computation of three-dimensional supersonic flow past complete, albeit quite oversimplified, forms of aircraft and spacecraft. The existing numerical methods can be successfully applied to solve this problem although they require the use of highly efficient computers.

References

2.1. G. P. Voskresensky and P. I. Chushkin, in: *Advances in Science and Technology, Fluid Mechanics*, vol. 11, VINITI, Moscow, 1978, p. 5-65 (in Russian).

2.2. G. P. Voskresensky and P. I. Chushkin, *Uspekhi Mekhaniki*, 3, 2: 47-95 (1980).

2.3. P. I. Chushkin and G. P. Voskresensky, *Review of numerical methods for the problem of the supersonic flow around bodies at angle of attack,¶ 12th Congress of ICAS, 12-17 oct. 1980, Munich*, in: ICAS Proceedings 1980, p. 444-54.

2.4. S. K. Godunov, A. V. Zabrodin, and G. P. Prokopov, *Zh. Vychisl. Mat. i Mat. Fiz.*, 1, 6: 1020-50 (1961).

2.5. M. Ya. Ivanov and A. N. Kraiko, *Zh. Vychisl. Mat. i Mat. Fiz.*, 12, 3: 805-13 (1972).

2.6. S. K. Godunov, A. V. Zabrodin, M. Ya. Ivanov, A. N. Kraiko, and G. P. Prokopov, *Numerical Solution of Multidimensional Problems in Gas Dynamics*, Nauka, Moscow, 1976 (in Russian).

2.7. A. E. Lutsky, G. P. Prokopov, and V. A. Cherkashin, Preprint No. 87, Keldysh Inst. Appl. Math., USSR Acad. Sc., Moscow, 1980 (in Russian).

2.8. M. Ya. Ivanov and A. N. Kraiko, *Zh. Vychisl. Mat. i Mat. Fiz.*, 13, 6: 1557-72 (1973).

2.9. M. Ya. Ivanov and T. V. Nikitina, *Uch. Zap. Tsentr. Aero-gidrodinam. Inst.*, 4, 4: 7-13 (1973).
2.10. A. V. Rozin, *Izv. Akad. Nauk SSSR, Ser. Mekh. Zhidk. i Gaza*, 1: 185-7 (1983).
2.11. M. K. Aukin and R. K. Tagirov, *Chisl. Metody Mekh. Sploshn. Sredy*, 11, 6: 23-35 (1980).
2.12. W. P. Nelms, R. L. Carmichael, and Ch. R. Castellano, *NASA Tech. Notes*, D-5272 (1969).
2.13. M. K. Aukin and R. K. Tagirov, *Uch. Zap. Tsentr. Aero-gidrodinam. Inst.*, 13, 3: 136-41 (1982).
2.14. V. P. Kolgan, *Uch. Zap. Tsentr. Aero-gidrodinam. Inst.*, 6, 2: 1-6 (1975).
2.15. A. P. Kosykh and A. N. Minailos, *Tr. Tsentr. Aero-gidrodinam. Inst.*, vyp. 1809 (1976).
2.16. A. P. Kosykh and A. N. Minailos, *Izv. Akad. Nauk SSSR, Ser. Mekh. Zhidk. i Gaza*, 3: 105-11 (1975).
2.17. A. P. Kosykh, *Uch. Zap. Tsentr. Aero-gidrodinam. Inst.*, 11, 4: 129-38 (1980).
2.18. A. N. Minailos, *Uch. Zap. Tsentr. Aero-gidrodinam. Inst.*, 11, 5: 7-17 (1980).
2.19. A. N. Minailos, *Uch. Zap. Tsentr. Aero-gidrodinam. Inst.*, 12, 3: 30-8 (1981).
2.20. A. A. Golubinsky and A. P. Kosykh, *Uch. Zap. Tsentr. Aero-gidrodinam. Inst.*, 9, 4: 35-48 (1978).
2.21. A. G. Zarubin, *Uch. Zap. Tsentr. Aero-gidrodinam. Inst.*, 13, 2: 123-8 (1982).
2.22. K. I. Babenko and G. P. Voskresensky, *Zh. Vychisl. Mat. i Mat. Fiz.*, 1, 6: 1051-60 (1961).
2.23. K. I. Babenko, G. P. Voskresensky, A. N. Lyubimov, and V. V. Rusanov, *Three-dimensional Ideal-gas Flow Past Smooth Bodies*, Nauka, Moscow, 1964 (in Russian).
2.24. K. I. Babenko and V. V. Rusanov, *Proc. 2nd All-Union Congress on Theor. and Appl. Mech., 1964*, Nauka, Moscow, 1965, vyp. 2 (in Russian).
2.25. V. V. Rusanov, *Zh. Vychisl. Mat. i Mat. Fiz.*, 8, 3: 616-33 (1968).
2.26. K. I. Babenko, V. N. Ivanova, E. P. Kazandzhan, M. A. Kukarkina, and Yu. B. Radvogin, *Unsteady Ideal-gas Flow Past the Nose Part of a Blunted Body*, Inst. Appl. Math. USSR Acad. Sc., Moscow, 1969 (in Russian).
2.27. V. N. Ivanova and Yu. B. Radvogin, Preprint No. 82, Keldysh Inst. Appl. Math., USSR Acad. Sc., Moscow, 1981 (in Russian).
2.28. Yu. N. Dyakonov, N. S. Kokoshinskaya, V. M. Lukashin, L. V. Pchelkina and I. D. Sandomirskaya, in: *Coll. Works of Comp. Center of Moscow Univ.*, Izd. MGU, Moscow, 1970, p. 85-91 (in Russian).
2.29. Yu. Ya. Mikhailov, *Zh. Vychisl. Mat. i Mat. Fiz.*, 10, 1: 233-5 (1970).
2.30. Yu. B. Radvogin, *Proc. of 2nd Intern. Coll. on Gas Dynamics of Explosion and Reacting Systems, sect. of Numer. Meth. in Gas Dynam.* Moscow, 1969 p. 228-36 (in Russian).
2.31. C. Weiland, *J. Comp. Phys.*, 29, 2: 173-98 (1978).
2.32. R. Gonidou, *Rech. Aérospat.*, 120: 11-19 (1967).
2.33. G. P. Voskresensky, V. S. Tatarenchik, and O. A. Shepetievsky, Preprint No. 16, Inst. Appl. Math., USSR Acad. Sc., Moscow, 1976 (in Russian).
2.34. V. N. Vetlutsky and V. P. Ganimedov, *Zh. Prikl. Mekh. i Tekhn. Fiz.*, 1: 114-20 (1975).
2.35. G. P. Voskresensky, *Zh. Vychisl. Mat. i Mat. Fiz.*, 7, 2: 389-400 (1967).
2.36. G. P. Voskresensky, O. V. Ivanov and V. A. Stebunov, Preprint No. 67, Keldysh Inst. Appl. Math., USSR Acad. Sc., Moscow, 1981 (in Russian).
2.37. G. P. Voskresensky, *Izv. Akad. Nauk SSSR, Ser. Mekh. Zhidk. i Gaza*, 4: 134-42 (1968).
2.38. G. P. Voskresensky, *Zh. Prikl. Mekh. i Tekhn. Fiz.*, 6: 76-81 (1973).

2.39. G. P. Voskresensky, A. S. Ilyina, and V. S. Tatarenchik, *Tr. Tsentr. Aero-gidrodinam. Inst.*, vyp. 1590 (1974).
2.40. G. P. Voskresensky, A. S. Ilyina, and V. S. Tatarenchik., *Zh. Prikl. Mekh. i Tekhn. Fiz.*, 6: 35-42 (1977).
2.41. Yu. N. Dyakonov, *Izv. Akad. Nauk SSSR, Ser. Mekhan. i Mashinostr.*, 4: 150-3 (1964).
2.42. Yu. N. Dyakonov, M. G. Lebedev, V. M. Lukashin, L. V. Pchelkina, and I. D. Sandomirskaya, in: *Some Applications of Grid Method in Gas Dynamics.* Vyp. V., Izd. MGU, Moscow, 1974, p. 4-139 (in Russian).
2.43. Yu. N. Dyakonov, L. V. Pchelkina, I. D. Sandomirskaya, and V. I. Uskov, in: *Coll. Works of Comp. Center of Moscow Univ.*, vyp. 15, Izd. MGU, Moscow, 1970, p. 72-84 (in Russian).
2.44. A. V. Antonets and V. P. Marinin, *Izv. Akad. Nauk SSSR, Ser. Mekh. Zhidk. i Gaza*, 1: 178-83 (1981).
2.45. S. L. Vishnevetsky and M. A. Ivanov, *Izv. Akad. Nauk SSSR, Ser. Mekh. Zhidk. i Gaza*, 1: 144-9 (1983).
2.46. Yu. Ya. Mikhailov, G. G. Nersesov, and I. F. Chelysheva, *Uch. Zap. Tsentr. Aero-gidrodinam. Inst.*, 5, 5: 106-10 (1974).
2.47. Yu. Ya. Mikhailov and G. G. Nersesov, *Tr. Tsentr. Aero-gidrodinam. Inst.*, vyp. 1808: 3-22 (1977).
2.48. G. G. Nersesov, *Uch. Zap. Tsentr. Aero-gidrodinam. Inst.*, 5, 1: 77-81 (1974).
2.49. A. P. Bazzhin and Yu. Ya. Mikhailov, *Lect. Notes Phys.*, 59: 96-100 (1976).
2.50. Yu. N. Dyakonov, *Dokl. Akad. Nauk SSSR*, 157, 4: 822-5 (1964).
2.51. A. V. Antonets, *Izv. Akad. Nauk SSSR, Ser. Mekh. Zhidk. i Gaza*, 2: 178-81 (1970).
2.52. Yu. M. Lipnitsky, Yu. Ya. Mikhailov, and K. G. Savinov, *Izv. Akad. Nauk SSSR, Ser. Mekh. Zhidk. i Gaza*, 3: 182-6 (1972).
2.53. A. K. Burdelnyi, V. B. Minostsev, A. F. Mosin, K. G. Savinov, and M. P. Falunin, *Nauch. Tr. Inst. Mekh. MGU*, 30: 157-67 (1973).
2.54. A. V. Antonets and Yu. M. Lipnitsky, *Izv. Akad. Nauk SSSR, Ser. Mekh. Zhidk. i Gaza*, 6: 155-9 (1976).
2.55. V. B. Minostsev and K. G. Savinov, *Izv. Akad. Nauk SSSR, Ser. Mekh. Zhidk. i Gaza*, 6: 174-6 (1982).
2.56. K. G. Savinov and V. P. Shkadova, *Izv. Akad. Nauk SSSR, Ser. Mekh. Zhidk. i Gaza*, 2: 140-5 (1976).
2.57. V. P. Shkadova, *Izv. Akad. Nauk SSSR, Ser. Mekh. Zhydk. i Gaza*, 1: 73-6 (1969).
2.58. A. K. Burdelnyi and V. B. Minostsev, *Izv. Akad. Nauk SSSR, Ser. Mekh. Zhidk. i Gaza*, 5: 124-9 (1972).
2.59. V. V. Rusanov, in: *Fluid Dynam. Transact.*, vol. 4, PWN, Warszawa, 1969.
2.60. A. N. Lyubimov, *Izv. Akad. Nauk SSSR, Ser. Mekh. Zhidk. i Gaza*, 2: 85-94 (1969).
2.61. A. N. Lyubimov, *Izv. Akad. Nauk SSSR, Ser. Mekh. Zhidk. i Gaza*, 1: 176-81 (1970).
2.62. A. N. Lyubimov and V. V. Rusanov, *Gas Flows past Blunted Bodies. Method of Calculation and Analysis of Flows* (Part 1). *Tables of Gasdynamic Functions* (Part 2), Nauka, Moscow, 1970 (in Russian).
2.63. K. I. Babenko, V. N. Ivanova, A. P. Kazandzhan, M. A. Kukarkina, and Yu. B. Radvogin, *Tables of Three-dimensional Supersonic Ideal Gas Flow past the Nose Part of Ellipsoids of Revolution*, Inst. Appl. Math. USSR Acad. Sc., Moscow, 1973 (in Russian).
2.64. V. N. Ivanova and Yu. B. Radvogin, Preprint No. 126, Keldysh Inst. of Appl. Math., USSR Acad. Sc., Moscow, 1980 (in Russian).
2.65. V. N. Ivanova and Yu. B. Radvogin, Preprint No. 28, Keldysh Inst. Appl. Math., USSR Acad. Sc., Moscow, 1981 (in Russian).
2.66. G. P. Voskresensky, *Comp. Meth. Appl. Mech. and Eng.* 19: 257-75 (1979).

2.67. G. P. Voskresensky, M. G. Orlova, and V. A. Stebunov, Preprint No. 67, Keldysh Inst. Appl. Math., USSR Acad. Sc., Moscow, 1981 (in Russian).
2.68. N. N. Yanenko, *Method of Fractional Steps for Solution of Multidimensional Problems in Mathematical Physics*, Nauka, Novosibirsk, 1967 (in Russian).
2.69. V. M. Kovenya and N. N. Yanenko, *Method of Splitting in Gasdynamic Problems*, Nauka, Novosibirsk, 1981 (in Russian).
2.70. R. W. MacCormac, *The Effect of Viscosity in Hypervelocity Impact Cratering*, AIAA Pap., No. 364, 1969.
2.71. A. P. Bazzhin and I. F. Chelysheva, *Uch. Zap. Tsentr. Aero-gidrodinam. Inst.*, 5, 5: 46-54 (1974).
2.72. I. F. Chelysheva, *Uch. Zap. Tsentr. Aero-gidrodinam. Inst.*, 8, 2: 103-5 (1977).
2.73. A. M. Blokhin, *Izv. Sib. Otd. Akad. Nauk SSSR, Ser. Tekhn. Nauk*, vyp. 1, 3: 84-6 (1974).
2.74. Yu. I. Lobanovsky, *Uch. Zap. Tsentr. Aero-gidrodinam. Inst.*, 8, 6: 22-33 (1977).
2.75. Yu. I. Lobanovsky, *Uch. Zap. Tsentr. Aero-gidrodinam. Inst.*, **11**, 6: 58-65 (1980).
2.76. V. F. Volkov, in: *Problems of Development and Exploitation of Applied Program Packets*, Novosibirsk, 1981, p. 98 (in Russian).
2.77. V. F. Volkov, Preprint No. 43, Inst. Theor. and Appl. Mech. Siberian Branch USSR Acad. Sc., Novosibirsk, 1981 (in Russian).
2.78. L. G. Vasenov, V. F. Volkov, and N. F. Vorobyev, in: *Problems of Aerodynamics of Bodies of Three-dimensional Configurations*, Inst. Theor. and Appl. Mech. Siberian Branch USSR Acad. Sc., Novosibirsk, 1981, p. 49 (in Russian).
2.79. V. P. Kotenev, V. I. Sakharov, and G. A. Tirsky, in: *Gas Dynamics of Nonequilibrium Processes*, Novosibirsk, 1981, p. 141-5 (in Russian).
2.80. J. Crank and P. Nicolson, *Proc. Cambridge Phil. Soc.*, 43, 50: 50-67 (1947).
2.81. V. I. Sakharov and G. A. Tirsky in: *Supersonic Three-dimensional Flows with Physico-chemical Transformations*, Izd. MGU, Moscow, 1981 (in Russian).
2.82. N. V. Pogorelov and Yu. D. Shevelev, *Chisl. Metody Mekh. Sploshn. Sredy*, 12, 6: 65-79 (1981).
2.83. V. I. Sakharov, V. P. Kotenev, and G. A. Tirsky, in: *Supersonic Three-dimensional Flows with Physico-chemical Transformations*, Izd. MGU, Moscow, 1981 (in Russian).
2.84. D. S. Chaussee, T. Holtz, and P. Kutler, *Inviscid Supersonic-Hypersonic Flow Fields and Aerodynamics Form Shock-capturing Technique Calculations*, AIAA Paper, No. 837, 1975.
2.85. V. I. Sakharov and Yu. D. Shevelev, *Izv. Akad. Nauk SSSR, Ser. Mekh. Zhidk. i Gaza*, 4: 172-5 (1980).
2.86. V. P. Galinsky and V. I. Timoshenko, *Uch. Zap. Tsentr. Aero-gidrodinam. Inst.*, 9, 6: 48-55 (1978).
2.87. V. P. Galinsky and V. I. Timoshenko, *Kosmich. Issled. na Ukraine*, 13: 43-8 (1979).
2.88. V. P. Galinsky and V. I. Timoshenko, *Kosmich. Issled. na Ukraine*, 15: 89-92 (1981).
2.89. G. A. Tarnavsky, *Chisl. Metody Mekh. Sploshn. Sredy*, 10, 6: 128-40 (1979).
2.90. V. M. Kovenya and G. A. Tarnavsky, *Chisl. Metody Mekh. Sploshn. Sredy*, 9, 1: 65-83 (1978).
2.91. V. M. Kovenya, G. A. Tarnavsky, and N. N. Yanenko, *Zh. Vychisl. Mat. i Mat. Fiz.*, 20, 6: 1465-82 (1980).
2.92. O. M. Belotserkovskii and Yu. M. Davydov, *Chisl. Metody Mekh. Sploshn. Sredy*, 1, 6: 19-43 (1970).

2.93. O. M. Belotserkovskii and Yu. M. Davydov, *Method of Coarse Particles in Gas Dynamics*, Nauka, Moscow, 1982 (in Russian).
2.94. Yu. M. Davydov, *Dokl. Akad. Nauk SSSR*, 247, 6: 1346-50 (1979).
2.95. J. Pyzik and A. Tarnogrodzki, *2nd, GAMM Conf. Numeric. Meth. Fluid Mech., Proc. DEVLR*: 144-51 Köln, 1978.
2.96. A. P. Bazzhin and S. V. Pirogova, *Uch. Zap. Tsentr. Aero-gidrodinam. Inst.*, 4, 5: 9-17 (1973).
2.97. A. P. Bazzhin and S. V. Pirogova, *Uch. Zap. Tsentr. Aero-gidrodinam., Inst.* 6, 6: 89-91 (1975).
2.98. P. D. Lax, *Communs. Pure Appl. Math.* 7: 159-93 (1954).
2.99. V. V. Rusanov, *Zh. Vychisl. Mat. i Mat. Fiz.*, 1, 2: 267-79 (1961).
2.100. N. S. Bachmanova, V. N. Lapygin, and Yu. M. Lipnitsky, *Izv. Acad. Nauk SSSR, Ser. Mekh. Zhidk. i Gaza*, 6: 79-84 (1973).
2.101. V. I. Lapygin, *Izv. Akad. Nauk SSSR, Ser. Mekh. Zhidk. i Gaza*, 3: 180-5 (1971).
2.102. V. I. Lapygin, *Izv. Akad. Nauk SSSR, Ser. Mekh. Zhidk. i Gaza*, 3: 114-19 (1973).
2.103. V. I. Lapygin and N. A. Ostapenko, *Izv. Akad. Nauk SSSR, Ser. Mekh. Zhidk. i Gaza*, 1: 112-21 (1973).
2.104. D. A. Babaev, *Zh. Vychisl. Mat. i Mat. Fiz.*, 2, 2: 278-89 (1962).
2.105. D. A. Babaev, *Zh. Vychisl. Mat. i Mat. Fiz.*, 2, 6: 1081-101 (1962).
2.106. A. P. Shashkin, *Chisl. Metody Mekh. Sploshn. Sredy*, 6, 1: 109-21 (1975).
2.107. A. A. Samarsky and Yu. P. Popov, *Difference Schemes in Gas Dynamics*, Nauka, Moscow, 1975 (in Russian).
2.108. V. V. Rusanov, in: *Theoretical Hydromechanics*, No. 11, vyp. 3, Oborongiz, Moscow, 1953 (in Russian).
2.109. V. V. Rusanov, *Zh. Vychisl. Mat. i Mat. Fiz.*, 3, 3: 508-27 (1963).
2.110. P. I. Chushkin, *Method of Characteristics for Three-dimensional Supersonic Flows*, Comp. Center USSR Acad. Sc., Moscow, 1968 (in Russian).
2.111. P. I. Chushkin, in: *Progress Aeronaut. Sc.*, Vol. 9, Pergamon Press, Oxford, 1968, p. 41.
2.112. Yu. N. Podladchikov, *Izv. Akad. Nauk SSSR, Ser. Mekhanika*, 4: 3-12 (1965).
2.113. V. B. Minostsev, *Izv. Akad. Nauk SSSR, Ser. Mekh. Zhidk. i Gaza*, 2: 126-33 (1967).
2.114. Z. D. Zapryanov and V. B. Minostsev, *Izv. Akad. Nauk SSSR, Ser. Mekhan. i Mashinostr.*, 5: 20-4 (1964).
2.115. V. B. Minostsev, G. F. Telenin, and G. P. Tinyakov, *Dokl. Akad. Nauk SSSR*, 179, 2: 304-7 (1968).
2.116. M. G. Lebedev, V. B. Minostsev, G. F. Telenin, and G. P. Tinyakov, *Izv. Akad. Nauk SSSR, Ser. Mekh. Zhidk. i Gaza*, 2: 107-11 (1969).
2.117. V. B. Minostsev and G. F. Telenin, *Nauchn. Trudy Inst. Mekh. MGU*, 5: 4-19 (1970).
2.118. Yu. N. Dyakonov and V. B. Minostsev, *Nauchn. Trudy Inst. Mekh. MGU*, 5: 20-25 (1970).
2.119. D. S. Butler, *Proc. Roy. Soc.*, London, A225, 1281: 232-52 (1960).
2.120. K. M. Magomedov, *Zh. Vychisl. Mat. i Mat. Fiz.*, 6, 2: 313-25 (1966).
2.121. K. M. Magomedov, *Izv. Akad. Nauk SSSR, Ser. Mekh. Zhidk. i Gaza*, 3: 130-7 (1967).
2.122. K. M. Magomedov, *Dokl. Akad. Nauk SSSR*, 171, 6: 1297-300 (1966).
2.123. V. V. Lunev, K. M. Magomedov, and V. G. Pavlov, *Supersonic Flow past Blunted Cones, Taking into Account Equilibrium Physical and Chemical Transformations*, Comp. Center USSR Acad. Sc., Moscow, 1968 (in Russian).
2.124. K. M. Magomedov and A. S. Kholodov, *Izv. Akad. Nauk SSSR, Ser. Mekh. Zhidk. i Gaza* 4: 159-63 (1967).
2.125. C. Ferrari. *J. Aeronaut, Sc.*, 16, 7: 411-34 (1949).

2.126. O. N. Katskova and P. I. Chushkin, *Dokl. Akad. Nauk SSSR*, **154**, 1: 26-9 (1964).
2.127. O. N. Katskova and P. I. Chushkin, *Zh. Vychisl. Mat. i Mat. Fiz.*, 5, 3: 503-18 (1965).
2.128. O. N. Katskova and P. I. Chushkin, *Izv. Akad. Nauk SSSR, Ser. Mekh. Zhidk. i Gaza*, 3, 124-30 (1967).
2.129. O. N. Katskova and P. I. Chushkin, in: *Aerospace Proceedings, 1966*, Vol. 1, Macmillan, London, 1967, p. 309.
2.130. O. N. Katskova and P. I. Chushkin, *Zh. Vychisl. Mat. i Mat. Fiz.*, 8, 5: 1049-62 (1968).
2.131. O. N. Katskova and P. I. Chushkin, *Izv. Akad. Nauk SSSR, Ser. Mekh. Zhidk. i Gaza*, 2: 182-5 (1970).
2.132. P. I. Chushkin, M. M. Golomazov and E. I. Grigoryev, *Proc. 9th Int. Symp. Space Technol. and Sc.*, Tokyo, 1971, p. 339-49.
2.133. P. I. Chushkin, *J. Comp. Phys.*, 5, 3: 572-86 (1970).
2.134. G. Moretti, *AIAA Journal*, **1**, 9: 2192-3 (1963).
2.135. J. V. Rakich, *AIAA Journal*, **5**, 10: 1906-8 (1967).
2.136. J. V. Rakich, H. E. Bailey, and C. Park, *AIAA Paper*, No. 835 (1975).
2.137. R. Camarero, *Aeronaut. Quart.*, **27**, 1: 75-86 (1976).
2.138. E. I. Grigoryev and K. M. Magomedov, *Zh. Vychisl. Mat. i Mat. Fiz*,. **9**, 6: 1413-19 (1969).
2.139. V. M. Borisov and I. E. Mikhailov, *Zh. Vychisl. Mat. i Mat. Fiz.*, **18**, 5: 1243-52 (1978).
2.140. K. M. Magomedov and A. S. Kholodov, *Zh. Vychisl. Mat. i Mat. Fiz.*, 9: 2, 373-86 (1969).
2.141. R. Courant, E. Isaacson, and M. Rees, *Communs Pure and Appl. Math.*, 5: 243-55 (1952).
2.142. O. M. Belotserkovskii, Yu. P. Golovachev, V. G. Grudnitsky, Yu. M. Davydov, V. K. Dushin, A. I. Tolstykh, V. N. Fomin, and A. S. Kholodov, *Numerical Analysis of Modern Problems in Gas Dynamics*, Nauka, Moscow, 1974 (in Russian).
2.143. V. I. Kosarev and K. M. Magomedov, *Zh. Vychisl. Mat. i Mat. Fiz.*, **13**, 4: 923-37 (1973).
2.144. V. I. Kosarev, *Zh. Vychisl. Mat. i Mat. Fiz.*, **11**, 5: 1262-71 (1971).
2.145. A. G. Reshetin, E. N. Lychkin, V. M. Kotov, and A. N. Shchelkonogov, *Chisl. Methody Mekh. Sploshn. Sredy*, **11**, 6: 110-22 (1980).
2.146. A. S. Kholodov, *Zh. Vychisl. Mat. i Mat. Fiz.*, 18, 6: 1476-92 (1978).
2.147. V. S. Kamenetsky and L. I. Turchak, *Supersonic Nonuniform Ideal Gas Flow past Bodies*, Comp. Center USSR Acad. Sc., Moscow, 1982 (in Russian).
2.148. O. A. Onufrieva, V. B. Pirogov, and A. S. Kholodov, in: *Jet Fluid Flows*, Proc. of All-Union Sc. Conf., Part 2, Novopolotsk, 1982, p. 60 (in Russian).
2.149. O. M. Belotserkovskii, S. D. Osetrova, V. N. Fomin, and A. S. Kholodov, *Zh. Vychisl. Mat. i Mat. Fiz.*, **17**, 4: 992-1003 (1974).
2.150. A. A. Kostuzik, *Proc. 7th Conf. of Young Sc., Moscow Physico-technical Inst.*, Part 2, MFTI, Moscow, 1982.
2.151. A. A. Dorodnitsyn, *Proc. 3rd All-Union Math. Congr.*, Vol. 3, 1956, Izd. Akad. Nauk SSSR, Moscow, 1958 (in Russian).
2.152. A. A. Dorodnitsyn, *Zh. Prikl. Mekh. i Tekhn. Fiz.*, 3: 11-118 (1960).
2.153. O. M. Belotserkovskii and P. I. Chushkin, *Zh. Vychisl. Mat. i Mat. Fiz.*, **2**, 5: 731-59 (1962).
2.154. O. M. Belotserkovskii, *Dokl. Akad. Nauk SSSR*, **113**, 3: 509-12 (1957).
2.155. O. M. Belotserkovskii, *The Analysis of Flow Past Axisymmetric Bodies with Detached Shock Wave (Computational Formulas and Tales of Flow Fields)*, Comp. Center, USSR Acad. Sc., Moscow, 1961.
2.156. O. M. Belotserkovkii, A. Bulekbaev, M. M. Golomazov, V. G. Grudnit-

sky, V. K. Dushin, V. F. Ivanov, Yu. P. Lun'kin, F. D. Popov, G. M. Ryabinkov, G. Ya. Timofeeva, A. I. Tolstykh, V. N. Fomin, and F. V. Shugaev, *Supersonic Gas Flow Past Blunted Bodies. Theoretical and Experimental Investigations*, 2nd. ed., Comp. Center USSR Acad. Sc., Moscow, 1967 (in Russian).
2.157. A. N. Minailos, *Zh. Vychisl. Mat. i Mat. Fiz.*, 4, 1: 171-7 (1964).
2.158. I. G. Kozlova and A. N. Minailos, *Zh. Vychisl. Mat. i Mat. Fiz.*, 7, 3: 594-608 (1967).
2.159. G. D. Waldman, *AIAA Pap.*, No. 28 (1965).
2.160. V. Ya. Mitnitsky, *Proc. 18th Sc. Conf. of Moscow Physico-Technical Inst., 1972, Ser. Aeromechanics., Control Pros.* Dolgoprudnyi, 1973 (in Russian).
2.161. P. I. Chushkin, *Zh. Vychisl., Mat. i Mat. Fiz.*, 20, 6: 1525-35 (1980).
2.162. M. M. Golomazov, *Zh. Vychisl. Mat. i Mat. Fiz.*, 11, 4: 1063-71 (1971).
2.163. M. M. Golomazov, in: *Numerical Methods of Mechanics of Continuous Medium*, Vol. 6, No. 4, Novosibirsk, 1975, p. 31, (in Russian).
2.164. P. I. Chushkin and V. V. Shchennikov, *Inzh.-fiz. Zh.*, 3, 7: 88-94 (1960).
2.165. P. I. Chushkin, in: *Collected Works on Hydromechanics*, Comp. Center USSR Acad. Sc., Moscow, 1970 (in Russian).
2.166. A. P. Bazzhin, *Inzh. Zh.*, 4, 2: 242-6 (1964).
2.167. H. Kennet, *The Inviscid Supersonic Flow on the Windward Side of a Delta Wing*, JAS Paper No. 55, 1963.
2.168. A. P. Bazzhin, *Izv. Akad. Nauk SSSR, Ser. Mekh. Zhidk. i Gaza*, 5: 104-5 (1966).
2.169. E. A. Akinrelere, *J. Fluid. Mech.*, 44, 1: 113-27 (1970).
2.170. P. I. Chushkin, *Zh. Vychisl. Mat. i Mat. Fiz.*, 8, 4: 853-64 (1968).
2.171. S. M. Gilinsky, G. F. Telenin, and G. P. Tinyakov, *Izv. Akad. Nauk SSSR, Ser. Mekh. i Mashinostr.*, 4: 9-28 (1964).
2.172. G. F. Telenin and G. P. Tinyakov, *Dokl. Akad. Nauk SSSR*, 154, 5: 1056-8 (1964).
2.173. G. P. Tinyakov, *Izv. Akad. Nauk SSSR, Ser. Mekhanika*, 6: 10-19 (1965).
2.174. V. P. Shkadova, *Nauchn. Trudy Inst. Mekh. MGU*, 5: 26-34 (1970).
2.175. O. N. Semenikhina and V. P. Shkadova, *Izv. Akad. Nauk SSSR, Ser. Mekh. Zhidk. i Gaza*, 2: 99-103 (1973).
2.176. A. K. Burdelnyi, V. B. Minostsev, and V. P. Shkadova, *Nauchn. Trudy Inst. Mekh. MGU*, 30: 149-56 (1973).
2.177. M. M. Golomazov and A. P. Zyuzin, *Zh. Vychisl. Mat. i Mat. Fiz.*, 15, 5: 1349-55 (1975).
2.178. M. M. Golomazov and A. P. Zyuzin, *Izv. Akad. Nauk. SSSR, Ser. Mekh. Zhidk. i Gaza*, 4: 143-5 (1979).
2.179. O. M. Belotserkovskii, M. M. Golomazov, and O. A. Zhuravleva, *Izv. Akad. Nauk SSSR, Ser. Mekh. Zhidk. i Gaza*, 1: 22-7 (1982).
2.180. O. M. Belotserkovskii, *Izv. Akad. Nauk SSSR, Ser. Mekh. Zhidk. i Gaza*, 1: 5-17 (1981).
2.181. N. A. Makhin and V. F. Syagaev. *Izv. Akad. Nauk SSSR, Ser. Mekh. Zhidk. i Gaza*, 1: 140-2 (1966).
2.182. A. P. Bazzhin and I. F. Chelysheva., *Izv. Akad. Nauk SSSR, Ser. Mekh. Zhidk. i Gaza*, 3: 119-23 (1967).
2.183. A. P. Bazzhin, O. N. Trusova, and I. F. Chelysheva, *Izv. Akad. Nauk SSSR, Ser. Mekh. Zhidk. i Gaza*, 4: 45-51 (1968).
2.184. A. P. Bazzhin, O. N. Trusova, and I. F. Chelysheva, *Uch. Zap. Tsentr. Aero-gidrodinam. Inst.*, 1, 2: 46-52 (1970).
2.185. M. Holt and D. E. Ndefo, *J. Comput. Phys.*, 5, 3: 463-86 (1970).
2.186. C. A. J. Fletcher, *Lect. Notes Phys.*, 35: 161-6 (1975).
2.187. Yu. N. Dyakonov and N. A. Zaitseva, *Izv. Akad. Nauk SSSR, Ser. Mekhan. i Mashinostr.*, 1: 118-23 (1963).
2.188. V. V. Rusanov, *Three-dimensional Supersonic Gas Flow Past Smooth Blunt Bodies*, Proc. II Internat. Congr. Appl. Mech., p. 774-8 (1964).
2.189. G. F. Voskresensky, *Zh. Vychisl. Matem. i Mat. Fiz.*, 24, 6: 900-15 (1984).

3 Grid-characteristic Methods in Multidimensional Problems of Gas Dynamics

O. M. Belotserkovskii, *Mem. USSR Acad. Sc.*
A. S. Kholodov, *D.Sc. (Phys.-Math.), and*
L. I. Turchak, *Cand. Sc. (Phys.-Math.)*

Multidimensional systems of hyperbolic equations are used for simulating a wide range of problems which are important from a practical point of view. These problems include nonstationary and supersonic stationary problems of gas dynamics and magnetic gas dynamics, dynamic problems of the mechanics of a deformable rigid body for many models in this field, and so on.

The basic notions of hyperbolic equations lie in their characteristic properties. The long experience of the use of various methods of characteristics ([3.1-3.7] and others; the simplest of these methods were proposed by Masso in the beginning of this century) shows that the finite difference approximation of not the original equations but the equivalent compatibility relations along certain characteristic directions gives them a certain advantage over the conventional grid methods. In particular, we can construct the computational algorithm in the most natural way on the integration domain boundaries, make a transition from one scalar equation to a system of hyperbolic equations, take into account the domain of dependence of solutions to a certain extent, and so on.

The advantages of the method of characteristics are manifested most completely in the case of one-dimensional equations, especially in combination with a fixed difference grid (inverse methods or grid-characteristic methods). In the multidimensional case, however, the positive aspects of the grid-characteristic method can be retained by applying quite universal and effective algorithms, for example, the methods of splitting in spatial parameters ([3.8-3.13], etc.), which can be used to extend almost any "one-dimensional" method to the multidimensional case.

When methods of splitting according to physical processes are used, the grid-characteristic approach can be advantageously applied for approximating the hyperbolic part of more general operators, the part frequently associated with the most difficult computational problem.

The methods developed for linear equations and systems, which ensure that the difference analogues of conservation laws are satisfied (this is important for a computation of discontinuous solutions), can be generalized to the nonlinear case by using the equally effective

and universal methods of Runge-Kutta type [3.14] or the integro-interpolation method [3.15].

The general methods listed above for constructing difference schemes for multidimensional nonlinear equations of hyperbolic type are used in this paper together with the method of indeterminate coefficients (developed here in a somewhat nontraditional form by introducing linear spaces of these coefficients) while constructing difference schemes for simplest scalar one-dimensional transport equations which form the basis of multidimensional nonlinear systems of hyperbolic equations. For such simple equations, we can carry out a detailed analysis of all linear difference schemes emerging from some grid model and choose the schemes that are most effective in certain respects. The introduction of free parameters (to be fixed later in accordance with certain considerations, which may even be purely heuristic) into difference schemes is quite common in computational practice, say, for regularizing the numerical solutions. In particular, we can mention the fundamental work [3.16] dealing with these problems. Using the methods described above for systematically generalizing these "elementary schemes" to the case of one-dimensional or multidimensional linear and nonlinear equations and systems, we can obtain effective algorithms by and large, which preserve some of the positive aspects of the "elementary schemes". We would like to emphasize once again the significant role of the characteristic properties of hyperbolic equations which form the basis of the approach used in this paper for constructing difference schemes. The theoretical constructions described in Secs. 3.1-3.3 are based on the works [3.17-3.20].

From the application point of view, the results mentioned in this paper are important for determining the aerogasdynamics of bodies having complex geometric forms in three-dimensional supersonic flows, including nonstationary problems and the related problems of plasma physics and mechanics of deformable rigid bodies. The main attention is devoted to the methodical aspect of the solution of such problems on the basis of various approaches and formulations, and to the effects connected with the multidimensional nature of the problems under consideration. A more detailed description of the results given in Sec. 3.4 can be found in [3.21-3.37].

3.1. DIFFERENCE SCHEMES FOR SIMPLE ONE-DIMENSIONAL HYPERBOLIC EQUATIONS

3.1.1. Let us first consider the transport equation

$$w_t + \lambda w_x = 0, \quad \lambda = \text{const}, \tag{3.1.1}$$

which is the simplest of hyperbolic equations. In the domain of integration, we introduce a difference grid which, say, is uniform

in x and t: $x_m = mh$, $m = 0, \pm 1, \pm 2, \ldots$, $t^n = n\tau$, $n = 0, 1, 2, \ldots$. As usual, we use the notation $w_m^n = w(t^n, x_m)$. To approximate (3.1.1), we choose an arbitrary grid model including a certain set of nodal points $\{t^{n+\nu}, x_{m+\mu}\}$, $\nu = 1, 0, -1, \ldots$, $\mu = 0, \pm 1, \ldots$ (Fig. 3.1) and write all admissible linear difference schemes corresponding to this model in the form

$$w_m^{n+1} = \sum_{\mu,\,\nu} \alpha_\mu^\nu w_{m+\mu}^{n+\nu}, \tag{3.1.2}$$

where α_μ^ν are indeterminate coefficients.

Using the expansion of $w_{m+\mu}^{n+\nu}$ into a Taylor series in the vicinity of any point (irrespective of what point it is for $\lambda = \text{const}$, for

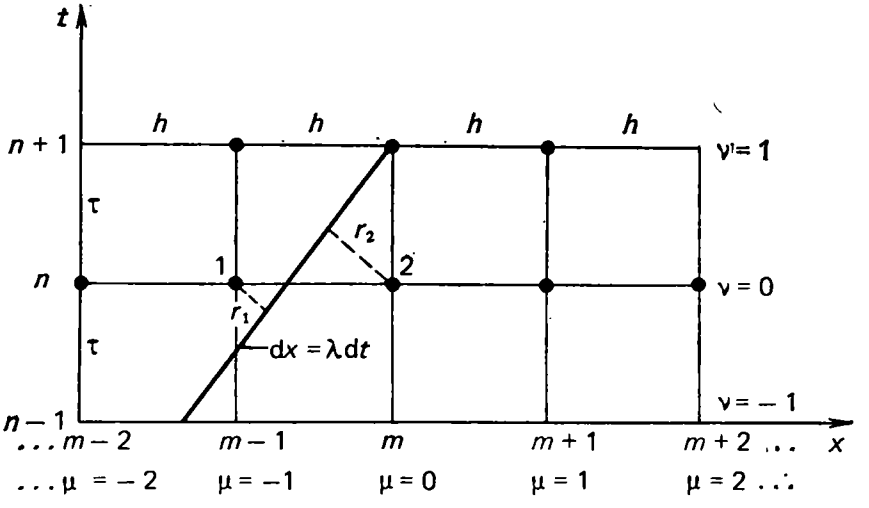

Fig. 3.1.

example, near (t^n, x_m)) and Eq. (3.1.1) as well as its corollary $\partial^{k+l} w/\partial t^k \partial x^l = (-1)^k \lambda^k \partial^{k+l} w/\partial x^{k+l}$, we obtain after substituting the expansion of $w_{m+\mu}^{n+\nu}$ into (3.1.2)

$$\begin{gathered} w_t + \lambda w_x = \frac{\delta_0 w}{\tau} + \frac{h\delta_1 w_x}{\tau} + \frac{h^2 \delta_2 w_{xx}}{2\tau} + \frac{h^3 \delta_3 w_{xxx}}{3!\,\tau} + \ldots, \\ \delta_k = -(-\sigma)^k + \sum_{\mu,\,\nu} (\mu - \nu\sigma)^k \alpha_\mu^\lambda, \quad \sigma = \lambda\tau/h, \\ k = 0, 1, 2, 3, \ldots. \end{gathered} \tag{3.1.3}$$

Then the conditions of approximation of Eq. (3.1.1) by the difference expression (3.1.2) (on the solutions of (3.1.1)) will be linear with respect to the indeterminate coefficients of the equation

$$\begin{gathered} \delta_k = c_k \alpha - b_k = 0, \quad c_k = \{c_{k\mu}^\nu\}, \\ c_{k\mu}^\nu = (\mu - \nu\sigma)^k, \quad b_k = (-\sigma)^k, \end{gathered} \tag{3.1.4}$$

where we consider the linear space of indeterminate coefficients $\alpha = \{\alpha_\mu^\nu\}$. The dimension p of this space is less by unity than the number of nodes in the grid model, and $\mathbf{c}_k$ are vectors having the same dimension as α, in particular, $\mathbf{c}_0 = \{1, 1, \ldots\}$.

It can be seen from (3.1.3) that the necessary and sufficient condition for approximation with the lowest, i.e. first, order of accuracy $O(\tau, h)$ is that Eq. (3.1.4) be satisfied for $k = 0, 1$, i.e.

$$\delta_0 = -1 + \sum_{\mu, \nu} \alpha_\mu^\nu = 0, \quad \delta_1 = \sigma + \sum_{\mu, \nu} (\mu - \nu\sigma)\, \alpha_\mu^\nu = 0. \tag{3.1.5}$$

For $k = 0, 1, \ldots, K$, the relations (3.1.4) serve as conditions for higher, viz. Kth-order approximations on the solutions of (3.1.1). Obviously, the approximation order K and the number $p + 1$ of points in the grid model must be connected through the relation $K \leqslant p - 1$ so that the linear system (3.1.4) has a solution. Moreover, this inequality should preferably be strict so that some type of optimization can be carried out.

Besides the space $\alpha = \{\alpha_\mu^\nu\}$, we shall also use the space $\tilde{\alpha} = \{\alpha_\mu^\nu\}$ whose dimension is less than that of α by two, and which is obtained by eliminating with the help of (3.1.5) any two coefficients, say, α_{-1}^0 and α_1^0:

$$\alpha_{-1}^0 = (1 + \sigma - \sum_{\mu, \nu} (1 - \mu + \nu\sigma)\, \alpha_\mu^\nu)/2,$$

$$\alpha_1^0 = (1 - \sigma - \sum_{\mu, \nu} (1 + \mu - \nu\sigma)\, \alpha_\mu^\nu)/2, \tag{3.1.6}$$

that are usually present in the grid model. In (3.1.6) and hereafter, whenever $\tilde{\alpha}$ is encountered, the sum naturally does not contain two points: $\mu = -1$, $\nu = 0$ and $\mu = 1$, $\nu = 0$. Any point in such a space corresponds to a certain difference scheme of the first order of accuracy, while conditions which have a higher order of accuracy than the first ((3.1.4) for $k \geqslant 2$) are also linear equations in the remaining free coefficients α_μ^ν:

$$\tilde{\delta}_k = \tilde{\mathbf{c}}_k \tilde{\alpha} - \tilde{b}_k = 0, \quad \tilde{\mathbf{c}}_k = \{\tilde{c}_{k\mu}^\nu\},$$

$$\tilde{\alpha} = \{\alpha_\mu^\nu\}, \quad k = 2, 3, \ldots, \tag{3.1.7}$$

$$\tilde{c}_{k\mu}^\nu = (\mu - \nu\sigma)^k - 1, \quad b_k = \sigma^k - 1 \text{ for even } k,$$

$$\tilde{c}_{k\mu}^\nu = (\mu - \nu\sigma)\,((\mu - \nu\sigma)^{k-1} - 1), \quad \tilde{b}_k = \sigma\,(1 - \sigma)^{k-1} \text{ for odd } k$$

and define a certain hyperplane in the space $\tilde{\alpha}$ for each k. In particular, the second-order approximation equations for solutions of (3.1.1) will be relations (3.1.4) for $k = 0, 1, 2$ or (3.1.7) for $k = 2$.

For third-order schemes, the role of such equations is played by relations (3.1.4) for $k = 0, 1, 2, 3$ or the intersection of two hyperplanes (3.1.7) for $k = 2$ and $k = 3$, and so on until the chosen grid model is completely exhausted.

Besides the approximation conditions, the foremost restriction that should be imposed on the indeterminate coefficients α_μ^ν is the requirement that the stability conditions be satisfied [3.16, 3.38], for example, by using the conventional approach for the investigation of stability of difference schemes, i.e. solution of the type $w_m^n = q^n \exp(im\varphi)$. In the space of coefficients $\boldsymbol{\alpha}$ or $\tilde{\boldsymbol{\alpha}}$, stability conditions of the type

$$|q(\alpha_\mu^\nu, \varphi)| \leqslant 1 \tag{3.1.8}$$

(or analogous conditions obtained by using other stability criteria) isolate a certain domain of stable difference schemes. The explicit determination of domains of the type (3.1.8) for arbitrary grid models is a quite cumbersome problem, although it has been sufficiently formalized (it is required to find in the space $\tilde{\boldsymbol{\alpha}} = \{\alpha_\mu^\nu\}$ the envelope of one-parametric family of curves $f(\varphi) = |q(\alpha_\mu^\nu, \varphi)| - 1 = 0$, where φ is eliminated as usual by employing the condition $\partial f/\partial\varphi = 0$). We shall not be considering this problem in the general form in the present paper.

The requirements imposed on the difference schemes from modern standpoint are not confined just to approximation and stability. We shall consider some of these requirements which are formulated as further restrictions on the remaining free coefficients α_μ^ν and which define certain subdomains in (3.1.8) in the space $\boldsymbol{\alpha}$ or $\tilde{\boldsymbol{\alpha}}$. In this case, we use a hypothesis which, to our mind, is quite natural and according to which the difference schemes having close points in the space of coefficients (for example, in the sense of the ordinary Euclidean metric)

$$r = |\tilde{\alpha}_1 - \tilde{\alpha}_2| = \sqrt{\sum_{\mu,\nu} (\alpha_{1\mu}^\nu - \alpha_{2\mu}^\nu)^2}, \tag{3.1.9}$$

have also similar properties.

3.1.2. Difference schemes of the type (3.1.2) having non-negative coefficients

$$\alpha_\mu^\nu \geqslant 0, \tag{3.1.10}$$

which were first introduced by Fridrichs [3.39] for hyperbolic equations, form an important class. Properties of such schemes (stability, convergence, etc.) have been discussed many times in

literature and are widely known (monotonic or majorant schemes in a different terminology). In particular, (3.1.10) is a sufficient condition for stability of difference schemes, and hence the domain defined by relations (3.1.10) is contained in (3.1.8).

Together with the first-order approximation conditions (3.1.5), inequalities (3.1.10) form a convex polyhedral set in the space $\alpha = \{\alpha_\mu^\nu\}$, the rank of the system of restrictions for this set being equal to the dimension of α, i.e. p. Let us now find the general solution of systems (3.1.5), (3.1.10). For this purpose, we have to determine the coordinates of the vertices of this closed polyhedron in the space of coefficients and use the well-known representation theorem.

It is well known from linear algebra that to find the vertices, we must consider all possible systems of p linearly indepedent equations including Eqs. (3.1.5) supplemented by $p - 2$ relations (3.1.10) in which the inequality is replaced by strict equality. The solution of each such system will define a vertex if the remaining two inequalities in (3.1.10) are satisfied. It can be seen that a possible vertex has a corresponding vector $\alpha_b = \{0, \ldots, 0, \alpha_{\mu_1}^{\nu_1}, 0, \ldots, 0, \alpha_{\mu_2}^{\nu_2}, 0, \ldots, 0\}$, in which only two components

$$\alpha_{\mu_1}^{\nu_1} = \bar{\mu}_2/(\bar{\mu}_2 - \bar{\mu}_1), \quad \alpha_{\mu_2}^{\nu_2} = -\bar{\mu}_1/(\bar{\mu}_2 - \bar{\mu}_1),$$
$$\bar{\mu}_l = \mu_l + (1 - \nu_l)\sigma, \quad l = 1, 2 \tag{3.1.11}$$

can assume nonzero values, while the remaining components α_μ^ν are equal to zero, i.e. all possible three-point models including the points (t^{n+1}, x_m), $(t^{n+\nu_1}, x_{m+\mu_1})$ and $(t^{n+\nu_2}, x_{m+\mu_2})$ correspond to possible vertices. Of all possible three-point models, the condition $\alpha_{\mu_1}^{\nu_1} \geqslant 0$, $\alpha_{\mu_2}^{\nu_2} \geqslant 0$ isolates only those for which the points $(t^{n+\nu_1}, x_{m+\mu_1})$ and $(t^{n+\nu_2}, x_{m+\mu_2})$ lie on opposite sides of the characteristic $dx = \lambda dt$ (one of these points may lie on the characteristic if $\sigma = \lambda\tau/h = j$ is an integer). In other words, (3.1.11) must be supplemented by the conditions

$$\bar{\mu}_1 < 0, \quad \bar{\mu}_2 > 0, \tag{3.1.12}$$

(if point *1* lies to the left of the characteristic $dx = \lambda\, dt$ and point *2* lies to the right of it, see Fig. 3.1).

After the coordinates of the vertices have been found, the representation theorem, which is applicable to system (3.1.5), (3.1.10), can be used to write the general solution (vector $\bar{\alpha}$) in the form of a linear combination of partial solutions (vectors α_b) with nonnegative coefficients γ_b whose sum is equal to unity, i.e.

$$\bar{\alpha} = \sum_b \gamma_b \alpha_b, \quad \gamma_b \geqslant 0, \quad \sum_b \gamma_b = 1. \tag{3.1.13}$$

Thus the relations (3.1.11)-(3.1.13) completely solve the problem of constructing the entire set of linear difference schemes with a positive approximation for arbitrary grid models.

By way of an example, we can consider the case $\lambda > 0$ and an implicit six-point model with nodes:

$$(t^{n+1}, x_{m-1}),\ (t^{n+1}, x_m),\ (t^{n+1}, x_{m+1}),$$
$$(t^n, x_{m-1}),\ (t^n, x_m),\ (t^n, x_{m+1}). \qquad (3.1.14)$$

Figures 3.2 and 3.3 show in coordinates $\tilde{\alpha} = \{\alpha_{-1}^1, \alpha_0^0, \alpha_1^1\}$ the domain of admissible values of these coefficients for first-order schemes

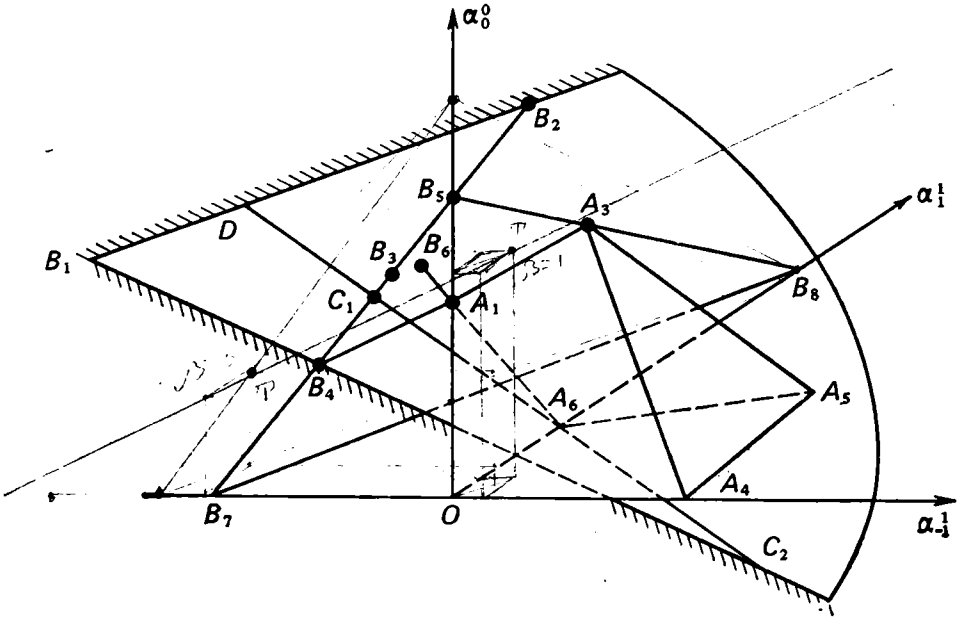

Fig. 3.2.

with restrictions (3.1.10): closed polyhedron with vertices O, A_1, A_3, A_4, A_5 and A_6 (Fig. 3.2, $\sigma = 0.5$) and pyramid $A_2A_3A_4A_5$ (Fig. 3.3, $\sigma = 2$). Point O corresponds to Lax's scheme [40] which is stable and monotonic for $|\sigma| \leqslant 1$:

$$\alpha_{-1}^1 = \alpha_0^0 = \alpha_1^1 = 0. \qquad (3.1.15)$$

Point A_1 is the scheme presented by Courant, Isaacson and Rees [3.1], which is stable and monotonic for $|\sigma| \leqslant 1$ ("explicit corner")

$$\alpha_{-1}^1 = \alpha_1^1 = 0, \quad \alpha_0^0 = 1 - |\sigma|. \qquad (3.1.16)$$

Point A_3 is the scheme proposed by Landau, Meiman and Khalatnikov [3.41], which is stable and monotonic for all σ ("implicit

corner")

$$\begin{aligned} &\text{for } \sigma > 0\text{: } \alpha^1_{-1} = \sigma/(1+\sigma),\ \alpha^0_0 = 1/(1+\sigma),\ \alpha^1_1 = 0,\\ &\text{for } \sigma < 0\text{: } \alpha^1_{-1} = 0,\ \alpha^0_0 = 1/(1-\sigma),\ \alpha^1_1 = -\sigma/(1-\sigma). \end{aligned} \tag{3.1.17}$$

Point A_1 for $|\sigma| \leqslant 1$ and point A_2 for $|\sigma| > 1$ together correspond to Carlsson's scheme (see [3.42]) which is stable and monotonic for all σ

$$\begin{aligned} &\text{for } |\sigma| \leqslant 1\text{: } \alpha^1_{-1} = \alpha^1_1 = 0,\ \alpha^0_0 = 1 - |\sigma|,\\ &\text{for } \sigma > 1\text{: } \alpha^1_{-1} = (\sigma-1)/\sigma,\ \alpha^0_0 = \alpha^1_1 = 0,\\ &\text{for } \sigma < -1\text{: } \alpha^1_{-1} = \alpha^0_0 = 0,\ \alpha^1_1 = (\sigma+1)/\sigma. \end{aligned} \tag{3.1.18}$$

The remaining coefficients α^0_{-1} and α^0_1 are defined by relations (3.1.6).

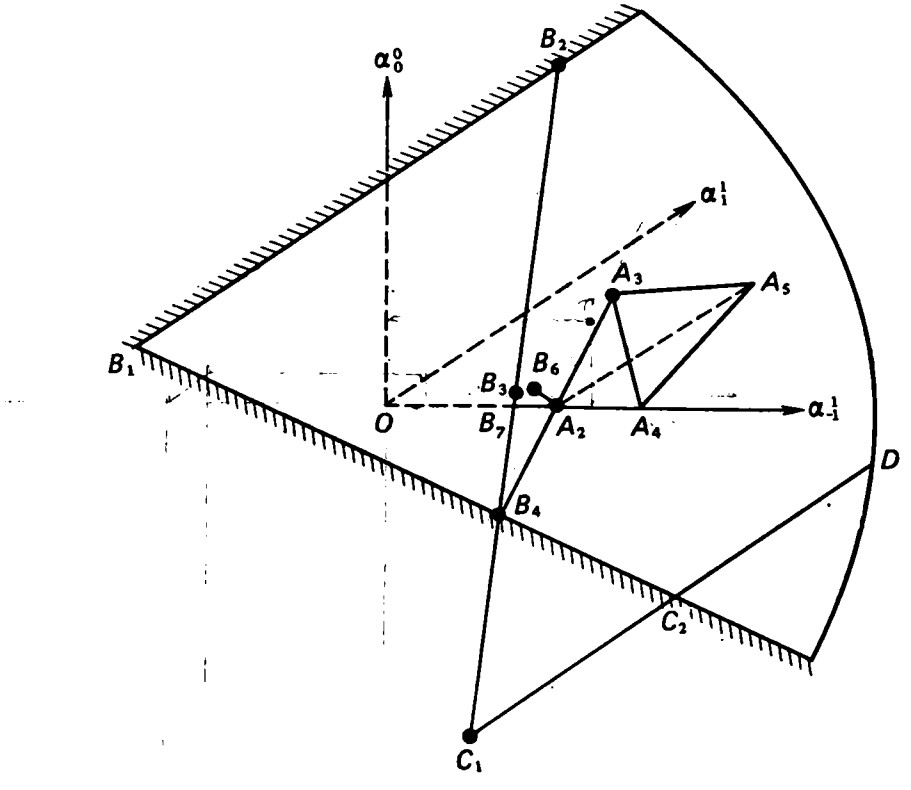

Fig. 3.3.

Analogous constructions for an explicit six-point model with nodes

$$(t^{n+1},\ x_m),\ (t^n,\ x_{m-2}),\ \ldots,\ (t^n,\ x_{m+2}) \tag{3.1.19}$$

are shown in Fig. 3.4 for $\sigma = 0.5$ and in Fig. 3.5 for $\sigma = 1.5$. These figures show in the space of coefficients $\tilde{\alpha} = \{\alpha^0_{-2}, \alpha^0_0, \alpha^0_2\}$ the do-

mains corresponding to difference schemes with a positive approximation (polyhedrons $OA_1A_3A_4A_5A_6$ and $A_7A_3A_4A_5$ respectively). Point O represents Lax's scheme (3.1.15), while point A_1 corresponds to the scheme (3.1.16) proposed by Courant, Isaacson and Rees.

3.1.3. Another quite general problem which can be formulated and solved by introducing a linear space of coefficients of difference

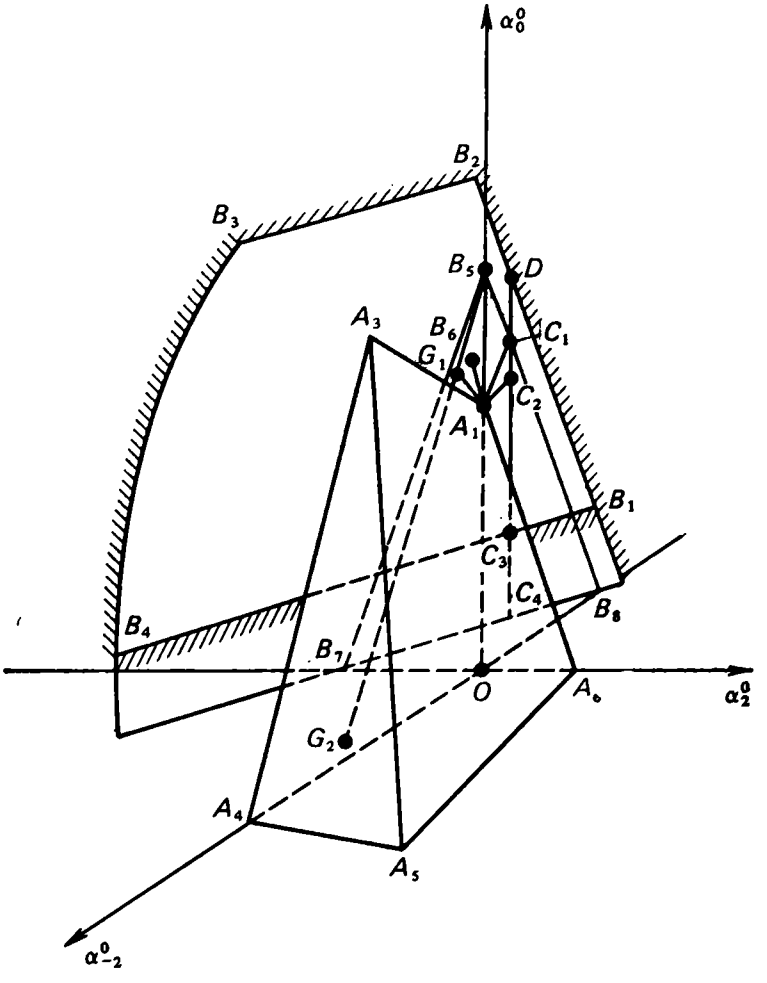

Fig. 3.4.

schemes consists in the following. For the first-order difference schemes with a positive approximation, the quantity $h^2\overline{\delta}_2/2\tau = h^2(c_2\overline{\alpha} - \sigma^2)/2\tau$ is the approximation viscosity coefficient in the first differential approximation (3.1.3) of scheme (3.1.2) when the restrictions (3.1.10) are satisfied, i.e. in $w_t + \lambda w_x = h^2\overline{\delta}_2 w_{xx}/2\tau$. On the other hand, $\overline{\delta}_2$ is the distance (with sign) from an arbitrary point $\overline{\alpha}$ of the polyhedron (3.1.5), (3.1.10) to the hyperplane $\delta_2 = 0$ ((3.1.4) for $k = 2$, on which all schemes of higher than the first-order

approximation lie). Directly calculating $\bar{\delta}_2$, we obtain

$$\bar{\delta}_2 = c_2\bar{\alpha} - \sigma^2 = \left(\sum_b \gamma_b c_2 \alpha_b\right) - \sigma^2 \sum_b \gamma_b$$

$$= \sum_b \gamma_b (c_2\alpha_b - \sigma^2) = \sum_b \gamma_b \delta_{2b} \geqslant 0, \tag{3.1.20}$$

since $\delta_{2b} = -\bar{\mu}_1\bar{\mu}_2 \geqslant 0$ and all $\gamma_b \geqslant 0 \left(\sum_b \gamma_b = 1\right)$ for each vertex. It follows from (3.1.20) that the closed polyhedron (3.1.5), (3.1.10) and the hyperplane (3.1.4) have no intersections for $k = 2$ except

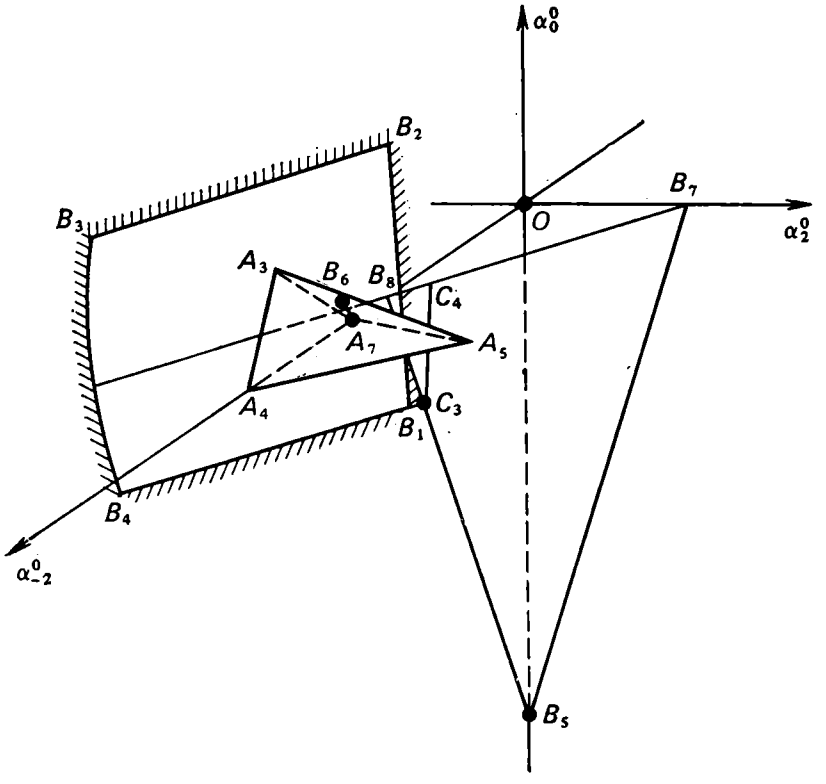

Fig. 3.5.

the practically unimportant case when the characteristic $dx = \lambda dt$ strictly passes through a node of the grid model (in this case they intersect at a vertex).

Consequently, there are no difference schemes of the type (3.1.2) that have a second-order accuracy on the solutions of (3.1.1) and satisfy inequalities (3.1.10). Since the validity of (3.1.4) for $k = 0$, 1, 2 is also a necessary condition for higher-order schemes, this conclusion applies to all schemes with higher than second-order approximation. Godunov [3.43] obtained a similar result (i.e. the absence of monotonic linear explicit two-layer second-order schemes

on the solutions of (3.1.1)) for explicit two-layer difference schemes in a different way.

For the explicit grid model (3.1.19), Figs. 3.4 and 3.5 show the plane $B_1, \ldots, B_8$ having the equation

$$\alpha_0^0 = 3(\alpha_{-2}^0 + \alpha_2^0) + (1 - \sigma^2). \tag{3.1.21}$$

On this plane lie all difference schemes with second-order accuracy on the solutions of (3.1.1), including the two-parametric family of stable schemes for $|\sigma| \leqslant 2$ (the boundaries of the stable scheme region are shown in Figs. 3.4 and 3.5 by hatched lines and are obtained from condition (3.1.8) by taking into account (3.1.21)). This plane also contains the straight line $DC_1 \ldots C_4$ which corresponds to difference schemes of third-order accuracy with the equation

$$\alpha_2^0 = \alpha_{-2}^0 + \sigma(1 - \sigma^2)/6, \quad \alpha_0^0 = 6\alpha_{-2}^0 + (1-\sigma^2)(\sigma + 2)/2. \tag{3.1.22}$$

For

$$(3 + 2\sigma)(\sigma^2 - 1)/24 \leqslant \alpha_{-2}^0 \leqslant \sigma(\sigma + 2)(\sigma^2 - 1)/24, \quad |\sigma| \leqslant 1, \tag{3.1.23}$$

this plane contains the segment DC_3 of stable schemes [3.14] and the only fourth-order scheme (point D) on this model, which is also stable for $|\sigma| \leqslant 1$, and for which

$$\alpha_{-2}^0 = (\sigma^2 - 1)\sigma(\sigma + 2)/24, \quad \alpha_0^0 = (\sigma^2 - 1)(\sigma^2 - 4)/9,$$
$$\alpha_2^0 = (\sigma^2 - 1)\sigma(\sigma - 2)/24. \tag{3.1.24}$$

Point B_5 corresponds to the well-known Lax-Wendroff scheme [3.44] with the coefficients

$$\alpha_{-2}^0 = \alpha_2^0 = 0, \quad \alpha_0^0 = 1 - \sigma^2. \tag{3.1.25}$$

Points C_1 and C_3 describe two difference schemes of third-order accuracy, for which

$$\alpha_{-2}^0 = -\sigma(1-\sigma^2)/6, \quad \alpha_0^0 = (1-\sigma^2)(2-\sigma)/2, \quad \alpha_2^0 = 0 \tag{3.1.26}$$

and

$$\alpha_{-2}^0 = (\sigma^2 - 1)(3 + 2\sigma)/24, \quad \alpha_0^0 = (1 - \sigma^2)/4,$$
$$\alpha_2^0 = (\sigma^2 - 1)(3 - 2\sigma)/24 \tag{3.1.27}$$

respectively.

Similar constructions for the implicit model (3.1.14) in the space of coefficients $\tilde{\alpha} = \{\alpha_{-1}^1, \alpha_0^0, \alpha_1^1\}$ are shown in Figs. 3.2 and 3.3. As in the previous case, the plane $B_1, \ldots, B_8$ of second-order difference schemes includes a certain two-parametric region of stable schemes (its boundaries are marked by a hatched line), a one-parametric

family of third-order schemes (the segment C_2D in Fig. 3.2 for $\sigma = 0.5$ and the ray C_2D in Fig. 3.3 for $\sigma = 2$ are stable schemes).

The Lax-Wendroff scheme [3.44] is marked by point B_5; point B_4 corresponds to another well-known second-order ("left rectangle") scheme with coefficients

$$\alpha^1_{-1} = (\sigma - 1)/(\sigma + 1), \quad \alpha^0_0 = (1 - \sigma)/(1 + \sigma), \quad \alpha^1_1 = 0. \tag{3.1.28}$$

Point B_2 also represents a second-order scheme with coordinates

$$\alpha^1_{-1} = \sigma/(2 + \sigma), \quad \alpha^0_0 = 1, \quad \alpha^1_1 = 0. \tag{3.1.29}$$

Point C_1 corresponds to a third-order difference scheme which is stable for $|\sigma| \leqslant 1$:

$$\alpha^1_{-1} = (\sigma - 1)/(\sigma + 2), \quad \alpha^0_0 = 1 - \sigma, \quad \alpha^1_1 = 0. \tag{3.1.30}$$

3.1.4. Taking into account the results of Sec. 3.1.3 according to which the sets of schemes with positive approximation (3.1.2), (3.1.10) and schemes with higher than first-order accuracy on the solutions of (3.1.1) do not intersect, we can formulate and solve for the general case the following two conjugate problems.

Firstly, we can formulate for the system (3.1.5), (3.1.10) with a general solution (3.1.11), (3.1.12), (3.1.13) the following ordinary problem of linear programming:

$$\bar{\delta}_2 \to \min, \tag{3.1.31}$$

i.e. the problem of minimization of approximation viscosity of schemes with positive approximation and hence of finding the most accurate difference scheme for an arbitrary grid model.

The solution of (3.1.5), (3.1.10), (3.1.31) is a difference scheme constructed on a three-point grid model including the point under consideration (t^{n+1}, x_m) and two nodes $(t^{n+\nu_1}, x_{m+\mu_1})$, $(t^{n+\nu_2}, x_{m+\mu_2})$ lying on the opposite sides of the characteristic $dx = \lambda\, dt$, and closest to it in the sense of usual geometric distance in the plane of independent variables (t, x). Indeed, $\bar{\delta}_2 = \sum_b \gamma_b \delta_{2b}$ assumes its smallest value for one of the vertices of the closed polyhedron (3.1.5), (3.1.10) (closest to the hyperplane $\delta_2 = 0$ of the difference schemes with a higher than first-order approximation). Since $\delta_{2b} = -\bar{\mu}_1\bar{\mu}_2$ ($\bar{\mu}_1 < 0$, $\bar{\mu}_2 > 0$) and, as can be easily verified,

$$\bar{\mu}_1 = -\sqrt{1+\lambda^2}\, r_1/h, \quad \bar{\mu}_2 = \sqrt{1+\lambda^2}\, r_2/h,$$

where r_1 and r_2 are the distances from points $(t^{n+\nu_1}, x_{m+\mu_1})$ and $(t^{n+\nu_2}, x_{m+\mu_2})$ to the characteristic $dx = \lambda\, dt$ in the (t, x)-plane (Fig. 3.1), $\delta_{2b} = \delta_{2\min}$ assumes its minimum value for such a vertex if r_1 and r_2 also have minimum values.

In particular, for two-layer difference schemes on a grid model including the points $(t^{n+1}, x_{m-K}), \ldots, (t^{n+1}, x_{m+R}), (t^n, x_{m-J}), \ldots, (t^n, x_{m+L})$ for $-L \leqslant j < \sigma = \lambda\tau/h < j+1 \leqslant J$, i.e. when the characteristic $dx = \lambda\, dt$ intersects the straight line $t = t^n = n\tau$ within the chosen model, the minimum value of $\overline{\delta}_2 = \delta_{2\,\min} = (\sigma - j)(1 + j - \sigma)$ is attained at the vertex $\alpha_b = \{0, \ldots, 0, \alpha^{\nu_1}_{\mu_1}, 0, \ldots, 0, \alpha^{\nu_2}_{\mu_2}, 0, \ldots, 0\}$, for which

$$\nu_1 = \nu_2 = 0, \quad \mu_1 = -j - 1, \quad \mu_2 = -j. \tag{3.1.32}$$

This corresponds to the case when the value of $\tilde{w} = w(t^n, \tilde{x})$, $\tilde{x} = x_m - \lambda\tau$ is calculated in the exact solution $w^{n+1}_m = \tilde{w}$ of (3.1.1) with the help of linear interpolation for values of w at the nodes (t^n, x_{m-j}) and (t^n, x_{m-j-1}) of the difference grid that are closest to the characteristic $dx = \lambda\, dt$ and lie on opposite sides of it. Such a scheme was applied to gasdynamic equations, for example, in [3.45]. For $J = 1$ and $L = 1$, i.e. when the condition $|\sigma| \leqslant 1$ is satisfied, (3.1.32) represents the scheme (3.1.15) proposed by Courant, Isaacson and Rees (point A_1 on Figs. 3.2 and 3.4).

For $\sigma > J$, the lowest value $\overline{\delta}_2 = \delta_{2\,\min} = \sigma - J$ is attained at

$$\mu_1 = \nu_1 = 1, \quad \mu_2 = -J, \quad \nu_2 = 0. \tag{3.1.33}$$

Accordingly, if $\sigma < -L$, we have $\overline{\delta}_2 = \delta_{2\,\min} = -\sigma - L$ for $\mu_1 = L$, $\nu_1 = 0$ and $\mu_2 = \nu_2 = 1$. If in this case $J = K = L = R = 1$, then, together with scheme (3.1.16) which is used for $|\sigma| \leqslant 1$, we obtain Carlsson's scheme (3.1.18) which was initially proposed for (3.1.1) and was extended in [3.46] to the general case of one-dimensional quasilinear systems of hyperbolic equations. It was mentioned above, that points A_1 (for $0 \leqslant \sigma \leqslant 1$) and A_2 (for $\sigma > 1$) correspond to this scheme in Figs. 3.2 and 3.3.

By way of an illustration, Fig. 3.6 shows the dependence of the quantity $h^2\overline{\delta}_2/2\tau$ on σ for some schemes with positive approximation (for the case $\lambda > 0$). Curves O, A_1, A_3, A_1-A_7-A_8, A_1-A_2 and A_1-A_7-A_9 correspond to the schemes (3.1.15), (3.1.16), (3.1.17), (3.1.32) for $J = 3$, Carlsson's scheme (3.1.18), and scheme (3.1.32), (3.1.33) for $J = 2$, $K = 1$. It can be seen that for small $\sigma \leqslant h$ (i.e. for $\tau \simeq h^2$), the quantity $h^2\overline{\delta}_2/2\tau$ in Lax's scheme is of the order of unity and the approximation is violated. It is known that this scheme is "unflexible" or conditionally approximating. The minimum value of $\overline{\delta}_2$ corresponds to the explicit scheme (3.1.32).

In Fig. 3.7, the exact solution of (3.1.1), $\lambda > 0$ (the broken line *1*) is compared with the results of calculations made by using some of the above difference schemes under the following initial conditions:

$$w(0, x) = 1 \text{ for } x \leqslant 0, \quad w(0, x) = 0 \text{ for } x > 0. \tag{3.1.34}$$

Curves O, A_1, A_7, A_3 and A_2 were obtained from schemes (3.1.15), (3.1.16), (3.1.32) for $J = 2$, (3.1.17) and (3.1.18) for values of $\sigma = \lambda\tau/h$ equal to 0.5, 0.5, 1.5, 2 and 2 respectively. It can be seen

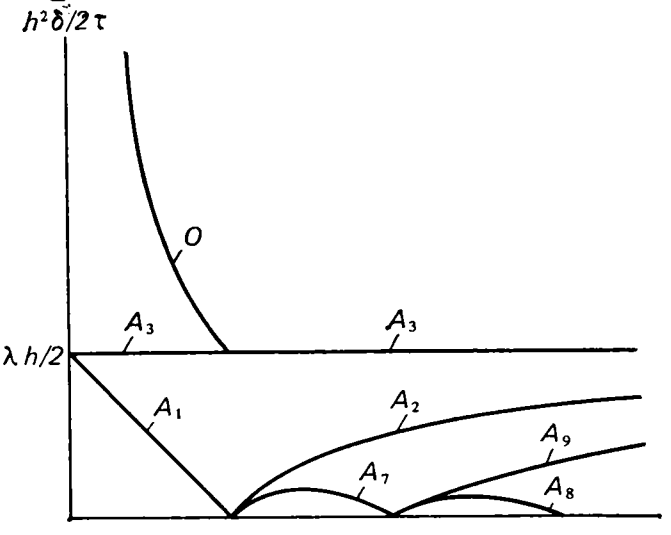

Fig. 3.6.

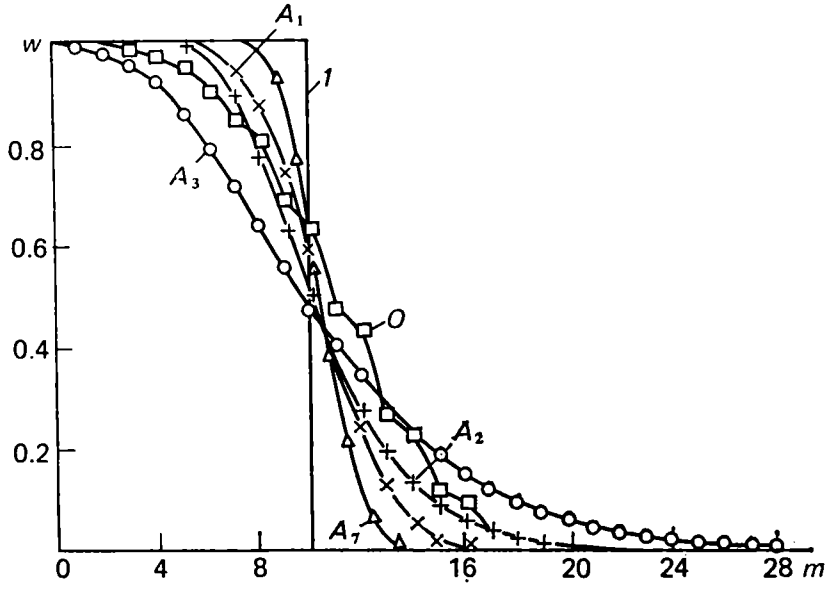

Fig. 3.7.

that the conclusions drawn in this section on the properties of the above schemes with positive approximation are confirmed by the numerical experiment as well. In particular, the effective width of the zone of spreading of the discontinuity of any difference scheme

with positive approximation (i.e. the slope of the curves near the discontinuity) is proportional to the approximation viscosity $h^2\overline{\delta}_2/2\tau$ or, in other words, to the distance from the point corresponding to this scheme in the space of coefficients to the hyperplane $\delta_2 = 0$. This is quite natural, since the magnitude of the coefficient of w_{xx} in the first differential approximation (3.1.2) affects the dissipative properties of difference schemes.

3.1.5. The difference schemes with a positive approximation considered in Secs. 3.1.2 and 3.1.4 have undoubtedly several advantages, the most important among these being the absence of oscillations of difference origin on nonsmooth solutions. However, it was shown in Sec. 3.1.3 that all these difference schemes have first order of accuracy, and even when the best of these schemes (having the lowest approximation viscosity, see Sec. 3.1.4) is used, a large number of computational points must be chosen on the difference grid and this, naturally, requires a large amount of computations. On the other hand, in higher-order schemes, oscillations of different kinds appear on nonsmooth solutions due to the fact that some of the coefficients α_μ^ν in these schemes become negative. Hence when a grid model admits a certain set (one-parametric, two-parametric, etc.) of schemes of second (or higher) order of accuracy, we can formulate the problem of constructing higher-order difference schemes which are "closest" to the schemes with positive approximation in a certain sense. In other words, we can formulate a problem conjugate to the one formulated and solved in Sec. 3.1.4.

Naturally, it can be assumed that the behaviour of a specific higher-order scheme on nonsmooth solutions (amplitude of oscillations, mode of their damping, etc.) is determined by the distance (in the space of indeterminate coefficients $\tilde{\alpha}$) from a point corresponding to this scheme to the domain of difference schemes with positive approximation (polyhedrons $OA_1A_3A_4A_5A_6$ (Figs. 3.2, 3.4), $A_7A_3A_4A_5$ (Fig. 3.5), $A_2A_3A_4A_5$ (Fig. 3.3), etc). In other words, the "nonmonotonicity" of difference schemes should be characterized by the quantity (3.1.9)

$$r = |\tilde{\alpha} - \tilde{\alpha}_A| \tag{3.1.35}$$

which is then minimized for the chosen grid model and the order of approximation of the set of difference schemes (3.1.2). Here $\tilde{\alpha} = \{\alpha_\mu^\nu\}$ is the set of coefficients in (3.1.2) corresponding to the higher-order difference scheme under consideration (these lying on the hyperplane (3.1.7) for $k = 2$), while $\tilde{\alpha}_A = \{\alpha_{\mu A}^\nu\}$ is the set of coefficients in (3.1.2) corresponding to that vertex of polyhedron of schemes with a positive approximation which is closest to this hyperplane

(for the schemes constructed in Sec. 3.1.4, for example, this vertex is point A_1 in Figs. 3.2, 3.4, point A_7 in Fig. 3.5, point A_2 in Fig. 3.3, and so on).

For second-order difference schemes on the solutions of (3.1.1), the coefficients α_μ^ν are determined by ordinary geometrical construction, in the space $\tilde{\alpha} = \{\alpha_\mu^\nu\}$, of the point of intersection of the normal drawn from point $\tilde{\alpha}_A$ with the hyperplane (3.1.7), $k = 2$. In other words, these coefficients are determined from the relations

$$\tilde{\alpha} = \tilde{\alpha}_A + r_2\tilde{c}_2, \quad r_2 = (\tilde{b}_2 - \tilde{c}_2\tilde{\alpha}_A)/(\tilde{c}_2\tilde{c}_2),$$
$$\tilde{\alpha}_A = \{\alpha_{\mu A}^\nu\}, \quad \tilde{c}_2 = \{\tilde{c}_{2\mu}^\nu\}, \quad \tilde{c}_{2\mu}^\nu = (\mu - \nu\sigma)^2 - 1, \tag{3.1.36}$$
$$\tilde{b}_2 = \sigma^2 - 1, \quad r = |r_2|\,|\tilde{c}_2|.$$

Let us consider some examples of such schemes. For the model (3.1.19) at $0 \leqslant \sigma \leqslant 1$ $\tilde{\alpha}_A = \{\alpha_{-2}^0, \alpha_0^0, \alpha_2^0\} = \{0, 1 - \sigma, 0\}$, and from (3.1.36) we obtain a difference scheme with coefficients (point B_6 in Fig. 3.4)

$$\alpha_{-2}^0 = \alpha_2^0 = 3\sigma(\sigma - 1)/19, \quad \alpha_0^0 = (1 - \sigma)(19 + \sigma)/19. \tag{3.1.37}$$

For the same model we also obtain for $1 < \sigma \leqslant 2$ $\tilde{\alpha}_A = \{\sigma - 1, 0, 0\}$, point B_6 in Fig. 3.5

$$\alpha_{-2}^0 = (\sigma - 1)(13 + 3\sigma)/19, \quad \alpha_0^0 = (\sigma - 1)(2 - \sigma)/19,$$
$$\alpha_2^0 = -3(\sigma - 1)(2 - \sigma)/19. \tag{3.1.38}$$

For the implicit model (3.1.14) at $0 \leqslant \sigma \leqslant 1$ $\tilde{\alpha}_A = \{\alpha_{-1}^1, \alpha_0^0, \alpha_1^1\} = \{0, 1 - \sigma, 0\}$ and from (3.1.36), we obtain a difference scheme corresponding to point B_6 in Fig. 3.2

$$\alpha_{-1}^1 = \sigma^2(\sigma - 1)(\sigma + 2)/a, \quad \alpha_0^0 = 1 - \sigma - \sigma(\sigma - 1)/a,$$
$$\alpha_1^1 = \sigma^2(\sigma - 1)(\sigma - 2)/a, \quad a = 2\sigma^2(\sigma^2 + 4) + 1. \tag{3.1.39}$$

For $\sigma > 1$, we obtain point B_6 in Fig. 3.3 with coordinates ($\tilde{\alpha}_A = \{(\sigma - 1)/\sigma, 0, 0\}$)

$$\alpha_{-1}^1 = (\sigma - 1)/\sigma - \sigma(\sigma - 1)(\sigma + 2)/a, \quad \alpha_0^0 = (\sigma - 1)/a,$$
$$\alpha_1^1 = \sigma(1 - \sigma)(\sigma - 2)/a, \quad a = 2\sigma^2(\sigma^2 + 4) + 1. \tag{3.1.40}$$

For a nonsymmetric five-point model including the points

$$(t^{n+1}, x_{m-1}), (t^{n+1}, x_m), (t^n, x_{m-1}),$$
$$(t^n, x_m), (t^n, x_{m+1}) \tag{3.1.41}$$

the difference scheme with the minimum value of r in (3.1.35) for $0 \leqslant \sigma \leqslant 1$ has coordinates in the space of coefficients $\tilde{\alpha} = \{\alpha^1_{-1}, \alpha^0_0\}$ ($\tilde{\alpha}_A = \{0, 1 - \sigma\}$, point B_3 in Fig. 3.2)

$$\alpha^1_{-1} = -\sigma(1-\sigma)(2+\sigma)^2/a, \quad \alpha^0_0 = (1-\sigma)[1+(\sigma+2)/a],$$
$$a = \sigma^2(\sigma+2)^2+1, \tag{3.1.42}$$

while for $\sigma > 1$ this scheme corresponds to point B_3 in Fig. 3.3 ($\tilde{\alpha}_A = \{(\sigma - 1)/\sigma, \ 0\}$)

$$\alpha^1_{-1} = (\sigma-1)[1+\sigma^2(\sigma+1)(\sigma+2)]/a,$$
$$\alpha^0_0 = (\sigma-1)/a, \quad a = [\sigma^2(\sigma+2)^2+1]. \tag{3.1.43}$$

For third-order difference schemes, the scheme with the minimum value of r in (3.1.35) is determined by constructing in the space of coefficients $\tilde{\alpha}$ the point of intersection of (3.1.7) for $k = 2, 3$ with the normal dropped from point A to this "straight line". In other words, this value is determined from the relations

$$\tilde{\alpha} = \tilde{\alpha}_A + r_2\tilde{c}_2 + r_3\tilde{c}_3, \quad r = |r_2\tilde{c}_2 + r_3\tilde{c}_3|,$$
$$r_2 = [(\tilde{b}_2 - \tilde{\alpha}_A\tilde{c}_2)(\tilde{c}_3\tilde{c}_3) - (\tilde{b}_3 - \tilde{\alpha}_A\tilde{c}_3)(\tilde{c}_2\tilde{c}_3)]/a,$$
$$a = (\tilde{c}_2\tilde{c}_2)(\tilde{c}_3\tilde{c}_3) - (\tilde{c}_2\tilde{c}_3)^2, \tag{3.1.44}$$
$$r_3 = [(\tilde{b}_3 - \tilde{\alpha}_A\tilde{c}_3)(\tilde{c}_2\tilde{c}_2) - (\tilde{b}_2 - \tilde{\alpha}_A\tilde{c}_2)(\tilde{c}_2\tilde{c}_3)]/a.$$

Here $\tilde{c}_i\tilde{c}_j$, $\tilde{\alpha}_A\tilde{c}_i$, $i, j = 2, 3$ are the scalar products of the vectors $\tilde{\alpha}_A$, $\tilde{c}_2$ and $\tilde{c}_3$ from (3.1.7), and the scalars $\tilde{b}_2$ and $\tilde{b}_3$ are also defined by formulas (3.1.7).

For the explicit model (3.1.19), we have at $0 \leqslant \sigma \leqslant 1$ $\tilde{\alpha}_A = \{\alpha^0_{-2}, \alpha^0_0, \alpha^0_2\} = \{0, 1 - \sigma, 0\}$ and from (3.1.44) the following third-order scheme on the solutions of (3.1.1) (point C_2 in Fig. 3.4)

$$\alpha^0_{-2} = \sigma(\sigma - 1)(55 + 19\sigma)/228, \quad \alpha^0_0 = (1 - \sigma)(19 + \sigma)/19,$$
$$\alpha^0_2 = \sigma(\sigma - 1)(17 - 19\sigma)/228. \tag{3.1.45}$$

Figures 3.8-3.10 ($\sigma = 0.5$) and Fig. 3.11 ($\sigma = 2$) show the results of numerical solution of the simulation problem (3.1.1), (3.1.34) by using some of the higher-order difference schemes described above. It can be seen from the data presented in Fig. 3.8, where the exact solution (broken line *1*) is compared with the numerical solution obtained from the third-order schemes (3.1.26), (3.1.45), and (3.1.27) corresponding to points C_1, C_2, and C_3 in Fig. 3.4 (curves C_1, C_2, C_3 respectively), as well as from the fourth-order scheme (3.1.24)

(curve D), that the amplitude of oscillations on a given discontinuous solution and the nature of their damping depend significantly on the proximity of these schemes (points C_1, C_2, C_3 and D) to the

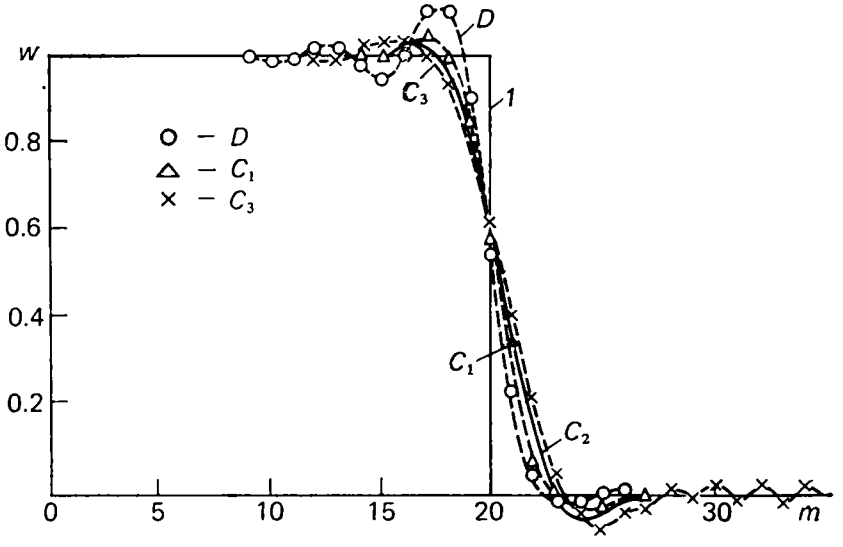

Fig. 3.8.

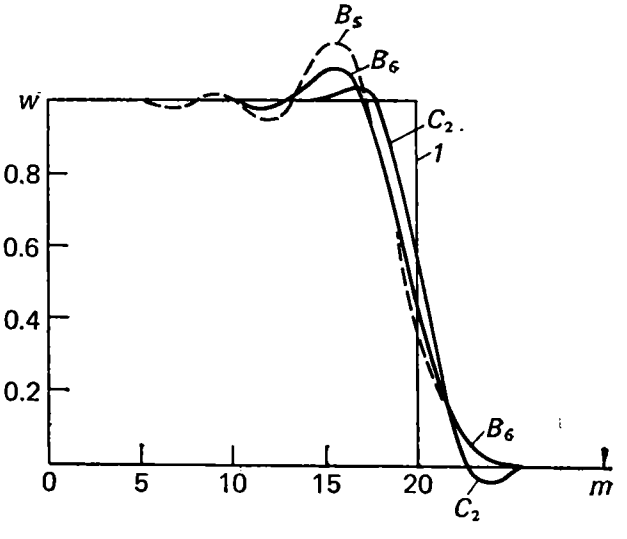

Fig. 3.9.

difference schemes with positive approximation (i.e. to point A_1 in Fig. 3.4). As expected, the difference scheme (3.1.45) corresponds to oscillations with the smallest amplitude and a rapid damping. In Fig. 3.9, an analogous comparison is made for explicit difference schemes (3.1.25), (3.1.37), (3.1.45) corresponding to points B_5, B_6, C_2

in Fig. 3.4 (curves B_5, B_6, C_2 respectively). It can also be seen that the numerical solution for scheme (3.1.37) behaves better than that for Lax-Wendroff scheme (3.1.25) and other second-order schemes in the model (3.1.19) where the oscillations are even more noticeable than for scheme (3.1.25).

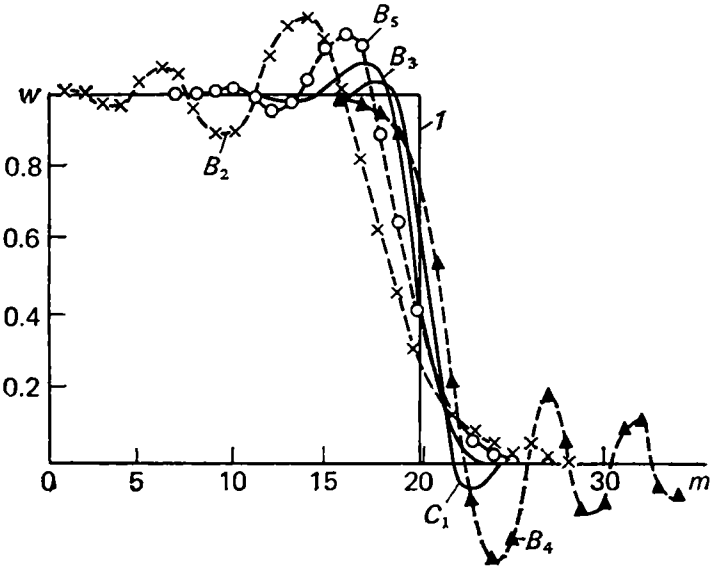

Fig. 3.10.

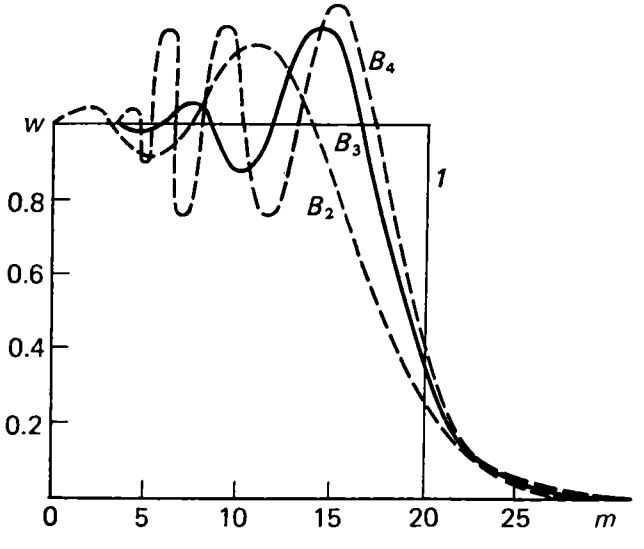

Fig. 3.11.

For the five-point model (3.1.41) chosen for considering the simulation problem in such a way that it is possible to carry out a through count without resorting to any marching relations (nonsymmetric grid models are also essential for calculating boundary points).

Figures 3.10 and 3.11 show a comparison of the exact solution (broken line *1*) with the results of calculations by using the second-order schemes (3.1.25), (3.1.28), (3.1.29), (3.1.42)-(3.1.43) (curves B_5, B_4, B_2, B_3 respectively), and also by using the only third-order scheme (3.1.30) for this model, corresponding to point C_1 in Fig. 3.2 (curve C_1). For $0 \leqslant \sigma \leqslant 1$, the difference between second-order schemes being compared is even more noticeable and the advantages of scheme (3.1.42) become more apparent. It can also be seen that for $\sigma > 1$, it is not possible to significantly improve the oscillating properties of implicit second- (and higher-)order schemes on the given model.

3.1.6. Since the well-known work of Neumann [3.47], various methods have been used for regularizing the discontinuous numerical solutions for stable, though not monotonic, difference schemes in which non-physical oscillations appear on nonsmooth solutions. These methods are introduced either over the entire domain of integration or only in the vicinity of discontinuities (an explicit introduction into artificial viscosity schemes, for example, [3.47-3.49], the use of smoothing operators and hybrid schemes, for example, [3.50-3.60]). The fundamental theory of regularization of discontinuous numerical solutions has been worked out in [3.16].

In spite of all the diversity of methods, the essence of various regularization techniques is quite simple and involves the choice of two reference schemes. One of them has a very high order of accuracy but is not monotonic and oscillates on the discontinuous solutions. The other scheme is positive definite or close to it, but has a first order of accuracy. The regularization process involves the organization of a transition between these two reference schemes depending on the behaviour of the required solution. The difference schemes described in [3.51-3.54] and some other schemes are based on this approach. We can similarly treat those difference schemes involving an explicit or indirect introduction of terms which correspond to the difference approximation and are missing in the hyperbolic-type equations of even-order spatial derivatives (w_{xx}, w_{xxxx}, etc.) with small coefficients. It was noted long ago that this leads to a stabilization of the numerical solution.

For the approach developed in this paper and involving the introduction of the linear space of coefficients of difference schemes, various methods of regularization are associated with the choice of two reference points (difference schemes). One of these points (point B) lies on the hyperplane (3.1.7), $k = 2$ (second-order approximation) or on the intersection of two hyperplanes (3.1.7), $k = 2, 3$ (third-order approximation) and so on. The second point (point A) belongs to the set of schemes (3.1.2), (3.1.5), (3.1.10) with positive approximation. The regularization method involves the construction of a one-

parametric family of difference schemes

$$\tilde{\alpha} = (1-\gamma)\tilde{\alpha}_B + \gamma\tilde{\alpha}_A, \quad 0 \leqslant \gamma \leqslant 1, \tag{3.1.46}$$

which corresponds to the segment AB in the space of coefficients. Parameter γ should be associated with the behaviour of the required solution in such a way that $\gamma = 1$ in the vicinity of discontinuities while in the domain of a smooth solution, $\gamma = 0$. Such hybrid schemes (apparently, Fedorenko [3.51] was the first to introduce such a scheme) combine the positive properties of both reference schemes, as is borne out by their numerous applications ([3.51-3.60] and others).

Naturally, it can be expected that the best results will be obtained by using for the reference schemes the first-order approximation schemes with the lowest approximation viscosity discussed in Sec. 3.1.4 (i.e. which blur the discontinuity fronts to a smaller extent than other monotonic schemes), as well as higher-order schemes which are closest to schemes with positive approximation (i.e. schemes which give the least-oscillating solution among higher-order schemes). It should also be emphasized that for many difference schemes, the coordinates of the points corresponding to them in the space of coefficients (in particular, the points A_1, A_2, A_4, A_7 in Figs. 3.2, 3.3, 3.4, 3.5) depend on local values of the parameter $\sigma = \lambda\tau/h$, i.e. $\tilde{\alpha}_A = \tilde{\alpha}_A(\sigma)$. Consequently, when hybrid systems of the type (3.1.46) are generalized to a system of hyperbolic equations, their characteristic properties should be used.

3.2. GRID-CHARACTERISTIC METHODS FOR ONE-DIMENSIONAL QUASILINEAR HYPERBOLIC SYSTEMS

3.2.1. The difference schemes of the type (3.1.2) considered in Sec. 3.1 are generalized to one-dimensional systems of hyperbolic equations

$$\mathbf{u}_t + A\mathbf{u}_x = \mathbf{f}, \quad \mathbf{u} = \{u_1, \ldots, u_I\}, \quad \mathbf{f} = \{f_1, \ldots, f_I\}, \tag{3.2.1}$$
$$A = \Omega^{-1}\Lambda\Omega = \{a_{ij}\} \ (i, j = 1, \ldots, I), \quad \Omega = \{\omega_i\}, \quad \Lambda = \{\lambda_i\},$$

($a_{ij} = \text{const}$ and $\mathbf{f} = 0$) quite formally, in such a way that their properties are conserved. System (3.2.1) is premultiplied by the matrix Ω and reduced to the characteristic form $\mathbf{w}_t + \Lambda\mathbf{w}_x = 0$, $\mathbf{w} = \Omega\mathbf{u}$ or, in scalar notation, to the form

$$w_{it} + \lambda_i w_{ix} = 0, \quad w_i = \omega_i \mathbf{u}, \quad i = 1, \ldots, I. \tag{3.2.2}$$

For each of the equations (3.2.2) we then choose some difference scheme of the type (3.1.2) from the schemes considered above (this choice

may be different for different characteristic directions $dx = \lambda_i\, dt$) and carry out the reverse transition from $\mathbf{w}$ to $\mathbf{u} = \Omega^{-1}\mathbf{w}$. In (3.2.1) and (3.2.2), Λ is a diagonal matrix of eigenvalues of matrix A, defined by the characteristic equation $\mathrm{Det}\,(A - \lambda E) = 0$ (for a system of equations of hyperbolic type, all λ_i are real), Ω is a nonsingular matrix whose rows are linearly independent left eigenvectors ω_i of matrix A, defined to within their length from the set of linear homogeneous system of equations $\omega_i\,(A - \lambda_i E) = 0$, Ω^{-1} is the matrix inverse to Ω, w_i are Riemann's invariants, and E is a unit matrix.

For system (3.2.1), such difference schemes have the following form for $a_{ij} = \mathrm{const}$ and $\mathbf{f} = \mathrm{const}$:

$$\mathbf{u}_m^{n+1} = \sum_{\mu,\,\nu} B_\mu^\nu \mathbf{u}_{m+\mu}^{n+\nu} + \tau R\mathbf{f},$$

$$B_\mu^\nu = \Omega^{-1} A_\mu^\nu \Omega,\quad A_\mu^\nu = \{\alpha_{\mu i}^\nu\}, \tag{3.2.3}$$

$$R = \{r_{ij}\} = E - \sum_{\mu,\,\nu} \nu B_\mu^\nu = \Omega^{-1}\left(E - \sum_{\mu,\,\nu} \nu A_\mu^\nu\right)\Omega,$$

where A_μ^ν are diagonal matrices formed by the coefficients α_μ^ν analyzed in Sec. 3.1. In particular, the analogue of difference schemes (3.1.2), (3.1.5), (3.1.10) with non-negative coefficients α_μ^ν will be the schemes with non-negative definite matrices B_μ^ν which were first introduced by Fridrichs [3.39] and for which the scalar products

$$(B_\mu^\nu \mathbf{v},\ \mathbf{v}) \geqslant 0 \tag{3.2.4}$$

for arbitrary nonzero vectors $\mathbf{v}$. In the case of symmetric matrices A, conditions (3.2.4) and (3.1.10), i.e. $\alpha_{\mu i}^\nu \geqslant 0$ for matrices B_μ^ν in (3.2.3), are known to be equivalent. However, for systems of Eqs. (3.2.1) with nonsymmetric matrices A, which can be symmetrized, i.e. we can reduce Eqs. (3.2.1) to the form $A_1\mathbf{v}_t + A_2\mathbf{v}_x = \varphi$ with symmetric matrices A_1, A_2 and a positive definite matrix A_1 (t being Fridrichs' hyperbolic systems [3.39]), it is quite possible to use (3.1.10) instead of conditions (3.2.4). Examples of such systems are time-dependent equations of gasdynamics and magnetogasdynamics, time-dependent equations of the theory of elasticity, etc. (see, for example, [3.61]). Note that for $a_{ij} = \mathrm{const}$, all difference schemes (3.2.3), as well as the initial system (3.2.1), are conservative if we put $\mathbf{F} = A\mathbf{u}$.

3.2.2. To generalize the difference schemes considered above to the quasilinear system (3.2.1) with $A = A\,(t, x, \mathbf{u})$, $\mathbf{f} = \mathbf{f}\,(t, x, \mathbf{u})$, including the divergent form

$$\mathbf{u}_t + \mathbf{F}_x\,(t, x, \mathbf{u}) = \varphi\,(t, x, \mathbf{u}),$$

$$\mathbf{F}_\mathbf{u} = A,\quad \varphi = \mathbf{f} + \partial\mathbf{F}/\partial x, \tag{3.2.5}$$

of such equations, the Runge-Kutta method and the integro-interpolation method are the most universal and effective techniques for constructing the grid-characteristic schemes of type (3.2.3) (including those ensuring the validity of the difference analogues of the conservation laws, i.e. the conservative scheme) (see, for example, [3.14, 3.15, 3.62]). If these methods are used to construct on some grid model the corresponding set of difference schemes with the same number of free parameters as in (3.2.3), and the notation of (3.2.3) is then employed by taking a system with $a_{ij} = \text{const}$ as an example (putting $\mathbf{F} = A\mathbf{u}$), we can establish a connection between these free parameters and B_μ^ν and thus obtain analogues of some difference schemes considered in Sec. 3.1 for the general quasilinear case.

As a first example of such a generalization, let us consider the widely used six-point implicit model (3.1.14) and use the integro-interpolation method [3.15].

Writing the initial divergence equations (3.2.5) for the difference cell $t^n \leqslant t \leqslant t^{n+1}$, $x_{m-1/2} \leqslant x \leqslant x_{m+1/2}$ in integral form

$$\int_{x_{m-1/2}}^{x_{m+1/2}} \mathbf{u}(t^{n+1}, x)\,dx - \int_{x_{m-1/2}}^{x_{m+1/2}} \mathbf{u}(t^n, x)\,dx + \int_{t^n}^{t^{n+1}} \mathbf{F}(t, x_{m+1/2}, \mathbf{u}(t, x_{m+1/2}))\,dt - \int_{t^n}^{t^{n+1}} \mathbf{F}(t, x_{m-1/2}, \mathbf{u}(t, x_{m-1/2}))\,dt = \int_{t^n}^{t^{n+1}} \int_{x_{m-1/2}}^{x_{m+1/2}} \varphi(t, x, \mathbf{u})\,dx\,dt \tag{3.2.6}$$

and using some interpolation formulas for approximating the integrands $\mathbf{u}$ (identical formulas on upper and lower edges of a cell) and $\mathbf{F}$ (identical formulas on the left and right boundaries of a cell) in (3.2.6), we can ensure that the difference scheme thus obtained is conservative and has the appropriate order of accuracy (within the limits admissible for the chosen grid model). In particular, the difference scheme

$$(\mathbf{u}_m^{n+1} - \mathbf{u}_m^n)/\tau + (\mathbf{F}_{m+1/2}^{n+1/2} - \mathbf{F}_{m-1/2}^{n+1/2})/h = \varphi_m^{n+1/2}$$

approximates the initial system (3.2.5) with first or second order of accuracy for an appropriate choice of an interpolation formula of first or second order for calculating $\mathbf{F}_{m\pm1/2}^{n+1/2} = \mathbf{F}(t^{n+1/2}, x_{m\pm1/2}, \mathbf{u}_{m\pm1/2}^{n+1/2})$. A certain connection with the values of this vector at the

mesh points of the difference grid is required also for $\varphi_m^{n+1/2}$, for example, the simplest relation $\varphi_m^{n+1/2} = \varphi_m^n$ for first-order schemes.

Putting

$$\mathbf{F}_{m+1/2}^{n+1/2} = \sum_{\mu=0}^{1} \sum_{\nu=0}^{1} (D_\mu^\nu)_{m+1/2}^{n+1/2} \mathbf{F}_{m+\mu}^{n+\nu} \tag{3.2.7}$$

and using a similar interpolation formula for $\mathbf{F}_{m-1/2}^{n+1/2}$, and requiring the fulfilment of the condition

$$\sum_{\mu=0}^{1} \sum_{\nu=0}^{1} D_\mu^\nu = E, \tag{3.2.8}$$

which can be used for eliminating one of the matrix coefficients, say, D_0^0, we obtain a three-parametric family of conservative first-order difference schemes with arbitrary matrix coefficient D_0^1, D_1^0, D_1^1

$$\begin{aligned}
&-(\tilde{D}_0^1)_{m-1/2}^{n+1/2} \mathbf{F}_{m-1}^{n+1} + \{\mathbf{u}_m^{n+1} + [(\tilde{D}_0^1)_{m+1/2}^{n+1/2} \\
&-(\tilde{D}_1^1)_{m-1/2}^{n+1/2}]\, \mathbf{F}_m^{n+1}\} + (\tilde{D}_1^1)_{m+1/2}^{n+1/2} \mathbf{F}_{m+1}^{n+1} = \mathbf{b}_m^n \\
= \mathbf{u}_m^n + \tau\varphi_m^{n+1/2} &+ \{[-\tilde{D}_1^0 + (-\tilde{D}_0^1 - \tilde{D}_1^1 + \tau E/h)/2]_{m+1/2}^{n+1/2} (\mathbf{F}_{m+1}^n - \mathbf{F}_m^n) \\
&-[-\tilde{D}_1^0 + (-\tilde{D}_0^1 - \tilde{D}_1^1 + \tau E/h)/2]_{m-1/2}^{n+1/2} (\mathbf{F}_m^n - \mathbf{F}_{m-1}^n)\} \\
&+[(\tilde{D}_1^1 + \tilde{D}_0^1 - \tau E/h)_{m+1/2}^{n+1/2} (\mathbf{F}_{m+1}^n + \mathbf{F}_m^n)/2 \\
&-(\tilde{D}_1^1 + \tilde{D}_0^1 - \tau E/h)_{m-1/2}^{n+1/2} (\mathbf{F}_m^n + \mathbf{F}_{m-1}^n)/2], \\
&\tilde{D}_\mu^\nu = \tau D_\mu^\nu / h,
\end{aligned} \tag{3.2.9}$$

where E is a unit matrix.

Comparing (3.2.9) in the linear case $\mathbf{F} = A\mathbf{u}$, $A = \{a_{ij}\}$, $a_{ij} =$ const, with (3.2.3) (for the grid model (3.1.14)), we can easily establish a connection between the matrix coefficients D_0^1, D_1^0, D_1^1 in (3.2.9) and the matrix coefficients B_μ^ν in (3.2.3), i.e. B_{-1}^0, B_0^0, B_1^1 (as before, the coefficients B_{-1}^0 and B_1^0 are defined by relations (3.1.6)). This connection can be expressed as follows:

$$\begin{aligned}
&D_\mu^\nu = \Omega^{-1} \mathrm{d}_\mu^\nu \Omega, \quad \mathrm{d}_\mu^\nu = \{(\mathrm{d}_\mu^\nu)_i\}, \\
&i = 1, \ldots, I, \quad \mu, \nu = 0, 1, \\
&(\mathrm{d}_1^1)_i = -(\alpha_1^1)_i/\beta_i, \quad (\mathrm{d}_0^1)_i = (\alpha_{-1}^1)_i/\beta_i, \\
&(\mathrm{d}_1^0)_i = 0.5\,[(\alpha_0^0)_i + 2\,(\alpha_1^1)_i - 1 + \beta_i]/\beta_i, \\
&\beta_i = \sigma_i\,[1 - (\alpha_{-1}^1)_i - (\alpha_1^1)_i], \\
&\sigma_i = \lambda_i \tau/h,
\end{aligned} \tag{3.2.10}$$

(d_μ^ν are diagonal matrices), after the matrices A and B_μ^ν have been represented in the form $A=\Omega^{-1}\Lambda\Omega$, $B_\mu^\nu=\Omega^{-1}A_\mu^\nu\Omega$ with diagonal matrices $\Lambda=\{\lambda_i\}$ and $A_\mu^\nu=\{(\alpha_\mu^\nu)_i\}$.

In accordance with the analysis carried out in Secs. 3.1.2 and 3.1.4, we choose $(\alpha_{-1}^1)_i$, $(\alpha_1^1)_i$ and $(\alpha_0^0)_i$ to be non-negative; this leads to conservative analogues of difference schemes with positive approximation for the divergent quasilinear system (3.2.5).

In particular, if we choose $(\alpha_{-1}^1)_i$, $(\alpha_0^0)_i$ and $(\alpha_1^1)_i$ in accordance with (3.1.15)-(3.1.18), we respectively obtain Lax's difference scheme [3.40], and conservative versions proposed in [3.18] for the schemes of Courant, Isaacson and Rees [3.1], Landau, Meiman, and Khalatnikov [3.41], and Carlsson (see (3.1.18)). Note that for $\sigma_i = 0$, indeterminacy of the type 0/0 appears in the relations (3.2.10) in some cases. This indeterminacy, however, can be easily eliminated by replacing the differences $\mathbf{F}_{m+1}^n - \mathbf{F}_m^n$ and $\mathbf{F}_m^n - \mathbf{F}_{m-1}^n$ in the third term on the right-hand side of (3.2.9) by $A_{m+1/2}^{n+1/2}(\mathbf{u}_{m+1}^n - \mathbf{u}_m^n)$ and $A_{m-1/2}^{n+1/2}(\mathbf{u}_m^n - \mathbf{u}_{m-1}^n)$, or by some other appropriate method which does not violate the conservative nature of the scheme. For example, while choosing the coefficients $(\alpha_{-1}^1)_i$, $(\alpha_0^0)_i$ and $(\alpha_1^1)_i$ in accordance with (3.1.16), we can obtain the following version of scheme (3.2.9), (3.2.10) [3.18, 3.33]:

$$\begin{aligned}\mathbf{u}_{m+1}^{n+1} &= \mathbf{u}_m^n + \tau\varphi_m^n - \tau(\mathbf{F}_{m+1}^n - \mathbf{F}_{m-1}^n)/2h \\ &+ \tau[(\Omega^{-1}|\Lambda|\Omega)_{m+1/2}^n(\mathbf{u}_{m+1}^n - \mathbf{u}_m^n) \\ &- (\Omega^{-1}|\Lambda|\Omega)_{m-1/2}^n(\mathbf{u}_m^n - \mathbf{u}_{m-1}^n)]/2h.\end{aligned} \tag{3.2.11}$$

As was shown above, among all the explicit two-layer schemes of the first-order of accuracy with positive approximation, this scheme has the lowest approximation viscosity if the condition of its stability is satisfied:

$$\sigma_* = \tau \max_{i,\,m} |(\lambda_i)_m^n|/h \leqslant 1. \tag{3.2.12}$$

Requiring that the difference expression (3.2.7) approximates the corollary

$$\mathbf{F}_t + A\mathbf{F}_x = A\varphi + \partial\mathbf{F}/\partial t, \quad A = \mathbf{F}_\mathbf{u},$$

of (3.2.5) with first order of accuracy, we find that an additional condition is imposed on the indeterminate matrix coefficients D_μ^ν:

$$\sum_{\mu=0}^{1}\sum_{\nu=0}^{1}[(2\mu-1)E-(2\nu-1)\widetilde{A}]D_\mu^\nu = 0, \quad \widetilde{A} = \tau A/h.$$

Using this condition in (3.2.9), we can eliminate another matrix coefficient, for example, $D_1^0 = (E - \widetilde{A})/2 + \widetilde{A}D_0^1 - (E - \widetilde{A})D_1^1$

and obtain a two-parametric family of conservative difference schemes having second order of accuracy (for an appropriate choice of $\varphi_m^{n+1/2}$) with arbitrary matrix coefficients $\tilde{D}_0^1$, $\tilde{D}_1^1$. The same result can be obtained by expressing the coefficients $(\alpha_0^0)_i$ in (3.2.10) in terms of $(\alpha_{-1}^1)_i$, $(\alpha_1^1)_i$ and using the second-order approximation conditions (3.1.7), $k = 2$, for the given model (3.1.14). Choosing some values of the coefficients $(\alpha_{-1}^1)_i$ and $(\alpha_1^1)_i$ from those considered in Secs. 3.1.3 and 3.1.5, we can obtain conservative versions of these schemes for quasilinear divergent systems of equations (3.2.5). For example, if we choose $(\alpha_{-1}^1)_i$ and $(\alpha_1^1)_i$ in accordance with (3.1.39) and (3.1.40) for $\sigma_i > 0$ and similar expressions for $\sigma_i < 0$, we can obtain an analogue of the difference scheme that is "the closest" on the grid model (3.1.14) to schemes with positive approximation. Such a scheme is presented in [3.20]. Finally, using the results of Sec. 3.1.6 and choosing in (3.2.9) and (3.2.10) the coefficients $(\alpha_{-1}^1)_i$, $(\alpha_0^0)_i$, $(\alpha_1^1)_i$ in accordance with (3.1.46), we obtain hybrid versions of these conservative difference schemes with first order of accuracy for $\gamma = 1$ (monotonic if $\tilde{\alpha}_A$ is chosen in accordance with the conditions (3.1.11)-(3.1.13)) and having second order of accuracy for $\gamma = 0$. In particular, we choose in (3.1.46) Carlsson's scheme (3.1.18) for $\tilde{\alpha}_A$, the scheme (3.1.39), (3.1.40) for $\tilde{\alpha}_B$ when $\sigma_i > 0$ and a similar scheme when $\sigma_i < 0$. In other words, we put in (3.2.10)

$$\text{for } \sigma_i > 1: \quad (\alpha_{-1}^1)_i = (\sigma_i - 1)/\sigma_i - (1-\gamma)(\sigma_i - 1)\sigma_i(\sigma_i + 2)/c_i,$$
$$(\alpha_0^0)_i = (1-\gamma)(\sigma_i - 1)/c_i,$$
$$(\alpha_1^1)_i = (1-\gamma)(1-\sigma_i)\sigma_i(\sigma_i - 2)/c_i,$$

$$\text{for } |\sigma_i| \leqslant 1: \quad (\alpha_{-1}^1)_i = (1-\gamma)|\sigma_i|(|\sigma_i| - 1)\sigma_i(\sigma_i + 2)/c_i, \tag{3.2.13}$$
$$(\alpha_1^1)_i = (1-\gamma)|\sigma_i|(|\sigma_i| - 1)\sigma_i(\sigma_i - 2)/c_i,$$
$$(\alpha_0^0)_i = 1 - |\sigma_i| - (1-\gamma)|\sigma_i|(|\sigma_i| - 1)/c_i,$$

$$\text{for } \sigma_i < -1: \quad (\alpha_{-1}^1)_i = (1-\gamma)(\sigma_i + 1)\sigma_i(\sigma_i + 2)/c_i,$$
$$(\alpha_1^1)_i = (\sigma_i + 1)/\sigma_i + (1-\gamma)(\sigma_i + 1)\sigma_i(\sigma_i - 2)/c_i,$$
$$(\alpha_0^0)_i = -(1-\gamma)(\sigma_i + 1)/c_i,$$
$$c_i = 1 + 2\sigma_i^2(\sigma_i^2 + 4), \quad 0 \leqslant \gamma \leqslant 1.$$

The system (3.2.9), (3.2.10), (3.2.13) is then transformed for $\gamma = 1$ into a conservative version of Carlsson's scheme for system (3.2.5) having the lowest approximation viscosity among monotonic first-order systems on the grid model (3.1.14). For $\gamma = 0$, we get the conservative analogue of scheme (3.1.39), (3.1.40) having the least oscillating solution among all second-order difference schemes for

(3.1.14). In the linear scalar case for $0 \leqslant \gamma \leqslant 1$ segments A_1B_6 (Fig. 3.2) and A_2B_6 (Fig. 3.3) correspond to this scheme in the space of coefficients. It is also worth noting that if we choose for $\tilde{\alpha}_A$ the difference scheme (3.1.18), for $\tilde{\alpha}_B$ the "left (right) rectangle" (3.1.28)

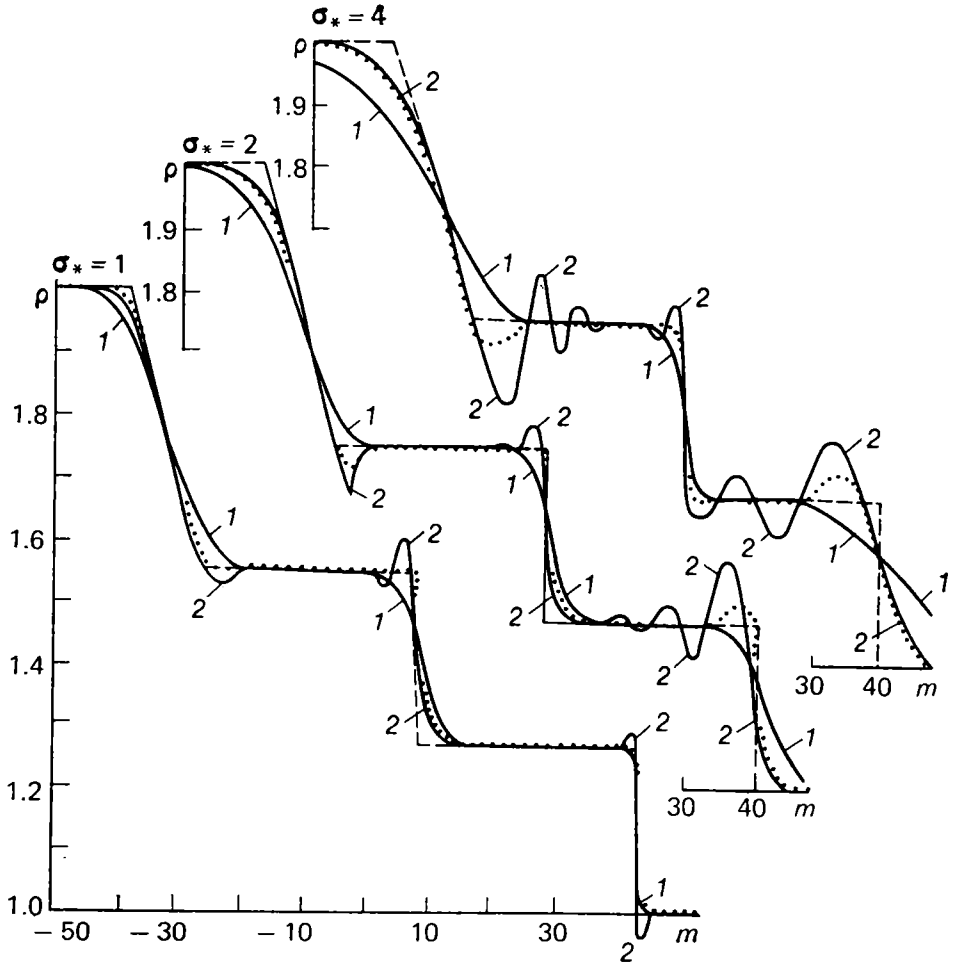

Fig. 3.12.

for $\sigma_i > 0$ ($\sigma_i < 0$), we obtain a generalization to system (3.2.5) of the difference scheme presented in [3.52] (this system is not suitable for $\gamma \ll 1$, since the difference schemes of type (3.1.28) behave badly on discontinuous solutions). In the linear scalar case, segments A_1B_4 (Fig. 3.2) and A_2B_4 (Fig. 3.3) correspond to the scheme presented in [3.52].

By way of an example, Fig. 3.12 shows the results of calculations carried out by using the scheme (3.2.9), (3.2.10), (3.2.13) for the problem of splitting a discontinuity for one-dimensional time-

dependent equations of gas dynamics

$$\mathbf{u} = \{\rho, \rho v, \rho E\}, \ \mathbf{F} = \{\rho v, \rho v^2 + p, (\rho E + p)v\},$$
$$E = \varepsilon + v^2/2, \ p = (\varkappa - 1)\rho\varepsilon,$$
$$\rho(0, x) = p(0, x) = 2 \text{ for } x \leqslant 0, \qquad (3.2.14)$$
$$\rho(0, x) = p(0, x) = 1 \text{ for } x > 0, \ v(0, x) = 0,$$
$$\rho(t, x_1) = p(t, x_1) = 2, \ \rho(t, x_2) = p(t, x_2) = 1,$$
$$v(t, x_1) = v(t, x_2) = 0, \ x_1 \leqslant x \leqslant x_2, \ t \geqslant 0,$$

where ρ is the density, p the pressure, v the velocity, ε the specific internal energy, and $\varkappa = 1.4$ the adiabatic exponent. The domain of integration $0 \leqslant t \leqslant T$, $x_1 \leqslant x \leqslant x_2$ was chosen in such a way that the perturbations did not reach its boundary during the time $0 \leqslant t \leqslant T$. The density profiles, which correspond to the instant $t = 2.5$, were obtained in calculations by using the Courant number (3.2.12) $\sigma_* = 1$, 2 and 4. Curves *1* and *2* in Fig. 3.12 correspond to $\gamma = 1$ and $\gamma = 0$. The points in the figure correspond to the calculations in which the value of the parameter γ was associated with the behaviour of the numerical solution in such a way that $\gamma \approx 1$ in the vicinity of discontinuities, while in the domain of a smooth solution, $\gamma \approx 0$. The exact solution is shown by dashed lines. The initial discontinuity is split into an expansion wave (on the left), a contact discontinuity (at the centre), and a shock wave (on the right). The nonlinear system (3.2.9), (3.2.10), (3.2.13) of difference equations was solved by iterations (with linearization according to Newton's method), and matrix sweep was used at each iteration for solving the corresponding linear system. For Courant's numbers $\sigma_* \leqslant 1$, two or three iterations were required for convergence with $\varepsilon' = 10^{-6}$. For $\sigma_* > 1$ the required number of iterations increased, but convergence was observed in all versions for which calculations were made (this was verified up to $\sigma_* = 8$). For $\sigma_* \leqslant 1$, such a hybrid scheme can be used to completely get rid of oscillations, in the same way as in Carlsson's monotonic scheme ($\gamma = 1$, curve *1*). The width of the blurring zone (the slope of the curves at the discontinuities) remains the same as in second-order schemes ($\gamma = 0$, curve *2*). For $\sigma_* > 1$, the oscillation amplitude and penetration depth increases, as in the linear case (Fig. 3.11), at first behind the shock wave front, where Courant's number has its maximum value, and then in the vicinity of the expansion wave in the second-order scheme (and as a consequence, in the hybrid scheme also, but to a lesser extent). This, however, does not mean that implicit schemes are not applicable for calculating discontinuous solutions. For example, Courant's number quite often changes sharply in the integration domain and attains large values (which restrict the time step τ in explicit schemes) in the region of smooth solution, the values at the discontinuities being

much smaller. Implicit schemes have an undisputed advantage over explicit schemes in problems of this type. It is interesting to note that at a contact discontinuity, the properties of all three versions of this sheme ($\gamma = 0$, $\gamma = 1$, and hybrid) are practically independent of the value of Courant's number.

3.2.3. Another, equally effective approach towards the generalization of difference schemes is the Runge-Kutta method which was developed for linear and nonlinear equations (for explicit schemes as a rule) and forms the basis of many predictor-corrector multistep schemes. Such a method was used, for example, in [3.14] and by many other authors ([3.63-3.66], etc.) for third-order schemes. It is also applicable for second-order schemes of Lax-Wendroff [3.44], MacCormac [3.67] and others. A common feature of all these schemes is that they employ a grid model of the type (3.1.19) for which various difference schemes of Secs. 3.1.5 and 3.1.6 are generalized to (3.2.5).

By way of the first example, let us consider a one-parametric family of explicit conservative schemes for (3.2.5) (for the sake of simplicity, we shall consider the case $\varphi = 0$)

$$\mathbf{u}_m^{n+1} = \tilde{\mathbf{u}}_m + [(\Omega^{-1}B\Omega)_{m+1/2}(\bar{\mathbf{u}}_{m+1} - \bar{\mathbf{u}}_m) - (\Omega^{-1}B\Omega)_{m-1/2}(\bar{\mathbf{u}}_m - \bar{\mathbf{u}}_{m-1})], \tag{3.2.15}$$

where $B = \{b_i\}$ is a certain diagonal matrix and $\tilde{\mathbf{u}}$ is calculated, for example, from the well-known Lax-Wendroff second-order scheme [3.44] or the analogous MacCormac scheme [3.67] which correspond in the linear case to the point B_5 in Figs. 3.2, 3.4; $\bar{\mathbf{u}} = \mathbf{u}^n$ or $\tilde{\mathbf{u}}$ depending on the time layer which is used for smoothing with the help of the operator in brackets on the right-hand side of (3.2.15). Relations of the type (3.2.15) are frequently used in computations but with a scalar smoothing coefficient ($b_i \equiv b$) which is chosen on the basis of different, often heuristic, concepts. If instead of the same smoothing coefficient b for all characteristic directions $dx = \lambda_i dt$ of the system (3.2.5) we use different values b_i for each of the compatibility relations to which the system (3.2.5) can be reduced, the possibilities of choosing optimal values of these coefficients are considerably enhanced (these optimal values depend on $\sigma_i = \lambda_i \tau/h$ and are different for different characteristic directions $dx = \lambda_i dt$).

If we use the data on the layer $t = t^n$ for smoothing, i.e. if $\bar{\mathbf{u}} = \mathbf{u}^n$ in (3.2.15), and

$$b_i = \gamma \mid \sigma_i \mid (1 - \mid \sigma_i \mid)/2, \quad \gamma \geqslant 0 \tag{3.2.16}$$

is chosen in the linear case for each compatibility relation (3.1.1) to which the system (3.2.5) is reduced, an increase in the value of γ in (3.2.16), i.e. an increase in b_i, leads to a downward displacement

of the point corresponding to this scheme in Fig. 3.4 from B_5 (for $\gamma = 0$) along the vertical axis (since $(\alpha_{-2}^0)_i = (\alpha_2^0)_i = 0$). For $\gamma = 1$, this point coincides with point A_1 (scheme (3.2.11) with positive approximation is an analogue of the scheme closest to higher-order schemes on the given model). A further increase in the value of γ leads only to an excessive smoothing of the numerical solution. In particular, for $b_i = (1 - \sigma_i^2)/2$, we obtain a difference scheme which is analogous to Lax's scheme [3.40] (point O in Fig. 3.4), while for still higher values of γ the space of coefficients of the difference scheme (3.2.15) will have corresponding points below the polyhedron of schemes with positive approximation (unstable schemes). This leads to an upper bound on the value of b when scalar smoothing coefficient is used in (3.2.15) (for $\bar{\mathbf{u}} = \mathbf{u}^n$):

$$0 \leqslant b \leqslant (1 - \sigma_{\max}^2)/2, \quad \sigma_{\max} = \max_i |\lambda_i| h, \quad \sigma_{\max} \leqslant 1.$$

When smoothing in (3.2.15) is carried out from the data of the time layer $t = t^{n+1}$, i.e. $\bar{\mathbf{u}} = \tilde{\mathbf{u}}$, the linear scalar case (3.1.1) for $\lambda > 0$ has in the space of coefficients a correspoding ray with its origin at point B_5 (for $b_i = b = 0$). This ray is directed towards point G_2 (for $b > 0$) and does not intersect the polyhedron $OA_1A_3A_4A_5A_6$ of difference schemes with positive approximation for any values of b, although it may pass quite close to this polyhedron (Fig. 3.4). The point on the ray B_5G_2 closest to this polyhedron is G_1 for which $b = \sigma/(2 + 5\sigma)$. In this case, if we choose

$$b_i = \gamma |\sigma_i|/(2 + 5|\sigma_i|), \quad 0 \leqslant \gamma \leqslant 1 \tag{3.2.17}$$

in (3.2.15), the points on the segment B_5G_1 in Fig. 3.4 will correspond to such a difference scheme.

Other widely used examples of explicit recalculation schemes which use smoothing on the upper time layer are some versions of the flow correction technique (FCT), proposed for one scalar equation (3.1.1) with variable values of λ [3.54], including the sign-changing values. The main idea behind these schemes is the calculation of $\tilde{w}_m$ according to a positive-approximation scheme, say

$$\tilde{w}_m = w_m^n - [\sigma_{m+1/2}(w_{m+1}^n + w_m^n) - \sigma_{m-1/2}(w_m^n + w_{m-1}^n)]/2$$
$$+ [\nu_{m+1/2}(w_{m+1}^n - w_m^n) - \nu_{m-1/2}(w_m^n - w_{m-1}^n)],$$
$$|\sigma|/2 \leqslant \nu \leqslant (1+\sigma^2)/4, \quad \sigma = \lambda\tau/h, \quad |\sigma| \leqslant 1,$$

followed by restoration in the domain of the second-order smooth solution with the help of recalculation

$$w_m^{n+1} = \tilde{w}_m - [\mu_{m+1/2}(\tilde{w}_{m+1} - \tilde{w}_m)$$
$$- \mu_{m-1/2}(\tilde{w}_m - \tilde{w}_{m-1})], \quad 0 \leqslant \mu \leqslant \nu - \sigma^2/2.$$

In the space of the coefficients of the difference schemes on the model (3.1.19) (Fig. 3.4), the first stage is represented by a certain point on the segment A_1O (the position of this point depends on the choice of ν), while the second stage marks a transition of the second-order schemes from this point to some point on the plane B_j, $j = 1, 2, \ldots$. The direction of this transition and the position of the transition point on the plane B_j, $j = 1, 2, \ldots$ is uniquely defined by the shape of the "antismoothing" operator used for scaling and depends on the quantity $\sigma = \lambda\tau/h$. Apparently, such an approach is preferable to (3.2.15), (3.2.17), since it always permits (whereever necessary) the use of a positive approximation scheme. Besides, together with the computation of $\tilde{\mathbf{u}}$ with the help of two-step schemes of Lax-Wendroff type, (3.2.15) is essentially a three-step scheme, while a scheme with third-order accuracy could be constructed with the help of two recalculations. For the first-order monotonic schemes in explicit flow-correction schemes, it is preferable to choose a difference scheme corresponding to point A_1 which is closest to the plane B_j, $j = 1, 2, \ldots$. Then the final stage will also be represented on this plane by a point (difference scheme) which is not very far from the point B_6 closest to the polyhedron $OA_1A_3A_4A_5A_6$. For system (3.2.5) such a difference scheme will be (3.2.15) for $\bar{\mathbf{u}} = \tilde{\mathbf{u}}$, computation of $\tilde{\mathbf{u}}$ by the scheme (3.2.11) and the choice of

$$b_i = -(1-\gamma)\,|\,\sigma_i\,|\,(1-|\,\sigma_i\,|)/2,\quad 0 \leqslant \gamma \leqslant 1. \tag{3.2.18}$$

For $\gamma = 1$, we then get the monotonic scheme (3.2.11), while the scheme (3.2.11), (3.2.15), (3.2.18) for $\gamma = 0$ will have the second order of accuracy on the solutions of (3.2.5). For intermediate values of γ in the linear case and for $0 \leqslant \sigma_i \leqslant 1$, this scheme will be represented by segment A_1C_1 in Fig. 3.4 (point C_1 falls on the straight line corresponding to third-order difference schemes only for $\sigma_i = 0.5$ as shown in Fig. 3.4).

Let us consider another example of the hybrid explicit two-step scheme for (3.2.5), which corresponds in the linear scalar case to a one-parametric family of difference schemes lying on segment A_1B_6 (it was shown in Secs. 3.1.4 and 3.1.5 that the terminal points A_1 and B_6 of this segment in Fig. 3.4 correspond to the most accurate first-order monotonic scheme and the least-oscillating second-order scheme respectively). Such a difference scheme can be realized in different ways, for example,

$$\tilde{\mathbf{u}}_m = \mathbf{u}_m^n - \tau(\mathbf{F}_{m+1}^n - \mathbf{F}_{m-1}^n)/2h,$$

$$\mathbf{u}_m^{n+1} = \tilde{\mathbf{u}}_m + [(\Omega^{-1}B\Omega)_{m+1/2}(\mathbf{u}_{m+1}^n - \mathbf{u}_m^n)$$

$$-(\Omega^{-1}B\Omega)_{m-1/2}(\mathbf{u}_m^n - \mathbf{u}_{m-1}^n)] + [(\Omega^{-1}C\Omega)_{m+1/2}(\tilde{\mathbf{u}}_{m+1} - \tilde{\mathbf{u}}_m)$$

$$-(\Omega^{-1}C\Omega)_{m-1/2}\,(\tilde{u}_m-\tilde{u}_{m-1})]+\{(\Omega^{-1}D\Omega)_{m+1/2}\,[(\tilde{u}_{m+1}+\tilde{u}_m)$$

$$-(u^n_{m+1}+u^n_m)]-(\Omega^{-1}D\Omega)_{m-1/2}\,[(\tilde{u}_m+\tilde{u}_{m-1})-(u^n_m+u^n_{m-1})]\},$$

$$B=\{b_i\},\ C=\{c_i\},\ D=\{d_i\},\quad i=1,\ \ldots,\ I. \tag{3.2.19}$$

Here B, C, and D are diagonal matrices with elements

$$\text{for } |\sigma_i|\leqslant 1:\ b_i=|\sigma_i|\,[1+5\,(1-\gamma)\,(1-|\sigma_i|)/19]/2,$$

$$c_i=0,\ d_i=6\,(1-\gamma)\,\sigma_i\,(1/|\sigma_i|-1)/19,$$

$$\text{for } 1<|\sigma_i|\leqslant 2:\ b_i=1/|\sigma_i|-[|\sigma|_i$$

$$+5\,(1-\gamma)\,(2-|\sigma_i|)\,(1-|\sigma_i|)/19]/2, \tag{3.2.20}$$

$$c_i=(|\sigma_i|-1)/|\sigma_i|,$$

$$d_i=(1-|\sigma_i|)\,[1-6\,(1-\gamma)\,(2-|\sigma_i|)/19]/\sigma_i.$$

It can be seen that although the unstable scheme for calculating $\tilde{u}_m$ is used as the predictor in this realization, the scheme (3.2.19), (3.2.20) is stable on the whole for Courant's numbers $\sigma_*\leqslant 2$ and any values of γ in the interval [0, 1]. For $\gamma=1$ this scheme is transformed into a certain monotonic scheme (in particular, for $\sigma_*\leqslant 1$ into (3.2.11)), while for $\gamma=0$ it has the second order of accuracy on the solutions of (3.2.5) and is analogous to the least oscillating second-order explicit scheme from [3.20]. This example once again emphasizes the well-known fact from computational practice which states that the properties of multistep difference schemes (as well as schemes with artificial viscosity, smoothing, etc.) must be judged as a whole and not separately for their individual steps. In other words, a favourable element in some scheme may lead to quite undesirable consequences in another (and vice versa, of course). This is due to the fact that each combination of the values of grid functions (at the mesh points of a grid model having a free parameter) which is added to a certain reference sheme, i.e. to a point in the space of coefficients, defines in this space a certain straight line passing through this point (called the reference scheme). By changing the reference scheme we displace this straight line parallel to itself in the space of coefficients, and different values of the free parameter will now have corresponding difference schemes with altogether different properties, resembling neither the reference scheme nor the initial family of schemes. For example, this straight line may now lie almost everywhere in the region of unstable schemes, may not intersect the set of schemes with positive approximation, and so on.

Let us consider another example of a hybrid (three-step) difference scheme for (3.2.5):

$$\tilde{\mathbf{u}}_{m+1/2} = (\mathbf{u}^n_m + \mathbf{u}^n_{m+1})/2 - \alpha\tau\,(\mathbf{F}^n_{m+1} - \mathbf{F}^n_m)/h, \tag{3.2.21}$$

$$\tilde{\tilde{\mathbf{u}}}_m = \mathbf{u}^n_m - \beta\tau\,(\tilde{\mathbf{F}}_{m+1/2} - \tilde{\mathbf{F}}_{m-1/2})/h, \tag{3.2.22}$$

$$\mathbf{u}^{n+1}_m = \mathbf{u}^n_m - 3\tau\,(\tilde{\tilde{\mathbf{F}}}_{m+1} - \tilde{\tilde{\mathbf{F}}}_{m-1})/4h - \tau\,(\mathbf{F}^n_{m+1} - \mathbf{F}^n_{m-1})/4h$$
$$+ \tau\,(\mathbf{F}^n_{m+2} - 2\mathbf{F}^n_{m+1} + 2\mathbf{F}^n_{m-1} - \mathbf{F}^n_{m-2})/12h + \delta, \quad \alpha = 1/3, \quad \beta = 2/3, \tag{3.2.23}$$

$$\delta = [(\Omega^{-1}B\Omega)^n_{m+1/2}\,(\mathbf{u}^n_{m+1} - \mathbf{u}^n_m) - (\Omega^{-1}B\Omega)^n_{m-1/2}\,(\mathbf{u}^n_m - \mathbf{u}^n_{m-1})]$$
$$+ [(\Omega^{-1}G\Omega)^n_{m+1/2}\,(-\mathbf{u}^n_{m-1} + 3\mathbf{u}^n_m - 3\mathbf{u}^n_{m+1} + \mathbf{u}^n_{m+2})$$
$$- (\Omega^{-1}G\Omega)^n_{m-1/2}\,(-\mathbf{u}^n_{m-2} + 3\mathbf{u}^n_{m-1} - 3\mathbf{u}^n_m + \mathbf{u}^n_{m+1})]$$
$$+ [(\Omega^{-1}D\Omega)^n_{m+1/2}\,(\mathbf{u}^n_{m-1} - \mathbf{u}^n_m - \mathbf{u}^n_{m+1} + \mathbf{u}^n_{m+2})$$
$$- (\Omega^{-1}D\Omega)^n_{m-1/2}\,(\mathbf{u}^n_{m-2} - \mathbf{u}^n_{m-1} - \mathbf{u}^n_m + \mathbf{u}^n_{m+1})],$$
$$B = \{b_i\}, \quad G = \{g_i\}, \quad D = \{d_i\}, \quad i = 1, \ldots, I,$$
$$b_i = \gamma|\sigma_i|\,(1 - |\sigma_i|)/2,$$
$$g_i = 3\gamma\,|\sigma_i|\,(1 - |\sigma_i|)/19 - |\sigma_i|\,(24 - 5|\sigma_i|)/152,$$
$$d_i = \gamma\sigma_i\,(\sigma_i^2 - 1)/24, \quad 0 \leqslant \gamma \leqslant 1. \tag{3.2.24}$$

For $\gamma = 1$, this scheme is transformed into the monotonic scheme (3.2.11). For $\gamma = 0$ and with a scalar g (as the coefficient in the expression for δ) instead of the matrix coefficient $\Omega^{-1}G\Omega$ as in (3.2.24), i.e. for

$$\delta = g\,(\mathbf{u}^n_{m+2} - 4\mathbf{u}^n_{m+1} + 6\mathbf{u}^n_m - 4\mathbf{u}^n_{m-1} + \mathbf{u}^n_{m-2}), \tag{3.2.25}$$

this scheme is a one-parametric family of third-order difference schemes on the solutions of (3.2.5), proposed in [3.14] where it is also shown (see (3.1.23) as well) that this family is stable for

$$\sigma_* = \tau \max_{m,\,i} |\lambda_i|/h \leqslant 1 \quad \text{and}$$
$$-1/8 \leqslant g \leqslant \sigma_*^2\,(\sigma_*^2 - 4)/24.$$

Figure 3.13 shows the domain of values of parameter g allowed by this stability condition (this domain lies between the dashed lines D and C_3). The dashed lines D and C_1 in this figure show the values of parameter g in (3.2.25) recommended in [3.65] and obtained from an analysis of the dissipative and dispersive properties of a difference scheme of the type (3.2.21), (3.2.22), (3.2.23), (3.2.25) (the relations (3.2.21) and (3.2.22) have been replaced by the MacCormac scheme

[3.67] which is more convenient for generalization to the multidimensional case). For the scheme with the minimum dissipation, $g = \sigma^2_{max}(\sigma^2_{max} - 4)/24$ (point D in Fig. 3.4), while for the scheme with minimum dispersion, $g = (4\sigma^2_{max} + 1)(\sigma^2_{max} - 4)/120$ (point C_1 in Fig. 3.4), where $\sigma_{max} = \tau \max_i |(\lambda_i)^n_m|/h$. Comparing the relations (3.2.21)-(3.2.23) and (3.2.25) in the linear scalar case with (3.1.2), (3.1.5), (3.1.22) on the grid model (3.1.19), we can establish a relation between the free parameters g and α^0_{-2}:

$$g = \alpha^0_{-2} - \sigma(\sigma + 2)(2\sigma - 1)/24.$$

This gives the following optimal value of this parameter for a version of the scheme (3.2.21)-(3.2.24), $\gamma = 0$ (which is "closest" to positive

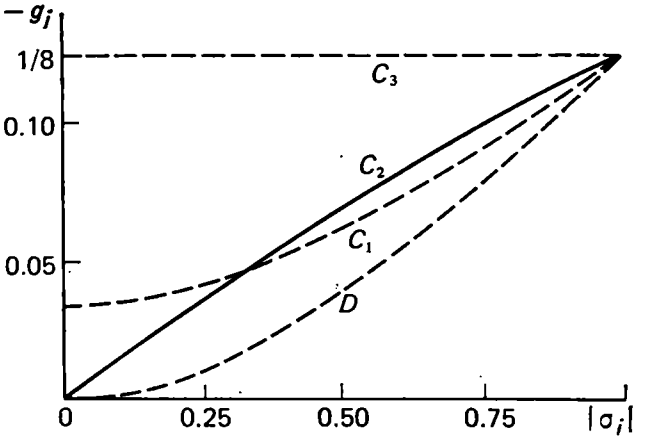

Fig. 3.13.

approximation schemes) obtained from (3.1.24) for $\sigma > 0$ and an analogous expression for $\sigma < 0$:

$$g_i = |\sigma_i|(5|\sigma_i| - 24)/152. \qquad (3.2.26)$$

The dependence of parameter g_i on $|\sigma_i|$ in this expression is shown by a solid line in Fig. 3.13 (curve C_2). The segment A_1C_2 in Fig. 3.4 corresponds to the scheme (3.2.21)-(3.2.24) in the linear scalar case and $\sigma > 0$ for values of γ lying between 0 and 1.

In Fig. 3.14, the density profiles ρ are plotted as functions of $m = y/h$ at the cross section $x = 2.77$ (after 120 steps). These profiles have been calculated by using various schemes of self-simulating stationary problem on the interaction of the rectilinear shock wave AC with the contact discontinuity BC (Fig. 3.15). After the interaction at point C, the refracted shock wave $1'$, contact discontinuity $2'$,

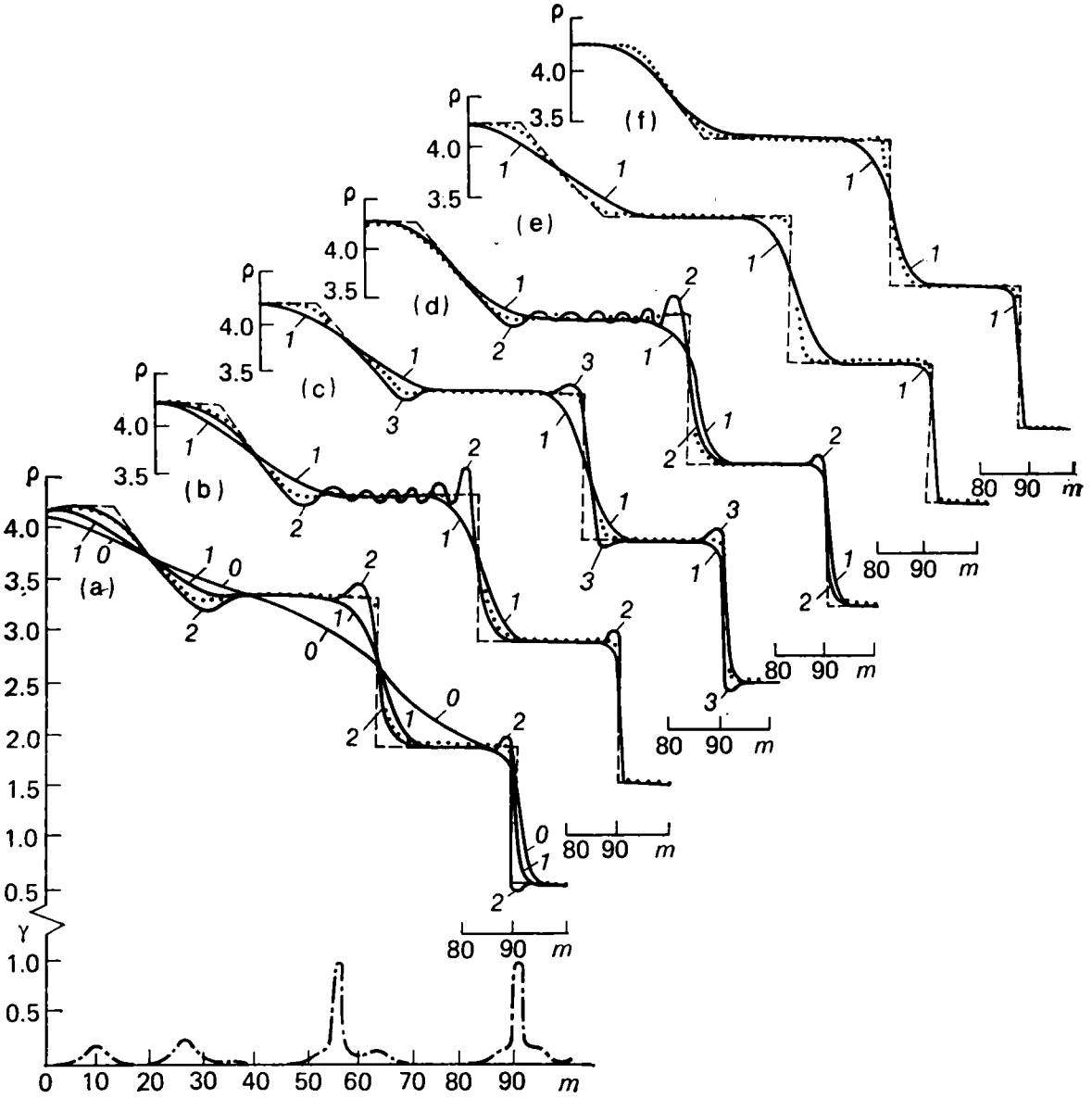

Fig. 3.14.

and fan of expansion waves *3* and *4* are formed. For the problem under consideration, we obtain in (3.2.5)

$$\mathbf{u} = \{\rho u, \ \rho u^2 + p, \ \rho uv, \ (\rho E + p)\, u\},$$
$$\mathbf{F} = \{\rho v, \ \rho uv, \ \rho v^2 + p, \ (\rho E + p)\, v\}, \qquad (3.2.27)$$
$$p = (\varkappa - 1)\, \rho\varepsilon, \quad E = \varepsilon + (u^2 + v^2)/2,$$
$$\mathbf{u}\,(0, \ y) = \mathbf{u}^0\,(y).$$

The spatial coordinate x plays the role of the hyperbolic variable t, while another spatial coordinate y is used instead of x in (3.2.5). The following initial values were chosen for the components u and v of the velocity vector along x- and y-axes, the internal energy ε, and the pressure p:

in domain I : $u = 0.967$, $v = -0.259$, $\varepsilon = 0.348$, $p = 0.007$,

in domain II : $u = 0.967$, $v = -0.259$, $\varepsilon = 0.174$, $p = 0.007$,

in domain III: $u = 0.944$, $v = 0.000$, $\varepsilon = 0.585$, $p = 0.095$.

The data in Figs. 3.14*a-e* correspond to calculations for $\sigma_* = 1$, and in Fig. 3.14*f* to calculations for $\sigma_* = 2$. The exact solution is shown by dashed lines.

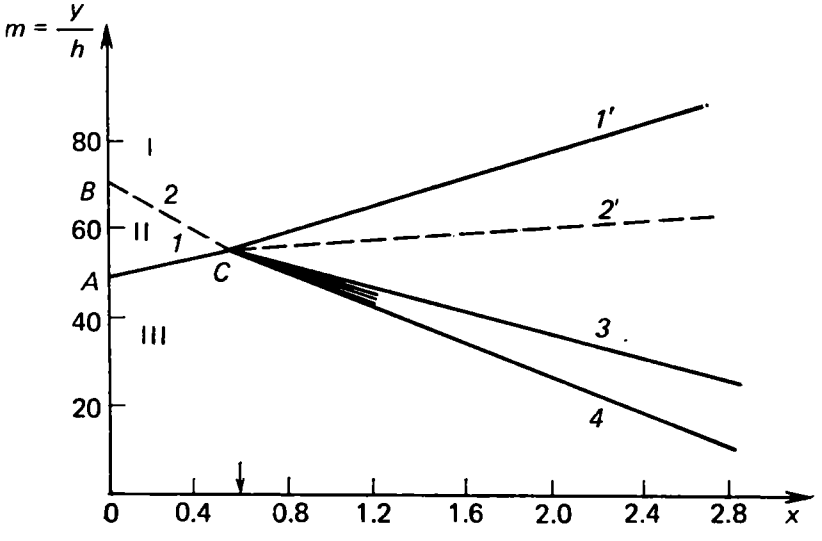

Fig. 3.15.

Curves *1* in Figs. 3.14*a-c*, *e* correspond to calculations according to the first-order monotonic scheme with the minimum approximation viscosity (3.2.11), curve *O* in Fig. 3.14*a* represents Lax's scheme (point *O* in Figs. 3.2-3.5 corresponds to the difference scheme which is not optimal in the sense of the value of approximation viscosity). As in the linear scalar case (Fig. 3.7), we can clearly note here the advantages of positive-approximation schemes (which are "closest" to higher-approximation schemes in the space of coefficients) over schemes that are not optimal in this sense. While scheme (3.2.11) gives quite a satisfactory solution and can successfully compete with higher-order schemes at discontinuities like shock waves, Lax's scheme and other non-optimal schemes with positive approximation are practically unsuitable for this type of problems.

The effect of closeness of second- and higher-order schemes to the set of positive approximation schemes in the space of coefficients can be judged by comparing the results of calculations made by using the second-order scheme (3.2.19), (3.2.20), $\gamma = 0$ (curve *2* in Fig. 3.14*a*) and the third-order scheme (3.2.21)-(3.2.24), $\gamma = 0$ (curve *3* in Fig. 3.14*c*), (these schemes are optimal) with the results obtained by using the non-optimal second-order Lax-Wendroff scheme [3.44] and the analogous MacCormac scheme [3.67] (curves *2* in Figs. 3.14*d* and 3.14*b* respectively). It can be seen that the use of optimal schemes considerably decreases the amplitude of oscillations and the extent of their propagation. However, it follows from the results of [3.18-3.20] and Sec. 3.1.3 that it is not possible to completely eliminate these quantities.

The results of calculations of problem (3.2.27) by using the hybrid grid-characteristic schemes (with $0 \leqslant \gamma \leqslant 1$) (3.2.15), (3.2.16) (Fig. 3.14*b*); (3.2.15), (3.2.17) (Fig. 3.14*d*); (3.2.11), (3.2.15), (3.2.18) (Fig. 3.14*e*); (3.2.19), (3.2.20) (Fig. 3.14*a*, 3.14*f*); and (3.2.21)-(3.2.24) (Fig. 3.14*c*) are shown by dots. Curves *1* in Fig. 3.14*f* represent the results of calculations by using the first-order monotonic scheme (3.2.19), (3.2.20), $\gamma = 1$, for $\sigma_* = 2$. We see that in all hybrid grid-characteristic schemes it is possible to practically get rid of oscillations while the width of the discontinuity spreading zone in these schemes remains the same as in the second- and third-order reference schemes. The scheme (3.2.19), (3.2.20) (Fig. 3.14*a*) gives somewhat better results. This is quite natural since the solution obtained has small oscillations even without regularization (Fig. 3.14*a*, curve *2*). The positive properties of this scheme are retained right up to $\sigma_* = 2$ (Fig. 3.14*f*). Curve *1* in Fig. 3.14*d* represents the results of calculations using the scheme (3.2.15), (3.2.17) with the scalar smoothing coefficient $b_i = b = 0.3$. The choice of a universal smoothing coefficient suitable for all compatibility conditions is a quite complicated problem. The same applies to the scheme (3.2.21), (3.2.22), (3.2.23), (3.2.25).

In the hybrid schemes considered above, the question of the choice of specific values of the scalar parameter $0 \leqslant \gamma \leqslant 1$ was left unresolved, since its choice, which usually depends on the nature of the solution, is an independent problem. The general requirements concerning the choice of this parameter are quite apparent: it must assume the value 0 in the domain of smooth solution and the value 1 near the discontinuities. For this purpose, we need effective algorithms for localizing the positions of discontinuities. The parameter γ can actually be chosen in different ways and the final result depends to a certain extent on the successful choice of the algorithm for determining this parameter. Some methods of choosing γ (or its analogues) are described in [3.51-3.54]. It should be emphasized that in constructing all the hybrid schemes considered here, characteristic

properties of systems of hyperbolic equations were essentially used, while the choice of a single (universal) parameter γ for all equations ensures for $\gamma = 1$ the attainment of some reference monotonic difference scheme with the lowest approximation viscosity. This distinguishes the method described here from other existing methods of regularization of discontinuous numerical solutions. In the computations presented in Figs. 3.12 and 3.14, the algorithm for the choice was analogous to that in [3.53] for example

$$\gamma_{m\pm1/2} = [1 + (2\mu_{m\pm1/2} - 1)\,(|\,2\mu_{m\pm1/2} - 1\,| + \varepsilon')^{1/k-1}]/2,$$
$$\mu_{m\pm1/2} = (\mu_m + \mu_{m\pm1})/2,$$
$$\mu_m = (|\,\delta_{m+1/2} - \delta_{m-1/2}\,|)/[(\delta_{m+1/2} + \delta_{m-1/2}) + \varepsilon'], \qquad (3.2.28)$$
$$\delta_{m\pm1/2} = |\,|\,\mathbf{u}_{m\pm1}\,| - |\,\mathbf{u}_m\,|\,|,$$
$$|\,\mathbf{u}\,| = \sqrt{\sum_{i=1}^{I} u_i^2}, \quad \mathbf{u} = \mathbf{u}^n = \{u_1^n, \ldots, u_I^n\}, \quad \varepsilon' = 10^{-6}, \quad k = 2\text{-}10,$$

and some other versions of the same choice can be taken. The dot-and-dash line in Fig. 3.14 shows the typical behaviour of γ in numerical computations.

3.2.4. The difference schemes considered in Secs. 3.2.2 and 3.2.3 were constructed from the divergent equations (3.2.5) and are of conservative nature. This property is known [3.15] to play an important role in through calculations of discontinuous solutions. The nondivergent versions of all these schemes can be easily obtained, for example, by replacing differences of the type $\mathbf{F}_{m+1} - \mathbf{F}_m$ by

$$A_{m+1/2}\,(\mathbf{u}_{m+1} - \mathbf{u}_m).$$

The exact solutions (dashed lines) of the problem (3.2.14) are compared in Fig. 3.16 with the results of calculations (of the density profile ρ) for divergent (Fig. 3.16*a*) and nondivergent (Fig. 3.16*b*) versions of the scheme (3.2.19), (3.2.20). Curves *1* correspond to calculations made with the help of a first-order scheme ($\gamma = 1$), while curves *2* are obtained by using a version having the second-order accuracy ($\gamma = 0$). The dots represent the results obtained by using the hybrid scheme (γ given by (3.2.28)). It can be seen that for low shockwave intensities (up to pressure ratio $\simeq 1.5$), the nondivergent schemes quite satisfactorily reproduce such a discontinuous solution, in particular, for the parameters behind the shock wave, although the velocity of the shock wave is reproduced in these schemes with a much lower accuracy than in the divergent versions (in other words, relations at discontinuities are satisfied in nondivergent schemes with a considerable error). With an increasing intensity of discontinuities, however, nondivergent schemes become practically unsuitable for a through calculation of discontinuous solutions and require for their application an explicit isolation of high-intensity discontinuities.

From the velocity profiles, v, presented in Fig. 3.17 for the divergent (curve *1*) and nondivergent (curve *2*) versions of the hybrid scheme (3.2.19), (3.2.20), (3.2.28) for the same problem (3.2.14) but with stronger discontinuities ($\rho\,(0,\ x) = p\,(0,\ x) = 10$ for $x \leqslant 0$), we see that the nondivergent scheme quite unsatisfactorily reproduces

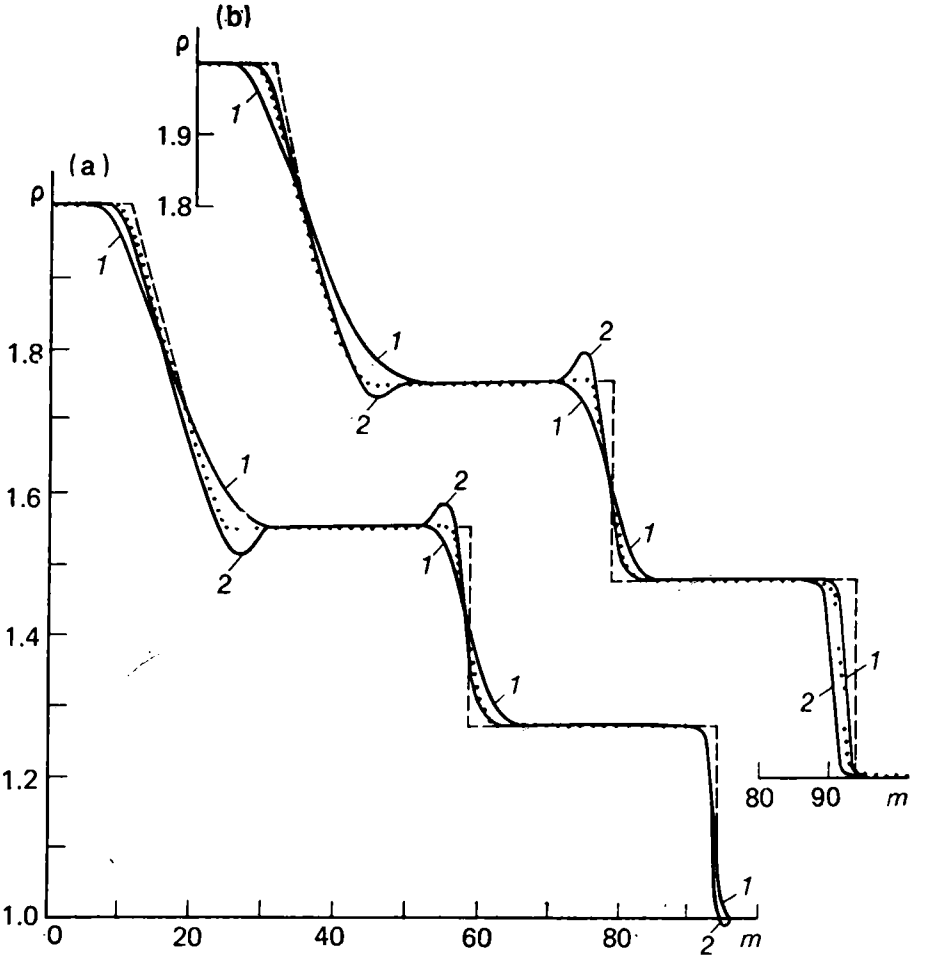

Fig. 3.16.

discontinuities, including the contact discontinuity for which the velocity, v, must be continuous. The exact solution is shown in Fig. 3.17 by a dashed line.

On the other hand, the application of conservative difference schemes for strictly divergent equations (3.2.5) (with the right-hand side φ equal to zero) may also lead to unpleasant consequences in some cases. For example, if the equations can be written in the divergent form (3.2.5) with $\varphi = 0$ in at least one coordinate system, an arbitrary one-to-one transformation of independent variables $t = t\,(\tau,\ \eta)$, $x = x\,(\tau,\ \eta)$ transforms the system (3.2.5) (with the

help of the substitution $\mathbf{w} = (1/\eta_x)\,\mathbf{u}$, $\Phi = (1/\eta_x)\,(\eta_t \mathbf{u} + \eta_x \mathbf{F})$ into the following divergent form in terms of new variables τ and η, which is equivalent to (3.2.5):

$$\mathbf{w}_\tau + \Phi_\eta = 0. \tag{3.2.29}$$

This remark is also valid for the multidimensional case. Let us consider the simplest Cauchy problem for (3.2.5), $\varphi = 0$, viz.

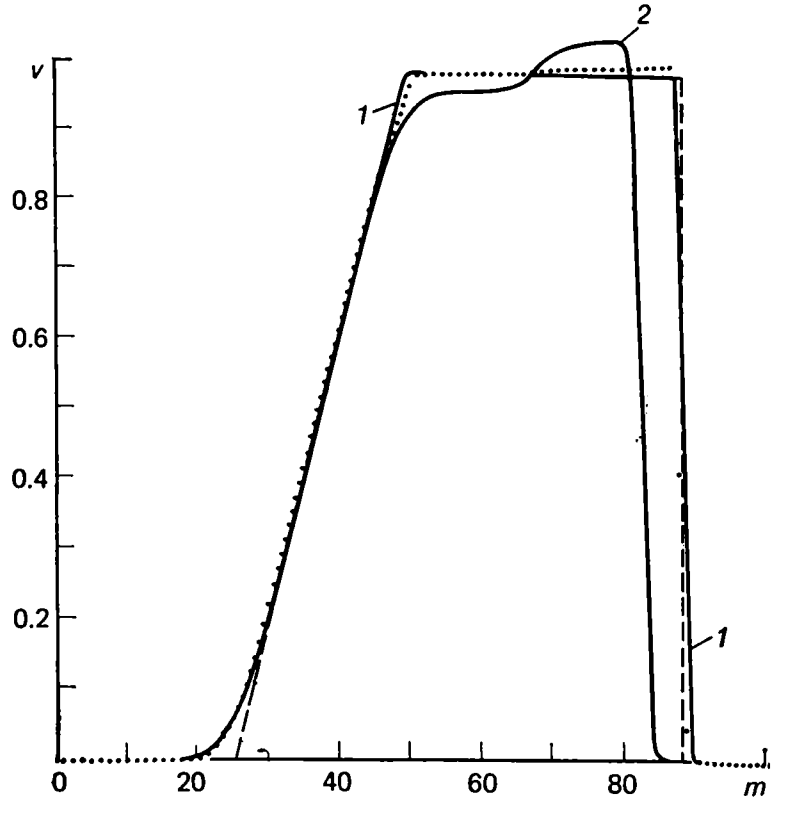

Fig. 3.17.

$\mathbf{u}\,(0, x) = \mathbf{u}^0$, $u_i^0 = \text{const}$, $i = 1, \ldots, I$. Then $\mathbf{u}\,(t, x) = \mathbf{u}^0$ for all $t > 0$. However, for a certain nonlinear change of variables, for example, $t = \tau$, $x = x\,(\tau, \eta)$, $\eta_x \neq 0$ and $\eta_x \neq \infty$, we find that $\mathbf{w}\,(0, \eta)$ and $\Phi\,(0, \eta)$ become functions of η. In this case, due to approximation errors, no conservative scheme will give $\mathbf{u}\,(t, x) = \mathbf{u}^0$, while nondivergent schemes do not suffer from this drawback. This effect is especially noticeable near the axis of a cylindrical system of coordinates, near the centre of a spherical system, and so on, corresponding to the sharpest change in the transformed function Φ and to the largest approximation errors which are proportional to some spatial derivatives of Φ. In such situations, intermediate forms of equations between (3.2.1) and (3.2.5) are usually employed. Other approaches, however, are also possible. Besides the problem of finding

a generalized solution (the use of conservative through-count schemes is an analogue of this problem), another approach is also widely used for the divergent equations (3.2.5). This involves the splitting of the integration domain into subdomains of smooth solutions separated by explicitly treated discontinuity surfaces, and the formulation on such surfaces of the boundary conditions following from the corresponding limiting transition in the conservation laws of the type (3.2.5). In other words, the divergent form of Eqs. (3.2.5) is used in this method only at the discontinuity surfaces. This approach, based on nondivergent numerical methods, is used widely and successfully (especially for first order schemes). It leads to quite accurate results on rather coarse grids if the number of high-intensity discontinuities is comparatively small, since weak discontinuities are satisfactorily reproduced by nondivergent schemes. When such an approach becomes too cumbersome (due to a large number of sharp discontinuities, the complexity of their form, etc.), we can resort to through-count schemes. However, conservative versions of the schemes are employed only when they are really required, i.e. near the discontinuities and other surfaces of the nonsmooth solution, while nondivergent schemes are used in the region of smooth solution in the same way as in hybrid schemes with an approximation order. Such locally divergent schemes are also advantageous because the computations for the conservative versions (usually requiring a much larger number of arithmetical operations than for the nondivergent versions) are made for a relatively small number of nodes among the total number of such points in the domain of integration. An example of the solution of problem (3.2.14) with $\rho(0, x) = p(0, x) = 10$ for $x \leqslant 0$ with the help of the hybrid scheme (3.2.19), (3.2.20), (3.2.28) is shown by dots in Fig. 3.17. The scheme (3.2.19), (3.2.20) was directly used for calculating the values of $\gamma_m > 0.5$ in accordance with (3.2.28). For $\gamma_m \leqslant 0.5$, this point was computed with the help of the nondivergent version of the same scheme (there was about 87-90% such points on the layer $t = \text{const}$). We see that such a locally divergent scheme is not inferior in its properties to the purely conservative scheme (3.2.19), (3.2.20).

3.3. GRID-CHARACTERISTIC METHODS FOR MULTIDIMENSIONAL SYSTEMS OF HYPERBOLIC EQUATIONS

3.3.1. The grid-characteristic methods considered in Sec. 3.2 can be generalized to multidimensional systems of hyperbolic equations of the type

$$\mathbf{u}_t + \sum_{p=1}^{P} A_p(t, x_1, \ldots, x_P, \mathbf{u})\,\mathbf{u}_{x_p} - \mathbf{f}(t, x_1, \ldots, x_P, \mathbf{u}) = 0,$$

$$A_p = \Omega_p^{-1} \Lambda_p \Omega_p, \quad \Lambda_p = \{\lambda_i^p\}, \quad \Omega_p = \{\omega_i^p\},$$
$$i = 1, \ldots, I, \quad p = 1, \ldots, P, \tag{3.3.1}$$

or to their divergent form

$$\mathbf{u}_t + \sum_{p=1}^{P} (\mathbf{F}_p)_{x_p} - \varphi = 0, \tag{3.3.2}$$

in different ways. From linear algebra, it is known that in the particular case of pairwise commuting matrices A_p, i.e. when $A_{p_1} A_{p_2} = A_{p_2} A_{p_1}$ (unfortunately, this situation is encountered rarely in computational practice), there exists a single transformation which diagonalizes matrix A_p (in this case, all $\Omega_p = \Omega$). We can then directly use the approach proposed in Sec. 3.1 and carry out constructions analogous to those in Sec. 3.1 for the multidimensional transport equation $w_t + \sum_{p=1}^{P} \lambda^p w_{x_p} = 0$. These constructions are then naturally extended to the case of systems (3.3.1) or (3.3.2). Sometimes, the generalizations to the multidimensional case are obvious (for example, for scheme (3.2.11) or its nondivergent version [3.1]) and can be obtained without much difficulty (see, for example, [3.17, 3.33]). The most universal and effective among these methods, apparently, involve the use of various versions of the method of splitting into various spatial coordinates, although some properties of the schemes obtained in this way (in particular, for one-dimensional equations following from their analysis in the space of coefficients) can be judged in this case from the results of their practical applications, or from the analysis for the case of one equation in (3.3.1).

3.3.2. For generalization of the first-order difference schemes with positive approximation to the multidimensional case, we express (3.3.1) in the form of a linear combination of one-dimensional operators with positive coefficients γ_p whose sum is equal to unity:

$$\sum_{p=1}^{P} \gamma_p (\mathbf{u}_t + D_p \mathbf{u}_{x_p} - \mathbf{f}) = 0 \quad \gamma_p \geqslant 0, \quad \sum_{p=1}^{P} \gamma_p = 1,$$
$$D_p = A_p/\gamma_p = \Omega_p^{-1} L_p \Omega_p, \quad L_p = \Lambda_p/\gamma_p = \{l_i^p\}, \quad l_i^p = \lambda_i^p/\gamma_p.$$

Introducing the difference grid

$$t^n = n\tau, n = 0, 1, \ldots, \quad x_{m_p} = m_p h_p, m_p = 0, \pm 1, \ldots,$$

in the domain of integration, we approximate the expressions within parentheses to the difference expressions (3.2.3)

$$\tau^{-1} \Big[\Omega_p^{-1} \Big(E - \sum_{\mu_p, \nu_p} \nu_p A_{\mu_p}^{\nu_p}\Big)^{-1} \Omega_p \mathbf{u}^{n+1}_{m_1, \ldots, m_P}$$
$$- \sum_{\mu_p, \nu_p} \Omega_p^{-1} \Big(E - \sum_{\mu_p, \nu_p} \nu_p A_{\mu_p}^{\nu_p}\Big)^{-1} A_{\mu_p}^{\nu_p} \Omega_p$$
$$\times \mathbf{u}^{n+\nu_p}_{m_1, \ldots, m_p + \mu_p, \ldots, m_P} - \tau \mathbf{f}\Big] = \mathbf{u}_t + D_p \mathbf{u}_{x_p} - \mathbf{f} + O(\tau, h_p, h_p^2/\tau),$$

where $A_{\mu_p}^{\nu_p} = \{(\alpha_{\mu_p}^{\nu_p})_i\}$ are diagonal matrices whose elements for all $p = 1, 2, \ldots, P$ and $i = 1, 2, \ldots, I$ are determined from Eqs. (3.1.5) and inequalities (3.1.10) (i.e. from (3.1.11)-(3.1.13)), where $\lambda = \lambda_i^p/\gamma_p$ in (3.1.11)-(3.1.13) are now eigenvalues of matrices D_p.

As a result, we obtain first-order difference schemes of the type

$$\Big[\sum_{p=1}^{P} \gamma_p \Omega_p^{-1} \Big(E - \sum_{\mu_p,\, \nu_p} \nu_p A_{\mu_p}^{\nu_p}\Big)^{-1} \Omega_p\Big] \mathbf{u}_{m_1, \ldots, m_P}^{n+1} = \tau \mathbf{f}$$

$$+ \sum_{p=1}^{P} \gamma_p \Big[\sum_{\mu_p, \nu_p} \Omega_p^{-1} \Big(E - \sum_{\mu_p, \nu_p} \nu_p A_{\mu_p}^{\nu_p}\Big)^{-1} A_{\mu_p}^{\nu_p} \Omega_p\Big] \mathbf{u}_{m_1, \ldots, m_p + \mu_p, \ldots, m_P}^{n+\nu_p} \tag{3.3.3}$$

in which (in the case of symmetric matrices A_p of the initial system (3.3.1)) all matrices

$$\gamma_p \Omega_p^{-1} \Big(E - \sum_{\mu_p, \nu_p} \nu_p A_{\mu_p}^{\nu_p}\Big)^{-1} A_{\mu_p}^{\nu_p} \Omega_p,$$

$$\sum_{p=1}^{P} \gamma_p \Omega_p^{-1} \Big(E - \sum_{\mu_p, \nu_p} \nu_p A_{\mu_p}^{\nu_p}\Big)^{-1} A_{0p}^{0p} \Omega_p$$

are non-negative definite (the matrix $\sum_{p=1}^{P} \gamma_p \Omega_p^{-1} \Big(E - \sum_{\mu_p, \nu_p} \nu_p A_{\mu_p}^{\nu_p}\Big)^{-1} \Omega_p$ is positive definite) in view of the fact that all $\gamma_p \geqslant 0$ and the fact known from linear algebra that the sum of non-negative (positive) definite matrices is also a non-negative (positive) definite matrix.

If for all $p = 1, \ldots, P$, one-dimensional difference operators (3.2.3) are explicit ($\nu_p \leqslant 0$), scheme (3.3.3) will also be explicit on the whole, for example, for the two-layer schemes

$$\nu_p = 0, \quad \sum_{\mu_p, \nu_p} \nu_p A_{\mu_p}^{\nu_p} = 0:$$

$$\mathbf{u}_{m_1, \ldots, m_P}^{n+1} = \tau \mathbf{f} + \sum_{p=1}^{P} \gamma_p \sum_{\mu_p, \nu_p} \Omega_p^{-1} A_{\mu_p}^{0p} \Omega_p \mathbf{u}_{m_1, \ldots, m_p + \mu_p, \ldots, m_P}^{n+\nu_p}.$$

In particular, for $P = 2$, by using the nondivergent versions of one-dimensional schemes (3.2.11) for each direction, we obtain the following scheme [3.17] on the six-point model $(t^{n+1}, x_{m_1}, x_{m_2})$, (t^n, x_{m_1}, x_{m_2}), $(t^n, x_{m_1 \pm 1}, x_{m_2})$, $(t^n, x_{m_1}, x_{m_2 \pm 1})$:

$$\mathbf{u}_{m_1 m_2}^{n+1} = \tau \mathbf{f} + \Big[\gamma_1 \Omega_1^{-1} \Big(E - \frac{\tau}{h_1} |\, L_1 \,|\Big) \Omega_1$$

$$+ \gamma_2 \Omega_2^{-1} \Big(E - \frac{\tau}{h_2} |\, L_2 \,|\Big) \Omega_2\Big] \mathbf{u}_{m_1 m_2}^{n}$$

$$+ \frac{\gamma_1 \tau}{2h_1} \Omega_1^{-1} (|\, L_1 \,| - L_1) \Omega_1 \mathbf{u}_{m_1+1,\, m_2}^{n}$$

$$
\begin{aligned}
&+\frac{\gamma_1\tau}{2h_1}\,\Omega_1^{-1}\,(|\,L_1\,|+L_1)\,\Omega_1\mathbf{u}^n_{m_1-1,\,m_2}\\
&+\frac{\gamma_2\tau}{2h_2}\,\Omega_2^{-1}\,(|\,L_2\,|-L_2)\,\Omega_2\mathbf{u}^n_{m_1,\,m_2+1}\\
&+\frac{\gamma_2\tau}{2h_2}\,\Omega_2^{-1}\,(|\,L_2\,|+L_2)\Omega_2\mathbf{u}^n_{m_1,\,m_2-1}=\tau\mathbf{f}\\
&+\left(E-\frac{\tau}{h_1}\,\Omega_1^{-1}\,|\,\Lambda_1\,|\,\Omega_1-\frac{\tau}{h_2}\,\Omega_2^{-1}\,|\,\Lambda_2\,|\,\Omega_2\right)\mathbf{u}^n_{m_1m_2}\\
&+\frac{\tau}{2h_1}\,\Omega_1^{-1}\,(|\,\Lambda_1\,|+\Lambda_1)\,\Omega_1\mathbf{u}^n_{m_1+1,\,m_2}\\
&+\frac{\tau}{2h_1}\,\Omega_1^{-1}\,(|\,\Lambda_1\,|+\Lambda_1)\,\Omega_1\mathbf{u}^n_{m_1-1,\,m_2}\\
&+\frac{\tau}{2h_2}\,\Omega_2^{-1}\,(|\,\Lambda_2\,|-\Lambda_2)\,\Omega_2\mathbf{u}^n_{m_1,\,m_2+1}\\
&+\frac{\tau}{2h_2}\,\Omega_2^{-1}\,(|\,\Lambda_2\,|+\Lambda_2)\,\Omega_2\mathbf{u}^n_{m_1,\,m_2-1}.
\end{aligned}
\tag{3.3.4}
$$

This scheme contains no explicit dependence on the coefficients $\gamma_1=\gamma>0$ and $\gamma_2=1-\gamma>0$, although their introduction allows us to find the admissible values of τ. Indeed, the condition of nonnegative definiteness of the matrices appearing in (3.3.4) has the form (in the case of symmetric A_1 and A_2)

$$
\begin{aligned}
&(\gamma h_1)^{-1}\,\tau\max_i\,|\,\lambda_i^1\,|=\tau/(\gamma\tau_1)\leqslant 1,\\
&[(1-\gamma)\,h_2]^{-1}\,\tau\max_i\,|\,\lambda_i^2\,|=\tau/((1-\gamma)\,\tau_2)\leqslant 1,
\end{aligned}
\tag{3.3.5}
$$

whence the maximum admissible value $\tau=(1/\tau_1+1/\tau_2)^{-1}$ is obtained for $\gamma=\tau_2/(\tau_1+\tau_2)$, $\tau_p=h_p/\max_i\,|\,\lambda_i^p\,|$, $p=1,\ 2$.

For (3.3.2), the conservative version of scheme (3.3.4) has the form [3.18, 3.33]

$$
\begin{aligned}
&\mathbf{u}^{n+1}_{m_1m_2}=\tau\boldsymbol{\varphi}^n_{m_1m_2}+\mathbf{u}^n_{m_1m_2}\\
&-\frac{\tau}{2h_1}\,[(\mathbf{F}_1)^n_{m_1+1,\,m_2}-(\mathbf{F}_1)^n_{m_1-1,\,m_2}]\,\frac{\tau}{2h_2}\,[(\mathbf{F}_2)^n_{m_1,\,m_2+1}-(\mathbf{F}_2)^n_{m_1,\,m_2-1}]\\
&+\frac{\tau}{2h_1}\,[(\Omega_1^{-1}\,|\,\Lambda_1\,|\,\Omega_1)^n_{m_1+1/2,\,m_2}\,(\mathbf{u}^n_{m_1+1,\,m_2}-\mathbf{u}^n_{m_1m_2})\\
&-(\Omega_1^{-1}\,|\,\Lambda_1\,|\,\Omega_1)^n_{m_1-1/2,\,m_2}\,(\mathbf{u}^n_{m_1m_2}-\mathbf{u}^n_{m_1-1,\,m_2})]\\
&+\frac{\tau}{2h_2}\,[(\Omega_2^{-1}\,|\,\Lambda_2\,|\,\Omega_2)^n_{m_1,\,m_2+1/2}\,(\mathbf{u}^n_{m_1,\,m_2+1}-\mathbf{u}^n_{m_1m_2})\\
&-(\Omega_2^{-1}\,|\,\Lambda_2\,|\,\Omega_2)^n_{m_1,\,m_2-1/2}\,(\mathbf{u}^n_{m_1m_2}-\mathbf{u}^n_{m_1,\,m_2-1})].
\end{aligned}
\tag{3.3.6}
$$

From (3.3.5), it can be seen that for $\tau_1\ll\tau_2$, for example, we have $\tau\simeq\tau_1$ and it is interesting to choose one of the one-dimensional differ-

ence operators (corresponding to the direction $p = 1$) in an implicit form. If for one-dimensional operators we choose Carlsson's scheme for $p = 1$ and the nondivergent version of scheme (3.2.11) for $p = P = 2$, we obtain the following explicit-implicit difference scheme from (3.3.3) [3.18]:

$$-\Omega_1^{-1}S_{-11}^1\Omega_1\mathbf{u}_{m_1-1,\,m_2}^{n+1}+\Omega_1^{-1}S_{01}^1\Omega_1\mathbf{u}_{m_1m_2}^{n+1}$$
$$-\Omega_1^{-1}S_{11}^1\Omega_1\mathbf{u}_{m_1+1,\,m_2}^{n+1}=\tau\mathbf{f}+\sum_{\mu=-1}^{1}\Omega_1^{-1}S_{\mu_1}^0\Omega_1\mathbf{u}_{m_1+\mu,\,m_2}^{n}$$
$$+\sum_{m=-1}^{1}\Omega_2^{-1}S_{\mu_2}^0\Omega_2\mathbf{u}_{m_1,\,m_2+\mu}^{n}. \qquad (3.3.7)$$

Here, $S_{\mu p}^{\nu}=\{(s_{\mu p}^{\nu})_i\}$ are diagonal matrices with non-negative elements (when weaker restrictions are imposed on $\tau\leqslant(1-\gamma)\tau_2$ than in (3.3.5)):

$$(s_{-11}^1)_i=\sigma_i^1-\gamma,\quad (s_{01}^1)_i=1-\gamma+\sigma_i^1,$$
$$(s_{11}^1)_i=(s_{01}^0)_i=(s_{11}^0)_i=0,\ (s_{-11}^0)_i=\gamma \text{ for } \sigma_i^1>\gamma,$$
$$(s_{-11}^1)_i=(s_{11}^1)_i=(s_{11}^0)_i=0,\ (s_{01}^1)_i=1,$$
$$(s_{-11}^0)_i=\sigma_i^1,\ (s_{01}^0)_i=\gamma-\sigma_i^1 \text{ for } \gamma\geqslant\sigma_i^1\geqslant 0,$$
$$(s_{-11}^1)_i=(s_{-11}^0)_i=(s_{11}^0)_i=0,\ (s_{01}^1)_i=1,$$
$$(s_{01}^0)_i=\gamma+\sigma_i^1,\ (s_{11}^0)_i=-\sigma_i^1 \text{ for } 0>\sigma_i^1\geqslant-\gamma,$$
$$(s_{-11}^1)_i=(s_{-11}^0)_i=(s_{01}^0)_i=0,\ (s_{01}^1)_i=1-\gamma-\sigma_i^1,$$
$$(s_{11}^1)_i=-\sigma_i^1-\gamma,\ (s_{11}^0)_i=\gamma \text{ for } -\gamma>\sigma_i^1,$$
$$(s_{-12}^0)_i=\sigma_i^2,\ (s_{02}^0)_i=1-\gamma-\sigma_i^2,\ (s_{12}^0)_i=0 \text{ for } \sigma_i^2\geqslant 0,$$
$$(s_{-12}^0)_i=0,\ (s_{02}^0)_i=1-\gamma+\sigma_i^2,$$
$$(s_{12}^0)_i=-\sigma_i^2 \text{ for } 0>\sigma_i^2,\ \sigma_i^p=\tau\lambda_i^p/h_p,\ p=1,\ 2.$$

3.3.3. More diverse possibilities, including the possibility of generalizing second- and higher-order grid-characteristic schemes, hybrid schemes, etc. to the multidimensional case, arise if we represent multidimensional difference operators as products of the corresponding one-dimensional operators rather than their sum, as was done before. For some first-order monotonic schemes, this approach has been adopted, for example, in [3.68]. Other general methods of splitting are described, for example, in [3.12, 3.13].

By way of an example, we can mention the generalization to the multidimensional case constructed in [3.65] for the third-order explicit scheme of the type (3.2.21), (3.2.22), (3.2.23), (3.2.25) in which the multidimensional version of MacCormak's scheme [3.67] is used instead of the Lax-Wendroff scheme in the first two stages (of the type (3.2.21), (3.2.22). If, as in (3.2.24) ($\gamma = 0$), we replace

the scalar coefficients g^p from (3.2.25) in such a scheme by the matrix coefficients $\Omega_p^{-1}G_p\Omega_p$ with diagonal matrices $G_p = \{g_i^p\}$ given by the relations $g_i^p = -|\sigma_i^p|(24 - 5|\sigma_i^p|)/152$, $\sigma_i^p = \tau\lambda_i^p/h_p$, $p = 1, 2, 3$, $i = 1, \ldots, I$, we can obtain for the behaviour of the difference solutions in the multidimensional case a curve similar to curve 3 in Fig. 3.14*c*. Such a modification does not change the third order of approximation of the difference scheme [3.65].

As an example of an explicit hybrid scheme, we consider the two-dimensional version of the conservative scheme (3.2.11), (3.2.15), (3.2.18) for the divergent scheme (3.3.2) in which the multidimensional version of the monotonic scheme (3.2.11), i.e. (3.3.6), is used as the predictor for computing $\tilde{\mathbf{u}}_{m_1m_2}$, while for the corrector we take

$$\tilde{\tilde{\mathbf{u}}}_{m_1m_2} = \tilde{\mathbf{u}}_{m_1m_2} - [(\Omega_1^{-1}B_1\Omega_1)_{m_1+1/2,\,m_2}$$
$$\times(\tilde{\mathbf{u}}_{m_1+1,\,m_2} - \tilde{\mathbf{u}}_{m_1m_2}) - (\Omega_1^{-1}B_1\Omega_1)_{m_1-1/2,\,m_2}(\tilde{\mathbf{u}}_{m_1m_2} - \tilde{\mathbf{u}}_{m_1-1,\,m_2})],$$
$$\mathbf{u}_{m_1m_2}^{n+1} = \tilde{\tilde{\mathbf{u}}}_{m_1m_2} - [(\Omega_2^{-1}B_2\Omega_2)_{m_1,\,m_1+1/2}$$
$$\times(\tilde{\tilde{\mathbf{u}}}_{m_1m_2\pm1} - \tilde{\tilde{\mathbf{u}}}_{m_1m_2}) - (\Omega_2^{-1}B_2\Omega_2)_{m_1,\,m_2-1/2}(\tilde{\tilde{\mathbf{u}}}_{m_1m_2} - \tilde{\tilde{\mathbf{u}}}_{m_1,\,m_2-1})],$$
$$B_p = \{b_i^p\},\quad b_i^p = (1-\gamma_p)|\sigma_i^p|(1-|\sigma_i^p|)/2,$$
$$\sigma_i^p = \tau\lambda_i^p/h_p,\quad 0 \leqslant \gamma_p \leqslant 1,\quad p = 1, 2,\quad i = 1, \ldots, I. \qquad (3.3.8)$$

In order to ensure the second-order approximation for $\gamma_p = 0$ in the case on non-commuting matrices A_p ($A_1A_2 \neq A_2A_1$), we should carry out cyclic permutation of independent variables x_1 and x_2 in the corrector (3.3.8) as usual (see [3.13]). For each direction x_p in space, the scalar parameters γ_p are chosen independently in accordance with (3.2.28).

3.4. SOME RESULTS OF NUMERICAL INVESTIGATIONS OF MULTIDIMENSIONAL PROBLEMS

On the basis of some of the grid-characteristics methods considered above, a systematic analysis was carried out over the last few years of the aerodynamics of blunt bodies of complex geometric shapes (including spatial and nonstationary problems), numerical simulation of one- and two-dimensional nonstationary problems in plasma physics, as well as some dynamic problems in the mechanics of a deformable rigid body, including problems in which finite deformations are taken into account. Characteristic features of these problems are the complex stucture of the required solution, existence of domains with large gradients, discontinuity surfaces, etc.

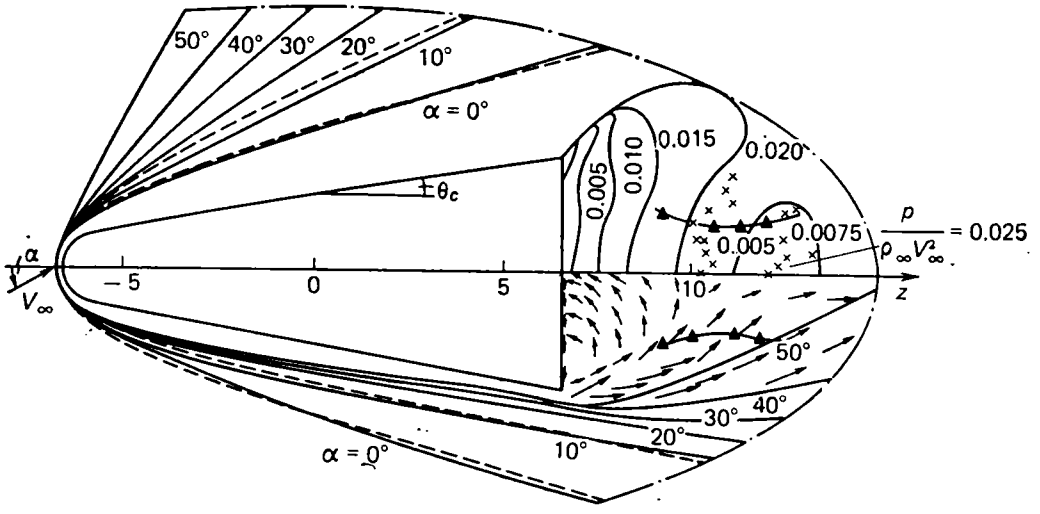

Fig. 3.18. Flow pattern in the symmetry plane; $M_\infty = 6$, $\varkappa = 1.4$, $\theta_c = 10°$.

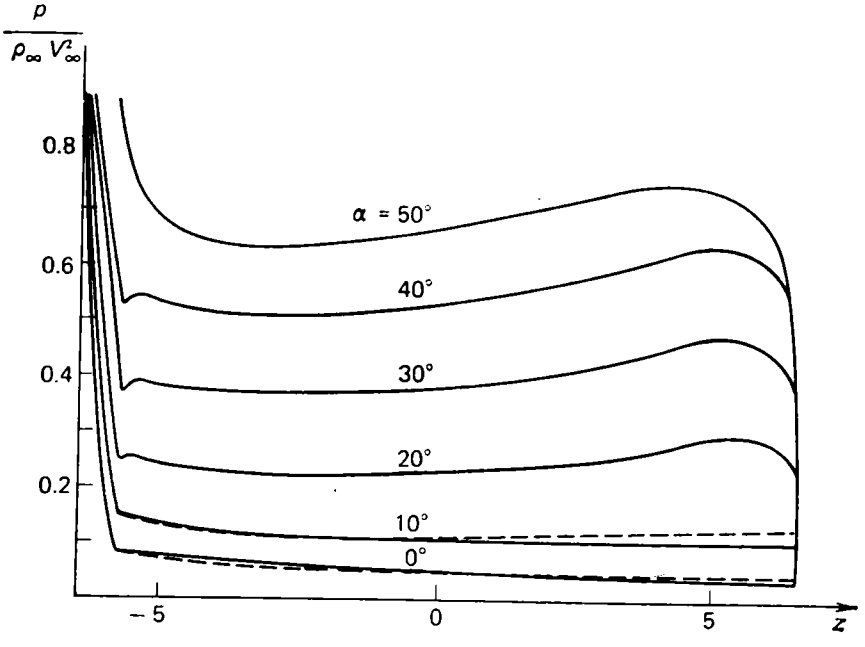

Fig. 3.19. Pressure distribution along the windward generatrix of a body; $M_\infty = 6$, $\varkappa = 1.4$, $\theta_c = 10°$.

3.4.1. The first-order nondivergent scheme (3.3.4) from [3.17] having the lowest approximation viscosity and the property of monotonicity, was found to be quite effective for numerical solution of problems with a comparatively small number of high-intensity discontinuity surfaces which can be explicitly treated by imposition of appropriate boundary conditions. As an example, Figs. 3.18 and 3.19 show in the flow symmetry plane the pattern of steady superso-

nic flow past a spherically blunted cone of finite length with a half-angle $\theta_c = 10°$ for Mach number $M_\infty = 6$ for the forward air flow (adiabatic exponent $\varkappa = 1.4$) (Fig. 3.18), and pressure distribution along the windward generatrix (referred to twice the velocity head $\rho_\infty V_\infty^2$, Fig. 3.19). Calculations were carried out proceeding from some initial conditions for the body as a whole. On each generatrix,

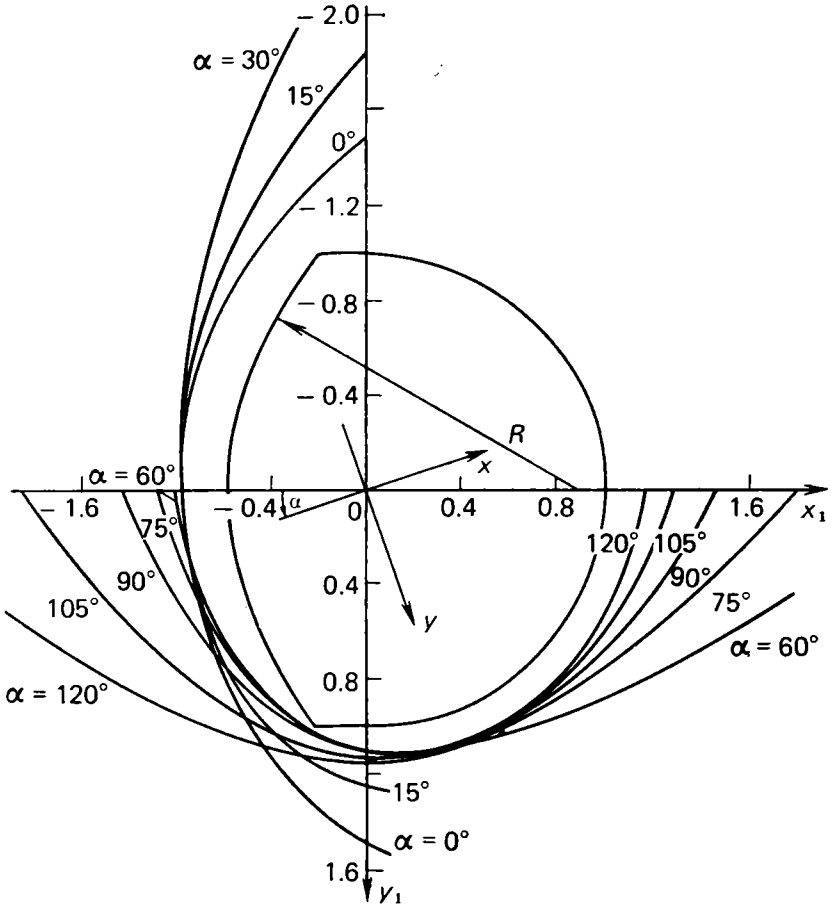

Fig. 3.20. Flow pattern in the symmetry plane; $M_\infty = \infty$, $\varkappa = 1.4$, $R = 1.5$.

30 points of the difference grid were taken in the meridional planes $\varphi = \text{const}$ $(0 \leqslant \varphi \leqslant \pi)$, including 8 points on the bluntness and 16 points on the lateral surface. The domain of integration was bounded by a time-independent segment of the ellipsoid of revolution (shown by a dot-and-dash line) and a region of the bow shock wave which was explicitly treated in calculations. The parameters of the incoming flow served as the boundary conditions on the closing surface (ellipsoid). Dashed lines show the results obtained in [3.69] for $\alpha = 0°$ and 10° by separate calculations of the transonic zone in the

vicinity of the bluntness, and of the supersonic flow near the lateral surface with the help of the time-marching method (over the layers $z = \text{const}$). It is well known that such an approach is possible only for comparatively small angles of attack, when the flow in the vicinity of the lateral surface of the body is completely supersonic. It can be seen from the pressure distribution, for example, that such a method is inapplicable for large angles of attack. For a zero angle of

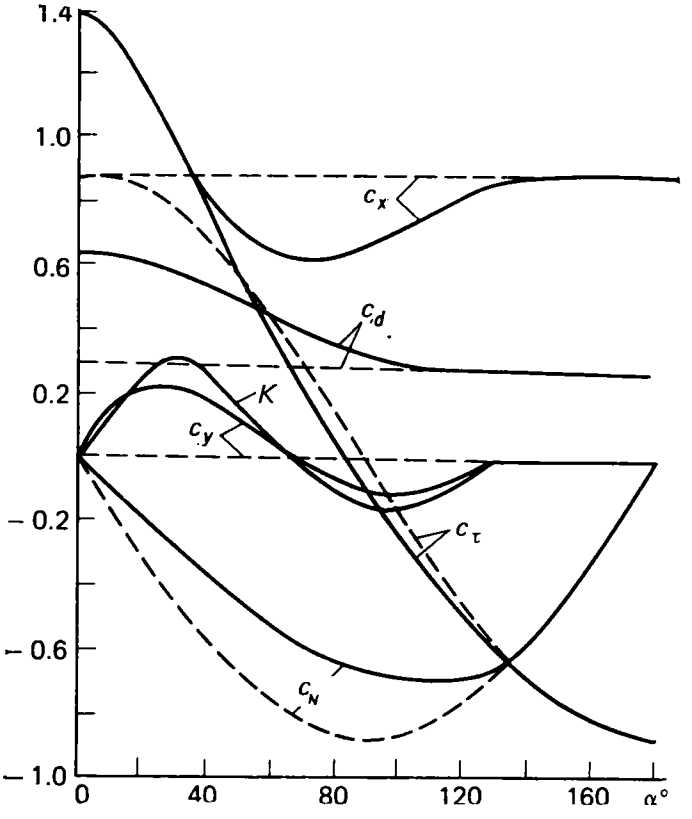

Fig. 3.21. Aerodynamic coefficients; $M_\infty = \infty$, $\varkappa = 1.4$, $R = 1.5$.

attack, the arrows in Fig. 3.18 show the calculated values of the velocity field in the neighbouring wake (below the z-axis), while the solid lines above the z-axis represent the isometric lines $p/\rho_\infty V_\infty^2 = \text{const}$. The isometric lines $p/\rho_\infty V_\infty^2 = 0.005$ and 0.0075 obtained experimentally (in [3.70]) are marked in the figure by crosses, while the curves with triangles show the form of the wake constriction obtained in the same work. We can see that the results (at least qualitative) of such a complicated flow obtained by using (3.3.4) do not contradict the experimental data.

For a body with a small elongation consisting of a segment with radius $R = 1.5$, a hemisphere with radius 1 and a cylindrical insertion of length 0.2, the flow pattern in the flow symmetry plane ($M_\infty = \infty$, $\varkappa = 1.4$) is shown in Fig. 3.20 for various angles of

attack $\alpha = 0°$-$120°$ (still larger angles of attack correspond to the normal flow past a spherical bluntness). Figure 3.21 shows the dependence of the overall aerodynamic characteristics on the angle of attack (these characteristics are: longitudinal and normal force coefficients C_τ and C_N, the wavedrag coefficient C_x, lifting force coefficient C_y, coefficient C_d of the centre of pressure, and the quality factor K). The data corresponding to a sphere are shown in Fig. 3.21 by dashed lines.

Many other problems of three-dimensional flow past bodies, including those which involve equilibrium and nonequilibrium physical and chemical processes, radiation transport, time dependence, etc., were investigated on the basis of scheme (3.3.4) in [3.21-3.32] and in other works.

3.4.2. If the integration domain contains, besides the basic discontinuity surfaces, additional discontinuity surfaces (contact discontinuities, secondary shock waves, etc.) whose explicit treatment

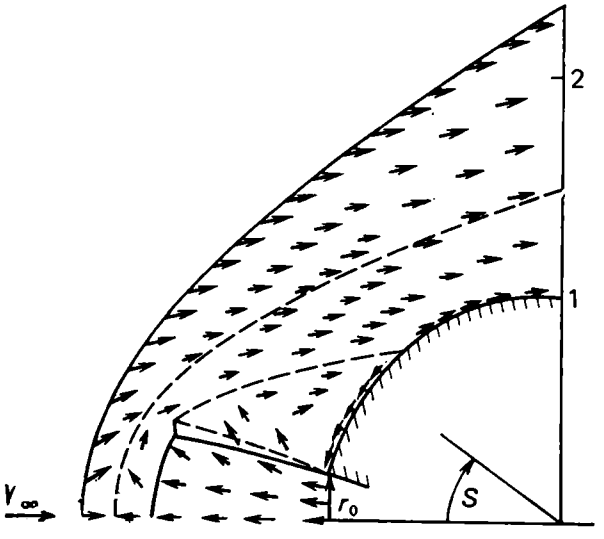

Fig. 3.22. Flow pattern in the velocity field; $M_\infty = 2.5$, $M_0 = 1.5$, $\varkappa = 1.4$, $r_0 = 0.2$.

would make the computational algorithm too complicated on the whole, it is expedient to go over to the divergent form of equations and conservative schemes. However, if the intensity of such discontinuities is not too high (as in the one-dimensional case considered in Sec. 3.2.4), quite satisfactory results can be obtained with the help of through calculations of such singularities with the help of the nondivergent scheme (3.3.4). Examples of such calculations are shown in Figs. 3.22-3.25 for the problem on supersonic flow past a blunted body with a central jet injection into the shock layer (sta-

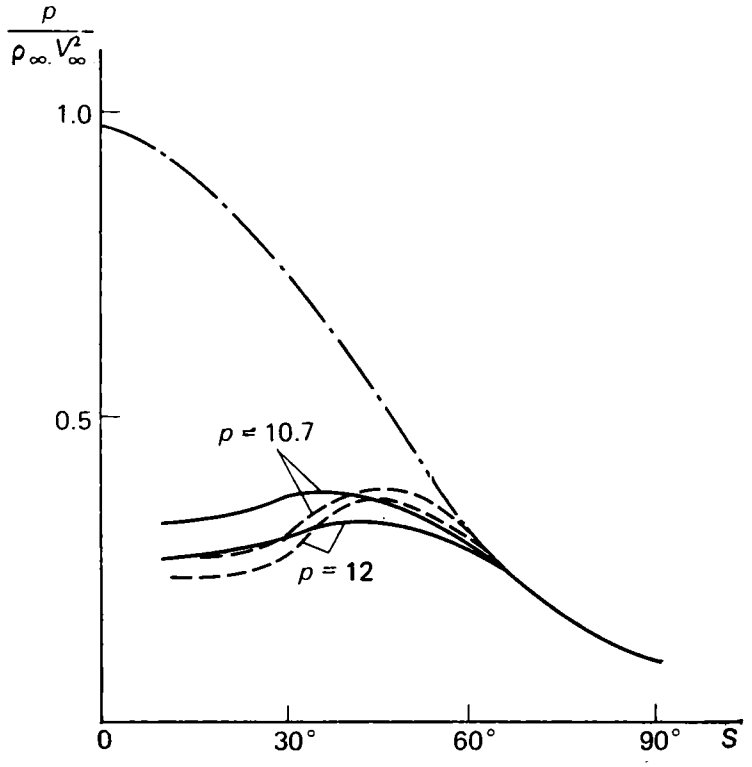

Fig. 3.23. Pressure distribution over a body.

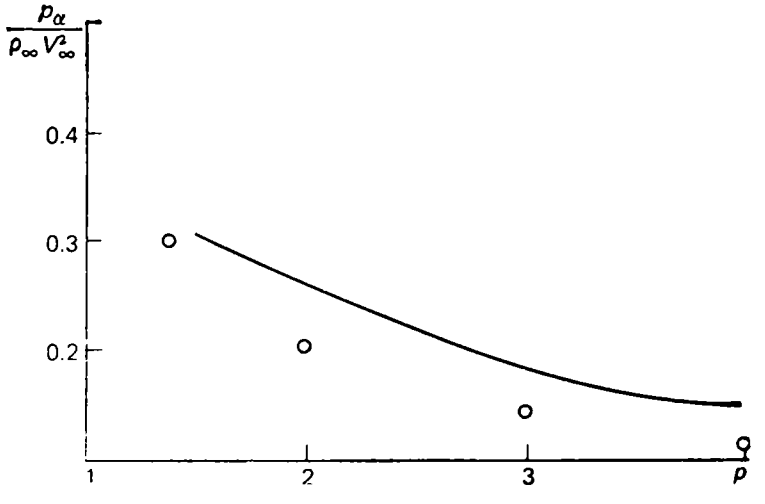

Fig. 3.24. Pressure in the stagnation zone.

tionary axisymmetric problem), and in Figs. 3.26-3.28 for problems of supersonic flow past a spherically blunted cone; an intensive non-uniform time-dependent blowing of vapours of the breaking heat-

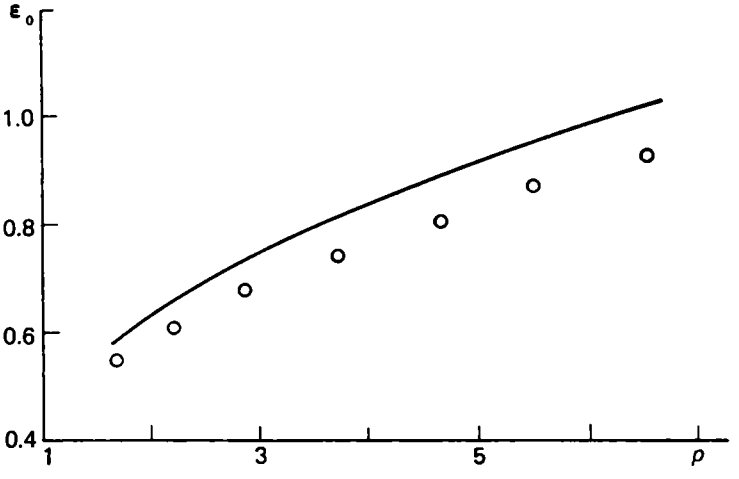

Fig. 3.25. Detachment of the shock wave.

insulating covering takes place from a part of the surface of this cone (nonstationary spatial problem on intensive jet injection). For the first problem which was numerically solved by Kozlov and Fin-

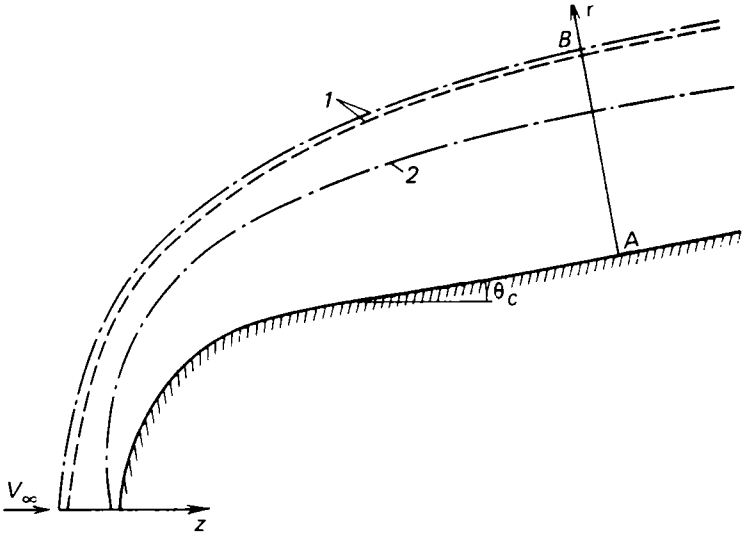

Fig. 3.26. Stream line pattern in the symmetry plane of the flow.

chenko by using scheme (3.3.4) Fig. 3.22 shows the experimentally observed [3.71] flow pattern with a bow shock wave and a system of internal shock waves (solid curves). The contact discontinuities separating the incoming flow from the injected gas and bounding the

stagnation zone with inverse flow in it are shown by dashed lines. The stationary velocity field obtained in computations (by treating only the bow shock wave) is shown by arrows. The Mach number for the incoming gas flow ($\varkappa = 1.4$) is $M_\infty = 2.5$. The value M_0 at the nozzle edge of radius $r_0 = 0.2$ is equal to 1.5, while the pressure ratio at the nozzle edge and in the incoming flow $p = 20$. Gas with the same composition as in the incoming flow is injected. Solid curves in Fig. 3.23 show the calculated pressure distribution over the

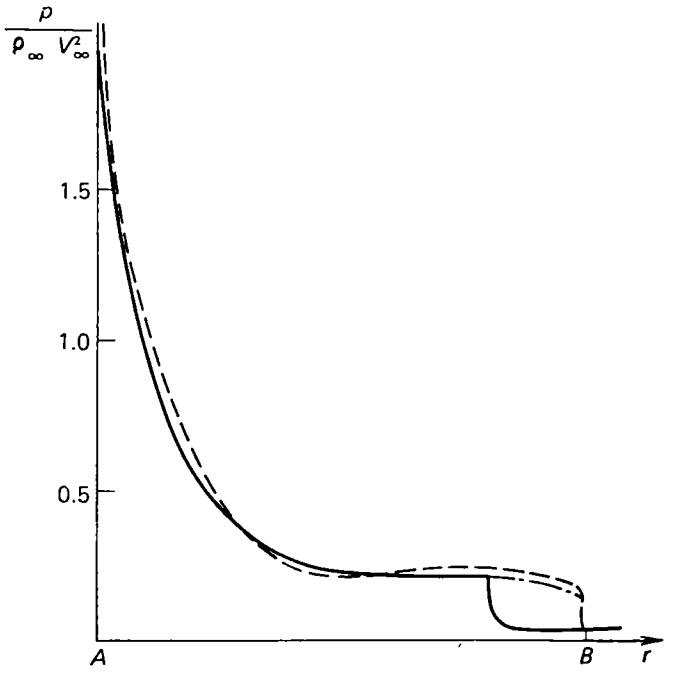

Fig. 3.27. Pressure profile along AB.

body for $p = 10.7$ and 12. Experimental results obtained in [3.71] are shown by dashed lines, while dot-and-dash lines show the pressure distribution over a sphere in the absence of gas injection. Figures 3.24 and 3.25 represent the calculated (solid lines) and experimental [3.71] (points) values of pressure $p_\alpha/\rho_\infty V_\infty^2$ in the stagnation zone and the detachment ε_0 of the bow shock wave on the flow symmetry axis respectively as functions of the pressure drop p. It is seen that many characteristics of such a complex flow (detachment, pressure, in the stagnation zone, flow junction point, etc.) are in quite good agreement with the experimental results.

For the three-dimensional nonstationary problem of a strong injection calculations were carried out by using the nondivergent scheme (3.3.4) in the three-dimensional formulation by treating only the bow shock wave *1* (in this case, the velocity of the gas injected along the normal to the surface of the body depended on the meridio-

nal coordinate φ: $\mathbf{V} \approx \mathbf{V}_0(t, z) \cos\varphi$ for $0 \leqslant \varphi \leqslant \pi/2$, and $\mathbf{V} = 0$ for $\pi/2 \leqslant \varphi \leqslant \pi$), as well as in the two-dimensional formulation by treating the bow shock wave *1* and the contact discontinuity *2* (in this case, it was assumed that $\mathbf{V} = \mathbf{V}_0(t, z)$ [3.31]). The time-dependence $\mathbf{V}_0(t, z)$ had a triangular shape. Figure 3.26 shows the flow pattern in the meridional plane $\varphi = 0$ at a certain instant of time. Figure 3.27 represents the pressure profile $p/\rho_\infty V_\infty^2$ along AB,

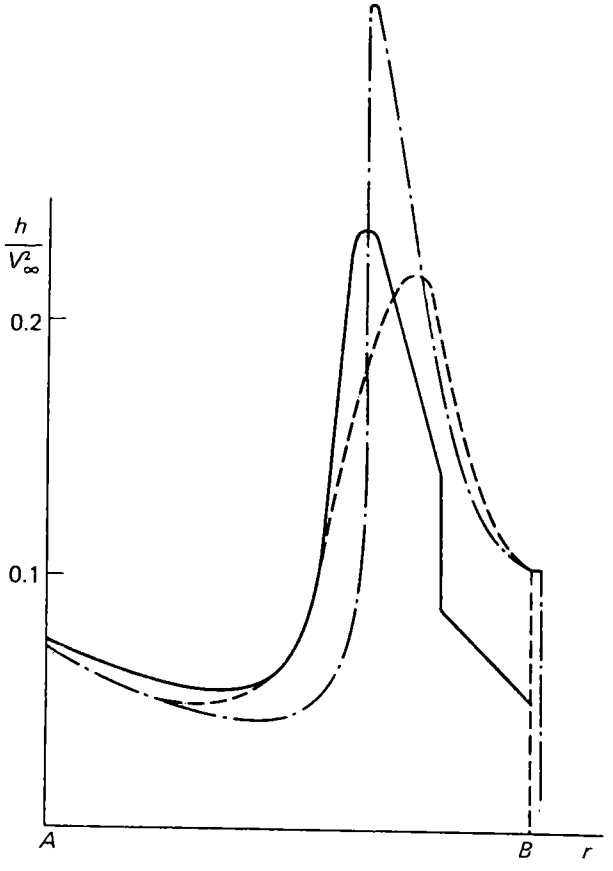

Fig. 3.28. Enthalpy profile along AB.

while Fig. 3.28 shows the enthalpy profile h/V_∞^2 in the same cross section. The dashed curves in Figs. 3.26-3.28 correspond to the three-dimensional problem, while dot-and-dash lines represent calculations in two dimensions. Solid curves are based on the results of one-dimensional model calculation according to the conservative version of the grid-characteristic method (3.2.11) without explicit treatment of the bow shock wave and the contact discontinuity. We see that the results of calculations based on all three formulations are quite close in respect of several parameters, and the basic differences (mainly in the enthalpy profile) are localized in the vicinity of the contact dis-

continuity which is not treated in the one- and three-dimensional cases.

These and many other computations of similar problems indicate that the range of practical applicability of nondivergent schemes is much wider than the range usually assumed, although such schemes should be used with care for a computation of problems.

3.4.3. If the intensity of discontinuities which are being subjected to through calculations is quite high, we must go over to conservative schemes and, in particular, the conservative versions of grid-characteristics methods. A satisfactory solution of such problems

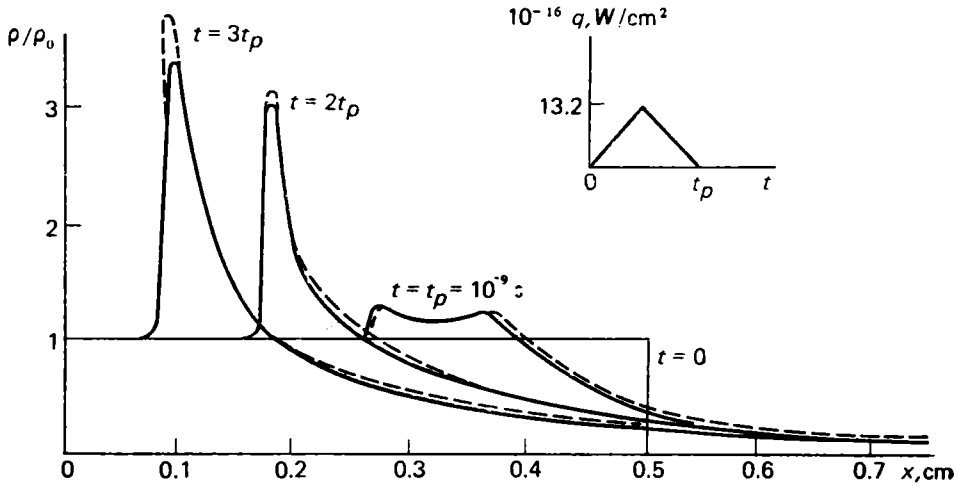

Fig. 3.29. Density profiles. One-dimensional problem.

is possible only on the basis of conservative schemes and, perhaps, locally divergent schemes of the type considered in Sec. 3.2.4. As an example of the computation of such problems, with the help of the conservative scheme (3.3.6) Figs. 3.29-3.34 show the results corresponding to the numerical simulation of the plane one-dimensional problem (Figs. 3.29, 3.30), and one- and two-dimensional problems in spherical geometry (Figs. 3.31, 3.32, 3.34) on the compression and heating of microscopic particles by a powerful laser pulse. The complexity of this type of problems (besides the difficulties associated with the construction of processes adequate to real physics and mathematical simulation compatible with the computational techniques) associated with their strong time-dependence and spatial inhomogeneity (characteristic times are $\simeq 10^{-9}$ s and the spatial scale is in micrometers), as well as with the considerably nonlinear nature of the processes (like electron thermal conductivity, etc.). Without going into a detailed formulation of these problems and the computational algorithm as a whole (see [3.33] for details, the results

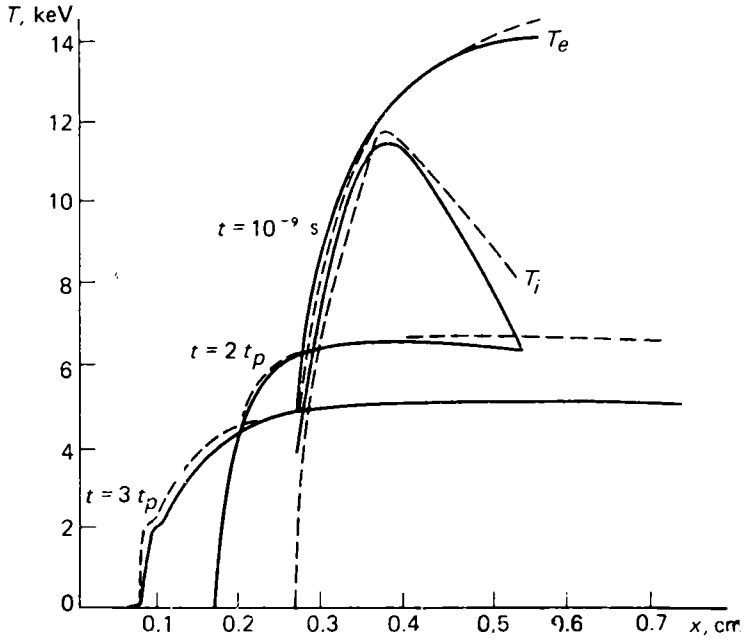

Fig. 3.30. Electron (T_e) and ion (T_i) temperature profiles.

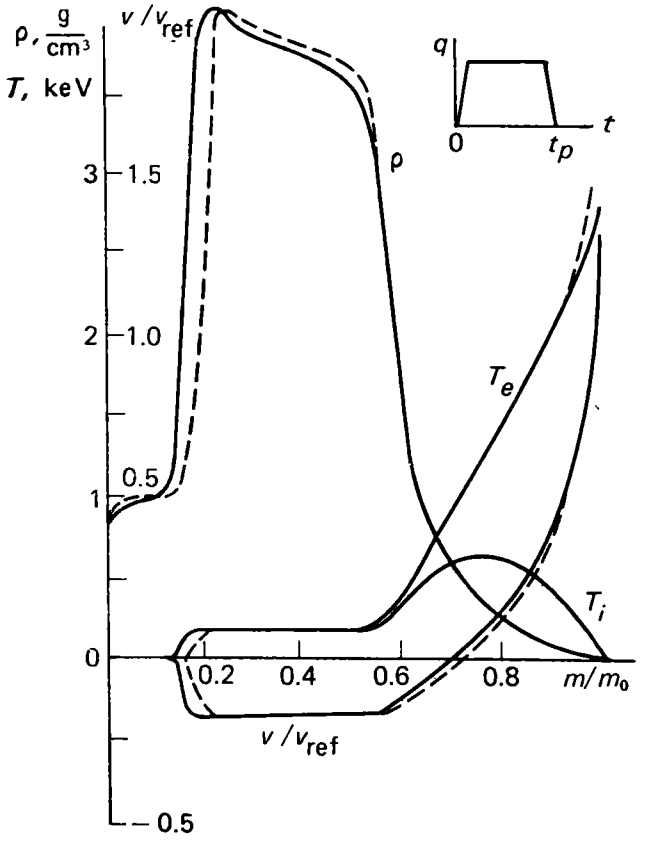

Fig. 3.31. Parameter profiles. Spherical shell.

described here are borrowed from this work), we shall just mention that the mathematical model contained two-temperature one-velocity gasdynamic equations. The energy equations for ion and elec-

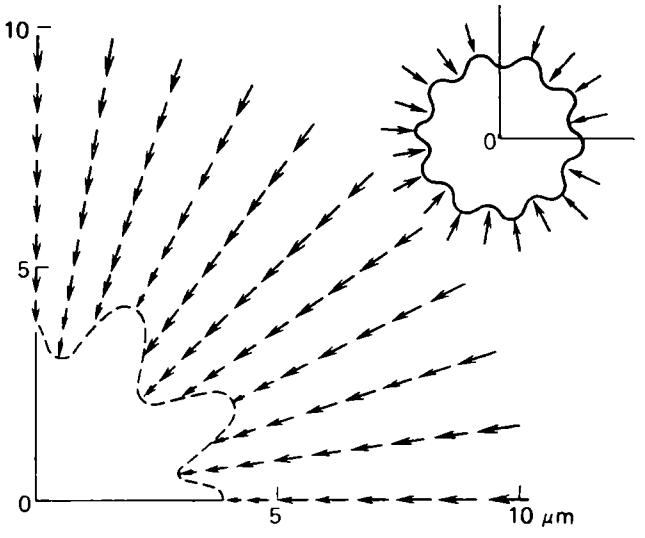

Fig. 3.32. Velocity field in the central zone.

tron components of a fully ionized ideal plasma were supplemented by terms which take into account the electron thermal conductivity, electron-ion collision relaxation, and the absorption of external la-

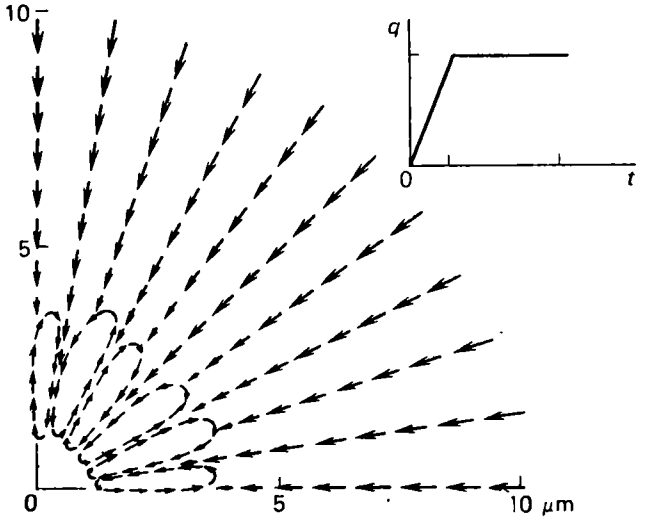

Fig. 3.33. Velocity field in the central zone.

ser radiation. Scheme (3.3.6) was employed for approximating the hyperbolic part (excluding the electron thermal conductivity) of this on the whole parabolic system at the first stage. After this, the

complete energy equations were solved with the help of the traditional implicit scheme, i.e. "splitting into physical processes" was employed.

The results of calculation of density profiles (Fig. 3.29), electron- and ion-temperatures T_e and T_i (Fig. 3.30) from scheme (3.2.11) by using Euler coordinates that are fixed in space (solid curves) were compared at different instants of time with the results of calculations in Lagrangian variables (dashed curves) by using Kosarev's explicit

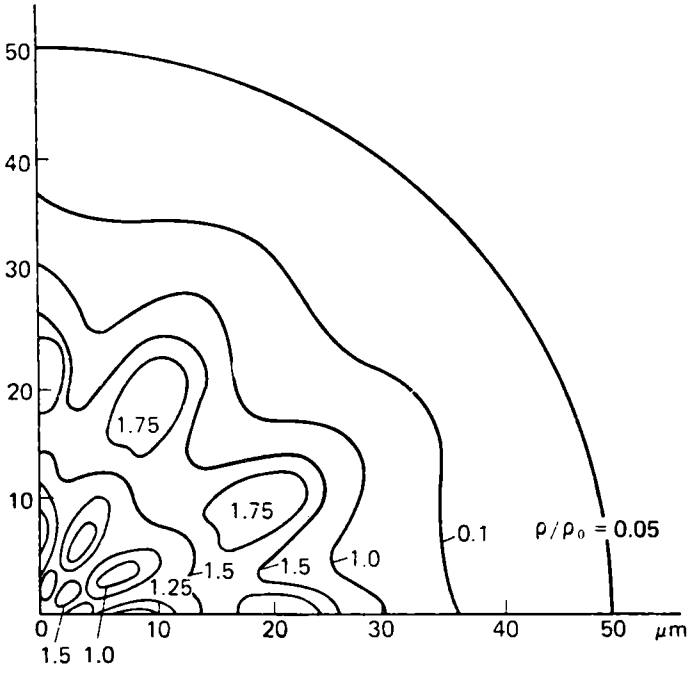

Fig. 3.34. Isometric lines $\rho/\rho_0 = \text{const}$.

fully-conservative second-order scheme (to a certain extent, this scheme is analogues in its properties to the schemes described in [3.62,3.72]). A quite satisfactory agreement was observed in the case of the plane one-dimensional problem under consideration. The parameters for the target and the laser pulse in these calculations are borrowed from [3.73].

The use of Lagrangian variables in scheme (3.2.11) which are more traditional for the given class of problems concerning the flow of a finite mass of a substance, brings the results of calculations of one-dimensional problems by the first-order grid characteristic scheme still closer to the results of analogous calculations by the fully conservative second-order scheme [3.62]. This can be seen from a comparison (Fig. 3.31) of the profiles of density ρ, electron and ion temperatures T_e and T_i, and velocity v for a one-dimensional problem on the compression and heating of a hollow spherical shell by a laser

pulse. Solid curves represent the results obtained by using scheme (3.2.11), while the dashed lines correspond to the values calculated by using the scheme presented in [3.62]. The same grid parameters were used in both cases. This example also indicates the importance of the choice of independent variables for the problem under consideration (as for the familiar case of numerical solution, where the choice of the required parameters is certainly not immaterial). Figures 3.32-3.34 show as an example the calculation of a two-dimensional problem (on compression and heating by a laser pulse of a hollow spherical shell with an initial disturbance of its shape with an amplitude $\simeq 5\%$) by the conservative scheme (3.3.6). Calculations were made by using Euler variables that were fixed in space. This enables us to trace the evolution of the initial perturbations right up to the formation of cumulative jets in the vicinity of the central part of the target (traced over the velocity field shown in Fig. 3.32 at some instant of time), their interaction and the creation of inverse-circular flow regions in the central part of the target (Fig. 3.33, velocity field after the "collision of jets"). The isometric lines $\rho/\rho_0 = \text{const}$ for this instant of time are shown in Fig. 3.34.

3.4.4. Let us briefly consider the computational peculiarities of the solution of multidimensional dynamic problems of a deformable rigid body, which are simulated by systems of hyperbolic equations (for example, the time-dependent equations in the linear and nonlinear theory of elasticity, etc.). Petrov [3.36, 3.37] and others have carried out numerical investigation of these problems by using the grid-characteristic methods (3.3.4), (3.3.8).

In many problems of this type having clearly manifested shock wave properties, we have to calculate the discontinuity surfaces spreading over the deformable medium and interacting with the boundaries as well as with one another. These discontinuity surfaces appear due to the discontinuous nature of the boundary conditions (for example, during an impulsive loading of structural elements, etc.). In the computational sense, such discontinuities are analogous to contact discontinuities in gas dynamics. It is well known that their prolonged computation over time is much more complicated than the computation count of, say, gasdynamic shock waves. In this case, the question of dissipation and dispersion properties of the numerical method becomes very important in the through calculation of such "linear" discontinuities, and the advantages of hybrid difference schemes discussed in Sec. 3.2.3 become quite noticeable.

As an example, Fig. 3.35 shows the isometric lines $\sigma_{22} = \text{const}$ (normal component of the stress tensor in the direction x_2) obtained at a certain instant of time while calculating the problem of sudden loading (which then remains constant in time along OA) of a part

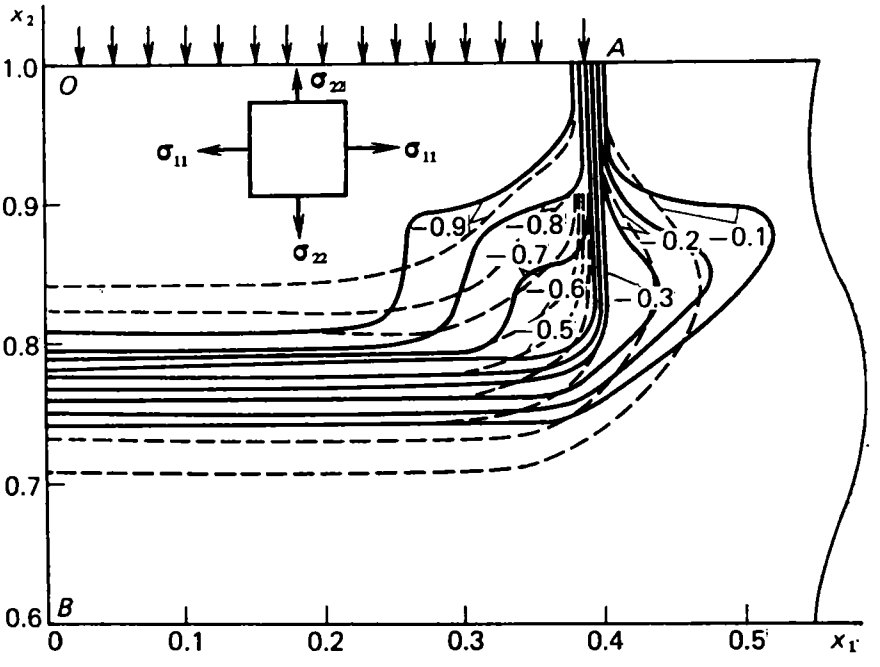

Fig. 3.35. Isometric lines $\sigma_{22} = \text{const}$.

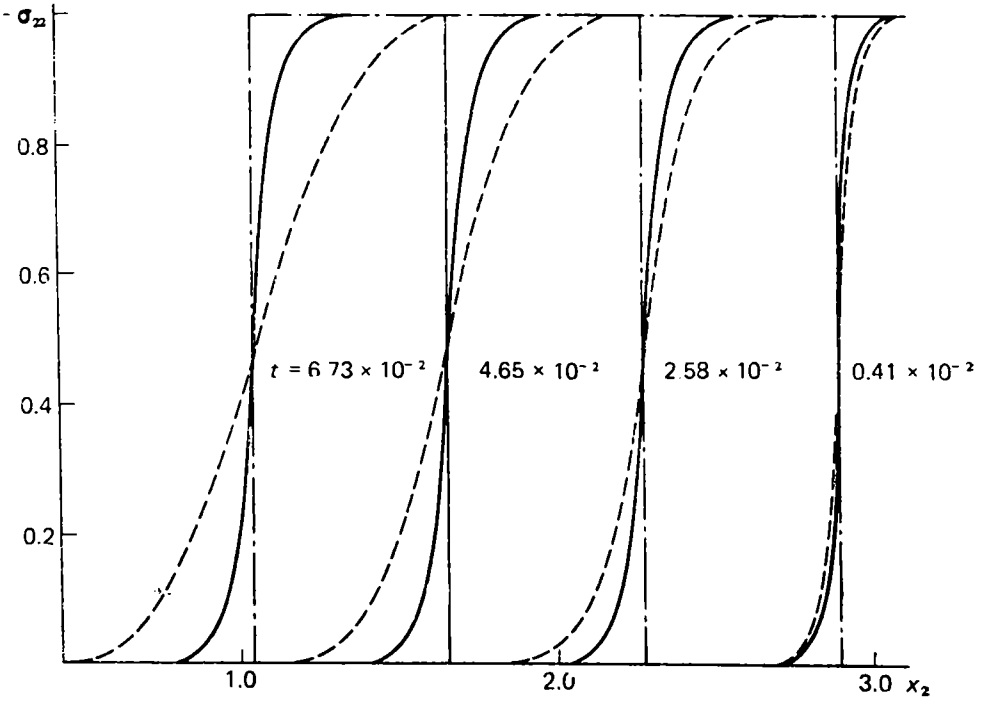

Fig. 3.36. σ_{22} profiles in one-dimensional problem.

of the boundary of elastic half-space by pressure normal to this boundary (plane problem). Solid curves in Figs. 3.35 and 3.36 show the results of calculations by using the nondivergent version of the hybrid scheme (3.3.8), while the dashed lines represent the results obtained from the first-order monotonic scheme (3.3.4). Figure 3.36 shows the distribution of σ_{22} along the symmetry plane of the problem at different instants of time. The dot-and-dash lines correspond to the exact solution of the one-dimensional problem (when the entire boundary of the half-space is being loaded) whose solution coincides with the solution of the two-dimensional problem along OB up to the moment when perturbations arrive from point A. It can be seen that the hybrid scheme permits a more detailed reproduction of the given discontinuous solution.

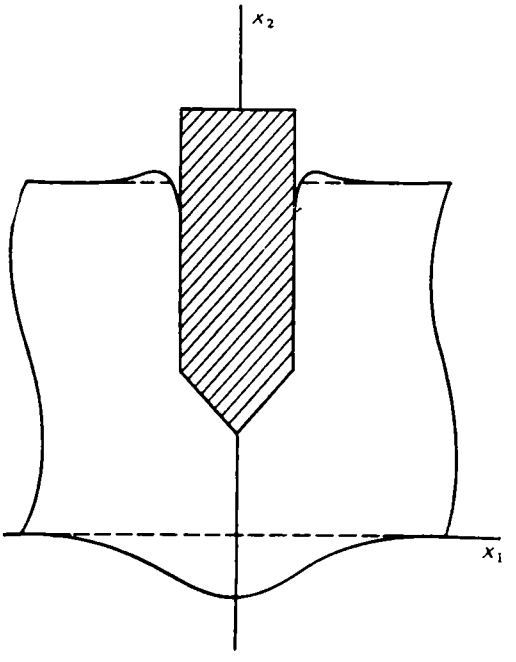

Fig. 3.37. Deformed state pattern at the instant when the conical striker comes to a halt.

Another example of this type of problems illustrates the potentialities of scheme (3.3.4) for solving the problem of the high-speed impingement of an absolutely rigid cylindrical striker on a deformable plate of a finite thickness, when large shear strains appear. The rheology of the material was described by the Prandtl-Reiss ideal elastic-plastic flow theory under Mises' plasticity condition, which is widely used for this type of problems.

The pattern of the strained state for one of the versions at the instant when the striker comes to a halt is shown in Fig. 3.37. For various types of impingements (elastic, low impingement velocities—curve *1*, two regimes in which the striker comes to a halt—curves *2*, *3*, and a regime involving the piercing of the obstacle—curve *4*), Fig. 3.38 shows the time-dependence of the velocity of penetration of the striker into the obstacle. Calculations were carried out in moving coordinates connected to the mobile boundaries of the obstacle.

Besides the explicit schemes (3.3.4) and the nondivergent version of the scheme (3.3.8), many time-independent two-dimensional problems in the mechanics of a deformable rigid body were solved by the grid-characteristic scheme (3.3.7), which was implicit

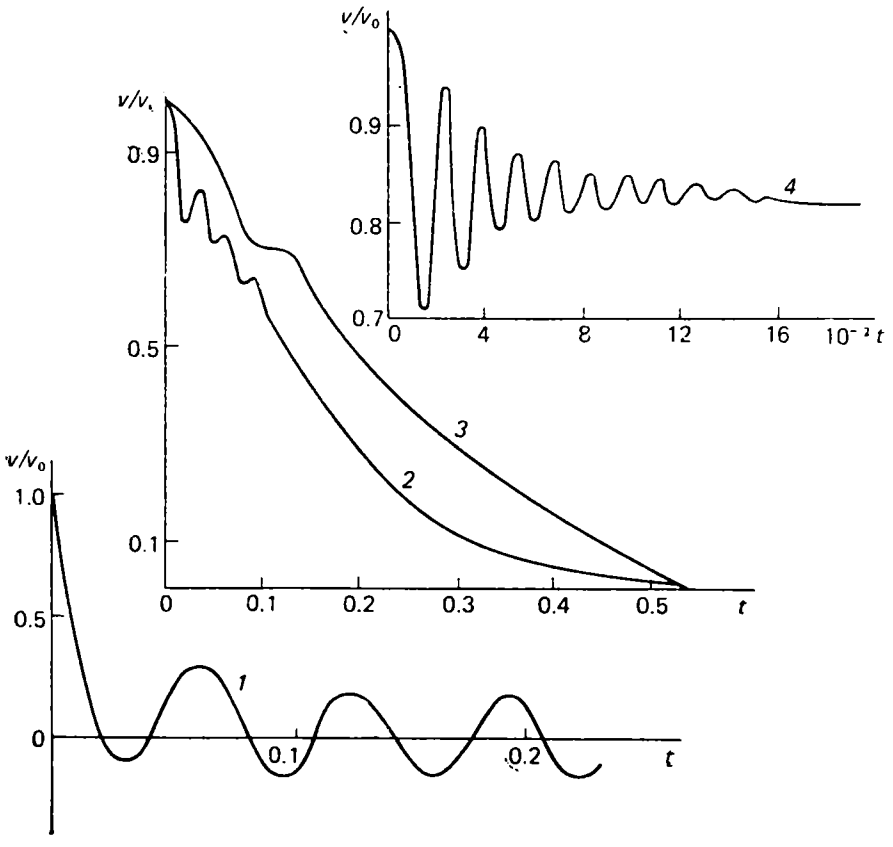

Fig. 3.38. Dependence of the striker velocity on t.

in one of its coordinates, in conjunction with the stabilization method for obtaining steady-state solutions [3.35].

3.5. CONCLUSION

In conclusion, let us summarize the main results presented in this paper.

The method proposed by us for constructing difference schemes for multidimensional quasilinear equations of hyperbolic type as well as the hyperbolic part of more complicated equations is based on a successive transition from the simplest one-dimensional transport equation to a system of linear, and then quasilinear, one-dimensional hyperbolic equations followed by multidimensional equations. The approach involves the introduction of linear spaces of coefficients of difference schemes and the use of characteristic properties of systems of hyperbolic equations. This allows us:

(i) to construct the entire set of schemes with positive approximation (of monotonic or majorant schemes) for arbitrary grid models;

(ii) to prove that in general there are no schemes with second or higher order of approximation on the solutions of original equations;

(iii) to find the most accurate scheme among monotonic schemes for each grid model and, conversely, to find among second- and higher-order nonmonotonic schemes the one that is least oscillating at the discontinuities of the solution; and

(iv) to construct the analogues of all these schemes for a quite general case of linear and nonlinear systems of hyperbolic equations.

The grid-characteristic methods constructed in this way present a wide range of computational algorithms with different properties. These algorithms, which are required for solving the boundary-value problems for hyperbolic equations, include explicit and implicit schemes with first- or higher-order approximation, intermediate hybrid schemes, etc.

The application of several of these grid-characteristic methods for numerical investigation of modern multidimensional problems of gas dynamics, plasma physics and mechanics of a deformable body has proved their effectiveness in solving problems with a quite complicated structure of the required solution.

The authors are deeply indebted to K. M. Magomedov, who started investigations of the grid-characteristic methods. Sincere thanks are also due to V. I. Kosarev, V. B. Pirogov, V. N. Fomin, A. N. Nikulin, S. M. Khololov, S. D. Osetrova, V. S. Kostrykin, V. S. Finchenko, I. A. Kozlov, V. V. Demchenko, I. B. Petrov and many other colleagues who participated in the solution of the problems discussed in this paper, as well as many other problems, and facilitated a successful extension of grid-characteristic methods to various problems that can be simulated by multidimensional equations of hyperbolic type.

References

3.1. R. Courant, E. Isaacson and M. Rees, *Communs Pure and Appl., Math.*, 5, 5: 243-54 (1952).
3.2. A. I. Zhukov, *Trudy Matem. Inst. Akad. Nauk SSSR*, 58 (1960).
3.3. D. S. Butler, *Proc. Roy. Soc., A*255, 1281: 232 (1960).
3.4. V. V. Rusanov, *Zh. Vychisl. Mat. i Mat. Fiz.*, 3: 508-27 (1963).
3.5. Z. D. Zapryanov and V. B. Minostsev, *Izv. Akad. Nauk SSSR, Ser. Mekh. i. Mashinostr.*, 5: 20-4 (1964).
3.6. O. N. Katskova and P. I. Chushkin, *Zh. Vychisl. Mat. i Mat. Fiz.*, 5, 3: 503-18 (1965).
3.7. K. M. Magomedov, *Zh. Vychisl. Mat. i Mat. Fiz.*, 6, 2: 313-25 (1966).
3.8. D. W. Peaceman and H. H. Rachford, *J. Soc. Industr. Appl. Math.*, 3, 1: 28-42 (1955).
3.9. K. A. Bagrinovsky and S. K. Godunov, *Dokl. Akad. Nauk SSSR*, **115**, 3: 131-3 (1957).
3.10. E. G. Dyakonov, *Dokl. Akad. Nauk SSSR*, **138**, 2, 271-4 (1961).
3.11. A. A. Samarsky, *Zh. Vychisl. Mat. i Mat. Fiz.* 4, 4: 638-48 (1964).
3.12. N. N. Yanenko, *Method of Fractional Steps for Solution of Multidimensional Problems in Mathematical Physics*, Nauka, Novosibirsk, 1973 (in Russian).

3.13. G. I. Marchuk, *Methods of Computational Mathematics*, Nauka, Novosibirsk, 1973 (in Russian).
3.14. V. V. Rusanov, *Dokl. Akad. Nauk SSSR*, 180, 6: 1303-5 (1968).
3.15. A. N. Tikhonov and A. A. Samarsky, *Zh. Vychisl. Mat. i Mat. Fiz.* 1, 1: 5-63 (1961).
3.16. A. A. Samarsky, *Zh. Vychisl. Mat. i Mat. Fiz.*, 7, 1: 62-93 (1967).
3.17. K. M. Magomedov and A. S. Kholodov, *Zh. Vychisl. Mat. i Mat. Fiz.*, 9, 2: 373-86 (1969).
3.18. A. S. Kholodov, *Zh. Vychisl. Mat. i Mat. Fiz.*, 18, 6: 1476-92 (1978).
3.19. O. M. Belotserkovskii and A. S. Kholodov, in: *Proc. 6th Intern. Conf. on Numer. Meth. in Hydrodynamics, Tbilisi, 1978*, vol. 2, Izd. Inst. Prikl. Matem. Akad. Nauk SSSR, Moscow, 1978, (in Russian).
3.20. A. S. Kholodov, *Zh. Vychisl. Mat. i Mat. Fiz.*, 20, 6: 1601-20 (1980).
3.21. O. M. Belotserkovskii, F. D. Popov, A. I. Tolstykh, V. N. Fomin, and A. S. Kholodov, *Zh. Vychisl. Mat. i Mat. Fiz.*, 10, 2: 401-16 (1970).
3.22. O. M. Belotserkovskii (Ed.), *Numerical Analysis of Modern Problems in Gas Dynamics*, Nauka, Moscow, 1974, (in Russian).
3.23. A. V. Krasilnikov, A. N. Nikulin and A. S. Kholodov, *Izv. Akad. Nauk SSSR, Ser. Mekh. Zhidk. i Gaza*, 5: 179-81 (1975).
3.24. A. N. Nikulin, *Proc. Moscow Physico-Techn. Inst., Ser. Aerophysics and Control Processes*, part. 1: 5-9 (1974).
3.25. O. M. Belotserkovskii, S. D. Osetrova, V. N. Fomin, and A. S. Kholodov, *Zh. Vychisl. Mat. i Mat. Fiz.*, 14, 4: 992-1003 (1974).
3.26. V. S. Kostrykin, V. N. Fomin, and A. S. Kholodov, *Zh. Vychisl. Mat. i Mat. Fiz.*, 16, 2: 451-9 (1976).
3.27. O. M. Belotserkovskii, L. I. Turchak, and A. S. Kholodov, *Izv. Akad. Nauk SSSR, Ser. Mekh. Zhydk. i Gaza*, 5: 110-15 (1975).
3.28. L. I. Turchak, *Izv. Akad. Nauk SSSR, Ser. Mekh. Zhidk. i Gaza*, 1: 166-70 (1976).
3.29. L. I. Turchak, *Dokl. Akad. Nauk SSSR*, 229, 2: 318-21 (1976).
3.30. V. F. Kamenetsky and L. I. Turchak, *Supersonic Nonuniform Flow of Ideal Gas past Bodies*, Comp. Center, USSR Acad. Sc., Moscow, 1982 (in Russian).
3.31. O. A. Onufrieva, V. B. Pirogov and A. S. Kholodov, *Abstr. of All-Union Conf. on Jet Fluid Flows, Novopolotsk, 1982*, Izd. BPI, Minsk, 1982 (in Russian).
3.32. O. M. Belotserkovskii and A. S. Kholodov, in: *Gas and Wave Dynamics*, vyp. 3, Izd. MGU, Moscow, 1979 (in Russian).
3.33. O. M. Belotserkovskii, V. V. Demchenko, V. I. Kosarev, and A. S. Kholodov, *Zh. Vychisl. Mat. i Mat. Fiz.*, 18, 2: 420-44 (1978).
3.34. O. M. Belotserkovskii, in: *Modern Problems in Mathematical Physics and Computational Mathematics*, Nauka, Moscow, 1982 (in Russian).
3.35. V. D. Ivanov and A. S. Kholodov, *On Utilization of Grid-Characteristic Schemes with a Positive Approximation for Solving Linear Problems in the Theory of Elasticity*, VINITI, Dep. No. 2826-78, 1980.
3.36. I. B. Petrov and A. S. Kholodov, *Numerical Investigation of Nonstationary Problems on Small Two-dimensional Thermoelastoplastic Deformations of Solids*, VINITI, Dep. No. 104-82, 1982.
3.37. I. B. Petrov, *Numerical Investigation of Penetration Processes with the Help of Movable Calculation Grids*, VINITI, Dep. No. 103-82, 1982.
3.38. V. F. Dyachenko, *Basic Concepts of Computational Mathematics*, Nauka, Moscow, 1972 (in Russian).
3.39. K. O. Fridrichs, *Communs Pure and Appl. Math.*, 7, 2: 345-92 (1954).
3.40. P. D. Lax, *Communs Pure and Appl. Math.*, 7, 1: 159-93 (1954).
3.41. L. D. Landau, I. N. Meiman and I. M. Khalatnikov, *Proc. 3rd All-Union Math. Congress*, vol. 3, Izd. Akad. Nauk SSSR, Moscow, 1958 (in Russian).

3.42. R. Richtmyer, and K. Morton, *Difference Methods for Initial-value Problems*, 2nd ed., New York, 1967.
3.43. S. K. Godunov, *Matem. Sbornik*, vyp. 3, 47: 271-306 (1959).
3.44. P. D. Lax and B. Wendroff, *Communs Pure and Appl. Math.*, **13**, 2: 217-37 (1960).
3.45. C. A. Kot, *Intense Underwater Explosions*, ITT Research Institute, Chicago, USA (preprint).
3.46. H. B. Keller, B. Wendroff, *Communs Pure and Appl. Math.*, **10**, 4: 567-82 (1957).
3.47. J. von Neumann, R. D. Richtmuer, *J. Appl. Phys.*, **21**: 232-7 (1950).
3.48. R. Latter. *J. Appl. Phys.*, **26**, 8: 955-60 (1955).
3.49. A. A. Samarsky and V. Ya. Arsenin, *Zh. Vychisl. Mat. i Mat. Fiz.*, **1**, 2: 357-60 (1961).
3.50. V. F. Dyachenko, *Zh. Vychisl. Mat. i Mat. Fiz.*, **1**, 6: 1127-9 (1961).
3.51. R. P. Fedorenko, *Zh. Vychisl. Mat. i Mat. Fiz.*, **2**, 6: 1128-8 (1962).
3.52. V. Ya. Goldin, N. N. Kalitkin and T. V. Shishova, *Zh. Vychisl Mat. i Mat. Fiz.*, 5, 5: 938-44 (1965).
3.53. B. Van Leer, *J. Appl. Phys.*, **14**, 4: 361-70 (1974).
3.54. D. L. Book, J. P. Boris and K. Hain, *J. Comp. Phys.*, 18, 3: 248-83 (1975).
3.55. A. Lerat, R. Peyret, *Comput. and Fluids*, 2: 35-50 (1974).
3.56. P. A. Voinovich et al., *On Calculation of Discontinuous Gas Flows*, Izd. LFTI, Leningrad, 1977 (in Russian).
3.57. A. N. Minailos, *Zh. Vychisl. Mat. i Mat. Fiz.*, **17**, 4: 1058-63 (1977).
3.58. V. P. Kolgan, *Zh. Vychisl. Mat. i Mat. Fiz.*, 18, 5: 1340-5 (1978).
3.59. Yu. N. Lobanovsky, *Zh. Vychisl. Mat. i Mat. Fiz.*, **19**, 4; 1063-9 (1979).
3.60. A. I. Zhmakin and A. A. Fursenko, *Zh. Vychisl. Mat. i Mat. Fiz.*, **20**, 4: 1021-31 (1980).
3.61. S. K. Godunov, A. V. Zabrodin, M. Ya. Ivanov, A. N. Kraiko, and G. P. Prokopov, *Numerical Solution of Multidimensional Problems in Gas Dynamics*, Nauka, Moscow, 1976 (in Russian).
3.62. A. A. Samarsky and Yu. P. Popov, *Difference Schemes in Gas Dynamics*, Nauka, Moscow, 1975 (in Russian).
3.63. V. B. Balakin, *Zh. Vychisl. Mat. i Mat. Fiz.*, **10**, 6: 1512-19 (1970).
3.64. S. Z. Burstein and A. A. Mirin, *J. Comp. Phys.*, 5: 547-71 (1970).
3.65. R. F. Warming, P. Kutler, H. Lomax, *AIAA Journal*, **11**, 2: 189-96 (1973).
3.66. V. V. Eremin and Yu. M. Lipnitsky, *Zh. Vychisl. Mat. i Mat. Fiz.*, **14**, 2: 379-89 (1974).
3.67. R. W. MacCormac, *AIAA Paper* No. 69-354 (1969).
3.68. N. N. Anuchina, *Trudy Matem. Inst. Akad. Nauk SSSR, XXIV. Difference Methods of Solving Problems in Mathematical Physics*, part 1, Nauka, Moscow, 1966 (in Russian).
3.69. V. V. Lunev, K. M. Magomedov, and V. G. Pavlov, *Hypersonic Flow past Blunted Cones, Involving Equilibrium Physico-chemical Transformations*, Comp. Center, USSR Acad. Sc., Moscow, 1968 (in Russian).
3.70. A. I. Shwets and I. T. Shwets, *Gas Dynamics of Close-range Wake*, Naukova Dumka, Kiev, 1976 (in Russian).
3.71. P. J. Finley, *J. Fluid. Mech.*, **26**, 2: 337-68 (1966).
3.72. A. A. Samarsky *et al.*, *Zh. Vychisl. Mat. i Mat. Fiz.*, 8, 5: 1025-38 (1968).
3.73. Yu. V. Afanasyev *et al.*, *Heating of Deuterium-tritium Plasmas to Thermonuclear Temperatures with the Help of Laser Radiation*, Preprint FIAN SSSR, No. 66, Moscow, 1972.

4 Method of Difference Potentials for Numerical Solution of Problems in Mechanics of Continuous Media

V. S. Ryaben'ky, *D.Sc. (Phys.-Math.)*

The method of difference potentials (or difference projectors, or internal boundary conditions) is intended for numerical solution of boundary value problems and some other problems in mathematical physics for linear differential equations with variable coefficients in irregular multidimensional domains. The method of difference potentials (MDP) combines the reduction in the problem dimensionality and the simplicity of taking into account given boundary conditions, which is typical of the methods of reduction of boundary value problems to integral equations at the domain boundary, with algorithmic solution of difference equations in convenient auxiliary mesh domains under convenient auxiliary boundary conditions. On the other hand, the MDP differs from traditional methods of solving boundary integral equations mainly in that it does not require the knowledge of the fundamental solution of a considerable modification depending on the type of boundary condition and does not involve quadrature formulas for the replacement of improper or singular integrals. The version of MDP considered in this article differs from the conventional method of solving differential boundary value problems by approximating them to difference boundary value problems in the following main aspects: firstly, there is no need to construct a difference approximation of boundary conditions of the initial problem; secondly, it is not necessary to solve any difference boundary value problem in the initial curvilinear mesh domain; and thirdly, the dimensionality of the problem is reduced.

In special cases when the capacitance matrix methods can be successfully used for solving a boundary value problem [4.41], the effectiveness of the two approaches is the same in the order of magnitude of the number of memory cells and in the number of arithmetic operations. Wider potentialities of the MDP are ensured, in particular, by using Green's difference formula constructed by the author [4.1, 4.3, 4.4, 4.11, 4.13, 4.18, 4.19, 4.21, 4.25].

The method of difference potentials was proposed in [4.1-4.8] for numerical solution of difference boundary value problems. A new idea appearing in [4.10] made it possible to manage without difference approximation of boundary conditions in solving differential boundary value problems. Later, the MDP was developed in [4.11-

4.31]. Here we shall outline the general idea behind this method, which permits the numerical solution of differential equations with additional conditions that are not necessarily boundary conditions. These problems are reduced to the problem of determining the values of a solution on a special (multilayer) boundary of a mesh domain. In an important particular case, when additional conditions are the boundary conditions, the MDP is used for numerical solution of modified and generalized [4.26] boundary pseudodifferential Calderón-Seeley equations [4.38, 4.39].

The version of MDP presented here appeared through a development of the results described in [4.1-4.31]. However, many essential results of these works are not mentioned in this article.

The proofs of the theorems are omitted since we aimed to acquaint the reader with most of basic constructions and ideas of MDP within the framework of the limited volume of the paper. The application of the general idea is illustrated by using as examples the problems in the potential theory, external problems for the Helmholtz equation, and the internal Stokes problem on the slow flow of a viscous incompressible liquid.

I worked on the development and applications of the method together with my colleagues from the Keldysh Institute of Applied Mathematics, USSR Academy of Sciences, L. V. Bad'in (with whom we made first computer calculations in 1975), A. V. Voronkov, V. I. Turchaninov, and students and research scholars at the Moscow Physico-Technical Institute A. Ya. Belyankov, A. A. Reznik, I. L. Sofronov, and also with A. A. Alekseev, M. Yu. Lokhanov, A. M. Fedorovsky and D. V. Yanushevich. Collaboration with some of them is still being continued.

The method of difference potentials was worked out at the Keldysh Institute of Applied Mathematics more than 15 years ago. This method is still being developed with active support from the governing body of the Institute and, in particular, Prof. O. V. Lokutsievsky.

The work presented in this article was informally discussed many times at the seminar under the guidance of K. I. Babenko, A. V. Zabrodin, and O. V. Lokutsievsky. L. R. Volevich, Ya. M. Kazhdan, Yu. B. Radvogin, R. P. Fedorenko, L. G. Khazin, and other participants of the seminar also took part in the discussions which proved very helpful.

I am extremely grateful to all these colleagues.

It gives me great pleasure to express my deep gratitude to O. M. Belotserkovskii for many useful discussions of the material presented, for providing me with an opportunity to involve students and research scholars from the Moscow Physico-Technical Institute, and for inviting me to contribute an article to this collection.

4.1. AN EXAMPLE ILLUSTRATING THE METHOD

A preliminary acquaintance with the method can be made with the help of boundary value problems for the Laplace equation

$$\frac{\partial^2 u}{\partial x_1^2}+\frac{\partial^2 u}{\partial x_2^2}=0, \quad x=(x_1, x_2)\in D^+ \tag{4.1.1}$$

in a bounded curvilinear domain D^+ lying in a unit square $D = \{x \mid |x_1|<1, \ |x_2|<1\}$, $D^+ \Subset D$. We shall assume that the boundary $\Gamma = \partial D^+$ is sufficiently smooth.

1. Reduction of the Calderón problem in the domain to equations on its boundary. Let us consider in the square D, $D^+ \subset D$ an auxiliary Dirichlet problem

$$\left.\begin{aligned} \Delta u := \Delta_{D\overline{D}} u_{\overline{D}}\,|_x = \frac{\partial^2 u}{\partial x_1^2}+\frac{\partial^2 u}{\partial x_2^2}=f(x_1, x_2), \ x\in D \\ u\,|_{\partial D}=0. \end{aligned}\right\} \tag{4.1.2}$$

We denote by $G(x, y) = G(x_1, x_2, y_1, y_2)$ its Green function and consider in the domain D^+ the classical Green identity:

$$\int\limits_\Gamma \left(G\frac{\partial u}{\partial n}-\frac{\partial G}{\partial n}u\right) ds = u - \int\limits_{D^+}\int G(x, y)\left(\frac{\partial^2 u}{\partial y_1^2}+\frac{\partial^2 u}{\partial y_2^2}\right) dy. \tag{4.1.3}$$

Then we denote by u_Γ a space of pairs of functions $u_\Gamma = (u_\Gamma^0(s), u_\Gamma^1(s))$ defined on the boundary $\Gamma = \partial D^+$ and such that there exists a function $u_{\overline{D}^+}|_x = u(x)$, $x\in \overline{D}^+$, which is sufficiently smooth for the Green identity to be fulfilled and for which $u\,|_\Gamma = u_\Gamma^0(s)$, $\left.\frac{\partial u}{\partial n}\right|_\Gamma = u_\Gamma^1(s)$. We shall call the space U_Γ the Cauchy space for Laplace equation (4.1.1).

The expression

$$P_{\overline{D}^+\Gamma} u_\Gamma\,|_{x\in\overline{D}^+} \equiv u(x) - \int\limits_{D^+}\int G(x, y)\,\Delta u(y)\,dy, \quad x\in\overline{D}^+, \tag{4.1.4}$$

where $u\,|_\Gamma = u_\Gamma^0$, $\left.\frac{\partial u}{\partial n}\right|_\Gamma = u_\Gamma^1(s)$, will be called the potential with the vector density u_Γ. It follows from the Green identity (4.1.3) that expression (4.1.4) depends only on u_Γ and not on the choice of $u(x_1, x_2)$, $u\,|_\Gamma = u_\Gamma^0$, $\left.\frac{\partial u}{\partial n}\right|_\Gamma = u_\Gamma^1$, and can be written in the form of a contour integral.

Let us juxtapose each $v_\Gamma = (v_\Gamma^0, v_\Gamma^1)$ with a pair of functions $u_\Gamma = (u_\Gamma^0, u_\Gamma^1)$, by putting

$$u_\Gamma^0 = P_{\overline{D}^+\Gamma} v_\Gamma\,|_\Gamma, \quad u_\Gamma^1 = \frac{\partial}{\partial n}\left(P_{\overline{D}^+\Gamma} v_\Gamma\right)|_\Gamma.$$

This pair of equations will be written as follows: $u_\Gamma = P_\Gamma v_\Gamma$. It follows from the Green identity (4.1.3) that the equality $u_\Gamma - P_\Gamma u_\Gamma = 0$ holds for those and only those $u_\Gamma \in U_\Gamma$, for which there exists a solution u of Laplace equation (4.1.1), such that $u\,|_\Gamma = u_\Gamma^0$ and $\partial u/\partial n\,|_\Gamma = u_\Gamma^1$.

In this respect, the equation

$$u_\Gamma - P_\Gamma u_\Gamma = 0 \tag{4.1.5}$$

is equivalent to Laplace equation (4.1.1) in the domain D^+. Equation (4.1.5) is an example of pseudodifferential Calderón-Seely equations constructed for a common elliptical operator in [4.38, 4.39].

Let us now consider a boundary value problem for the Laplace equation in the domain D^+, supplementing Eq. (4.1.1) by a boundary condition of the form

$$lu_\Gamma\,|_{x\in\Gamma} \equiv u(x) - a\,\frac{\partial u(x)}{\partial n}\Big|_{x\in\Gamma} = \varphi(s). \tag{4.1.1'}$$

We shall assume for the sake of definiteness that $a \equiv 0$ or $a \equiv 1$. Obviously, problem (4.1.1), (4.1.1′) is equivalent to the problem

$$u_\Gamma - P_\Gamma u_\Gamma = 0,\ lu_\Gamma = \varphi,\ \varphi \in \Phi, \tag{4.1.6}$$

where Φ is a given space of functions, on the boundary $\Gamma = \partial D^+$ in the sense that the boundary values $u_\Gamma = \left(u|_\Gamma, \frac{\partial u}{\partial n}\Big|_\Gamma\right)$ of the solution of problem (4.1.1), (4.1.1′) satisfy Eqs. (4.1.6), and the solution $u_\Gamma = \left(u\,|_\Gamma, \frac{\partial u}{\partial n}\Big|_\Gamma\right)$ of system (4.1.6) allows us to construct the solution $u(x_1, x_2)$ of problem (4.1.1), (4.1.1′) for which the Cauchy values coincide with the solution u_Γ of system (4.1.6). Namely, $u_{\overline{D}^+} = P_{\overline{D}^+\Gamma} u_\Gamma$.

Here we shall solve two problems: the problem of calculating the potential $u_{\overline{D}^+} = P_{\overline{D}^+\Gamma} v_\Gamma$ for a given v_Γ and the problem of approximately calculating the solution u_Γ of Calderón's equation (4.1.6).

The difference potential, which will be constructed below, will be used for solving these two problems.

2. Construction of the difference potential. Let us choose a natural h^{-1} and introduce a mesh $m = (m_1 h, m_2 h)$, where m_1, m_2 are integers. The numerical solution of (different!) boundary value problems for Eq. (4.1.1) will be reduced to the multiple solution of (the same!) auxiliary Dirichlet difference problem with zero boundary values for the simplest difference analog of the Poisson equation in the rectangle D. This auxiliary difference problem can be written as follows:

$$\sum_{n\in N_m} a_{mn} u_n = f_m,\ m \in M, \tag{4.1.7}$$

$$u_n\,|_{n\in\partial D} = 0. \tag{4.1.8}$$

Here N_m is a five-point pattern applied to the point m and consisting of the points (m_1h, m_2h), $((m_1 \pm 1)\,h, m_2h)$, $(m_1h, (m_2 \pm 1)\,h)$; and the coefficients

$$a_{mn} = \begin{cases} h^{-2}, & \text{if } m \neq n,\ n \in N_m, \\ -4h^{-2}, & \text{if } m = n,\ n \in N_m. \end{cases}$$

The set M consists of all points of the mesh which fall inside the square D.

Let us introduce the space F_M of all functions f_M defined on M. We put $N = UN_m$, $m \in M$, and introduce the space U_N of all functions u_N defined on N and vanishing at all points $n \in N$ that lie on the sides of the square D. We introduce the operator Δ_{MN}: $U_N \to F_M$, which juxtaposes each u_N to an f_M in accordance with formula (4.1.7). The problem (4.1.7), (4.1.8) can be written in the following concise form:

$$\Delta_{MN}u_N = f_M, \quad f_M \in F_M, \quad u_N \in U_N. \tag{4.1.9}$$

Problem (4.1.7), (4.1.8) or (4.1.9) has the unique solution $u_N \in U_N$ for any $f_M \in F_M$.

Let us denote by G_{NM} the operator which puts each f_M in correspondence with the solution u_N of problem (4.1.9). We shall call this operator the Green operator of problem (4.1.9). It should be noted that $u_N = G_{NM}f_M$ can be calculated by solving problem (4.1.7), (4.1.8) by the Fourier method or in some other manner.

We put $M^+ = M \cap D^+$ and $N^+ = UN_m$, $m \in M^+$. Let us consider the spaces F_{M^+} and U_{M^+} of all functions f_{M^+} and u_{N^+} defined on M^+ and N^+ respectively. We define the operator $\Delta_{M^+N^+}$: $U_{N^+} \to F_{M^+}$ by specifying for an arbitrary $u_{N^+} \in U_{N^+}$ the value f_m of the function f_{M^+} at the point $m \in M^+$ in accordance with formula (4.1.7). We also define $G_{N^+M^+}$: $F_{M^+} \to U_{N^+}$ by juxtaposing each $f_{M^+} \in F_{M^+}$ to the function $u_{N^+} \in U_{N^+}$ according to the following rule. We additionally define f_{M^+} so that it is zero everywhere on M, solve problem (4.1.7), (4.1.8), and consider the obtained solution u_N only on N^+, denoting this contraction of the function by u_{N^+}.

Determination of the two-layer boundary Γ_h. We denote $M^- = M \setminus M^+$ and $N^- = UN_m$, $m \in M^-$, and determine the boundary Γ_h of the domain N^+ by putting $\Gamma_h = N^+ \cap N^-$.

Determination of the difference potential. Let us introduce the space U_{Γ_h} of all functions u_{Γ_h} defined on Γ_h.

We define the operator $P_{N^+\Gamma_h}$: $U_{\Gamma_h} \to U_{N^+}$ by putting for a given $v_{\Gamma_h} \in U_{\Gamma_h}$:

$$u_{N^+} = P_{N^+\Gamma_h}v_{\Gamma_h} \overset{\text{def}}{=} v_{N^+} - G_{N^+M^+}\Delta_{M^+N^+}v_{N^+},$$

where v_{N^+} is an arbitrary extension of v_{Γ_h} everywhere on N^+. It can be shown that $u_{N^+} = P_{N^+\Gamma_h}v_{\Gamma_h}$ depends only on v_{Γ_h} rather

than on the chosen extension v_{N^+}. We shall call the expression $P_{N^+\Gamma_h} v_{\Gamma_h}$ the difference potential with the density v_{Γ_h}. Obviously, its calculation is reduced to solving the problem of the type (4.1.7), (4.1.8).

3. Approximation of the continual potential by the difference potential. Let $\rho_\Gamma = (\rho_\Gamma^0(s), \rho_\Gamma^1(s))$ be the vector density of the potential $u_{\bar{D}^+} = P_{\bar{D}^+\Gamma}\rho_\Gamma$, where $\rho_\Gamma^0(s)$ and $\rho_\Gamma^1(s)$ are sufficiently smooth functions. We denote by $u(x_1, x_2)$ a smooth function for which $u|_\Gamma = \rho^0(s)$, $\left.\frac{\partial u}{\partial n}\right|_\Gamma = \rho^1(s)$ and $\Delta u|_\Gamma = 0$. The latter requirement uniquely defines $\frac{\partial^2 u}{\partial n^2}$ in terms of the values ρ_Γ^0, $\frac{d}{ds}\rho_\Gamma^0$ and ρ_Γ^1. Let us consider the difference potential $u_{N^+} = P_{N^+\Gamma_h}\rho_{\Gamma_h}$ with the density ρ_{Γ_h} which is defined at an arbitrary point $\nu \in \Gamma_h$ from the following formula:

$$\rho_{\Gamma_h}|_\nu = \rho_\Gamma^0(s_\nu) + r\rho_\Gamma^1(s_\nu) + \frac{r^2}{2!}\left.\frac{\partial^2 u}{\partial n^2}\right|_{s_\nu}. \tag{4.1.10}$$

Here s_ν is the point on the boundary Γ, through which the normal to the boundary containing $\nu \in \Gamma_h$ passes, and r is the distance between ν and s_ν. The symbol s_ν denotes simultaneously the length of the arc s at the point s_ν.

We define the set $Y^+ \subset N^+$ as a totality of points $y = (y_1, y_2)$, for which each of the following nine points

$$(y_1, y_2),\ (y_1 \pm h, y_2),\ (y_1, y_2 \pm h),\ (y_1 \pm h, y_2 \pm h),$$
$$(y_1 \pm h, y_2 \mp h) \tag{4.1.11}$$

belongs to N^+. Let $x \in \bar{D}^+$ be an arbitrary point and y_x one of its neighbouring points from Y^+. We denote the corresponding set of nine points (4.1.11) by N_x^+. We then construct an interpolation polynomial $\mathcal{P}_{2,2}(t_1, t_2)$ of a degree not higher than second in each of its arguments, which assumes at the points of N_x^+ the values of the difference potential $P_{N^+\Gamma_h}\rho_{\Gamma_h}$. The results obtained in [4.24] and [4.31] show that

$$|P_{\bar{D}^+\Gamma}\rho_\Gamma|_x - \mathcal{P}_{2,2}(x)| \leqslant ch^2,$$

$$\left|\frac{\partial}{\partial l}P_{\bar{D}^+\Gamma}\rho_\Gamma\right|_x - \frac{\partial}{\partial l}\mathcal{P}_{2,2}(x)| \leqslant ch^2,$$

where $\partial/\partial l$ is the derivative with respect to any direction l and c is a constant independent of x and h.

Hence it is clear that the difference potential $P_{N^+\Gamma_h}\rho_{\Gamma_h}$ can be used for calculating the continual potential $P_{\bar{D}^+\Gamma}\rho_\Gamma$ and its derivative everywhere in $\bar{D}^+$ up to the boundary.

4. Discretization of Calderón equations. Here we shall describe the method of discretization of Eqs. (4.1.6). We split the boundary

Γ into a certain number K of arcs having the same length H. Let the ends of these arcs, viz. the splitting points, be points $s_i = iH$, $i = 1, 2, \ldots, K$. The set of splitting points will be also denoted by K. Let us consider the space U_K of vector functions u_K, $u_K|_{s=s_i} = \mathbf{u}_i = (u_i^0, u_i^1)$, $i = 1, 2, \ldots, K$, which are defined on K.

We shall additionally define u_K^0 and u_K^1 specified at points s_i of the set K so that everywhere on Γ they are equal to $u^0_{\Gamma, K}(s)$ and $u^1_{\Gamma, K}(s)$, which have bounded fourth and third derivatives everywhere on $\Gamma \setminus K$ and continuous third and second derivatives everywhere on Γ, including the points of the set K. For this completion we shall use, for example, the formulas for a local smooth completion [4.34].

Similarly, we consider the space Φ_K of mesh functions φ_K and their completions $\varphi_{\Gamma K} \in \Phi$ given by formulas of [4.34]. These functions have derivatives up to the fourth order, bounded on $\Gamma \setminus K$ and third-order derivatives which are continuous everywhere on Γ if $a = 0$. If $a \equiv 1$, the requirement to the smoothness of $\varphi_{\Gamma K}(s)$ should be reduced by unity.

Let us consider, instead of (4.1.6), the following discrete system of equations in $2K$ components $u_K \in U_K$:

$$\left.\begin{aligned} &u_{\Gamma K} - P_\Gamma u_{\Gamma K}|_{s_i} = 0|_{s_i}, \\ &l u_{\Gamma K}|_{s=s_i} = \varphi(s_i), \quad i = 1, 2, \ldots, K. \end{aligned}\right\} \tag{4.1.12}$$

This system contains $3K$ linear algebraic equations and is hence overdetermined.

We introduce in the space U_Γ a scalar product by putting

$$(u_\Gamma, v_\Gamma) = \int_\Gamma \left[u^0_\Gamma(s)\, v^0_\Gamma(s) + \frac{du^0_\Gamma}{ds} \cdot \frac{dv^0_\Gamma}{ds} + u^1_\Gamma(s)\, v^1_\Gamma(s) \right] ds.$$

We also introduce a scalar product in the space Φ by putting

$$(\varphi_\Gamma, \psi_\Gamma) = \begin{cases} \displaystyle\int_\Gamma \varphi_\Gamma \psi_\Gamma\, ds, & \text{if } a \equiv 1, \\ \displaystyle\int_\Gamma (\varphi_\Gamma \psi_\Gamma + \varphi'_\Gamma \psi'_\Gamma)\, ds & \text{if } a \equiv 0. \end{cases}$$

These scalar products induce Hilbert norms

$$\|u_\Gamma\|^2_{U_\Gamma} = \int_\Gamma \left[\left(u^0 - \frac{d^2 u^0}{ds^2} \right) u^0 \right] ds + \int_\Gamma |u^1|^2\, ds, \tag{4.1.13}$$

$$\|\varphi_\Gamma\|^2_\Phi = \begin{cases} \displaystyle\int_\Gamma \varphi^2_\Gamma\, ds, & \text{if } a \equiv 1, \\ \displaystyle\int_\Gamma \left(\varphi_\Gamma - \frac{d^2 \varphi_\Gamma}{ds^2} \right) \varphi_\Gamma\, ds, & \text{if } a \equiv 0. \end{cases} \tag{4.1.14}$$

We shall treat the solution $u_K \in U_K$ of the overdetermined system (4.1.12) in the sense of the least squares method, i.e. as an element minimizing the expression

$$\| u_{\Gamma K} - P_\Gamma u_{\Gamma K} \|^2_{U_\Gamma} + \| l u_{\Gamma K} - \varphi_{\Gamma K} \|^2_\Phi. \qquad (4.1.15)$$

The norms $\| \cdot \|_{U_\Gamma}$ and $\| \cdot \|_\Phi$ are chosen so that in view of the properties of problem (4.1.1), (4.1.1′) and the corresponding properties of problem (4.1.6), and also the properties of the chosen method of completion $u_K \to u_{\Gamma K}$, the conditionality number of the linear system of the least squares method corresponding to (4.1.15) is independent of K. Hence gradient methods used for its solution require a certain number of iterations which is independent of K in order to reduce the error by a factor of ε^{-1}.

However, the actual application of the matrix of this system to the element $v_K \in U_K$ involves, in particular, the calculation of the results of application of P_Γ and P^*_Γ and is therefore nonconstructive.

5. **The algorithm of the method.** The essence of the algorithm consists in the replacement of the nonconstructive element $P_\Gamma u_{\Gamma K}$ in system (4.1.12) by a constructive element by approximating the continual potential to a difference potential which can be effectively calculated. Let us perform some auxiliary constructions.

(a) Let us define the operator $\pi_{\Gamma_h K}$: $U_K \to U_{\Gamma_h}$. Suppose that $u_K \in U_K$. The element $u_{\Gamma_h} = \pi_{\Gamma_h K} u_K$ is obtained as a result of the following constructions. On the basis of u_K, $u_{\Gamma K} \in U_\Gamma$ is constructed with the help of the smooth completion described in Subsec. 4. Then the difference potential density $u_{\Gamma_h K}$ is constructed on the basis of $u_{\Gamma K}$ as described in Subsec. 3.

The operator $\pi_{\Gamma_h K}$ is local. For calculating the value of $u_{\Gamma_h K}$ at a point $\nu \in \Gamma_h$, the values at a certain number of points are used, this number being independent of K or h. Hence the result of application of the conjugate operator $\pi^*_{K\Gamma_h}$: $U_{\Gamma_h} \to U_K$ can be easily calculated.

(b) We denote $N^+_K = UN^+_{s_i}$ (N^+_x was introduced in Subsec. 3). Let us consider the space $U^+_{N_K}$ of all functions defined on N^+_K. We denote by $P_{N^+_K \Gamma_h}$: $U_{\Gamma_h} \to U_{N^+_K}$ the operator which juxtaposes to a given $u_{\Gamma_h} \in U_{N^+_K}$ the contraction $v_{N^+} = P_{N^+ \Gamma_h} u_{\Gamma_h}$ of the potential to the set N^+_K.

Thus, the result of application of this operator is calculated by solving the auxiliary problem (4.1.7), (4.1.8).

(c) The operator $P^*_{\Gamma_h N^+_K}$: $U_{N^+_K} \to U_{\Gamma_h}$ is conjugate to the operator $P_{N^+_K \Gamma_h}$ (in the sense that their matrices are conjugate). The result of application of this operator to the element $u_{N^+_K}$ is also calculated by solving the auxiliary problem (4.1.7), (4.1.8). Indeed, let us use the

obvious formula

$$P_{N_K^+\Gamma_h} v_{\Gamma_h} = (I_{N_K^+\Gamma_h} - G_{\Gamma_h M^+} L_{M^+\Gamma_h})\, v_{\Gamma_h}. \tag{4.1.16}$$

Here the operator $I_{N_K^+\Gamma_h}$: $U_{\Gamma_h} \to U_{N_K^+}$, $w_{N_K^+} = I_{N_K^+\Gamma_h} v_{\Gamma_h}$ juxtaposes to v_{Γ_h} the function $w_{N_K^+}$ which is defined by the following expressions:

$$w_\nu = \begin{cases} v_\nu, & \text{if } \nu \in \Gamma_h, \\ 0, & \text{if } \nu \bar{\in} \Gamma_h, \end{cases} \tag{4.1.17}$$

$$L_{M^+\Gamma_h} v_{\Gamma_h} = L_{M^+N^+} \theta_{\Gamma_h} v_{N^+},$$

and $G_{\Gamma_h, M^+} f_{M^+}$ is the contraction of $G_{NM^+} f_{M^+}$ to Γ_h. It follows from (4.1.16) that

$$(P_{N_K^+\Gamma_h})^* = P^*_{\Gamma_h N_K^+} = I^*_{\Gamma_h N_K^+} - (L_{M^+\Gamma_h})^* \cdot (G_{\Gamma_h M^+})^*.$$

The function $v_{\Gamma_h} = I^*_{\Gamma_h N_K^+} w_{N_K^+}$ is obviously determined from the given $w_{N_K^+}$ in accordance with formula (4.1.17). The calculation of

$$(G_{\Gamma_h M^+})^* v_{\Gamma_h} = G^*_{M^+\Gamma_h} v_{\Gamma_h} = G_{M^+\Gamma_h} v_{\Gamma_h} = G_{M^+M^+} \theta_{\Gamma_h} v_{M^+}$$

is reduced to the solution of problem (4.1.1.7), (4.1.8), where $f_{M^+} = \Theta_{\Gamma_h} v_{M^+}$ and v_{M^+} is an arbitrary completion of v_{Γ_h}. Finally,

$$(L_{M^+\Gamma_h})^* v_{M^+} = L^*_{\Gamma_h M^+} v_{M^+} = L_{\Gamma_h M^+} v_{M^+} = L_{\Gamma_h N^+} (\theta_{M^+} v_{N^+})$$

is the contraction of $L_{MN^+}(\theta_{M^+} v_{N^+})$ to the set $\Gamma_h \subset M \subset N$.

(d) The operator $r_{KN_K^+}$: $U_{N_K^+} \to U_K$ transforms the function $v_{N_K^+} \in U_{N_K^+}$ to the vector function $u_K = r_{KN_K^+} v_{N_K^+}$ which is defined at the $s_i = x \in K$ by the formulas

$$u_i^0 = \mathcal{P}_{2,2}(x); \quad u_i^1 = \frac{\partial \mathcal{P}_{2,2}(x)}{\partial n},$$

where $\mathcal{P}_{2,2}(x)$ is the operator introduced in Subsec. 3. Obviously, $r_{K,\, N_K^+}$ is a local operator used for calculating $u_i = (u_i^0, u_i^1)$, viz. the value of $u_{N_K^+}$ at nine points of the set N_x^+.

Consequently, the result of application of the operator $(r_{K,\, N_K^+})^*$: $U_K \to U_{N_K^+}$ to $u_K \in U_K$ can be easily calculated.

(e) The operator l: $U_K \to \Phi_K$ is local. Therefore, l^*: $\Phi_K \to U_K$ is such that $l\varphi_K = u_K$ can be easily calculated for any $\varphi_K \in \Phi_K$.

Instead of system (4.1.12), we shall consider the system

$$\left.\begin{aligned} &u_k - r_{KN_K^+} P_{N_K^+\Gamma_h} \pi_{\Gamma_h K} u_K = 0_K, \\ &l u_K = \varphi_K. \end{aligned}\right\} \tag{4.1.18}$$

We introduce into U_K a norm similar to (4.1.13) by putting

$$\| u_K \|^2_{U_K} = H \sum_{i=1}^{K} \left[\left(u_i^0 - \frac{u_{i+1}^0 - 2u_i^0 + u_{i-1}^0}{H^2} \right) u_i^0 + (u_i^1)^2 \right], \quad u_0^0 \equiv u_K^0.$$

The norm for Φ_K is introduced by putting, in analogy with (4.1.14),

$$\| \varphi_K \|^2_{\Phi_K} = \begin{cases} H \sum \varphi_i^2 \text{ if } a \equiv 1, \\ H \sum \left[\left(\varphi_i - \frac{\varphi_{i+1} - 2\varphi_i + \varphi_{i-1}}{H^2} \right) \varphi_i \right], \text{ if } a \equiv 0. \end{cases}$$

For the generalized solution of system (4.1.18) we shall take $u_K \in U_K$ which minimizes the expression

$$\| u_K - r_{KN_K^+} P_{N_K^+\Gamma_h} \pi_{\Gamma_h K} u_K \|^2_{U_K} + \| l u_K - \varphi_K \|^2_{\Phi_K}.$$

For the chosen norms, the corresponding linear system is found to be determined in the sense $\| \cdot \|_{U_K}$ by a number which is independent of K only if $h \leqslant bH^{3/2}$ and b is sufficiently small. Let us write this system $C_{KK} u_K = g_K$, using the following brief notations:

$$Q_{KK} u_K \equiv u_K - r_{KN_K^+} P_{N_K^+\Gamma_h} \pi_{\Gamma_h K} u_K,$$

$$A_{KK} u_K \,|_i = \mathbf{v}_i = (v_i^0, v_i^1)$$

$$= \left(u_i^0 - \frac{u_{i+1}^0 - 2u_i^0 + u_{i-1}^0}{H^2}, u_i^1 \right), \quad i = 1, 2, \ldots, K,$$

$$B_{KK} \varphi_K \,|_i \equiv \psi_K \,|_i = \varphi_i - (1 + a) \frac{\varphi_{i+1} - 2\varphi_i + \varphi_{i-1}}{H^2}.$$

We obtain

$$g_K = A_{KK}^{-1} l^* B_{KK} \varphi_K, \quad \varphi_K \in \Phi_K,$$

$$C_{KK} = A_{KK}^{-1} [Q_{KK}^* A_{KK} Q_{KK} + l^* B_{KK} l].$$

In view of the above constructions and remarks, the application of the matrix C_{KK} to the vector $u_K \in U_K$ is the operation to be realised. The calculation of $v_K = A_{KK}^{-1} f_K$ is reduced to the solution of the equation of the type

$$\left.\begin{aligned} v_i^0 - \frac{v_{i+1}^0 - 2v_i^0 + v_{i-1}^0}{H^2} &= f_i^0, \\ v_i^1 &= f_i^1, \end{aligned}\right\} \quad i = 1, 2, \ldots, K,$$

which is carried out by the sweep ("progonka") method.

The computational procedure which does not involve the matrix C_{KK}, is similar to that used in [4.41].

After the value of u_K has been found, $u_{\Gamma_h} = \pi_{\Gamma_h K} u_K$ is calculated, and the approximate solution is $u_{N^+} = P_{N^+ \Gamma_h} u_{\Gamma_h}$.

6. The effectiveness of the method. In order to obtain u_{N^+} such that

$$|u^{(h, H)}(x) \equiv u(x, h, H) = r_{x N^+} u_{N^+}$$

and its first derivatives differ from the exact solution $u(x)$ and from its corresponding derivatives by less than ε we need to store $O(\varepsilon^{-1})$ computer words and $O(\varepsilon^{-2} \ln |\varepsilon|)$ arithmetic operations, i.e. as many as in the capacitance matrix method. However, the range of applicability of the MDP is much wider.

4.2. GREEN'S FORMULA, POTENTIAL, PROJECTOR, AND CALDERÓN'S BOUNDARY CONDITIONS GENERALIZED ON THE BASIS OF THE CONCEPT OF SHARP TRACE

The MDP algorithm is based on the combined application of Green's difference formula and difference projectors on the one hand and classical Green's formula and Calderón projectors specially modified and generalized for this purpose on the other hand. Here we shall introduce the concept of sharp trace and construct the required modifications of Green's formula, surface potentials, projectors, and boundary pseudodifferential Calderón-Seeley equations.

We shall consider linear differential equations or systems of equations

$$L_{D^+ \overline{D}^+} u_{\overline{D}^+} = f_{D^+},$$

defined in an arbitrary domain D^+ of a certain multidimensional manifold. We shall assume that the boundary ∂D^+ is sufficiently smooth and that the differential equation under consideration has also a sense in the extended domain D, $D^+ \subset D$, of this manifold which will be required. In this case, we shall use the notation $L_{D\overline{D}} u_{\overline{D}} = f_D$, where $\overline{D}$ is the closure of D. The material will be divided into subsections 1, 2, etc. Besides some subsections will be labelled by the numbers with asterisks, e.g. 1*. These subsections contain the illustrations of the main text with the help of Poisson's equation on a plane. This section presents in a concise form the results of [4.26], the concept of the sharp trace introduced there being somewhat refined.

1. Auxiliary boundary value problem and Green's operator. Suppose that a domain $D \supset D^+$ and its closure $\overline{D}$ are given. We shall assume that we are given linear spaces $U_{\overline{D}}$, $V_{\overline{D}}$, and F_D of the functions

$u_{\overline{D}}$, $v_{\overline{D}}$ and f_D defined on $\overline{D}$ or D respectively. Suppose that the linear differential equation

$$L_{D\overline{D}}u_{\overline{D}} = f_D, \quad u_{\overline{D}} \in U_{\overline{D}}, \tag{4.2.1}$$

is given in the domain D, where $f_D \in F_D$. We shall assume that problem (4.2.1) has one and only one solution $u_{\overline{D}} \in U_{\overline{D}}$ for every $f_D \in F_D$. Then Eq. (4.2.1) defines the operator $G_{\overline{D}D}$: $F_D \to U_{\overline{D}}$ called Green's operator of problem (4.2.1).

As regards $V_{\overline{D}}$, we shall assume that the differential operation $L_{D\overline{D}}$ is applicable to each $v_{\overline{D}} \in V_{\overline{D}}$ so that $L_{D\overline{D}}v_{\overline{D}} \in F_D$ and the extension of the operator $L_{D\overline{D}}$: $U_{\overline{D}} \to F_D$ to the space $V_{\overline{D}}$ has sense. As before, we shall denote this extension by the symbol $L_{D\overline{D}}$, $L_{D\overline{D}}$: $V_{\overline{D}} \to F_D$.

We shall assume that F_D is the Hölder class $C_{k+\alpha, D}$ where k is a nonnegative integer, $0 < \alpha < 1$, and $U_{\overline{D}}$ is a set of functions continuous in $\overline{D}$, vanishing on the boundary of the square $\overline{D}$ having continuous second derivatives, and such that Δu belongs to F_D as a function considered on D. The operator $G_{\overline{D}D}$: $F_D \to U_{\overline{D}}$ can in this case be defined by the formula

$$u(x) \equiv u(x_1, x_2) = \int\int_D G(x, y) f(y)\, dy, \tag{4.2.2}$$

where $G(x, y)$ is a classical Green's function for problem (4.2.1) under the boundary condition $u|_{\partial D} = 0$. Let $V_{\overline{D}}$ be the class of functions such that $\Delta v_{\overline{D}} \in F_D$, vanishing at $x_1 = 0$, $x_1 = 1$, $x_2 = 0$, and being arbitrary in other respects.

2. Contractions of spaces and equations to subdomains. Suppose that $D^+ \subset D$ and $\overline{D}^+$ is the closure of D^+. We denote by $(u_{\overline{D}})_{\overline{D}^+} = u_{\overline{D}^+}$, $(v_{\overline{D}})_{\overline{D}^+} = v_{\overline{D}^+}$, and $(f_D)_{D^+} = f_{D^+}$ the contractions of the functions $u_{\overline{D}}$, $v_{\overline{D}}$ and f_D to the corresponding sets.

Let $\mathcal{F}_D$ be a certain subspace of F_D, $\mathcal{F}_D \subset F_D$. We denote $\mathcal{F}_{D^+} = \{f_{D^+} \mid f_D \in \mathcal{F}_D\}$ and introduce

$$\mathcal{F}^+_D = \{f_D \mid f_D \in \mathcal{F}_D \text{ and } \Theta_{D^+} f_D \in \mathcal{F}_D\}. \tag{4.2.3}$$

Here and below Θ_X is the eigenfunction of the set X, i.e. the function which is equal to 1 on X and zero outside it. For a given $\mathcal{F}_D$ we define a subspace $\mathcal{U}_{D^+} = \mathcal{U}_{\overline{D}}(\mathcal{F}^+_D) \subset U_D$ by putting

$$\mathcal{U}^+_{\overline{D}} = \{u_{\overline{D}} \mid L_{D\overline{D}}u_{\overline{D}} \in \mathcal{F}^+_D\}. \tag{4.2.4}$$

For each subspace $\mathcal{U}_{\overline{D}} \subset U_{\overline{D}}$ we define $\mathcal{U}_{\overline{D}^+}$ by putting $\mathcal{U}_{\overline{D}^+} = \{u_{\overline{D}^+} \mid u_{\overline{D}} \in \mathcal{U}_{\overline{D}}\}$. In particular,

$$\mathcal{U}^+_{D^+} = \{u_{\overline{D}^+} \mid u_{\overline{D}} \in \mathcal{U}^+_{\overline{D}}\}. \tag{4.2.5}$$

We define the operator $G_{\overline{D}D^+}$: $\mathcal{F}^+_{D^+} \to \mathcal{U}^+_{\overline{D}}$ by putting for each $f_{D^+} \in \mathcal{F}^+_{D^+}$

$$u_{\overline{D}} = G_{\overline{D}D^+} f_{D^+} \overset{\text{def}}{=} G_{\overline{D}D} \tilde{f}_D,$$

where $\tilde{f}_D$ is the additional definition of f_{D^+} equal to zero outside D^+. We define the operator $G_{\overline{D}^+D^+}$: $\mathcal{F}^+_{D^+} \to \mathcal{U}^+_{\overline{D}^+}$ by putting for every $f_{D^+} \in \mathcal{F}^+_{D^+}$

$$u_{\overline{D}^+} = G_{\overline{D}^+D^+} f_{D^+} = (G_{\overline{D}D^+} f_{D^+})_{\overline{D}^+}.$$

Thus, the operator $G_{\overline{D}^+\overline{D}^+}$ is defined on $F^+_{D^+}$ and on each of its subspaces $\mathcal{F}^+_{D^+}$ which is generated by an arbitrary $\mathcal{F}_D \subset F_D$ in accordance with (4.2.3). Let us introduce the notation $\mathcal{V}_{\overline{D}} = \mathcal{V}_{\overline{D}}(\mathcal{F}_D)$ for the inverse image $\mathcal{F}_D$ in $V_{\overline{D}}$. We shall denote

$$\mathcal{V}^+_{\overline{D}} = \mathcal{V}_{\overline{D}}(\mathcal{F}^+_D). \tag{4.2.6}$$

3. Let us define the operator $P_{\overline{D}^+\overline{D}^+}$: $V^+_{\overline{D}^+} \to V^+_{\overline{D}^+}$ by putting for an arbitrary $v_{\overline{D}^+} \in V^+_{\overline{D}^+}$

$$P_{\overline{D}^+\overline{D}^+} v_{\overline{D}^+} \overset{\text{def}}{=} v_{\overline{D}^+} - G_{\overline{D}^+D^+} L_{D^+\overline{D}^+} v_{\overline{D}^+}, \tag{4.2.7}$$

where $L_{D^+\overline{D}^+} v_{\overline{D}^+} = (L_{D\overline{D}} v_D)_{\overline{D}^+}$, and $v_{\overline{D}} \in V_{\overline{D}}$ is an arbitrary completion of $v_{\overline{D}^+}$ to $v_{\overline{D}} \in V_{\overline{D}}$.

Theorem 4.2.1. *For any $\mathcal{F}_D \subset F_D$, the space $\mathcal{V}^+_{\overline{D}^+} = \mathcal{V}_{\overline{D}^+}(\mathcal{F}^+_D)$ generated by it in accordance with* (4.2.6), *is the eigen subspace of the operator $P_{\overline{D}^+\overline{D}^+}$.*

Theorem 4.2.2. *The following statements are true.*

1°. *For any $v_{\overline{D}^+} \in V^+_{\overline{D}^+}$, the function $u_{\overline{D}^+} = P_{\overline{D}^+\overline{D}^+} v_{\overline{D}^+}$ satisfies the homogeneous equation $L_{D^+\overline{D}^+} v_{\overline{D}} = O_{D^+}$.*

2°. *If $v_{\overline{D}^+} \in V_{\overline{D}^+}$ satisfies the homogeneous equation $L_{D^+\overline{D}^+} v_{\overline{D}^+} = O_{D^+}$, then $v_{\overline{D}^+} \in V^+_{\overline{D}^+}$ and $P_{\overline{D}^+\overline{D}^+} v_{\overline{D}^+} = v_{\overline{D}^+}$.*

3°. $P^2_{\overline{D}^+\overline{D}^+} = P^1_{\overline{D}^+\overline{D}^+}$, *i.e. $P_{\overline{D}^+\overline{D}^+}$ is a projector.*

Remark. According to Theorem 4.2.1, for any $\mathcal{F}_D \subset F_D$ under the conditions of Theorem 4.2.2 $V^+_{\overline{D}} = V_{\overline{D}}(F^+_D)$ can be replaced everywhere by $\mathcal{V}^+_{\overline{D}} = \mathcal{V}_{\overline{D}}(\mathcal{F}^+_D)$.

4. **The boundary Γ, sharp trace.** Let $\Gamma \subset \overline{D}^+$ be an arbitrary subset, V_Γ a certain linear space of vector functions defined on Γ, and γ: $V_{\overline{D}^+} \to V_\Gamma$ be a certain linear operator.

The element $v_\Gamma = \gamma v_{\overline{D}^+} \in V_\Gamma$ will be called the trace of $v_{\overline{D}^+}$ (and also of any $v_{\overline{D}} \in V_{\overline{D}}$, coinciding with $v_{\overline{D}^+}$ on $\overline{D}^+$) on Γ and the operator γ will be called the trace operator.

Theorem 4.2.3. *Let $U_{\overline{D}}$, $V_{\overline{D}}$, Γ, V_Γ, and γ be matched so that each $v_{\overline{D}} \in V^+_{\overline{D}}$ for which $v_\Gamma = \gamma v_{\overline{D}} = 0_\Gamma$ belongs to $U_{\overline{D}}$ as well. Then the following four properties are equivalent.*

1°. *For any two $v_{\overline{D}} \in V^+_{\overline{D}}$ and $v'_{\overline{D}} \in V^+_{\overline{D}}$ whose traces coincide ($v_\Gamma = v'_\Gamma$) the equality $P_{\overline{D}^+\overline{D}^+} v_{\overline{D}^+} = P_{\overline{D}^+\overline{D}^+} v'_{\overline{D}^+}$ is valid.*

2°. *For any $v_{\overline{D}}$, $v_{\overline{D}} \in V^+_{\overline{D}}$, $v_\Gamma = 0$ the equality $P_{\overline{D}^+\overline{D}^+} v_{\overline{D}^+} = O_{D^+}$ is satisfied.*

3. *For any $v_{\overline{D}}$ such that $v_{\overline{D}} \in V^+_{\overline{D}}$ and $v_\Gamma = 0$ the condition $G_{\overline{D}^+D^+} L_{D^+\overline{D}^+} v_{\overline{D}^+} = v_{\overline{D}^+}$ is fulfilled.*

4°. *For any $v_{\overline{D}}$, $v_{\overline{D}} \in V^+_{\overline{D}}$, $v_\Gamma = 0$, there exists $u_{\overline{D}} \in U_{\overline{D}}$ such that $v_{\overline{D}^+} = u_{\overline{D}^+}$ and $(L_{D\overline{D}} u_{\overline{D}})_{D \setminus D^+} = O_{D \setminus D^+}$.*

Definition. We shall say that $V^+_{\overline{D}}$ leaves a sharp trace $V^+_\Gamma = \{v_\Gamma \mid \gamma v_{\overline{D}^+},\ v_{\overline{D}^+} \in V^+_{\overline{D}^+}\}$ on the boundary Γ if each $v_D \in V^+_{\overline{D}}$ whose trace $v_\Gamma = \gamma v_{\overline{D}^+}$ is equal to zero belongs to $U_{\overline{D}}$ as well and if any one of four (equivalent) conditions 1°-4° formulated in Theorem 4.2.3 is satisfied.

Theorem 4.2.4 (sufficient test for a sharp trace). *Let the hypothesis of Theorem 4.2.3 be satisfied and let for each $v_{\overline{D}} \in V^+_{\overline{D}}$, whose trace v_Γ is equal to zero ($v_\Gamma = 0$), the function $w_{\overline{D}} = \Theta_{\overline{D}^+} v_{\overline{D}}$ belongs to $U_{\overline{D}}$. Then V^+_Γ is the sharp trace of $V^+_{\overline{D}}$ on Γ.*

Remark. Let $\mathcal{F}_D$, $\mathcal{F}_D \in F_D$ be any subspace and $\mathcal{U}_{\overline{D}}$, $\mathcal{V}_{\overline{D}}$ be the corresponding subspaces, $\mathcal{U}_{\overline{D}}(\mathcal{F}_D)$, $\mathcal{V}_{\overline{D}}(\mathcal{F}_D)$. Obviously, $\mathcal{U}_{\overline{D}} \subset \mathcal{V}_{\overline{D}}$; a contraction of the operator $G_{\overline{D}D}$: $F_D \to U_{\overline{D}}$ on $\mathcal{F}_D$ will be the operator $G_{\overline{D}D}$: $\mathcal{F}_D \to \mathcal{U}_{\overline{D}}$, the contraction $L_{D\overline{D}}$: $V_{\overline{D}} \to F_D$ on $\mathcal{V}_{\overline{D}}$ will be the operator $L_{D\overline{D}}$: $\mathcal{V}_{\overline{D}} \to \mathcal{F}_D$; the contraction $L_{D\overline{D}}$: $U_{\overline{D}} \to F_D$ on $\mathcal{U}_{\overline{D}}$ will be the operator $L_{D\overline{D}}$: $\mathcal{U}_{\overline{D}} \to \mathcal{F}_D$. From the proposition that any $v_{\overline{D}} \in V_{\overline{D}}$ for which $v_\Gamma = 0$ belongs to $U_{\overline{D}}$ as well, $v_{\overline{D}} \in U_{\overline{D}}$, it follows that each $v_{\overline{D}} \in \mathcal{V}_{\overline{D}}$ for which $v_\Gamma = 0$ belongs to $\mathcal{U}_{\overline{D}}$ as well, $v_{\overline{D}} \in \mathcal{U}_{\overline{D}}$.

Hence we may consider all the concepts introduced in this section by replacing F_D by the subspace $\mathcal{F}_D$, and $U_{\overline{D}}$, $V_{\overline{D}}$ and V^+_Γ respectively by the subspaces $\mathcal{U}_{\overline{D}}$, $\mathcal{V}_{\overline{D}}$, and $\mathcal{V}^+_\Gamma = \{v_\Gamma \mid v_\Gamma = \gamma v_{\overline{D}},\ v_{\overline{D}} \in \mathcal{V}^+_{\overline{D}}\}$.

Theorem 4.2.5. *Let $V^+_{\overline{D}}$ leave a sharp trace V^+_Γ on Γ and let $\mathcal{F}_D \subset F_D$ be an arbitrary subspace. Then $\mathcal{V}^+_\Gamma = \mathcal{V}_\Gamma(\mathcal{F}^+_D)$ is the sharp trace of the space $\mathcal{V}^+_{\overline{D}}$ on Γ.*

1*. Let us consider two examples illustrating the concept of sharp trace. In both examples D is a circle $x_1^2 + x_2^2 < 1$, $F_D = C_{k+\alpha, D}$,

$$U_{\overline{D}} = (u_{\overline{D}} \mid u_{\overline{D}} \in C_{k+\alpha+2,\,\overline{D}},\ u_{\overline{D}}|_{\partial D} = 0),$$

$$L_{D\overline{D}}u_{\overline{D}}|_x = \Delta_{D\overline{D}}u_{\overline{D}}|_x = \frac{\partial^2 u}{\partial x_1^2} + \frac{\partial^2 u}{\partial x_2^2}.$$

Example 4.2.1. Let us take for D^+ the domain bounded by a smooth non-selfintersecting curve $\Gamma = \partial D^+$ and put $V_{\overline{D}} = U_{\overline{D}}$. For V_Γ we take the space of pairs of functions $v_\Gamma = (\varphi_0, \varphi_1)$ defined on the boundary Γ, $\varphi_0 \in C_{k+\alpha+2,\,\Gamma}$, $\varphi_1 \in C_{k+\alpha+1,\,\Gamma}$. The operator γ will be defined by putting $v_\Gamma = \gamma v_{\overline{D}} = \left(v|_\Gamma, \frac{\partial v_{\overline{D}}}{\partial n}\Big|_\Gamma\right)$. In other words, for the image of $v_{\overline{D}}$ upon the transformation γ we shall take "Cauchy data" for the function $v_{\overline{D}}$. For any $k = 0, 1, \ldots$, V_Γ^+ will be the sharp trace of $V_{\overline{D}}^+$ on Γ.

Example 4.2.2. Let us take for D^+ the part of D which lies outside the contour ∂D^+ and for $V_{\overline{D}}$ the entire space $C_{k+\alpha+2,\,\overline{D}}$. Then, in order that $v_{\overline{D}} \in U_{\overline{D}}$ follow from $v_{\overline{D}} \in V_{\overline{D}}$, $v_\Gamma = 0$, we must assume that $\Gamma = \partial D^+ \cup \partial D$ and take for V_Γ the space of triplets of functions $\varphi_\Gamma = (\varphi_0|_{\partial D^+}, \varphi_1|_{\partial D^+}, \varphi_2|_{\partial D})$, $\varphi_2 \in C_{k+\alpha+2,\,\partial D}$. For γ we take the operator $\gamma v_{\overline{D}} = \left(v|_{\partial D^+}, \frac{\partial v}{\partial n}\Big|_{\partial D^+}, v|_{\partial D}\right)$. Then V_Γ^+ is a sharp trace.

5. Generalized surface potential and generalized Calderón-Seeley projector. Let V_Γ^+ be a sharp trace of the space $V_{\overline{D}}^+$ on Γ. We introduce the operators $P_{\overline{D}^+\Gamma}$: $V_\Gamma^+ \to V_{\overline{D}^+}^+$; $P_\Gamma = V_\Gamma^+ \to V_\Gamma^+$ by putting for $v_\Gamma \in V_\Gamma^+$

$$u_{\overline{D}^+} = P_{\overline{D}^+\Gamma}v_\Gamma \overset{\text{def}}{=} P_{\overline{D}^+\overline{D}^+}v_{\overline{D}^+},$$

$$u_\Gamma = P_\Gamma v_\Gamma \overset{\text{def}}{=} \gamma\,(P_{\overline{D}^+\Gamma}v_\Gamma),$$

where $v_{\overline{D}^+}$ is an arbitrary element from $V_{\overline{D}^+}^+$ whose trace is v_Γ.

The correctness of the definitions of $P_{\overline{D}^+\Gamma}$ and P_Γ follows from the definition of the sharp trace.

We shall call the expression $u_{\overline{D}} = P_{\overline{D}^+\Gamma}v_\Gamma$ the generalized potential with the density $v_\Gamma \in V_\Gamma^+$. The operator P_Γ is a modification and generalization of the Calderón-Seeley projector introduced in [4.38, 4.39] for general elliptic equations. For V_Γ^+ we take the space of Cauchy data, and γ is the operator that juxtaposes to a function defined in the domain its Cauchy data. For a second-order equation, we have

$$\gamma u_{\overline{D}^+} = \left(u|_\Gamma, \frac{\partial u}{\partial n}\Big|_\Gamma\right).$$

Theorem 4.2.6. *The operators* $P_{\overline{D}^+\Gamma}$ *and* P_Γ *have the following properties.*

1°. *For any* $v_\Gamma \in V_\Gamma^+$ *the element* $u_{\overline{D}^+} = P_{\overline{D}^+\Gamma} v_\Gamma$ *satisfies the homogeneous equation* $L_{D^+\overline{D}^+} v_{\overline{D}^+} = 0_{D^+}$.

2°. *If* $v_{\overline{D}^+} \in V_{\overline{D}^+}^+$ *satisfies the equation*

$$L_{D^+\overline{D}^+} v_{\overline{D}^+} = 0_{D^+},$$

then

$$P_{\overline{D}^+\Gamma} v_\Gamma = v_{\overline{D}^+}.$$

3°. *The equality* $u_\Gamma = P_\Gamma u_\Gamma$ *is satisfied for those and only those* $u_\Gamma \in V_\Gamma^+$ *which are the trace* $u_\Gamma = \gamma u_{\overline{D}^+}$ *of a certain solution* $u_{\overline{D}^+}$ *of the equation*

$$L_{D^+\overline{D}^+} u_{\overline{D}^+} = 0_{D^+}.$$

4°. *If* u_Γ *satisfies the condition* $u_\Gamma = P_\Gamma u_\Gamma$, *the solution* $u_{\overline{D}^+}$, $u_{\overline{D}^+} \in V_{\overline{D}^+}^+$, $\gamma u_{\overline{D}^+} = u_\Gamma$ *of the equation* $L_{D^+\overline{D}^+} u_{\overline{D}^+} = 0_{D^+}$ *is unique and is given by* $u_{\overline{D}^+} = P_{\overline{D}^+\Gamma} u_\Gamma$.

5°. *The operator* P_Γ *is a projector, i.e.* $P_\Gamma^2 = P_\Gamma$.

2*. For the case of the first example of Subsec. 1*, $v_\Gamma = \left(v\,|_\Gamma, \frac{\partial v}{\partial n}\Big|_\Gamma\right)$ and $P_{\overline{D}^+\Gamma} v_\Gamma$ assumes the form

$$P_{\overline{D}^+\Gamma} v_\Gamma\,|_x = v_{\overline{D}^+}\,|_x - G_{\overline{D}^+ D^+} L_{D^+\overline{D}^+} v_{\overline{D}^+}\,|_x$$
$$= v(x) - \iint\limits_{D^+} G(x, y)\,\Delta v\,dy, \quad x \in \overline{D}^+.$$

On the other hand, classical Green's formula for the Poisson equation is valid

$$\int\limits_\Gamma \left(v \frac{\partial G}{\partial n} - \frac{\partial v}{\partial n} G\right) ds = v(x) - \iint\limits_{D^+} G(x, y)\,\Delta v\,dy, \quad x \in D^+.$$

The right-hand sides of both equations coincide at the internal points $x \in D^+$. Consequently, the generalized potential $P_{\overline{D}^+\Gamma}\varphi_\Gamma$ coincides at the internal points with the contour potential $\int\limits_\Gamma \left(\varphi_0 \frac{\partial G}{\partial n} - \varphi_1 G\right) ds$. At the boundary points the values of $P_{\overline{D}^+\Gamma}\varphi_\Gamma = w_{\overline{D}^+}$ are obtained by passing to the limit inside the domain, taking into account the potential drop in the double layer. Further,

$w_\Gamma = P_\Gamma \varphi_\Gamma$ at the point $x_0 \in \Gamma$ is a vector with the components $w|_\Gamma$, $\left.\frac{\partial w}{\partial n}\right|_\Gamma$

$$w|_\Gamma = \lim_{x \to x_0} \int_\Gamma \left(\varphi_0 \frac{\partial G}{\partial n} - \varphi_1 G\right) ds,$$

$$\left.\frac{\partial w}{\partial n}\right|_\Gamma = \lim_{x \to x_0} \frac{\partial}{\partial n_x} \int_\Gamma \left(\varphi_0 \frac{\partial G}{\partial n} - \varphi_1 G\right) ds.$$

6. Generalized Green's formula. Let $v_{\bar{D}^+} \in V^+_{\bar{D}^+}$. We shall call the identity

$$v_{\bar{D}^+} = P_{\bar{D}^+\Gamma} v_\Gamma + G_{\bar{D}^+ D^+} L_{D^+\bar{D}^+} v_{\bar{D}^+}$$

the generalized Green identity. In view of this identity, the following equation is valid for each solution $v_{\bar{D}^+} \in V^+_{\bar{D}^+}$ of the equation $L_{D^+\bar{D}^+} v_{\bar{D}^+} = f_{D^+}$, $f_{D^+} \in F^+_{D^+}$:

$$v_{\bar{D}^+} = P_{\bar{D}^+\Gamma} v_\Gamma + G_{\bar{D}^+ D^+} f_{D^+}. \tag{4.2.8}$$

This relation will be called generalized Green's formula.

3*. For the case of Example 4.2.1 from Subsec. 1*, Green's formula is transformed into classical one for the Poisson equation.

7. The generalization of Calderón-Seeley boundary conditions.

Theorem 4.2.7. *Suppose that $v_\Gamma \in V^+_\Gamma$ and $f_{D^+} \in F^+_{D^+}$. For the existence of the solution $v_{\bar{D}^+} \in V^+_{\bar{D}^+}$ of the equation $L_{D^+\bar{D}^+} v_{\bar{D}^+} = f_{D^+}$, whose trace coincides with $v_\Gamma = \gamma v_{\bar{D}^+}$, it is necessary and sufficient that the following equality hold:*

$$v_\Gamma = P_\Gamma v_\Gamma + \gamma (G_{\bar{D}^+ D^+} f_{D^+}), \tag{4.2.9}$$

which is a modification and generalization of the Calderón-Seeley conditions.

If this equality is satisfied, the solution $v_{\bar{D}^+}$ is unique and can be reconstructed from its trace v_Γ from Green's formula (4.2.8).

8. Differential equations with (nonboundary) additional conditions. For the equation $L_{D^+\bar{D}^+} v_{\bar{D}^+} = 0$ we specify additional (in particular, boundary) conditions of the type $l_{Q D'} v_{D'} = \varphi_Q$, $\varphi_Q \in \Phi_Q$. Here Φ_Q is a certain linear space of functions or vector functions defined on a certain (abstract) set Q, the set D' is a subset of $\bar{D}^+$, and $l_{Q D'}$ is the operator $l_{Q D'}$: $V_{D'} \to \Phi_Q$.

Let us consider the problem

$$L_{D^+\bar{D}^+} v_{\bar{D}^+} = 0; \quad l_{QD'} v_{D'} = \varphi_Q. \tag{4.2.10}$$

In view of Theorem 4.2.7, it is equivalent to the system of equations

$$v_\Gamma - P_\Gamma v_\Gamma = 0, \quad l_{QD'} P_{D'\Gamma} v_\Gamma = \varphi_Q \tag{4.2.11}$$

for a vector density v_Γ of the potential. If the additional conditions are the boundary conditions specified on Γ, then $Q = \Gamma$, and Eq. (4.2.11) assumes the form

$$v_\Gamma - P_\Gamma v_\Gamma = 0, \quad l_{\Gamma\Gamma} v_\Gamma = \varphi_\Gamma, \quad l_{\Gamma\Gamma} \equiv l_{\Gamma D'} P_{D'\Gamma}, \quad \varphi_\Gamma \in \Phi_\Gamma.$$

9. Metric properties of potentials and projectors.

Theorem 4.2.8. *Let the spaces F_D, $U_{\overline{D}}$, $V_{\overline{D}}$, and V_Γ^+ be normalized and the spaces and the norms are matched so that the operator $L_{D\overline{D}}$: $V_{\overline{D}} \to F_D$ is bounded. Suppose that the operator of multiplication by the eigenfunction Θ_{D^+}: $F_D^+ \to F_D^+$ is bounded on F_D^+ and the operator γ: $V^+ \to V_\Gamma^+$ is bounded. We shall assume that there exists the continuation operator from the boundary $R_{\overline{D}\Gamma}$: $V_\Gamma^+ \to V_{\overline{D}}^+$ which is bounded and such that for any $v_\Gamma \in V_\Gamma^+$ we have $\gamma R_{\overline{D}\Gamma} v_\Gamma = v_\Gamma$.*

Let us also introduce the norms into $V_{D^+}^+$ and $U_{\overline{D}^+}^+$ by putting for each $v_{\overline{D}^+} \in V_{\overline{D}^+}$ and $u_{\overline{D}^+} \in U_{\overline{D}^+}$

$$\| v_{\overline{D}^+} \|_{V_{\overline{D}^+}^+} = \inf \| v_{\overline{D}} \|_{V_{\overline{D}}^+},$$

$$\| u_{\overline{D}^+} \|_{U_{\overline{D}^+}^+} = \inf \| u_{\overline{D}} \|_{U_{\overline{D}}^+},$$

where the lower bounds are taken over all $v_{\overline{D}} \in V_{\overline{D}}^+$ and $u_{\overline{D}} \in U_{\overline{D}}^+$ which are the completions of $v_{\overline{D}^+}$ and $u_{\overline{D}^+}$ respectively. Let $G_{\overline{D}^+ D}$: $F_D^+ \to U_{\overline{D}^+}$ be a bounded operator. Then the operators $P_{\overline{D}^+\Gamma}$: $V_\Gamma^+ \to V_{\overline{D}^+}^+$, P_Γ: $V_\Gamma^+ \to V_\Gamma^+$ are bounded.

4.3. DIFFERENCE GREEN'S FORMULA, POTENTIAL, PROJECTOR, AND INTERNAL BOUNDARY CONDITIONS ON THE BASIS OF THE CONCEPT OF SHARP DIFFERENCE TRACE

Let $\widetilde{M}$ and $\widetilde{N}$ be two meshes (two discrete sets) lying on a certain multidimensional manifold $\widetilde{D}$. The elements of $\widetilde{M}$ will be denoted by m, m', etc., and the elements of $\widetilde{N}$ by n, n', etc. We suppose that $u_{\widetilde{N}}$ and $f_{\widetilde{M}}$ are any vector functions defined on $\widetilde{N}$ and $\widetilde{M}$ and assume the following values for $m \in \widetilde{M}$ and $n \in \widetilde{N}$:

$$(u_{\widetilde{N}})_n = u_n, \quad (f_{\widetilde{M}})_m = f_m,$$

where u_n and f_m are vector columns of a height $k \geqslant 1$. Suppose that we are given the subsets

$$M^+ \subset \widetilde{M}, \quad N_m \subset \widetilde{N}, \quad m \in \widetilde{M},$$

and the difference equation

$$(L_{M^+N^+}u_{N^+})_m = \sum_{n\in Nm} a_{mn}u_n = f_m, \quad m \in M^+, \tag{4.3.1}$$

or, in the brief form, $L_{M^+N^+}u_{N^+} = f_{M^+}$. Here a_{mn} are given $k \times k$ matrices, $N^+ = UN_m$, $m \in M^+$. We shall assume that the difference equation under consideration also has sense in any extended region of the mesh M, $M^+ \subset M \subset \tilde{M}$, which we shall require. In this case, we shall write

$$L_{MN}u_N = f_M \ (N = UN_m, m \in M).$$

1. Auxiliary boundary value problem and Green's difference operator. In view of the analysis associated with the difference equation $L_{M^+N^+}u_{N^+} = f_{M^+}$, we choose and fix the auxiliary set M, $M^+ \subset M \subset \tilde{M}$, and construct $N = UN_m$, $m \in M$. Let F_M, U_N, V_N, $U_N \subset V_N$ be some (auxiliary) linear spaces of the elements $f_M \in F_M$, $u_N \in U_N$, $v_N \in V_N$.

We shall assume that for any $u_N \in U_N$ and $v_N \in V_N$ the functions f_M defined by the equalities $f_m = \sum a_{mn}u_n$ or $f_m = \sum a_{mn}v_n$ belong to F_M so that the mapping L_{MN}: $U_N \to F_M$ and its extension L_{MN}: $V_N \to F_M$ are defined. We shall call the problem

$$L_{MN}u_N = f_M, \ f_M \in F_M, \ u_N \in U_N \tag{4.3.2}$$

the auxiliary problem. For this problem, we shall assume that for any $f_M \in F_M$ there exists a unique solution $u_N \in U_N$. In view of this assumption, there exists a linear operator G_{NM}: $F_M \to U_N$ which will be called Green's operator for problem (4.3.2).

2. Contraction of spaces and equations to subspaces and subdomains. Let $M^+ \in M$, $N^+ = UN_m$, $m \in M^+$, and f_M and u_N be any functions. We shall denote by f_{M^+} and u_{N^+} their contractions to the sets M^+ and N^+. Let $\mathcal{F}_M$ be a certain subspace of the space F_M (in particular, it is possible that $\mathcal{F}_M = F_M$). We shall denote $\mathcal{F}_{M^+} = \{f_{M^+} \mid f_M \in \mathcal{F}_M\}$,

$$\mathcal{F}_M^+ = \{f_M \mid f_M \in \mathcal{F}_M, \ \Theta_{M^+}f_M \in \mathcal{F}_M\}.$$

Let us introduce the notation $\mathcal{U}_N = \mathcal{U}_N(\mathcal{F}_M)$ for the inverse image $\mathcal{F}_M$ of the mapping L_{MN}: $U_N \to F_M$. We shall denote $\mathcal{U}_N^+ = \mathcal{U}_N(\mathcal{F}_M^+)$. For any subspace $\mathcal{U}_N \subset U_N$ we define $\mathcal{U}_{N^+} \overset{\text{def}}{=} \{u_{N^+} \mid u_N \in \mathcal{U}_N\}$. In particular, $\mathcal{U}_{N^+} = \{u_{N^+} \mid u_N \in \mathcal{U}_N^+\}$. For an arbitrary $\mathcal{F}_M \subset F_M$ we define the operator G_{NM^+}: $\mathcal{F}_{M^+}^+ \to \mathcal{U}_N^+$ by putting $u_N = G_{NM^+}f_{M^+} = G_{NM}f_M$, for any $f_{M^+} \in F_{M^+}^+$, where f_M is the completion of f_{M^+} by zero on $M \setminus M^+$. We define the operator

$G_{N^+M^+}$: $\mathcal{F}^+_{M^+} \to \mathcal{U}^+_{N^+}$ by putting for an arbitrary $f_{M^+} \in \mathcal{F}^+_{M^+}$:

$$u_{N^+} = G_{N^+M^+} f_{M^+} = (G_{NM^+} f_{M^+})_{N^+}.$$

Thus, the operator $G_{N^+M^+}$ is defined on $F^+_{M^+}$, and for an arbitrary $\mathcal{F}_M \subset F_M$ is a contraction to the corresponding $\mathcal{F}^+_{M^+}$. Let us also introduce the notation $\mathcal{V}_N = \mathcal{V}_N(\mathcal{F}_M)$ for the inverse image $\mathcal{F}_M$ in V_N for the mapping L_{MN}: $V_N \to F_M$. We shall denote $\mathcal{V}^+_N = \mathcal{V}_N(\mathcal{F}^+_M)$.

3. Definition of operator $P_{N^+N^+}$. Let us introduce $P_{N^+N^+}$: $V^+_{N^+} \to V^+_{N^+}$ by putting for an arbitrary $v_{N^+} \in V^+_{N^+}$:

$$P_{N^+N^+} v_{N^+} \overset{\text{def}}{=} v_{N^+} - G_{N^+M^+} L_{M^+N^+} v_{N^+}.$$

Theorem 4.3.1. *For any $\mathcal{F}_M \subset F_M$, the space $\mathcal{V}^+_{N^+} = \mathcal{V}_{N^+}(\mathcal{F}^+_M)$ it generates is the eigensubspace of the operator $P_{N^+N^+}$: $V^+_{N^+} \to V^+_{N^+}$.*

Theorem 4.3.2. *The following properties hold for the operator $P_{N^+N^+}$, $w_{N^+} = P_{N^+N^+} v_{N^+}$, $v_{N^+} \in V^+_{N^+}$:*

1°. *For any $v_{N^+} \in V^+_{N^+}$ we have $L_{M^+N^+} w_{N^+} = 0_{M^+}$;*

2°. *If $L_{M^+N^+} v_{N^+} = 0_{M^+}$, then $P_{N^+N^+} v_{N^+} = v_{N^+}$;*

3°. $P^2_{N^+N^+} = P_{N^+N^+}$.

It should be noted that according to Theorem 4.3.1, for any $\mathcal{F}_M \subset F_M$, $V^+_{N^+} = V_{N^+}(F^+_M)$ can be replaced everywhere by $\mathcal{V}^+_{N^+} = \mathcal{V}_{N^+}(\mathcal{F}^+_M)$ under the conditions of Theorem 4.3.2.

4. The boundary Γ, sharp trace. Let $\Gamma \subset N^+$ be an arbitrary set. The linear space V_Γ of contractions v_Γ of the elements $v_{N^+} \in V_{N^+}$ on Γ will be called the trace of V_N on Γ.

Theorem 4.3.3. *Let U_N, V_N, and the decomposition $M = M^+ \cup M^-$ be matched so that each v_N, $v_N \in V^+_N$, whose trace v_Γ is equal to zero, also belongs to U_N. Then the following four properties either hold or do not hold simultaneously:*

1° *for any two $v_N \in V^+_N$ and $v'_N \in V^+_N$ whose traces coincide, $v_\Gamma = v'_\Gamma$, the equality*

$$P_{N^+N^+} v_{N^+} = P_{N^+N^+} v'_{N^+}$$

is valid;

2° *for any v_N, $v_N \in V^+$ whose trace is equal to zero, $v_\Gamma = 0$, the condition*

$$P_{N^+N^+} v_{N^+} = 0_{N^+}$$

is satisfied;

3° *for any $v_{N^+} \in V^+_{N^+}$ whose trace is equal to zero, $v_\Gamma = 0$, the equality*

$$G_{N^+M^+} L_{M^+N^+} v_{N^+} = v_{N^+}$$

is satisfied;

4° *for any* v_N, $v_N \in V^+$ *whose trace is equal to zero, there exists* $w_N \in U_N$ *such that* $w_{N^+} = v_{N^+}$ *and*

$$L_{M^-N^-}w_{N^-} = 0_{M^-},$$

where $M^- = M \setminus M^+$, $N^- = UN_m$, $m \in M^-$.

Definition. We shall say that $V^+_{N^+}$ leaves sharp difference trace V^+_Γ, $V^+_\Gamma = \{v_\Gamma \mid v_{N^+} \in V^+_N\}$, if the condition of Theorem 4.3.3 is fulfilled and one of the properties 1°-4° whose equivalence is stated in Theorem 4.3.3 holds.

Theorem 4.3.4 (sufficient criterion for a sharp difference trace). *Suppose that* $\Gamma = N^+ \cap N^-$, *the condition of Theorem* 4.3.3 *is satisfied, and for any* $v_N \in V^+_N$ *whose trace is equal to zero the function* w_N, $w_N = \Theta_{N^+}v_N$, *constructed for it belongs to* U_N. *Then* $V^+_\Gamma = \{v_\Gamma \mid v_{N^+} \in V^+_{N^+}\}$ *is a sharp difference trace of* V^+_N *on* Γ.

5. Difference potential and difference projector. Let V_Γ be a sharp difference trace on Γ. Let us introduce the operators

$$P_{N^+\Gamma}\colon V_\Gamma \to V^+_{N^+}; \quad P_\Gamma\colon V_\Gamma \to V_\Gamma$$

by putting for $v_\Gamma \in V^+_\Gamma$:

$$u_{N^+} = P_{N^+\Gamma}v_\Gamma \overset{\text{def}}{=} P_{N^+N^+}v_{N^+},$$

$$u_\Gamma = P_\Gamma v_\Gamma \overset{\text{def}}{=} (P_{N^+\Gamma}v^-_\Gamma)_\Gamma,$$

where v_{N^+} is an arbitrary element from $V^+_{N^+}$ whose trace is v_Γ.

The correctness of the definitions (in particular, their independence of the choice of v_{N^+}) follows from the properties of the sharp difference trace.

Theorem 4.3.5. *The operators* $P_{N^+\Gamma}$ *and* P_Γ *have the following properties:*

1° *for any* $v_\Gamma \in V_\Gamma$ *the function* $w_{N^+} = P_{N^+\Gamma}v_\Gamma$ *satisfies the equation* $L_{M^+N^+}w_{N^+} = 0_{M^+}$;

2° *if* v_{N^+} *satisfies the homogeneous equation* $L_{M^+N^+}v_{N^+} = 0_{M^+}$, *then* $P_{N^+\Gamma}v_\Gamma = v_{N^+}$;

3° *the equality* $v_\Gamma = P_\Gamma v_\Gamma$ *holds if and only if there exists* $v_{N^+} \in V^+_{N^+}$ *such that it satisfies the equation* $L_{M^+N^+}v_{N^+} = 0_{M^+}$ *and its trace coincides with* v_Γ;

4° *if* v_Γ *satisfies the equation* $v_\Gamma = P_\Gamma v_\Gamma$, *then its additional definition as the solution* v_{N^+} *of the equation* $L_{M^+N^+}v_{N^+} = 0_{M^+}$ *is unique and is given by* $v_{N^+} = P_{N^+\Gamma}v_\Gamma$;

5° *the operator* P_Γ *is a projector, i.e.* $P^2_\Gamma = P_\Gamma$.

Definition. The expression $P_{N^+\Gamma}v_\Gamma$, $v_\Gamma \in V_\Gamma$, will be called the difference potential with the density v_Γ. The operator P_Γ will be called the difference projector of the boundary projection operator.

It should be noted that the calculation of $P_{N^+\Gamma}v_\Gamma$ is reduced to solving the auxiliary problem (4.3.2) with the known right-hand side f_M: it is sufficient to additionally define v_Γ for $v_{N^+} \in V^+_{N^+}$ (normally, equal to zero) and note that the subtrahend in the formula $P_{N^+\Gamma}v_\Gamma = v_{N^+} - G_{N^+M^+}L_{M^+N^+}v_{N^+}$ is the solution of problem (4.3.2) with $f_M = \{f_{M^+}, f_{M^-}\}$ on the right-hand side, where $f_{M^+} = L_{M^+N^+}v_{N^+}$, $f_{M^-} = 0_{M^-}$.

6. **Difference Green's formula.** Let $v_{N^+} \in V_{N^+}$. The identity

$$v_{N^+} = P_{N^+\Gamma}v_\Gamma + G_{N^+M^+}L_{M^+N^+}v_{N^+}$$

will be called the Green identity. In view of this identity, for each solution v_{N^+} of the equation $L_{M^+N^+}v_{N^+} = f_{M^+}$ the following equality holds:

$$v_{N^+} = P_{N^+\Gamma}v_\Gamma + G_{N^+M^+}f_{M^+}. \tag{4.3.3}$$

This expression is called Green's difference formula.

7. **Internal boundary conditions.**

Theorem 4.3.6. *Let $v_\Gamma \in V_\Gamma$ and $f_{M^+} \in F^+_{M^+}$. In order that the solution $v_{N^+} \in V^+_{N^+}$ of the problem $L_{M^+N^+}v_{N^+} = f_{M^+}$ whose trace is v_Γ exist, it is necessary and sufficient that the following equality hold:*

$$v_\Gamma = P_\Gamma v_\Gamma + G_{\Gamma M^+}f_{M^+}. \tag{4.3.4}$$

If this is satisfied, the solution v_{N^+} is unique and can be reconstructed from v_Γ with the help of difference Green's formula.

Following [4.1] we shall call condition (4.3.4) the internal boundary condition.

8. **Metric properties of difference potentials.** We shall assume that the sets M, N, N_m, M^+, N^+, and Γ the spaces F_M, U_N, V_N, F^+_M, U^+_N, V^+_N, and V_Γ and also the elements of these spaces depend on the parameter h, viz. the mesh spacing, $0 < h < h_0$. We shall assume the spaces F_M, V_N, V_Γ to be normalized. Then the norms in all their subspaces will also be defined. Let us define the norm

$$\| v_{N^+} \|_{V_{N^+}} = \inf \| v_N \|_{V_N},$$

where v_{N^+} coincides with v_N on the set N^+. The operators

$$G_{N^+M}\colon F_M \to U_{N^+},$$

$$\gamma_{\Gamma N^+}\colon V_{N^+} \to V_\Gamma, \quad \| v_\Gamma \|_{V_\Gamma} \leqslant \| \gamma_{\Gamma N^+} \| \cdot \| v_N \|$$

will be assumed to be bounded uniformly in h.

Theorem 4.3.7. *Let V_Γ and V_Γ coincide. Suppose that $c > 0$ and $s \geqslant 0$ are such two numbers that for any $v_\Gamma \in V_\Gamma$ and any h there exists a completion $v_N \in V_N^+$ of the element v_Γ for which the following two inequalities simultaneously hold:*

$$\| v_{N^+} \|_{V_{N^+}} \leqslant ch^{-s} \| v_\Gamma \|_{V_\Gamma};$$

$$\| \Theta_{M^+} L_{MN} v_N \|_{F_M} \leqslant ch^{-s} \| v_\Gamma \|_{V_\Gamma}.$$

Then

$$\| P_{N^+\Gamma} v_\Gamma \|_{V_{N^+}} \leqslant ch^{-s} (1 + \| G_{N^+M} \|) \cdot \| v_\Gamma \|_{V_\Gamma},$$

$$\| P_\Gamma v_\Gamma \|_{V_\Gamma} \leqslant ch^{-s} (1 + \| G_{N^+M} \|) \cdot \| \gamma_{\Gamma N^+} \| \cdot \| v_\Gamma \|.$$

Difference Green's formulas, potentials, projectors, and internal boundary conditions were first introduced in [4.1-4.6] and were considerably developed in [4.11, 4.13, 4.18, 4.19, 4.21, 4.25]. In subsections 1-7, we followed [4.25]. The analysis of the metric properties of difference potentials was initiated by Reznik [4.24, 4.31] who obtained the proof for the boundedness of the operators $P_{N^+\Gamma}$, P_Γ for difference elliptic operators on the scale of Hölder mesh spaces and the mesh analogues of Sobolev spaces introduced by him. He also developed the theory of these spaces, including the theorems on traces.

4.4. SCHEME OF APPROXIMATION OF GENERALIZED CONTINUAL POTENTIALS BY DIFFERENCE POTENTIALS

1. The similarity of forms of continual (see Sec. 4.2) and difference (see Sec. 4.3) potentials suggests that continual potentials can be approximated by difference potentials whose calculation is reduced to solving the auxiliary problem of type (4.3.2). The calculation of potentials and their derivatives up to the boundary where the vector density is concentrated is itself an interesting and complicated problem. Besides, we shall use the approximation of continual potentials by difference potentials for the numerical solution of boundary value problems. Such an approach was jointly worked out by Reznik and the author [4.14-4.17] for refining, substantiating, and constructing effective algorithms for realization of the idea expressed in [4.10]. The first and in a certain sense the best results of approximation of the potentials of general elliptical operators in the norms of Hölder spaces and Sobolev spaces in the domains $D^+ \Subset D$ were obtained by Reznik in [4.24, 4.31] from an analysis of Green's difference operators.

2. **Matching of spaces of continuous and mesh functions.** Let $\mathscr{V}_{\overline{D}}$ be a normalized space embedded into the normalized space $V_{\overline{D}}$: if $v_{\overline{D}} \in \mathscr{V}_{\overline{D}}$, then $v_{\overline{D}} \in V_{\overline{D}}$ so that $\| v_{\overline{D}} \|_{\mathscr{V}_{\overline{D}}} \geqslant \| v_{\overline{D}} \|_{V_{\overline{D}}}$. The subspace $\mathscr{V}^+_{\overline{D}}$, $\mathscr{V}^+_{\overline{D}} \subset \mathscr{V}_{\overline{D}}$ is defined as

$$\mathscr{V}^+_{\overline{D}} = \{v_{\overline{D}} \mid v_{\overline{D}} \in \mathscr{V}_{\overline{D}},\ G_{\overline{D}D}\Theta_{D^+}L_{D\overline{D}}v_{\overline{D}} \in \mathscr{V}_{\overline{D}}\}.$$

We shall assume that

$$\| G_{\overline{D}D}\Theta_{D^+}L_{D\overline{D}}v_{\overline{D}} \|_{\mathscr{V}_{\overline{D}}} \leqslant c \| v_{\overline{D}} \|_{\mathscr{V}_{\overline{D}}},\quad v_{\overline{D}} \in \mathscr{V}^+_{\overline{D}}.$$

Further,

$$\mathscr{U}_{\overline{D}} = \mathscr{V}_{\overline{D}} \cap U_{\overline{D}},\quad \mathscr{U}^+_{\overline{D}} = \mathscr{V}^+_{\overline{D}} \cap U_{\overline{D}}.$$

We denote by $r_{N\overline{D}}$: $V_{\overline{D}} \to V_N$ and r_{MD}: $F_D \to F_M$ some operators of descent on the mesh, which put each function $v_{\overline{D}} \in V_{\overline{D}}$ or $f_D \in F_D$ in correspondence with the functions v_N or f_M on the mesh N or M, and so on. Moreover, we shall require that $r_{N\overline{D}}$ is such that in this case $v_N \in V_N$ and if $v_{\overline{D}} \in U_{\overline{D}}$, then $v_N \in U_N$.

We denote by $r_{\Gamma_h\overline{D}}$: $V_{\overline{D}} \to V_{\Gamma_h}$ the descent of the function $v_{\overline{D}}$ on the mesh boundary Γ_h.

3. **Definitions of approximation and stability for auxiliary difference problem.**

Definition. We shall say that the operator L_{MN} approximates $L_{D\overline{D}}$ on the subspace $\mathscr{V}_{\overline{D}} \subset V_{\overline{D}}$ with the order of accuracy h^l if for any $v_{\overline{D}} \in \mathscr{V}_{\overline{D}}$ we have

$$L_{MN}(r_{N\overline{D}}v_{\overline{D}}) = r_{MD}L_{D\overline{D}}v_{\overline{D}} + h^l\delta_M,$$

$$\delta_M \in F_M,\quad \| \delta_M \|_{F_M} \leqslant c \| v_{\overline{D}} \|_{\mathscr{V}_{\overline{D}}},\quad c = \text{const}.$$

Definition. We shall say that the problem $L_{MN}u_N = f_M$, $u_N \in U_N$ is stable in the domain Q, $Q \subset D$, if for any $f_M \in F_M$ the contraction u_{Q_h} of the solution u_N to the set $Q_h = N \cap Q$ satisfies the inequality

$$\| u_{Q_h} \|_{U_{Q_h}} \leqslant c \| f_M \|_{F_M},\quad c = \text{const}.$$

The stability with respect to N^+ is determined in a similar way. This definition of stability is less restricted than the conventional definition [4.35]

$$\| u_N \|_{V_N} \leqslant c \| f_M \|_{F_M}$$

and makes it possible to take into account the properties of interior regularity of solutions expressed by the Thomée estimates [4.40] for

elliptic difference equations which are similar to the Schauder estimates for the elliptic differential equations.

4. Approximation of potentials. Let $\mathscr{V}_\Gamma \subset V_\Gamma$ be a subspace of the space of sharp traces, which is the trace of the subspace $\mathscr{V}^+_{\bar{D}} \subset V^+_{\bar{D}}$ on Γ. Suppose that the operator L_{MN} approximates $L_{D\bar{D}}$ on $\mathscr{V}^+_{\bar{D}}$ with a certain order of accuracy h^l. Let us consider the function

$$w_{\bar{D}} \equiv P_{\bar{D}\Gamma} v_\Gamma = v_{\bar{D}} - G_{\bar{D}D} \Theta_{\bar{D}^+} L_{D\bar{D}} v_{\bar{D}},$$

where $v_{\bar{D}} \in \mathscr{V}^+_{\bar{D}}$, $\gamma v_{\bar{D}} = v_\Gamma$, which coincides on $\bar{D}^+$ with the continual potential $P_{\bar{D}^+\Gamma} v_\Gamma$ for the vector density v_Γ. Let us introduce the function $\tilde{u}_N \in U_N$ as a solution of the difference equation

$$L_{MN} \tilde{u}_N = \tilde{f}_M,$$

$$\tilde{f}_M = r_{MD} (L_{D\bar{D}} v_{\bar{D}}) - L_{MN} (r_{N\bar{D}} v_{\bar{D}}) \equiv f_M - L_{MN} v_N, \quad v_N = r_{N\bar{D}} v_{\bar{D}}.$$

We construct the element $\tilde{v}_N = v_N + \tilde{u}_N$. As before, we put $M^+ = M \cap D^+$. Then M^-, N^+, and N^- are defined. Let us specify Γ_h and assume that $V^+_{\Gamma_h}$ is a sharp difference trace of V^+_N on Γ_h. We consider the mesh function $\tilde{w}_N \in V_N$,

$$\tilde{w}_N \overset{\text{def}}{=} P_{N\Gamma_h} \tilde{v}_{\Gamma_h} = \tilde{v}_N - G_{NM^+} L_{M^+N^+} \tilde{v}_{N^+},$$

which coincides with the difference potential for the density v_{Γ_h} on N^+.

Lemma. *Let $Q^+ \subset D$, $Q_h = Q \cap N$, and the difference problem $L_{MN} u_N = f_M$, $u_N \in U_N$ is stable in the domain Q_h. Then the following estimate is valid:*

$$\| r_{Q_h \bar{D}} w_{\bar{D}} - \tilde{w}_{Q_h} \|_{V_{Q_h}} \leqslant c h^l \| v_{\bar{D}} \|_{\mathscr{V}_{\bar{D}}}.$$

Theorem. *Let the element v_Γ be an element in the space of sharp traces with the following property. There exists a $v_{\bar{D}} \in \mathscr{V}^+_{\bar{D}}$, $\gamma v_{\bar{D}} = v_\Gamma$ such that the operator L_{MN} approximates $L_{D\bar{D}}$ on $v_{\bar{D}}$ with a certain given order h^l. Suppose that the difference equation is stable on N^+.*

Let us consider the function $w_{\bar{D}} \in V_{\bar{D}}$,

$$w_{\bar{D}} \equiv P_{\bar{D}\Gamma} v_\Gamma = v_{\bar{D}} - G_{\bar{D}\bar{D}} (\Theta_{D^+} L_{D\bar{D}} v_{\bar{D}}),$$

which coincides on $\bar{D}^+$ with the continual potential for the vector density v_Γ.

Suppose that $v_{\Gamma_h} = r_{\Gamma_h \overline{D}} v_{\overline{D}}$ *is the trace of* $v_{\overline{D}}$ *on* Γ_h *and* $v'_{\Gamma_h} \in V_{\Gamma_h}$ *is an arbitrary function from* V_{Γ_h} *satisfying the condition*

$$\| v_{\Gamma_h} - v'_{\Gamma_h} \|_{V_{\Gamma_h}} \leqslant ch^l \| v_{\Gamma_h} \|_{\mathcal{V}_{\Gamma_h}}, \quad c = \text{const}.$$

Let the conditions of theorem 4.3.7 *be satisfied. Then the difference potential with the density* v'_{Γ_h}, $w'_{N^+} = P_{N^+\Gamma_h} v'_{\Gamma_h}$ *approximates the continual potential* $w_{\overline{D}^+} = P_{\overline{D}^+\Gamma} v_\Gamma$ *in the sense that the following inequality holds*:

$$\| w_{N^+} - w'_{N^+} \| \leqslant ch^{l-s} \| v_\Gamma \|_{\mathcal{V}_\Gamma}, \quad c = \text{const}.$$

4.5. PRELIMINARY NONCONSTRUCTIVE DISCRETIZATION OF BOUNDARY EQUATIONS

The method of reducing the boundary value problem $L_{D^+\overline{D}^+} v_{\overline{D}^+} = 0_{D^+}$, $lu_\Gamma = \varphi$ in the domain D^+ to the generalized pseudodifferential equations

$$u_\Gamma - P_\Gamma u_\Gamma = 0_\Gamma, \quad lu_\Gamma = \varphi \tag{4.5.1}$$

was suggested in Sec. 4.2. Here to solve it we shall consider a nonconstructive method of discretization of system (4.5.1) which leads to a substantiated algebraic system and also a nonconstructive but probably rapidly diverging iterative process. This presentation will explain some of the basic circumstances and will help us go over to the real algorithm of the method of difference projectors.

1. Basic lemma. Suppose that we are given abstract linear normalized spaces U and Φ and two linear operators P: $U \to U$ and l: $U \to \Phi$, where P is a projector, $P^2 = P$, and l: $U \to \Phi$ is bounded.

Let us decompose U into a direct sum of the spaces ker P and Im P:

$$\Psi = \ker P = \{u \mid u \in U,\ Pu = 0\},$$
$$V = \operatorname{Im} P = \{u \mid u \in U,\ u = Pu\}.$$

Any vector $u \in U$ can be obviously represented, and in a unique way, in the form $u = \psi + v$, $\psi \in \Psi$, $v \in V$. Namely, $u = (u - Pu) + Pu$, $\psi = u - Pu$, $v = Pu$. Let us introduce the space $\Psi \oplus \Phi$ with the elements (ψ, φ), $\psi \in \Psi$, $\varphi \in \Phi$ and the norm in it by putting

$$\| \{\psi, \varphi\} \|^2_{\Psi \oplus \Phi} = \| \psi \|^2_\Psi + \| \varphi \|^2_\Phi.$$

We introduce the operator (Q, l): $U \to \Psi \oplus \Phi$ which puts each $u \in U$ in correspondence with the element $(\psi, \varphi) \in \Psi \oplus \Phi$ according to the formula

$$\psi = Qu \equiv u - Pu; \quad \varphi = lu.$$

Lemma 4.5.1 (basic lemma). *Suppose that the system of equations*

$$u - Pu = 0, \quad lu = \varphi \tag{4.5.2}$$

has a unique solution $u \in U$ *for any* $\varphi \in \Phi$ *such that*

$$\| u \|_U \leqslant c \| \varphi \|_\Phi, \quad c = \text{const}. \tag{4.5.3}$$

Then,

1° *The operator* (Q, l) *has an inverse operator* $(Q, l)^{-1}: \Psi \oplus \Phi \to U$, *such that*

$$\| u \|_U = \| (Q, l)^{-1} \{\psi, \varphi\} \|_U \leqslant (1 + c \| l \|) \| \psi \|_{U^+} + c \| \varphi \|_\Phi \leqslant \max \{c, c \| l \| + 1\} \cdot \| (\psi, \varphi) \|_{\Psi \dotplus \Phi}. \tag{4.5.4}$$

2° *Any element* $u \in U$ *satisfies an a priori estimate*

$$\| u \|_U \leqslant c (\| l \| + 1) \| u - Pu \|_U + c \| lu \|_\Phi.$$

For every $v \in U$ *we define the number* $\delta = \delta(v)$ *by putting*

$$\delta^2 = \| v - Pv \|^2_\Psi + \| lv - \varphi \|^2_\Phi. \tag{4.5.5}$$

Lemma 4.5.2. *Suppose that the conditions of Lemma* 4.5.1 *are satisfied and* u *is the solution of problem* (4.5.1), *while* v *is an arbitrary element,* $v \in V$. *Then*

$$\| u - v \|^2_U \leqslant 2M^2\delta^2, \quad M = \max \{c, c \| l \| + 1\}. \tag{4.5.6}$$

2. Discretization. Suppose that the conditions of Lemma 4.5.1 are satisfied. Let $e_1, e_2, \ldots, e_k \in U$ be a certain system of linearly independent elements. We denote by $u_c = \sum c_j e_j$ the linear combination with the coefficients $c = (c_1, c_2, \ldots, c_k)$. We also denote $\varepsilon_K = \min \| u - u_c \|_U$. Let u_α, $c = \alpha$ be the linear combination $u_\alpha = \sum^c \alpha_j e_j$, for which $\varepsilon_K = \| u - u_\alpha \|$ and u_β be the linear combination which minimizes expression (4.5.5):

$$\delta^2_K (u_\beta) \leqslant \delta^2_K (u_c) \tag{4.5.7}$$

for any c.

Theorem 4.5.1 (on the discretization of Eqs. (4.5.1)). *Suppose that the conditions of Lemma* 4.5.1 *are satisfied. Then*

$$\| u - u_\beta \|_U \leqslant \sqrt{2}\, MN\varepsilon_K, \quad M = \max \{c, 1 + c \| l \|\},$$
$$N^2 = (1 + \| P \|)^2 + \| l \|^2. \tag{4.5.8}$$

This theorem corroborates the theorem on discretization [4.14] obtained by the author and A. Ya. Belyankov. The basic lemma somewhat corroborates one of the results of [4.1].

Henceforth, we shall assume that the norms in U and Φ are the Hilbert norms, $\| u \|^2_U = (u, u)_U$, $\| \varphi \|^2 = (\varphi, \varphi)_\Phi$. The problem

of determining the minimum of the quadratic functional (4.5.5) leads to a linear system of equations in $c_1, c_2, \ldots, c_K$.

Suppose that the nondegeneracy of the basis $e_1, e_2, \ldots, e_K$ of the subspace U_K spanned on them is characterized by a pair of numbers A'_K and A''_K such that for any $u_c = \sum c_j e_j$ the following condition is satisfied:

$$A'_K \sum c_j^2 \leqslant \| u_c \|_U^2 \leqslant A''_K \sum c_j^2. \tag{4.5.9}$$

We denote by $\| P_K \|$ the norm of the contraction P_K: $U_K \to U$ of the operator P onto the subspace U_K.

Theorem 4.5.2. *Let the conditions of Lemma* 4.5.1 *be satisfied. The conditionality number* μ *of the matrix of the linear system for determining the coefficients* $c_1, c_2, \ldots, c_K$ *that define the minimum of the quadratic form* (4.5.5) *satisfies the estimate*

$$\mu_K \leqslant A_K (1 + \| P_K \| + \| l \|)^2 \{\max [c, 1 + c \| l \|]\}^2, \quad A_K = A''_K : A'_K.$$

For a system of type (4.5.1) emerging as a result of reduction of well-posed boundary value problems or other problems with additional conditions to pseudodifferential equations on the boundary of the domain ∂D^+, it is usually possible to choose the Hilbert norms in U_Γ and Φ so that the operators P_Γ: $V_\Gamma \to V_\Gamma$ and l: $V_\Gamma \to \Phi$ are bounded and there exists the constant c appearing in inequality (4.5.3). Moreover, it is possible to choose the basis $e_1, e_2, \ldots, e_K$ for each K so that the numbers $A_K = A''_K : A'_K$ are bounded altogether, $A_K < A$ for $K \to \infty$. Then the conditionality numbers μ_K, $\mu_K < \mu$, are also bounded altogether.

If we solve the system obtained for $c_1, c_2, \ldots, c_K$ by gradient methods and decrease the error by a given number of times ε^{-1}, the required number of iterations is $\nu = O(\ln | \varepsilon^{-1} |)$, where the constant $O(| \ln \varepsilon^{-1} |)$ depends only on μ and not on K.

When solving the linear system by iterations using gradient methods, one should be able to calculate the result of application of the matrix of the system to a vector. In the case under consideration, in particular, we should have to calculate the result of application of the operator P_Γ to $\sum c_j e_j$, which is difficult to do directly. However, we managed to do this roughly by approximating the continual potentials to difference potentials.

We shall not consider here the construction of the scheme for a real algorithm in the general case and only point out the examples contained in Secs. 4.1 and 4.6.

4.6. EXAMPLES OF SPECIFIC ALGORITHMS

1. On nonclassical auxiliary boundary value problems. An important point in all concrete MDP algorithms is the choice of auxiliary domains D, N and spaces $U_{\overline{D}}$, U_N determining the auxil-

iary differential and difference boundary value problems (4.2.1) and (4.3.2). In the examples considered below, some nonclassical auxiliary boundary value problems are found to be convenient. Although these problems have no meaning themselves, they become important just as an element of MDP.

2. Exterior problems for the equation $\Delta u + \mu^2 u = 0$ on a plane. We shall consider the problems which are external relative to the bounded domain Q with a smooth boundary ∂Q and satisfy the radiation condition at infinity. Let us choose a point O inside Q and introduce the polar system of coordinates ρ, α with the pole at the point O. Let $\rho = r$ and $\rho = R$ be the equations of two circumferences the first of which lies, together with the circle $\rho < r$, inside Q, while the second contains Q inside it. We replace the part of the plane external relative to Q by the domain D^+ bounded by the circumference $\rho = R$ and the curve ∂Q. We replace the radiation conditions at infinity by an equivalent partial boundary conditions on the circumference $\rho = R$, which are quite similar to those specified in [4.33] for the three-dimensional case.

Namely, by denoting

$$v_k(\rho) = \frac{1}{2\pi} \int_0^{2\pi} u(\rho, \alpha)\, e^{-ik\alpha}\, d\alpha, \quad k = 0, \pm 1, \ldots,$$

where $u(\rho, \alpha)$ is the required solution for $\rho \geqslant R$, we obtain from the radiation condition $v_k(\rho) = c_k H_{|k|}^{(2)}(\mu, \rho)$, where $c_k = \text{const}$, and the radiation conditions for $\rho = R$ can be written as follows:

$$\begin{vmatrix} v_k(R) & H_{|k|}^{(2)}(\mu\rho)\,|_{\rho=R} \\ v_k'(R) & \frac{d}{d\rho} H_{|k|}^{(2)}(\mu\rho)\,|_{\rho=R} \end{vmatrix} = 0, \quad k = 0, \pm 1, \pm 2, \ldots . \tag{4.6.1}$$

The additional conditions $lu_\Gamma = \varphi$ determining the exterior boundary value problem are specified on ∂Q. For the sake of definiteness, suppose that we are given $u\,|_{\partial Q} = \varphi(s)$. We shall consider the auxiliary problem on the ring D, $r < \rho < R$. For F_D we take the class of functions $f_D \in C_{k+a,\,D}$ which can be equal to zero outside the ring D without leaving the class $C_{k+a,\,E^2}$. We define the class $U_{\overline{D}}$ as a totality of all functions $u_{\overline{D}}$, which are continuous together with their first derivatives in the domain $\overline{D}$, are transformed to the elements of F_D upon the application of the Laplace operator and satisfy conditions (4.6.1) for $\rho = R$, and for $\rho = r$, the conditions of the type

$$A_k v_k(r) + B_k v_k'(r) = 0, \quad |k| = 0, 1, \ldots, \tag{4.6.2}$$

where A_k, B_k are certain numbers such that $A_k^2 + B_k^2 = 1$. These numbers are somewhat arbitrary, it is only important that the ho-

mogeneous Bessel equation determining the solutions $H_k^{(1)}$ and $H_k^{(2)}$ for the given conditions (4.6.1) and (4.6.2) has no nontrivial solution.

Moreover, it is important that the closest-to-zero eigenvalue of the Bessel operator on the functions satisfying conditions (4.6.1) and (4.6.2) be "as large as possible". Practically it is sufficient to impose condition (4.6.2) with the numbers A_k and B_k satisfying the equality

$$\begin{vmatrix} -B_k & H_k^{(2)}(\mu r) \\ A_k & \frac{d}{d\rho} H_k^{(2)}(\mu r) \end{vmatrix} = 0, \quad |k| = 0, 1, \ldots . \tag{4.6.3}$$

In order to apply the method of difference potential, let us use the simplest five-point difference equations on the mesh in polar coordinates with a constant angular spacing h_α ($2\pi/h_\alpha$ is an odd integer) and a constant radial spacing h_ρ. For simplicity we shall assume that the circumferences $\rho = r$ and $\rho = R$ are the mesh lines. We take for M the set of mesh points that lie inside D, and for M^+, the set of mesh points that are inside D^+. Then M^-, N^+, N^-, and N are defined. We put $\Gamma_h = N^+ \cap N^-$.

The auxiliary problem is formulated as follows. We take for F_M the space of all mesh functions and for U_N the space of all mesh functions satisfying on the circumferences $\rho = r$ and $\rho = R$ the conditions which will be now specified.

Let us consider the solutions of a difference equation which have the form

$$u_{s,l}^{(k)} = v_s^{(k)} e^{iklh_\alpha},$$

where (sh_ρ, lh_α) are the mesh points. Obviously, $v_s^{(k)}$ is a solution of the difference analogue of the Bessel equation defining the functions $H_k^{(1)}$ and $H_k^{(2)}$. For $\rho = R$, we impose the condition which is similar to (4.6.1):

$$\begin{vmatrix} \frac{1}{2}(v_{s_1-1}^{(k)} + v_{s_1}^{(k)}) & H_k^{(2)}\left(\mu\left(R - \frac{h_\rho}{2}\right)\right) \\ h_\rho^{-1}(v_{s_1}^{(k)} - v_{s_1-1}^{(k)}) & \frac{d}{d\rho} H_k^{(2)}\left(\mu\left(R - \frac{h_\rho}{2}\right)\right) \end{vmatrix} = 0, \tag{4.6.4}$$

$$s_1 = R : h_\rho; \quad |k| = 0, 1, \ldots, \frac{\pi}{h_\alpha} - \frac{1}{2}.$$

For $\rho = r$ we impose the condition which ensures the uniqueness of the solution of an ordinary difference equation which is similar to the Bessel equation. This condition has the form

$$\frac{1}{2} A_k^{(h)}(v_{s_2}^{(k)} + v_{s_2+1}^{(k)}) + h_\rho^{-1} B_k^{(h)}(v_{s_2+1}^{(k)} - v_{s_2}^{(k)}) = 0,$$

$$s_2 = r : h_\rho; \quad |k| = 0, 1. \ldots, \frac{\pi}{h_\alpha} - \frac{1}{2}.$$

Here $v_s^{(k)}$ is the solution of the resulting homogeneous difference equation, which satisfies condition (4.6.4). The numbers $A_k^{(h)}$ and $B_k^{(h)}$ can be determined from a condition similar to (4.6.3):

$$\begin{vmatrix} \frac{1}{2}(v_{s_2}^{(k)}+v_{s_2+1}^{(k)}) & -B_k^{(h)} \\ h_\rho^{-1}(v_{s_2+1}^{(k)}-v_{s_2}^{(k)}) & A_k^{(h)} \end{vmatrix} = 0,$$

$$k = 0,\ 1,\ \ldots,\ \frac{\pi}{h_\rho} - \frac{1}{2}$$

Other constructions are exactly similar to those in Sec. 4.1. In [4.32] we have constructed and realized on a computer an MDP algorithm for the exterior three-dimensional problems with the radiation conditions at infinity for the equation $\Delta u + \mu^2 u = 0$.

4. Interior problems for the Stokes system.

$$\begin{aligned} &\Delta v - \frac{\partial p}{\partial x_1} = f_1(x_1,\ x_2), \\ &\Delta w - \frac{\partial p}{\partial x_2} = f_2(x_1,\ x_2), \\ &\frac{\partial v}{\partial x_1} + \frac{\partial w}{\partial x_2} = f_3(x_1,\ x_2) \end{aligned} \tag{4.6.5}$$

in the bounded domain D^+, $\bar{D}^+ \subset D = \{0 < x_1,\ x_2 < 1\}$. We take for the auxiliary domain the square D and fix an integer k, $k \geqslant 0$ and α, $0 < \alpha < 1$. Let us consider the spaces F_{E^2} and U_{E^2} of the vector functions

$$f_{E^2} = \{f_{1E^2}, f_{2E^2}, f_{3E^2}\} \text{ and } u_{E^2} = \{v_{E^2},\ w_{E^2},\ p_{E^2}\},$$

defined on the entire plane E^2, periodic with the period 2 in x_1 and in x_2 and such that $v_{E^2}(x_1, x_2)$ and $f_{1E^2}(x_1,\ x_2)$ are even in x_1 and odd in x_2, while w_{E^2} and f_{2E^2} are odd in x_1 and even in x_2, and p_{E^2} and f_{3E^2} are odd both in x_1 and in x_2. Besides, we shall assume that

$$\begin{aligned} &f_{1E^2},\ f_{2E^2} \in C_{k+\alpha,\,E^2}; \\ &p_{E^2},\ f_{3E^2} \in C_{k+1+\alpha,\,E^2},\ v_{E^2},\ w_{E^2} \in C_{k+2+\alpha,\,E^2}, \end{aligned}$$

where $c_{\nu,\,E^2}$ is the Hölder space with the index ν.

Let us define the spaces F_D and $U_{\bar{D}}$ participating in the formulation of the auxiliary differential problem in the domain D by assigning them the vector functions $f_D = \{f_{1D}, f_{2D}, f_{3D}\}$ and $u_{\bar{D}} = \{v_{\bar{D}}, w_{\bar{D}}, p_{\bar{D}}\}$ obtained from the analysis of the vector functions $f_{E^2} \in F_{E^2}$ and $u_{E^2} \in U_{E^2}$ not on the entire plane but only on D and $\bar{D}$ respectively. We introduce the space $V_{\bar{D}}$ by putting $V_{\bar{D}} = U_{\bar{D}}$. We take ∂D^+ for the boundary Γ. The space of traces $V_\Gamma = U_\Gamma$ will

be defined as the space of the vector functions φ_0, φ:

$$\varphi_\Gamma = (\varphi_0|_\Gamma, \varphi_1|_\Gamma, \varphi_2|_\Gamma, \varphi_3|_\Gamma);$$

$$\varphi_0, \varphi_1 \in C_{k+\alpha+2,\Gamma};\ \varphi_2, \varphi_3 \in C_{k+\alpha+1,\Gamma}.$$

We define the operator γ: $U_{\overline{D}} \to V_\Gamma$ by putting for an arbitrary $u_{\overline{D}}$

$$\gamma u_{\overline{D}} = \left(v|_\Gamma, w|_\Gamma, \frac{\partial (v, w)_\tau}{\partial n}\Big|_\Gamma, p|_\Gamma\right),$$

where $(v, w)_\tau = v\cos\xi + w\cos\eta$ is the velocity in the direction τ tangential to the contour Γ.

In view of the sufficient criterion from Sec. 4.2, it turns out that the space U^+_Γ is a space of sharp traces of U^+_{D+} on Γ. The reconstruction of $u_{\overline{D}} \in U^+_{\overline{D}}$ from its trace u_Γ in the vicinity of the boundary Γ can be done quite accurately from

$$v|_\Gamma, \frac{\partial v}{\partial n}\Big|_\Gamma, \frac{\partial^2 v}{\partial n^2}\Big|_\Gamma;$$

$$w|_\Gamma, \frac{\partial w}{\partial n}\Big|_\Gamma, \frac{\partial^2 w}{\partial n^2}\Big|_\Gamma;$$

$$p|_\Gamma, \frac{\partial p}{\partial n}\Big|_\Gamma, \frac{\partial^2 p}{\partial n^2}\Big|_\Gamma$$

using the Taylor formula. These values themselves and the values of the normal derivatives at the points on Γ are calculated with the help of the Stokes system as follows. The functions u, v, and p are given.

For the sake of simplicity, we shall assume that a segment of the boundary under consideration lies on the straight line $x_2 = \text{const}$. Then

$$\frac{\partial (v, w)_\tau}{\partial n} = \frac{\partial v}{\partial n} = \frac{\partial v}{\partial x_2}$$

is a given function of x_1 and

$$\frac{\partial w}{\partial x_2} = -\frac{\partial v}{\partial x_1}$$

is known. From the third equation, we shall obtain

$$\frac{\partial^2 w}{\partial x_2^2} = -\frac{\partial}{\partial x_1}\left(\frac{\partial v}{\partial x_2}\right),$$

where the right-hand side is a known function of x_1. Then from the first equation we get

$$\frac{\partial^2 v}{\partial x_2^2} = \frac{\partial p}{\partial x_1} - \frac{\partial^2 w}{\partial x_2^2},$$

from the second equation we have

$$\frac{\partial p}{\partial x_2}\Big|_\Gamma = -\frac{\partial^2 w}{\partial x_1} - \frac{\partial^2 w}{\partial x_2^2},$$

and so on; we can find the normal derivatives of any order if k is sufficiently large.

Let us construct the auxiliary difference (nonclassical) boundary value problem. We specify h (h^{-1} is an integer) and construct three meshes with the points

$$(n_1h,\ n_2h),\ \left(n_1+\frac{h}{2},\ n_2+\frac{h}{2}\right),$$

$$\left(\left(n_1+\frac{1}{2}\right)h,\ n_2h\right),\quad n_1,\ n_2=0,\ \pm 1,\ \ldots\ .$$

On each of these meshes, the corresponding scalar function

$$v_n=v_{n_1n_2},\quad w_{n_1+1/2,\ n_2+1/2},\quad p_{n_1+1/2,\ n_2},$$

and the scalar function

$$f^{(1)}_{m_1m_2},\ f^{(2)}_{m_1+1/2,\ [n_2+1/2},\ f^{(3)}_{m_1+1/2,\ m_2}$$

are specified.

At each point with integers m_1, m_2 the scalar difference equation

$$\Delta v_{m_1m_2}-\tilde{\Delta}_{x_1}p_{m_1m_2}=f^{(1)}_{m_1,\ m_2}$$

is specified. The scalar equation

$$\Delta w_{m_1+1/2,\ m_2+1/2}-\tilde{\Delta}_{x_2}p_{m_1+1/2,\ m_2+1/2}=f^{2}_{m_1+1/2,\ m_2+1/2}$$

is specified at the points $m_1+1/2$, $m_2+1/2$, and the scalar equation

$$\tilde{\Delta}_{x_1}v_{m_1+1/2,\ m_2}+\tilde{\Delta}_{x_2}w_{m_1+1/2,\ m_2}=f^{(3)}_{m_1+1/2,\ m_2}$$

at the points $m_1+1/2$, m_2. Here Δ is the difference analogue of the Laplace operator

$$\tilde{\Delta}_x f_t=h^{-1}(f_{t+1/2}-f_{t-1/2}).$$

The set M will include all the mesh points which fall strictly inside D. The set N will incorporate all the points swept by a five-point pattern applied to the points of the set M. The space F_M will include the triplets of arbitrary functions

$$f^{(1)}_{m_1,\ m_2},\ f^{(2)}_{m_1+1/2,\ m_2+1/2},\ f^{(3)}_{m_1+1/2,\ m_2},$$

while U_N includes the triplets of arbitrary functions permitting the completion on the entire mesh in the plane E^2 provided that the parity and periodicity conditions indicated above for the elements of the space U_{E^2} are satisfied. We put $M^+=M\cap D^+$, $\Gamma_h=N^+\cap N^-$. The procedure for solution is the same as in Sec. 4.1.

For obtaining the same effectiveness of the method as in the example of Sec. 4.1, we must assume that $k=2$, use the three terms of the Taylor functions for calculating v_{Γ_h} and w_{Γ_h} and two terms for

calculating p_{Γ_h}, use the fourth-order interpolation for $v \mid_\Gamma$ and $w \mid_\Gamma$ and the cubic interpolation for $\partial (v, w)_\tau/\partial n \mid_\Gamma$ and $p \mid_\Gamma$, and finally, construct the operator r_{K, Γ_h} so that all the quantities at the points of the set K (see Sec. 4.1) are calculated to within h^2. As in Sec. 4.1, the numbers h and H should be related as $h < aH^2$, where a is sufficiently small.

In the case of the Stokes problem, $v \mid_\Gamma$ and $w \mid_\Gamma$ are given, and $v \mid_\Gamma = \varphi_0 (s)$; $w \mid_\Gamma = \varphi_1 (s)$; the space Φ consists of the pairs of functions $\varphi_\Gamma = (\varphi_1 (s), \varphi_2 (s))$. The norms are given by

$$\left\| \begin{matrix} v \\ w \\ \dfrac{\partial (v, w)_\tau}{\partial n} \\ p \end{matrix} \right\|^2_{U_\Gamma} = \int_\Gamma \left[v^2 + w^2 + \left(\frac{dv}{ds}\right)^2 + \left(\frac{dw}{ds}\right)^2 + \left(\frac{\partial (v, w)_\tau}{\partial n}\right)^2 + p^2 \right] ds,$$

$$\left\| \begin{matrix} \varphi_1 \\ \varphi_2 \end{matrix} \right\|_\Phi = \oint_\Gamma \left[\varphi_1^2 + \varphi_2^2 + \left(\frac{d\varphi_1}{ds}\right)^2 + \left(\frac{d\varphi_2}{ds}\right)^2 \right] ds.$$

The required quantities are

$$\left(\begin{matrix} v \\ w \\ \dfrac{\partial (v, w)_\tau}{\partial n} \\ p \end{matrix} \right)_{s_i}, \qquad i = 1, 2, \ldots, K.$$

Here the role of transformations A and B from Sec. 4.1 is played by

$$A_{KK} \left(\begin{matrix} v \\ w \\ \dfrac{\partial (v, w)_\tau}{\partial n} \\ p \end{matrix} \right)_i = \left(\begin{matrix} v_i - h^{-2} (v_{i+1} - 2v_i + v_{i-1}) \\ w_i - h^{-2} (w_{i+1} - 2w_i + w_{i-1}) \\ \dfrac{\partial (v, w)_\tau}{\partial n}\Big|_i \\ p_i \end{matrix} \right),$$

$$B_{KK} \begin{pmatrix} \varphi_1 (s_i) \\ \varphi_2 (s_i) \end{pmatrix} = \begin{pmatrix} \varphi_1 (s_i) - h^{-2} (\varphi_1 (s_{i+1}) - 2\varphi_1 (s_i) + \varphi_1 (s_{i-1})) \\ \varphi_2 (s_i) - h^{-2} (\varphi_2 (s_{i+1}) - 2\varphi_2 (s_i) + \varphi_2 (s_{i-1})) \end{pmatrix}.$$

References

4.1. V. S. Ryaben'ky, *D. Sc. Thesis*, Inst. Appl. Math. USSR Acad. Sci., Moscow, 1969.
4.2. V. S. Ryaben'ky, *Dokl. Akad. Nauk SSSR* 185, 3 (1969).
4.3. V. S. Ryaben'ky, *Matem. Zametki* 5, 5 (1969).

4.4. V. S. Ryaben'ky, *Matem. Zametki*, 6, 2 (1969).
4.5. V. S. Ryaben'ky, VINITI Dep. No. 635-69 (1969).
4.6. V. S. Ryaben'ky, *Matem. Sb.* 79. 1 (1969).
4.7. V. S. Ryaben'ky, *Matem. Zametki* 7, 5 (1970).
4.8. V. S. Ryaben'ky, *Uspekhi Mat. Nauk* 26, 3 (1971).
4.9. V. S. Ryaben'ky, *Dokl. Akad. Nauk SSSR* 202, 4 (1972).
4.10. V. S. Ryaben'ky, in: *Proc. All-Union Conf. (January 1976) on Partial Differential Equations*, Izd. MGU, Moscow, 1978 (in Russian).
4.11. A. Ya. Belyankov, in: *Problems of Mechanics and Mathematical Physics*, Nauka, Moscow, 1976 (in Russian).
4.12. V. S. Rayben'ky, in: *Problems of Mechanics and Mathematical Physics*, Nauka, Moscow, 1976 (in Russian).
4.13. A. D. Belyankov, Cand. Thesis. Inst. Appl. Math. USSR Acad. Sci., Moscow, 1977.
4.14. V. S. Ryaben'ky, in: *The Theory of Cubature Formulas and Computational Mathematics*, Nauka, Moscow, 1980 (in Russian).
4.15. A. A. Reznik and V. S. Ryaben'ky, *Uspekhi Mat. Nauk* 34, 4, (1979).
4.16. A. A. Reznik and V. S. Ryaben'ky, Preprint of Inst. Appl. Math. USSR Acad. Sci., No. 54, Moscow, 1979.
4.17. A. A. Reznik. Diploma, Moscow Physico-Technical Inst., Moscow, 1979.
4.18. V. S. Ryaben'ky and A. Ya. Belyankov, *Dokl. Akad. Nauk SSSR* 254, 5 (1980).
4.19. A. D. Belyankov and V. S. Ryaben'ky, *Uspekhi Mat. Nauk* 36, 4 (1981).
4.20. I. L. Sofronov, Diploma, Moscow Physico-Technical Inst., Moscow (1981).
4.21. A. D. Belyankov and V. S. Ryaben'ky, Preprint No. 70 of Keldysh Inst. Appl. Math., USSR Acad. Sci., Moscow (1981).
4.22. A. Ya. Belyankov, A. A. Reznik, and V. S. Ryaben'ky, Preprint No. 105 of Keldysh Inst. Appl. Math., USSR Acad. Sci., Moscow (1981).
4.23. M. Yu. Lokhanov, Diploma, Moscow Physico-Technical Inst., Moscow (1982).
4.24. A. A. Reznik, *Dokl. Akad. Nauk SSSR* 263, 6 (1982).
4.25. V. S. Ryaben'ky, Preprint No. 15 of Keldysh Inst. Appl. Math., Moscow (1983).
4.26. V. S. Ryaben'ky, *Dokl. Akad. Nauk SSSR* 270, 2 (1983).
4.27. A. Ya. Belyankov and V. S. Ryaben'ky, *Tr. Mosk. Matem. Obshch.* 46 (1983).
4.28. V. S. Ryaben'ky and I. L. Sofronov, Preprint No. 30 of Keldysh Inst. Appl. Math., USSR Acad. Sci., Moscow (1983).
4.29. I. L. Sofronov, Preprint No. 35 of Keldysh Inst. Appl. Math., USSR Acad. Sci., Moscow (1983).
4.30. V. S. Ryaben'ky, *Uspekhi Mat. Nauk* 42, 1 (1983).
4.31. A. A. Reznik, Cand. Thesis, Moscow Physico-Technical Inst. (1983).
4.32. V. S. Ryaben'ky and I. L. Sofronov, Preprint No. 80 of Keldysh Inst. Appl. Math., USSR Acad. Sci., Moscow (1983).
4.33. A. G. Sveshnikov, *Dokl. Akad. Nauk SSSR* 73, 5 (1950).
4.34. V. S. Ryaben'ky, Cand. Thesis, MGU, Moscow (1952).
4.35. V. S. Ryaben'ky and A. F. Filippov, *On Stability of Difference Equations*, Gostekhizdat, Moscow, 1956 (in Russian).
4.36. A. A. Samarsky and V. B. Andreev, *Difference Methods for Elliptic Equations*, Nauka, Moscow, 1976 (in Russian).
4.37. S. K. Godunov and V. S. Ryaben'ky, *Difference Schemes (Introduction to the Theory)*, Nauka, Moscow, 1977 (in Russian).
4.38. A. P. Calderón, *Outlines of the Joint Soviet-American Symposium on Partial Differential Equations*, August, 1963, Novosibirsk.
4.39. R. T. Seeley, *Amer. J. Math.*, 88, 4: 781 (1966).
4.40. V. Thomée, *SIAM J. Numer. Analysis* 5, 3: 626 (1968).
4.41. Proskurowski and Widlund, *Math. Comp.*, 30: 125 (1976).

5 Higher-accuracy Methods for Solving Fluid Dynamics Problems

A. I. Tolstykh, *D.Sc. (Phys.-Math.)*

5.1. INTRODUCTION

The complexity of modern problems in mathematical physics calls for stringent requirements on computer systems as well as computational methods. One of the trends of improving the effectiveness of algorithms is to increase their accuracy and make it compatible with the structure of modern computers. As regards the problems on fluid flows (as well as similar problems), a sufficient accuracy of computations is essentially ensured by two factors: the accuracy of "resolution" of elementary parts of the phenomenon under consideration and the accuracy of the algorithm itself.

In the case of difference methods, the first factor is associated with the construction of difference meshes ensuring a sufficient number of points in the subdomains of computational domain which have their local characteristic size. One of the methods of constructing difference meshes consists in the coordinate transformation, which provides a unique characteristic scale in the new variables, with a subsequent uniform distribution of mesh points. Henceforth we shall assume that precisely this method is being used.

The approximation error of the difference algorithm on a mesh with a characteristic size h depends on the order of accuracy of the scheme and on higher-order derivatives of the solutions of initial differential equations with respect to new variables. Hence the "resolution" of meshes is directly related with the real accuracy of the difference scheme: an appropriate transformation of coordinates may result not only in the optimal arrangement of mesh-points, but also in smoothing of abruptly-varying functions. In this case, the computational accuracy can be increased for admissible values of h by increasing the order of approximation of the scheme.

By a higher-accuracy method, we shall mean the algorithm including the construction of difference meshes with an appropriate distribution of nodes in the physical computational domain as well as the scheme having an approximation order higher than the second.

This paper is mainly devoted to the construction and substantiation of third-order implicit compact schemes applicable, in particular, to the analysis of viscous fluid flows (Secs. 5.2-5.4). Symmetrization of such schemes may lead to fourth-order schemes described, in particular, in [5.1-5.3].

A systematic application of third-order implicit compact schemes to the analysis of viscous gas flows was initiated by the author in 1972 [5.4]. It was combined with the utilization of adaptable difference meshes in which the mesh-points were automatically concentrated in the process of solution in the regions with high gradients. Without considering in detail the construction of such meshes, we note that it was based on the transformation of one of the spatial coordinates, the transformation being determined by the required function that varies rapidly in the direction of this coordinate.

The examples illustrating the combined application of adaptable meshes and higher-accuracy schemes are considered in Secs. 5.3.2 and 5.5.1. For more complicated versions of the algorithm, a preliminarily fixed concentration of mesh-points has been used. Some results of calculations, in particular those associated with numerical simulation of separated flows, are described in Sec. 5.5.2.

5.2. NONSYMMETRIC COMPACT SCHEMES FOR ONE-DIMENSIONAL TRANSPORT EQUATIONS

5.2.1. Basic Operators and Principles of Constructing Third-order Schemes

1. Let us introduce on a uniform difference grid w_h: $x_n = nh$ the following pairs of difference operators [5.4-5.8]:

$$\begin{aligned} &\Delta_+ f_i = f_{i+1} - f_i, \\ &A_- f_i = \frac{5}{12} f_{i+1} + \frac{8}{12} f_i - \frac{1}{12} f_{i-1}, \end{aligned} \tag{5.2.1.1a}$$

and

$$\begin{aligned} &\Delta_- f_i = f_i - f_{i-1}, \\ &A_+ f_i = \frac{5}{12} f_{i-1} + \frac{8}{12} f_i - \frac{1}{12} f_{i+1}. \end{aligned} \tag{5.2.1.1b}$$

Using the Taylor expansion in the vicinity of the point $x = x_i$, we can easily obtain the following symbolic representations for $A_\pm$ and $\Delta_\pm$:

$$\begin{aligned} \frac{1}{h} \Delta_\mp f_i &= \left(E \mp \frac{h}{2} D_x + \frac{h^2}{6} D_x^2\right) D_x f_i + O(h^3), \\ A_\pm f_i &= \left(E \mp \frac{h}{2} D_x + \frac{h_2}{6} D_x^2\right) f_i + O(h^3), \end{aligned} \tag{5.2.1.2}$$

where D_x and D_x^2 are operators of the first- and second-order derivatives with respect to x.

Suppose that we have a nonlinear transport equation written in the form of a conservation law (in "divergent form"):

$$\frac{\partial u}{\partial t}+\frac{\partial \varphi(u)}{\partial x}=f(u, x, t). \tag{5.2.1.3}$$

Applying operators (5.2.1.1), we can construct on the grid $\omega_\tau \times \omega_h$ (ω_τ: $t_m = m\tau$) a family of difference schemes which approximate (5.2.1.3) to the third order of accuracy with respect to the spatial step h. In particular, by introducing the weight factors $\sigma_1, \sigma_2, \ldots, \sigma_k$ ($\sigma_1 + \sigma_2 + \ldots + \sigma_k = 1$), we write the k-level scheme for (5.2.1.3) in the form

$$A_\pm \left\langle \frac{\partial u}{\partial t} \right\rangle^{m+1} + \Delta_\mp \left(\sum_{j=0}^{k-1} \sigma_j \varphi^{m+1-j} \right) \Big/ h = A_\pm \left(\sum_{j=0}^{k-1} \sigma_j f^{m+1-j} \right). \tag{5.2.1.4}$$

Here $\varphi^{m+1-j} = \varphi(u^{m+1-j})$, and $\langle \partial u/\partial x \rangle^{m+1}$ stands for a certain approximation of the derivative $\partial u/\partial t$, in which the values of the function u for $t = t_p$ ($p = m+1, m, \ldots, m-k+2$) are used. By an appropriate choice of the factors σ_j ($j = 1, 2, \ldots, k$), we can obtain the required order of accuracy for the time-step τ. In this case, the approximation error with respect to step h will always have the order $O(h^3)$. This can be easily verified by substituting representation (5.2.1.2) into (5.2.1.4) and premultiplying both sides by $(E \pm (h/2) D_x + (h^2/6) D_x^3)^{-1}$. The obtained result can be represented in the form

$$\left\langle \frac{\partial u}{\partial x} \right\rangle_n^{m+1} + \sum_{j=0}^{k-1} \sigma_j \left(\frac{\partial \varphi}{\partial x} \right)_n^{m+1-j} = \sum_{j=0}^{k-1} \sigma_j f_n^{m+1-j} + O(h^3).$$

Henceforth, we shall confine the analysis to the simplest (mainly two-point) approximations of time derivatives. Such approximations are convenient when we are interested in the stationary solution of the initial equations. For $k = 2$, scheme (5.2.1.4) can be written in the form

$$A_\pm \frac{u^{m+1}-u^m}{\tau} + \frac{1}{h} \Delta_\mp (\sigma_1 \varphi(u^{m+1}) + \sigma_2 \varphi(u^m)) = A_\pm f, \quad \sigma_1 + \sigma_2 = 1. \tag{5.2.1.5}$$

The problem of the choice of an operator pair from (5.2.1.2) that should be used in (5.2.1.5) is solved by a simple stability analysis.

Suppose that $\varphi(u) = au$ and $a = \text{const}$. Using the spectral method, we obtain the following expression for the eigenvalue λ of the

transition operator:

$$\lambda = \frac{1 - ar\sigma_2 W_{\pm}(\alpha)}{1 + ar\sigma_1 W_{\pm}(\alpha)}, \quad 0 \leqslant \alpha \leqslant 2\pi, \quad r = \frac{\tau}{h}. \tag{5.2.1.6}$$

Here

$$W_+(\alpha) = \frac{12\,[1 - \exp(-i\alpha)]}{5\exp(-i\alpha) - \exp(i\alpha) + 8},$$

$$W_-(\alpha) = \frac{12\,[\exp(i\alpha) - 1]}{5\exp(i\alpha) - \exp(-i\alpha) + 8}$$

are the functions of a complex argument which satisfy the conditions

$$\operatorname{Re} W_+ = -\operatorname{Re} W_- \geqslant 0, \quad \operatorname{Im} W_+ = \operatorname{Im} W_-.$$

Choosing from (5.2.1.2) the pair for which $\operatorname{Re} W_l \geqslant 0$ (l stands for plus or minus), we obtain the absolutely stable scheme (5.2.1.5) for $\sigma \geqslant 0.5$. Henceforth, by the stability of a scheme we shall mean its stability in the "frozen" coefficient approximation.

In the nonlinear case, a simple criterion for choosing the required operator pair at the node $x_j = jh$ is the condition

$$\varphi'(u_j^m) \operatorname{Re} W_l \geqslant 0. \tag{5.2.1.7}$$

When $\varphi'(u_j^m)$ changes sign (upon a transition to the node x_{j-1} or x_{j+1}), a "reorientation" of operators is required as in the case of ordinary nonsymmetric schemes.

In can be shown [5.8] that if condition (5.2.1.7) is satisfied, absolute stability will also be observed for the three-deck scheme (5.2.1.4) of the order $O(\tau^2 + h^3)$, for which

$$\left\langle \frac{\partial u}{\partial t} \right\rangle^{m+1} = \frac{3u^{m+1} - 4u^m + u^{m-1}}{2\tau}, \quad \sigma_1 = 1, \ \sigma_2 = \sigma_3 = 0.$$

However, the three-deck scheme (5.2.1.4) of the order $O(\tau^3 + h^3)$ for

$$\left\langle \frac{\partial u}{\partial t} \right\rangle^{m+1} = \frac{u^{m+1} - u^m}{\tau}, \quad \sigma_1 = \frac{5}{12}, \quad \sigma_2 = \frac{8}{12}, \quad \sigma_3 = -\frac{1}{12} \tag{5.2.1.8}$$

is stable only if the Courant criterion $a\tau/h < \text{const}$, const $\simeq 1$ [5.9] is satisfied. In this paper, we shall consider as a rule only absolutely stable schemes of the type (5.2.1.4).

2. Let us consider some properties of these schemes. The third order of accuracy of scheme (5.2.1.4) with respect to the step h is attained on a three-point pattern in the x-direction irrespective of the change in the sign of the derivative $\varphi'(u_j^m)$. In this case, the difference equations for determining u_j^{m+1} have the form

$$a_j u_{j+1}^{m+1} + b_j u_j^{m+1} + c_j u_{j-1}^{m+1} = d_j. \tag{5.2.1.9}$$

Considering the case of constant coefficients $a_j = a$, $b_j = b$, $c_j = c$, we can show that the roots of the characteristic equation $aq^2 + bq + c = 0$ are real and satisfy the inequalities

$$4 - \sqrt{21} < q_1 < 1 < q_2.$$

This means that for appropriate boundary conditions at $j = 1$ and $j = N \geqslant 3$, the system (5.2.1.9) is, in accordance with [5.16], well defined and the sweep (progonka) method of its solution is stable.

When the coefficients a_j, b_j, and c_j are constant, the general solution of the homogeneous system (5.2.1.9) can be written in the form

$$u_j = C_1 q_1^j + C_2 q_2^j.$$

Hence we may conclude that the oscillations of the function u_j, which appear for negative values of q_1, rapidly attenuate since $|q_1| < 1$.

Thus, it can be naturally assumed that the nonmonotonicity of the schemes under consideration will not be clearly manifested while solving problems with varying coefficients (e.g., nonlinear problems). The conclusion that the oscillations are rapidly damped was confirmed by the analysis of discontinuous solutions (see the next subsection).

Another property of the schemes is their conservative nature. Indeed, the operators A_+ and A_- determine the quadrature formulas of the form

$$\frac{1}{h}\int_{x_i}^{x_{i+1}} f(x)\,dx = A_+ f + O(h^3), \quad \frac{1}{h}\int_{x_{i-1}}^{x_i} f(x)\,dx = A_- f + O(h^3). \tag{5.2.1.10}$$

Hence schemes of the type (5.2.1.3) can be treated as an approximation of the balance of fluxes through the cell boundaries in the (x, t)-plane. The integrals for the fluxes through the boundaries parallel to the x-axis are calculated by formulas (5.2.1.10).

Let us now establish the relation between the third-order approximations based on operators (5.2.1.1) and symmetric fourth-order approximations which were earlier reported in some papers [5.1-5.3]. In this connection, we note that the derivative $f = \partial u/\partial x$ in terms of (5.2.1.1) on a uniform grid ω_h is calculated by the formulas

$$A_\mp f = (\Delta_\mp u)/h. \tag{5.2.1.11}$$

We denote by A_0 and $0.5\Delta_0$ the half-sums $0.5(A_+ + A_-)$ and $0.5(\Delta_- + \Delta_+)$ respectively. Then, substituting A_0 and Δ_0 for $A_\mp$ and $\Delta_\mp$ into (5.2.1.11), we obtain representations of the form

$$A_0 f = (f_{i-1} + 4f_i + f_{i+1})/6 = (u_{i+1} - u_{i-1})/2h + O(h^4). \tag{5.2.1.12}$$

This equality can also be obtained as a result of approximation of the function f by cubic splines or Hermite interpolation polynomials [5.2, 5.3]. Suppose now that we have an equation of the form

$$\frac{\partial u}{\partial t}+a\frac{\partial u}{\partial x}=F. \tag{5.2.1.13}$$

Denoting $\partial u/\partial x$ by f and using (5.2.1.12), we write its approximation on the mesh $\omega_\tau \times \omega_h$ in the form of the system of equations for the pair (u_i, f_i):

$$\left\langle\frac{\partial u}{\partial t}\right\rangle_j^{m+1}+af_j^{m+1}=F_j, \quad A_0 f^{m+1}=\Delta_0 u^{m+1}/2h. \tag{5.2.1.14}$$

This is just the higher-accuracy scheme for (5.2.1.13) from the class of the schemes considered in [5.1-5.3]. Premultiplying the first equations in (5.2.1.14) by A_0 at a constant a and taking into account the second equation in (5.2.1.14), we obtain a scheme of the type (5.2.1.4) with symmetrized operators A_0 and Δ_0 instead of $A_\pm$ and $\Delta_\pm$. Such schemes were used by the author for methodical calculations (in particular, in the case of discontinuous solutions) [5.9]. As expected, these schemes exhibited inferior monotonic properties in comparison with their nonsymmetric counterparts. However, they are easier to realize since they do not require an analysis of signs of the coefficients of $\varphi'(u)$ at each point. When $a = a(x, u)$, scheme (5.2.1.14) is not equivalent to scheme (5.2.1.4) with A_0 and Δ_0. Its nonsymmetrical analogue can be obtained by replacing the second equation in (5.2.1.14) by Eq. (5.2.1.11) where A_+ and Δ_- are used for $a_i \geqslant 0$ and A_- and Δ_+ for $a_i < 0$:

$$\begin{aligned}&\left\langle\frac{\partial u}{\partial t}\right\rangle_j^{m+1}+a_j f_j^{m+1}=F_j,\\ &A_\pm f^{m+1}=\Delta_\mp u^{m+1}/h.\end{aligned} \tag{5.2.1.15}$$

Below, we shall write schemes of the type (5.2.1.5) in the equivalent form

$$A\left\langle\frac{\partial u}{\partial t}\right\rangle^{m+1}+\frac{1}{h}\Delta\bar{\varphi}=Au, \quad \bar{\varphi}=\sum_{j=0}^{k-1}\sigma_j\varphi^{m+1-j}, \tag{5.2.1.16}$$

where

$$A=A_0-0.25\operatorname{sgn}\varphi'(u_i^m)\Delta_0,$$

$$\Delta=(\Delta_0-\operatorname{sgn}\varphi'(u_i^m)\Delta_2)/2.$$

In such a representation, the operators A and Δ pass into a pair (A_+, Δ_-) or (A_-, Δ_+) upon a change in the sign of $\varphi'(u_i^m)$. If we formally put $\operatorname{sgn}\varphi'(u_j^m) = 0$, we shall obtain a symmetric scheme with the operators A_0 and Δ_0.

5.2.2. Examples of Through Computation of Discontinuous Solutions

The conservative nature of the above schemes allows us to use them for solving problems admitting discontinuities and, in particular, for solving gasdynamic problems. In order to estimate dissipative properties of approximations and monotonicity of obtained solutions, we consider simple model examples.

Suppose that for the equation

$$\frac{\partial u}{\partial t}+\frac{\partial (u^2/2)}{\partial x}=0 \qquad (5.2.2.1)$$

the problem with the following boundary conditions

$$u(x,\ 0)=1 \quad (x\leqslant\Theta), \quad u(x,0)=2-x/\Theta \quad (\Theta\leqslant x\leqslant 2\Theta),$$
$$u(x,\ 0)=0 \quad (2\Theta<x) \qquad (5.2.2.2)$$

is formulated. The exact solution of this problem is such that a discontinuity is formed at $t>0$. This discontinuity propagates in the positive direction of the x-axis at a constant velocity $x/t=0.5$. For numerical solution of (5.2.2.1)-(5.2.2.2), the conditionally stable scheme (5.2.1.4), (5.2.1.8) was used on the mesh ω: $t_m=m\tau$, $x_n=nh$ [5.9] with the approximation order $O(\tau^3+h^3)$. Since the function is positive, the operator pair $(A_+,\ \Delta_-)_0$ was used.

Figure 5.1 shows the variation of function u in the vicinity of the discontinuity front at fixed instants of time, obtained with the help of the implicit scheme (5.2.1.4), (5.2.1.8) for $\tau/h=0.7$ and third-order explicit schemes [5.10, 5.11]. A peculiar feature of the results of calculations presented in the figure is the arrangement of the regions of nonmonotonic solutions for small values of the function u_0. The rapid damping of oscillations is consistent with the presence of the component $(-1)^n q_1^n$ $(0<q_1<1,\ n=0,\ \mp 1,\ \mp 2,\ \ldots)$ in the solution of homogeneous difference schemes for the linearized equation (5.2.2.1). It should be noted that unlike third-order explicit schemes, a stable computation via the scheme (5.2.1.4), (5.2.1.8) does not involve the introduction of out-of-order dissipative terms. The introduction of such terms (or some other kind of filtration) may reduce the amplitude of oscillation of the solution [5.9].

Let us consider the Riemann breakdown problem for gasdynamic equations

$$\frac{\partial \rho u}{\partial t}+\frac{\partial (\rho u^2+p)}{\partial x}=0, \quad \frac{\partial \rho}{\partial t}+\frac{\partial \rho u}{\partial x}=0,$$
$$\frac{\partial \rho\left(\frac{h}{\gamma}+\frac{u^2}{2}\right)}{\partial t}+\frac{\partial \rho u\left(h+\frac{u^2}{2}\right)}{\partial x}=0, \quad p=\frac{\gamma-1}{\gamma}\rho h. \qquad (5.2.2.3)$$

Here ρ, u, and p are the gas density, velocity, and pressure respectively. System (5.2.2.3) was approximated by the scheme (5.2.1.4), (5.2.1.8) so that the choice of the operator pair (5.2.1.1) was based on the analysis of characteristic directions of system (5.2.2.3). It can be shown [5.5] that for $u \geqslant c$, where c is the velocity of sound, the spectral stability condition will be satisfied if all three equations in

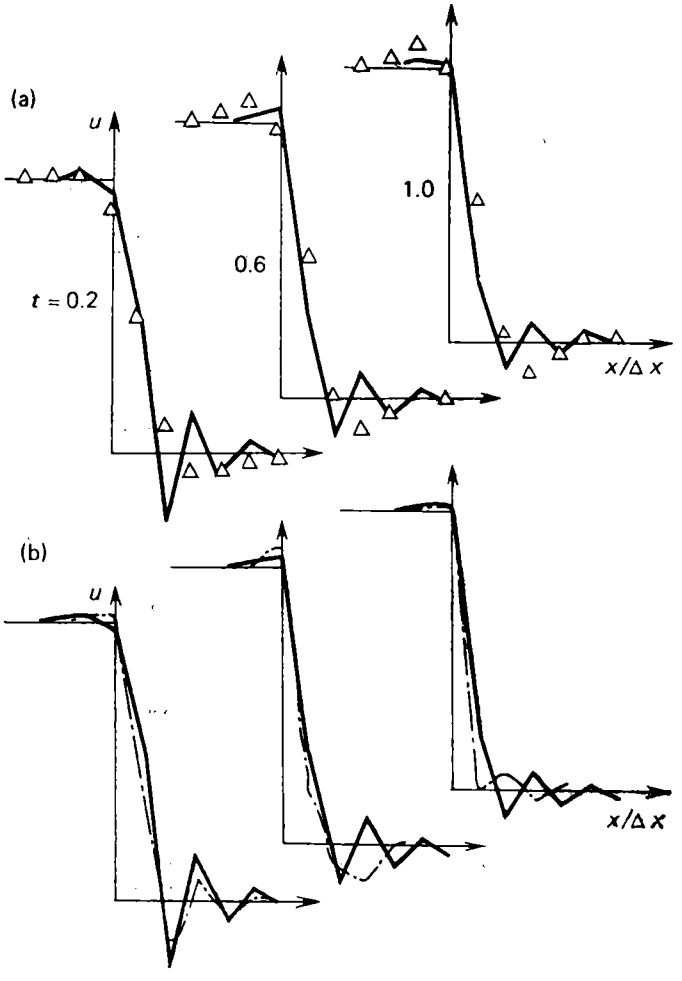

Fig. 5.1. Propagation of discontinuity for a model equation: — third-order implicit scheme, Δ scheme from [5.10, 5.11], — — scheme (5.2.1.4), (5.2.1.8) with out-of-order dissipation.

(5.2.2.3) are approximated by operators (5.2.1.3) for $\operatorname{sgn} \varphi'(u_n^m) = \operatorname{sgn} u_n^m$. If $u < c$, these operators should be used in the difference analogues of the second and third equations in (5.2.2.3). In this case, the first equation in (5.2.2.3) should be approximated with the help of operators (5.2.1.3) for $\operatorname{sgn} \varphi'(u) = -\operatorname{sgn} u_n^m$.

Figure 5.2 shows two examples of calculation. One of them is characterized by the appearance of a relatively strong expansion wave,

and the other by the presence of a shock wave and contact discontinuity of a high intensity. In the former case (Fig. 5.2*a*), the initial parameters for $t = 0$ were chosen in the following manner: $\rho = p = 2$, $u = 0$ for $x < 0$ and $\rho = p = 1$, $u = 0$ for $x \geqslant 0$. In the second case (Fig. 5.2*b*), the initial data were borrowed from [5.10].

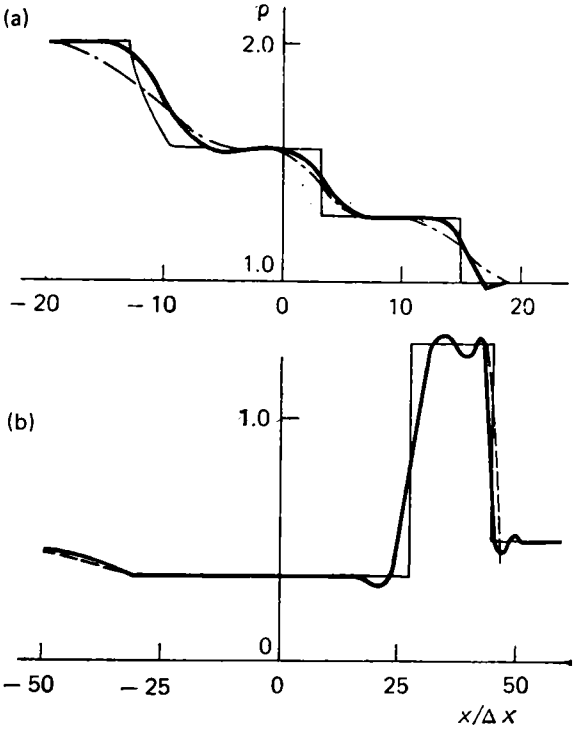

Fig. 5.2. Calculation of discontinuity disintegration: — third-order implicit scheme (5.2.1.4), (5.2.1.8), —·— first-order scheme from [5.12], — — third-order scheme from [5.10].

Calculations were made for $\tau/h = 0.5$. For the sake of comparison, Figs. 5.2*a* and *b* contain the results obtained by using the first [5.12] and third [5.10] order schemes.

The analysis of Figs. 5.1 and 5.2 reveals that the solutions obtained with the help of the compact scheme (5.2.1.4), (5.2.1.8) and the explicit third-order scheme [5.10] practically coincide and indicate a considerably smaller scheme dissipation than in the case of first-order schemes.

5.2.3. Approximation of Hyperbolic Systems

1. While solving the Riemann problem for one-dimensional gasdynamic equations (Sec. 5.2.2), the choice of operators (5.2.1.1) was based on simple stability estimates. In the general case of hyperbolic systems, higher-accuracy non-symmetric stable

schemes can be constructed, as in the case of the first-order schemes, by diagonalizing the matrices of coefficients. Let us consider a system of the form

$$\frac{\partial \mathbf{u}}{\partial t}+\frac{\partial \boldsymbol{\varphi}(\mathbf{u}, x)}{\partial x}=\mathbf{F}(\mathbf{u}, x, t), \tag{5.2.3.1}$$

where $\mathbf{u}$, $\boldsymbol{\varphi}$, and $\mathbf{F}$ are p-component vectors. We shall assume that in the corresponding nondivergent system

$$\frac{\partial \mathbf{u}}{\partial t}+K\frac{\partial \mathbf{u}}{\partial x}=\mathbf{F}, \quad K=\varphi'_{\mathbf{u}}, \tag{5.2.3.2}$$

the matrix K has real eigenvalues $\mu_1, \mu_2, \ldots, \mu_p$. To begin with, we assume that the components of K are constant. Let us transform (5.2.3.2) into

$$\frac{\partial \mathbf{v}}{\partial t}+\Lambda\frac{\partial \mathbf{v}}{\partial x}=S^{-1}\mathbf{F} \tag{5.2.3.3}$$

where $\mathbf{u}=S\mathbf{v}$, $\Lambda=\operatorname{diag}\{\mu_1, \mu_2, \ldots, \mu_p\}=S^{-1}KS$, and S is the matrix whose columns are eigenvectors of the matrix K. Now each individual equation from (5.2.3.3) can be approximated in accordance with the sign of μ_i $(i=1, 2, \ldots, p)$. We shall write for (5.2.3.3), for example, the simplest two-deck scheme with $\sigma_1=1$ and $\sigma_2=0$ in the form (5.2.1.16):

$$(A_0-0.25\operatorname{sgn}\mu_i\Delta_0)\frac{v_i^{m+1}-v_i^m}{\tau}+\frac{(\Delta_0-\operatorname{sgn}\mu_i\Delta_2)\mu_i\Delta_i v_i^{m+1}}{2h}$$

$$=(A_0-0.25\operatorname{sgn}\mu_i\Delta_0)S^{-1}F_i^{m+1}, \quad i=1, 2, \ldots, p. \tag{5.2.3.4}$$

Returning now to the vector variable $\mathbf{u}$, we obtain a scheme of the form [5.14]

$$(A_0-0.25M\Delta_0)\frac{\mathbf{u}^{m+1}-\mathbf{u}^m}{\tau}+(\Delta_0-M\Delta_0)\frac{K\mathbf{u}^{m+1}}{2h}=(A_0-0.25\Delta_0)\mathbf{F}^m, \tag{5.2.3.5}$$

where $M=SDS^{-1}$ and $D=\operatorname{diag}\{\operatorname{sgn}\mu_1, \operatorname{sgn}\mu_2, \ldots, \operatorname{sgn}\mu_p\}$. If the matrix K is varying, scheme (5.2.3.5) loses the third order of accuracy with respect to the step h. However, the third order of accuracy can be retained upon the following modification of (5.2.3.5):

$$(A_0-0.25\Delta_0 M)\frac{\mathbf{u}^{m+1}-\mathbf{u}^m}{\tau}+[\Delta_0-\Delta_-(T_{1/2}M)\Delta_+]\frac{\varphi^{m+1}}{2h}$$

$$=(A_0-0.25\Delta_0 M)\mathbf{F}. \tag{5.2.3.6}$$

In this expression, $T_{1/2}$ denotes the operator of displacement by $h/2$ in the positive direction of the x-axis so that $\Delta_-(T_{1/2}M)\Delta_+ f=M_{i+1/2}(f_{i+1}-f_i)-M_{i-1/2}(f_i-f_{i-1})$, $M_{i\mp1/2}=0.5(M_i+M_{i\mp1})$. Scheme (5.2.3.6) has the order $O(\tau+h^3)$. In order to

verify that, it is sufficient to use the symbolic representation

$$(A_0 - 0.25\Delta_0 M) f = \left(E - \frac{h}{2} D_x M + \frac{h^2}{6} D_x M D_x\right) f + O(h^3),$$

$$\frac{1}{2h}[\Delta_0 - \Delta_-(T_{1/2}M)\Delta_+] f = \left(E - \frac{h}{2} D_x M + \frac{h^2}{6} D_x M D_x\right) D_x f + O(h^3). \tag{5.2.3.7}$$

2. For estimating the stability of (5.2.3.6), we shall assume that $\varphi(\mathbf{u}, x) = K\mathbf{u}$, where K is a constant matrix. In order to avoid the introduction of different boundary conditions for different problems, we shall assume that the Cauchy problem is formulated for the initial system in the unbounded domain $t \geqslant 0$ with the initial parameters vanishing outside a certain interval on the x-axis.

Under the above assumptions, the absolute stability of (5.2.3.6) follows from the stability of schemes (5.2.3.4) for each scalar equation.

However, we shall be using henceforth the technique employing the energy norms, which was developed in [5.13] for the stability analysis. This helps to avoid cumbersome expressions for the eigenvalues of the transition operator.

Let us consider the space H of finitely supported mesh functions with the scalar product

$$(\mathbf{f} \cdot \mathbf{g}) = \sum_{i=-\infty}^{\infty} \mathbf{f}_i \cdot \mathbf{g}_i h,$$

where $\mathbf{f}_i \cdot \mathbf{g}_i$ is the inner product of the p-component vectors $\mathbf{f}$ and $\mathbf{g}$.

Assuming that the operator A defined on H is positive if the inequality $(A\mathbf{v}, \mathbf{v}) > 0$ is satisfied for any nonzero element $\mathbf{v} \in H$, we shall take into consideration the following properties of the matrix-difference operators appearing in (5.2.3.6):

$$\begin{aligned} &M' = M, \\ &M^2 = I \text{ for } \mu_i \neq 0 \ (i = 1, 2, \ldots, p) \\ &MK = (MK)' > 0, \end{aligned} \tag{5.2.3.8}$$

$$\Delta_0^2 = 4\Delta_2 + \Delta_2^2, \ A_0 = E + \Delta_2/6, \ 0 < -\Delta_2 \leqslant 4E. \tag{5.2.3.9}$$

Here I and E are the unit matrix and the unit operator respectively. The first three of the above properties follow from the definition of the matrix $M = SDS^{-1}$ and representation $K = S\Lambda S^{-1}$.

On the basis of these properties, we can easily establish the inequalities [5.14]

$$B > E/3, \ CK > 0, \ B(CK)^* > 0 \ (B^*CK > 0) \tag{5.2.3.10}$$

for the operators

$$B = A_0 - 0.25\,\Delta_0 M,\quad C = (\Delta_0 - M\Delta_2)/2h.$$

Henceforth we shall be using the following result from [5.14]. Suppose that the operators $\mathscr{B}$ and $\mathscr{A}$ are independent of t and satisfy the conditions $\mathscr{B} > 0$, $\mathscr{A} = \mathscr{A}^* > 0$. Then, to ensure the stability of the scheme

$$\mathscr{B}\frac{\mathbf{u}^{m+1}-\mathbf{u}^m}{\tau} + \mathscr{A}\mathbf{u}^m = 0 \qquad (5.2.3.11)$$

with respect to the norm $\|\cdot\|$ (i.e. for the inequality $(\mathscr{A}^{m+1}, \mathbf{u}^{m+1}) \leqslant (\mathscr{A}\mathbf{u}^m, \mathbf{u}^m)$ to be satisfied), it is necessary and sufficient that $\mathscr{B} \geqslant 0.5\tau\mathscr{A}$.

Let us write the scheme (5.2.3.5) with constant matrices for $\mathbf{F} = 0$ in a more general form by introducing the weight factor σ ($0 \leqslant \sigma \leqslant 1$):

$$(B + \tau\sigma CK)\frac{\mathbf{u}^{m+1}-\mathbf{u}^m}{\tau_i} + CK\mathbf{u}^m = 0. \qquad (5.2.3.12)$$

When $\sigma = 1$, this scheme is transformed to (5.2.3.5).

Multiplying both sides of (5.2.3.12) by $A_1^* = (CK)^*$, we obtain the scheme

$$(A_1^*B + \sigma\tau A_1^*A_1)\frac{\mathbf{u}^{m+1}-\mathbf{u}^m}{\tau} + A_1^*A_1\mathbf{u}^m = 0.$$

which satisfies for $\sigma > 0.5$ all conditions imposed on the operators $\mathscr{B}$ and $\mathscr{A}$ in (5.2.3.11) and hence is stable in the norm $\|\cdot\|_{A_1^*A_1}$ for all values of τ. It should be noted that scheme (5.2.3.12) is absolutely stable in the norm $\|\cdot\|_H$ in view of the inequality $CK > 0$ for $\sigma \geqslant 0.5$ as a weighted scheme [5.13].

Scheme (5.2.3.6) for a system of equations is an analogue of scheme (5.2.1.16) which approximates the scalar equation (5.2.1.3). Difference equations can be solved with the help of the three-point vector sweep method after some linearization of the function φ. In this case, the determination of the sign of the derivative $\varphi'(u)$ at each point in scheme (5.2.1.16) is replaced by the calculation of the matrix M. It should be noted that the introduction of the matrix M into the operators B and C is equivalent to constructing a scheme with a positive operator CK in (5.2.3.10) in the same way as it is done when applying all stable nonsymmetrical schemes.

3. Vector sweeps with $p \times p$ matrices for inversion of operators $B + \tau\sigma CK$ from (5.2.3.12) can be replaced by scalar ones if "Riemann invariants" $S^{-1}\mathbf{u}$ are taken for the required functions. For this purpose, it is sufficient to represent these operators in the form

$$G = B + \tau\sigma CK = S\,[A_0 - 0.25D\Delta_0 + \tau\sigma\,(\Delta_0 - D\Delta_2)\,\Lambda]S^{-1} = SRS^{-1}$$

where $\Lambda = \operatorname{diag}\{\lambda_i\}$, $D = \operatorname{diag}\{\operatorname{sgn}\lambda_i\}$, and reduce the problem to the inversion of the operator R in the brackets with the diagonal matrices D and Λ.

When the matrices K are varying, the operator G is transformed to the "nondiagonalizable" operator G_1. However, for solving equations of the type $G_1\xi = \mathbf{F}$, where $\mathbf{F}$ is a known mesh function, we can construct an iterative process of the type

$$SRS^{-1}\xi^h = \mathbf{F} + (SRS^{-1} - G_1)\,\xi^{h-1},$$

where the matrices S generally change from point to point in the mesh. Putting $S^{-1}\xi^h = \mathbf{z}$ and multiplying this equality by S^{-1}, we obtain the equality $R\mathbf{z} = \mathbf{F}_1$ with a known right-hand side and the operator R invertible as a result of scalar sweeps.

Henceforth, while mentioning vector sweeps with $p \times p$ matrices, we shall always imply the possibility of such a reduction without specially stipulating it.

5.2.4. Dispersive and Dissipative Properties of Third-order Approximations for Time-dependent Problems

1. So far, we mainly considered the approximation and stability of nonsymmetric "compact" schemes: the properties which are important for obtaining higher-accuracy steady solutions. On the other hand, it is interesting to find out to which extent the introduced spatial discretization may be helpful for solving time-dependent problems. In this case, there is no need to attain the absolute stability of the algorithm and to eliminate the error of approximation depending on the step τ for the steady solution.

For the sake of simplicity, let us consider the transport equation

$$\frac{\partial u}{\partial t} + c\frac{\partial u}{\partial x} = 0, \quad c = \text{const}. \tag{5.2.4.1}$$

In order to eliminate the errors introduced by the discretization of the time derivative, we shall first investigate the difference-differential equation

$$\frac{\partial u_j}{\partial t} + A^{-1}\Delta c u_j/h = 0, \tag{5.2.4.2}$$

where in operators A and Δ from (5.2.1.16) $\operatorname{sgn}\varphi'(u_j) = \operatorname{sgn} c$. Equation (5.2.4.2) is the above approximation of the order $O(h^3)$, where instead of approximate formula $\langle \partial u/\partial t\rangle$ the exact value of the derivative $\partial u/\partial t$ is used and all the terms are multiplied by A^{-1}. Seeking the solution of (5.2.4.1) in the form $u_n = v(t)\,e^{ikhn}$, we obtain the ordinary differential equation

$$\frac{dv}{dt} + \left[\frac{c}{h}W_0(kh) + i\frac{c}{h}W_1(kh)\right]U = 0, \tag{5.2.4.3}$$

where $W_0 = \operatorname{Re} W_+$, $W_1 = \operatorname{Im} W_+$ and W_+ is a function of the complex argument defined in formulas (5.2.1.6) (for $c < 0$, we must use W_- instead of W_+). The functions $W_0(\alpha)$ and $W_1(\alpha)$ have the form

$$W_0(\alpha) = 96 \sin^4 \frac{\alpha}{2} \Phi(\alpha),$$

$$W_1(\alpha) = 24 \sin \alpha (7 - \cos \alpha) \Phi(\alpha), \qquad (5.2.4.4)$$

$$\Phi(\alpha) = [(8 + 4\cos\alpha)^2 + 36 \sin^2 \alpha]^{-1}.$$

Comparing (5.2.4.3) with a similar relation for the exact solution ($v = v(t)\, e^{ikx}$)

$$\frac{dv}{dt} + ickv = 0,$$

where c is the phase velocity, we obtain the expression for the "scheme" phase velocity c^*:

$$c^* = c \frac{W_1(\alpha)}{\alpha}, \quad \alpha = kh. \qquad (5.2.4.5)$$

The second term in (5.2.4.3), which is non-negative for all α's, characterizes dissipation leading to damping of harmonics.

For not very short waves ($\alpha = kh \ll 1$), we have the following representation:

$$c^* = c[1 + O(\alpha^4)], \quad d = ch^{-1} W_0(\alpha) = ch^{-1} O(\alpha^4).$$

These formulas indicate that for long and medium waves the "phase" error introduced by the replacement of the differential operator $\partial/\partial x$ by the difference operator $A^{-1}\Delta/h$ is negligibly small and is fourth-order infinitesimal. The dissipation for these waves, which determines the decrease in the amplitude ("amplitude error"), is also very small.

For the shortest waves that can be resolved by a mesh ($kh = \pi$), the phase velocity c^* vanishes, and the phase error is large. At the same time, however, dissipation becomes significant, and such waves are simply damped. Figure 5.3 shows the relations $c^*(kh)/c$, $dh/c = f(kh)$, as well as $c_g(kh)/c$, where c_g is the group velocity equal to $d\alpha c(\alpha)/d\alpha$. The corresponding curves for the widely-used central differences are shown on the same figure by dashed curves for the sake of comparison.

It can be seen from Fig. 5.3 that for $kh \leqslant \pi/4$, the group velocity slightly differs from its exact value c. For the shortest waves it assumes relatively large negative values which indicate the propagation of wave packets in the "reverse" direction. This, however, is practically not observed due to a rapid damping of short-wave harmonics.

2. The approximation of spatial derivatives with the help of the operator $A^{-1}\Delta/h$ can be used in constructing various higher-accuracy schemes for solving time-dependent problems. Such schemes can be constructed if, for example, we replace the derivative $\partial u/\partial t$ in (5.2.4.2) by a difference approximation $\langle \partial u/\partial t \rangle$ introduced on the

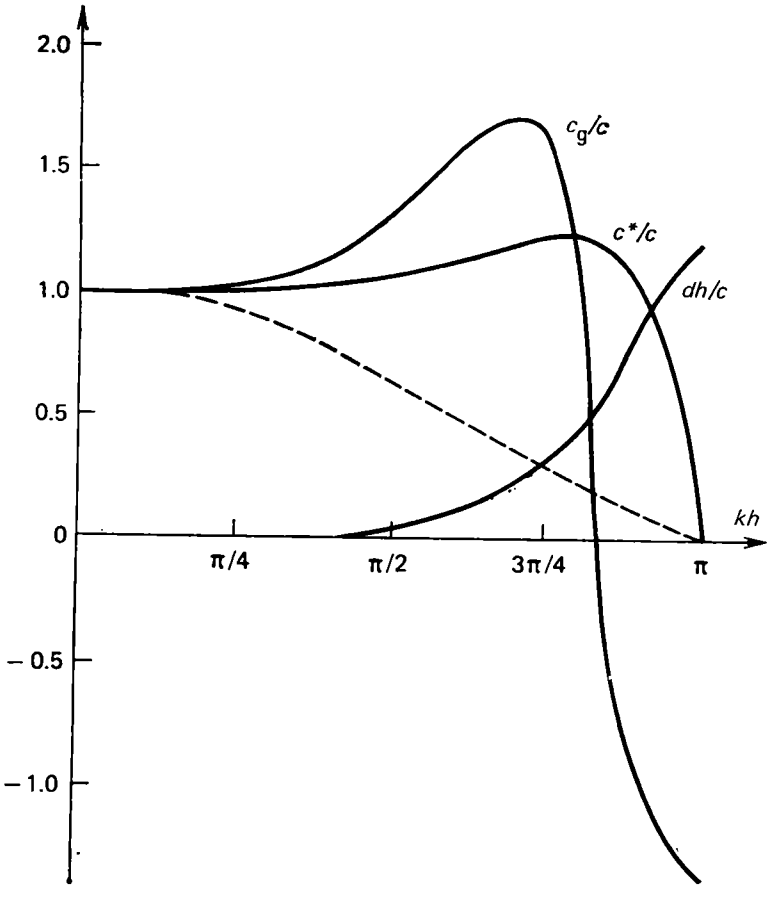

Fig. 5.3. Dispersive and dissipative properties of the third-order approximation.

mesh ω_τ: $t_m = m\tau$. In this case, the difference form $\langle \partial u/\partial t \rangle$ must ensure a stable algorithm for solving the ordinary differential equation (5.2.4.3).

Let us consider, for example, a family of three-deck schemes of the form

$$\alpha_1 u_n^{m+1} + \alpha_2 u_n^m + \alpha_3 u_n^{m-1} + \frac{c\tau}{h} A^{-1}\Delta\,(\beta_1 u_n^{m+1} + \beta_2 u_n^m + \beta_3 u_n^{m-1}) = 0, \tag{5.2.4.6}$$

where a part of the coefficients α_i and β_i $(i = 1, 2, 3)$ is chosen from the condition of approximation of the order $O(\tau^l)$, $l \leqslant 2$, while the other part remains free. A peculiar feature of such schemes

consists in that even for an "explicit" approximation ($\beta_1 = 0$), the inversion of the operator A is required for calculating the mesh function on the $(m+1)$th level. Practically, this can be done in the following way. We denote by Y_n the terms of the form $A^{-1}\Delta \times (\beta_2 u_n^m + \beta_3 u_n^{m-1})/h$. Then for Y_n we have a three-point difference equation of the type $AY_n = \Delta(\beta_2 u_n^m + \beta_3 u_n^{m-1})/h$, which can be easily solved by the method of sweeps. The obtained mesh function Y_n, being substituted into (5.2.4.6), immediately yields u_n^{m+1} $(n = 1, 2, \ldots, N)$. Another method consists in multiplying (5.2.4.6) by A and solving three-point equations for the complex $(\alpha_1 u_n^{m+1} + \alpha_2 u_n^m + \alpha_3 u_n^{m-1})$.

An alternative to schemes (5.2.4.6) is two-deck schemes (with the operators $A^{-1}\Delta$) which are similar to the Lax-Wendroff schemes. Expanding the function u into a series in τ with respect to the value $t = t_m$ and replacing the time derivatives by spatial derivatives, we can obtain from the initial equation a conditionally stable scheme of the type

$$\frac{u_n^{m+1} - u_n^m}{\tau} + \frac{c}{h} A^{-1}\Delta u_n^m - \frac{\tau c^2}{2h^2}\Delta_2 u_n^m = 0, \qquad (5.2.4.7)$$

having the error of the order $O(\tau^2 + h^3 + \tau h^2)$. For realizing this scheme, a three-point sweep is required with the inversion of the operator A. In this case, the mesh function $z_n = A^{-1}\Delta u_n^m$ is first determined, after which we find $u_n^{m+1} = u^m - (\tau c/h)\, z_n + \tau (c/h)^2\, \Delta_2 u^m/2$.

Scheme (5.2.4.7) is inferior to the above implicit schemes (for example, schemes (5.2.4.6) for $\alpha_3 = \beta_3 = 0$, $\alpha_1 = 1/\tau$, $\alpha_2 = -1/\tau$, $\beta_1 = \sigma$, $\beta_2 = 1 - \sigma$, $\sigma \geqslant 0.5$) in the stability margin, since it is only conditionally stable. However, for multidimensional problems which are solved by using computers with vector or matrix processors, operators A corresponding to different spatial directions can be inverted simultaneously rather than consecutively as in the case of implicit splitting schemes. Moreover, such an inversion may turn out to be preferable to the inversion of operators of the type $A + (\tau/h)\, c\, \Delta$ in implicit schemes $(\beta_1 \neq 0)$.

3. Substituting the solutions of the form $u_n^m = \lambda^m e^{i\alpha n}$, $0 \leqslant \alpha \leqslant 2\pi$ into schemes of the type (5.2.4.6), (5.2.4.7) or into some other schemes with the operators $A^{-1}\Delta$ (for example, implicit schemes (5.2.1.5)), we obtain the expressions for phase and amplitude errors determined both by approximations over the space and discretization of the time derivative. These errors may deteriorate the estimates (5.2.4.6). To avoid this, the order of approximation of a scheme with respect to the step τ should be increased. This can be done with the help of the following heuristic considerations.

Suppose that

$$\langle \partial u/\partial t \rangle = \left(\frac{\partial u}{\partial t}\right)_{t=t_m} + \gamma \tau^q \frac{\partial^{q+1} u}{\partial t^{q+1}} + O(\tau^{q+1}),$$

where γ is a certain coefficient. Then, replacing dv/dt in (5.2.4.3) by the approximation $\langle dv/dt \rangle$, we obtain after the substitution $v = e^{-i\omega t}$ the following dispersion relation for the differential approximation:

$$-i\omega + \gamma\tau^q (-i\omega)^{q+1} + \frac{c}{h} W_0(kh) + i\frac{c}{h} W_1(kh) = 0. \tag{5.2.4.8}$$

The ratio ω/k from this relation is given by the equation

$$-\left(\frac{\omega}{k}\right) - \gamma\left(-\frac{\tau\alpha}{h}\right)^q \left(\frac{\omega}{k}\right)^{q+1} i^q + cW_1(\alpha)/\alpha - icW_0(\alpha)/\alpha = 0. \tag{5.2.4.9}$$

Assuming that for small α the second term in this equation is a small correction to the value $\omega/k = cW_1(\alpha)/\alpha$ (formula (5.2.4.5)), we obtain the estimate $c_* = cW_1(\alpha)/\alpha + O(\alpha^q)$ for the phase velocity $c_* = \operatorname{Re} \omega/k$. The imaginary part of ω determines the contribution to the scheme dissipation.

A more detailed analysis of relation (5.2.4.9) leads to the following table for amplitude and phase errors, introduced by the time discretization with the error $O(\tau^q)$:

Approximation order	Amplitude errors	Phase errors
q is even	—	$O(\alpha^q)$
q is odd	$O(\alpha^{q+1})$	$O(\alpha^{2q})$

This table shows that the estimates (5.2.4.6) will not be distorted upon a transition to a difference scheme on the mesh $\omega_\tau \times \omega_h$ if the order of this scheme with respect to the step τ is not lower than the third. In particular, it is sufficient to use scheme (5.2.1.9) of the order $O(\tau^3 + h^3)$ [5.9]. For this scheme $\alpha_1 = 1$, $\alpha_2 = -1$, $\alpha_3 = 0$, $\beta_1 = 5/12$, $\beta_2 = 8/12$, and $\beta_3 = -1/12$. The choice of the coefficients α_i and β_i ($i = 1, 2, 3$) corresponds to Adams' method for ordinary differential equations. Such a scheme will only be conditionally stable.

Another way consists in the application of the methods of improving the accuracy with respect to the step τ using different meshes for calculations [5.18]. This way seems to be more promising due to two circumstances. Firstly, it permits calculations with large steps τ

by using absolutely stable algorithms (for example, in multidimensional cases, the schemes based on the idea of splitting [5.19, 5.20]). Secondly, it permits additional parallel computation while using modern computers.

5.3. COMPACT SCHEMES FOR EQUATIONS CONTAINING DIFFUSIVE TERMS

5.3.1. Construction of Difference Schemes

1. Let us consider a system of equations with second-order derivatives of the form

$$\frac{\partial \mathbf{u}}{\partial t}+\frac{\partial \varphi(\mathbf{u}, x)}{\partial x}=\frac{\partial}{\partial x} \mu \frac{\partial \mathbf{u}}{\partial x}+\mathbf{F}, \tag{5.3.1.1}$$

which differs from (5.2.3.1) in that it contains diffusive terms with a positive $p \times p$ matrix μ on its right-hand side. By introducing a new vector function of "fluxes" $q = \partial \mathbf{u}/\partial x$, we write (5.3.1.1) in the form of a system of $2p$ first-order equations:

$$\begin{aligned} &\frac{\partial \mathbf{u}}{\partial t}+\frac{\partial \varphi}{\partial x}-\frac{\partial \mu \mathbf{q}}{\partial x}=\mathbf{F}, \\ &\frac{\partial \mathbf{u}}{\partial x}=\mathbf{q}. \end{aligned} \tag{5.3.1.2}$$

Limiting ourselves to a two-level scheme of the order $O(\tau + h^3)$, we shall approximate (5.3.1.2) in the following manner. We write the difference analogue of the first equation in (5.3.1.2) with the help of operators

$$\begin{aligned} &B=A_0-0.25\Delta_0 M, \\ &C=(\Delta_0-\Delta_-(T_{1/2}M)\,\Delta_+)/2h, \end{aligned} \tag{5.3.1.3}$$

used in scheme (5.2.3.6). They are completely determined by "convective" terms $\partial\varphi/\partial x$ in (5.3.1.1). When approximating the second equation in (5.3.1.2), we apply conjugate operators B^* and C^*. Then the scheme of the order $O(\tau + h^3)$ for (5.3.1.1) will be written in the form [5.14]

$$\begin{aligned} &B\frac{\mathbf{u}^{m+1}-\mathbf{u}^m}{\tau}+C(\varphi^{m+1}-\mu\mathbf{q}^{m+1})=B\mathbf{F}, \\ &\widetilde{C}\mathbf{u}^{m+1}-\widetilde{B}\mathbf{q}^{m+1}=0, \quad \widetilde{C}=-C^*, \quad \widetilde{B}=B^*. \end{aligned} \tag{5.3.1.4}$$

In scalar case ($p = 1$), the operator pair from (5.2.1.1) is used for approximating the first equation in (5.3.1.2) in accordance with the sign of the derivative φ'_u while the second equation from (5.3.1.2) is approximated by the second pair of operators from (5.2.1.1).

For investigating the stability of scheme (5.3.1.4) for constant matrices K and μ it is convenient to eliminate vector $\mathbf{q}^{m+1}$ from the second equation in (5.3.1.4) by writing the scheme for $F = 0$ in a more general form

$$[E + \tau\sigma(NK + V)]\frac{\mathbf{u}^{m+1} - \mathbf{u}^m}{\tau} + (NK + V)\mathbf{u}^m = 0, \tag{5.3.1.5}$$

where $0 \leqslant \sigma < 1$ is the weight factor, $N = B^{-1}C$, and $V = B^{-1}C\mu\,(B^*)^{-1}C^*$. The fact that the operator NK is positive follows from the chain of equalities $(B^{-1}CK\mathbf{u}, \mathbf{u}) = (CK\mathbf{u}, B^{*-1}\mathbf{u}) = (CKB^*\mathbf{v}, \mathbf{v}) = (B^*CK\mathbf{v}, \mathbf{v})$ where $\mathbf{v} = B^{*-1}\mathbf{u}$, and from the third inequality in (5.2.3.10). The fact that the operator V is positive and self-conjugate can also be easily established. Thus, the operator $A_1 = NK + V$ is positive. Hence scheme (5.3.1.5) is absolutely stable in the norm $\|\cdot\|_H$ for $\sigma \geqslant 0.5$ as a scheme with weights [5.14]. Multiplying (5.3.1.5) by $A_1^* = (NK + V)^*$, we arrive at a scheme of the form (5.2.3.11) where $\mathscr{A} = A_1^*A_1^*$, $\mathscr{B} = A_1 + \tau\sigma A_1^*A_1$. Thus, for $\sigma \geqslant 0.5$, the stability takes place in the norm $\|\cdot\|_{A_1^*A_1}$ as well.

2. In the scalar case ($p = 1$), the difference equations (5.3.1.4) can be easily solved after the function φ has been linearized. It is only necessary to formulate the difference boundary conditions for $i = 1$ and $i = N$ for the system

$$A_i\mathbf{Z}_{i-1} + B_i\mathbf{Z}_i + C_i\mathbf{Z}_{i+1} = d_i \quad (i = 2, 3, \ldots, N - 1) \tag{5.3.1.6}$$

where $\mathbf{Z} = (u, q)$, A_i, B_i and C_i are the 2×2 matrices, and d_i is the two-component vector. Then we can show that with an "appropriate" choice of the boundary conditions, system (5.3.1.6) will be well-defined in the sense [5.16], and the sweep method used for its solution is stable.

If, however, $p > 1$, the dimension $2p \times 2p$ of matrices in (5.3.1.6) leads to a considerable increase in the number of arithmetic operations in the calculation of sweep coefficients in comparison with the case of hyperbolic systems ($\mu \equiv 0$). There are several ways of using the inversion of matrices of dimensions not higher than $p \times p$ in the algorithm. One of these methods consists in the following.

Instead of scheme (5.3.1.4), we write the scheme

$$(B + \tau kD)\frac{\mathbf{u}^{m+1} - \mathbf{u}^m}{\tau} + C(\varphi^{m+1} - \mu\mathbf{q}^m) = B\mathbf{F}$$

$$\widetilde{C}\mathbf{u}^m - \widetilde{B}\mathbf{q}^m = 0, \tag{5.3.1.4a}$$

where $Df = \Delta_+(T_{1/2}\mu)\,\Delta_- f = [\mu_{i+1/2}(f_{i+1} - f_i) - \mu_{i-1/2}(f_i - f_{i-1})]/h^2$ is the "traditional" approximation of diffusive terms, and k is a certain coefficient.

Scheme (5.3.1.4a) differs from scheme (5.3.1.4) in the terms of the order $O(\tau)$ and coincides with it in the case of a steady solution. When employing this scheme, we must first determine the vector $\mathbf{q}^m$ from the second equation in (5.3.1.4a) and then find the required vector $\mathbf{u}^{m+1}$ from the first equation in (5.3.1.4a). At each of these stages, we must solve three-point vector equations with $p \times p$ matrices.

When estimating the stability of scheme (5.3.1.4a) in the case of constant matrices, we write it in a form similar to (5.3.1.5):

$$(E + \tau\sigma NK + \tau kW)\frac{\mathbf{u}^{m+1} - \mathbf{u}^m}{\tau} + (NK + V)\,\mathbf{u}^m = 0. \tag{5.3.1.7}$$

Here $W = -B^{-1}\mu\Delta_2 = B^{-1}\mu C^*C$. Multiplying (5.3.1.7) by $A_1^* = (NK + V)^*$, having transformed the expression in the first parentheses we obtain the following equality:

$$[A_1^* + A_1^*A_1 + A_1^*(kW - \sigma V)]\,\frac{\mathbf{u}^{m+1} - \mathbf{u}^m}{\tau} + A_1^*A_1\mathbf{u}^m = 0. \tag{5.3.1.8}$$

This scheme is absolutely stable in $\|\cdot\|_{A_1^*A_1}$ if the last term in the brackets is positive. If the matrices μ and K (and hence μ and M) commute, it can be shown by direct calculations using the properties (5.2.3.10) of the operators appearing in this term that the inequality $A_1^*(kW - \sigma V) > 0$ holds when

$$k \geqslant 3\sigma. \tag{5.3.1.9}$$

The matrices μ and K are undoubtedly commutative in the scalar case ($p = 1$), when the absolute stability of (5.3.1.7) under the condition (5.3.1.9) can be easily established by the Fourier method as well.

In cases of practical importance (such as viscous fluid flows), the matrices μ and k are noncommutative. Moreover, they are varying and may depend on the solution at any instant of time. Therefore, the above substantiation of stability of scheme (5.3.1.6), like similar substantiations described in this work, is of estimating nature. However, under appropriate boundary conditions, the scheme is expected to have sufficient stability "margin" making it possible to perform calculations for large ratios τ/h.

3. Let us consider a simplified version of scheme (5.3.1.4) which is realized by three-point sweeps by $p \times p$ matrices. Instead of approximating the third-order diffusive term in (5.3.1.1), we introduce the conventional approximation of the second derivatives by using the operator D from (5.3.1.6). In this case, the difference scheme for (5.3.1.1) will have the form

$$(B + \tau D)\frac{\mathbf{u}^{m+1} - \mathbf{u}^m}{\tau} + C\varphi^{m+1} + D\mathbf{u}^m = B\mathbf{F}. \tag{5.3.1.10}$$

It can be easily established that this scheme has the order of accuracy $O(\tau + h^3 + h \| \mu \|)$. The meaning of such an approximation consists in the following. Terms of the order $O(h)$ appear as a result of introducing the operator D for the diffusive term and are not the "scheme" viscosity. For $\mu \equiv 0$ they vanish. When the elements of matrix μ are small (for example, for the equations of motion for a low-viscosity medium), the terms of the order $O(h)$ are also small, at least outside the domains in which the function varies rapidly (such as boundary layers or shock waves). If the first approximation for diffusive terms in these domains is admissible, the advantage in scheme (5.3.1.10) may be advantageous in that a more exact representation of the solution is possible for a considerable part of the computational domain as compared to lower-order schemes.

In the commutative case, the absolute stability of (5.3.1.10) can be easily proved: the corresponding equation with constant matrices differs from (5.3.1.5) only in that the positive operator $W = -B^{-1}\mu\Delta_2$ is used in it instead of the positive operator V.

5.3.2. Examples of Calculations for Equations with Small Coefficients of the Diffusive Terms

1. The effect of combined application of adaptable meshes and higher-accuracy schemes becomes especially noticeable in the numerical solution of equations with small coefficients of the second derivatives [5.16].

Let the coefficient μ in (5.3.1.1) be so small that regions of the type of shock waves or boundary layers with characteristic sizes of the order $O(\mu)$ may appear in the computational domain. In this case, the application of higher-accuracy schemes for a direct approximation of (5.3.1.1) may turn out to be not very effective. Indeed, for kth-order schemes the approximation error at some node can be represented in the form $C_k h^k$, where the constant C_k depends on higher-order derivatives $\partial u^l/\partial x^l$ $(l > k)$ of the exact solution of (5.3.1.1). For small μ's we can expect that owing to high values of these derivatives, the inequality $C_2 h^2 < C_k h^k$, $k > 2$, will be satisfied for a certain interval h. This inequality indicates that for $k > 2$ the error in the schemes will be larger than for second-order schemes.

While constructing the effective "stretching" transformation $\xi(x)$ which ensures the "resolution" of the domains having small characteristic sizes, we can hope that the derivatives $\partial u^l/\partial \xi^l$ will be uniformly bounded in l (for example, they will be equal to zero for $\xi = u$) or at least they will not increase very rapidly with l. Then we can expect that for real steps h the inequality $C_k h^k < C_2 h^2$ will be fulfilled.

For $\xi(x)$ we can use transformations adaptable to the solution [5.4, 5.15, 5.17, 5.18].

Let us introduce a new variable ζ of the form [5.4, 5.15]

$$\zeta = \psi(u) + bx, \quad \zeta(x_0) = 0, \quad \zeta(x_N) < 1, \quad b > 0, \quad (5.3.2.1)$$

where x_0 and x_N are the boundaries of the computational domain $x_0 \leqslant x \leqslant x_N$. Then Eq. (5.3.1.1) can be written in the form

$$\frac{\partial}{\partial t}\left(\frac{u}{\chi} + \frac{1}{b}\frac{\partial \psi_1}{\partial \zeta}\right) + \frac{\partial \varphi(u)}{\partial \zeta} = \frac{\partial}{\partial \zeta}\mu\chi\frac{\partial u}{\partial \zeta} + \frac{p}{\chi}, \quad (5.3.2.2)$$

where

$$\psi_1 = \int \psi^1(u)\, u\, du, \quad \chi = \frac{\partial \zeta}{\partial x}, \quad \chi^{-1} = \left(1 - \frac{\partial \varphi}{\partial \zeta}\right) b^{-1}.$$

If we are interested only in the steady solution of (5.3.2.2), then instead of (5.3.2.2) it is expedient to consider the equation

$$\frac{\partial u}{\partial t} + \frac{\partial \varphi(u)}{\partial \zeta} = \frac{\partial}{\partial \zeta}\mu\chi\frac{\partial u}{\partial \zeta} + \frac{F}{\chi}, \quad (5.3.2.3)$$

which has the form (5.3.1.1).

For approximating Eq. (5.3.2.3) on the mesh $\omega = \omega_\tau \times \omega_h$ (ω_h: $x_i = i(x_N - x_0)/N$), we use the scheme (5.3.1.4), supplementing it by the equality

$$\chi^{m+1} = b\left[1 - \left(\frac{\partial \psi}{\partial \zeta}\right)^m\right]^{-1},$$

which allows us to determine the "Jacobian" χ on each time step.

2. For solving three-point vector equations (5.3.1.6) for the vector $\mathbf{z}_i = (u_i, q_i)_i$ ($i = 0, 1, \ldots, N$), we must know the boundary conditions for the mesh function q_i (the values u_0 and u_N are assumed to be known from the formulation of the mathematical problem). Let us point out one of the possible constructions of the difference boundary conditions for q, which has been used in calculations [5.16]. We shall derive the conditions, for example, for $x = x_0$ (i.e. $\zeta = 0$).

Suppose that $\operatorname{sgn} \varphi'(u_1^m) < 0$ at node $\zeta_1 = h$. Then for $i = 1$ we can interpret the first equation in (5.3.1.4), approximated by using the operator A, as the balance equation for fluxes across a one-dimensional cell $h \leqslant \zeta \leqslant 2h$, while the second equation in (5.3.1.4) is treated as the balance equation for fluxes across the cell $0 \leqslant \zeta \leqslant h$. Writing the balance equation for fluxes across the cell $0 \leqslant \zeta \leqslant h$ in the form of the first equation in (5.3.1.4), but using the operator A_+, we obtain the relation

$$q_1^{m+1} - q_0^{m+1} = \varphi(u_1^{m+1}) - \varphi(u_0^{m+1})$$

$$+ hA\left[\left\langle\frac{\partial u}{\partial t}\right\rangle^{m+1} - \frac{p}{\chi}\right]_1^{m+1} = 0. \quad (5.3.2.4a)$$

Conversely, if $\operatorname{sgn} \varphi'(u_1^m) \geqslant 0$, the second equation in (5.3.1.4) can be interpreted as the balance equation for flows through the cell $h \leqslant \zeta \leqslant 2h$. Writing this equation for the cell $0 \leqslant \zeta \leqslant h$ with the help of the operator A_+, we obtain the relation

$$(q/\mu\chi)_1^{m+1} = (u_1^{m+1} - u_0^{m+1})/h. \qquad (5.3.2.4b)$$

Similarly, we can formulate the conditions for $x = x_N$ (i.e. $\zeta = 1$). It should be noted that in some cases one of the boundaries (e.g. $\zeta = 1$) lies in the domain where the function u is practically "unperturbed" ($u = \text{const}$). Then the condition $q_N = 0$ may turn out to be acceptable.

Conditions (5.3.2.4a) and (5.3.2.4b) at $\zeta = 0$ and the similar conditions at $\zeta = 1$ can be written in the form

$$P_0\mathbf{z}_0 + Q_0\mathbf{z}_1 + R_0\mathbf{z}_2 = \mathbf{l}_0, \quad P_1\mathbf{z}_{N-2} + Q_1\mathbf{z}_{N-1} + R_1\mathbf{z}_N = l_1, \qquad (5.3.2.5)$$

where P_j, Q_j, and R_j are 2×2 matrices, and $\mathbf{l}_j$ are two-component vectors ($j = 0, 1$).

An analysis of the boundary conditions for (5.2.3.4) in the "frozen" coefficient approximation showed that these conditions satisfy the Babenko-Gelfand stability criterion [5.17] if for the mesh function we take the pair $(u, q)_i$. We can also demonstrate that the corresponding systems of difference equations are well-defined.

3. By way of an example, let us consider some model problems [5.16].

Bürgers' equation. We put in (5.3.1.1) $\varphi(u) = u^2/2$, $\mu(u, x) = \nu = \text{const} > 0$, $F = 0$. Substituting $x_1 = x - t/2$, we arrive at the equation

$$\frac{\partial u}{\partial t} + \frac{\partial}{\partial x_1}\left(\frac{u^2}{2} - \frac{u}{2}\right] = \nu \frac{\partial^2 u}{\partial x_1^2}. \qquad (5.3.2.6)$$

Since we are interested in the steady solution of this equation with the boundary conditions $u(-\infty) = 1$ and $u(\infty) = 0$, we apply the transformation of the type (5.3.2.1) with $\psi(u) = au$, $a = \text{const}$, preliminarily replacing the infinite range of variation of x_1 by a finite one. For small values of ν it is sufficient, for example, to consider the interval $-1 \leqslant x_1 \leqslant 1$ by mapping it onto the interval $-1 \leqslant \zeta \leqslant 1$.

Figure 5.4 and Table 5.1 present some results of calculations for the scheme (5.3.1.4) with the boundary conditions (5.3.2.4). It follows from Fig. 5.4 that irrespective of the value of ν, the function $u(\zeta)$ determines the characteristic thickness of the "shock wave" $\Delta\zeta = O(1)$, which corresponds to the thickness $\Delta x_1 = O(\nu)$ on the physical plane. The actual value of $\Delta\zeta$ depends on the relation $b/a = C$ in (5.3.2.1) which is defined quite arbitrarily. The contri-

Table 5.1

$h = 0.1$				$h = 0.025$				
ζ	$x_1(\zeta)$	$u(\zeta)$	$u'_{x_1}(\zeta)$	ζ	$x_1(\zeta)$	$u(\zeta)$	$u_e(x_1)$	$u'_e(x_1)$
−0.0	0.0000	0.50000	125.092	0.00000	0.50000	124.999	0.50000	125.000
−0.1	0.000467	0.55997	123.296	0.000482	0.55995	123.202	0.56002	123.198
−0.2	0.000968	0.61992	117.902	0.000979	0.61990	117.810	0.62004	117.795
−0.3	0.00149	0.67986	108.915	0.00150	0.67984	108.826	0.68003	108.792
−0.4	0.00208	0.73980	96.337	0.00209	0.73979	96.249	0.74001	96.196
−0.5	0.00276	0.79973	80.168	0.00277	0.79972	80.082	0.79995	80.014
−0.6	0.00359	0.85965	60.414	0.00362	0.85963	60.329	0.85983	60.259
−0.7	0.00443	0.91956	37.071	0.00487	0.91951	37.003	0.91961	36.962
−0.8	0.00721	0.98482	7.55180	0.00741	0.97925	10.154	0.97603	11.693
−0.9	0.39785	1.00021	0.92862	0.39995	1.00000	0.92870	1.00000	0.00000
−1.0	1.00000	1.00000	0.02346	1.00000	1.00000	0.03662	1.00000	0.00000

bution from the physical coordinate x_1 to ζ (u, x_1) increases and the value of $\Delta\zeta$ decreases with increasing C. The accuracy of the method is illustrated in Table 5.1 which presents the values of x_1 (ζ), u (ζ),

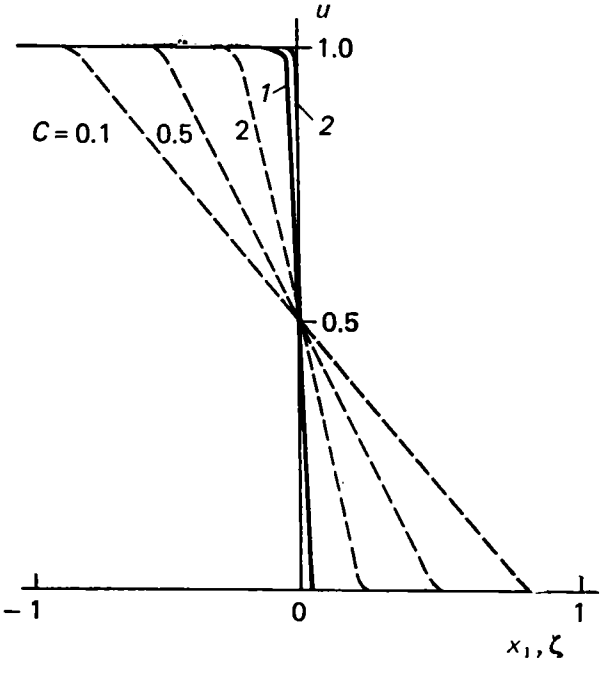

Fig. 5.4. Solution of Bürgers' equations: (*1*) $\nu = 0.01$, (*2*) $\nu = 0.001$.

and $u'_{x_1}(\zeta)$ on the interval $-1 \leqslant \zeta \leqslant 0$, obtained for $\nu = 10^{-3}$, $C = 0.1$ and $h = 0.1$, 0.025 (in the latter case, the exact values of $u_e(x_1)$ and $u'_e(x)$ are also given). Even for $h = 0.1$, the coincidence

with the case of $h = 0.025$ is attained in almost entire range to 3-4 significant digits both for the functions and their derivatives. A certain decrease in accuracy is observed near the asymptote ($\zeta \simeq 0.9$ at $C = 0.1$), where higher-order derivatives of $u(\zeta)$ become large.

Couette flow with injection. We put $F = \partial p/\partial x$, $\mu(u, y) = \mathrm{Re}^{-1}$, $\varphi(u) = v_0 u$, where the constants F, v_0, and Re are the longitudinal pressure gradient, injection velocity, and Reynolds number respectively. The role of the coordinate x in (5.3.1.1) is played by the

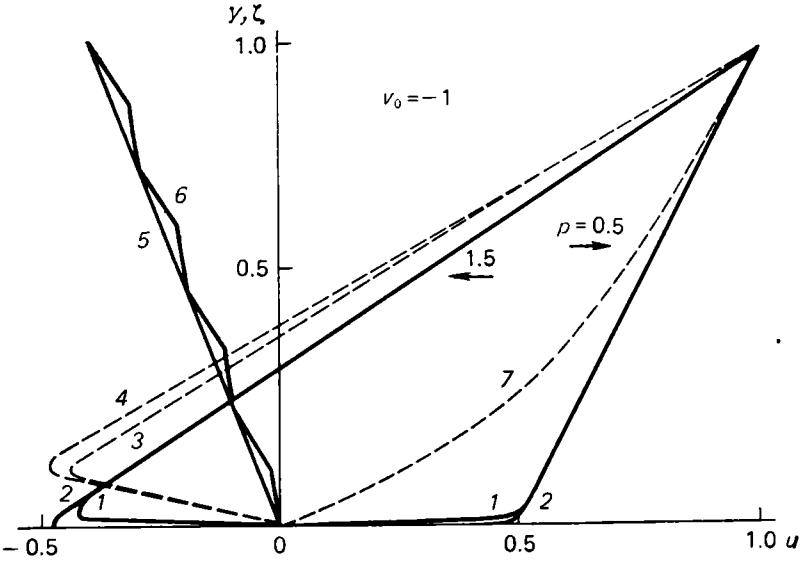

Fig. 5.5. Couette flow with injection. (*1*), (*3*) $\mathrm{Re} = 10^2$, (*2*), (*4*) $\mathrm{Re} = 10^3$, (*5*), (*6*) $u(\zeta/20)$; (*1*), (*2*) $u(y)$, (*3*), (*4*) $u(\zeta)$, (*6*) fourth-order implicit scheme, (*7*) $u(\zeta)$, $\mathrm{Re} = 10^2$, 10^3.

y-coordinate which is normal to the surface. The boundary conditions have the form $u(0) = 0$, $u(1) = 1$.

In accordance with the exact solution of this problem, a boundary layer of thickness $O(\mathrm{Re}^{-1})$ is formed either on the fixed wall $y = 0$ ($v_0 < 0$), or on the movable wall $y = 1$ ($v_0 > 1$). Depending on the values of F, velocity profiles may be either monotonic or with well-pronounced extrema (Fig. 5.5). Assuming that we know nothing about the position and dimensions of the boundary layer, we shall use transformation (5.3.2.1) with the linear function $\psi(u)$ and constants that depend on the monotonicity interval for the function $u(y)$ [5.15].

Figure 5.5 shows the results of calculations for two typical cases of a monotonic profile ($F = 0.5$) and "return" flow ($P = 1.5$). As in the previous example, the functions $u(\zeta)$ weakly depend on the

parameter Re ($10^{-2} \leqslant \mathrm{Re}^{-1} \leqslant 10^{-3}$, and the boundary layer thickness in the computational domain has the order $O(1)$.

Table 5.2 presents the values of $y(\zeta)$, $u(\zeta)$, and $u'_y(\zeta)$ for some typical values of ζ together with the exact values $u_e(y)$ and $u'_e(y)$. These data were obtained for $\mathrm{Re}^{-1} = 10^{-3}$, $h = 0.025$ and $v_0 = 1$

Table 5.2

ζ	$y(\zeta)$	$u(\zeta)$	$u'_y(\zeta)$	$u_e(y)$	$u'_e(y)$
0.000	0.00000	0.00000	—498.50	0.00000	—498.50
0.025	0.000219	—0.09854	—399.62	—0.09820	—399.96
0.050	0.000500	—0.19696	—300.78	—0.19589	—301.86
0.075	0.000881	—0.29518	—201.99	—0.29144	—205.73
0,100	0.000505	—0.39490	—102.83	—0.19778	—299.96
0.125	0.00258	—0.48976	—4.8596	—0.45848	—36.139
0.150	0.03827	—0.46142	—2.0336	—0.44259	1.50000
0.175	0.06112	—0.40768	0.87417	—0.40831	1.50000
0.200	0.08987	—0.36562	1.94439	0.36518	1.50000
0.250	0.14667	—0.28009	1.60525	0.27999	1.50000
0.300	0.20353	—0.19472	1.52637	—0.19469	1.50000
0.400	0.31731	—0.02403	1.50112	—0.02403	1.50000
0.500	0.43109	—0.146640	1.49934	0.146641	1.50000

for the most "unfavourable" of the above cases, when $P = 1.5$, significant computational errors may be expected. In accordance with Table 5.2, a considerable decrease in accuracy is observed in the region where the derivative u_ζ changes sign ($\zeta \simeq 0.13$, Fig. 5.5). Here the value of y even "falls out" of a monotonic sequence of the values of y due to inaccurate results for u (0.1). This behaviour of the solution of the difference problem can be explained by large values of higher-order derivatives in this region. Besides, it can be due to a variation of the transformation constants upon a transition from one monotonicity interval to another. However, the functions and their derivatives are calculated with a sufficiently high degree of accuracy in the remaining part of the computational domain.

Table 5.3 contains the results of calculations of a version of Table 5.2 for a smaller step $h = 0.0125$. These data point towards a noticeable increase in accuracy everywhere, in particular, in the "unfavourable" region mentioned above. It should be noted that in contrast to the case of the monotonic profile of u in Table 5.1, a comparison of the data contained in Tables 5.2 and 5.3 for the same values of ζ is ineffective since the extremal values of u, and

Table 5.3

ζ	$y(\zeta)$	$u(\zeta)$	$u'_y(\zeta)$	$u_e(y)$	$u'_e(y)$
0.0000	0.00000	0.00000	—498.50	0.00000	—498.50
0.0125	0.000104	—0.04924	—449.10	—0.04923	—449.11
0.0250	0.000220	—0.09846	—399.70	—0.09843	—399.73
0.0375	0.000351	—0.14765	—350.31	—0.14759	—350.37
0.0500	0.000502	—0.19680	—300.93	—0.19670	—301.04
0.0625	0.000680	—0.24590	—251.57	—0.24573	—251.74
0.0750	0.000896	—0.29492	—202.22	—0.29462	—202.52
0.0875	0.00117	—0.34383	—152.90	—0.34322	—153.51
0.1000	0.00154	—0.39255	—103.63	—0.39082	—105.36
0.1125	0.00176	—0.44157	—54.286	—0.41130	—84.556
0.1250	0.00277	—0.48901	—5.3229	—0.46475	—2.9578
0.1375	0.02186	—0.47731	11.614	—0.46720	1.4999
0.1500	0.03305	—0.44999	1.0788	—0.45041	1.5000
0.1625	0.04746	—0.42904	1.7327	—0.42881	1.5000
0.2000	0.0900	—0.36492	1.4806	—0.36493	1.5000

hence transformation (5.3.2.1), somewhat differ for $h = 0.025$ and $h = 0.0125$.

In addition to the third-order schemes, fourth-order schemes with the operator $A_0 = 0.5\,(A_- + A_+)$ were also used in methodical calculations as well as conventional central-difference schemes. Mesh functions obtained with the help of symmetric schemes exhibited a tendency to oscillations near the surface even for small h's. Figure 5.4 compares the solutions, which correspond to the third- and fourth-order schemes ($h = 0.0125$), near the wall.

Thus, nonsymmetric compact schemes may give quite accurate results when the mesh points are appropriately arranged in the physical plane. The advantage of these schemes over symmetric second-order schemes (even when the accuracy is not taken into account) is a higher monotonicity of solutions, which follows from the scheme "orientation" in accordance with the direction of propagation of perturbations.

5.3.3. Nonsymmetric Compact Schemes with Higher-than-the-third Order of Accuracy

1. The equality $A_{\pm} f^{m+1} = \Delta_{\mp} u^{m+1}/h$ in scheme (5.2.1.15) can be treated as "compact" numerical differentiation formulas which determine the derivative $f = \partial u/\partial x$ with the third order of accuracy. From this point of view, the general family of "compact"

higher-accuracy schemes for the equation

$$\frac{\partial u}{\partial t}+a(u,\ x)\frac{\partial u}{\partial x}=\varepsilon(u,\ x)\frac{\partial^2 u}{\partial x^2} \tag{5.3.3.1}$$

on the mesh $\omega_\tau \times \omega_h$ can be written in the form

$$\left\langle \frac{\partial u}{\partial t}\right\rangle_j^{n+1}+a_j m_j^{n+1}=\varepsilon_j M_j^{n+1}, \tag{5.3.3.2a}$$

$$P_1 m^{n+1}=D_1 u^{n+1}/h^2,\quad P_2 M^{n+1}=D_2 u^{n+1}/h^2, \tag{5.3.3.2b}$$

where P_1 and P_2 are the three-point operators and D_1 is the operator of either central difference or two-point one-sided difference. For central differences, we obtain symmetric schemes of the type [5.1-5.3], while for $P_1 = A_\pm$ we get the nonsymmetric schemes considered above.

The operators P_2 and D_2 may be quite different for different schemes. For example, for the fourth-order schemes the relation

$$Q_0 M=\Delta_2 u/h,\quad Q_0 M=(M_{j-1}+10M_j+M_{j-1})/12, \tag{5.3.3.3}$$

is widely used. It can be obtained, for example, on the basis of Hermite interpolation polynomials or spline approximations. For a scheme of the type (5.3.1.4) we have $P_2 = A$, $D_2 = \widetilde{A}^{-1}\Delta_2$.

The family of schemes (5.3.3.2) is a particular case of a more general class of compact schemes up to and including the sixth order of accuracy, which is obtained by replacing (5.3.3.2b) by the equalities

$$P_1 m^{n+1}+Q_1 M^{n+1}=D_1 u^{n+1}/h,\ P_2 m^{n+1}+Q_2 M^{n+1}=D_2 u^{n+1}/h^2. \tag{5.3.3.2c}$$

Approximations (5.3.3.2a) and (5.3.3.2c) contain both known and new schemes.

2. For determining the form of the operators P_1, Q_1, P_2, Q_2, we introduce "compact" numerical differentiation formulas of the form

$$\begin{aligned}&\sum_{i=1}^{3}\alpha_i^{(1)}m_i+\sum_{i=1}^{3}\beta_i^{(1)}M_i=0.5\,(\Delta_0-s\Delta_2)\,u/h,\\ &\sum_{i=1}^{3}\alpha_i^{(2)}m_i+\sum_{i=1}^{3}\beta_i^{(2)}M_i=\Delta_2 u/h^2,\end{aligned} \tag{5.3.3.4}$$

where $\alpha_i^{(1)}$ and $\beta_i^{(1)}$ $(i = 1, 2, 3)$ are the coefficients which are unknown so far, and the values $s = 0, 1, -1$ correspond to central, left, and right differences determined by the operator $0.5\,(\Delta_0 - s\Delta_2)$. In order to find $\alpha_i^{(j)}$ and $\beta_i^{(j)}$, we shall use the method of indeterminate coefficients (see, for example [5.30]) and require that equalities (5.3.3.4) be satisfied identically for $u = x, x^2, \ldots, x^6$ (the case $u = x^0$ leads to trivial relations). Having solved the system of linear

equations for $\alpha_i^{(j)}$, $\beta_i^{(j)}$ $(i = 1, 2, 3;\ j = 1, 2)$, we write formulas (5.3.3.4) in the form

$$\left[\left(E + \frac{7}{30}\Delta_2\right) - \frac{3}{16}s\Delta_0\right] m$$

$$+h\left[-\frac{5}{8}\left(E - \frac{1}{6}\Delta_2\right) - \frac{1}{30}\Delta_0\right] M = \frac{1}{2h}(\Delta_0 - s\Delta_2)\, u, \qquad (5.3.3.5)$$

$$\frac{3}{8h}\Delta_0 m + \frac{1}{4}\left(E - \frac{1}{6}\Delta_2\right) M = \frac{\Delta_2 u}{h^2}. \qquad (5.3.3.6)$$

It is interesting to note that if we consider (5.3.3.5) and (5.3.3.6) simultaneously, the terms with the coefficient s in (5.3.3.5) vanish in view of (5.3.3.6). Then formulas (5.3.3.5) and (5.3.3.6) determine for $s = 0$ the approximations m_j and M_j of the derivatives $(\partial u/\partial x)_{x=x_j}$ and $(\partial^2 u/\partial x^2)_{x=x_j}$ with an accuracy up to the order $O(h^6)$. The same result can be obtained on the basis of Hermite interpolation polynomials [5.2].

Using (5.3.3.5), we can construct a nonsymmetric fifth order approximation for the derivative $(\partial u/\partial x)_{x=x_j}$. For this purpose, we shall use the following heuristic considerations. For expressing m_j from (5.3.3.5) so that $m_j = (\partial u/\partial x)_{x=x_j} + O(h^5)$, it is sufficient to use any representation of the form $M_j = (\partial^2 u/\partial x^2)_{x=x_j} + O(h^4)$, since the second term on the left-hand side of (5.3.3.5) contains the factor h. For such a representation, we can use formula (5.3.3.2a) with the operators $P_2 = Q_0$ from (5.3.3.3) and $D_2 = \Delta_2$. This yields the following equality:

$$M_j = \left(E + \frac{1}{12}\Delta_2\right)^{-1} \Delta_2 u/h^2. \qquad (5.3.3.7)$$

Substituting this expression into (5.3.3.5) and multiplying the result by $(E + \Delta_2/12)$, we obtain after simple transformations the relation

$$\left[E + \frac{19}{60}\Delta_2 + \frac{7}{360}\Delta_2^2 - \frac{3}{16}s\Delta_0\left(E + \frac{1}{12}\Delta_2\right)\right] m$$

$$= \left[(-s\Delta_2)\left(\frac{3}{8}E + \frac{1}{16}\Delta_2\right) + \Delta_0\left(\frac{1}{2}E + \frac{3}{40}\Delta_2\right)\right] u/h.$$

Expanding the smooth functions u and $m = (\partial u/\partial x)$ into a Taylor series in the vicinity of the point $x = x_j$, we see that $m_j = (\partial u/\partial x)_{x=x_j} + O(h^5)$.

In actual practice, for determining $(\partial u/\partial x)_{x=x_j}$ with the accuracy of the order $O(h^5)$ and $(\partial^2 u/\partial x^2)_{x=x_j}$ to within $O(h^4)$ for a given function, it is sufficient to solve two three-point difference equations (5.3.3.5) and (5.3.3.3) together (first the second equation and then the first equation) for m_j and M_j.

3. The formulas of numerical differentiation obtained in this way can be used for constructing difference schemes approximating

(5.3.3.1). Here we shall be interested only in nonsymmetric approximations ($s = \mp 1$) which have better properties in many respects than their symmetric counterparts ($s = 0$).

We put $s_j = \operatorname{sgn} a_j$. Considering (5.3.3.2a), (5.3.3.5) for $s = s_j$, and (5.3.3.3) we obtain the spatial approximation of the order $O(h^5 + \max \varepsilon_j h^4)$. For equations without diffusive terms ($\varepsilon \equiv 0$), such a scheme will have the order $O(h^5)$. When $\varepsilon \neq 0$, its order will be formally lowered to fourth. However, this scheme has the following advantages over fourth-order symmetric schemes:

(a) improved monotonicity,

(b) higher accuracy for small values of ε in the domains where the derivatives $\partial^2 u/\partial x^2$ are small.

A practical transition from the mth to $(m+1)$th temporal layer using the scheme (5.3.3.2a), (5.3.3.3) and (5.3.3.5) can be reduced to three-point vector sweeps with 2×2 matrices. For this purpose, it is sufficient, for example, to exclude the mesh function u_j^{m+1} from the basic equation (5.3.3.2a).

The absolute stability of the above scheme for $\langle \partial u/\partial x \rangle^{m+1} = (u^{m+1} - u^m)/\tau$ and constant coefficients $a_j = a$ and $\varepsilon_j = \varepsilon$ can be easily substantiated either by the spectral method or by the method of operator inequalities [5.13]. In the latter case, the proof which will be omitted here, is reduced to writing the scheme in the form

$$[E + \tau(aS + \varepsilon T)] \frac{u^{m+1} - u^m}{\tau} + (aS + \varepsilon T)\, u^m = 0$$

and to establishing the fact that the operators S and T are nonnegative.

The scheme (5.3.3.2a), (5.3.3.3), and (5.3.3.5) can be generalized to systems of equations with symmetric matrices in the same way as third-order schemes.

5.4. HIGHER-ACCURACY ALGORITHMS FOR MULTIDIMENSIONAL PROBLEMS

5.4.1. Approximations of Systems of Equations in Several Spatial Coordinates

1. Let us consider a system of the type

$$\frac{\partial \mathbf{u}}{\partial t} + \sum_{j=1}^{n} \frac{\partial \Phi_j(\mathbf{u}, \mathbf{x})}{\partial x_j} = F(u, \mathbf{x}) \qquad (5.4.1.1)$$

with the corresponding nondivergent system

$$\frac{\partial u}{\partial t} + \sum_{j=1}^{n} K_j \frac{\partial u}{\partial x_j} = F_1(\mathbf{u}, x) \qquad (5.4.1.1a)$$

where the matrices $K_j = \partial\Phi_j/\partial\mathbf{u}$ are symmetric. Let us construct a spatial mesh ω_h with constant steps h_j along each coordinate x_j. We introduce the matrix difference operators B_j and C_j corresponding to the coordinate x_j and having the structure of the type (5.3.1.3):

$$B_j = (A_0^j - 0.25\Delta_0^j M_j), \quad C_j = 0.5\,(\Delta_0^j - \Delta_-^j\,(T_{1/2}^j M_j)\,\Delta_+^j)/h_j.$$

Here the superscript on the operators Δ_0, Δ_-, Δ_+, A_0, and T indicates that an operator belongs to the variable x_j; $M_j = S_j D_j S_j^{-1}$, where S_j and D_j are the matrices appearing in the diagonalization of the matrices K_j.

If all the matrices K_j and M_j were constant, a natural way of approximation of (5.4.1.1) with the third order of accuracy with respect to steps h_j would be the following [5.15]:

$$B\,\frac{\mathbf{u}^{m+1}-\mathbf{u}^m}{\tau} + \sum_{j=1}^{n} G_j \Phi_j^{m+1} = B\mathbf{F}, \qquad (5.4.1.2)$$

where $B = B_1 \ldots B_n$, $G_j = B_1 \ldots B_{j-1} C_j B_{j+1} \ldots B_n$. Indeed, for each operator B_j and C_j the following representation is valid:

$$B_j f = \left(E - \frac{h_j}{2} D_j M_j + \frac{h_j^2}{6} D_j M_j D_j\right) f + O(h_j^3),$$

$$C_j f = \left(E - \frac{h_j}{2} D_j M_j + \frac{h_j^2}{6} D_j M_j D_j\right) D_j + O(h_j^3),$$

where D_j are the operators of differentiation with respect to x_j. Substituting these operators into (5.4.1.2), we see that all the terms in (5.4.1.2) contain products of the type

$$\prod_{j=1}^{n} \left(E - \frac{h_j}{2} D_j M_j + \frac{h_j^2}{2} D_j M_j D_j\right)$$

as factors. The operators D_j can be transposed by putting them in front of Φ_j. Multiplying both sides of the equality thus obtained by

$$\left[\prod_{j=1}^{n} \left(E - \frac{h_j}{2} D_j M_j + \frac{h_j^2}{6} D_j M_j D_j\right)\right]^{-1}$$

we find that (5.4.1.2) differs from (5.4.1.1) in the terms of the order $O(\tau + h_1^3 + h_2^3 + \ldots + h_n^3)$.

In the general case, we can retain the form of (5.4.1.2) by supplementing it with an additional term Ω that takes into account the noncommutative nature of the corresponding operators. In order

to find the form of this term, we note that

$$D_jB_k = B_kD_j + (h_k/2)\, a_{kj} + (h_k^2/6)\, b_{kj}, \qquad (5.4.1.3)$$

where $a_{kj} = (D_kM_kD_j - D_jD_kM_k)$,

$b_{kj} = (D_jD_kM_kD_k - D_kM_kD_kD_j)$.

Let $a_{kj}^{(h)}\Psi$ and $b_{kj}^{(h)}\Psi$ be the second- and first-order approximations of the terms of the type $a_{kj}\Psi$ and $b_{kj}\Psi$ respectively. Then, according to (5.4.1.3), the transposition of the differentiation operator D_j with any other operator B_k with an accuracy of the order $O(h_k^3)$ would not change the order of approximation of the term containing Φ_j, if we supplement the right-hand side of (5.4.1.2) with the term $\omega_{kj}\Phi_j = -(a_{kj}^{(h)}h_k/2 + b_{kj}^{(h)}h_k^2/6)\left(\prod_{i=k+1}^{n} B_i\right)\Phi_j$. Carrying out such transpositions in each term of $\sum_{j=1}^{n} G_j\Phi_j^{m+1}$ until the operator D_j stands in front of Φ_j, we finally find that the scheme (5.4.1.2) has the order $O(\tau + h_1^3 + \ldots + h_n^3)$ if instead of $\mathbf{F}$ we introduce on the right-hand side of (5.4.1.2) $\bar{\mathbf{F}}^{m+1} = \mathbf{F}^{m+1} + \Omega^m$, where

$$\Omega^m = \sum_{j=1}^{n} \frac{1}{k_j} \sum_{k>j}^{n} \{(\Delta_0^k M_k \Delta_0^j - \Delta_0^j \Delta_0^k M_j)/8 + [\Delta_0^j \Delta_-^k (T_{1/2}^k M_k)\, \Delta_+^k$$

$$- \Delta_-^k (T_{1/2}^k M_k)\, \Delta_+^k \Delta_0^j]/12\}\, \Psi_{kj}^m, \qquad \Psi_{kj}^m = \left(\prod_{i=k+1}^{n} B_i\right)\Phi_j. \qquad (5.4.1.4)$$

The term Ω contains the values of the functions Φ_j ($j = 1, 2, \ldots, n$) at three points in each spatial direction x_j. This term vanishes for constant matrices M_j and hence is not considered while analyzing the stability of the scheme in the "frozen coefficients" approximation.

2. Let us consider another way of utilizing the operators B_j and C_j for approximating the time-independent equation

$$\sum_{j=1}^{n} \frac{\partial \Phi_j(\mathbf{u}, x)}{\partial x_j} = \mathbf{F}(\mathbf{u}, x). \qquad (5.4.1.5)$$

Considering that $B_j^{-1}C_j\Phi_j = \partial\Phi_j/\partial x_j + O(h_j^3)$ at each mesh point, we write the third-order difference analogue of (5.4.1.5) in the form

$$\sum_{j=1}^{n} B_j\mathbf{Y}_j = \mathbf{F}, \quad B_i\mathbf{Y}_i = C_i\Phi_i \quad (i = 1, 2, \ldots, n). \qquad (5.4.1.6)$$

These formulas indicate that even when the mesh functions Φ_j are known, the three-point operators B_j should be inverted for the

approximation of each term on the left-hand side of (5.4.1.5). This method does not involve the introduction of a "compensating" term Ω, and can be used for constructing splitting schemes.

5.4.2. Application of Coordinate Splitting

1. Although scheme (5.4.1.2) is absolutely stable [5.14], its realization in a multidimensional case imposes too stringent requirements on the computer power. Hence we shall consider more economical difference algorithms connected with factorization of difference-matrix operators acting on the function $\mathbf{u}^{m+1}$ [5.19-5.21]. Here we shall be interested in only those schemes which can be applied as iterative schemes, i.e. which ensure complete approximation in the sense of [5.20].

Using the Jacobi matrices $K_j = \partial\Phi_j/\partial\mathbf{u}$, we write the factorized scheme corresponding to (5.4.1.2):

$$\prod_{i=1}^{n} (B_j + \tau C_j Q_j) \frac{\mathbf{u}^{m+1} - \mathbf{u}^m}{\tau} + \sum G_j \Phi_j^m = B\mathbf{F}^m. \quad (5.4.2.1)$$

This scheme can be realized, in particular, in the following form:

$$\begin{aligned}
&(B_1 + \tau C_1 K_1)\,\xi^{1/n} = -\tau\Big(\sum_{j=1}^{n} G_j \Phi_j^m - B\mathbf{F}^m - \Omega^m\Big),\\
&\qquad\qquad \cdots\cdots\cdots\cdots\cdots\cdots\cdots\cdots\\
&(B_n + \tau C_j K_j)\,\xi^{j/n} = \xi^{(j-1)/n}, \quad j = 2, 3, \ldots, n, \qquad (5.4.2.2)\\
&\xi^1 = \mathbf{u}^{m+1} - \mathbf{u}^m.
\end{aligned}$$

The error of this scheme for a steady-state solution has the order $O(h_1^3 + h_2^3 + \ldots + h_n^3)$. It can be seen from (5.4.2.2) that this algorithm can be realized as a result of n "one-dimensional" vector sweeps with $p \times p$ matrices.

Using approximation (5.4.1.6) of a time-independent problem, we can write another splitting scheme in the form

$$\begin{aligned}
&(E + \tau B_1^{-1} C_1 K_1)\,\xi^{1/n} = -\tau\Big(\sum_{i=1}^{n} \mathbf{Y}_i^m - \mathbf{F}^m\Big),\\
&\qquad\qquad \cdots\cdots\cdots\cdots\cdots\cdots\cdots\cdots\\
&(E + \tau B_j^{-1} C_j K_j)\,\xi^{j/n} = \xi^{(j-1)/n}, \quad j = 2, 3, \ldots, n,
\end{aligned} \qquad (5.4.2.3)$$

where the mesh functions Y_1^m are calculated beforehand by the formulas

$$B_j \mathbf{Y}_j^m = \Phi_j^m, \quad j = 1, 2, \ldots, n. \qquad (5.4.2.4)$$

Multiplying each jth equation from (5.4.2.3) by B_j, we find that n one-dimensional operators B_j and n one-dimensional operators

$B_j + \tau C_j K_j$ appearing on the left-hand side of (5.4.2.2) should be inverted in order to realize algorithm (5.4.2.3)-(5.4.2.4).

Computer calculations with consecutive operations involving scheme (5.4.2.3)-(5.4.2.4) are less economical than those involving scheme (5.4.2.2) due to a large number of sweeps. Utilization of computers with vector and matrix processors may considerably increase the effectiveness of the two schemes and make them approximately equivalent from the point of view of computer time. The parallelism of calculations on the basis of algorithms in (5.4.2.2) and (5.4.2.3)-(5.4.2.4) is determined by three factors: the presence of sweeps of the same type along each line $x_j = \text{const}$ ($j = 1, 2, \ldots, n$) containing the nodes of the difference mesh, the parallelism of inversion of $p \times p$ matrices during the calculation of sweep coefficients, and a certain parallelism in the realization of sweeps.

2. While estimating the stability of the above schemes for Cauchy's multidimensional problems, the inner product $(\mathbf{u} \cdot \mathbf{v})$ of finitely supported functions $\mathbf{u}$ and $\mathbf{v}$ will be defined as the sum

$$\sum_{i_1, i_2, \ldots, i_n = -\infty}^{\infty} (\mathbf{u} \cdot \mathbf{v})_{i_1 i_2 \ldots i_n} h_1 h_2 \ldots h_n).$$

We can then easily establish that the operators B_i and C_i ($i = 1, 2, \ldots, n$) have the same properties (5.2.3.10) as the operators B and C. The absolute stability of implicit scheme (5.4.1.2) follows from these properties [5.14].

Let us consider the factorized schemes (5.4.2.1) and (5.4.2.3). For two dimensions ($n = 2$), (5.4.2.3) can be treated as a splitting scheme with non-negative operators ($B_i^{-1} C_i K_i \geqslant 0$, $i = 1, 2$), for which the absolute stability is established in a certain energy norm [5.20]. If the constant matrices K_1 and K_2 (and hence the matrices M_1 and M_2) are commutative, the schemes (5.4.2.1) and (5.4.2.3) are equivalent. Their absolute stability in this case can also be established in the norm $\|\cdot\|_{A_1^* A_1}$, $A_1 = B_1^{-1} C_1 K_1 + B_2^{-1} C_2 K_2$ [5.14].

Unfortunately, for $n > 2$ splitting schemes are not absolutely stable in any reasonable norm in the general case of non-self-conjugate, but non-negative operators [5.20]. An example illustrating this fact is considered in [5.14].

3. The third-order approximation for one-dimensional equations (5.3.1.1) with diffusive terms, as well as splitting algorithms considered above, can be used [5.14] for constructing compact nonsymmetric schemes for systems of the form

$$\frac{\partial \mathbf{u}}{\partial t} + \sum_{i=1}^{N} \frac{\partial \Phi_i(\mathbf{u})}{\partial x_i} = \sum_{i, j=1}^{n} \frac{\partial}{\partial x_i} \mu_{ij} \frac{\partial \mathbf{u}}{\partial x_j} + \mathbf{F}(\mathbf{u}, x), \qquad (5.4.2.5)$$

where μ_{ij} are positive matrices. The absolute stability of such schemes can be easily established under some additional assumptions

about the matrices μ_{ij} at least for the cases when the corresponding scheme is stable for $\mu_{ij} \equiv 0$ [5.14]. Without considering the general case of (5.4.2.5), we note that the terms with mixed derivatives can be approximated in several ways when $\mu_{ij} \neq 0$, $i \neq j$.

The realization of each splitting stage is in fact equivalent to the solution of a problem of the type (5.3.1.4) for isolated directions in space.

5.4.3. Application of Internal Iterations for Increasing Algorithm Stability

1. For solving the time-independent problem (5.4.1.5) with the help of the approximations considered above, we can construct an algorithm which is absolutely stable irrespective of the number n of spatial variables. Let us consider this algorithm in the general form [5.22].

Suppose that we have the difference problem

$$(E + \tau\sigma A)\frac{\mathbf{u}^{m+1} - \mathbf{u}^m}{\tau} + A\mathbf{u}^m = \mathbf{f}^m, \tag{5.4.3.1}$$

where $\mathbf{u}^m$, $\mathbf{u}^{m+1}$, $\mathbf{f}^m$ are the vectors, E and A are the unit and the linear matrix operators respectively, and $0 \leqslant \sigma \leqslant 1$ is a certain weight factor. We shall assume that operator A can be represented in the form

$$A = \sum_{i=1}^{N} A_i, \quad A_i \geqslant 0$$

and is independent of the index m.

To go over from the mth to $(m+1)$th layer, we introduce an internal iterative process of the type

$$\prod_{i=1}^{N} (E + \tau^2 D_i)\frac{\mathbf{u}^{m+1,\,k+1} - \mathbf{u}^m}{\tau} + \sigma A\mathbf{u}^{m+1,\,k} + (1-\sigma)A\mathbf{u}^m = \mathbf{f}^m \tag{5.4.3.2}$$

and put $\mathbf{u}^{m+1} = \mathbf{u}^{m+1,\,l}$, where l is the number of iterations. We shall assume that the operators D_i $(i = 1, 2, \ldots, N)$ in (5.4.3.2)

1° commute with all operators A_j $(j = 1, 2, \ldots, N)$,

2° are self-conjugate and positive, and

3° satisfy inequalities $D_i \geqslant NA_i^* A_i$.

Calculating the norm of the operator T of transition from the kth to $(k+1)$th iteration $(\mathbf{u}^{m+1,k+1} = T\mathbf{u}^{m+1,k} + \mathbf{F})$, we can show that the following estimate is valid:

$$q = \| T \|_{l_2^{(n)}} \leqslant \sigma / \sqrt{2}.$$

Determining successively $\mathbf{u}^{m+1,1}$, $\mathbf{u}^{m+1,2}$, . . ., $\mathbf{u}^{m+1,l} = \mathbf{u}^{m+1}$, we obtain after simple transformations the scheme:

$$(R+\sigma\tau A)\frac{\mathbf{u}^{m+1}-\mathbf{u}^m}{\tau}+(E-T^l)A\mathbf{u}^m=(E-T^l)\mathbf{f}^m, \tag{5.4.3.3}$$

$$R=\prod_{i=1}^{N}(E+\tau^2 D_i),$$

which possesses the following approximation properties:

(a) during the establishment of the "external" iterative process ($\mathbf{u}^{m+1}=\mathbf{u}^m=\mathbf{u}$, $\mathbf{f}^m=\mathbf{f}$), scheme (5.4.3.3) is transformed to the equality $A\mathbf{u}=\mathbf{f}$ irrespective of the number l of internal iterations (complete approximation in the sense of [5.19]);

(b) for a sufficiently large number l, when $T_g^l=O(\tau^2)$, scheme (5.4.3.3) differs from (5.4.3.1) in the terms of the order $O((\sigma-0.5)\tau, \tau^2)$; thus, scheme (5.4.2.3) is applicable for solving time-dependent problems as well.

The absolute stability of (5.4.3.3) can be easily established when the operator $C=(E-T^l)A$ is non-negative and the weight factor σ is bounded from below. Calculating the norm of the transition operator $S=(R+\tau\sigma A)^{-1}(R+\tau\sigma A-\tau C)$, we find that the inequality $\|S\|_{l_2^{(n)}}\leqslant 1$ holds for any τ if

$$\tau R(C^*+C)+\tau^2A^*A[(2\sigma-1)E$$
$$+(1-\sigma)(T^l+T^{*l})-2(T^*T)^l]\geqslant 0.$$

This inequality will be valid for

$$\sigma>0.5(1+q^l),\quad q\leqslant\sigma/\sqrt{2}. \tag{5.4.3.4}$$

Using one iteration in the Newton method for solving the equation $\sigma=0.5[1+(\sigma/\sqrt{2})^l]$, we find the minimal value $\sigma_{\min}$ ensuring that inequality (5.4.3.4) is satisfied. This value $\sigma_{\min}=0.5[1+(2^{3l/2}-1)^{-1}]$ just exceeds 0.5.

Using the results of [5.13], we can also show that the conditions $C\geqslant 0$ and (5.4.3.4) are also sufficient for the stability of (5.4.3.3) in the norm $\|\cdot\|_{C^*C}$.

Thus, the main factor determining the stability of scheme (5.4.3.3) is the non-negativeness of the operator C. Let us write some sufficient conditions for $C\geqslant 0$ without giving any proof.

1°. $A\geqslant\delta E$, $\delta=\text{const}>0$: $q^l<\delta/\|A\|$.

2°. Self-conjugate and skew-symmetric components of the operator A commute; $q^l<\sin\pi/(l+1)$ for $l=2k$ or $q^l<\sin\pi/[2(l+1)]$ for $l=4k-1$ ($k=1, 2, 3, \ldots$).

The second condition indicates that in the case of commutation (in particular, when the operator A is skew-symmetric), only 2 or 3 iterations are required for the condition $C\geqslant 0$ to be satisfied.

2. In order to apply the results described above to higher-accuracy difference schemes, let us consider the structure of the operators G_i ($i = 1, \ldots, n$) in (5.4.1.2). We shall assume that all eigenvalues of the constant matrices K_i in (5.4.1.1a) differ from zero ("strictly" zero eigenvalues are unlikely). Then $M_j^2 = I$, where I is a unit $p \times p$ matrix, and the following equalities hold:

$$B_i^* B_i = [(A_0^j)^2 - (1/16)(\Delta_0^j)^2], \quad C_i^* C_i = -\Delta_{2i}/h_i^2, \quad i = 1, 2, \ldots, N. \tag{5.4.3.5}$$

Multiplying (5.4.1.2) with $\Phi_j = K_j u$ by $B^{-1} = (B_1, B_2, \ldots, B_N)^{-1}$, we obtain scheme (5.4.3.1) with $A_j = B^{-1} G_j K_j$. Calculating $A_j^* A_j$ and taking into account (5.4.3.5) where the operators $B_i^* B_i$ and $C_i^* C_i$ commute with the same operators which, however, have different indices, we obtain the following inequalities:

$$A_j^* A_j \leqslant c_j I(-\Delta_{2j}) = D_j, \quad j = 1, 2, \ldots, N, \tag{5.4.3.6}$$

where c_j are constants depending on the norms of matrices K_j. Similar results can be obtained for the scheme

$$\frac{\mathbf{u}^{m+1} - \mathbf{u}^m}{\tau} + \sum_{j=1}^{N} B_j^{-1} C_j K_j \mathbf{u}^{m+1} = 0, \quad A_j = B_j^{-1} C_j K_j,$$

corresponding to approximation (5.4.1.6) for $\Phi_j = K_j \mathbf{u}$. The operator D_j from (5.4.3.6) obviously satisfies all properties 1°-3° of (5.4.3.2) and can be used for the internal iterative process. In this case, each iteration is reduced to the inversion of the three-point operators $E + \tau^2 D_i$ ($i = 1, 2, \ldots, N$), which can be carried out with the help of a three-point scalar sweep. Thus, the advantage of internal iterations may consist, firstly, in the absolute stability of the algorithm and secondly, in a more economical transition from one time level to another in comparison with the schemes of splitting by vector sweeps. It should be borne in mind, however, that in order to accelerate the convergence of "external" iterations associated with increasing the index m in (5.4.3.2), we must optimize the parameter τ, taking into account the lower and upper bounds of the operators A_i ($0 = 1, 2, \ldots, N$).

It can be shown that the operators D_j from (5.4.3.6) are also suitable for internal iterations of systems with diffusive terms. Besides, they can be used in conventional second-order approximations [5.22].

5.5. APPLICATION OF COMPACT SCHEMES TO THE ANALYSIS OF VISCOUS GAS FLOWS

5.5.1. Application of Algorithms with Scalar Sweeps

1. The methods of constructing compact third-order schemes considered above can be used in different ways for solving concrete problems. For example, the following possibilities exist for gasdynamic equations or the Navier-Stokes equations:

(a) the initial system of equations is treated as a nonlinear system of the type (5.4.1.1) or (5.4.2.5),

(b) the initial system is considered to be a set of scalar equations in the functions contained in time derivatives, while the remaining functions are assumed to be known (for example, they are taken from the preceding temporal layer).

In the first case involving vector sweeps, "characteristic" matrices M_j corresponding to the spatial direction x_j should be calculated at each point. If we go over to a fourth-order symmetric version of the schemes considered above, this is no longer necessary. In this case, it is sufficient to formally put $M_j = 0$ $(i = 1, 2, \ldots, N)$ in the entire computational domain. Despite certain additional expenditure of time associated with the inversion of matrices, simultaneous solution of the groups of three-point difference equations was successfully used in solving problems on a viscous gas flow [5.23, 5.24].

In the second case connected with scalar sweeps, it is sufficient to use only the signs of velocities appearing in the coefficients of the equations. This considerably reduces the number of arithmetic operations. However, the calculation of pressure gradients on the preceding temporal layer (or the previous iteration), which makes it possible to solve the equations independently, markedly reduces the scheme stability.

The application of modern computers may significantly reduce the difference in computer time for completing a computational cycle (time step or iteration) in cases (a) and (b). If we also take into account the possibility of convergence to a steady state over a smaller number of cycles, the possibility (a) seems to be more promising than the possibility (b) for solving time-independent problems.

On the other hand, it should be noted that splitting in accordance with physical properties is found to be very effective. Here the absolute stability is attained by increasing the number of fractional steps without altering the scalar nature of sweeps [5.19, 5.25].

It should be borne in mind, however, that the effectiveness of an algorithm for a specific problem is determined by many factors some

of which are not taken into account in this paper, e.g. the nature of obtained solutions and boundary conditions. When considering time-independent problems in fluid mechanics, we must speak about a "sufficient stability" margin which allows us to obtain solutions after a comparatively small number of computational cycles, rather than about the absolute stability of a method as in the linear case.

2. While solving a number of problems on two-dimensional steady-state flows of a viscous gas, it is sometimes possible to isolate a certain "main" direction in which a disturbance propagates. Suppose that in the (x, y) coordinate system this direction coincides with the x-axis. Then the algorithm can be simplified by constructing, instead of the stabilization scheme, an iterative process where an equation of the type (5.3.1.1) with the variable x instead of t is solved in each iteration according to the "time marching" scheme. The implicit approximation of the order $O\ (\Delta y)^3$ is constructed here only for the transverse coordinate y, while for the longitudinal coordinate with relatively slow variations of solutions, three-point one-sided differences of the order $O\ (\Delta x^2)$ may turn out to be sufficient (Δx and Δy are the mesh steps along the x- and y-axes respectively). Considering each Navier-Stokes equation independently of the remaining equations (case (b)), we can determine the parameters of the flow field at each iteration by the method of sweeps by going over from one "layer" $x = \text{const}$ to another. The values of functions which correspond to the cross section in front of a given one are taken from the previous iteration [5.15]. This method, which can be conditionally referred to the "relaxation in lines" type, is absolutely stable for an individual equation with constant coefficients. The following problems illustrate the effectiveness of this approach: hypersonic flow of a viscous gas past blunted bodies, a flow field around a finite-length plate in a hypersonic flow of weakly rarefied gas. In both cases, it is natural to take for the x-coordinate the direction of the body profile.

Figures 5.6 and 5.7 show the results of calculations of such flows [5.15] with the help of automatic concentration of the mesh points near the surface. The concentration was attained by a transformation of the type (5.3.2.1) with $\psi\ (u) = au$, $a = \text{const}$, where u is the velocity component corresponding to the x-coordinate.

Figure 5.6 illustrates the solution of the complete system of Navier-Stokes equations for a flow between a spherically blunted body and a detached shock wave. Profiles of the tangential components of velocity, calculated for the parameters of the unperturbed flow, are shown for the Mach number $M_\infty = 10$ and various Reynolds numbers Re_∞. For $x/R = 0.6$, the profiles u/u_1 as functions of variables y/y_1 and ξ (R is the radius of the sphere and the subscript 1 marks the value on the shock wave) illustrate the mapping of the boundary layer irrespective of the Reynolds number onto a sufficiently wide

band in the computational domain $\{0 \leqslant x,\ 0 \leqslant \xi < 1\}$. Using a shorter step and comparing with the known solutions for an inviscid core of the boundary layer (for large Reynolds numbers Re_∞), we find that a fairly high accuracy can be attained for a comparatively small number of nodes along the normal to the surface.

The flow past a finite-length plate for $\mathrm{M}_\infty \gg 1$ and comparatively small Reynolds numbers Re_∞ was investigated in detail on the

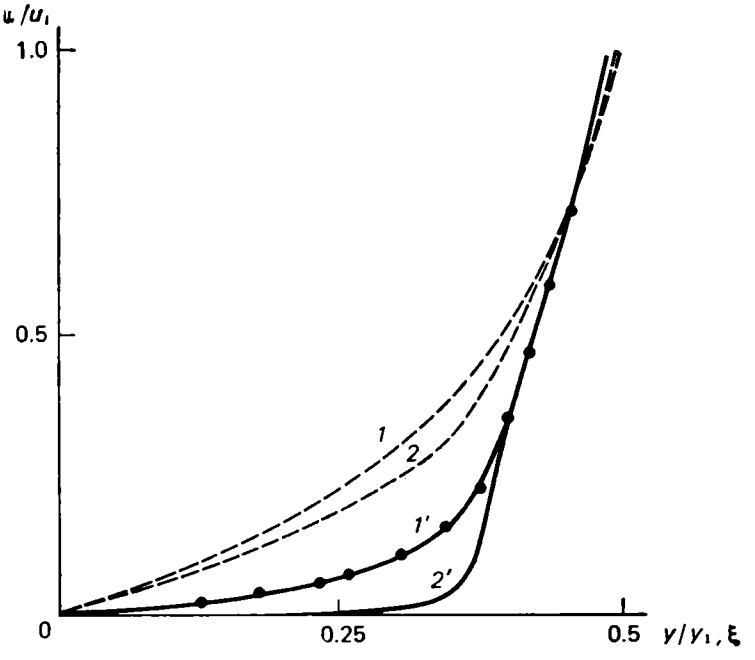

Fig. 5.6. Distribution of shear velocities in the neighbourhood of a spherical blunting. (*1*) Re = 640, $u(\xi)$, (*2*) Re = 640, $u(y)$; (*1*) Re = 64 000, $u(\xi)$, (*2*) Re = 64 000, $u(y)$.

basis of Navier-Stokes equations under the conditions of slip and a temperature jump at the surface. In addition to automatic concentration of mesh points along the y-coordinate using a transformation of the type (5.3.2.1), a preliminarily fixed node concentration was maintained along the plate in the vicinity of its leading edge. According to the obtained results, the trailing edge considerably affects the entire flow field in the regime under consideration. This is especially typical of pressure whose variation along the plate surface is shown in Fig. 5.7 for various values of Re_∞ and various ratios between the wall temperature T_w and the stagnation temperature T_0 ($\mathrm{M}_\infty = 10$; the adiabatic exponents $\gamma = 7/5,\ 5/3$), This result as well as other characteristics are in good agreement with the numerical solutions of the Boltzmann equation [5.26] obtained

by Bird's method. This allows us to speak about practical applicability of Navier-Stokes equations for sufficiently small Reynolds numbers.

From the methodical point of view, the above calculations have shown that the application of iteration algorithm enables us to obtain a steady-state solution to within 3-4 significant digits over

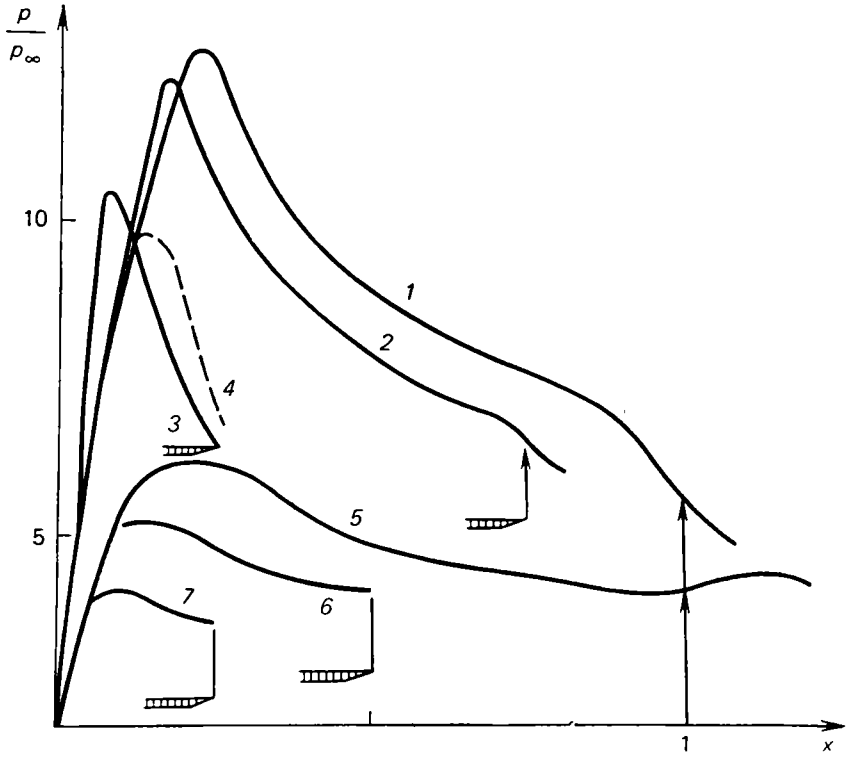

Fig. 5.7. Pressure distribution along a finite-length plate in a hypersonic flow. (*1*) Re = 6700, (*2*) Re = 5000, (*3*) Re = 1670; — — — calculations by Monte-Carlo method [5.26]; (*1*)—(*4*) for $\gamma = 5/3$, $T_w = T_0$, $\mu \propto T$, (*5*) Re = 640, (*6*) Re = 320, (*7*) Re = 160, (*5*)-(*7*) for $\gamma = 7/5$, $T_w = 0.1\ T$, Sutherland's law for T.

200-500 cycles for the total number of nodes of the order of 10^3 unless reverse flows appear in the computational domain. For separated flows, however, fairly small values of relaxation parameter were required, and stabilization was attained much more slowly. This is probably due to the absence of a "preferred" direction of the flow in separation zones and more stringent stability criteria since the derivatives of pressure are calculated by using the results of the previous iteration.

5.5.2. Splitting Algorithm with Vector Sweeps

1. For complete Navier-Stokes equations describing the behaviour of a compressible gas, let us consider a symmetrized scheme of the type (5.4.2.1), $M_j \equiv 0$, with a simplified approximation of diffusive terms [5.27]. Such a scheme retains the basic structure of a complete algorithm for $M_j \neq 0$ and at the same time it is sufficiently simple to realize.

Confining ourselves for the sake of simplicity to two dimensions, we write the initial equations in a curvilinear system of coordinates in divergent form, retaining the Cartesian components of momentum:

$$\frac{\partial \widetilde{\mathbf{v}}}{\partial t} + \frac{\partial \widetilde{\mathbf{F}}}{\partial \xi} + \frac{\partial \widetilde{\mathbf{G}}}{\partial u} + \widetilde{\mathbf{H}} = 0, \tag{5.5.2.1}$$

$$\widetilde{\mathbf{v}} = I^{-1}\mathbf{v}, \quad \widetilde{\mathbf{F}} = I^{-1}(\mathbf{F}\xi_x + \mathbf{G}\xi_y),$$

$$\widetilde{\mathbf{G}} = I^{-1}(\mathbf{F}\eta_x + \mathbf{G}\eta_y), \quad \widetilde{\mathbf{H}} = I^{-1}\mathbf{H},$$

$$\xi_x = Iy_\eta, \quad \xi_y = -Ix_\eta, \quad \eta_x = -Iy_\xi, \quad \eta_y = Ix_\xi.$$

Here x and y are Cartesian coordinates, $I = D(\xi, \eta)/D(x, y)$ is assumed to be different from zero, and $\mathbf{v}$, $\mathbf{F}$, $\mathbf{G}$, and $\mathbf{H}$ are the vectors which depend on the vector of unknown functions, $\mathbf{u}$ (vector $\mathbf{H}$ differs from zero only in axisymmetric case). The form of vectors $\widetilde{\mathbf{v}}$, $\widetilde{\mathbf{F}}$, $\widetilde{\mathbf{G}}$, and $\widetilde{\mathbf{H}}$ is given in many papers devoted to the numerical solution of Navier-Stokes equations and hence is not discussed here.

Representing $\widetilde{\mathbf{F}}$, $\widetilde{\mathbf{G}}$ and $\widetilde{\mathbf{H}}$ in the form

$$\widetilde{\mathbf{F}} = \mathbf{F}_0 + \mu\left(\frac{\partial \mathbf{F}_1}{\partial \xi} + \frac{\partial \mathbf{F}_2}{\partial \eta}\right), \quad \widetilde{\mathbf{G}} = \mathbf{G}_0 + \mu\left(\frac{\partial \mathbf{G}_1}{\partial \xi} + \frac{\partial \mathbf{G}_2}{\partial \eta}\right),$$

$$\widetilde{\mathbf{H}} = \mathbf{H}_0 + \mu\left(\frac{\partial \mathbf{H}_1}{\partial \xi} + \frac{\partial \mathbf{H}_2}{\partial \eta}\right),$$

where $\mathbf{F}_0$, $\mathbf{G}_0$ and $\mathbf{H}_0$ are the vectors which do not contain viscosity μ, we can write on the mesh $\omega_{h_1 h_2} \times \omega_\tau$ $\{\xi_i = h_1 i, \eta_j = h_2 j, t_n = n\tau, h_1, h_2 = \text{const}\}$ the difference analogue of (5.5.2.1) in the form

$$A_\xi A_y \frac{\widetilde{\mathbf{U}}^{n+1} - \widetilde{\mathbf{U}}^n}{\tau} + L\widetilde{\mathbf{U}}^{n+1} = 0, \tag{5.5.2.2}$$

where

$$L\mathbf{U}^{n+1} = A_\eta \Delta_\xi \mathbf{F}_0^{n+1} + A_\xi \Delta_\eta \mathbf{G}_0^{n+1} + A_\xi A_\eta \mathbf{H}_0^{n+1} + \mu A_\eta \Delta_\xi \mathbf{H}_1^{n+1} + \mu A_\eta \Lambda_{11} \mathbf{F}_1^{n+1}$$
$$+ \mu \Lambda_{12} \mathbf{F}_2^{n+1} + \mu A_\xi \Lambda_{22} \mathbf{G}_2^{n+1} + \mu \Lambda_{21} \mathbf{G}_1^{n+1}.$$

Here A_ξ, A_η are symmetric operators from (5.2.1.12) which correspond to the coordinates ξ and η, while Λ_{pq} $(p, q = 1, 2)$ are the

operators used for approximating the terms containing viscosity, for example

$$\Lambda_{11}(\mu f) = [\mu_{i+1/2,\,j}(f_{i+1,\,j} - f_{i,\,j}) - \mu_{i-1/2,\,j}(f_{i,\,j} - f_{i-1,\,j})]/h_1^2,$$
$$\Lambda_{12}(\mu f) = [\mu_{i+1,\,j}(f_{i+1,\,j+1} - f_{i+1,\,j-1}) - \mu_{i-1,\,j}(f_{i-1,\,j+1} - f_{i-1,\,j-1})]/2h_1h_2.$$

It can be easily seen that scheme (5.5.2.2) written on a nine-point pattern, has the approximation order $O(h^4 + \mu h^2)$, on the stationary solution (5.5.2.1), where $h = \max(h_1, h_2)$. For Euler's equations ($\mu = 0$), scheme (5.5.2.2) will have the fourth order. For small μ, scheme (5.5.2.2) will be a fourth-order scheme practically everywhere except the regions where viscosity plays a significant role (in such regions the order becomes equal to two). A decrease in accuracy to the second order inside viscous layers seems to be quite natural if we use the equations for turbulent flows where the terms containing the turbulent viscosity have an approximate nature themselves.

Going over from (5.5.2.2) to the corresponding splitting scheme, we introduce the following matrices:

$$A = \frac{\partial \mathbf{F}_0}{\partial \mathbf{u}}, \quad B = \frac{\partial \mathbf{G}_0}{\partial \mathbf{u}}, \quad C = \frac{\partial \mathbf{U}}{\partial \mathbf{u}}, \quad R = \frac{\partial \mathbf{F}_1}{\partial \mathbf{u}}, \quad S = \frac{\partial \mathbf{G}_2}{\partial \mathbf{u}} \tag{5.5.2.3}$$

and write the algorithm in the form [5.27]

$$(A_\xi C + \tau\Delta_\xi A + \tau\Lambda_{11}R)\,C^{-1}(A_\eta C + i\Delta_\eta B + \tau\Lambda_{22}S)\,\frac{\mathbf{u}^{n+1} - \mathbf{u}^n}{\tau} = -L\tilde{\mathbf{U}}^n. \tag{5.5.2.4}$$

The factorized scheme (5.5.2.3) can be realized in two stages:

$$\begin{aligned}(A_\xi C + \tau\Delta_\xi A + \tau\Lambda_{11}R)\,\boldsymbol{\xi}^{1/2} &= -\tau L\tilde{\mathbf{U}}^n,\\ (A_\eta C + \tau\Delta_\eta B + \tau\Lambda_{22}S)\,(\mathbf{u}^{n+1} - \mathbf{u}^n) &= C\boldsymbol{\xi}^{1/2},\end{aligned} \tag{5.5.2.5}$$

where the operators in the parentheses are inverted as a result of three-point vector sweeps. The stability of scheme (5.5.2.4) can be substantiated in the frozen coefficient approximation with the help of an analysis similar to that carried out in Sec. 5.4.

When scheme (5.5.2.4) was used in practice, we chose as a vector $\mathbf{u}$ of required functions the vector whose components were the density ρ, the Cartesian velocity components u and v, and the internal energy e. Choosing other dependent variables, other Jacobian matrices A, B and C defined by formulas (5.5.2.3) can be obtained, which leads to a change in the factorized operator on the left-hand side of (5.5.2.4) without altering its "stationary" part $L\tilde{U}^n$. The experience shows that, in particular, it is expedient to choose in many problems the vector with the components $\{\rho, \rho u, \rho v, \rho[e + (u^2 + v^2)/2]\}$. Then C becomes a unit matrix.

2. In spite of its simplicity, scheme (5.5.2.4) is inferior to the nonsymmetric scheme of the type (5.4.2.1) as regards the monoto-

nicity of solutions. In order to reduce or eliminate undesirable oscillations of required functions, which are inherent in symmetric schemes and appear in high-gradient flows, "smoothing" was utilized (the approximation order of the scheme on smooth solutions remained unchanged in this case). Various smoothing operators (filters), similar to the operators Λ_{11} and Λ_{22} were introduced implicitly into the initial scheme on a three-point (in each direction) pattern. Their form is given in [5.27]. Upon a transition to the factorized scheme (5.5.2.4), the smoothing involved an additional term on the right-hand side (which was calculated on the nth time layer), as well as additions to the viscosity μ in the operators Λ_{11} and Λ_{22} on the left-hand side. Smoothing required a large number of methodical calculations aimed, on the one hand, at choosing the minimum artificial viscosity constants (so that this viscosity is much smaller than the physical viscosity), and on the other hand, at ensuring complete elimination of saw-tooth oscillations (or at least weakening them significantly).

3. The formulation of difference boundary conditions has a strong effect on the properties of an algorithm and on the quality of the obtained solutions (e.g., their monotonicity). For the factorized scheme (5.5.2.5), the boundary conditions should be specified not only for vector $\mathbf{u}^n$ of the required functions but also for the vector $\xi^{1/2}$ of intermediate quantities. A large number of methodical calculations were made to elucidate the effectiveness of various boundary approximations and, in particular, the algorithm for determining the density on solid surfaces. Some results of these investigations are described in [5.27]. This work also presents the estimates of the accuracy of the method, obtained from a comparison with the exact solutions for internal flows [5.28] as well as with the known solution for the boundary layer on a flat plate. Besides, the applicability of the algorithm to the case of through computation of discontinuous solutions and the effects of smoothing which does not reduce the approximation order were investigated for the problem of an oblique shock wave in an inviscid gas.

4. The application of curvilinear coordinates makes it possible to apply algorithm (5.5.2.5) to flows with a quite arbitrary configuration of solid boundaries in the framework of a single computer program. Various types of flows were calculated. Some of them have already been studied and may serve as the basis for comparison with the obtained results. Much attention was paid to numerical simulation of steady-state separation as one of complex phenomena in viscous gas mechanics.

In some of the cases under investigation, Reynolds numbers turned out to be quite large (of the order of 10^5). The fixed coordinate transformation used for concentrating the mesh nodes was such that the region of significant viscosity contained not less than ten nodes in

each direction. In the regions where viscosity was insignificant, the fourth approximation order of the scheme permitted reasonably large steps in calculations. A certain inconvenience in the application of scheme (5.5.2.4) for large Reynolds numbers was associated with the necessity to control the artificial viscosity introduced by smoothing, so that its value was always less than the physical viscosity. For small Reynolds numbers, smoothing was not required.

Interaction of an oblique shock wave with the boundary layer on a plane plate [5.27]. This problem was considered in a number of

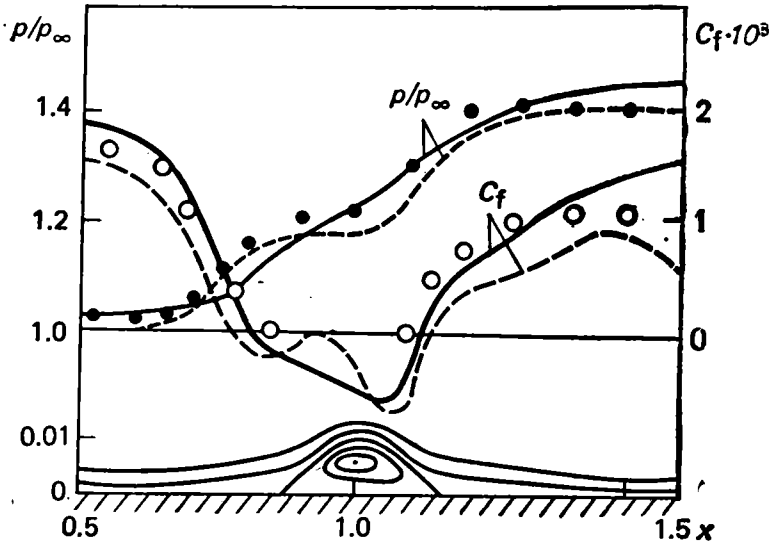

Fig. 5.8. Interaction of an oblique shock wave with the boundary layer.

papers (see for example [5.29]). In our case this problem was formulated as follows. In a certain initial section on a flat plate, the Blasius profiles and the parameter of incoming flow in the boundary layer and above it were specified. The parameters were fixed in front of and behind an oblique shock wave on the upper boundary of the computational domain. As in [5.29] these parameters correspond to the angle 32.6° of incidence of the shock wave.

Figure 5.8 shows the streamlines near the plate. The shape of these lines reveals the formation of detached wave and the reverse flow regions in the vicinity of the incidence of the shock wave. The figure also contains the distributions of the friction coefficient C_f, pressure p/p_∞ as well as the calculated (circles) and experimental (dashed lines) results obtained in [5.29]. The calculations were made for Mach number $M_\infty = 2$ and Reynolds number $Re_\infty = 10^5$. The latter was calculated from the distance between the initial cross section and the point of incidence of the shock wave.

Flow past the main part of a body of revolution [5.27]. Figure 5.9 presents the results of calculations for a flow along the curvilinear generatrix of a body of revolution. These results were obtained for $M_\infty = 1.7$, $Re = 10^4$, and $T_w/T_\infty = 1.225$ (T_w and T_∞ are the temperatures of the wall and the incoming flow).

A typical feature of the flow under consideration is the presence of an extended backward flow in the region where the curvilinear

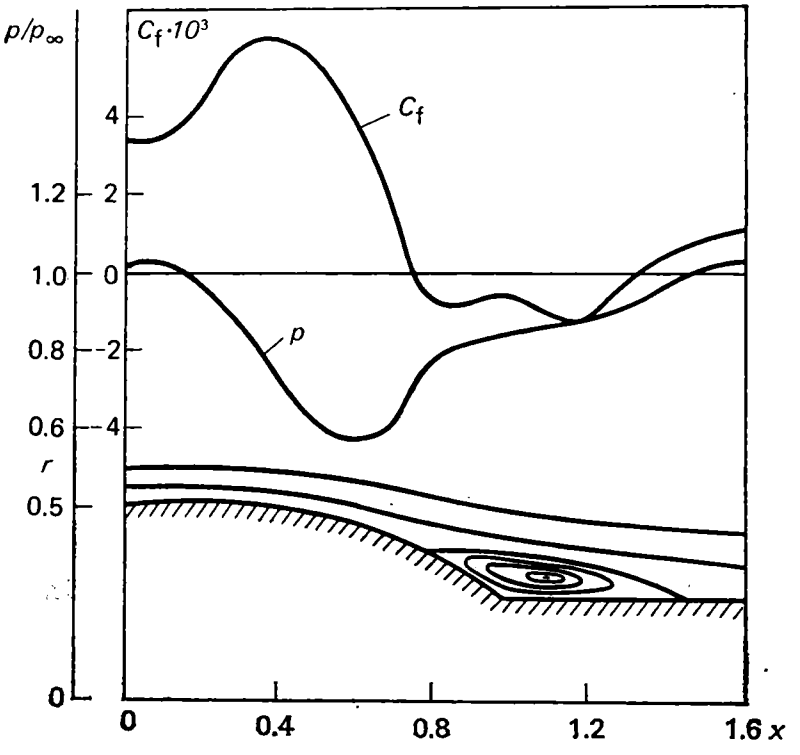

Fig. 5.9. Pressure and friction coefficient distribution in the main part of a body of revolution.

part of the surface meets the cylindrical part. The plateau on the pressure curve, corresponding to this region, is more pronounced than in the previous example.

The results presented in Figs. 5.8 and 5.9 were obtained on a mesh containing about 10^3 mesh points after about 150 cycles preceding the stabilization (the choice of the parameter was not optimized).

Flows in channels [5.27]. By way of an example, we shall consider the results of calculations for a plane channel having a constant cross section. The problem is formulated as follows. At the channel inlet, the pressure p_1 and temperature T_1 were considered to be known, and at outlet, the pressure p_2 was specified. Thus, we have to find the gas flow rate through the channel cross section and the problem is similar to that concerning the flow of a viscous gas from

a large volume (where the gas pressure is p_1) through a nozzle of small cross section to a medium with a present pressure p_2.

Since the flow parameters at the channel outlet may rapidly change, the downstream boundary conditions are of great importance. Numerical experiments have shown that the suitable conditions for

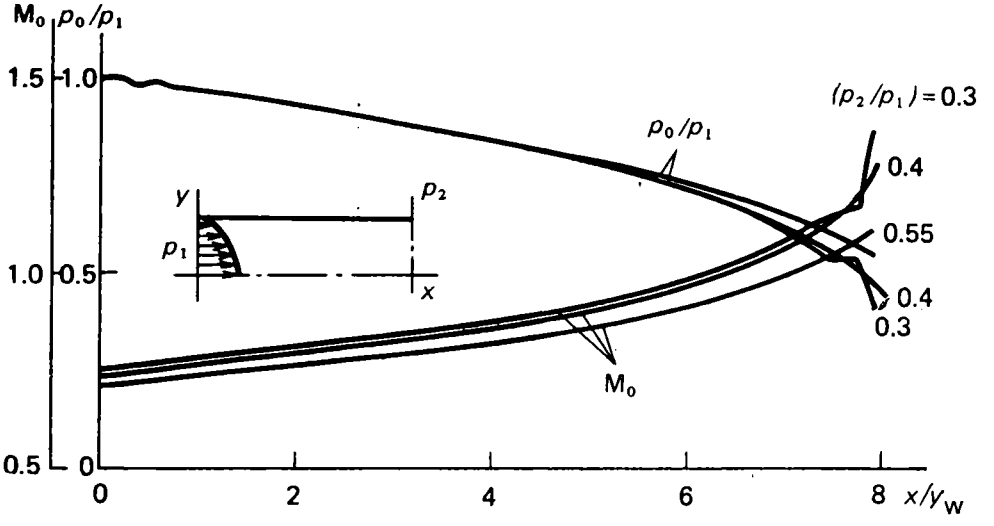

Fig. 5.10. Distribution of pressure and Mach number along the channel axis.

this problem involve extrapolation according to formulas with a high order accuracy, which corresponds to the differential conditions $\partial^k f/\partial x^k = 0$, $k = u$.

Figure 5.10 shows steady-state distributions of pressure p_0 and Mach number M_0 along the channel axis. These distributions were obtained by using a 41×18 mesh after 300 time cycles for the following parameters of the problem: the ratio of the length L of the channel to half its height H, $L/H = 8$, $T_w = T_0$, where T_0 is the deceleration temperature, and the Reynolds number calculated from the gas parameters at the channel inlet and the average velocity is $Re = 50$.

5.6. CONCLUSION

The algorithms considered above and their possible modifications can be applied for solving many problems in fluid dynamics as well as other problems in mathematical physics, containing equations with convective and diffusion terms. At present, such algorithms are used for the analysis of incompressible liquid flows and turbulent flows described by semi-empirical models. Moreover, calculations are also being made for three-dimensional flows.

It should be noted that the effectiveness of these methods can be considerably improved by using the parallelism contained in these problems for calculations on computers with vector and matrix processors.

References

5.1. E. Krauss, E. H. Hirschel, and W. Kordulla, in: *Proc. AIAA Computational Fluid Dynamics Conf.*, Palm Springs, Calif. 1973, p. 92.
5.2. S. G. Rubin and R. A. Graves, *Computers and Fluids* 3, 1: 1 (1975).
5.3. R. Hirsh, *J. Comput. Phys.* 19, 1: 90 (1975).
5.4. A. I. Tolstykh, *Uch. Zap. TsAGI* 3, 6: 78 (1972).
5.5. A. I. Tolstykh, *Uch. Zap. TsAGI* 4, 2: 36 (1973).
5.6. A. I. Tolstykh, *Dokl. Akad. Nauk SSSR* 210, 1: 48 (1973).
5.7. O. M. Belotserkovskii (ed.), *Numerical Solution of Current Problems in Gas Dynamics*, Nauka, Moscow, 1975 (in Russian).
5.8. A. I. Tolstykh, *Zh. Vychisl. Matem. i Mat. Fiz.* 16, 5: 1182 (1976).
5.9. A. N. Minailos and A. I. Tolstykh, *Zh. Vychisl. Matem. i Mat. Fiz.* 15, 2: 527 (1975).
5.10. V. V. Rusanov, *Dokl. Akad. Nauk SSSR* 180, 6: 1303 (1968).
5.11. P. Kutler, H. Lomax, and R. Warming, Computations of Space Shuttle Flow Fields Using Noncentered Finite-difference Schemes. AIAA Paper, 1972, 72-193.
5.12. S. K. Godunov, *Matem. Sb.* 47 (89), No. 3, 271 (1959).
5.13. A. A. Samarsky and A. V. Gulin. *Stability of Difference* Schemes, Nauka, Moscow, 1973 (in Russian).
5.14. A. I. Tolstykh, *Zh. Vychisl. Matem. i Mat. Fiz.* 21, 2: 339 (1981).
5.15. A. I. Tolstykh, *Zh. Vychisl. Matem. i Mat. Fiz.* 18, 4: 139 (1978).
5.16. S. K. Godunov and V. S. Ryaben'ky, *Difference Schemes*, Nauka, Moscow, 1973 (in Russian).
5.17. N. N. Yanenko, N. G. Danaev and V. D. Lisetskin, *Chisl. Metody Mekhan. Sploshnoi Sredy* 8, 4: 157 (1977).
5.18. N. N. Yanenko and V. M. Kovenya, *Dokl. Akad. Nauk SSSR* 232, 6: 1273 (1977).
5.19. N. N. Yanenko, *Fractional Step Method of Solving Multidimensional Problems in Mathematical Physics*, Nauka, Novosibirsk, 1967 (in Russian).
5.20. G. I. Marchuk, *Methods of Computational Mathematics*, Nauka, Moscow, 1980 (in Russian), p. 53.
5.21. A. A. Samarsky, *The Theory of Difference Schemes*, Nauka, Moscow, 1977 (in Russian).
5.22. A. I. Tolstykh, *Dckl. Akad. Nauk SSSR*, 272, 3 (1983).
5.23. W. B. Briley, *J. Comput. Phys.* 24, 4: 327 (1977).
5.24. R. M. Beam and R. F. Warming, *An Implicit Factored Scheme for the Compressible Navier-Stokes Equations*, AIAA Paper, 77-645.
5.25. V. M. Kovenya and N. N. Yanenko, *Splitting Method in Gasdynamics Problems*, Nauka, Novosibirsk, 1981 (in Russian).
5.26. A. I. Erofeev and V. A. Perepukhov, *Uch. Zap. TsAGI* 6, 3: 51 (1975).
5.27. O. M. Belotserkovskii, A. N. Byrkin, A. P. Mazurov, and A. I. Tolstykh, *Zh. Vychisl. Matem. i Mat. Fiz.*, 22, 6: 1480 (1982).
5.28. A. P. Byrkin, *Uch. Zap. TsAGI* 7, 2: 25 (1976).
5.29. C. P. Li, *A Numerical Study of Separated Flows Induced by Shock Wave/ Boundary-layer Interaction.* AIAA Paper, 77-168.

6 Three-dimensional Boundary Layer at the Surface of a Dihedral Corner

V. P. Shidlovsky, D.Sc. (Phys.-Math.)

6.1. INTRODUCTION

The dihedral corner formed by two semi-infinite plates represents the simplest configuration on whose surface the boundary layer is essentially three-dimensional. The problem of such a boundary layer represents a natural generalization of the Blasius problem, and the numerous efforts to build up its closed solution have appeared at rather early stage of the development of boundary layer theory. In this connection we could mention the papers by Loitsianskii [6.1, 6.2], Loitsianskii and Bolshakov [6.3], Carrier [6.4], Sowerby and Cooke [6.5], Sowerby [6.6], Howarth [6.7], Stewartson and Howarth [6.8], where some approximate solutions were proposed either for the general problem of a dihedral corner of arbitrary size, or for particular problems of right-angle corner or "quarterinfinite" plate. In spite of differences in their approach, the authors listed above have highlighted the most important features of boundary layers along the dihedral corners.

The purely quantitative factor, that is, an increase in the number of arguments, is not the only source of the difficulties involved in solving this problem. As a matter of fact, formal application of the transformation of variables generally accepted in boundary layer theory, leads here to an incomplete set of equations. In some of the references cited this difficulty was avoided by using integral relations instead of differential equations, while other authors tried to complete the set of equations by some artificial ways, for example, by splitting the continuity equation. The rigorous mathematical formulation of the problem of boundary layer along the right-angle corner was proposed by Rubin [6.9], who suggested that the set should be completed by using those equations, which degenerate in the classical theory and indicate only the absence of pressure changes across the boundary layer. Such a technique might seem purely formal, but it has quite logical substantiation. In fact, the boundary layer under consideration must possess the usual properties in any streamwise cross section parallel to the edge of a dihedral corner. If, however, the normal cross section is considered, then it becomes clear that the classical theory will not be adequate for a description of flow in this section just because of the existence of the corner point, where one cannot meet the usual requirement that the

radius of curvature of the surface be of the order not less than unity. If so, then in this cross section the viscous, inertial terms and the terms related to the pressure change should be of the same order. Just such a hypothesis forms the basis for the derivation of those equations, which Rubin calls "corner-layer equations", though in their real meaning they still remain the boundary layer equations.

6.2. FORMULATION OF THE PROBLEM

Consider the configuration of somewhat more general type than that of Rubin, which represents the dihedral corner of arbitrary size β (Fig. 6.1). The leading edge of such a configuration

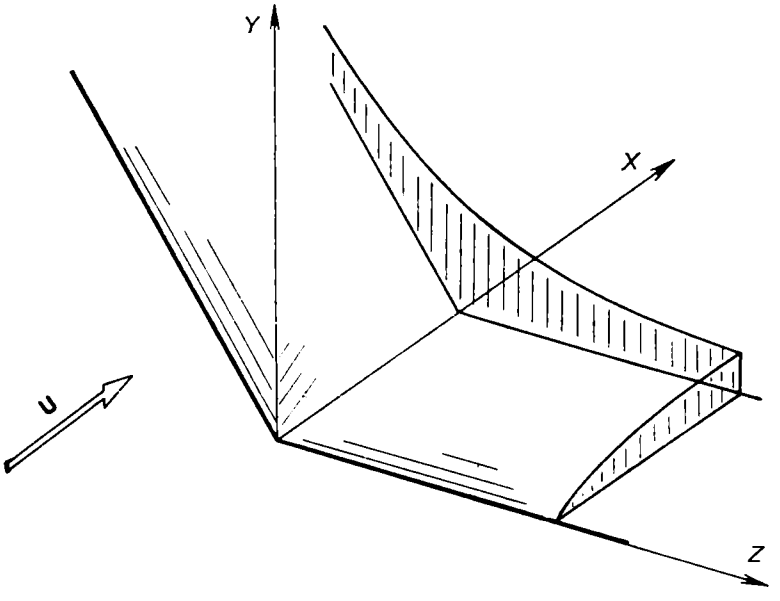

Fig. 6.1.

is perpendicular to the oncoming stream direction, while the stream itself is directed along the corner's edge. The flow is considered to be steady.

A dimensionless cartesian coordinate system is chosen in such a way that the X-axis coincides in direction with the mainstream velocity and has a unit scale of length, while the Y- and Z-axes are scaled in accordance with the rules of boundary layer theory. Upon the introduction of the notation

$$n = \beta/\pi \tag{6.1}$$

we are going to change the coordinates z and y for new independent variables ξ and η. To do that the conformal transformation is carried out, which maps the interior of the corner to the upper half-plane (Fig. 6.2). If the complex variables are introduced

$$x = z + iy, \quad \Lambda = \xi + i\eta \tag{6.2}$$

then the transformation corresponds to a formula

$$x = n^{-1}\Lambda^n,$$

or

$$z + iy = n^{-1}(\xi^2 + \eta^2)^{n/2}(\cos n\varphi + i \sin n\varphi), \tag{6.3}$$

where $\varphi = \arctan(\eta/\xi)$.

Taking into account scaling of the coordinates and projections of velocities, and denoting by u, v and w the velocity components in orthogonal directions x, η and ξ, correspondingly, we obtain

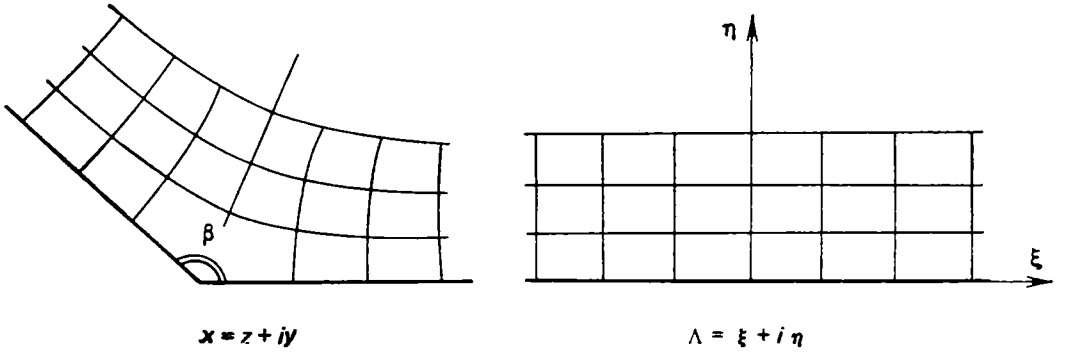

Fig. 6.2.

the continuity equation and the longitudinal projection of the momentum equation in the form

$$\frac{\partial(e^2u)}{\partial x} + \frac{\partial(ev)}{\partial \eta} + \frac{\partial(ew)}{\partial \xi} = 0, \tag{6.4}$$

$$e^2u\frac{\partial u}{\partial x} + ev\frac{\partial u}{\partial \eta} + ew\frac{\partial u}{\partial \xi} = \frac{\partial^2 u}{\partial \eta^2} + \frac{\partial^2 u}{\partial \xi^2} \tag{6.5}$$

which include the metric complex of the transformation

$$e = (\eta^2 + \xi^2)^{(n-1)/2}. \tag{6.6}$$

In accordance with what was said earlier on the order of different terms of equations, two remaining projections of the momentum equation contain a new variable—pressure—and together with Eqs. (6.4) and (6.5) form a closed set of equations. However, it would be more convenient to complete the set of equations in somewhat different way, by first using the properties of the problem for decreasing the number of arguments.

Like the Blasius problem, the problem of a flow about dihedral corner does not involve any characteristic length, so that its solution should depend only on such a combination of initial arguments,

which contains no characteristic length. In the present case such new arguments have the form

$$\lambda = \eta x^{-1/2n}, \quad \sigma = \xi x^{-1/2n}. \tag{6.7}$$

After introducing the notations

$$h = (\lambda^2 + \sigma^2)^{(n-1)/2} = e x^{(1-n)/2n}, \tag{6.8}$$

$$V = x^{1/2} h v - (2n)^{-1} \lambda h^2 u, \quad W = x^{1/2} h w - (2n)^{-1} \sigma h^2 u. \tag{6.9}$$

Eqs. (6.4) and (6.5) can be reduced to the form

$$\frac{\partial V}{\partial \lambda} + \frac{\partial W}{\partial \sigma} = -h^2 u \tag{6.10}$$

$$V \frac{\partial u}{\partial \lambda} + W \frac{\partial u}{\partial \sigma} = \frac{\partial^2 u}{\partial \lambda^2} + \frac{\partial^2 u}{\partial \sigma^2}. \tag{6.11}$$

Following Rubin's idea, we complete the set of equations by using the Helmholtz equation for vorticity diffusion rather than the momentum equation. Let us recall the vectorial form of this equation:

$$(\mathbf{v} \cdot \nabla)\, \boldsymbol{\omega} - (\boldsymbol{\omega} \cdot \nabla)\, \mathbf{v} = \nabla^2 \boldsymbol{\omega}. \tag{6.12}$$

In particular, the longitudinal component of the vorticity vector $\boldsymbol{\omega}$ is expressed as

$$\omega_x = e^{-2} [\partial (ew)/\partial \eta - \partial (ev)/\partial \xi]. \tag{6.13}$$

In the same way as Eqs. (6.10) and (6.11), Eq. (6.12) in its projection on the x-axis is transformed to variables λ and σ. If the function responsible for vorticity effects is defined as

$$\theta = x\omega_x + (2n)^{-1} (\lambda\, \partial u/\partial \sigma - \sigma\, \partial u/\partial \lambda), \tag{6.14}$$

then in addition to Eqs. (6.10) and (6.11) we obtain the following equations:

$$\frac{\partial W}{\partial \lambda} - \frac{\partial V}{\partial \sigma} = h^2 \theta, \tag{6.15}$$

$$V \frac{\partial \theta}{\partial \lambda} + W \frac{\partial \theta}{\partial \sigma} - h^2 u \left(\frac{\sigma}{2n} \frac{\partial u}{\partial \lambda} - \frac{\lambda}{2n} \frac{\partial u}{\partial \sigma} + \theta \right) = \frac{\partial^2 \theta}{\partial \lambda^2} + \frac{\partial^2 \theta}{\partial \sigma^2}. \tag{6.16}$$

Thus we have obtained the set of Eqs. (6.10), (6.11), (6.15), and (6.16) which determine the distribution of velocities and vorticity within the boundary layer at the surface of a dihedral corner. The highest derivatives enter this set in linear form, though Eqs. (6.11) and (6.16) also contain nonlinear terms. It is clearly seen that the equations are elliptic, which is in complete agreement with the modern notions on three-dimensional boundary layers, in whose cross-sections the local disturbances propagate instantaneously, that is, in accordance with the laws of elliptical equations.

One of the main advantages of the curvilinear coordinates used here is the simplicity of formulation of boundary conditions. The surface $\lambda = 0$ always coincides with a solid surface, while the surface $\sigma = 0$ corresponds to the symmetry plane of the corner. Further on, by any fixed value of σ the outer boundary of a boundary layer corresponds to an asymptotic condition $\lambda \to \infty$ whereas a condition $\sigma \to \infty$ with finite λ means a transition to the Blasius boundary layer, where the solution is known.

While the boundary conditions for velocities, that is, for u, V, and W, are sufficiently clear from the physical point of view, this is not true for the vorticity conditions. Nevertheless, one can state that the vorticity will vanish at the outer boundary of a layer and far away from the ridge of the corner (as $\sigma \to \infty$), and also at the symmetry plane ($\sigma = 0$).

However, before giving such a formulation of the boundary conditions which would permit to pass on to the numerical solution of the problem, it is necessary to analyze the asymptotic behaviour of the unknown functions, first of all at the large values of the argument σ.

6.3. ASYMPTOTIC BEHAVIOUR OF THE SOLUTION

As we have already mentioned, at sufficiently large values of σ the solution for all the four of unknown functions must asymptotically turn into the Blasius solution for a semi-infinite plate. First of all, it is clear that the longitudinal velocity component u within this region should approximately correspond to an expression

$$u_a = f'(\zeta), \tag{6.17}$$

where $f(\zeta)$ is the Blasius function, and

$$\zeta = \lambda \sigma^{n-1} \tag{6.18}$$

for $\sigma \gg \lambda$.

Turning to the second of Eqs. (6.9), it should be noted that as σ grows the quantity w should remain finite, and therefore the predominant role will be played by the second term of the expression for W, that is

$$W_a = -(2n)^{-1} \sigma^{2n-1} f'(\zeta). \tag{6.19}$$

Using Eqs. (6.17) and (6.19) we can obtain from Eq (6.10)

$$V_a = (2n)^{-1} \sigma^{n-1} [-nf(\zeta) + (n-1)\, \zeta f'(\zeta)] \tag{6.20}$$

whereas Eq. (6.15) makes it possible to obtain the main term in σ for modified vorticity:

$$\theta_a = -(2n)^{-1} \sigma^n f''(\zeta). \tag{6.21}$$

Substituting Eqs. (6.17), (6.19), (6.20), and (6.21) into Eqs. (6.11) and (6.16) we can obtain either the classical Blasius equation (from Eq. (6.11)) or its differentiated version (from Eq. (6.16)) up to the neglected terms of the order σ^{-2n}. This confirms the validity of the asymptotic formulas we have suggested. At the same time, the fact that the unbalanced terms in some of the governing equations are of the order σ^{-2n} suggests the possibility of using asymptotic expansions in the form

$$u = f'(\zeta) + \sigma^{-2n} u_1(\zeta) + \ldots,$$
$$V = \sigma^{n-1}\left[-\frac{1}{2} f(\zeta) + \frac{n-1}{2n}\zeta f'(\zeta) + \sigma^{-2n} V_1(\zeta) + \ldots\right], \tag{6.22}$$
$$W = \sigma^{2n-1}\left[-\frac{1}{2n} f'(\zeta) + \sigma^{-2n} W_1(\zeta) + \ldots\right],$$
$$\theta = \sigma^{n}\left[-\frac{1}{2n} f''(\zeta) + \sigma^{-2n}\theta_1(\zeta) + \ldots\right].$$

Substitution of expansions (6.22) into Eqs. (6.10), (6.11), (6.15), and (6.16) permits us to obtain the differential equations for the first-order terms. After determining these terms, one could similarly obtain the equations for second-order terms, etc. The linear ordinary differential equations containing first-approximation terms are as follows:

$$u_1'' + \frac{1}{2} f u_1' - f' u_1 - f'' V_1 - (n-1)\zeta f'' W_1$$
$$= -(n-1)\zeta[(n-2) f'' + (n-1)\zeta f'''], \tag{6.23}$$
$$\theta_1'' + \frac{1}{2} f\theta_1' + \frac{1}{2} f'\theta_1 + \frac{1}{2n} f' u_1' + \frac{1}{2n} f''' V_1 + \frac{1}{2n}[n f'' + (n-1)\zeta f'''] W_1$$
$$= \frac{(n-1)}{2n}[n f'' + (3n-2)\zeta f''' + (n-1)\zeta^2 f^{\mathrm{IV}} + \zeta^2 f' f''], \tag{6.24}$$
$$V_1' + (n-1)\zeta W_1' = W_1 - u_1, \tag{6.25}$$
$$W_1' = \theta_1 + \frac{n-1}{2n}[-n f + (n-2)\zeta f' + (n-1)\zeta^2 f'']. \tag{6.26}$$

By the numerical solution of a complete boundary value problem the necessity of determining of the first-order or higher-order approximations is stipulated by the magnitude of actual limit value σ_N, as well as by that of parameter n. It seems that for the cases of practical interest there is always possibility to choose σ_N in such a way that $\sigma_N^{-2n} \ll 1$ and that the main terms of expansions (6.22) provide the necessary accuracy of calculations.

It should be noted that the asymptotic analysis for the right-angle dihedral corner was conducted by Pal and Rubin [6.10].

These authors did not use the transformation (6.3), and their results practically coincide with ours for the particular value of parameter $n = 1/2$.

At the outer boundary of a boundary layer, that is, as $\lambda \to \infty$ the longitudinal velocity component should approach unity. If so, then the asymptotic expressions for functions V and W will be, correspondingly,

$$V_b = -(2n)^{-1} (\lambda^2 + \sigma^2)^{n-1} \lambda, \tag{6.27}$$

$$W_b = -(2n)^{-1} (\lambda^2 + \sigma^2)^{n-1} \sigma. \tag{6.28}$$

Taking into account the algebraic character of the asymptotic behaviour of V and W, from the structure of Eqs. (6.11) and (6.16) one can deduce that functions u and θ will approach their limiting values exponentially.

6.4. NUMERICAL SOLUTION AND RESULTS OF CALCULATIONS

Our ultimate aim is to construct a numerical solution of Eqs. (6.10), (6.11), (6.15) and (6.16) with boundary conditions resulting from the physical considerations, properties of symmetry of the flow, and the results of the asymptotic analysis of Sec. 6.3.

$$\begin{aligned}
&u = V = W = 0, \quad \theta = \sigma^{2(1-n)} \partial W/\partial\lambda \text{ at } \lambda = 0,\\
&u \to 1, \quad \theta \to 0, \quad V \to -(2n)^{-1} \lambda (\lambda^2 + \sigma^2)^{n-1},\\
&W \to -(2n)^{-1} \sigma (\lambda^2 + \sigma^2)^{n-1} \text{ as } \lambda \to \infty,\\
&W = \theta = \partial u/\partial\sigma = \partial V/\partial\sigma = 0 \quad \text{at} \quad \sigma = 0,\\
&u \to f'(\zeta), \quad V \to -(2n)^{-1} \sigma^{n-1} [nf(\zeta) - (n-1)\, \zeta f'(\zeta)],\\
&W \to -(2n)^{-1} \sigma^{2n-1} f'(\zeta), \quad \theta \to -(2n)^{-1} \sigma^n f''(\zeta) \text{ as } \sigma \to \infty.
\end{aligned} \tag{6.29}$$

When choosing the method of numerical computation we proceeded from the possibilities of the BESM-6 computer used. The method applied here was based on the principle of attaining time-independence with directional splitting. Moreover, the program included an iterative cycle which permitted to deal with the linear difference equations within each iteration. The matrices of coefficients in these equations being tri-diagonal, satisfaction of boundary conditions was ensured by the application of sweep method.

For carrying out the iterations the complete set of equations is divided in two groups. The first group includes the momentum equations (Eq. (6.11)) and the vorticity diffusion equation (Eq. (6.16)). If functions V and W are given by some approximate expressions, then Eq. (6.11) becomes linear and can be used for finding u (λ, σ),

after which from Eq. (6.16) one might determine $\theta(\lambda, \sigma)$. With the functions u and θ known, the numerical solution of Eqs. (6.10) and (6.15) is considerably simplified: their cross-differentiation allows to obtain two Poisson-like equations for more accurate determination of the functions V and W, which once again are substituted into Eq. (6.11), and the whole cycle is repeated. The iterations are stopped either after the achievement of convergence, or after the prescribed number of cycles. Computations have shown that the convergence is eventually achieved with any choice of initial approximations for V_0 and W_0 compatible to the conditions (6.29), but the rate of convergence will be different for different versions. One of the versions closest to optimum was realized with the initial approximations

$$\begin{aligned} V_0 &= -(2n)^{-1}\,\lambda\,(\lambda^2+\sigma^2)^{n-1}\,u, \\ W_0 &= -(2n)^{-1}\,\sigma\,(\lambda^2+\sigma^2)^{n-1}\,u. \end{aligned} \tag{6.30}$$

Substitution of Eqs. (6.30) into Eq. (6.11) leads to the following type of quasilinear equation for determining the initial approximation u_0:

$$\frac{(\lambda^2+\sigma^2)^{n-1}}{2n}\left(\lambda u_0\frac{\partial u_0}{\partial\lambda}+\sigma u_0\frac{\partial u_0}{\partial\sigma}\right)+\frac{\partial^2 u_0}{\partial\lambda^2}+\frac{\partial^2 u_0}{\partial\sigma^2}. \tag{6.31}$$

The existence of nonlinear terms requires an additional iteration cycle to be introduced into the block scheme (see [6.12]). However, this cannot be considered as a drawback of the approximation (6.30), since the need for additional iterations is more than compensated by a decrease in the number of iterations in the outer cycle as compared to the initial approximation version which does not involve functions u.

In order to ensure the stability of the algorithm at all stages of computation, implicit difference schemes were employed. If we disregard the above-mentioned initial approximation for velocity u, the computation of a specific approximation for each of the required functions is reduced to inversion of the difference analogue of the purely linear form, of the two-dimensional Poisson equation. According to the number of unknown functions, four kinds of such equations were encountered and solved by the method of attaining time-independence. Each step on the artificial time scale was split into two half-steps for the purpose of directional splitting in accordance with the principles of the fractional-step method [6.13, 6.14]. Naturally, to attain time-independence, it was necessary to make a sufficiently large number of steps along the artificial time scale. Nevertheless, both simplicity and uniformity of the algorithms at each half-step permitted to confine the total computational time for each version within reasonable limits. With a computer of moderate power, like an BESM-6, this computational time was not, as a rule, larger than one hour.

The computational program was compiled for an arbitrary value of the parameter n, that is, for an arbitrary size of a dihedral corner. However, it is necessary to keep in mind that for very small values of n the theory presented here will not hold, because the boundary layers on each of the edges of the corner might merge with each other.

Two discrete values of the parameter n were taken in the calculations (1) $n = 2$, (2) $n = 1/2$. The first of these values corresponds to the case of the "quarterinfinite" plate, that is, a plate with a leading

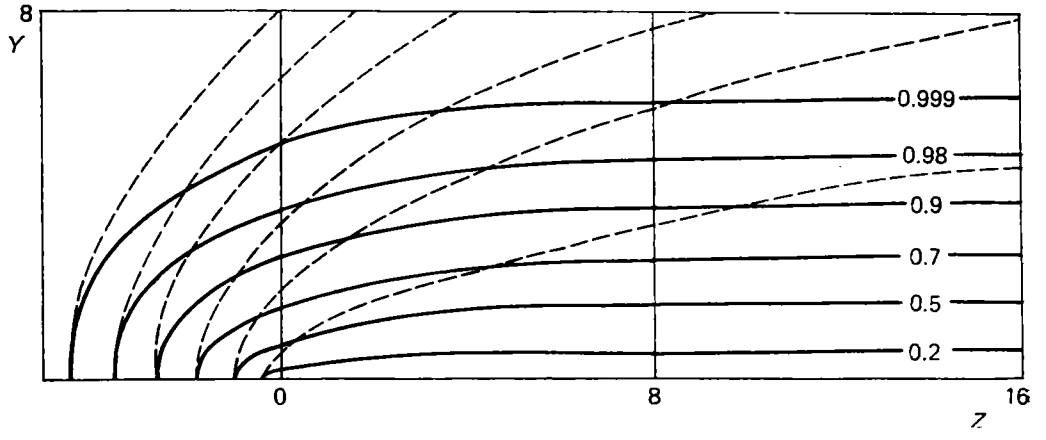

Fig. 6.3.

edge coinciding with a positive semi-axis Z, and with a side edge aligned to the semi-axis X (see Fig. 6.1). The second version is just the right-angle corner, the numerical study of the flow about which, conducted by a different method, was described by Rubin and Grossman [6.11].

The numerical results for quarterinfinite plate ($n = 2$) are illustrated in the figures. Figure 6.3 shows isovels of a streamwise velocity component, where the dashed curves show for comparison the coordinate lines $\lambda = \text{const}$ passing through the same points of the symmetry plane of the corner. Figure 6.4 shows the profiles of a streamwise velocity in three curvilinear cross-sections $\sigma = \text{const}$. Figure 6.5 shows the streamlines of the secondary flow, or, more exactly, the intersections of streamsurfaces with the plane $x = \text{const}$. It can be seen that the highest vorticity of the secondary flow is achieved at a certain distance from the side edge and is gradually decaying both when approaching the edge and when moving away from it.

The diagram of variation of a friction stress at the surface of a quarterinfinite plate is shown in Fig. 6.6. As is the case with all obtuse corners ($n > 1$), at $z = 0$ the friction stress becomes infinitely

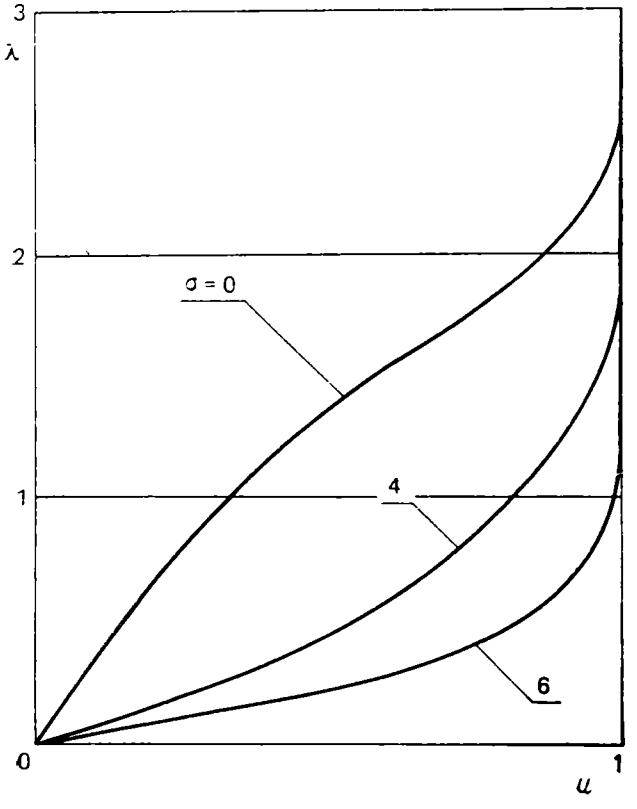

Fig. 6.4.

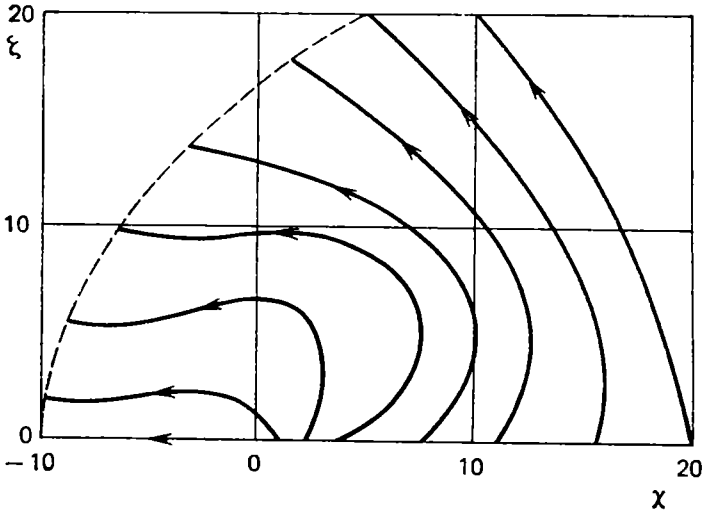

Fig. 6.5.

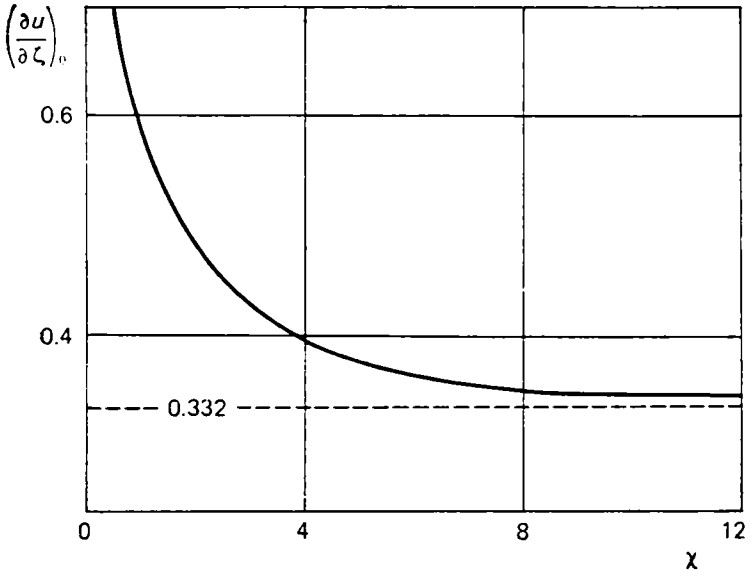

Fig. 6.6.

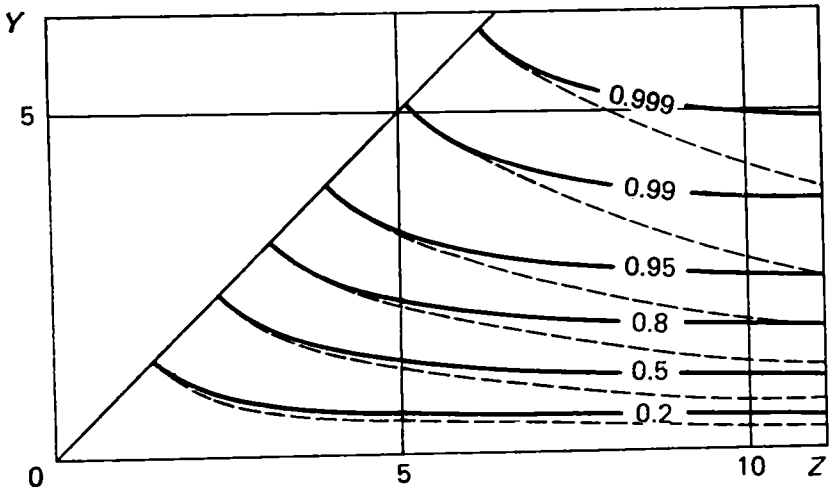

Fig. 6.7.

large, though the singularity is integrable and the relative variation in the friction force is expressed as ($\chi = zx^{-1/2n}$)

$$\delta F = \int_0^\infty \left[\left(\frac{\partial u}{\partial \zeta_0}\right) - f''(0)\right] d\chi = 2.961 \quad (n = 2). \tag{6.32}$$

Similar results for a right-angle corner ($n = 1/2$) are shown in Figs. 6.7-6.10. Most of the results basically coincide with those obtained by Rubin and Grossman, but where the latter differ notice-

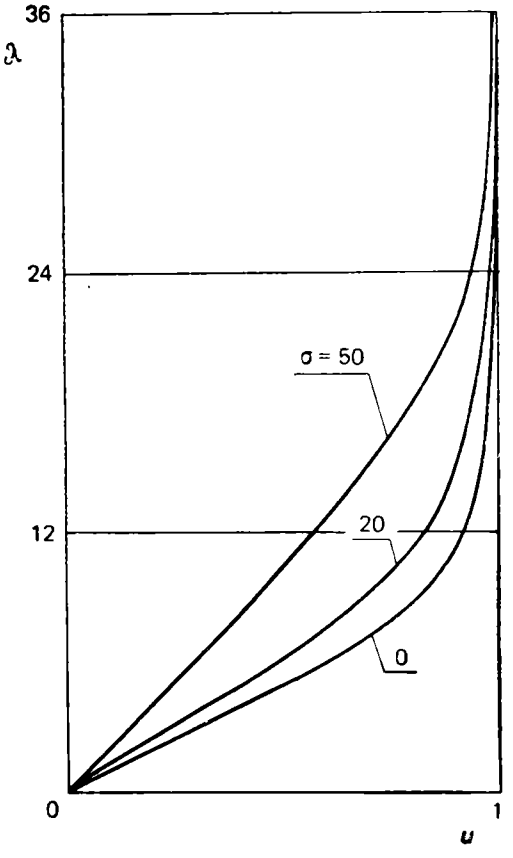

Fig. 6.8.

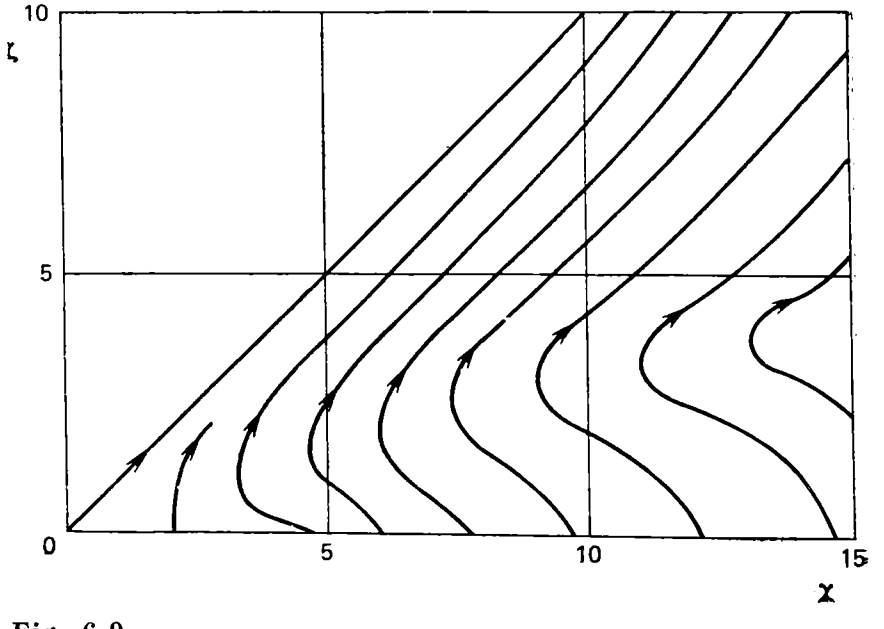

Fig. 6.9.

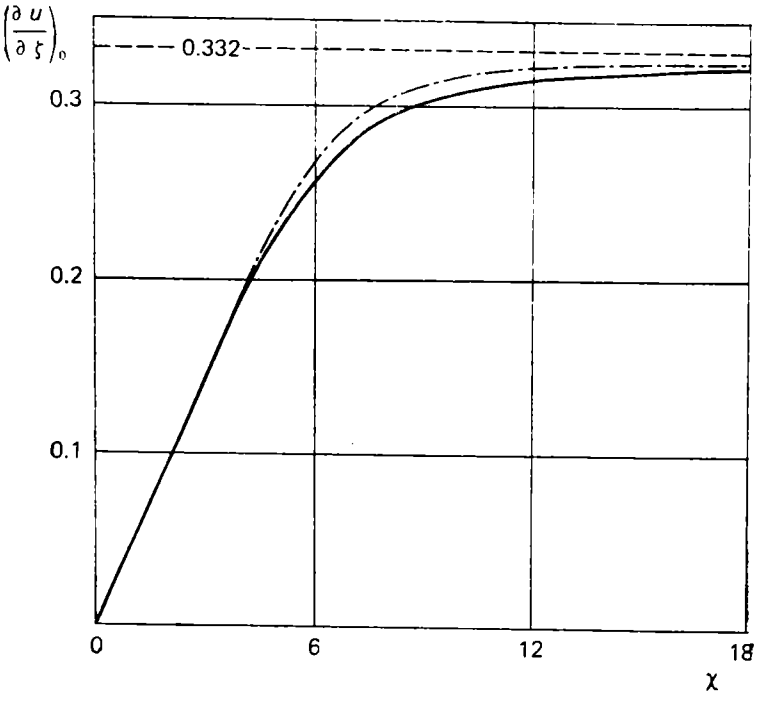

Fig. 6.10.

ably from our results, the data of these authors are indicated by dotted lines. We also give below the result of calculation of the change in total friction force for this case:

$$\delta F = -1.486 \quad (n = 1/2). \tag{6.33}$$

References

6.1. L. G. Loitsianskii, *Proceedings of TSAGI*, No. 249, 1936 (in Russian).
6.2. L. G. Loitsianskii, *Proceeding of the Leningrad Industrial Institute, Section of Physics and Mathematics*, No. 1, 1937 (in Russian).
6.3. L. G. Loitsianskii and V. P. Bolshakov, *Proceedings of TsAGI*, No. 279, 1937 (in Russian).
6.4. G. F. Carrier, *Quart. Appl. Math.*, 4, 367-370, 1947.
6.5. L. Sowerby and Cooke J. C. *Quart J. Mech. and Appl. Math.*, 6, part 1, 50-70, 1953.
6.6. L. Sowerby, *Quart. J. Mech. and Appl. Math.*, 11, part 3, 390-301, 1958.
6.7. L. Howarth, *Proc. of the Cambr. Phil. Soc.*, 46, part 1, 127-140, 1950.
6.8. K. Stewartson and L. Howarth, *J. Fluid Mech.*, 7, part 1, 1-21, 1960.
6.9. S. G. Rubin, *Fluid Mech.*, 26, part 1, 97-110, 1966.
6.10. A. Pal and S. G. Rubin, *Quart. Appl. Math.*, 29, No. 1, 91-108, 1971.
6.11. S. G. Rubin and B. Grossman, *Quart. Appl. Math.*, 29, No. 2, 169-186, 1971.
6.12. A. A. Samarsky, *Introduction into the Theory of Difference Schemes*, Nauka, Moscow, 1971 (in Russian).
6.13. N. N. Yanenko, *Fractional-step Method for Multidimensional Problems in Mathematical Physics*, Nauka, Novosibirsk, 1967 (in Russian).
6.14. V. M. Kovenya and N. N. Yanenko, *The Splitting Method in Gas Dynamics Problems*, Nauka, Novosibirsk, 1981 (in Russian).

7 On the Stability of a Compressible Boundary Layer Against Three-dimensional Disturbances with Self-induced Pressure Gradient

O. S. Ryzhov, *D.Sc. (Phys.-Math.)*,
and V. I. Zhuk, *Cand. Sc. (Phys.-Math.)*

In some cases, the problem on the boundary layer stability can be formulated in the framework of the free interaction theory [7.1-7.3]. The time-dependent version of this theory [7.4-7.7] makes it possible to analyze long-wave disturbances on the basis of the Prandtl equations, with self-induced pressure included, instead of complete Navier-Stokes equations. It was shown [7.8, 7.9] that internal waves in an incompressible boundary layer, which give rise to an intrinsic pressure gradient, are the asymptotic form of the Tollmien-Schlichting waves in the limit when the Reynolds number tends to infinity. Numerous applications of the free-interaction triple-deck theory are discussed in recent reviews [7.10, 7.11].

The splitting of the boundary layer into several sublayers with different properties made it possible to determine the shape of the lower and upper branches of the neutral curve to a high degree of accuracy, including non-parallel flow effects [7.12, 7.13]. A generalization of the classical concept of neutral stability curve to the three-dimensional case is given in [7.14-7.16].

The three-dimensional nature of disturbances is observed in their evolution stage preceding transition. It was noted in [7.17] that many features of this process can be explained on the basis of the existing linear or weakly nonlinear theories. This article presents a detailed linear analysis of the three-dimensional boundary layer equations with self-induced pressure.

7.1. STATEMENT OF THE PROBLEM

Suppose that the evolution in time of the amplitudes, wavelengths, and frequencies of three-dimensional disturbances in the boundary layer of a compressible gas are described by free-interaction theory asymptotic equations [7.1-7.7]. In this case the velocity field is divided into three sublayers, the pressure gradient produced by a change in the boundary-layer displacement thickness being an unknown function.

Let us place the origin of Cartesian coordinates at a distance L from the leading edge of a body with the x- and y-axes directed

along the unperturbed velocity vector and the normal to the tangential plane respectively. To nondimensionalize the problem, we denote time by $(L/U_\infty)\,t$, the Cartesian coordinates by Lx, Ly and Lz, the corresponding velocity components by $U_\infty u$, $U_\infty v$ and $U_\infty w$, the dynamic pressure by $\rho_\infty U_\infty^2 p$, and the gas density by $\rho_\infty \rho$, the subscript ∞ indicating the oncoming flow parameters. The velocity U_∞ at infinity may be either subsonic or supersonic, the Mach numbers $M_\infty \neq 1$ only are considered.

Designating the Reynolds number for the distance L by Re_1, let us introduce the small parameter $\varepsilon = Re_1^{-1/8}$. The free-interaction regime takes place under the condition that the following representation is valid for the main part of the boundary layer:

$$(u,\ v,\ w,\ p,\ \rho) = (U_0 + \varepsilon u',\ \varepsilon^2 v',\ \varepsilon^2 w',\ \varepsilon^2 p',\ R_0 + \varepsilon\rho'). \tag{7.1.1}$$

Here, the longitudinal component of the velocity vector U_0 and the density R_0 in the unperturbed boundary layer depend on the variable $y' = \varepsilon^{-4}y$. While the arguments of the primed perturbation functions are $t' = \varepsilon^{-2}t$, $x' = \varepsilon^{-3}x$, $y' = \varepsilon^{-4}y$, and $z' = \varepsilon^{-3}z$. Thus, the flow is characterized by rapid variations of gas parameters in the longitudinal (x) and lateral (z) directions, the perturbation wavelengths being much larger than the boundary layer thickness (which is of the order of ε^4) but much smaller than the length of the body.

From the inviscid flow equations, to which the Navier-Stokes equations are reduced if the solution is sought in the form (7.1.1) the primed functions are obtained in the form of explicit expressions containing an arbitrary function $A\,(t',\ x',\ z')$ [7.1-7.7]. This function defines the instantaneous displacement of streamline projections onto the xy-plane relative to their unperturbed position.

In the nonlinear viscous sublayer near the wall, the perturbation of the longitudinal velocity component becomes of the order of the velocity itself. Hence, instead of (7.1.1), one should write for $y' = O(\varepsilon)$

$$(u,\ v,\ w,\ p,\ \rho) = (\varepsilon u'',\ \varepsilon^3 v'',\ \varepsilon w'',\ \varepsilon^2 p'',\ \rho''), \tag{7.1.2}$$

where the dependence on the vertical coordinate is given in terms of the variable $y'' = \varepsilon^{-5}y$. The scales of other independent variables remain the same as in the main part of the boundary layer.

Substitution of expressions (7.1.2) into the Navier-Stokes system leads to the equations for double-primed functions. The latter equations have the form of Prandtl's time-dependent equations with a pressure gradient that is not known beforehand.

In the outer region of a weakly perturbed flow resulting from the displacement thickness change, the Euler equations are valid. Since

in this region the length scales along the x-, y-, and z-axes are the same and have the order of ε^3, the excess pressure satisfies the wave equation for $M_\infty > 1$ or the Laplace equation for $M_\infty < 1$.

The characteristic scale of the order of ε^{-2} for the frequency of unsteady disturbances is chosen so that the flow is quasistationary everywhere except for the near-wall region where the time derivatives are significant even in the first approximation.

For further analysis it is convenient to write the above equations, as well as the boundary conditions obtained by matching with expressions (7.1.1), in canonical form. For simplicity, consider the body in a flow to be a flat heat-insulated plate. Suppose that the viscosity λ_1 depends on the temperature T in accordance with the Chapman law $\lambda_1/\lambda_{1\infty} = CT/T_\infty$, $C = \text{const}$, and the Prandtl number is equal to unity. For a heat-insulated plate, the derivative $dR_0(0)/dy' = 0$. Hence for the solution we can put $\rho'' = R_0(0) + O(\varepsilon^2)$. Consequently, the first-order equation for density from the Prandtl system is satisfied identically.

Let us perform an affine transformation in the equations for the near-wall region:

$$
\begin{aligned}
t &= \varepsilon^2 t'' = \varepsilon^2 C^{1/4}\lambda^{-3/2}\,|M_\infty^2 - 1|^{-1/4}\left(\frac{T_w}{T_\infty}\right) t_1,\\
x &= \varepsilon^3 x'' = \varepsilon^3 C^{3/8}\lambda^{-5/4}\,|M_\infty^2 - 1|^{-3/8}\left(\frac{T_w}{T_\infty}\right)^{3/2} x_1,\\
y &= \varepsilon^5 y'' = \varepsilon^5 C^{5/8}\lambda^{-3/4}\,|M_\infty^2 - 1|^{-1/8}\left(\frac{T_w}{T_\infty}\right)^{3/2} y_1,\\
z &= \varepsilon^3 z'' = \varepsilon^3 C^{3/8}\lambda^{-5/4}\,|M_\infty^2 - 1|^{-3/8}\left(\frac{T_w}{T_\infty}\right)^{3/2} z_1,\\
u &= \varepsilon u'' = \varepsilon C^{1/8}\lambda^{1/4}\,|M_\infty^2 - 1|^{-1/8}\left(\frac{T_w}{T_\infty}\right)^{1/2} u_1,\\
v &= \varepsilon^3 v'' = \varepsilon^3 C^{3/8}\lambda^{3/4}\,|M_\infty^2 - 1|^{1/8}\left(\frac{T_w}{T_\infty}\right)^{1/2} v_1,\\
w &= \varepsilon w'' = \varepsilon C^{1/8}\lambda^{1/4}\,|M_\infty^2 - 1|^{-1/8}\left(\frac{T_w}{T_\infty}\right)^{1/2} w_1,\\
p &= \varepsilon^2 p'' = \varepsilon^2 C^{1/4}\lambda^{1/2}\,|M_\infty^2 - 1|^{-1/4} p_1,\\
A' &= C^{5/8}\lambda^{-3/4}\,|M_\infty^2 - 1|^{-1/8}\left(\frac{T_w}{T_\infty}\right)^{3/2} A_1.
\end{aligned}
\tag{7.1.3}
$$

In the region adjacent to the boundary layer from above, we make a substitution according to the formulas

$$
\begin{aligned}
y &= \varepsilon^3 C^{3/8}\lambda^{-5/4}\,|M_\infty^2 - 1|^{-7/8}\left(\frac{T_w}{T_\infty}\right)^{3/2} \hat{y}_1,\\
v &= \varepsilon^2 C^{1/4}\lambda^{1/2}\,|M_\infty^2 - 1|^{-1/4}\,\hat{v}_1
\end{aligned}
\tag{7.1.4}
$$

and formulas (7.1.3) for x, z and p. In these transformations, the constant $\lambda = 0.3321$ defined by the equation $dU_0(0)/dy' = \lambda C^{-1/2}(T_w/T_\infty)^{-1}$ is calculated from the Blasius solution for an unperturbed boundary layer and T_w is the wall temperature.

The problem for perturbation functions is finally formulated as follows. In the new variables, the system of equations for the wall sublayer is

$$\begin{aligned} &\frac{\partial u}{\partial x}+\frac{\partial v}{\partial y}+\frac{\partial w}{\partial z}=0, \quad \frac{\partial p}{\partial y}=0, \\ &\frac{\partial u}{\partial t}+u\frac{\partial u}{\partial x}+v\frac{\partial u}{\partial y}+w\frac{\partial u}{\partial z}=-\frac{\partial p}{\partial x}+\frac{\partial^2 u}{\partial y^2}, \\ &\frac{\partial w}{\partial t}+u\frac{\partial w}{\partial x}+v\frac{\partial w}{\partial y}+w\frac{\partial w}{\partial z}=-\frac{\partial p}{\partial z}+\frac{\partial^2 w}{\partial y^2} \end{aligned} \tag{7.1.5}$$

(here and below, the subscript 1 will be omitted).

The no-slip conditions for $y = 0$ are

$$u = 0, \; v = 0, \; w = 0. \tag{7.1.6}$$

The limiting conditions for $y \to \infty$ are

$$\begin{aligned} &p \to \hat{p}\,(t, x, 0, z), \\ &u \to y + A, \\ &w \to 0. \end{aligned} \tag{7.1.7}$$

The potential flow region above the boundary layer is described by

$$\begin{aligned} &\mp\frac{\partial^2 \hat{p}}{\partial x^2}+\frac{\partial^2 \hat{p}}{\partial \hat{y}^2}+|M_\infty^2-1|^{-1}\frac{\partial^2 \hat{p}}{\partial z^2}=0, \\ &\frac{\partial \hat{v}}{\partial x}=-|M_\infty^2-1|^{1/2}\frac{\partial \hat{p}}{\partial \hat{y}}. \end{aligned} \tag{7.1.8}$$

Here the upper or lower sign of the derivative $\partial^2\hat{p}/\partial x^2$ is chosen when the oncoming flow is supersonic or subsonic respectively. The second equation in system (7.1.8) follows from the equation of conservation of the momentum vertical component, written in terms of the new variables. Besides, the limit of the expression for the velocity vertical component in the boundary layer when $y' \to \infty$ is the boundary condition for $\hat{y} = 0$:

$$\hat{v}\,(t, x, 0, z) = -|M_\infty^2-1|^{1/2}\frac{\partial A}{\partial x}. \tag{7.1.9}$$

For the upstream boundary condition (as $x \to -\infty$) one may demand either damping or periodicity of all the required functions.

In contrast to the planar boundary layer, where the boundary condition of interaction for the wall-sublayer equations can be expressed in terms of the function $A\ (t,\ x,\ z)$, the three-dimensional disturbance equations (7.1.5) and (7.1.8) should be integrated simultaneously.

Similarity transformation (7.1.3) and (7.1.4) permits to exclude the number Re_1 from the equations and the boundary conditions as well as the constants associated with viscosity, friction and temperature in the unperturbed boundary layer for $y' = 0$. The dependence on the Mach number M_∞ is retained as a consequence of the three-dimensional nature of the flow.

7.2. DISPERSION RELATION

Let us seek the solutions of the systems (7.1.5) and (7.1.8) in the linear approximation. We put

$$\begin{aligned} u &= y - a\frac{df}{dy}e^{i(\alpha x+\beta z-\omega t)},\\ v &= age^{i(\alpha x+\beta z-\omega t)},\\ w &= -a\frac{dh}{dy}e^{i(\alpha x+\beta z-\omega t)},\\ p &= ae^{i(\alpha x+\beta z-\omega t)},\\ \hat{p} &= a\Pi(\hat{y})\,e^{i(\alpha x+\beta z-\omega t)},\\ \hat{v} &= aV(\hat{y})\,e^{i(\alpha x+\beta z-\omega t)}, \end{aligned} \tag{7.2.1}$$

where the amplitude factor a is considered to be small. First consider the region near the wall. Substituting expressions (7.2.1) into system (7.1.5) and neglecting terms of the order of a^2, one gets

$$\begin{aligned} &\frac{d^3f}{dy^3}+i(\omega-\alpha y)\frac{df}{dy}+i\alpha f+i\beta h+i\alpha=0,\\ &\frac{d^3h}{dy^3}+i(\omega-\alpha y)\frac{dh}{dy}+i\beta=0. \end{aligned} \tag{7.2.2}$$

The continuity equation leads to the finite relation

$$g = i(\alpha f + \beta h). \tag{7.2.3}$$

The boundary conditions on the surface give

$$\frac{df(0)}{dy}=0,\quad \frac{dh(0)}{dy}=0,\quad \alpha f(0)+\beta h(0)=0. \tag{7.2.4}$$

We denote

$$F=\frac{d^2f}{dy^2},\quad H=\frac{dh}{dy}. \tag{7.2.5}$$

Let us differentiate the first of equations (7.2.2) with respect to y and introduce the new complex variable $Z = (i\alpha)^{1/3} y - i^{1/3} \times (\omega/\alpha^{2/3})$. In order to fix the regular branch of the multiple-valued power function, one must cut the complex plane α along the positive imaginary semiaxis and put $-3\pi/2 < \arg \alpha < \pi/2$ (here and below $i = e^{i\pi/2}$). As a result, the system of equations (7.2.2) can be written in the form

$$\frac{d^2F}{dZ^2} - ZF + i^{1/3} \frac{\beta}{\alpha^{2/3}} H = 0, \tag{7.2.6}$$

$$\frac{d^2H}{dZ^2} - ZH + i^{1/3} \frac{\beta}{\alpha^{2/3}} = 0. \tag{7.2.7}$$

Differentiation of Eq. (7.2.7) with respect to the variable Z gives

$$\frac{d^3H}{dZ^3} - Z \frac{dH}{dZ} - H = 0. \tag{7.2.8}$$

A comparison of Eqs. (7.2.6) and (7.2.8) shows that the function $\tilde{F} = F + i^{1/3} \frac{\beta}{\alpha^{2/3}} \frac{dH}{dZ}$ satisfies the Airy homogeneous equation

$$\frac{d^2\tilde{F}}{dZ^2} - Z\tilde{F} = 0. \tag{7.2.9}$$

The transition to the function $\tilde{F}$ is an analogue of the Squire transformation [7.18], which is applicable since the initial system (7.1.5) does not contain an equation for the gas density.

Neglecting the exponentially increasing solutions of Eq. (7.2.9), one obtains

$$F(Z) = C_0 \mathrm{Ai}(Z) - i^{1/3} \frac{\beta}{\alpha^{2/3}} \frac{dH}{dZ}. \tag{7.2.10}$$

In accordance with the selection rule for a single-valued branch of the function $\alpha^{1/3}$, the complex variable Z lies in the sector $-\pi/3 < \arg Z < \pi/3$ as $y \to \infty$. The Airy function exponentially decreases in this sector. For the determination of the constant C_0, note that the no-slip conditions (7.2.4) and Eqs. (7.2.2) lead to the following relations on the surface

$$\frac{dF}{dZ} = -(i\alpha)^{2/3}, \quad \frac{d^2H}{dZ^2} = -i^{1/3} \frac{\beta}{\alpha^{2/3}} \quad \text{for } Z = -i^{1/3} \frac{\omega}{\alpha^{2/3}}. \tag{7.2.11}$$

Differentiating (7.2.10) once and taking into account (7.2.11), one gets

$$C_0 = \frac{\alpha^2 + \beta^2}{(i\alpha)^{4/3}} \left[\frac{d\mathrm{Ai}\left(-i^{1/3} \frac{\omega}{\alpha^{2/3}} \right)}{dZ} \right]^{-1}, \tag{7.2.12}$$

whence

$$\frac{df}{dZ} = -\frac{\alpha^2+\beta^2}{\alpha^2}\left[\frac{d\mathrm{Ai}(\zeta)}{dZ}\right]^{-1}\int_{\zeta}^{Z}\mathrm{Ai}(Z')\,dZ' - \frac{\beta}{i^{1/3}\alpha^{4/3}}H(Z), \tag{7.2.13}$$

$$\zeta = -i^{1/3}\frac{\omega}{\alpha^{2/3}}.$$

Expression (7.2.13) is written under the conditions $df/dZ = 0$, $H = 0$ for $Z = -i^{1/3}(\omega/\alpha^{2/3})$.

It follows from the third limiting condition (7.1.7) for the lateral component of the velocity vector that $H(Z) \to 0$ as $|Z| \to \infty$. (The solution of the Airy inhomogeneous equation for the function $H(Z)$, satisfying the above condition, is given in [7.9].) Consequently, as $y \to \infty$ we have

$$\frac{df}{dy} = \frac{\alpha^2+\beta^2}{(i\alpha)^{5/3}}\left[\frac{d\mathrm{Ai}(\zeta)}{dZ}\right]^{-1}\int_{\zeta}^{\infty}\mathrm{Ai}(Z)\,dZ. \tag{7.2.14}$$

Let us now consider the external region where the flow is governed by the system of equations (7.1.8). Substituting into this system the last two formulas from (7.2.1), one obtains

$$\Pi = e^{-\mu\hat{y}}, \quad V = \frac{\mu}{i\alpha}|\mathrm{M}_\infty^2 - 1|^{1/2}e^{-\mu\hat{y}}. \tag{7.2.15}$$

The complex parameter μ is defined as follows:

$$\mu = \begin{cases} [\beta^2|\mathrm{M}_\infty^2-1|^{-1} - \alpha^2]^{1/2}, & \mathrm{M}_\infty > 1, \\ [\beta^2|\mathrm{M}_\infty^2-1|^{-1} + \alpha^2]^{1/2}, & \mathrm{M}_\infty < 1. \end{cases} \tag{7.2.16}$$

In these expressions, the branch of the square root with $\mathrm{Re}\,\mu > 0$ is taken. This requirement ensures the damping of disturbances as $\hat{y} \to \infty$. The arbitrary factor in (7.2.15), up to which the functions Π and V from system (7.1.8) are determined, is chosen by taking into account the first boundary condition from (7.1.7) for pressure. For $\hat{y} = 0$, condition (7.1.9) allows us to determine the function $A(t, x, z)$:

$$A = -a\frac{\mu}{(i\alpha)^2}e^{i(\alpha x+\beta z-\omega t)}. \tag{7.2.17}$$

The second boundary condition for matching (7.1.7) for the longitudinal component of the velocity vector assumes the form

$$\frac{df}{dy} \to \frac{\mu}{(i\alpha)^2} \quad \text{for } y \to \infty. \tag{7.2.18}$$

Using the limiting expression (7.2.14) obtained from the solution of system (7.2.2) in the near-wall region, we arrive at the dispersion

relation

$$\frac{d\mathrm{Ai}(\zeta)}{dZ}\left[\int_{\zeta}^{\infty}\mathrm{Ai}(Z)\,dZ\right]^{-1}=(i\alpha)^{1/3}\frac{\alpha^2+\beta^2}{\mu},\quad \zeta=-i^{1/3}\frac{\omega}{\alpha^{2/3}}. \qquad (7.2.19)$$

As shown in [7.9], the matching of solutions in the viscous wall-sublayer and in the external region of the potential flow to within terms of the order of y^{-1} as $y\to\infty$ occurs automatically and leads to no new restrictions on disturbance parameters compared to (7.2.19).

Expression (7.2.19) relates the complex frequency $\omega=\omega_r+i\omega_i$ with the complex wave numbers $\alpha=\alpha_r+i\alpha_i$, $\beta=\beta_r+i\beta_i$. It also contains the Mach number M_∞ which does not affect the relation for two-dimensional disturbances $\beta=0$. For a fixed Mach number, the dispersion relation (7.2.19) consists of two real relations between six real-valued parameters α_r, α_i, β_r, β_i, and ω_r, ω_i. Hence, any four of these parameters are independent.

The procedure, proposed in [7.6] for numerical solution of the transcedental equation (7.2.19) is based on the representation of the derivative and the integral of the Airy function appearing on its left-hand side in the form of series. If the modulus of the complex parameter ζ is of the order of unity, it is natural to use the Taylor expansion [7.21]:

$$\mathrm{Ai}(Z)=\frac{1}{3^{2/3}}\left[\sum_{m=0}^{\infty}\frac{Z^{3m}}{3^{2m}m!\Gamma(m+2/3)}-\frac{Z}{3^{1/3}}\sum_{m=0}^{\infty}\frac{Z^{3m}}{3^{2m}m!\Gamma(m+4/3)}\right]. \qquad (7.2.20)$$

The series converges on the entire complex plane. With increasing $|Z|$ the number of summands in the Taylor series required for exact calculations should also be increased. For this reason, the asymptotic representation [7.19]

$$\mathrm{Ai}(Z)=\frac{1}{2\sqrt{\pi}}e^{-(2/3)Z^{3/2}}\left[Z^{-1/4}+\sum_{m=1}^{\infty}c_mZ^{-3m/2-1/4}\right], \qquad (7.2.21)$$

$$c_m=\frac{(-1)^m}{(2m)!\,72^m}\prod_{s=1}^{3m}(2s-1),$$

was used for large $|Z|$. This formula holds for $-\pi<\arg Z<\pi$. Since the asymptotic expansion (7.2.21) diverges in the conventional sense, the number of its terms ensuring the accuracy of calculations depends on $|Z|$. For $|Z|\geq 10$, the calculations were made with 6 terms of the asymptotic series, and for $|Z|<10$, with 35 terms of the Taylor series.

Using (7.2.21), we obtain

$$\frac{d\mathrm{Ai}(Z)}{dZ} = -\frac{1}{2\sqrt{\pi}} e^{(-2/3)Z^{3/2}} \left\{ Z^{1/4} + \sum_{m=0}^{\infty} \left[c_{m+1} + c_m \left(\frac{3}{2} m + \frac{1}{4} \right) \right] Z^{-3m/2-5/4} \right\},$$

$$\int_{\infty}^{Z} \mathrm{Ai}(Z)\, dZ = \frac{1}{2\sqrt{\pi}} e^{(-2/3)Z^{3/2}} \sum_{m=0}^{\infty} Z^{-3m/2-3/4} \sum_{\sigma=0}^{m} c_\sigma S_{m-\sigma}^{(\sigma)}, \qquad (7.2.22)$$

$$S_n^{(m)} = (-1)^{n+1} \left(\frac{3}{4} \right)^n \prod_{\sigma=1}^{n} (2m + 2\sigma - 1),\ n \geqslant 1,\ S_0^{(m)} = -1.$$

In the vicinity of the Stokes ray $\arg Z = \pm\pi$, where expressions (7.2.21) and (7.2.22) are inapplicable, the following asymptotic formula is valid:

$$\mathrm{Ai}(Z) = \frac{1}{2\sqrt{\pi}} \left\{ e^{-(2/3)Z^{3/2}} \sum_{m=0}^{\infty} c_m Z^{-3m/2-1/4} + ie^{(2/3)Z^{3/2}} \sum_{m=0}^{\infty} (-1)^m c_m Z^{-3m/2-1/4} \right\},\ \frac{\pi}{3} < \arg Z < \frac{5\pi}{3}. \qquad (7.2.23)$$

This relation follows from the identity

$$\mathrm{Ai}(Z) = -e^{2\pi i/3} \mathrm{Ai}(e^{2\pi i/3} Z) - e^{-2\pi i/3} \mathrm{Ai}(e^{-2\pi i/3} Z). \qquad (7.2.24)$$

The solution of the dispersion equation (7.2.19) was found by Newton's method, convergence to within eight significant digits having been attained after three or four iterations.

7.3. THREE-DIMENSIONAL STEADY DISTURBANCES IN SUPERSONIC BOUNDARY LAYER

Henceforth, while considering disturbances that are periodic in the direction of the z-coordinate, we shall assume that β is a real quantity.

Let us investigate the dispersion equation for a supersonic boundary layer and find the relation between the parameters α and β for $\omega = 0$. Lighthill [7.20] was the first to discover the existence of a nontrivial solution for two-dimensional steady disturbances. In this case, the wave number α is determined uniquely and is a purely imaginary quantity, which defines disturbances damping

exponentially upstream. As was shown in [7.1, 7.2] this solution describes a gas flow before separation and is an asymptotic form of the solution of the nonlinear problem on global separation from a smooth surface.

Put $\omega = 0$ on the left-hand side of the dispersion equation $\Phi(\zeta)$, $\zeta = -i^{1/3}(\omega/\alpha^{2/3})$. For the Airy function the equalities from [7.21] are valid:

$$\int_0^\infty \mathrm{Ai}(Z)\,dZ = \frac{1}{3}, \quad \frac{d\mathrm{Ai}(0)}{dZ} = -\frac{1}{3^{4/3}\Gamma(4/3)}, \tag{7.3.1}$$

whence

$$\Phi(0) = -\frac{3^{2/3}}{\Gamma(1/3)}. \tag{7.3.2}$$

Let $\alpha = -i\,|\,\alpha\,|$ be a purely imaginary quantity. The dispersion relation then assumes the form

$$\Phi(0) = |\alpha|^{1/3}\,\frac{\beta^2 - |\alpha|^2}{[\beta^2(M_\infty^2-1)^{-1} + |\alpha|^2]^{1/2}}. \tag{7.3.3}$$

Solving this equation for β, one obtains

$$\beta^2 = |\alpha|^2 + \frac{1}{2}(M_\infty^2-1)^{-1}\Phi^2(0)\,|\alpha|^{-2/3} - \sqrt{\frac{1}{4}(M_\infty^2-1)^{-2}\Phi^4(0)\,|\alpha|^{-4/3} + M_\infty^2(M_\infty^2-1)^{-1}\Phi^2(0)\,|\alpha|^{4/3}}. \tag{7.3.4}$$

The minus sign is chosen in front of the radical in this expression since it follows from the inequality $\Phi(0) < 0$ and relation (7.3.3) that $|\alpha|^2 > \beta^2$. As $|\alpha| \to \infty$, formula (7.3.4) gives

$$\beta^2 = |\alpha|^2 - \frac{3^{2/3}}{\Gamma\left(\frac{1}{3}\right)}\,\frac{M_\infty}{(M_\infty^2-1)^{1/2}}\,|\alpha|^{2/3}. \tag{7.3.5}$$

The quantity β vanishes at $|\alpha| = \alpha^*$, α^* being the Lighthill root, which is numerically equal to

$$\alpha^* = [-\Phi(0)]^{3/4} = 3^{1/2}\Gamma^{-3/4}\left(\frac{1}{3}\right) = 0.82715. \tag{7.3.6}$$

Figure 7.1 shows $|\alpha|$ as a function of β. The weak dependence of these curves on the Mach number deserves attention. This effect is retained in the initial dimensionless system of units since the scale on the x- and z-axes change similarly upon transformation (7.1.3). In the three-dimensional case, the values of $|\alpha|$ always lie above the Lighthill root α^*. A decrease in the wavelength of disturbances

periodic in z-coordinate leads to a faster exponential increment of the amplitude downstream.

It should be noted that the formation of three-dimensional steady vortex structures superimposed on the basic two-dimensional flow is observed in different experimental situations. In particular, lateral periodic pressure disturbances and systems of streamwise vortices appear in the vicinity of the attachment point in a two-dimensional or axisymmetric flow over a wide range of Mach and Reynolds numbers [7.22]. In this case, the characteristic radius of the streamline

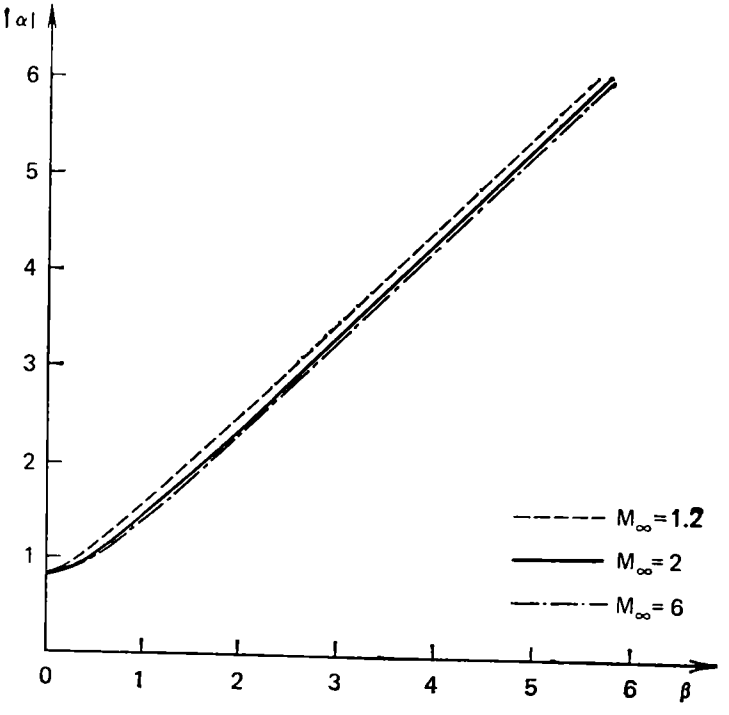

Fig. 7.1

curvature in the observed flows exceeds the minimal radius of curvature in the Taylor-Görtler theory by more than an order of magnitude. Possible physical mechanisms explaining the birth of three-dimensional disturbances of this type are associated either with the assumption about the intensification of vortices penetrating into the flow from outside or with the concept of "vortex instability" of the initial two-dimensional flow. The above-mentioned steady disturbances (periodic along the z-axis), being the eigensolutions of the equations for the supersonic boundary layer with self-induced pressure, may give evidence to the latter assumption. The existence of such solutions is not connected with the surface curvature.

7.4. SUPERSONIC BOUNDARY LAYER INSTABILITY TO THREE-DIMENSIONAL PERIODIC DISTURBANCES

Now suppose that both wave numbers α and β are real quantities. It is sufficient to confine to positive values of α since the substitution $\alpha \to -\alpha$ leads to a simple frequency transformation $\omega \to -\bar{\omega}$ where the bar denotes complex conjugation. In this case, formulas (7.2.1) specify an oblique wave propagating at an angle of $\Psi = \arctan(\beta/\alpha)$ relative to the x-axis. The condition $\operatorname{Re}\mu > 0$ in (7.2.16) for $M_\infty > 1$ indicates that admissible spatially periodic disturbances in the supersonic boundary layer necessarily fit the inequality

$$\alpha_i' < \frac{|\beta|}{(M_\infty^2 - 1)^{1/2}}. \tag{7.4.1}$$

Consequently, the angle of wave propagation is restricted from below:

$$|\Psi| > \Psi_0, \quad \Psi_0 = \arctan[(M_\infty^2 - 1)^{1/2}]. \tag{7.4.2}$$

The dispersion relation (7.2.19) does not hold for disturbances whose wave vector does not satisfy inequality (7.4.2). The limiting angle Ψ_0 determines the boundary of continuous spectrum. Condition (7.4.1) means that the projection of the oncoming flow velocity onto the direction of the wave vector must be subsonic.

Let us show that for $M_\infty > 1$, the solutions of the dispersion equation contain eigenvalues corresponding to unstable eigenfunctions in the form of oblique waves. Indeed, let the complex parameter $\zeta = -i^{1/3}(\omega/\alpha^{2/3})$ tend to infinity. Using the asymptotic representations (7.2.22), the left-hand side of (7.2.19) can be expanded into the series:

$$\Phi(\zeta) = -\zeta - \zeta^{-1/2} + O(\zeta^{-2}). \tag{7.4.3}$$

The assumption that $|\zeta| \gg 1$ means that

$$\alpha^{1/3} \frac{\alpha^2 + \beta^2}{[\beta^2 (M_\infty^2 - 1)^{-1} - \alpha^2]^{1/2}} \gg 1. \tag{7.4.4}$$

The dispersion equation takes the form

$$\zeta = -(i\alpha)^{1/3} \frac{\alpha^2 + \beta^2}{\mu} [1 - \zeta^{-3/2} + O(\zeta^{-3})]. \tag{7.4.5}$$

Since the asymptotic formulas (7.2.22) are valid within the sector $-\pi < \arg\zeta < \pi$, we must put $\zeta = \exp\left(-\frac{5}{6}\pi i\right) \alpha^{1/3}(\alpha^2 + \beta^2)/\mu$ while calculating the correction term $\zeta^{-3/2}$ in (7.4.5) in the first

approximation. In two approximations, we finally obtain

$$\zeta = -e^{\pi i/6}\alpha^{1/3}\frac{\alpha^2+\beta^2}{\mu} - e^{5\pi i/12}\left[\alpha^{1/3}\frac{\alpha^2+\beta^2}{\mu}\right]^{-1/2}. \quad (7.4.6)$$

Taking into account the definition of ζ one finds the expression for the frequency:

$$\omega = \alpha\frac{\alpha^2+\beta^2}{\mu} + e^{\pi i/4}\alpha^{1/2}\left[\frac{\mu}{\alpha^2+\beta^2}\right]^{1/2}. \quad (7.4.7)$$

The asymptotic solution (7.4.7) describes unstable oscillations with the time increment

$$\omega_i = \frac{1}{\sqrt{2}}\frac{\alpha^{1/2}\left[\beta^2(M_\infty^2-1)^{-1}-\alpha^2\right]^{1/4}}{(\alpha^2+\beta^2)^{1/2}}. \quad (7.4.8)$$

Now consider some limiting cases which do not violate condition (7.4.4). If $\alpha \sim \beta$ (in accordance with (7.4.4), the two wave numbers α and β must be sufficiently large), then $\omega_i = O(1)$. For $\beta \to \infty$ and a fixed α, we have $\omega_i \to 0$. Finally, when $\alpha \sim \beta$, but $\mu \to 0$, we have $\omega_i \to 0$.

Let us find neutral eigenvalues for $M_\infty > 1$. For this purpose, note that the dispersion relation (7.2.19) can be written in the form

$$\frac{d\mathrm{Ai}\left(-i^{1/3}\frac{\Omega}{K^{2/3}}\right)}{dZ}\left[\int\limits_{-i^{1/3}\frac{\Omega}{K^{2/3}}}^{\infty}\mathrm{Ai}(Z)\,dZ\right]^{-1} = i^{1/3}K^{4/3}, \quad (7.4.9)$$

where the reduced wave number K and the reduced frequency Ω are:

$$K^{4/3} = \alpha^{1/3}\frac{\alpha^2+\beta^2}{\left[\beta^2(M_\infty^2-1)^{-1}-\alpha^2\right]^{1/2}}, \quad \Omega = -i^{-1/3}\zeta K^{2/3}. \quad (7.4.10)$$

For spatially periodic oscillations with real α and β, satisfying condition (7.4.1), the reduced wave number K is also a purely real number (since parameter K cannot be determined uniquely from the first relation in (7.4.10), the choice of $\arg K = 0$ is essentially a definition of K).

The dispersion relation (7.4.9) has the standard form encountered in the theory of planar flows. It was shown [7.8, 7.9] that each value of K corresponds to an infinite set of eigenvalues Ω. As the parameter K moves along the real positive semiaxis of the complex plane, the imaginary part of Ω for the first mode changes its sign. The value of the reduced wave number $K = K_*$, for which the reduced frequency is purely real ($\Omega = \Omega_*$), was obtained in [7.8], $K_* = 1.0005$ and $\Omega_* = 2.298$. It can be easily seen that these values of K and Ω determine the neutral solutions of the dispersion equation (7.2.19) in terms of the initial variables α, β, and ω. The second relation

from (7.4.10) leads to the following expression for frequency:

$$\omega = \omega_r = \frac{\Omega_*}{K_*^{2/3}} \alpha^{2/3}. \tag{7.4.11}$$

The variable α appearing in this expression is not independent. It is related to β through the first equation from (7.4.10) for $K = K_*$, which is the equation of a neutral curve in the (α, β)-plane. Thus, for neutral oscillations, the three real parameters α, β, and ω must satisfy two relations. The parameters β and α can be related explicitly:

$$\beta^2 = -\alpha^2 + \frac{1}{2}\alpha^{-2/3}(M_\infty^2 - 1)^{-1} K_*^{8/3}$$
$$\pm \sqrt{\frac{1}{4}\alpha^{-4/3}(M_\infty^2 - 1)^{-2} K_*^{16/3}\left[1 - 4\alpha^{8/3} M_\infty^2 (M_\infty^2 - 1) K_*^{-8/3}\right]}. \tag{7.4.12}$$

Both signs in front of the radical in this formula are valid. The vanishing of the radicand for $\alpha = \alpha_{max}$ restricts from above the range of the longitudinal wave number:

$$\alpha \leqslant \alpha_{max} = K_* [4M_\infty^2 (M_\infty^2 - 1)]^{-3/8}, \tag{7.4.13}$$

in which real values of β exist. The branch of the neutral curve $\beta = \beta(\alpha)$, corresponding to the plus sign of the radical, tends to infinity as $\alpha \to 0$ in accordance with the law

$$|\beta| \to \frac{K_*^{4/3}}{(M_\infty^2 - 1)^{1/2}} \alpha^{-1/3} + \ldots. \tag{7.4.14}$$

The choice of the minus sign for the radical fixes the branch emerging from the origin and having the following asymptotic form for $\alpha \to 0$:

$$|\beta| \to \alpha (M_\infty^2 - 1)^{1/2} + \frac{1}{2}\alpha^{11/3} M_\infty^4 (M_\infty^2 - 1)^{1/2} K_*^{-8/3} + \ldots. \tag{7.4.15}$$

This asymptotic form, just as the entire neutral curve, naturally lies in the part of the (α, β)-plane, which is admitted by inequality (7.4.1).

Figure 7.2 depicts the neutral curve $\alpha = \alpha(\beta)$ for $M_\infty = 1.5$ (solid line), with the wave number β in the lateral direction taken as independent variable. The limiting curve $\alpha = (M_\infty^2 - 1)^{-1/2} \beta$ is shown by the dashed line. The part of the plane below the neutral curve is the stability domain and corresponds to oscillations with damping amplitude. The instability domain, where the oscillation amplitude exponentially increases in time, lies between the limiting curve and the neutral curve. For illustrating the behaviour of the perturbation increment in various regions of the (α, β)-plane, Fig. 7.2 also depicts the curves $\omega_i = \omega_i(\alpha)$ for three given values of the transverse wave number β (0.7, 1, and 1.5). For each value

of α, the corresponding value of ω_i is plotted along the abscissa axis. It can be seen that the parts of the curves $\omega_i = \omega_i(\alpha)$ with positive and negative values of ω_i lie on different sides of the neutral curve,

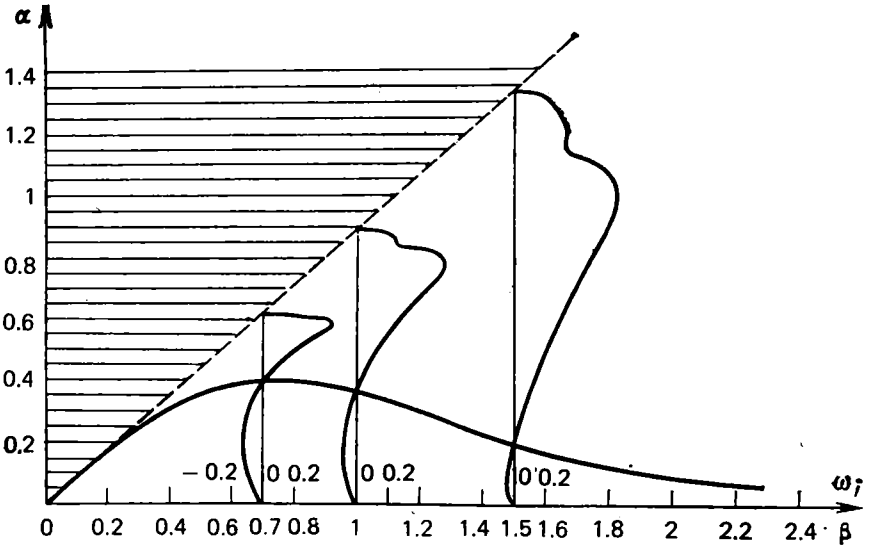

Fig. 7.2.

on which they change sign. The value of ω_i vanishes for the second time on the limiting curve near which the asymptotic form (7.4.8) is valid for $\mu \to 0$. As β increases, the neutral curve approaches the abscissa axis in accordance with (7.4.14), and the range of stable

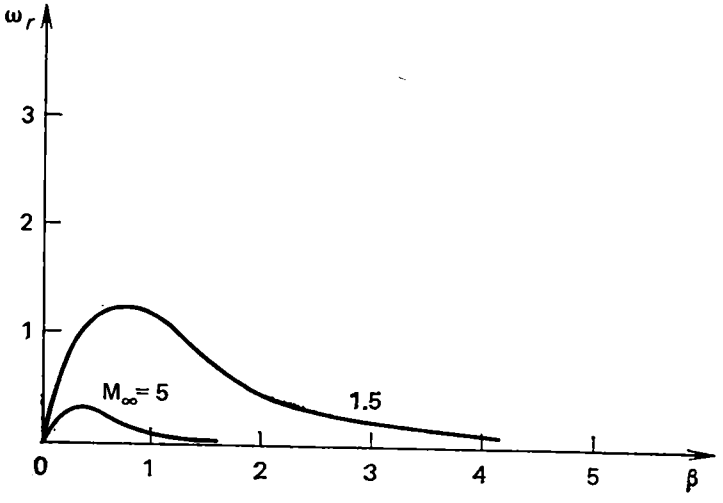

Fig. 7.3.

values of α becomes narrower. It should be noted that although for large β almost the entire region below the limiting curve corresponds to unstable oscillations, the maximum increment ω_i remains of the order of unity everywhere.

Figure 7.3 represents the neutral curves on the (β, ω_r)-plane for different Mach numbers. As the Mach number increases, the curves of neutral frequencies are shifted downwards. This can be explained by a similar behaviour of the neutral values of α which are related to ω_r via formula (7.4.11). The maximum of the neutral-frequency curve can be easily calculated by using expression (7.4.13) for α_{max}, which gives

$$\omega_{max} = \Omega_* [4M_\infty^2 (M_\infty^2 - 1)]^{-1/4}. \tag{7.4.16}$$

For a given Mach number, the stability domain in Fig. 7.3 is bounded by the corresponding neutral curve and the abscissa axis. The instability domain occupies the entire remaining part of the (β, ω_r)-plane above the neutral curve.

7.5. THREE-DIMENSIONAL DISTURBANCES IN A SUBSONIC BOUNDARY LAYER

In contrast to a supersonic boundary layer for which, as was shown above, there are no neutral solutions of the dispersion equation (7.2.19) in the limit $\beta \to 0$ (with the exception of the trivial solution $\alpha \to 0$, $\omega \to 0$), the first mode of spatially periodic disturbances in a subsonic boundary layer can be stable as well as unstable irrespective of the direction of wave propagation [7.9]. Using the transformation

$$K^{4/3} = \alpha^{1/3} \frac{\alpha^2 + \beta^2}{[\beta^2 (1 - M_\infty^2)^{-1} + \alpha^2]^{1/2}}, \quad \Omega = -i^{-1/3} \zeta K^{2/3}, \tag{7.5.1}$$

the dispersion relation for $M_\infty < 1$ and for real values of $\alpha > 0$ and β can be reduced to the standard form (7.4.9). Neutral solutions are generated by the aforementioned purely real eigenvalues of Eq. (7.4.9) $K = K_*$ and $\Omega = \Omega_*$. Substituting these eigenvalues into (7.5.1), we obtain the relation between the variables α, β, and ω for neutral oscillations. Let us solve the equation of the neutral curve in the (α, β)-plane (the first equation in (7.5.1) for $K = K_*$) for the transverse wave number:

$$\beta^2 = -\alpha^2 + \frac{1}{2} \alpha^{-2/3} (1 - M_\infty^2)^{-1} K_*^{8/3}$$

$$\pm \sqrt{\frac{1}{4} \alpha^{-4/3} (1 - M_\infty^2)^{-2} K_*^{16/3} [1 - 4\alpha^{8/3} M_\infty^2 (1 - M_\infty^2) K_*^{-8/3}]}. \tag{7.5.2}$$

First of all, note that the lower sign of the radical should be eliminated when $M_\infty^2 < 1/2$. As expected, all curves (7.5.2) intersect the axis $\beta = 0$, for any Mach number $M_\infty^2 < 1$, at a point where the longitudinal wave number assumes the critical value $\alpha = K_*$ for planar disturbances. The branch of the neutral curve (7.5.2) with the plus sign of the radical has an increasing asymptotic form for

$\alpha \to 0$:

$$|\beta| \to \frac{K_*^{4/3}}{(1-M_\infty^2)^{1/2}}\,\alpha^{-1/3} + \ldots. \tag{7.5.3}$$

Let us find the range of admissible values of α for the two branches of curve (7.5.2), which meet for $\alpha = \alpha_{max} = K_* [4M_\infty^2 (1 - M_\infty^2)]^{-3/8}$. It can be seen that $\alpha_{max} \geqslant K_*$, and the equality is attained for $M_\infty^2 = 1/2$. The substitution of $\alpha = \alpha_{max}$ into expression (7.5.2) leads to the formula $\beta^2 = \alpha_{max}^2 (2M_\infty^2 - 1)$. Hence it

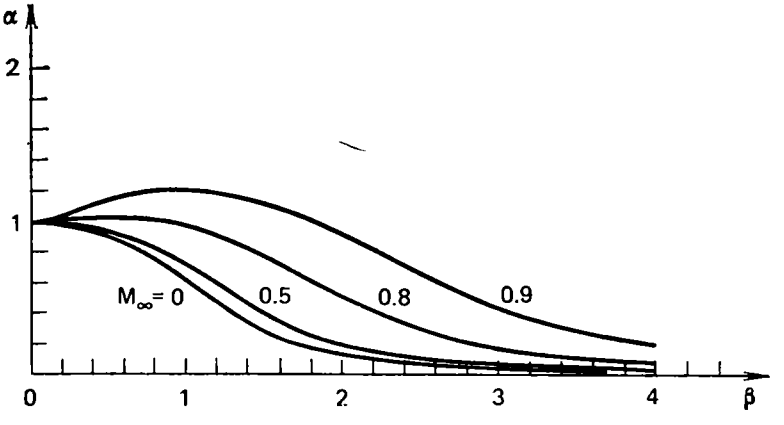

Fig. 7.4.

follows that for $M_\infty^2 < 1/2$, all acceptable solutions are described by the branch with the plus sign of the radical in the interval $0 < \alpha \leqslant K_*$. For $1/2 < M_\infty^2 < 1$, the choice of the minus sign of the radical leads to real values of β in the interval $K_* < \alpha < \alpha_{max}$, and the choice of the plus sign corresponds to the interval $0 < \alpha < \alpha_{max}$.

Figure 7.4 depicts the neutral curves $\alpha = \alpha(\beta)$ for different Mach numbers, the value of β being taken as independent variable. Since the curves $\alpha = \alpha(\beta)$ have maxima for $1/2 < M_\infty^2 < 1$, two different values of β correspond to each α from the interval (K_*, α_{max}).

Figure 7.5 represents the results of calculations of the increment ω_i as a function of α for two fixed values of β, equal to 1 and 4, and the Mach number $M_\infty = 0.8$, as well as the neutral curve $\alpha = \alpha(\beta)$. The parameter ω_i (plotted on the same axis on which the value of β is plotted) is negative in the stability domain below the neutral curve. As the value of α increases, the parameter ω_i getting into the instability domain above the neutral curve becomes positive, attains its maximum value and then remains constant. The value of the latter can be determined from the asymptotic formula

$$\omega_i = \frac{1}{\sqrt{2}} \frac{\alpha^{1/2} [\beta^2 (1-M_\infty^2)^{-1} + \alpha^2]^{1/4}}{(\alpha^2+\beta^2)^{1/2}} \tag{7.5.4}$$

which is valid under the condition

$$\alpha^{1/3}\frac{\alpha^2+\beta^2}{[\beta^2(1-M_\infty^2)^{-1}+\alpha^2]^{1/2}}\gg 1. \tag{7.5.5}$$

The derivation of formula (7.5.4) is identical to that of the similar expression (7.4.8) for a supersonic flow. Thus, the limiting value of ω_i for $\alpha\to\infty$ and a given β turns out to be equal to $1/\sqrt{2}$.

The neutral-frequency curves for several values of the Mach number are represented in Fig. 7.6. For $\beta = 0$, all the curves converge

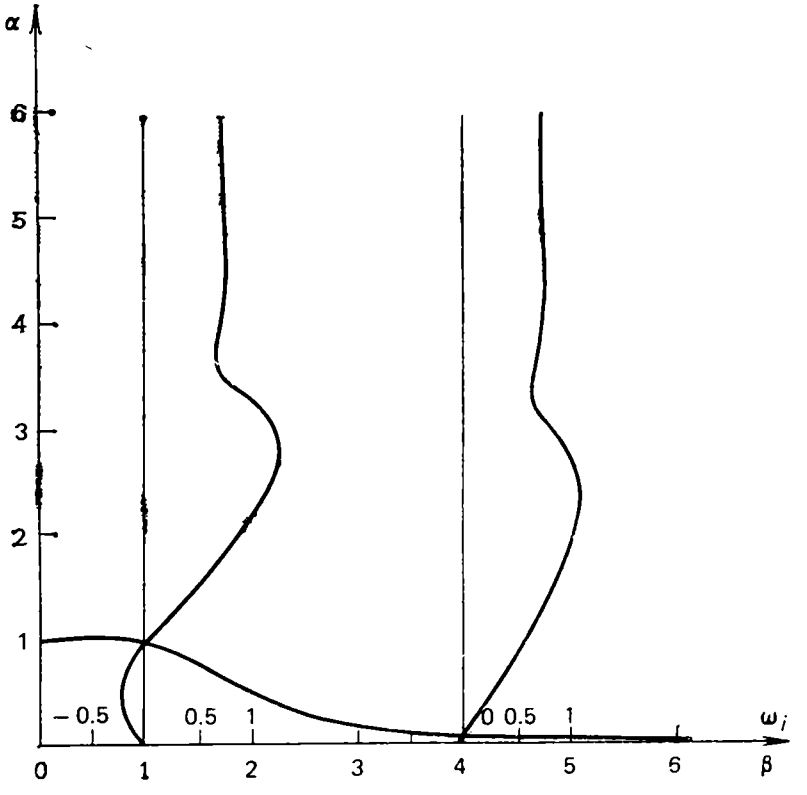

Fig. 7.5.

to the point $\omega_r = \Omega_*$, viz. the critical value of the frequency for the first mode of planar oscillations. The stability and instability domains lie below and above the neutral curve $\omega_r = \omega_r(\beta)$ as in Fig. 7.3 for the supersonic flow.

So far, the problem of the evolution of spatial disturbances was formulated in terms of "time stability", when the wave numbers α and β are assumed to be purely real. The results of calculation of the imaginary part α_i of the longitudinal wave number for the first mode as a function of the frequency ω (assumed to be purely real), depicted in Fig. 7.7, may be treated as an example of the solution

of the problem of "spatial stability". As before, the transverse wave number here is purely real ($\beta = 1$) and the Mach number $M_\infty = 0$. If the frequency does not exceed the neutral value (which can be

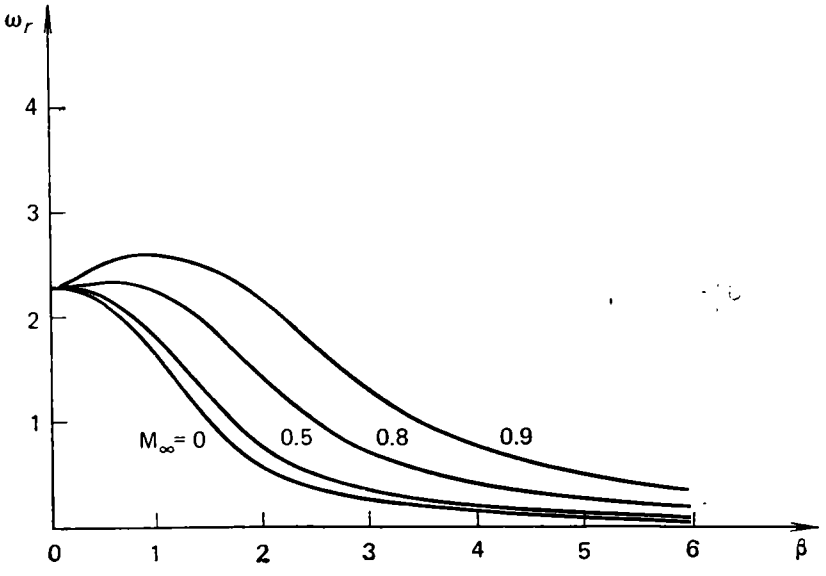

Fig. 7.6.

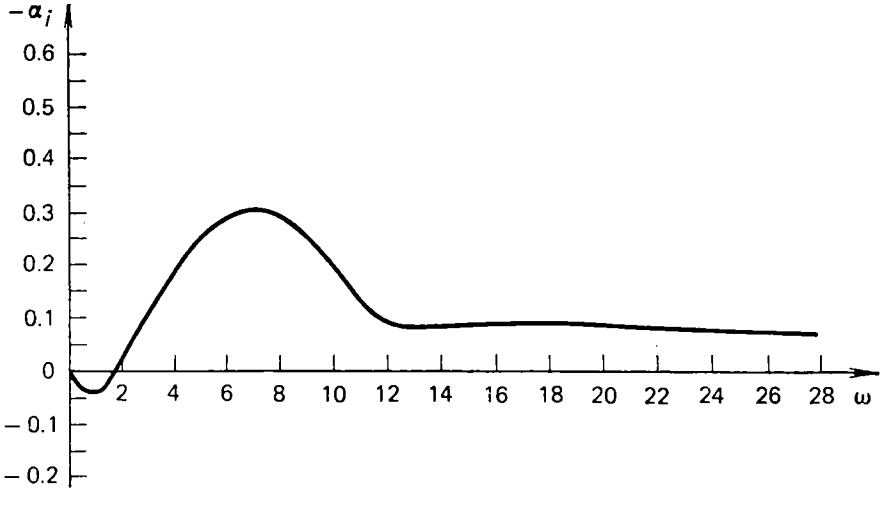

Fig. 7.7.

found with the help of the curves in Fig. 7.6), the perturbations damp for $x \to \infty$. Otherwise, perturbations exponentially increase downstream. The solution of the boundary value problem on the spatial instability of two-dimensional oscillations induced in a subsonic boundary layer by a harmonic oscillator placed on its bottom, was

constructed in [7.23]. In that work, both subcritical ($\omega < \Omega_*$) and supercritical ($\omega > \Omega_*$) regimes were analyzed. It follows from Fig. 7.7 that as ω increases, the spatial increment $-\alpha_i$ passes through the maximum in the instability domain and then slowly decreases.

Let us find the asymptotic form of α_i as $\omega \to \infty$. It can be concluded from the form of the dispersion equation (7.2.19) that as the frequency increases, the two parameters ζ and α increase in their magnitude. Now expand the complex quantity μ into a series for $M_\infty < 1$:

$$\mu = \pm\alpha\left(1 + \frac{1}{2}\frac{\beta^2}{\alpha^2}\frac{1}{1-M_\infty^2} + \ldots\right). \tag{7.5.6}$$

The upper sign here corresponds to $\operatorname{Re}\alpha > 0$, and the lower sign to $\operatorname{Re}\alpha < 0$. This sign rule is equivalent to the condition $\operatorname{Re}\mu > 0$. The dispersion relation

$$\frac{d\mathrm{Ai}(\zeta)}{dZ}\left[\int_\zeta^\infty \mathrm{Ai}(Z)\,dZ\right]^{-1} = \pm i^{1/3}\alpha^{4/3}\frac{1+\beta^2/\alpha^2}{1+\frac{1}{2}\frac{\beta^2}{\alpha^2}\frac{1}{1-M_\infty^2}+\ldots}, \tag{7.5.7}$$

with its left-hand side being replaced by the asymptotic form (7.4.3) to within the terms of the order of $\zeta^{-2} \sim \alpha^{-8/3}$, can be written in the form

$$-\zeta - \zeta^{-1/2} = \pm i^{1/3}\alpha^{4/3}\left[1 + \frac{1}{2}\frac{\beta^2}{\alpha^2}\frac{1-2M_\infty^2}{1-M_\infty^2}\right]. \tag{7.5.8}$$

Suppose, for the sake of definiteness, that $\omega = \omega_r > 0$. In the first approximation, $\zeta = \mp i^{1/3}\alpha^{4/3}$, whence $\omega = \pm\alpha^2$. The numerical calculation of the first mode shows that the real part α_r of the longitudinal wave number is large for large ω's. Consequently, we must take the upper sign in formulas (7.5.6)-(7.5.8) (otherwise, the first approximation gives $\alpha_r = 0$). As a result, the argument of the wave number α is uniquely determined from the condition $\operatorname{Re}\mu > 0$. The correction terms $\zeta^{-1/2}$ can be calculated from the first approximation by representing it in the form $\zeta = \exp(-5\pi i/6)\,\omega^{2/3}$ in accordance with the condition $-\pi < \arg\zeta < \pi$. The dispersion equation is transformed as follows:

$$\zeta = -i^{1/3}\alpha^{4/3} - i^{1/3}\alpha^{-2/3}\left[\frac{1}{2}\beta^2\frac{1-2M_\infty^2}{1-M_\infty^2} + e^{\pi i/4}\right]. \tag{7.5.9}$$

Introducing the expression $\zeta = -i^{1/3}\omega/\alpha^{2/3}$ into this formula and solving the obtained equation for α, we get

$$\alpha = \omega^{1/2} - \frac{1}{4}\frac{\beta}{\omega^{1/2}}\frac{1-2M_\infty^2}{1-M_\infty^2} - \frac{1}{2\omega^{1/2}}e^{\pi i/4}. \tag{7.5.10}$$

A direct result of formula (7.5.10) concerns the limiting behaviour of the spatial disturbance increment as $\omega \to \infty$:

$$-\alpha_i \to \frac{1}{2\sqrt{2}}\,\omega^{-1/2}. \tag{7.5.11}$$

Figure 7.8 depicts the dependence of α_i on the transverse wave number $\beta > 0$ for a fixed frequency $\omega = \omega_r$. If the frequency ω is smaller than the critical value Ω_*, as is the case for the curve calculated for $M_\infty = 0$, $\omega = 1$ (solid line), then oscillations that are stable for small β become unstable as its value increases. For $1/2 < M_\infty^2 < 1$ but $\Omega_* < \omega < \omega_{max}$, the initially unstable oscillations become stable as β increases over a finite interval, after which α_i

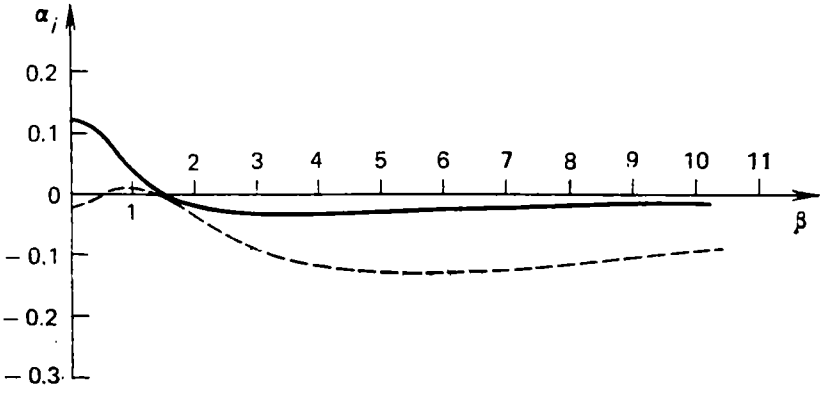

Fig. 7.8.

changes its sign for the second time. Such a behaviour of α_i is illustrated in Fig. 7.8 by the dashed curve for $M_\infty = 0.9$, $\omega = 2.5$. Since the neutral-frequency curve has a maximum, the line $\omega = \text{const}$ intersects this curve twice on the (β, ω_r)-plane (see Fig. 7.6).

In the limit $\beta \to \infty$, the increment tends to zero. Let us prove this statement. The dispersion relation for a subsonic flow with a large positive β is transformed as follows:

$$\zeta + \zeta^{-1/2} = -(i\alpha)^{1/3}\beta\,(1-M_\infty^2)^{1/2}\left[1 + O\left(\frac{\alpha^2}{\beta^2}\right)\right]. \tag{7.5.12}$$

We can ignore the correction term $O(\alpha^2/\beta^2)$ and put $\zeta = \exp(-\pi i)\,(i\alpha)^{1/3}\,\beta\,(1 - M_\infty^2)^{1/2}$ in the term $\zeta^{-1/2}$ on the left-hand side of (7.5.12). This leads to an asymptotic expression for the longitudinal wave number as $\beta \to \infty$:

$$\alpha = \frac{\omega}{\beta}\,(1-M_\infty^2)^{-1/2} - \frac{\omega^{1/2}}{\beta^2}\,(1-M_\infty^2)^{-1}\,e^{\pi i/4}, \tag{7.5.13}$$

whence

$$\alpha_i = -\frac{1}{\sqrt{2}}\,\frac{\omega^{1/2}}{1-M_\infty^2}\,\beta^{-2}. \tag{7.5.14}$$

It can be seen from Fig. 7.4 that the possibility for a stable two-dimensional wave in a subsonic boundary layer to become unstable upon the rotation of its wave vector relative to the direction of the main flow does not contradict the Squire theorem. The Squire transformation puts a two-dimensional wave into correspondence with each three-dimensional wave for a larger Reynolds number. This does not mean, however, that two-dimensional disturbances are the most unstable for a fixed Reynolds number. This fact is emphasized in [7.24]. It should also be noted that although the range of unstable frequencies becomes wider for large values of the transverse wave number (as follows from the shape of neutral curves), the coefficients of time and spatial amplification of disturbances remain of the order of unity everywhere for the variables under consideration.

References

7.1. V. Ya. Neiland, *Tr. TsAGI.* No 1529 (1974).
7.2. K. Stewartson, in: *Advances of Appl. Mech.*, V. 14, Acad. Press, New-York-San Francisco-London, 1974.
7.3. A. I. Ruban and V. V. Sychev, *Uspekhi Mekhaniki* 2, 4 (1979).
7.4. W. Schneider, *J. Fluid Mech.* 63, 3: 465 (1974).
7.5. F. T. Smith, *Mathematika* 23, pt. 1, No. 45: 62 (1976).
7.6. O. S. Ryzhov and E. D. Terent'ev, *Prikl. Matem. i Mekh.* 41, 6: 1007 (1977).
7.7. O. S. Ryzhov, *Prikl. Matem. i Mekh.* 44, 6: 1035 (1980).
7.8. V. I. Zhuk and O. S. Ryzhov, *Dokl. Akad. Nauk SSSR* 253, 6: 1326 (1980).
7.9. V. I. Zhuk and O. S. Ryzhov, *Prikl. Matem. i Mekh.* 45, 3: 552 (1981).
7.10. K. Stewartson, *SIAM Review* 23, 3: 309 (1981).
7.11. F. T. Smith, *IMA J. of Appl. Math.* 28: 207 (1982).
7.12. F. T. Smith, *Proc. Roy. Soc.* A366, 1724: 91 (1979).
7.13. R. J. Bodonyi and F. T. Smith, *Proc. Roy. Soc.* A375, 1760: 65 (1981).
7.14. T. Cebeci and K. Stewartson, *AIAA Journal* 18, 4: 398 (1980).
7.15. H. Nayfeh Ali, *AIAA Journal* 18, 4: 406 (1980).
7.16. T. Cebeci and K. Stewartson, *AIAA Journal* 19, 6: 806 (1981).
7.17. A. D. D. Craik, *J. Fluid. Mech.* 99, pt. 2: 247 (1980).
7.18. C. C. Lin, *The Theory of Hydrodynamic Stability.* Cambridge University Press, Cambridge, 1955.
7.19. W. Wasow, *Asymptotic Expansions for Ordinary Differential Equations*, John Wiley and Sons Inc., New York-London-Sydney, 1965.
7.20. M. J. Lighthill, *Proc. Roy. Soc.* A217, 1131: 478 (1953).
7.21. A. Erdélyi, W. Magnus, F. Oberhettinger, and F. G. Tricomi, *Higher Transcendental Functions*, vol. 2, McGraw-Hill, New York-Toronto-London, 1953.
7.22. J. Ginoux, *AIAA Journal* 9, 4: 759 (1971).
7.23. E. D. Terent'ev, *Prikl. Matem. i Mekh.* 45, 6: 1049 (1981).
7.24. T. Cebeci and K. Stewartson, "On the prediction of transition in three-dimensional flows", in: *Laminar-turbulent Transitions*, Symposium Stuttgart, Springer-Verlag, Berlin-Heidelberg-New York, 1980.

Name Index

Afanasyev, Yu. V., 189
Akinrelere, E. A., 114, 124
Alder, B., 12
Alekseev, A. A., 191
Ali, H. N., 307
Amsden, A. A., 69
Andreev, V. B., 224
Antonets, A. V., 85f, 120
Anuchina, N. N., 189
Arnold, V. I., 70
Arsenin, V. Ya., 189
Aukin, M. A., 76, 119

Babaev, D. A., 97, 122
Babakov, A. V., 43, 68, 70, 83
Babenko, K. I., 81, 86, 88, 119f
Bachmanova, N. S., 96, 122
Bad'in, L. V., 191
Bagrinovsky, K. A., 187
Bailey, H. E. 123
Belakin, V. B., 189
Bazhenov, D. V. 69f
Bazhenova, L. A., 69f
Bazzhin, A. P., 86, 91, 95, 113f, 117, 120ff, 124
Beam, R. M., 272
Belotserkovskii, O. M., 7f, 68, 70, 95, 106, 108, 110f, 116, 121ff, 188, 191, 272
Belotserkovskii, S. O., 23, 47, 55, 68ff
Belyankov, A. Ya., 191, 216, 224
Bird, G. A., 68
Birkhoff, G., 70
Blokhin, A. M., 92, 121
Bodonyi, B. J., 307
Bolshakov, V. P., 273, 285
Bondarenko, N. F., 70
Book, D. L., 189
Boris, J. P., 189
Borisov, V. M., 106, 123
Briley, W. B., 272
Brissaud, A., 69
Bulenbaev, A., 123
Burdelnyi, A. K., 86, 88, 120, 124
Burstein, S. Z., 189
Butler, D. S., 122, 187
Byrkin, A. P., 70, 272

Calderón, A. P., 224
Camarero, R., 105, 123
Cantwell, B. J., 69
Carmichael, R. L., 119
Carrier, G. F., 273, 285
Castellano, Ch. R., 119
Cebeci, T., 307
Chapman, D. R., 69
Chaussée, D. S., 121
Chelysheva, I. F., 85, 91, 117, 120f, 124
Cheremisin, 19
Cherkashin, V. A., 74, 118
Chushkin, P. I., 8, 98, 103f, 108, 110ff, 114, 118, 122ff, 187
Chusov, M. A., 70
Cooke, J. C., 273, 285
Courant, R., 106, 123, 131, 133, 137, 149, 187
Craik, A. D. D., 307
Crank, J., 121

Daly, B. J., 70
Danaev, N. G., 272
Davydov, Yu. M., 34, 66, 68ff, 95, 121ff
Deardoff, J. W., 69
Demchenko, V. V., 187f
Dolzhanskii, F. V., 70
Dorodnicyn *see* Dorodnitsyn
Dorodnitsyn, A. A., 69, 108, 123
Dushin, V. K., 123f
Dyachenko, V. F., 188f
Dyakonov, Yu. N., 82, 84, 86, 100, 119f, 122, 124, 187

Erdélyi, E., 307
Eremin, V. V., 189
Erofeev, A. I., 69, 272

Falunin, M. P., 120
Fedorovsky, A. M., 191
Fedorenko, R. P., 189, 191
Fernbach, S., 12
Ferrari, C., 102, 122
Ferziger, J. H., 69
Finchenko, V. S., 176, 187
Finley, P. J., 189
Fletcher, C. A. J., 117, 124
Fomin, V. N., 123f, 187f
Fridrichs, K. O., 129, 188
Frisch, V., 69
Fursenko, A. A., 189

Gak, M. Z., 70
Galinsky, V. P., 93, 121
Ganimedov, V. P., 83, 119
Gilinsky, S. M., 124
Ginoux, J., 307
Godunov, S. K., 74, 118, 134, 187, 189, 224, 272
Goldin, V. Ya., 189
Goldshtik, M. A. 69
Golomazov, M. M., 112, 115f, 123f
Golovachev, Yu. P., 123
Golubinsky, A. A., 80, 119
Gonidou, R., 83, 119
Graves, R. A., 272
Grigoryev, E. I., 105f, 123
Grossman, B., 285
Grudnitsky, V. G., 116, 123f
Gulin, A. V., 272
Gusev, 77
Gushchin, V. A., 47, 55, 68ff

Hain, K., 189
Harlow, F. H., 12, 69
Hinze, J. O., 69
Hirschel, E. H., 272
Hirsh, R., 272
Holt, M., 117, 124
Holtz, T., 121
Howarth, L., 273, 285

Ievlev, V. M., 32f, 69
Ilyina, A. S., 84, 120
Isaacson, E., 106, 123, 131, 133, 137, 149, 187
Ivanov, M. Ya., 74ff, 82ff, 118ff, 189
Ivanov, V. D., 188
Ivanov, V. F., 124
Ivanova, V. N., 81, 88, 119f

Kac, M., 68
Kalitkin, N. N., 189
Kamenetsky, V. S., 108, 123, 188
Katskova, O. N., 103f, 122, 187
Kazandzhan, E. P., 119f
Kazhdan, Ya. M., 191
Keller, H. B., 189
Kennet, H., 113, 124
Khalatnikov, I. M., 131, 149, 188
Khazin, L. G., 191
Kholodov, A. S., 8, 102, 106ff, 122f, 188
Khololov, S. M., 187
Klyatskin, V. I., 70
Kochin, N. E., 10
Kogan, M. N., 68
Kokoshinskaya, N. S., 119

Kolgan, V. P., 78, 119, 189
Kolmogorov, A. N., 54, 69
Kordulla, W., 272
Kosarev, V. I., 187f
Kostrykin, V. S., 187f
Kostuzik, A. A., 108, 123
Kosykh, A. P., 78, 119, 189
Kot, C. A., 189
Kotenev, V. P., 92f, 121
Kotov, V. M., 123
Kovenya, V. M., 90, 94, 121, 272, 285
Kozlov, I. A., 176, 187
Kozlova, I. G., 111, 124
Kraiko, A. N., 74f, 118, 189
Krasilnikov, A. V., 188
Krause, E., 272
Kubota, N., 69
Kuehn, D. M., 69
Kukarkina, M. A., 119f
Kutler, P., 121, 189, 272
Kuznetsov, O. M., 69

Ladyzhenskaya, O. A., 69
Landau, L. D., 54, 69, 131, 149, 188
Lapygin, V. I., 96, 122
Larson, H. K., 69
Latter, R., 189
Lax, P. D., 95, 122, 188f
Lebedev, M. G., 100, 120, 122
Leorat, I., 69
Lerat, A., 189
Li, C. P., 272
Lifshitz, E. M., 69
Lighthill, M. J., 294, 307
Lin, C. C., 307
Lipnitsky, Yu. M., 86, 96, 120, 122, 189
Lisetskin, V. D., 272
Lobanovsky, Yu. I., 92, 121, 189
Loitsianskii, L. G., 273, 285
Lokhanov, M. Yu., 191, 224
Lokutsievsky, O. V., 191
Lomax, H., 189, 272
Lukashin, V. M., 119f
Lunev, V. V., 102, 122, 189
Lun'kin, Yu. P., 124
Lutsky, A. E., 74, 77, 118
Lyakhter, V. M., 69
Lychkin, E. N., 123
Lyubimov, A. N., 81f, 88, 119

MacCormack, V. M., 91, 121, 189
Magnus, W., 307
Magomedov, K. M., 102, 105f, 122f, 187ff
Makhin, N. A., 117, 124
Marinin, V. P., 85, 120
Marchuk, G. I., 7, 188, 272
Mazurov, A. P., 70
McCarthy, J. F., Jr., 36, 69
Meiman, I. N., 131, 149, 188
Meshalkin, L. D., 70
Mikhailov, I. E., 106, 123
Mikhailov, Yu. Ya., 82, 85f, 119
Minailos, A. N., 78, 80, 111, 119, 124, 189, 224
Minostsev, V. B., 87f, 100, 115, 120, 122, 124, 187
Mirabel, A. P., 70
Mirin, A. A., 189
Mitnitsky, V. Ya., 124
Monin, A. S., 69
Moretti, G., 105, 123
Morton, K., 189
Mosin, 120

Nailand, V. Ya., 307
Naudasher, E., 70
Ndefo, D. E., 117, 124
Nelms, W. P., 119
Nersesov, G. G., 85, 120
Neumann, J. von, 144, 189
Nicolson, P., 121
Nikitina, T. V., 76, 119
Nikulin, A. N., 187f
Nisht, M. I., 23, 69

Oberhettinger, F., 307
Obukhov, A. M., 32, 70
Onufriev, A. T., 32, 70, 108
Onufrieva, O. A., 123, 188

Orlova, M. G., 89, 121
Osetrova, S. D., 123, 187f
Ostapenko, N. A., 96, 122

Pal, A., 278, 285
Panteleev, M. S., 66, 70
Park, C., 123
Pavlov, V. G., 102, 122, 189
Pchelkina, L. V., 119f
Peaceman, D. W., 187
Perepukhov, V. A., 272
Petrov, I. B., 183, 187f
Peyret, R., 189
Pirogov, V. B., 108, 123, 187f
Pirogova, S. V., 95, 122
Podladchikov, Yu. N., 100, 122
Pogorelov, N. V., 92, 121
Popov, F. D., 124, 188
Popov, S. G., 69
Popov, Yu. P., 97, 122, 189
Prokopov, G. P., 74, 118, 189
Proskurowski, 224
Pyzik, 95, 122

Rachford, H. H., 187
Radvogin, Yu. B., 81f, 119f, 191
Rakich, J. V., 105, 123
Rees, M., 106, 123, 131, 133, 137, 149, 187
Reshetin, A. G., 123
Reznik, A. A., 191, 212, 224
Richtmeyer, R., 189
Rimskii-Korsakov, A. V., 70
Rotenberg, M., 12
Rozin, A. V., 119
Ruban, A. I., 307
Rubin, S. G., 272ff, 278, 285
Rusanov, V. V., 82, 85, 88, 97, 99, 119f, 122, 124, 187f, 224
Ryaben'ky, V. S., 8, 223f, 272
Ryabinkov, G. M., 124
Rykov, 19
Ryzhov, O. S., 8, 27, 307

Sakharov, V. I., 92f, 121
Samarsky, A. A., 7, 97, 122, 187ff, 224, 272, 285
Sandomirskaya, I. D., 119f
Savinov, K. G., 86ff, 120
Schneider, W., 307
Seeley, R. T., 224
Semenikhina, O. N., 115, 124
Seminar, A. N., 70
Severinov, L. I., 68
Shashkin, A. P., 97, 122
Shchelkonogov, A. N., 123
Shchennikov, V. V., 68, 113, 124
Shepetievsky, O. A., 83, 119
Shevelev, Yu. D., 92f, 121
Shidlovsky, V. P., 8, 273
Shishova, T. V., 189
Shkadova, V. P., 88, 115, 120, 124
Shugaev, F. V., 124
Shwets, A. I., 189
Shwets, I. T., 189
Sinai, Ya. G., 70
Smith, F. T., 307
Sofronov, I. L., 191, 224
Sowerby, L., 273, 285
Stebunov, V. A., 83f, 89, 120
Stewartson, K., 273, 285, 307
Struminskii, V. V., 68f
Sveshnikov, A. G., 224
Syagaev, V. F., 117, 124
Sychev, T. V., 44
Sychev, V. V., 44, 307

Tagirov, R. K., 76, 119
Tarnavsky, G. A., 94, 121
Tarnogrodzki, A., 95, 122
Tatarenchik, V. S., 83f, 119f
Telenin, G. F., 100, 114f, 122, 124
Terent'ev, E. D., 307
Thomée, V., 224
Tikhonov, A. N., 7, 188
Timofeeva, G. Ya., 124
Timoshenko, V. I., 93, 121
Tinyakov, G. P., 100, 114f, 122, 124
Tirsky, G. A., 92f, 121

Tolstykh, A. I., 8, 44, 68, 70, 123f, 188, 272
Townsend, A., 27, 69
Tricomi, F. G., 307
Trusova, O. N., 124
Turchak, L. I., 8, 108, 123, 188
Turchaninov, V. I., 191

Uskov, V. I., 120

Van Dyke, M., 69
Van Leer, B., 189
Vasenov, L. G., 92, 121
Vetlutsky, V. N., 83, 119
Vishnevetsky, S. L., 85, 120
Voinovich, P. A., 189
Volevich, L. R., 191
Volkov, V. F., 92, 121
Vorobyev, N. F., 92, 121
Voronkov, A. V., 191
Voskresensky, G. P., 8, 81, 83f, 89f, 118ff, 124

Waldman, G. D., 124
Warming, R. F., 189, 272
Wasow, W., 307
Weiland, G., 119
Wendroff, B., 189
Widlund, 224

Yaglom, A. M., 69
Yanenko, N. N., 7, 91, 94, 121, 187, 272, 285
Yanitskii, V. E., 48, 68f
Yanushevich, D. N., 191
Yudovich, V. I., 70

Zabrodin, A. V., 74, 118, 189, 191
Zaitseva, N. A., 124
Zapryanov, Z. D., 100, 122, 187
Zarubin, A. G., 81, 119
Zhmakin, A. I., 189
Zhuk, V. I., 8, 307
Zhukov, A. I., 187
Zhuravleva, O. A., 116, 124
Zyuzin, A. P., 43, 70, 115f, 124

Subject Index

Algorithm,
  difference, 225
  higher-accuracy, 254
  splitting, 258, 266
angle,
  of attack, 83, 86f, 89, 96
  roll, 86
approximation(s), 229
  conventional second-order, 261
  finite-difference, 106, 125
  of frozen coefficients, 256, 267
  of hyperbolic system, 233
  Markov, 19
  nonsymmetric, 254
  quadratic, 113
  spatial, 254
  symmetric fourth-order, 229
  third-order, 237, 239, 258

Biocharacteristics, 102
Blasius boundary layer, 277
Blasius profile(s), 269, 273
Blasius solution, 277, 289
boundary condition(s),
  Calderón-Seeley, 206
  internal, 211f

Cauchy data, 204
Cauchy space, 192
Cauchy value, 193
characteristic lines, 102
Chebyshev polynomials, 114
coefficient(s),
  aerodynamic, 103f
  drag, 43
  normal force, 76
  pitch moment, 76
condition(s),
  Calderón boundary, 200ff
  Mises plasticity, 185
  spectral stability, 232
  stability, 157
corner,
  explicit, 131
  implicit, 131f
criterion(a),
  Babenko-Gelfand stability, 247
  Courant, 228
  stability, 129, 265

Density stratification, 47
difference projector(s), 190
disturbance(s), 301ff
  three-dimensional periodic, 297ff
  two-dimensional steady, 294

Equation(s)
  Airy homogeneous, 291f
  balance, 246f
  Blasius, 278
  Boltzmann's, 49f, 264
    kinetic, 15ff
  Boussinesq's, 25
  Bürgers, 247f
  Calderón's, 193
    discretization, 195
  Calderón-Seeley, 200, 204
  continuity, 12, 275, 290
  corner-layer, 274
  Crook's, 50

Equation(s)
difference, 228
dispersion, 294, 297, 301
elliptical, 276
difference, 213f
energy, 12
Euler, 24, 26, 37, 29, 71
difference, 12, 20f, 44, 267
finite-difference, 21
transport, 53
gasdynamic, 75, 103, 109, 137, 152
generalized pseudodifferential, 215, 217
Helmholtz, 191, 276
homogeneous Bessel, 219
difference, 220
hyperbolic, 129, 145, 162, 165, 183, 186
multidimensional, 125f
two-dimensional, 106
integral, 190
internal Stokes, 191
Kac, 17
kinetic, 24, 26
Laplace, 192f
linear,
difference, 190
ordinary differential, 278
momentum, 12, 275, 279
multidimensional,
quasilinear, 186
transport, 166, 186
Navier-Stokes, 14f, 23ff, 29, 31f, 44, 47, 55, 59, 66, 71, 94, 262
difference, 21
time-dependent, 25f
nonlinear transport, 227
one-dimensional, 186
gasdynamic, 233
transport, 226
Onufriev's relaxation kinetic, 49
Poisson, 193, 200, 205f
Poisson-type, 280
pseudodifferential Calderón-Seeley, 191, 193
relaxation, 104
Reynolds, 25, 44
averaged, 30
scalar differential, 222
in several spatial coordinates, 254
of state, 97
three-point,
difference, 240, 253, 262
vector, 244
time-dependent,
Boltzmann, 11
Euler, 11
of gas dynamics and magnetogasdynamics, 149
time-independent, 256
transcendental, 293
two-dimensional Poisson, 280
two-temperature one-velocity gasdynamic, 181
vorticity diffusion, 279
Euclidean metric, 129
Euler cell, 53
experiment,
McCarthy and Kubota, 36
Naudasher, 50f

Field,
isomach, 79
velocity, 181
flow,
in channels, 270
Couette, with injection, 249
mainstream, 56
past bodies of revolution, 270
Prandtl-Mayer, 97
supersonic, 84, 102
three-dimensional, 84ff
viscous,
fluid, 225, 244
gas, 262
flow-correction technique, 154
formula,
Green's difference, 190
Taylor, 221
function(s),
Airy, 291, 293, 295

function(s)
Bessel, 52
Blasius, 277
Green, 192, 200f
difference, 200, 205, 211f
grid, 156
mesh, 196, 219, 240
Taylor, 222
functional, quadratic, 217

Grid,
difference, 226
Euler, 12

Hermite interpolation polynomials, 230, 252f
Hilbert norms, 196, 216f
Hölder class, 201
hypothesis,
Kolmogorov's second similarity, 30
Millionshchikov's, 52

Identity, Green's classical, 192f, 211
instability,
Kelvin-Helmholtz, 34
Neumann, 105
Rayleigh-Taylor, 9, 66
supersonic boundary layer, 297ff
internal iterations, 259
interpolation expressions, 103

Jacobi matrices, 257, 267

Law(s),
Kolmogorov's, 25
Kolmogorov-Obukhov, 31
conservation, 74, 125, 165
in divergent form, 227

Mach line, 35
Mach triple, configuration, 97
mesh,
adaptable, 245
difference, 225
method(s),
Adams, 241
of approximating transverse derivatives, 106
Bird's, 265
of characteristics, 97ff, 102
three-dimensional, 118
two-dimensional, 105
coarse-particle, 11f, 34, 39, 66
computational, 225
difference, 225
of difference potentials (MDP), 190f, 219
algorithm of, 217, 220
of difference projectors, 215
Euler difference, 34
explicit first-order, 74
finite-difference, 25, 73ff, 101, 118
of finite elements, 72
of flows, 14
Fourier, 194, 244
spectral, 25
of fractional steps, 91
Galerkin's, 56
gradient, 197, 217
grid characteristic, 98, 106ff, 125, 145ff, 165, 170, 179, 183, 187
higher-accuracy, 225
implicit second-order, 81, 126
of indeterminate coefficients, 252
of integral relations, 72, 108ff, 113, 118
integro-interpolation, 126, 147
inverse, 125
linearization, 72
Monte-Carlo, 11, 48
numerical, 17f
Newton, 111, 260, 294
of operator inequalities, 254
of particles, 95
of regularization, 144
of discontinuous numerical solutions, 162
Reynolds, 29
Runge-Kutta, 126, 147, 153
scalar sweep, 94
spectral, 254, 227

method(s)
splitting, 11, 90f
in spatial parameters, 125
stabilization, 186
statistical, 29, 34, 53
of statistical simulation, 49
of straight lines, 72, 108, 114, 118
sweep ("progonka"), 82, 199, 229
time-marching, 72, 173
model,
cascade, 34
Euler nonstationary, 31
grid, 126ff, 131, 134ff, 147f, 158, 186f
nonsymmetric, 143
implicit six-point, 131
Kac, 17f
Navier-Stokes, 26
six-point, 167
implicit, 147
semi-empirical, 271
statistical, 16
thermodynamic equilibrium, 81
three-point, 130

Number
Courant, 152, 156
Knudsen, 9, 23
Mach, 19, 44, 76, 80, 83, 86, 89, 93, 103, 107, 115, 117, 172, 177, 263, 269, 271, 290, 293, 295f, 301ff
Reynolds, 16, 22, 24ff, 31f, 36, 46, 54, 56, 59, 61, 64f, 249, 263, 265, 268f, 271, 291f, 307
Struchal, 48

Operator,
antismoothing, 155
Bessel, 219
difference-matrix, 257
elliptical, 193
Green, 194, 200
Green's difference, 208
Laplace, 222
matrix difference, 255
multidimensional difference, 169
three-point, 252, 261
trace, 202

Parameter(s),
grid, 183
normalization, 17
point,
Ferri, 96
singular, 117
mesh, 165
nodal, 103
stagnation, 101f
potential(s), 207
continual, 197, 214, 217
difference, 193ff, 177, 211, 214, 217
metric properties of, 211
Green's 200
principle,
self-similar stationing, 72, 83
time-dependent stationing, 74, 77, 83, 89, 92
problem(s),
auxiliary difference, 213, 220
(nonclassical) boundary value, 222
Blasius, 275
boundary value, 82, 187, 215
difference, 190, 218
differential, 190
Calderón, 192
Cauchy, 164
multidimensional, 258
Dirichlet, 192
difference, 193
exterior, 218
boundary value, 218
gasdynamic, 231
multidimensional, 170
in gas dynamics, 125
Orr-Sommerfeld periodic, 56
Riemann breakdown, 231, 233
simulation, 141

problem(s)
stationary axisymmetric, 177
Stokes, 223
supersonic flow, 73
of supersonic flow past spherically blunted bodies, 176
three-dimensional nonstationary, 177
on three-dimensional supersonic flow of perfect gas, 78
time-dependent, 237, 260
time-independent, 257, 259, 262
in fluid mechanics, 263
two-dimensional, in mechanics of deformable rigid body, 185
of turbulence diffusion, 50
two-dimensional nonstationary, 95
process(es),
Ievlev's, 33
Markov, 17
projector(s), 205, 207
Calderón, 200
difference, 211
properties, metric, 207

Relation(s),
compatibility, 97ff, 105f, 153
dispersion, 290ff, 305
Rankine-Hugoniot, 74
relaxation,
collision, 17
collisionless, 17
Reynolds stress, 24
Riemann invariants, 146, 236

Schauder estimates, 214
scheme,
of approximation of generalized continual potential by difference potential, 212
with bicharacteristics, 99
Carlsson's 132, 137, 150, 168f
monotonic, 152
central difference, 251
Chapman's classical, 36
compact, 262
higher-accuracy, 251f
nonsymmetric, 251
conservative, 147, 179
difference, 74, 163
first-order, 148
scheme,
Crank-Nicolson implicit, 92
difference, 77, 126, 129, 141, 144, 146, 151
Euler, 31
explicit-implicit, 169
first-order, 166
third-order, 141, 157
explicit, 73, 153
flow-correction, 155
monotonic difference, 75
factorization, 267
finite-difference, 14, 91
first-order,
monotonic, 155
nondivergent, 171, 177, 179
grid-characteristic, 185
first-order, 182
higher-order, 169
higher-accuracy, 226, 245
non-symmetric stable, 233
homogeneous, 20
difference, 231
hybrid, 145, 165, 169
grid-characteristic, 161
two-step, 155
three-step, 157
implicit, 73, 153, 182
difference, 94, 231, 280
splitting, 240
through-counting, 94
Kosarev's explicit fully-conservative second-order, 182
Lax, 131, 133, 137, 154
difference, 149
Lax-Wendroff, 135f, 143, 155, 169, 240
second-order, 153
non-optimal, 161
least-oscillating second-order, 155
locally divergent, 165, 179

scheme,
MacCormack, 91, 93, 157, 169
two-step, 92
monotonic (majorant), 130, 156, 186
higher-order, 187
linear explicit two-dayer second-order, 134
second-order, 187
multistep difference, 91
nonsymmetric, 267
compact, 226ff
positive approximation, 154, 158, 161
Rusanov explicit difference, 96
second-order, 245
Shkadova's two-point implicit, 88
single-strip, 113
splittng, 267
symmetric, 230, 251, 268
third-order, 226, 254
explicit, 169, 231
implicit, 232f
compact, 225
three-deck, 239
three-step, 155
time-marching, 267
two-level, 240
two-step predictor-corrector, 73, 93
unstable, 154
shock wave, 46
oblique, 46
space,
of continuous functions, 213
Hölder, 220
mesh, 212
of mesh functions, 213
Sobolev, 212
Squire transformation, 291
stability,
absolute, 260
Courant, 73
stagnation zone, 39
Stokes ray, 294
structure(s)
coherent, 27
dynamic, 27
structure(s)
flow, 27
large scale, 28
sweep(s),
scalar, 262
three-point, 261
vector, 262, 266
three-point, 267
system,
Fridrich's hyperbolic, 146
Stokes, 221

Theorem
on discretization, 216
representation, 130
Squire, 307
theory,
boundary layer, 274
of elasticity, 146
Landau's turbulence evolution, 32
Prandtl-Reiss ideal elastic-plastic flow, 185
Taylor-Görtler, 296
Thomée estimates, 213
through counting, 75
trace,
sharp, 200, 202f, 209, 214
difference, 207, 214
transformation, 307
turbulence, small-scale, 29

Variable,
Euler, 183
Lagrangian, 182
velocity,
group, 238
mean flow, 64
phase, 241
vortex road, 39, 43
Karman, 48

Wave number, longitudinal, 301

TO THE READER

Mir Publishers would be grateful for your comments on the content, translation and design of this book. We would also be pleased to receive any other suggestions you may wish to make.

Our address is:
Mir Publishers
2 Pervy Rizhsky Pereulok
I-110, GSP, Moscow, 129820
USSR

Printed in the Union of Soviet Socialist Republics

УДК 531+681(022)=20

Сборник статей под редакцией

Олега Михайловича Белоцерковского и
Всеволода Павловича Шидловского

СОВРЕМЕННЫЕ ПРОБЛЕМЫ
ВЫЧИСЛИТЕЛЬНОЙ ГИДРОДИНАМИКИ

Научные редакторы Т. Д. Барановская и Е. Л. Трошнева
Редакторы Г. Б. Дяченко, Т. В. Лазарева, И. Я. Мельникова
Художник В. Б. Юдин
Художественный редактор Н. В. Зотова
Технический редактор Е. С. Потапенкова
Корректоры М. Э. Александрова, Н. Ф. Шлифер

ИБ № 5726

Сдано в набор 27.12.85. Подписано к печати 15.05.86.
Формат $60 \times 90^1/_{16}$. Бумага типографская № 1. Печать высокая.
Гарнитура обыкновенная. Объем 10,0 бум. л. Усл. печ. л. 20,0.
Усл. кр.-отт. 20,21. Уч.-изд. л. 20,95. Изд. № 10/4001.
Тираж 3970 экз. Зак. 0501. Цена 2 р. 45 к.

ИЗДАТЕЛЬСТВО «МИР»
129820, ГСП, Москва, И-110, 1-й Рижский пер., 2.

Ордена Трудового Красного Знамени
Московская типография № 7 «Искра революции»
Союзполиграфпрома Государственного комитета СССР
по делам издательств, полиграфии и книжной торговли.
103001, Москва, Трехпрудный пер., 9.

С $\frac{1703040000-367}{056(01)-86}$ 13—86, ч. 2

Current Problems in Computational Fluid Dynamics

Edited by O. M. Belotserkovskii, Mem. USSR Acad. Sc., and V. P. Shidlovsky, D. Sc. (Phys.-Math.)

This is a collection of articles by Soviet scientists on various problems in computational fluid dynamics. The articles involve those methods and applications which best meet today's requirements, that is those involving three-dimensional physical processes taking into account possible time-dependent physical processes or nonlinear effects. The aim of this collection is to make available in English results obtained by Soviet scientists in computational fluid dynamics.

Mir Publishers
2 Pervy Rizhsky Pereulok,
1-110, GSP, Moscow, 129820
USSR